“Catalytic upgrading of fast pyrolysis bio-oils applying nickel-based catalysts”

zur Erlangung des akademischen Grades einer

DOKTORIN DER INGENIEURWISSENSCHAFTEN

von der KIT-Fakultät für Chemieingenieurwesen und Verfahrenstechnik des

Karlsruher Instituts für Technologie (KIT)

genehmigte

DISSERTATION

von

M.Sc. Caroline Carriel Schmitt

aus

Curitiba (Brasilien)

Tag der mündlichen Prüfung: 16.Oktober 2020

Erstgutachter: Prof. Nicolaus Dahmen

Zweitgutachter: Prof. Jan-Dierk Grunwaldt

Declaration

I Caroline Carriel Schmitt, declare that this thesis represents my own work and that I have written this thesis independently by myself, without the use of other documents or sources beyond those stated in the references.

Caroline Carriel Schmitt

Acknowledgement

Once I had a dream of studying abroad. For me it was a long journey started in 2006, when I decided to be a Chemical Engineer. Later in 2013, I moved to Ireland to learn English with the goal of doing my PhD in an excellent university in the field of renewable energy. Therefore, finishing this journey at Karlsruhe Institute of Technology at the Institute of Catalysis Research and Technology is such a big accomplishments and I could not be happier.

There is no way to conclude such a journey yourself. It is definitely a teamwork, with the collaboration of many people and I am deeply grateful to all of you.

I am extremely grateful to Prof. Nicolaus Dahmen. I am such a lucky person for having a brilliant Professor guiding my work, contributing to my personal growth and always motivating me. I am very grateful for all freedom to develop my PhD work, for your support on my passion to build collaboration projects Brazil-Germany and for helping me to grow professionally. Thank you also for sharing your broad knowledge about biomass conversion contributing significantly to the development of my thesis. Thank you "Nico" for all!

I would like to say thank you to Dr. Klaus Raffelt. Klaus, thank you very much for supporting me every single day and for allowing me to develop my PhD thesis in your research group. Thank you for encouraging me to attend several International Conferences, building a scientific network, which significantly contributed to the development of my thesis. Thank you also for giving me the chance to supervise HiWi and Master Students, which definitely contributed to my project. Furthermore, thank you very much for your support with Brazil-Germany cooperation projects, for the emails late night full of valuable scientific ideas and for teaching me so many things, especially NMR.

I would like to thank Prof. Grunwaldt, for sharing your deep knowledge in catalysis. Thank you for helping me to learn more about catalysis, for supporting the characterization of my catalysts and for all deep review of my work during the TAC meetings as well as peer reviewed publications. Thank you also for supporting and encouraging my exchange period at Technical University of Denmark, which was an important experience that significantly contributed to my PhD project.

I would like to thank the BBW Forwerts – the Bioeconomy Graduate Program of the Baden-Württemberg state, especially Prof. Thomas Rausch, Dr. Ines Petersen and Dr. Annette Weidtmann. I am grateful for the soft skills courses, excursions, Summer Schools and Bioeconomy Conferences. During my time at the Graduate Program, I had the opportunity to learn a lot and see that Bioeconomy is one of my big passions. Thank you also for supporting my idea and enthusiasm of bringing Brazilian students and Brazilian professors for two of our Summer Schools.

I am also thankful to Prof. Anker Degn Jensen and Prof. Martin Høj from Technical University of Denmark for supporting and supervising my work during my exchange in Denmark. It was an excellent opportunity to develop part of my PhD thesis in Denmark learning more about continuous catalytic reactions. I am also thankful to Anders Kjersgaardo for helping me with any technical issue during the operation of the continuous reactor. Jeg har lært så meget takket være dig!

I want to thank Dr. Axel Funke, Daniel Richter, Renata Moreira and Dr. Renato Cruz Neves for the execution of the work with sugarcane bagasse. It was one of my favorite parts of the project and being part of such hard working team was really rewarding. Thank you all! There is more to come!

Big thanks to Maria Belén Gagliardi Reolón for accepting doing her Master thesis under my supervision and for significantly contribute to the overall project. We had a great hardworking time together! Thanks also to the HiWi students Mouhannad Moulla, Zeineb Yigit and Katharina Rieker.

Thanks to the IKFT analytical team that deeply supported my experiments: Pia Griesheimer, Jessica Maier, Jessica Heinrich, Petra Janke, Melanie Frank, Birgit Rolli, Gilbert Zwick, Michael Zimmermann, Hermann Köhler and Armin Lautenbach.

A big thank to Anna Zimina for the support with X-ray absorption spectroscopy analysis as well as for the review of my work and for the very insightful discussions.

I am also thankful to Bärbel Krause for the XPS analysis, Yakub Fam for the STEM-EDX analysis, Simon Wodarz for H_2-TPR measurements, Dr. Thomas Otto for BET measurements, Oliver Schade for the support with the catalyst reduction oven and Bernhard Hochstein for the viscosity measurement.

I also would like to thank all my PhD colleagues for the nice time together. Our lunchtime was full of fun and sharing these years with our very multicultural team thought me a lot!

I also would like to thank Dr. Michael Rapp for opening the doors of Germany to me.

A big thank to my friends in Karlsruhe, especially to Rafa, Guilherme, Halina, Gaby and Huey and Leo for the dinners full of fun. A big thank to the all my capoeira friends around Europe which energized me in every capoeira event we had the chance to attend. Thanks also to my family and to my husband for being always by my side.

Obrigado, Dankeschön, Gracias, Dziękuję Ci, 謝謝, Tak, جزيلا شكرا, teşekkür ederim, **Спасибо, terima kasih, Thank you all!**

"If I have seen further, it is by standing upon the shoulders of giants"

Sir Isaac Newton

Preface

Some of the chapters presented in this thesis have been previously published or are under preparation for peer-reviewed publications. Hence, the content may be identical to the content already published, with minor modifications, such as formatting, citation style or even modification of the figures, tables and layout. The chapters with previously published content or currently under preparation are described below:

Chapter 3: “Evaluation of high-loaded Ni-based catalysts for upgrading fast pyrolysis bio-oil”.

Chapter 4: “Hydrotreatment of fast pyrolysis bio-oil fractions over nickel-based catalyst”

Chapter 5: “Synthesis and regeneration of nickel-based catalysts for hydrodeoxygenation of beech wood fast pyrolysis bio-oil”.

Chapter 6: “From agriculture residue to upgraded product: the thermochemical conversion of sugarcane bagasse for fuel and chemical products”.

Chapter 7: “Evaluation of nickel-based catalysts for hydrotreatment of bio-oil model compound mixtures in a continuous flow reactor: selectivity and resistance to sulfur poisoning” (under preparation).

List of publications

Peer-reviewed manuscripts

Schmitt, C. C., Zimina, A., Fam, Y., Raffelt, K., Grunwaldt, J.D., Dahmen, N. (2019). Evaluation of High-Loaded Ni-Based Catalysts for Upgrading Fast Pyrolysis Bio-Oil. *Catalysts,* 9 (9), 784-812.

Schmitt, C. C., Raffelt, K., Zimina, A., Krause, B., Otto, T., Rapp, M., Grunwaldt, J.D., Dahmen, N. (2018). Hydrotreatment of Fast Pyrolysis Bio-oil Fractions over Nickel-based Catalyst. *Topics in Catalysis*, 61, 1769-1782.

Schmitt, C. C., Reolon, M.B.G., Zimmermann, M., Raffelt, Grunwaldt, J.D., Dahmen, N. (2018) Synthesis and Regeneration of Nickel-based Catalysts for Hydrodeoxygenation of Beech Wood Fast Pyrolysis Bio-oil. *Catalysts*, 8 (10), 449-477.

Schmitt, C. C., Moreira, R., Neves, R.C., Richter, D., Funke, A., Raffelt, K., Grunwaldt, J.D., Dahmen, N. (2020). From agriculture residue to upgraded product: The thermochemical conversion of sugarcane bagasse for fuel and chemical products. Fuel Processing Technology, 197, 106199.

Conference proceedings

Moreira, R., Neves, R.C., Schmitt, C.C., Breunig, M., Tambani, P.C., Ushima, A.H., Funke, A., Raffelt, K. (2017). Characterization of Brazilian sugarcane bagasse and sugarcane straw based on European methodologies to evaluate the potential for energy conversion. Conference proceeding at 25th European Biomass Conference in Stockholm 2017.

Schmitt, C.C., Boscagli, C., Rapp, M., Raffelt, K., Dahmen, N. (2017). Characterization of light and heavy phase of pyrolysis-oil from distinct biomass for further upgrading reactions. Conference proceeding at 25th European Biomass Conference in Stockholm 2017.

Schmitt, C.C., Reolon, M.B.G., Raffelt, K., Dahmen, N. (2018). Síntese e regeneração de catalisadores de níquel para hidrotratamento de bio-óleos de pirólise rápida. Conference proceedings at XXVI Congresso Íbero Americano de Catálise, Coimbra, 2018.

Conference oral presentations

Schmitt, C.C., Moreira, R., Neves, R.C., Richter, D., Funke, A., Raffelt, K., Grunwaldt, J-D., Dahmen, N. (2020). Thermochemical conversion of sugarcane bagasse and catalytic upgrading of fast pyrolysis bio-oil as a potential conversion route in sugarcane refineries. Oral presentation at 3rd International Bioeconomy Congress Baden-Württemberg, Stuttgart, 2020.

Schmitt, C.C. (2019). Institute of Catalysis Research and Technology: Research activities and Collaboration Potential. Oral presentation at Anpei Innovation Conference as part of the Innovation & Matchmaking Tour organized by Enrich in Brazil, Foz do Iguaçú, 2019.

Schmitt, C.C., Rapp, M., Raffel, K., Dahmen, N. (2018). Hydrotreatment of the Heavy Phase Fraction of Beech Wood Pyrolysis Oil Over Nickel Catalyst. Oral presentation at the 2nd International Conference on Catalysis and Chemical Engineering, Paris, 2018.

Schmitt, C.C., Boscagli, C., Raffelt, K., Rapp, M., Dahmen, N. (2018). Hydrotreatment of bio-oil for fuels and chemicals production. Oral presentation at the Biomass and Bioenergy Conference, Sorocaba, 2018. **Prize 1st place oral presentation.**

Schmitt, C.C., Yigit, Z., Moreira, R., Rapp, M., Raffelt, K., Dahmen, N. (2017). Extraction, characterization and evaluation of pyrolytic lignin from beech wood bio-oil for applications as a bio-based material. Oral presentation at the 13th International Conference on Renewable Resources & Biorefineries, Wroclaw, 2017.

Conference poster presentation

Schmitt, C.C., Raffelt, K., Dahmen, N. (2020). Sequential Hydrotreatment of Beech wood fast pyrolysis bio-oil with nickel-based catalysts. Poster presentation at the 28th European Biomass Conference and Exhibition, Marseille, 2020. **1st place best poster prize.**

Schmitt, C.C., Raffelt, K., Grunwaldt, J.D., Dahmen, N. (2019). Two steps upgrading of beech wood fast pyrolysis bio-oil with nickel-based catalysts. Poster presentation at the Pyroliq conference, Cork, 2019.

Schmitt, C.C., Moreira, R., Neves, R.C., Richter, D., Funke, A., Raffelt, K., Grunwaldt, J.D. (2019). Fast pyrolysis of sugarcane biomass and hydrotreatment of pyrolysis oil for production of renewable fuels and chemicals. Poster presentation at the 9th edition of the biennial Brazil-Germany Symposium on Sustainable Development, Stuttgart, 2019.

Schmitt, C.C., Reolon, M. B.G., Raffelt, K., Grunwaldt, J.D., Dahmen, N. (2018). Synthesis and reuse of nickel-based catalysts for upgrading of pyrolysis oil. Poster presentation at the 18th Nordic Symposium on Catalysis, Copenhagen, 2018. **1st place as the best poster prize.**

Schmitt, C.C., Moreira, R., Neves, R.C., Funke, A., Raffelt, K., Dahmen, N. (2018). Upgrading of pyrolysis-oil produced from sugarcane refinery residues. Poster presentation at the Biomass and Bioenergy Conference, Sorocaba, 2018.

Schmitt, C.C., Moreira, R., Neves, R.C., Funke, A., Raffelt, K., Dahmen, N.(2018). Upgrading of pyrolysis-oil produced from sugarcane biorefinery residues. Poster presentation at the Biomass and Bioenergy Conference, Sorocaba, 2018.

Schmitt, C.C., Rapp, M., Raffelt, K., Dahmen, N. (2018). Mild and deep hydrodeoxygenation of pyrolysis oil over nickel catalysts. Poster presentation at the 26th European Biomass Conference, Copenhagen, 2018.

Schmitt, C.C., Rapp, M., Raffelt, K., Dahmen, N. (2017). Hydrodeoxygenation of beech wood bio-oil over nickel catalyst. Poster presentation at the 2nd International Bioeconomy Congress, Stuttgart, 2017.

Schmitt, C.C., Boscagli, C., Rapp, M., Raffelt, K., Dahmen, N. (2017). Characterization of light and heavy phase of pyrolysis-oil from distinct biomass for further upgrading reactions. Poster Presentation at the 25th European Biomass Conference in Stockholm 2017.

Moreira, R., Neves, R.C., Schmitt, C.C., Breunig, M., Tambani, P.C., Ushima, A.H., Funke, A., Raffelt, K. (2017). Characterization of Brazilian sugarcane bagasse and sugarcane straw based on European methodologies to evaluate the potential for energy conversion. Poster presentation at the 25th European Biomass Conference in Stockholm 2017.

Abstract

Motivated by the population growth, climate change and limited fossil fuel resources, renewable alternatives for fuels and chemicals production are becoming more and more important. Biomass, especially residual lignocellulosic biomass shows a significant potential as feedstock for bioenergy, due to its high carbon content and short-term availability. Among the thermochemical conversion technologies, fast pyrolysis for biomass liquefaction can be considered already well stablished, as several commercial plants are spread worldwide. However, fast pyrolysis bio-oil, the main product of fast pyrolysis, currently shows limited bioenergy application as boiler fuel for heat production. It can be explained by its chemical composition and properties, as fast pyrolysis bio-oil is an acidic multi-component product, with low energetic density due to its high content of water and oxygenated compounds. Moreover, wood is the only feedstock currently used commercially.

In order to expand the feedstock range and application viability, an additional upgrading treatment may be required in order to improve the fast pyrolysis properties, meeting existing fuel standards. In order to do so, catalytic hydrotreatment is considered a promising upgrading treatment, as it is a well-known technology currently applied in petroleum refineries for heteroatoms removal from crude oil. However, due to the differences in chemical composition, the hydrotreatment conditions applied to crude oil cannot be simply applied to fast pyrolysis bio-oil. Although research in this field has been carried out for a few decades, there are still open questions to enable hydrotreatment to produce fuel oils from residual biomass in stable processes. By developing a robust fast pyrolysis bio-oil hydrotreatment process, small biorefineries units could be installed near to feedstock sourcing or even be installed in biorefinery units already stablished, such as a sugarcane biorefinery, in which high volumes of residual biomass are generated. Also, co-processing of crude oil and fast pyrolysis bio-oil in petroleum refineries may be a feasible option.

In view of the importance of the hydrotreatment for expansion of the range of chemicals obtained by thermochemical conversion of residual biomass, the presented work investigated the hydrotreatment of fast pyrolysis bio-oil applying nickel-based catalysts. In a systematic evaluation nickel-based catalysts with different metal loading, supports and promoters have been studied. Overall, six nickel-based catalyst were screened and compared to ruthenium supported in activated carbon. The hydrotreatment conditions in terms of reaction time, temperature and pressure were optimized and fast pyrolysis bio-oils derived from beech wood and residual biomass (sugarcane bagasse) were hydrotreated. Additionally, the heavy phase separated from beech wood bio-oil, characterized by its high content of lignin-derived compounds, was hydrotreated. The effect of deactivation by sulphur on the hydrotreatment was investigated by use of model substances in a continuously operated trickle bed reactor, since with this reactor the deactivation can be observed depending on time (in contrast to batch experiments). Finally, a 2-step upgrading approach of a previously upgraded fast pyrolysis bio-oil was proposed and verified.

Initially two high loaded nickel-based catalysts (monometallic nickel and nickel-chromium) were evaluated in comparison to Ru/C by batch hydrotreatment of beech wood bio-oil at 80 bar, 4 h, 175 °C and 225 °C. Both nickel-based catalysts revealed similar hydrodeoxygenation activities for the conditions applied and the nickel catalysts showed the higher hydrogenation activity compared to Ru/C. The nickel-chromium catalyst demonstrated

the highest activity for conversion of organic acids, ketones and sugars, attributed to the strength of the acid sites promoted by chromium oxide. When applied in a second hydrotreatment step of a previously upgraded oil, the oxygen content of the oil was reduced by 64.8 % in comparison to the original feedstock while the water concentration was reduced by 90 %. Nearly 96 % of the organic acids were converted and the higher heating value was increased by 90.1 %. Despite nickel-chromium demonstrated the best activity in the one step hydrotreatment reactions and contributed significantly in the 2-step upgrading, the oxygen content of 25.3 wt.% dry basis in the upgraded oil was still considered high. Thus, the upgrading conditions were further optimized, aiming to achieve higher hydrodeoxygenation performance.

The conditions of batch hydrotreatment were optimized with nickel-chromium catalyst considering two pressures (80 and 100 bar), four temperatures (175 °C, 225 °C, 275 °C and 325 °C), for both the complete beech wood fast pyrolysis bio-oil, as well as for the heavy phase after spontaneous separation induced by intentional ageing of the bio-oil. At higher temperatures, increased hydrodeoxygenation levels were reached, while at higher pressure larger hydrogen consumption was observed with no significant influence on hydrodeoxygenation. The best conditions among all tested was obtained by hydrotreating the beech wood bio-oil at 325 °C and 80 bar; in this case, 43 % of hydrodeoxygenation was reached. Although improved hydrodeoxygenation activity observed with nickel-chromium at optimized conditions, the results motivated the synthesis and evaluation of new nickel-based catalysts, targeting higher deoxygenation levels.

In the next part of this study, four nickel-based catalyst were synthesized by wet impregnation and evaluated for the hydrotreatment of beech wood fast pyrolysis bio-oil. The catalysts were supported in silica and zirconia and the influence of copper as promoter was studied. Among them, nickel-silica was the most active for hydrodeoxygenation, reducing the oxygen content of the upgraded beech wood fast pyrolysis bio-oil by more than 50 %. The highest degree of water removal as well as low gas and char production were also considered good properties attributed to this catalyst. The investigation on repeated cycles of hydrotreatment with the same catalyst showed a remaining activity even after the fourth reuse, in which 43 % of oxygen was removed. Thus, based on the results obtained with Ni/SiO_2, this catalyst was selected together with nickel-chromium catalyst to be used for hydrotreatment of fast pyrolysis bio-oil from residual biomass, as until this point the study had considered only wood-based fast pyrolysis bio-oil.

Based on the studies so far, the integration of hydrotreatment into a thermochemical conversion route of residues in a sugarcane refinery was proposed. For that, the study encompassed sugarcane bagasse characterization, fast pyrolysis and hydrotreatment of the so-derived bio-oils with nickel-chromium and nickel-silica catalyst. The detailed investigation of the bagasse and the fast pyrolysis bio-oil compositions allowed the correlation of the biomass building blocks with the monomers obtained. The hydrotreatment showed that nickel-chromium showed highest activity for organic acids conversion, as previously observed with beech wood bio-oil, whereas nickel-silica revealed more active for conversion of aromatics. Hydrodeoxygenation of 43.3 % was obtained with nickel-silica. Although both catalysts demonstrated to be active at the conditions evaluated, the high viscosities of the upgraded oils in comparison to those obtained from fast pyrolysis showed that polymerization took place and must be further investigated in detail, as it is one of the limiting factors for further application of

fast pyrolysis bio-oil hydrotreatment. Overall, this studied showed to be very promising and future studies are planned.

In the final part of the thesis, both high loaded nickel-based catalysts studied in the first chapters were selected for a detailed investigation in a continuous operated tricked bed hydrotreatment reactor, due to the similar nickel concentration, nickel particle size and support. The selection of both catalysts aimed to investigate the influence of sulfur on long term catalyst deactivation and the role of chromium in catalyst deactivation. Both catalysts were active for conversion of model substances over more than 48 h of reaction time. By the presence of sulfur, the selectivity of both catalysts changed, mainly towards alkene formation, while the activity remained in the same range. Formation of Ni_3S_2 was observed for both catalysts, but the highest intensity in the diffraction peak of metallic nickel in the nickel-chromium catalyst might be an indication of higher resistance to sulfur poisoning in comparison to Ni catalyst. In general, the catalysts were active for the conditions tested, although the hydrogenation activity was compromised by sulfur poisoning.

Overall, all the catalysts tested in this study were active for hydrotreatment of fast pyrolysis bio-oils. If only stabilization of reactive compounds such as aldehydes and furfurals is required, all of them could be considered suitable candidates. In terms of hydrodeoxygenation activity, Ni/SiO_2 showed the highest performance, while nickel-chromium showed to be the most active for conversion of organic acids and superior hydrogenation capacity than Ni/SiO_2.

Zusammenfassung

Aufgrund des Bevölkerungswachstums, des Klimawandels und der begrenzten Ressourcen fossiler Brennstoffe werden erneuerbare Alternativen für die Herstellung von Brennstoffen und Chemikalien immer wichtiger. Biomasse, insbesondere lignocellulosehaltige Restbiomasse, weist aufgrund ihres hohen Kohlenstoffgehalts und ihrer hohen Verfügbarkeit ein erhebliches Potenzial als Ausgangsmaterial für Bioenergie auf. Unter den thermochemischen Umwandlungstechnologien kann die Schnellpyrolyse zur Verflüssigung von Biomasse als bereits gut etabliert angesehen werden, da mehrere kommerzielle Anlagen weltweit in Betrieb sind. Bioöl ist das Hauptprodukt der Schnellpyrolyse, jedoch ist seine Anwendung als Brennstoff für die Wärmeerzeugung zur Zeit noch begrenzt. Dies lässt sich durch seine chemische Zusammensetzung und seine Eigenschaften erklären, da es sich bei Schnellpyrolyse-Bioöl um ein saures Mehrkomponentengemisch handelt, das aufgrund seines hohen Gehalts an Wasser und sauerstoffhaltigen organischen Molekülen eine niedrige Energiedichte aufweist. Holz ist das einzige derzeit kommerziell verwendete Ausgangsmaterial.

Um die Eigenschaften zu verbessern, Brennstoffnormen zu erfüllen und das Einsatzspektrum zu erweitern ist eine zusätzliche Aufbereitung erforderlich. Die katalytische Hydrierung ist eine vielversprechende Behandlung dafür, da es sich dabei um eine bekannte Technologie handelt, die derzeit in Erdölraffinerien zur Entfernung von Heteroatomen aus Rohöl angewandt wird. Aufgrund der unterschiedlichen chemischen Zusammensetzung können die bei Rohöl angewandten Bedingungen der Wasserstoffbehandlung jedoch nicht einfach auf Pyrolyseöl aus Biomasse übertragen werden und es gibt trotz jahrzehnte langer Forschung in diesem Bereich noch viele offene Fragen. Mit der Entwicklung eines robusten Hydrierverfahrens für Pyrolyseöl aus Biomasse könnte dieses Upgrading mit der Pyrolyseanlage gekoppelt sein und sich somit in der Nähe von Sammelpunkte für Biomassereststoffe oder Energieplantagen oder Verarbeitungsbetrieben (z.B. für Zuckerrohr) befinden. Alternativ ist die gemeinsame Verarbeitung von Rohöl und Bioöl der Schnellpyrolyse in einer Erdölraffinerie eine praktikable Option.

Angesichts der Bedeutung des hydrierenden Upgradings zur Erweiterung des Chemikalienspektrums, das durch thermochemische Umwandlung von Restbiomasse gewonnen werden kann, wird in der vorliegenden Arbeit die Hydrierung von Schnellpyrolyseölen auf Nickelbasis untersucht. Nickelhaltige Katalysatoren mit unterschiedlichen Metallbeladungen, Trägern und Promotoren werden systematisch untersucht und evaluiert. Insgesamt wurden sechs Katalysatoren auf Nickelbasis gescreent und mit Ruthenium auf Aktivkohle verglichen. Die Hydrierungsbedingungen wurden hinsichtlich Reaktionszeit, Temperatur und Druck optimiert und dann auf Schnellpyrolyseöl aus Buchenholz und Zuckerrohrbagasse angewandt. Zusätzlich wurde die aus dem Buchenholz-Bioöl abgetrennte schwere Phase, die sich durch ihren hohen Gehalt an Ligninverbindungen auszeichnet, einer Hydrierung unterzogen. Die Deaktivierung der Upgradingreaktion durch Schwefel wurde unter Verwendung von Modellsubstanzen in einem kontinuierlich betriebenen Rieselbettreaktor untersucht, da dort im Gegensatz zu Batch-Experimente auch die zeitliche Auflösung beschrieben werden kann. Schließlich wurde ein 2-stufiges Upgrading vorgeschlagen und verifiziert.

Im Weiteren wurden zwei hochbeladene Katalysatoren auf Nickelbasis charakterisiert und die Hydrierung von Pyrolyseöl im Batchreaktor bei 80 bar, 4 h Reaktionszeit, und einer Temperatur von 175 °C und 225 °C mit diesen beiden Katalysatoren und mit Ru/Aktivkohle als

Referenz verglichen. Beide Katalysatoren auf Nickelbasis zeigten ähnliche Hydrodesoxygenierungs-aktivitäten bei den genannten Bedingungen und hatten höhere Hydrierungsaktivität als Ru/C als Referenzkatalysator. Der Nickel-Chrom-Katalysator zeigte seine Aktivität vor allem in der Umwandlung von organischen Säuren, Ketonen und Zuckern, was darauf zurückzuführen ist, dass die sauren Positionen durch Chromoxid gefördert werden. Bei der weiteren Hydrierung eines zuvor schon upgegradeten Pyrolyseöls wurde der Sauerstoffgehalt im Vergleich zum ursprünglichen Ausgangsmaterial um 64,8 % reduziert, die Wasserkonzentration um 90 %. Nahezu 96 % der organischen Säuren wurden umgesetzt und der obere Heizwert um 90,1 % erhöht. Obwohl jedoch Nickel-Chrom die beste Aktivität in den einstufigen Hydrotreatment-Reaktionen zeigte und bei dem zweistufigen Upgrading einen hohen Anteil hatte, blieb der Sauerstoffgehalt bei 25,3 Gew.-% im hydrierten Öl immer noch hoch. Daher wurden die Reaktionsbedingungen weiter optimiert, mit dem Ziel, eine höhere Hydrodeoxygenierungs-leistung zu erreichen.

Dazu wurde der Paramtersatz erweitert auf Drücke von 80 und 100 bar und Temperaturen von 175 °C, 225 °C, 275 °C und 325 °C sowohl für das komplette Buchenholz-Schnellpyrolyseöl als auch für die schwere Phase nach Alterung. Bei höheren Temperaturen wurden erhöhte Werte der Hydrodeoxygenierung erreicht, während bei höherem Druck ein größerer Wasserstoffverbrauch ohne signifikanten Einfluss auf die Hydrodeoxygenierung beobachtet wurde. Die besten Resultate wurden bei der Hydrierung des Buchenholz-Schnellpyrolyseöls bei 325 °C und 80 bar erreicht (43 % Hydrodeoxygenierung). Trotz der verbesserten Hydrodeoxygenierungsaktivität beim Nickel-Chrom Katalysator motivierten die Ergebnisse zur Präparation und Evaluierung weiterer Katalysatoren auf Nickelbasis mit dem Ziel noch höherer Desoxygenierungsniveaus.

Im nächsten Teil dieser Arbeit wurden vier Katalysatoren auf Nickelbasis durch Nassimprägnierung hergestellt, charakterisiert und bewertet. Die Katalysatoren wurden auf Siliciumdioxid und Zirkoniumdioxid abgeschieden und der Einfluss von Kupfer als Promotor untersucht. Nickel auf Siliciumdioxid war bei der Hydrodeoxygenierung am aktivsten und reduzierte den Sauerstoffgehalt des upgegradeten Buchenholz-Schnellpyrolyseöls um mehr als 50 %. Der niedrigste Wassergehalt sowie eine geringe Gas- und Koksentstehung sind ebenfalls positiv zu bewerten. Die Untersuchung zu wiederholten Hydrotreatment-Zyklen mit dem gleichen Katalysator zeigte nach der vierten Wiederverwendung immernoch eine hohe Aktivität (43 % Sauerstoffentfernung). Auf Grundlage dieser Ergebnisse wurde Ni/SiO_2 zusammen mit dem vorher beschriebenen Nickel-Chrom-Katalysator für die Hydrierung von Schnellpyrolyseöl aus Restbiomasse ausgewählt.

Während die bisher vorgestellten Ergebnisse alle auf Buchenholz basierten, wurden im weiteren Rückstände einer Zuckerrohrraffinerie als Restbiomasse für die thermochemischen Umwandlung und anschließende Hydrierung ausgewählt. Die detaillierte Untersuchung der Bagasse und des Schnellpyrolyseöls ermöglichte die Korrelation der Biomassebausteine mit den erhaltenen Monomeren des Pyrolyseöls. Nickel-Chrom zeigte die höchste Aktivität für die Umwandlung organischer Säuren (wie zuvor bei Buchenholz-Pyrolyseöl beobachtet), während $Nickel/SiO_2$ aktiver bei der Umwandlung von Aromaten war. Mit $Nickel/SiO_2$ wurde eine Hydrodeoxygenierung von 43,3 % erzielt. Beide Katalysatoren waren unter den evaluierten Bedingungen aktiv. Die hohen Viskositäten der upgegradeten Öle zeigten aber, dass neben der Hydrierung auch eine Polymerisation stattgefunden haben muss. Da dies für die weitere Anwendung der Schnellpyrolyseöls unerwünscht ist, sollte dies näher untersucht werden.

Trotzdem war diese erste Untersuchung an Zuckerrohrbagasse vielversprechend und weitere Studien sind geplant.

Im letzten Teil der Arbeit wurden die beiden hochbeladenen Nickelkatalysatoren der ersten Kapitel für eine detaillierte Untersuchung in einem kontinuierlich betriebenen Rieselbetthydrierreaktor ausgewählt. Ziel der Untersuchung war, den Einfluss von Schwefel auf die langfristige Katalysatordeaktivierung und die Rolle von Chrom bei der Katalysatordeaktivierung zu untersuchen. Beide Katalysatoren waren bei der Umsetzung von Modellsubstanzen über 48 h Reaktionszeit aktiv. Durch die Anwesenheit von Schwefel änderte sich die Selektivität beider Katalysatoren, hauptsächlich in Richtung Alkenbildung, während die Reaktivität im gleichen Bereich blieb. Die Bildung von Ni_3S_2 wurde bei beiden Katalysatoren beobachtet, aber die hohe Intensität bei der Röntgenbeugung von metallischem Nickel im Nickel-Chrom-Katalysator könnte ein Hinweis auf dessen höhere Beständigkeit gegen Schwefelvergiftung im Vergleich zum Ni-Katalysator sein. Im Allgemeinen waren beide Katalysatoren unter den getesteten Bedingungen aktiv, obwohl die Hydrierungsaktivität durch eine Schwefelvergiftung beeinträchtigt wurde.

Insgesamt waren alle in dieser Studie getesteten Katalysatoren für die Hydrierung von Schnellpyrolyseölen aktiv. Wenn nur die Stabilisierung reaktiver Verbindungen wie Aldehyde und Furfurale erwünscht ist, könnten alle als geeignete Kandidaten betrachtet werden. Hinsichtlich der Hydrodeoxygenierungsaktivität zeigte Ni/SiO_2 die höchste Leistung, während sich Nickel-Chrom als am aktivsten für die Umwandlung organischer Säuren und mit einer besseren Hydrierungskapazität als Ni/SiO_2 erwies.

Content

Chapter 1. Thermochemical and thermo-catalytic conversion of biomass: an overview

List of abbreviation Chapter 1

FPBO: Fast Pyrolysis Bio-Oil

HDT: Catalytic hydrotreatment

HGF: Hot gas filtration system

1. Composition of biomass, thermochemical conversion and upgrading

In recent years, the search for renewable alternatives for petroleum-based fuels increased the interest of using biomass as a renewable energy carrier. This phenomenon is mainly due to the theoretical potential of biomass, accounting for $1{,}08 \cdot 10^{11}$ tons of oil equivalent, almost 10 times the energy required worldwide [1]. Biomass based products are considered almost neutral to CO_2 emissions, because it is consumed during the photosynthesis of biomass, closing the carbon cycle, differently of petroleum liquids, which contributes to more than 65 % of antropogenic CO_2 emission added to the carbon cycle [2–4].

By definition biomass is considered all organic material derived for example from plants, algae, crops, animals, etc [3]. Agriculture residues from production and processing, wood, wood residues i.e. sawdust, human wastes, animal wastes, food waste and other organic materials are classified as biomass [3,5]. The most abundant lignocellulosic biomass, on the other hand, comprises all plant derived biomass consisting of cellulose, hemicellulose and lignin [6].

The combustion of lignocelullosic biomass is considered the earliest "technical" application of biomass known. However, this biomass shows potential for not just combustion but also for a wider range of applications [3]. It is especially true for residues produced in large amounts as rice husk, sugarcane bagasse, residues of palm plantation, or crop straw [3,7]. Residual biomass is strategically interesting for production of fuels and chemicals for two main reasons: Firstly, biomass is the only renewable source of carbon and due to its chemical structure and composition, can be converted into valuable chemical products [3]. Secondly, a feedstock from residual lignocellulosic biomass does not compete with food production, avoiding the use of land for other than edible crops [8].

1.1 Lignocellulosic biomass composition

Lignocellulosic biomass is mainly composed by macromolecules also referred as building blocks: cellulose, hemicellulose and lignin. Depending on the type of the biomass (hardwood, softwood or grasses), the concentration of these units differs. Overall, 40-50 wt.% corresponds to cellulose, 20-30 wt.% to hemicellulose and 10-25 wt.% to lignin [9]. Depending on the biomass, low molecular weight substances (such as extractives) and inorganics are also constituents [2] (Figure 1).

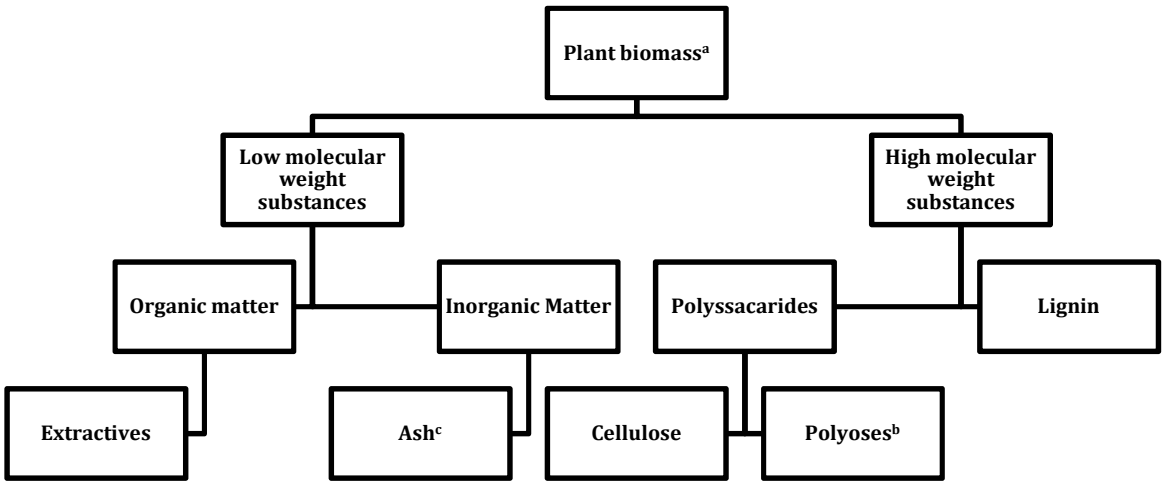

Figure 1. Main components of lignocellulosic biomass. Reproduced from reference [2] according to the terms of Creative Commons Attribution License.[a]: Lignocellulosic biomass; [b]: Hemicellulose; [c]:Inorganics are usually characterized as ash.

Each one of the building blocks shows a specific function. Cellulose is responsible for the plan strength and is mainly composed by cellobiose units (unhydride glucose units) while hemicellulose show a heteropolysaccaride structure composed by mannose, galactose, glucose, xylose and other carbohydrates [2,10]. Lignin, on the other hand, is a polyphenolic material wich provides fungal and microbial resistance to the plant and stabilizes the cell walls; p-coumaryl alcohol, sinapyl alcohol and coniferyl alcohol units are the main constituents in the lignin structures [2,9,10]. Extractives are responsible for the biomass defence and include pectins, waxes, essential oils, terpenes, mucilages and other components [2,11]. Some lignocellulosic biomass are mostly free of extractives, such as switchgrass, corn stover and wheat straw, while pine needles, mallee wood and forest residues can contain high concentration of extractives (5-12.6 wt.%) [11]. The ash composition includes Na, K, Mg, Ca, P and Si [2,11,12] and may vary significantly among different biomass. Usually the concentration of ash is higher in fast growing lignocellulosic biomass, for example miscanthus (12.9 wt.%) in comparison to wood, for example pine, with an ash content of 1.2 wt.% [13,14].

In terms of elemental analysis, the lignocellulosic biomass shows a carbon content in the range of 42.8-49.6 wt.%, hydrogen in the range of 5.4-6.0 wt.% and oxygen in the range of 38.9-43.2 wt.% (dry basis), depending of the source [13]. The higher heating value is usually in the range of 16.6 to 18.7 MJ/kg [13].

1.2 Thermochemical conversion of lignocellulosic biomass

A variety of biotechnological, physical-chemcial and thermochemical conversion routes have been proposed for lignocellulosic biomass valorization [15]. Among the thermochemical conversion routes currently investigated, hydrothermal liquefaction, gasification, combustion, pyrolysis, catalytic pyrolysis and others [1,2,4] can be mentioned. Due to the possibility to be optimized aiming different product yields (char and liquid condensate), pyrolysis has been considered one of the most robust well-developed technologies. The biomass liquefaction results in an energy dense, storable and easy to transport products.

During pyrolysis, the dry biomass (moisture below 15 wt.%) is thermically decomposed in inert atmosphere [15] to avoid combustion [16], even though also autothermal pyrolysis is investigated to provide the process heat required by partial combustion [17]. As detailed reported by Kan et al., 2016 [1] the decomposition mechanism occurring during pyrolysis is considered very complex due to the high number of parallel and consecutive reactions taking place. The lignocellulosic biomass bulding blocks are decomposed at different temperatures. Hemicellulose starts to decompose at the lowest temperatures (200-350 °C), leading to products such as acetic acid [2]; cellulose decomposes at medium temperatures (300-390 °C), leading to levoglucosan, anhydrocellulose [2] and others; lignin decomposes at the highest temperatures (200-450 °C), with higher contribution to char formation compared to cellulose and hemicellulose [2,7,18]. A complex range of reactions such as dehydration, decarboxylation, isomerization, depolymerization and charring occur during pyrolysis. Reactor design and reaction parameters such as, temperature, heating rate, residence time, biomass particle size and moisture content play a role in the pyrolysis mechanisms, leading to different liquid, gaseous and solid products [1,7,12]. The yield of each fraction can be classified depending on the pyrolysis parameters [7,12], accordingly to:

- Torrefaction is performed in inert atmosphere at temperatures in the range of 200-300 °C and residence time of around 2.5 min (Figure 2). Carbon rich solid fuels are targeted in this process [19];
- Slow pyrolysis is usually performed at the range of 300-700 °C, with residence time of hours or even days and biomass particle size in the range of 5-50 mm [1]. The non-condensable gas, condensate and solid product is nearly equally distributed, although slow pyrolysis is usually performed aiming solid production as the main product [7], with vapor and gas are used to produce process energy;
- Intermediate pyrolysis, in comparison to fast pyrolysis, operates with biomass containing higher concentration of water (up to 40 wt.%) and larger particle size (chips and pellets).

The heating rate is lower, around 100 K/min, while the residence time is higher, up to 10 min. Lower yields of organic liquids are obtained in comparison to fast pyrolysis and higher gas yield [13,20,21];

- Fast pyrolysis is characterized by the temperature around 500 °C, high heating rate (>10-200 K/s) and short gas residence time up to 2 seconds [1,22]. The aim of fast pyrolysis is to maximize the yield of liquid condensate (fast pyrolysis bio-oil and aqueous condensate in some cases, later discussed in details), usually in the range of 60 wt.% on dry basis [23];
- Gasification may be conducted by addition of a gasification agent considering partial oxidation or pyrolytic gasification (steam). The pyrolytic gasification is performed in two stages aiming the production of gas with heating value in the range of 15-20 MJ/m^3, mainly due to the methane rich composition [15]. Above 550 °C, the yield of non condensable gases in the products is increased [12].

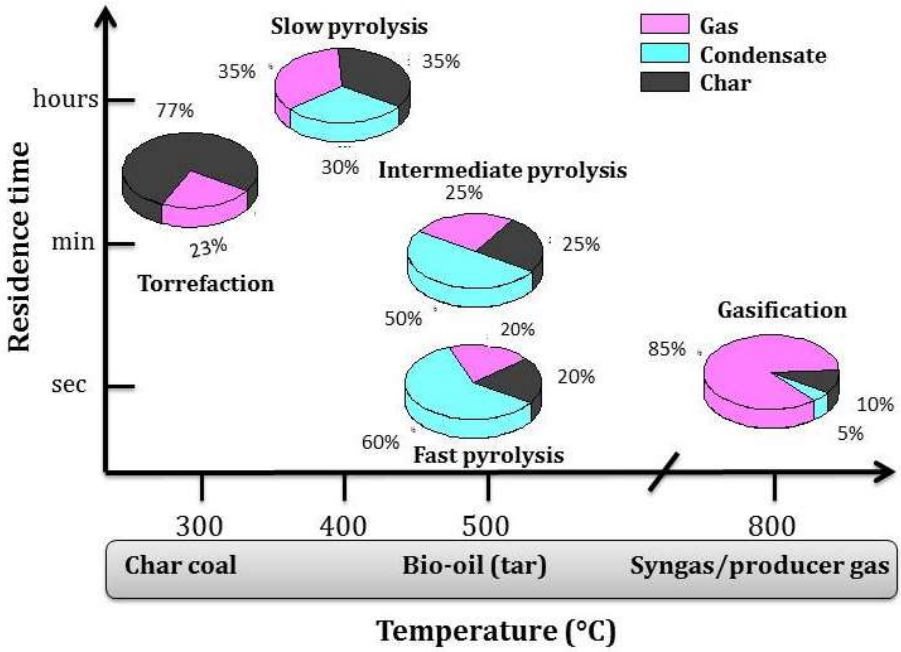

Figure 2. Product yields for different types of pyrolysis. Reproduced from ref. [24] according to the terms of Creative Commons Attribution License.

The biomass composition may also play a significant role during the pyrolysis. Inorganics such as Ca, Mg compounds, and especially K and Na compounds, may have a catalytic effect, reducing the yield of organic liquids, increasing char and gas formation [2,7,12,13]. Mostly, the inorganic substances will remain and enrich in the solid pyrolysis product. The distribution of building blocks in the biomass composition may result in organic liquids with increased viscosity and high yields of char. High concentration of lignin is attributed to high formation of char, as observed in softwood, whereas high concentration of cellulose and hemicellulose contribute to organic liquid yield [1,7]. The moisture content of the lignocellulosic biomass will be reflected in

the water content of the condensate; in some cases leading to phase separation, as well as lowering the energy efficiency of the conversion process [1,7]. For that reason, the biomass is usually dried before fast pyrolysis to moisture content below 10 wt.% [23].

1.2.1 Fast pyrolysis: process concept, reactors and main products

When the maximization of liquid products, usually referred to as bio-oil, bio crude, pyrolysis liquid or pyrolysis oil [25] is requested, fast pyrolysis is usually applied for dry lignocellulosic feedstock conversion. The liquid fraction is called fast pyrolysis bio-oil (FPBO) according for the existing standards for its use as heating fuel.

As previously reported, fast pyrolysis principally aims the maximization of FPBO, and minimization of non-condensible gas and solids. Typically, the moisture content is kept below 10 wt.% and particle size below 2 mm to minimize water formation allowing rapid pyrolysis reaction, respectively [15]. Rapid heating-up of the biomass, maintaining short gas/vapor residence times, and instant disruption of chemical reactions after solids separation by immediate cooling (quenching) of the condensable vapors [13] are characteristics of fast pyrolysis.

Different reactor designs have been proposed for fast pyrolysis, such as a fluidized bed reactor [13], ablative reactor, microwave reactor, rotating cone, auger reactor and others [5,7,8,11,16,26]. Most reactor designs make use of a heat carrier providing the heat required for warming up and pyrolyzing the biomass. Fluidized bed reactors, realized as bubbling or circulating fluidized-bed reactor, use a carrier gas and sand as heat carrier and shows good heat transfer and temperature control, resulting in high liquid yields [2,8,16,23]. In the rotating cone and auger reactors the heat carrier is brought in contact with the biomass mechanically. The centrifugal forces rotate the hot sand and biomass in the rotating cone reactor [23]. The design of auger reactors is attributed to reduction of operation costs and its capability for scale-up [2,11]. Ablative reactors, on the other hand, may operate with biomass chopped in larger diameter [16]. This is mainly possible due to the reactor configuration, where the biomass is heated by contact with a hot plate [2,27].

The twin screw mixer reactor, developed around 50 years ago, was initially designed for conversion of fossil-based feedstocks, such as coal and vaccum residue [16]. Currently it is developed for fast pyrolysis of a range of biomass feedstocks at KIT´s Institute of Catalysis Research and Technology, Germany. The high heating rate is reached by circulation of hot heat carrier material, such as steel balls [26] in the process development unit (10 kg/h) or hot sand [16] in the pilot plant (500 kg/h), which is mixed with the milled biomass as soon as it enters to

the fast pyrolysis reactor (Figure 3). Circulation is facilitated mechanically by a bucket elevator and by pneumatic lifting, respectively.

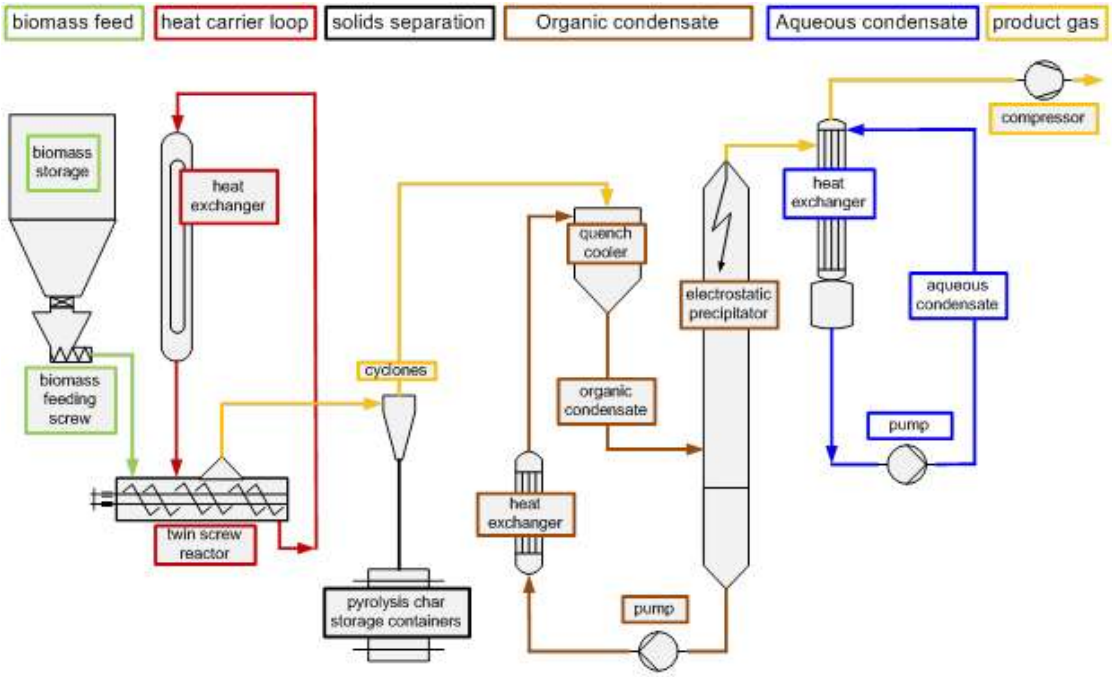

Figure 3. Schematic diagram of a fast pyrolysis process development unit at KIT with twin screw reactor. Reproduced from [28].

A variety of biomass has been already tested for fast pyrolysis, including forestry and agriculture residues such as wheat straw, eucalyptus, barley straw, olive pits, nut shells, miscanthus, sorghum and many others [2,7,25], resulting in a significant difference in products distribution between liquid, gas and char. Most of the investigations have considered wood biomass, due to the higher reproducibility when compared to agriculture residues [2] as well as the commercial interest. Currently the efforts are being dedicated in order to process residual biomass, usually complicated by the ash-rich composition, responsible for lowering the liquid yields and possible problems during processing [29].

Some commercial pyrolysis units are currently under operation worldwide. As example, Envergent Technology, founded in 2008, runs seven commercial plants based on circulating transported fluidized bed reactors in Canada and United States [30]. Fortum Otso, located in Finland operates a plant since 2013. The plant produces FPBO from forest residues, sawdust and wood chips and is integrated to a combined heat and power plant [31]. Empyro BV is under operation since 2015 in The Netherlands. The plant converts wood processing residues FPBO, process steam and electricity. The plant operates with a rotating cone reactor with 5 t/h capacity [32]. The bulk of FPBO produced today is used as heating/boiler fuel.

In fast pyrolysis is the product FPBO formed with the highest yield [23]. The non-condensable gas fraction is mainly composed by CO_2, CO, methane, ethane and other light hydrocarbons [2,7]. The solid product is composed of char with carbon content in the range of 61-93 wt.%, resulting in the high energetic value of this fraction [7]. The aqueous condensate is a single phase product with water in the range of 80-85 wt.%; it contains a significant amount of acetic acid, resulting in a pH value around 3 [2,16] and is formed when ash-rich materials or biomass with higher moisture content are used.

The FPBO is a characteristic dark brown liquid with high viscosity and presents significant environmental advantages. It generates nearly half of the NO_x generated by diesel and very low amounts of SO_x while is considered almost CO_2 neutral [2]. In terms of chemical composition, FPBO is a mixture of more than 300 mainly oxygenated compounds, comprising of carboxylic acids, ketones, aldehydes, alcohols, furans, sugars, phenolics, guaiacols, water, ash components, and partially depolymerized lignin, usually referred to as pyrolytic lignin [4,18,33]. The distribution of the main compounds observed in the FPBO is depicted in Figure 4.

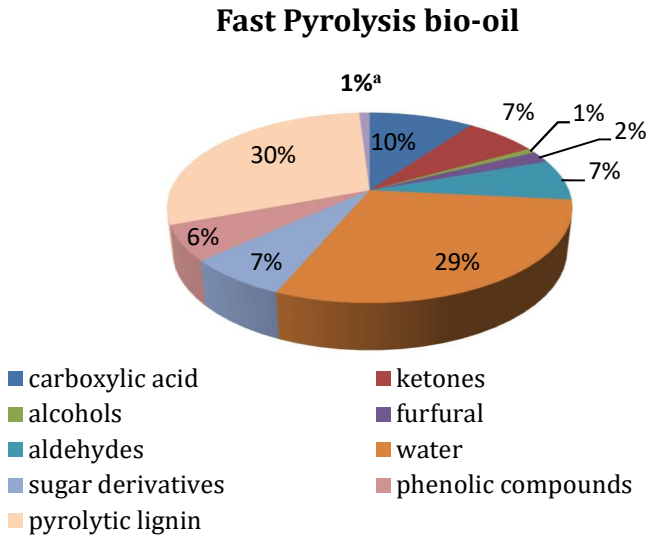

Figure 4. Distribution of the main constituents of the FPBO. Figure built based on ref. [8].

Different types of biomass may result in FPBO with different chemical composition. While FPBO derived from wood biomass usually results in single phase bio-oil, the high concentration of nitrogen, ash constituents in residual biomass may produce multi-phase FPBO due to high water formation [11,16,25]. Furthermore, the distribution of functional groups of the organic molecules is also dependent of the type of biomass used, with agriculture residues, in general, producing FBPO with higher concentrations of phenolic compounds and lower concentrations of ketones, furan and acetic acid in comparison to woody biomass [7]. However, independent of the feedstock or the reactor design, some undesired characteristics are common to all FPBO for fuel

applications: the high concentration of oxygen in comparison to conventional fuels (Table 1) contributes to the low energetic density of FBPO; the high concentration of organic acids results in its low pH value, usually in the range of 3-4 [34], and to the undesired high total acid number; the energy density is similar to biomass and it is roughly half that of the petroleum-derived conventional fuels; the high concentration of still reactive compounds leads to ageing and increasing viscosity during storage [8]; the high concentration of pyrolytic lignin oligomers, nearly 30 wt.%, tends to repolymerize [18]. Moreover, due to the polar composition FPBO is immiscible with petroleum-based oils, making it difficult to be directly co-processed in petroleum refineries.

Table 1. Comparison of the physicochemical properties and elemental composition of wheat straw, wheat straw FPBO, generic wood FPBO and a crude oil. Adapted from Funke et al., [13], Negahdar et al., [35] and Wang et al., [36] according to the terms of Creative Commons Attribution License.

	Wheat straw [13]	**Wheat straw FPBO** [35]	**Generic wood FPBO** [36]	**Crude Oil** [36]
Carbon (wt.%)	42.8	45.9	40-50	85
Hydrogen (wt.%)	5.4	7.69	6.0-7.6	11-13
Oxygen (wt.%)	38.9	41.3	36-52	0.1-1.0
Sulfur (wt.%)	n.a.	n.a.	0.00-0.02	1.0-1.8
Nitrogen (wt.%)	n.a.	2.19	0.00-0.15	0.1
Water (wt.%)	5.7	28.4	17-30	0.02-0.1
Solid (wt.%)	n.a.	n.a.	0.03-0.7	1
pH	n.a.	n.a.	2.4-2.8	n.a.
Viscosity at 323 K (cP)	n.a.	n.a.	13-30	180
HHV (MJ/Kg)	16.6	21.0	16-20	40
Density (kg/m^3)	n.a.	n.a.	1.2-1.3	0.9-1.0

n.a.: not available

Currently the direct application of FPBO is limited to boiler fuel for heat and power [7,25]. However, if replacement of fossil based liquid fuels, chemicals and other applications are intended, an additional upgrading step is necessary. Other problems related to FPBO such as changing of properties over the time, i.e. higher viscosity and phase separation during storage [11,37] also motivate the development and/or selection of upgrading technologies.

1.3 Fast pyrolysis bio-oil upgrading

In order to increase the range of FPBO applications, increase of storage stability, reduction of corrosiveness, oxygen and water content, further upgrading is required. So far, different physical, chemical and catalytic upgrading techniques have been proposed, such as filtration, esterification in supercritical fluids, addition of solvents, emulsification, separation of chemical groups by extraction and/or distillation and non-catalytic thermal treatment at high pressures as well as catalytic cracking [4,37–39]. Depending of the expected properties of the upgraded FPBO and the application intended, one or more upgrading technique may be proposed.

Filtration has been used targeting the removal of inorganic compounds from FPBO. A hot gas filtration system (HGF) used for this purpose can be installed directly at the fast pyrolysis unit, just before the vapours condensation; Elliott et al., [40] observed the reduction of ash constitutents, especially K and Ca compounds after HGF of FBPO, while higher stability due to the removal of char and minerals are reported [41].

Supercritical fluids are used targeting at viscosity reduction and higher energetic content of the FBPO [4,18]. Mainly water is used as supercritical fluid [4], but the use of supercritical ethanol and methanol was also reported by Zhan et al., [42] in addition to acid catalysts for complete esterification of organic acids. Xu et al., [43] performed the hydrogenation of FPBO with the addition of 1-butanol at supercrititat conditions and Ru/C catalyst. The energetic density was increased; the oxygen concentration of the upgraded oil was reduced and coke formation was minimized. Tang et al., [44] also performed hydrogenation of FPBO combined to the use of ethanol at supercritical conditions; the authors reported nearly complete conversion of aldehydes and ketones, with most of the organic acids converted. Hence, the upgraded FPBO showed improved properties.

Solvent addition has been proposed in order to improve the homogeneity, viscosity and stability of FBPO, at the same time that it is considered simple and effective [11,18,45]. Moreover, the better miscibility with petroleum-based fuels, reduced acidity and higher energetic density are observed after the addition of solvents [4,18,45]. Usually alcohols such as methanol, isopropanol and ethanol are used for this purpose; compounds such as carboxylic acids, aldehydes and ketones are reacted and stabilized by esterification with the solvents [11,45,46], as depicted in Figure 5. The acids present in the FPBO catalyze the reaction [47], but the use of other solid acid catalysts may be required [4].

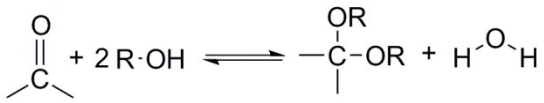

Figure 5. Simplified diagram of acetalization of aldehydes and ketones. Adapted from Oasmaa et al [47] and reproduced according to the terms of Creative Commons Attribution License.

Emulsification of FPBO with other mineral fuels by the use of surfactants is a relative simple process, aiming the use of the blend in boilers and in combustion engines [4,11]. Emulsions containing FPBO in the range of 5-30 % have been previously reported [45]. The corrosive properties, energetic value and cetane number of the emulsions need to be improved [4].

Non-catalytic thermal treatment is performed at temperatures higher than 250 °C and pressure above the partial pressure of water. In this treatment mainly condensation reactions

take place leading to polymerization [37,48]. Significant amounts of oxygen and water are removed, while the energetic content is increased in comparison to the feed [37]. However, the processability of the higher viscous product is one of the main limitations of the final thermal treated upgraded FPBO [49].

Catalytic cracking is performed at severe conditions of temperature, around 300 °C to 600 °C [50]. Usually silica-alumina, alumina or zeolites are the catalysts employed. Light deoxygenated compounds are targeted in this process [4], while a considerable amount of char is formed [37,39,51,52].

Analogous to the catalytic hydrotreatment (HDT) conducted in refineries for removal of sulfur and nitrogen from petroleum chains, FPBO may also undergo hydrotreatment [52]. In this case, the main objective is to remove oxygen completely or partially, in order to reach fuel specification and/or stabilization of reactive compounds. Further depolymerization of remaining oligomers also takes place. Sulfur and nitrogen, although also found in the FPBO in low concentration, usually in the range of 0.3 wt.% to 0.02 wt.% of sulfur and around 1.2 to 0.1 wt.% of nitrogen [8,52–54], are not the main target during the FPBO hydrotreatment; however, their concentration may impact the overall reaction performance.

In view of the notable differences in the crude oil and FBPO composition, the hydrotreatment conditions in terms of temperature and pressure (Table 2) as well as catalysts [8] differs. Usually the catalytic treatment of FPBO is performed at temperatures from 175 °C to 450 °C, hydrogen pressure in the range of 80-230 bar by employing a heterogeneous catalyst [8]. The reaction duration may vary from 1 up to 6 h [52,55].

Table 2. Comparison of HDT conditions of crude oil fractions and FPBO. Data obtained from Venderbosch et al., [37], Talmadge et al.,[56], and Dabros et al., [8] and reproduced according to the terms of Creative Commons Attribution License.

	Temperature (°C)	**Pressure (bar)**
Naphta	260-350	15-35
Light oil	290-400	17-35
Heavy oil	350-425	70-140
Residum hydrocracking	400-425	140-200
Fast pyrolysis bio-oil	175-450	80-230

Due to the complex composition of FPBO, many chemical reactions take place during the hydrotreatment. Reactions such as decarboxylation, decarbonylation, cracking, hydrocracking,

hydrogenation, hydrodeoxygenation, demethylation, demethoxylation and deoxygenation are observed [8]. Some of these reactions are represented in Figure 6.

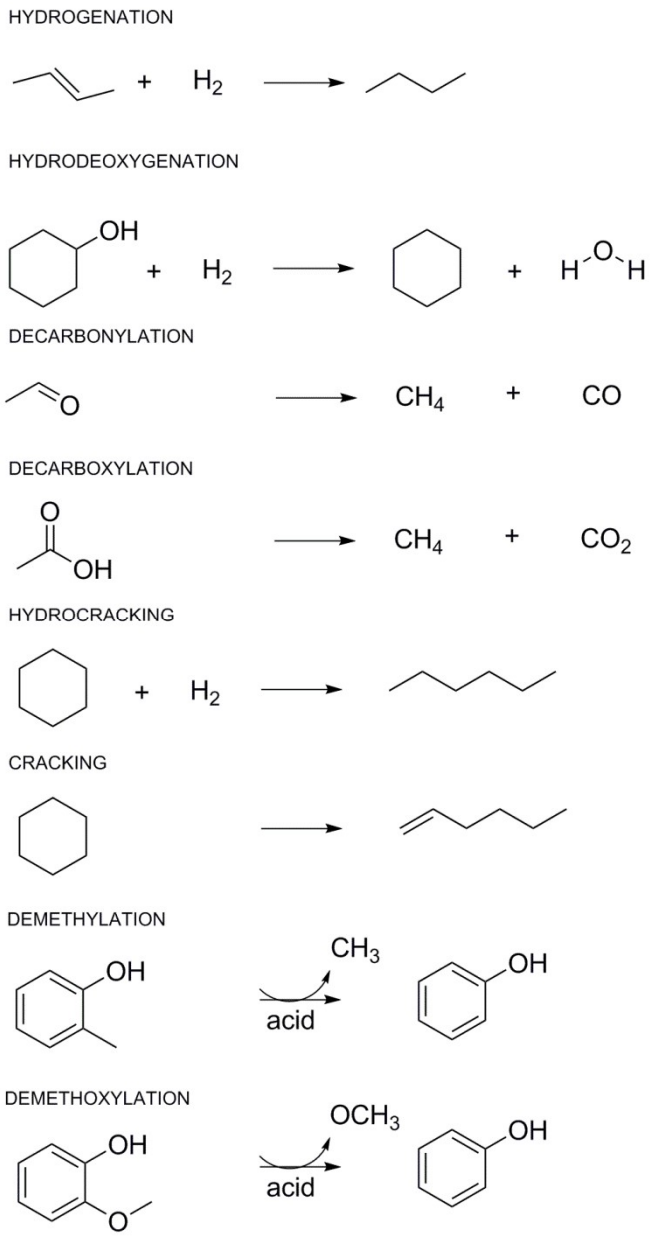

Figure 6. Schematic diagram of some of the main reactions taking place during the hydrotreatment of Fast Pyrolysis bio-oil. Drawn based on ref. [8,51].

Furthermore, undesirable reactions such as polymerization may also occur. Condensation and polymerization reactions compete with hydrogenation leading to water formation due to dehydration [37]. Hydrotreatment and polymerization are competitive reactions and molecules such as sugar derivatives are the ones undergoing polymerization [37].

Depending on the desired properties of the FBPO after upgrading, mainly in terms of oxygen content, different reaction conditions in terms of temperature, pressure and number of

hydrogenation stages may be employed. A general overview is presented in Figure 7. In general, the hydrotreatment can be classified in mild, hydrotreatment also referred as deep hydrotreatment and two or multi-steps hydrotreatment:

- Mild hydrotreatment: The mild hydrotreatment is performed at low temperatures, usually in the range of 175 °C to 225 °C. At this temperature mainly hydrogenation of ketones, aldehydes and olefins take place with minor hydrodeoxygenation [37,57,58]. Due to the conversion of these reactive compounds, mild hydrotreatment is also referred to as stabilization, whereas some authors classify both separately [57]. Although phase separation is not expected, it may occur during the stabilization treatment, depending on the temperature used [37]. The upgraded oil obtained after the mild hydrotreatment shows higher stability during storage, reduced plugging of lines and may be co-processed in petroleum refineries together with heavy petroleum chains [33,48].
- Hydrotreatment or deep hydrotreatment: It is performed at more severe conditions of temperature and pressure in comparison to mild upgrading, aiming complete hydrodeoxygenation. Usually high H_2 consumption is observed as well as high yields of gasous light compounds are formed; the costs are considered high [58].
- Two or multi-steps upgrading/hydrotreatment: Higher deoxygenation levels can be reached by consecutive upgrading of FPBO. The previously hydrotreated FPBO undergoes a second upgrading/hydrotreatment, which can be performed with the same catalyst used in the first upgrading step or another catalyst with different selectivity [59]. While the first step aims the stabilization and reduction of the tendency of char formation, the second step, usully at higher temperature, aims the hydrodeoxygenation [39,60]. Venderbosch et al., [37] reported higher deoxygenation levels, from 52.1 wt.% of O in the feed, 23.9 wt.% after first upgrading and 14.2 wt.% of O (wet basis) after multi-step upgrading, resulting in an upgraded oil with density lower than water. The authors reported upgraded aqueous phase after the 2nd upgrading was colorless and mainly composed by water.

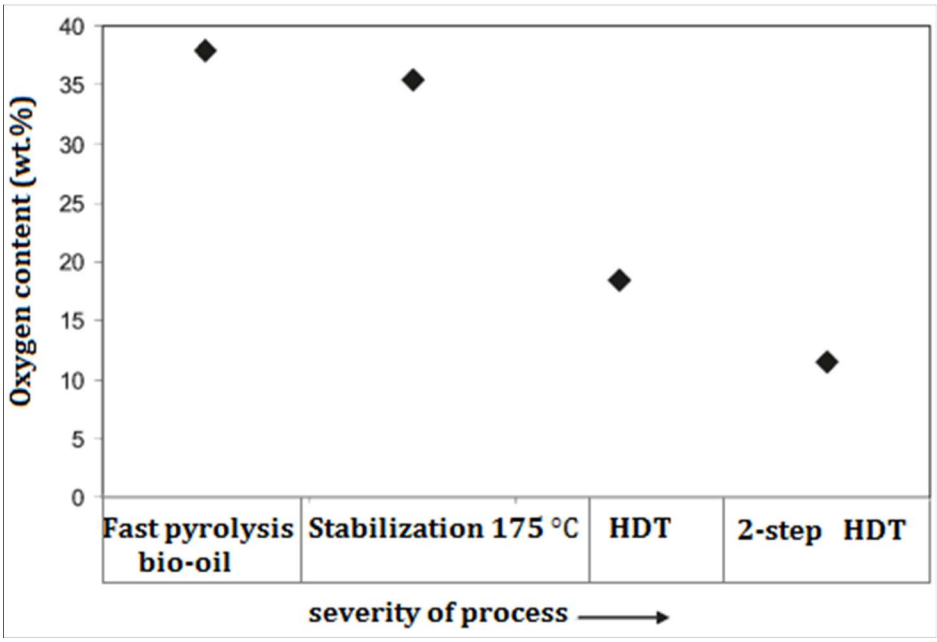

Figure 7. Concentration of oxygen as a function of the severity of the hydrotreatment. Addapted from ref. [57], according to the terms of Creative Commons Attribution License.

The efficiency of the HDT in terms of degree of deoxygenation is usually depicted by the Van Krevelen plot [37](Figure 8, (a)). By the O/C and H/C molar ratios, the elemental composition of feedstock, products and petroleum products are contrasted. Thus, the reduction of the oxygen concentration is observed by the low O/C ratio while the H/C ratio should ideally be in the range of 1.5-2.0 in case of hydrocarbon fuel [37]. Furthermore, the yield of upgraded FPBO is also another factor to be considered during the upgrading reactions; In general, the higher the degree of deoxygenation reached, the lower the upgraded oil yield [52], mostly because of higher water production and content of gas, as presented in Figure 8 (b).

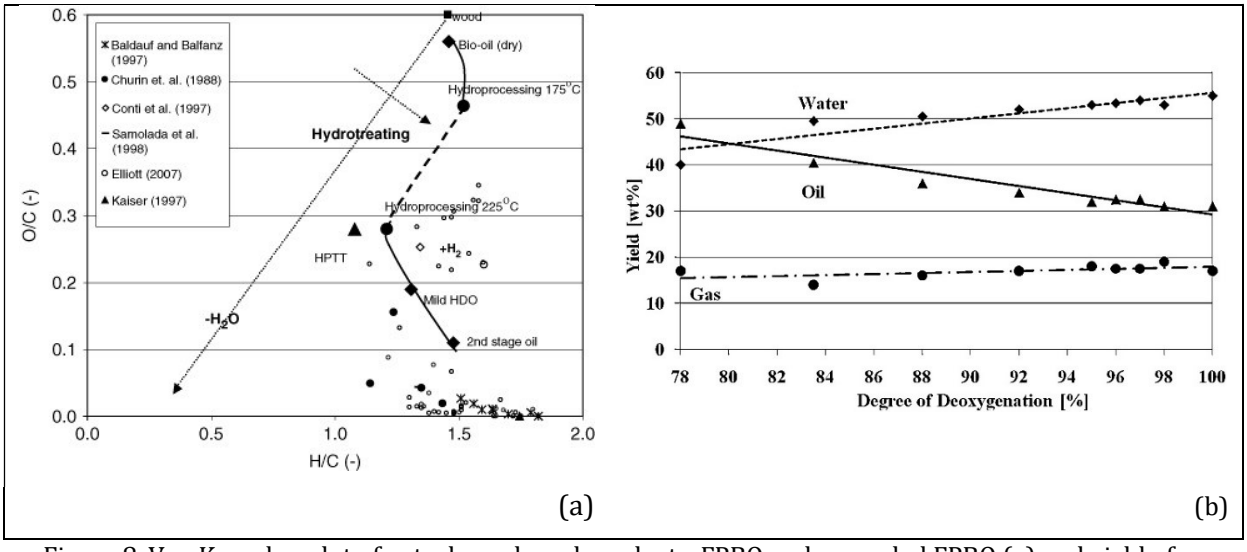

Figure 8. Van Krevelen plot of petroleum-based products, FPBO and upgraded FPBO (a) and yield of products as a function of the degree of deoxygenation (b). Figures reproduced from ref. [37] and ref. [52] according to the terms of Creative Commons Attribution License.

In summary, temperature, pressure of H_2, heating rate, residence time and catalyst contribute to the hydrotreatment efficiency independently and synergetically. A summary of the contribution of each individual parameter is presented below:

1.3.1 Temperature

Temperatures in the range of 175-450 °C are usually selected for hydrotreatment reactions. At higher hydrotreatment temperatures, higher degree of deoxygenation is obtained while lower yields of upgraded oil are observed. Moreover, the gas formation is also favored at high temperatures, i.e. above 350 °C, the formation of light volatile compounds is pronounced, without significant incluence over the hydrodeoxygenation [52]. The reactivity of the molecules is also dependent on the temperature. In general simple oxygenated compounds react at lower temperature and more complex molecules are converted at higher temperatures [8]. This can be observed by the reactivity scale proposed by Elliot et al., [61] for different constituents of FBPO under different temperatures (Figure 9) using a sulfided NiMo catalyst.

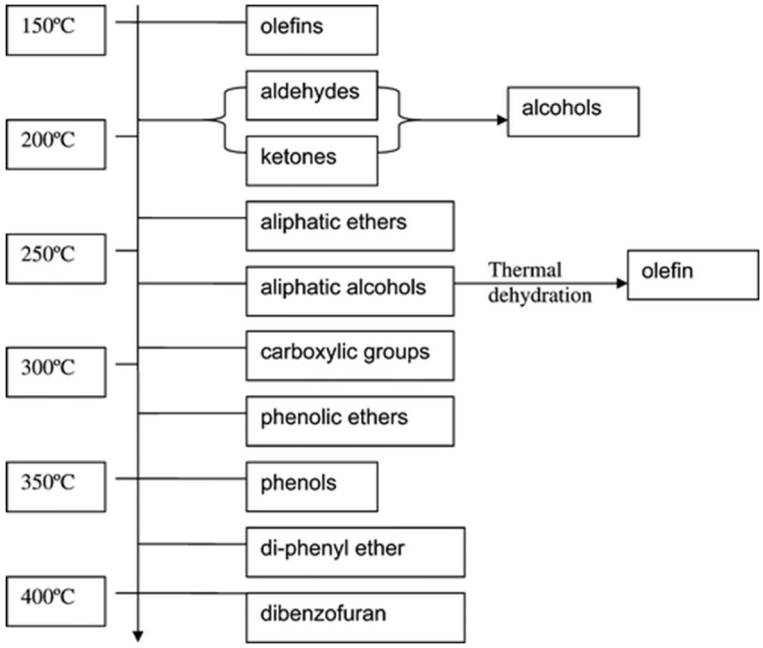

Figure 9. Reactivity scale of FPBO compounds at different temperatures with sulfided NiMo catalyst. Reproduced from ref. [61] according to the terms of Creative Commons Attribution License.

1.3.2 H_2 pressure and consumption

The high pressure of H_2 used during hydrotreatment, usually in the range of 80 to 230 bar is required in order to conduct hydrotreatment reactions, suppressing coke formation, increasing

the solubility and the availability of H_2 on the catalyst surface [8,52]. The H_2 consumption is reported to start already at low temperatures (80 °C) and increases at higher temperatures [48], due to hydrodeoxygenation and hydrogenation.

When higher degrees of deoxygenation are required, the hydrotreatment is performed at higher severity, consequently the pressure and consumption of H_2 is also higher [56,62]. However, if high temperatures are employed, the adsorption of H_2 over the catalyst surface can be compromised, reducing the hydrogenation activity and other reaction pathways, such as hydrogenolysis may occur preferentially [62].

1.3.3 Heating rate

The literature about the influence of the heating rate over the hydrotreatment of FPBO is very limited. In one of the very few investigation about this topic, Mercader et al., [48] observed lower consumption of H_2 at higher heating rate possibly indicating that polymerization is favoured at these conditions. The authors also observed that hydrogenation is mainly favoured at mild temperatures; thus, if the heating rate to temperatures above 200 °C is too high, the hydrogenation is unfavoured whereas polymerization prevails.

1.3.4 Reaction duration time in batch reactions

A few number of publications approached the influence of reaction time over hydrotreatment. Wildshut et al., [55] evaluated the influence of reaction time with Ru/C at 350 °C and 20 bar of H_2. The authors performed hydrotreatments from 1 to 6 h of duration. They observed that at longer reaction time the lowest yield of upgraded oil was obtained, whereas the highest amount of gas was formed. They assumed the optimum reaction time of 4 h of duration.

1.3.5 Catalysts

Although all parameters previously discussed are relevant, the selection of the catalyst is maybe the most important for HDT reactions [18]. The catalysts formulation has a significant impact on the conversion of the products, selectivity, costs and others, which in overall contribute to the HDT performance. Formulation parameters such as active metal, support, metal concentration and addition of promoters play a significant role in the upgraded FPBO composition.

In general, the catalyst already tested in early studies and currently under evaluation for hydrotreatment of FPBO may be classified in sulfided catalysts, noble metal catalysts and non noble transition metal catalysts.

The first hydrotreatment studies were performed with sulfided catalysts, due to the application of these catalysts in petroleum refineries for removal of sulfur and nitrogen [39]. Sulfided catalysts based on CoMo and NiMo have been extensively tested. Şenol et al., [63] evaluated the conversion of methyl heptanoate and methyl hexanoate in a continuous flow reactor applying sulphided $NiMo/\gamma\text{-}Al_2O_3$ and $CoMo/\gamma\text{-}Al_2O_3$. Both model compounds were hydrodeoxygenated to hydrocarbons, with $NiMo/\gamma\text{-}Al_2O_3$ showing the highest catalytic activity. However, both catalysts showed stability problems (loss of active sites and carbon deposition), affecting the distribution of compounds in the upgraded products. Auersvald et al., [27] studied the hydrotreatment of wheat straw fast pyrolysis bio-oil from ablative pyrolysis in a fixed bed reactor using sulphided $NiMo/Al_2O_3$ at different conditions of temperature (240-360 °C) and pressure (20-80 bars). The authors observed reduced viscosity and acidity for most of the conditions tested, as well as more than 85 % of the original energy content in the feedstock recovered in the upgraded oil. The upgraded oil obtained at 360 °C was completely missible with gas oil, with potential to be co-processed in petroleum refineries. Joshi et al., [60] studied the hydrotreatment of sawdust pyrolysis oil in a packed bed microreactor. The reactions performed with sulphided $NiMo/Al_2O_3$ evaluated different reaction parameters such as temperature, H_2 partial pressure and residence time. The authors observed that the hydrogenation pathway occurs simultaneously to hydrodeoxygenation during hydrotreatment. Furthermore, the authors observed coke formation at temperatures above 270 °C, indicating that a stabilization step below this temperature is required in order to stabilize reactive compounds minimizing coke formation. French et al., [59] evaluated the hydrotreatment of oak fast pyrolysis bio-oil in a semibatch reactor applying sulphided $NiMo/Al_2O_3$ and noble metal catalysts. The authors observed highest conversion of acids with $NiMo/Al_2O_3$ with low consumption of H_2 in comparison to noble metals. The highest amount of coke formed was observed with $NiMo/Al_2O_3$ in comparison to noble metal catalyst. Due to the differences in selectivity observed, the authors concluded that a 2-steps upgrading firstly applying a noble metal for minimize coke formation, followed by a second hydrotreatment reaction with sulphided catalyst for deoxygenation, aiming an optimized hydrotreatment process. Gholizadeh et al., [64] evaluated the hydrotreatment of malee wood bio-oil in a continuous fixed bed reactor at 375 °C and 70-80 bar. The authors observed that compounds with high molecular weight promoted fast deactivation of the catalyst, on the contrary of the observation for low molecular weight compounds.

A mechanism of hydrodeoxygenation of 2-ethylphenol over a sulfided $CoMo/Al_2O_3$ was presented in details by He and Wang [65]. Initially, the H_2S molecule is removed by the presence of H_2 resulting in a vacancy site of the catalyst; A molecule of H_2 is dissociated and S-H and Mo-H bondings are formed; the 2-ethylphenol molecule is adsorbed in the vacancy site by the oxygen atom; a H^+ is donated from S-H to the 2-ethylphenol molecule resulting in a carbocation; the C-O

bond is cleaved and the hydrodeoxygenated molecule is formed. The H_2O is formed and the active site is finally recovered (Figure 10). Furthermore, Ni and Co are commonly applied as promoters increasing the activity of the active sites for hydrotreatment reactions [52,65]. It is possible through the donation of electrons of the promoters to Mo atoms, weakening the S-Mo bonding and therefore resulting in the generation of the sulfur vacancy site. Contributions to the resistance to deactivation have been also attributed to Ni and Co [8].

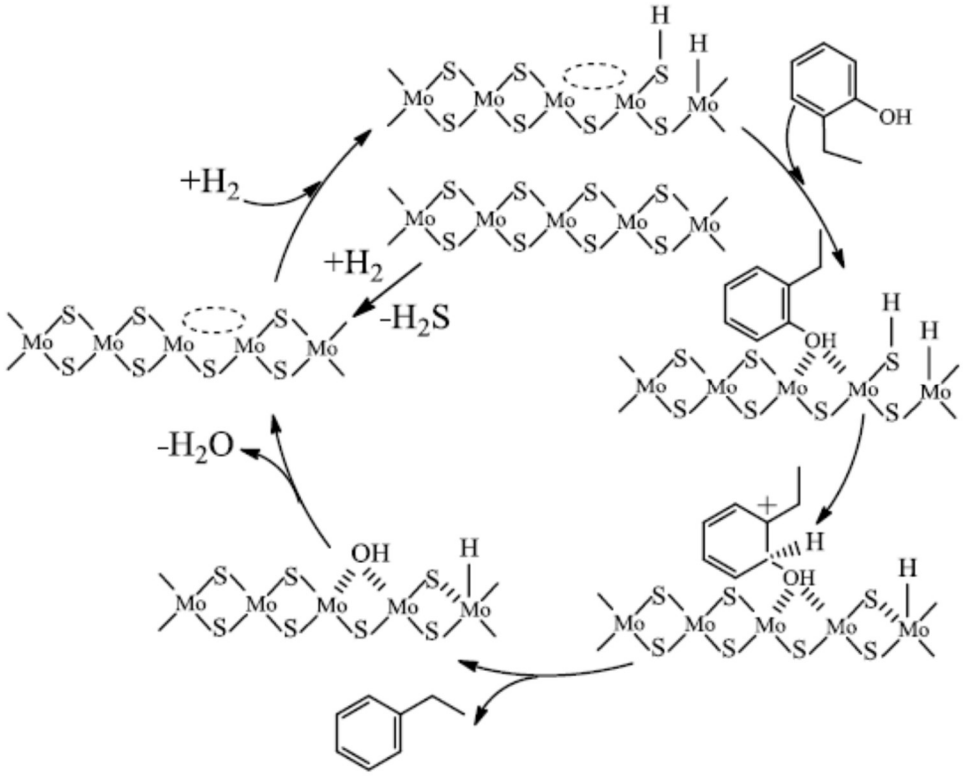

Figure 10. Hydrodeoxygenation mechanism of 2-ethylphenol over a sulfided $CoMo/Al_2O_3$ catalyst. Reproduced from ref. [65] according to the terms of Creative Commons Attribution License.

The use of sulfided catalysts requires an external source of sulfur continuously fed to the hydrotreatment reactor in order to maintain the catalyst activity [39,62]. Thus, the extra cost due to catalysts sulfidation in combination to environmental issues related to sulfur and poor resistance to water [8] are the main limitations regarding the application of these catalysts.

Noble metal catalysts have been also extensively used in hydrotreatment reactions. Platinum, palladium and ruthenium are among the noble metals already tested [50]. However, high H_2 consumption has been attributed to noble metals [39], as well as high yields of gas formed [59]. Thus, the high cost of these catalysts and the high consumption of H_2 are usually the main limitations for the establishment of hydrotreatment with noble metals. Consequently, it stimulates the search for low cost catalysts, mostly based in non noble transition elements.

French et al., [59] studied the catalytic activity of Pd/C, Ru/C and Pt/C in contrast to $NiMo/Al_2O_3$ for hydrotreatment of oak fast pyrolysis bio-oil in a semibatch reactor. The authors observed the highest gas formation with Pt/C, mainly composed by CH_4. Ru/C showed higher hydrogenation activity in comparison to $NiMo/Al_2O_3$ and poor hydrodeoxygenation activity. Additionally, significant amounts of CH_4 were produced with Ru/C. Pd/C demonstrated the highest consumption of H_2 and poor hydrodeoxygenation activity. Wan et al., [66] studied the catalytic activity of Ru/C, Ru/Al_2O_3, Pt/C, Pt/Al_2O_3 and Pd/C for hydrotreatment of acetic acid in water and in n-heptane. Furthermore, the influence of p-cresol over the hydrotreatment of acetic acetic was evaluated. Ru/C showed the highest activity among all the catalysts evaluated. At 150 °C acetic acid is mainly converted to ethanol while at around 300 °C mainly CO_2 and CH_4 are preferentially formed. Changing the solvent from water to n-heptane, esterification of ethanol to ethyl acetate is favored. When p-cresol was mixed with acetic acid, the hydrotreatment pathways previously observed are suppressed while hydrodeoxygenation of p-cresol resulting in methylcyclohexane is favored. Gholizadeh et al., [67] studied the continuous hydrotreatment of mallee wood pyrolysis oil at 70 bar and 375-450 °C using Pd/C in the upstream. The authors stated that even with stabilitization taking place at some extend in the upstream, the long term hydrotreatment operation was affected due to coke formation. Especially at higher temperatures the amount of coke formed inside the reactor was increased. The authors attributed the coke formation to polymerization and aromatic ring growth.

Non noble transition metal catalysts, such as Ni-based catalysts are used in a variety of catalytic process, as well as in a variety of hydrogenation reactions. Due to the good activity observed in other conversion routes, significant low cost in comparison to noble metal and high availability, they are promising candidates for FPBO hydrotreatment.

The most accepted mechanism for reduced transition metals (Figure 11) is the adsorption and activation of oxy compounds either over the support surface (non noble metals), metal surface (noble metals) as well as metal/support interface (noble metals), while the adsorption and dissociation of H_2 takes place on the metal surface, leading to hydrogenation or hydrodeoxygenation [52,65,68]. However, it is debated that the interaction between metal and support influences the overall catalytic mechanism, leading to ongoing discussions about the mechanism itself [8].

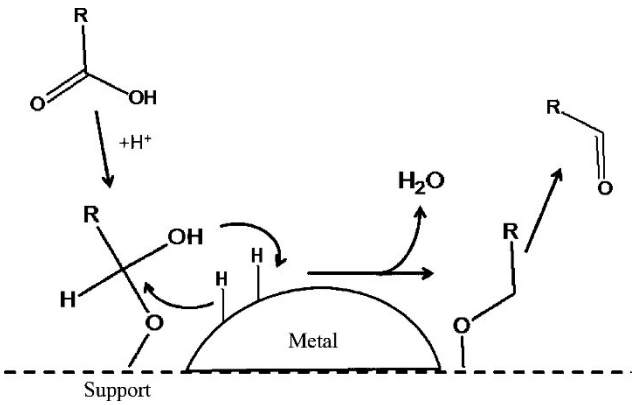

Figure 11. Mechanism of hydrotreatment over reduced transition metal catalysts. Reproduced from ref. [52] according to the terms of Creative Commons Attribution License.

Some previous studies have considered the application of nickel as the active metal of the catalyst. Ardiyanti, et al., [69] studied different nickel-based catalysts (NiCu and NiPd supported on SiO_2, La_2O_3, Kaolin and ZrO_2) with different nickel loadings ranging from 29-58 wt.% for hydrotreatment of pine wood bio-oil in a batch autoclave. The NiPd catalyst with 58 wt.% of nickel showed the best catalytic activity, producing the best upgraded oil in terms of lowest oxygen concentration, lowest tendency for coke formation and highest solubility in hydrocarbons. All the catalysts tested, with exception of the catalysts supported by zirconia, produced less methane in comparison to Ru/C. In another study, Ardiyanti, et al., [70] investigated the hydrotreatment performance of nickel-based catalysts promoted with copper in different supports (ZrO_2, CeO_2-ZrO_2, TiO_2, Al_2O_3, Sibunite and rice husk carbon) with different metal concentrations. The batch hydrotreatment reactions of pine wood bio-oil showed that NiCu/TiO_2 was the most active catalyst, based on the hydrogen consumption and on the highest H/C ratio of 1.43, although the lowest concentration of oxygen in the upgraded oil was obtained with NiCu/sibunite. Ardiyanti, et al., [71] also studied the hydrotreatment of anisole and pine wood bio-oil applying a range of NiCu/Al_2O_3 catalysts with different metal loadings (0.32-0.81 w/w). The best results in terms of hydrodeoxygenation of anisole and highest consumption of H_2 and highest H/C in the upgraded oil was obtained with the catalysts with a metal loading ratio (Ni/Cu) of eight. Another series of investigation was conducted by Mortensen et al., [68,72,73] encompassing nickel-based catalysts. Mortensen et al. [68] screened 23 catalysts in a batch autoclave at 275 °C and 100 bar for hydrodeoxygenation of phenol. The catalysts were classified accordingly to the catalytic activity as follow: Ni/ZrO_2 > Ni-V_2O_5/ZrO_2 > Ni-V_2O_5/SiO_2 > Ru/C > Ni/Al_2O_3 > Ni/SiO_2 ≫ Pd/C > Pt/C. The authors concluded that an oxide support is necessary in order to promote the heterolytic dissociation of O-H, facilitating the hydrogenation of phenol. In another study, Mortensen et al., [73] investigated the influence of nickel particles over the hydrodeoxygenation of phenol. The Ni/SiO_2 catalysts with metal particle sizes in the range of 5-22 nm were tested at

100 bar and 275 °C in a batch autoclave. The authors observed hat higher deoxygenation rates were obtained with smaller nickel particles (5 nm), favored by step/corner sites, while hydrogenation was promoted by larger regions. Mortensen et al., [72] also investigated the influence of poisoning substances over the catalytic activity of Ni/ZrO_2 for hydrodeoxygenation of guaiacol in a continuous trickle bed reactor.

Although some results have been previously obtained with nickel-based catalyst, the differences in reactor design, active metal loading, reaction conditions and feedstock applied are factors that limit the directly application of results previously obtained to new developments, demanding for continuous research and application studies.

In addition to the active metal, the selection of the right support material is fundamental for hydrotreatment catalyst formulations, as stabilization and dispersion of active metal, selectivity and activity of the catalysts are correlated to the support material [39]. Among the most common supports already tested, γ-Al_2O_3, SiO_2, ZrO_2, activated carbon, CeO_2 and in some cases, the combination of more than one support material can be mentioned [18].

γ-Al_2O_3 has been used as support for a variety of catalysts, especially for sulfided ones, previously described [27,59,60,63]. Despite its higher activity in comparison to silica and activated carbon, γ-Al_2O_3 also shows some limitations [39]. γ-Al_2O_3 is converted to boehmite in the presence of water; Furthermore, it catalyses the conversion of phenolics to coke, leading to catalyst deactivation [33,56].

Although lower activity in comparison to γ-Al_2O_3 [39], silica shows low coke formation tendency in comparison to alumina, being considered a promising support for hydrotreatment of FPBO [52,65]. Zirconia is also considered a promising support due to the low coke formation tendency and possible activation of oxy-compounds on the surface of the support [65].

Activated carbon usually shows higher surface area in comparison to other supports. It is an advantage if high dispersion of active metal is desired as well as high resistance to water [62]. In comparison to acidic supports, lower coke formation is observed with activated carbon, due to the low acidity [56]. However, renegeration techniques usually applied such as calcination are not suitable for activated carbon regeneration [56]. Hence, regeneration alternatives are required.

Supports considered less traditional in hydrotreatment, such as CeO_2, TiO_2, MgO and niobium oxides have been tested for hydrotreatment/hydrodeoxygenation reactions [18,74]. This is mainly due to the high dispersion, activitiy and reduced tendency for coke formation [65].

In general, the support must be stable in a water containing environment, due to the significant concentration of water in the FPBO composition in addition to the water formed during hydrotreatment. The support must show a high surface area, in order to promote a high dispersion of the active metal [39]; it also must show low propensity to coke formation. Acid sites are directly correlated to facilitates coke formation [8,39].

1.3.6 Deactivation mechanisms of hydrotreatment catalysts

Deactivation has been reported as one of the issues which must be addressed in hydrotreatment reactions. It is observed by the reduction of activity and/or changes in selectivity due to poisoning, sintering, coking, leaching and catalyst degradation [34,52,75]. However, deactivation due to water, coking and leaching is predominant in FPBO hydrotreatment reactions [8,34]. Inorganic compounds containing S, Cl, Ca and K are the main sources of catalyst poisoning during FPBO hydrotreatment. These compounds may adsorb irreversibly on the active sites, or may react with the active metal, leading to formation of a new chemical structure, leading to partial or complete deactivation [62]. The catalytic activity may also be compromised over the time due to agglomeration, sintering of active metal particles and loss of surface area [50], usually induced by high temperatures [62]. The composition of the FPBO also plays a role in deactivation mechanisms. For instance, the presence of carboxylic acids in the FBPO composition may induce the leaching of active metals, mostly later concentrated in the aqueous upgraded phase [50].

Although all these sources of deactivation are observed in hydrotreatment reactions, coke formation is one of the most important ones already reported for FPBO hydrotreatment. The main cause of coke formation is attributed to polymerization and polycondensation reactions taking place in parallel to hydrotreatment [39]. It is reported that oxygenated compounds containing more than one oxygen atom as well as lignin derivative compounds are attributed to coke formation [62]. The selection of catalyst with moderate acidity, high pressures of H_2 and moderate temperatures are some of the strategies previously adopted to reduce coke formation [8,39].

Hence the main challenge is the development of a stable catalyst, selective for deoxygenation, low H_2 consumption, resistant to poisoning substances and able to be regenerated [39]. As soon as this issue is overcome, a broad range of chemical products can be obtained and different biorefinery alternatives can be explored.

1.3.7 Application of upgraded pyrolysis oil

The upgraded FPBO can substitute fossil fuels, if deep deoxygenation levels are obtained, and can serve feedstock for the production of a variety of chemicals. For instance, FPBO with high

concentration of phenolic compounds may be used for resin production used in some specific petrochemical conversion routes, or binders, transportation fuels, power generation, btx (benzene, toluene and xylene), phenol and its derivatives productions [4,7,16,65](Figure 12).

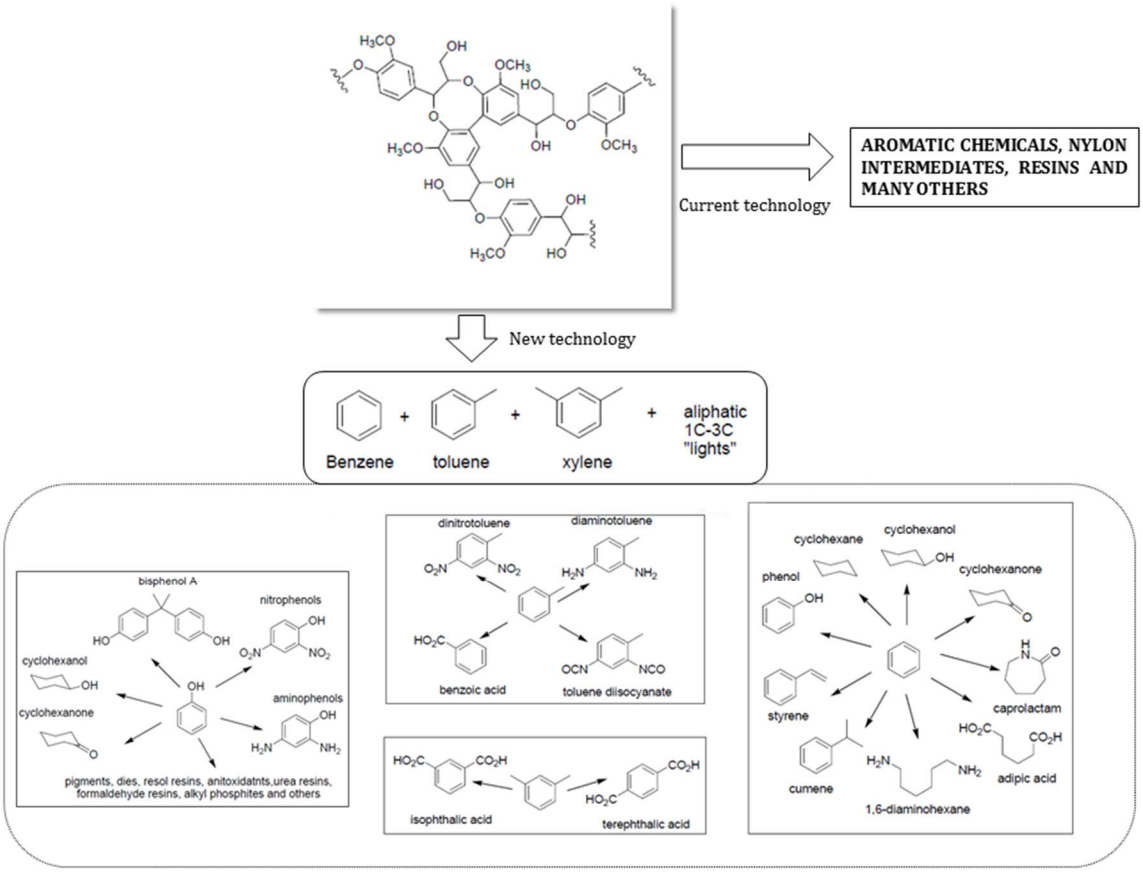

Figure 12. Summary of lignin derivative compounds and the range of chemical products from benzene, toluene, xylene and phenol. Addapted from ref. [76] according to the terms of Creative Commons Attribution License.

A variety of FPBO-derived products is nicely presented by Pires et al., [74]. The authors mentioned that antioxidants, carbon fibers, hydrogen, food aditives, olefins, fermentable sugars, surfactants and others are some of the potential products derived from FBPO.

1.4 Bio-oil biorefinery concepts

Different biorefinery concepts have been proposed for pyrolysis of lignocellulosic biomass and upgrading of liquid products. For agricultural residues valorization, decentralized pyrolysis is proposed as pre-treatment step, considering the low bulk density of biomass and the high cost for biomass transportation [3]. The FPBO is then easily stored and transported to biorefineries as the bulk energy is increased by a factor of 6 by fast pyrolysis in comparison to the biomass [8]. This concept is proposed for agricultural residues such as wheat straw.

In this co-processing concept, the FPBO is transported from the small pyrolysis unit to the refinery. It may undergo direct hydrotreatment whether to be fully deoxygenated or partially deoxygenated or stabilized. The main advantage of this concept is the utilization of the structure already available in the petroleum refinery for processing and distribution [49,56]. Hence, depending on the severity of the upgrading reaction, in terms of temperature, hydrogen pressure, feedstock and catalyst, the properties of the upgraded oil may vary significantly. The miscibility with petroleum derived products, might be acquired after the upgrading, allowing the co-feeding in different refinery streams (Figure 13). In this case, very low O/C ratio is not required [70,77]. Additionally, if deep hydrodeoxygenation is achieved, for example, after 2-step upgrading, the final upgraded product can be blended directly into the gasoline and diesel pools [78]. The production of functionalized aromatics is also interesting, considering that monomers applied in the petrochemical and pharmaceutical industry, polymers and resin production might be obtained [79–83]. Hence, part of the 1-step upgraded oil may undergo another conditioning/separation route.

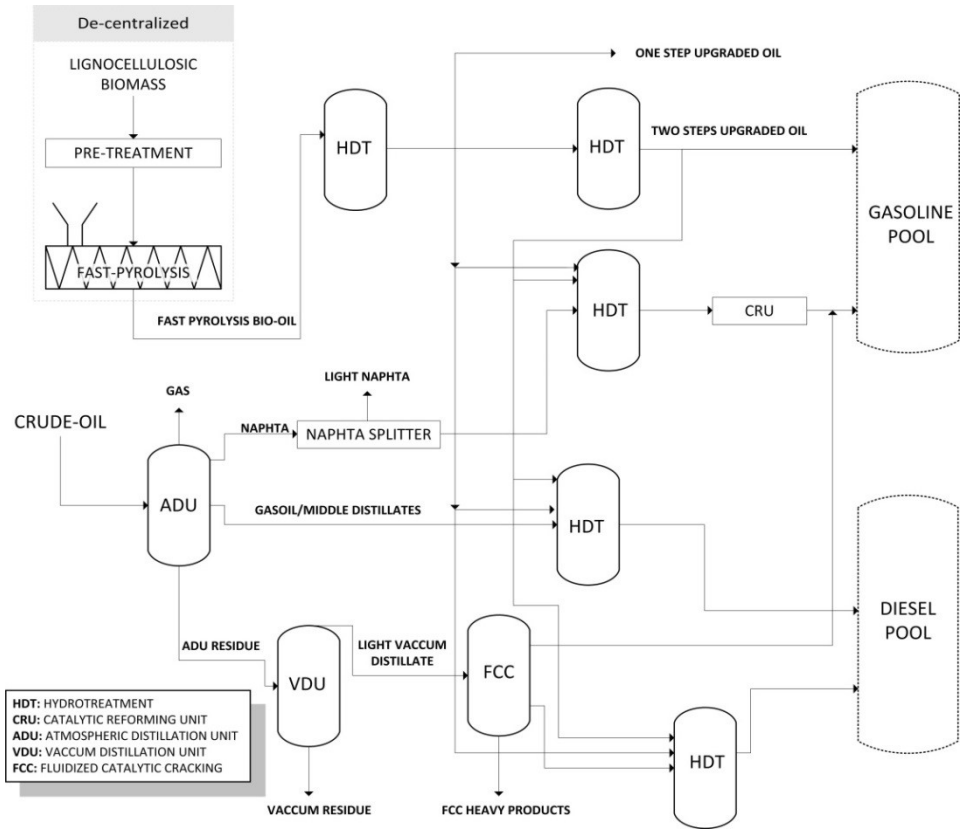

Figure 13. Diagram representing the decentralized production of fast pyrolysis bio-oil and the integration with crude-oil refining. The 2-step upgrading of fast pyrolysis bio-oil can be performed in a single 2-zone stages HDT reactor, here represented as two individual HDT units.

In the decentralized concept for FPBO production further processing/hydrotreatment is performed with the pure FBPO, in order to produce petroleum-like products, followed by refining of the products [37,84].

Another biorefinery concept proposes the integration of the thermochemical conversion unit to the chemical plants in which high amounts of lignocellulosic residues are produced. As example, the integration of a fast pyrolysis and hydrotreatment unit to the sugarcane biorefineries could expand the range of products other than sugar and ethanol to a wider range of fuels and chemicals by the conversion of the sugarcane bagasse (Figure 14). The centralized availability of this feedstock and the higher volumes generated annually are further discussed in the introduction of Chaper 6.

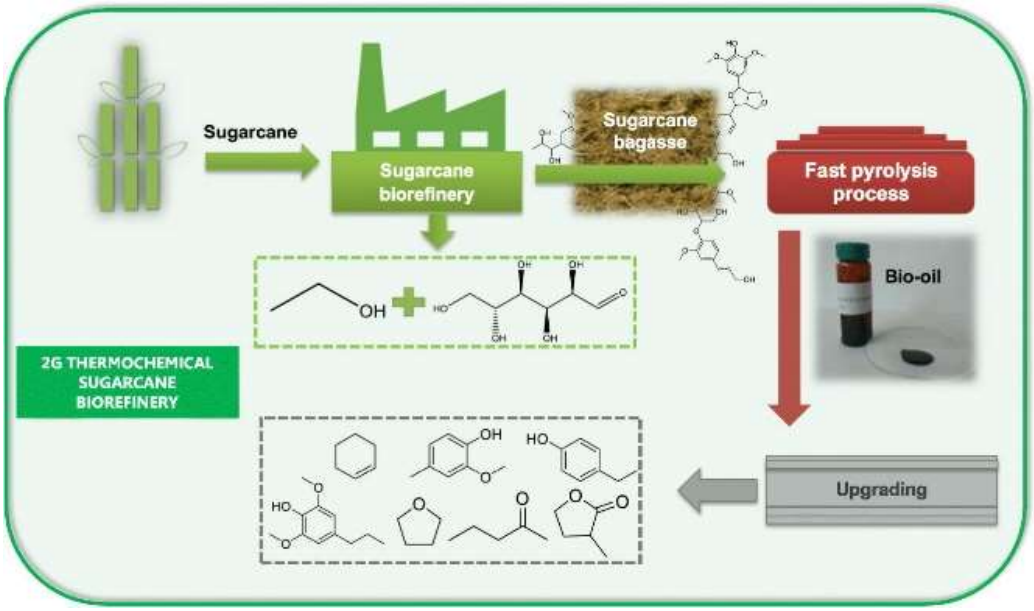

Figure 14. Integration of thermochemical conversion route to the sugarcane biorefinery. Reproduced from ref. [85] according to the terms of Creative Commons Attribution License.

The H_2 required for the hydrotreatment should be also taken into account when a biorefinery plant is designed. Currently H_2 is mainly produced by steam reforming of natural gas, but steam reforming of side products of the biorefinery could be considered, reducing the operation costs [58,86]. Furthermore, H_2 can be also sustainably produced by the hydrolysis of water. Currently many investigations are considering this conversion route, using electricity generated by other renewable sources, such as wind and solar energy [8]. Steam reforming of CO_2 and other feedstocks is also a current hot topic for H_2 production [18].

The future development, integration and operation of biorefineries based on residual lignocellulosic biomass still require significant effort in order to overcome the current challenges: The optimization in terms of biomass used as feedstock, the need to produce liquid yields during

the fast pyrolysis with improved properties (low inorganics and a stable homogeneousFPBO). Furthermore, the costs of the FPBO production are the main challenges to be addressed in terms of fast pyrolysis. The upgrading techniques must be selected according to the final products expected; the stability along the storage should be maximized; hydrotreatment still requires the development of robust catalysts, further investigation in continuously operating reactors and a strategy for product separation.

Chapter 2. Aims and outline of the thesis

2. Aims and outline of the thesis

2.1 Aims of the thesis

As introduced in Chapter 1, the thermochemical conversion of biomass is currently under development aiming production of renewable fuels and chemicals. Fast pyrolysis, considered a mature technology with commercial plants running worldwide, is a promising technology for this application. However, the main product of fast pyrolysis, the fast pyrolysis bio-oil, should undergo an upgrading treatment in order to improve its properties. Lower oxygen content, lower water content, higher energy density, lower viscosity and lower acidity are some of the improvements required if liquid fuels are targeted. In this context, the hydrotreatment is considered a promissing technology for fast FPBO upgrading, but up to now there are no industrial hydrotreatment plants in operation worldwide, requiring further studies in this field.

In order to investigate in details the hydrotreatment of fast pyrolysis bio-oil , the present work sistematically evaluate the application of nickel-based catalysts for this catalytic treatment, addressing the following questions below:

- What is the catalytic activity of nickel-based catalysts for hydrotreatment of fast pyroylsis bio-oil?
- What is the influence of promoters over the activity of the nickel-based catalyst?
- What is the role of Cr and Cu?
- What is the effect of the reaction parameters, such as temperature, pressure and reaction time on the HDT reactions?
- What is the effect of different supports over the hydrotreatment reaction?
- What will be the differences observed in the upgraded oil composition by using the complete FBPO *vs* the isolated heavy phase (low concentration of water and acids) as feedstocks for hydrotreatment reactions?
- Is the catalyst performance affected by the fast pyrolysis bio-oil source, considering woody (beech wood) and residual biomass (sugarcane bagasse) as pyrolysis feedstocks?
- How the catalytic activity and selectivity of the catalyts might be affected by sulfur in the feedstock? What is the role of Cr in terms of sulfur resistance?
- What would be the properties of the upgraded FBPO obtained by 2-step hydrotreatment?

By answering the above questions it is expected to understand the role of hydrotreatment catalysts, promoters, reaction parameters and influence of the feedstocks over the overall catalytic reaction performance.

2.2 Outline of the thesis

The outline of the thesis is organized as follow:

Chapter 1 introduces the use of biomass as renewable carbon source for bioenergy, giving an overview of thermochemical biomass conversion pathways to convert lignocellulose as the most abundant biomass into fuels or intermediates for energetic or chemical use. Concentrating on fast pyrolysis, the process characteristics are given and the product properties and possible application are described. Furthermore, the chapter presents the upgrading alternatives and expected upgraded products. Hydrotreatment concepts are presented as well as the catalysts used so far for FPBO upgrading. Upgrading strategies are then discussed within possible biorefinery concepts. Lastly, the current developments, limitations and future perspective regarding the upgrading of FPBO are presented as the background and motivation for the current thesis. From this, the research demand was identified, from which the question above listed were derived.

Chapter 2 presents the motivation, the questions to be answered in this work as derived from the research demand and the structure of this thesis.

Chapter 3 presents the comparison of two high-loaded benchmark nickel-based catalysts for hydrotreatment of a multiphase beech wood fast pyrolysis bio-oil. The catalytic activity of both catalysts is compared to Ru/C. The catalytic performance is addressed in terms of degree of deoxygenation, hydrogen consumption, upgraded oil yields and selectivity. The influence of Cr_2O_3 as promoter is also presented. Additionally, two sequential upgrading reactions are conducted, firstly with the best catalyst among the catalysts tested in Chapter 5 and in the sequence with the best catalyst presented in this chapter. For that, optimized conditions (Chapter 4) are used. The aim of this chapter is to investigate whether high-loaded catalysts may be a suitable alternative for fast pyrolysis bio-oil upgrading and to investigate the role of the promoters, especially Cr_2O_3, so far not evaluated for the application proposed in the thesis.

Chapter 4 presents the optimization of the hydrotreatment conditions with the catalyst considered more suitable for upgrading reactions, based on the results obtained in Chapter 3. Furthermore, the upgrading of the isolated heavy phase is presented. The aim of this chapter is to identify the best hydrotreatment conditions in terms of pressure and temperature as well as in terms of feedstock (complete beech wood fast pyrolysis bio-oil or isolated heavy phase, with reduced concentration of organic acids, water and aldehydes).

Chapter 5 presents the syntheses of four nickel-based catalysts and the influence of different supports (SiO_2 and ZrO_2) and Cu as promoter. This investigation was motivated in order to reach deeper deoxygenation levels in comparison to the previous results obtained in Chapter 3 and 4. In addition to the catalytic activitiy, the long term stability and activity were evaluated in four consecutive cycles of hydrogenation and catalyst regeneration.

Chapter 6 presents a holistic investigation of sugarcane bagasse characterization, fast pyrolysis, characterization and hydrotreatment of the fast pyrolysis bio-oil. Two of the catalysts tested in Chaper 3, 4 and 5 (a benchmark catalyst and an *in-house* synthesized catalyst) were selected for the hydrotreatment reactions. The aim of this chapter is to evaluate the catalytic performance of both nickel-based catalysts during the hydrotreatment of fast pyrolysis bio-oil from residual biomass and identify whether the thermochemical conversion of sugarcane bagasse followed by catalytic upgrading of the bio-oil can be a suitable technology to be integrated in the Brazilian sugarcane refineries.

Chapter 7 presents the evaluation of both high loaded nickel-based catalysts previously evaluated in Chapter 3 in terms of resistance to sulfur poisoning, considering that no conclusions could be derived from the results previously obtained. The investigation conducted with a model mixture in a continuous flow reactor at Technical University of Denmark aims to evaluate the catalytic activity of both catalysts as a function of time on stream and under the influence of sulfur over the conversion of model compounds and selectivity. The role of Cr_2O_3 is one of the focuses of this chapter, considering the poisoning effect of sulfur over nickel-based catalysts and the previously reported positive effect of Cr_2O_3 over the resistance of catalysts agains this poison substance, although in a different catalytic conversion process.

Chapter 8 presents the conclusion of this study, considering the research questions raised by aims of the thesis. Furthermore, suggestions for future research are presented.

Chapter 3. Evaluation of High-Loaded Ni-based Catalysts for Upgrading Fast Pyrolysis Bio-Oil

Chapter redrafted after:

Schmitt, C. C., Zimina, A., Fam, Y., Raffelt, K., Grunwaldt, J.D., Dahmen, N. (2019). Evaluation of High-Loaded Ni-Based Catalysts for Upgrading Fast Pyrolysis Bio-Oil. *Catalysts,* 9 (9), 784-812.

Declaration of contributions:

Caroline Carriel Schmitt performed the experimental design, conducted the hydrotreatment reactions, evaluated the data, discussed the results and wrote the manuscript.

Anna Zimina supported with the in-situ X-ray absorption spectroscopy.

Yakub Fam contributed with the transmission electron microscopy measurements.

Klaus Raffelt, Jan-Dierk Grunwaldt and Nicolaus Dahmen supervised the work, contributed to the discussion and corrected the manuscript.

List of abbreviation Chapter 3

BWBO: Beech wood fast pyrolysis bio-oil

HP: Heavy Phase

HP_{BWBO}: Heavy phase of beech wood fast pyrolysis bio-oil

LP: Light Phase

LP_{BWBO}: Light phase of beech wood fast pyrolysis bio-oil

Ni-Cr catalyst: benckmark high loaded nickel-based catalyst with Cr_2O_3 as promoter

Ni catalyst: benckmark high loaded nickel-based catalyst

UAP: Upgraded aqueous phase

$UAP_{Ni,\ 225\ °C}$: Upgraded aqueous phase with benchmark Ni catalyst at 225 °C

$UAP_{Ni\text{-}Cr,\ 225\ °C}$: Upgraded aqueous phase with benchmark Ni-Cr catalyst at 225 °C

$UAP_{2^{nd},\ Ni\text{-}Cr,\ 325\ °C}$: 2-step upgraded aqueous phase with benchmark Ni-Cr catalyst at 325 °C

UBWBO: Upgraded beech wood bio-oil

UOP: Upgraded oil phase

$UOP_{Ni,\ 225\ °C}$: Upgraded oil phase with benchmark Ni catalyst at 225 °C

$UOP_{Ni\text{-}Cr,\ 225\ °C}$: Upgraded oil phase with benchmark Ni-Cr catalyst at 225 °C

$UOP_{2^{nd},\ Ni\text{-}Cr,\ 325\ °C}$: 2-step upgraded oil phase with benchmark Ni-Cr catalyst at 325 °C

Abstract Chapter 3

The catalytic activity of high loaded Ni-based catalysts for beech wood fast-pyrolysis bio-oil hydrotreatment is compared to Ru/C. The influence of promoters, temperature, reaction time and consecutive upgrading is investigated. The catalytic activity is addressed in terms of elemental composition, pH value, H_2 consumption and water content, while the selectivity is based on the GC-MS/FID results. The catalysts showed similar deoxygenation activity, while the highest hydrogenation activity and the highest upgraded oil yields were obtained with Ni-based catalysts. The elemental composition of upgraded oils was comparable for 2 and 4 h of reaction, and the temperature showed a positive effect for reactions with Ni-Cr and Ru/C. Ni-Cr showed superior activity for conversion of organic acids, sugars and ketones being selected for the 2-step upgrading reaction. The highest activity correlates to the strength of the acid sites promoted by Cr_2O_3. Consecutive upgrading reduced by 64.8 % the content of oxygen and by 90 % of the water content, whereas the higher heating value increased by 90.1 %. While more than 96 % of the organic acid content was converted, the discrepancy of aromatics compounds quantified by ^{1}H-NMR and GC-MS/FID may indicate polymerization of aromatics taking place during the second upgrading step.

3.1 Introduction

As introduced in Chapter 1, the use of biomass may contribute to sustainable fuels and chemical production, considering that biomass is the only renewable carbon carrier available. Lignocellulosic biomass by far provides the largest mass potential of bio-feedstock for conversion into chemical, fuels and energy within a biorefinery [9,87].

Fast pyrolysis, conducted in an anoxic atmosphere typically at temperatures around 500 °C, is considered the most developed direct thermal liquefaction process for biomass conversion. The specific feature to yield high amounts of liquid condensate(s) is rapid heating up of the biomass ground to mm-size, short reaction time and instant cooling down the products at overall residence of a few seconds only [1].

Fast pyrolysis bio oil (FPBO) is a mixture of hundreds of oxygenated organic compounds including ketones, aldehydes, carboxylic acids, carbohydrates, phenolic derivative compounds and contains considerable amounts of water, ca. 15-35 wt.% [65,70].The presence of oligomers, high concentration of water and carboxylic acids are the main points to be improved [52].

Analogous to the hydrotreatment performed in petroleum refineries, where heteroatoms such as sulfur and nitrogen are removed by catalytic conversion, FPBO can also subjected to hydrotreatment [52]. However, due to the significant differences in petroleum and FPBO composition, the reaction conditions applied in petroleum refineries cannot be simply transferred to FPBO upgrading [8]. Different conditions of temperature, pressure and especially catalysts resistance to high water concentration and high acidity, are required [39]. Furthermore, in the case of FBPO, oxygen is the main heteroatom to be removed, usually corresponding to 35 to 50 wt.% of the pyrolysis oil composition [8]. Sulfur and nitrogen are also constituents of the FPBO, but in smaller amounts, usually in the range of 0.02 wt.% to 0.3 wt.% for sulfur [52–54] and around 0.1 wt.% to 1.2 wt.% for nitrogen [8,53,54], depending of the biomass pyrolyzed.

Therefore, the selection or development of appropriate catalysts maximizing desired pathways need to be accelerated. Consequently, the interest in catalytic upgrading of FPBOs has increased in the last years, leading to a significant number of catalysts tested. Noble metal catalysts such as ruthenium [48,55,71,88,89], palladium [67,90–93] and platinum [94,95] have been used in the early studies, whereas newer studies apply lower cost transition metals catalysts. The selection of the catalyst is a crucial step, considering that: the catalyst should be resistant to water, stable in an acid environment, resistant to poisons and active to hydrodeoxygenation with minimum consumption of hydrogen [61]. Moreover, the catalyst should be resistant to coke deposition and stable in consecutive reuses [65,96].

Among a variety of metallic catalysts available, Ni-based are interesting in terms of high activity versus at relatively low cost [97,98]. Additionally, high hydrodeoxygenation activity with low hydrogen consumption is attributed to Ni-based catalysts [99]. If the right support material is selected, high resistance to water is also obtained. For example, supports such as γ-Al_2O_3 can be converted to boehmite due to the high concentration of H_2O in the pyrolysis oil, resulting in loss of surface area [100]. Some of the previous studies have used Ni based catalysts with different metal loadings [101,102], different solid support materials [70,96,98,99,103] as well as with different feedstocks [53,104]. In terms of metal loading, Boscagli et al. [99] observed higher yields of upgraded oil and lower gas formation using Ni-based catalysts with Ni loading in the range of 20-22 wt.% in comparison to catalysts with Ni loading in the range of 3.2-5.8 wt.%. Ardiyanti et al. [69] reported that Ni-based catalysts with 58 wt.% of Ni loading and Pd and Cu as promoters showed superior performance compared to catalysts with lower concentration of Ni (29-37 wt.%). The Ni-based catalyst with 58 wt.% of Ni loading promoted by 0.7 wt.% of Pd showed the highest activity, lowest oxygen content, lowest char formation tendency and resulted in solubility of the upgraded oil in hydrocarbons. Furthermore, both high loading Ni based catalysts (58 wt.%) with Cu and Pd as promoters resulted in the highest H/C ratio of upgraded oils, considered a parameter as important as O/C ratio for hydrotreatment reactions. Jahromi and Agblevor [102] observed a significant increase in the liquid yields from 26.1 % to 68.6 %, reduction in the coke yield from 34.5 % to 4.2 % and lower gas yields from 35.2 % to 16.4 % by increasing the Ni loading from 10 wt.% to 40 wt.% in the red mud supported catalysts formulation. In addition, the hydrogen content in the upgraded oil was increased to 15.83 wt.% with 40 wt.% of Ni in contrast to 9.56 wt.% with 10 wt.% of Ni, while the oxygen was reduced from 19.72 wt.% to 1.35 wt.%, respectively.

However, the biggest challenges already reported using Ni-based catalyst are related to the degree of deoxygenation achievable as well as to deactivation due to poisons substances such as sulfur [53], coke deposition [98] and active metal leaching [105].

In order to overcome these limitations the addition of promoters and the sequential hydrotreatment applying different catalysts, each one with a specific purpose [39,65,67,106] can be adopted. Promoters included in the catalyst formulation are reported to play a role in hydrodeoxygenation [65] as well as increasing the resistance to poisoning substances [107]. Copper, iron, molybdenum, tungsten and phosphorous [65,70,99] are some of the promoters added to Ni-based catalysts, in order to improve H_2 spillover (Cu), C-O activation while C-C cleavage is inhibited (Cu and Fe), to reduce coke formation (Cu), to suppress sintering and activate oxygenated compounds (Mo), as well as to facilitate de C-O bond cleavage (P) [65,97,108,109].

Also, the inclusion of promoters in the catalysts formulation in order to increase the resistance of Ni-based catalysts in relation to sulfur should be addressed. As previously presented, sulfur deactivates Ni-based catalysts even in low concentrations [104]. Although the application of sulfided NiMo catalysts is usually considered a possibility to avoid sulfur deactivation, it requires an external source of sulfur, increasing the complexity and cost of the treatment [98,102].

One alternative is the addition of chromium promoters. Gómez-Cazalilla et al. [107] have reported increased sulfur tolerance and catalytic activity during hydrotreating of tetralin in the presence of dibenzothiophene. Additionally, Cr_2O_3 has been reported as a structural promoter, preventing sintering [110,111], and has been used in catalysts formulations for hydrogenation of carbonyl groups [112], usually attributed to bio-oil instability [37].

Another attractive possibility is sequential upgrading, which has been found to reduce the formation of coke [59], responsible for clogging the reactor during the upgrading reaction in continuously operated reactors. Additionally higher deoxygenation degree during 2-step upgrading than during 1-step upgrading has been observed. Usually in this 2-step hydrotreatment, the first step is conducted at lower temperature [37,106,113,114], aiming at conversion of reactive compounds, whereas the second step is performed at higher temperatures to hydrodeoxygenate the bio-oil [59]. The first step is referred to as stabilization step, where compounds related to bio-oil instability are converted, whereas in the second step a deep hydrodeoxygenation is performed [49,52,109]. Different catalysts and temperatures are usually used. For example, French et al. [59] suggested that the application of ruthenium based catalyst in the first step followed by nickel or platinum may result is reduced formation of coke and higher degree of deoxygenation in the final product.

Therefore, in the present chapter, two catalysts with high loading of nickel are evaluated for upgrading of fast pyrolysis bio-oil. Previous studies have reported higher yields of liquid products, and minimized production of coke and gas with high loading Ni-based catalyst, motivating the current study. The influence of Cr_2O_3 as promoter and its influence on the selectivity and activity is addressed and compared to Ru/C catalyst. Additionally, the beneficial role of 2-step upgrading with respect to the quality of the final upgraded oil is investigated and compared to the 1-step upgrading.

3.2 Materials and methods

3.2.1 Fast Pyrolysis Bio-oil

The reactions were performed using beech wood fast pyrolysis bio-oil produced in a rotating cone reactor, provided by BTG Biomass Technology Group BV, the Netherlands. The oil was composed by one denser phase, denominated heavy phase (HP) and a light phase (LP), concentrated in the top layer. The phase separation was initiated by intentional ageing at 80 °C for 24 h. The phases were stored separately and mixed again prior the reactions, in the same proportion as found in the original oil (41 wt.% HP and 59 wt.% LP). This bio-oil will be referred as BWBO; further information can be found elsewhere [115]. Additionally, the evaluation of Ni-based catalysts synthesized by wet impregnation for hydrotreatment of FBPO [96] is reported in Chapter 5; the best performance obtained with Ni/SiO_2 with 7.9 wt.% of Ni loading at 8 MPa of H_2 and 325 °C for 2 h resulted in upgraded oil with reduced oxygen content, although deep deoxygenation levels were not achieved. Furthermore, ketones were formed after upgrading. Then, in order to achieve deeper deoxygenation levels the previously upgraded FPBO was further upgraded in this study and referred as UBWBO (upgraded beech wood bio-oil). More information about the upgrading conditions of UBWBO is given in the Supplementary material (see Supplementary Material Chapter 3 section S.1.1). The composition of both pyrolysis oils used in this study are given in Table 3.

3.2.2 Catalysts

The upgrading reactions were conducted with three catalysts: Ru/C (Sigma Aldrich) with 5 wt.% of metal loading and specific surface area of 870 m^2 was selected as standard catalyst, considering the application of this catalyst in previous studies [53,71,88,104] and its higher activity for hydrodeoxygenation compared to other noble metals [68]. Additionally, two commercial catalysts with high loading of nickel were evaluated. The first Ni-based catalyst was composed by 50 wt.% of Ni, (30 wt.% metallic nickel and 26 wt.% NiO) 15 wt.% of Cr_2O_3, 1.5 wt.% of graphite in diatomaceous earth support (27 wt.%, mainly silica see ref. [116]). The catalyst shows a specific surface area of 94 m^2. The catalyst is referred to as Ni-Cr along the chapter. The second Ni-based catalyst was composed of 60 wt.% of nickel, from which around ≤25-<50 wt.% are present as NiO, along with smaller concentrations of ZrO_2 (≤1-<3 wt.%) and Al_2O_3 (≤3-<5 wt.%) in diatomaceous earth support. The catalyst shows a specific surface area of 190 m^2 and is referred as Ni catalyst along the chapter. The pre-reduced catalysts were used in the upgrading reactions as received from the supplier.

3.2.3 Methodologies

3.2.3.1 Reaction conditions

The reactions were conducted in a batch autoclave (200 ml, Tmax: 400 °C, pmax: 36 MPa). Approximately 50 g of the bio-oil to be upgraded was transferred to the autoclave with the addition of 2.5 g of catalyst to be tested. After purging with an inert gas (N_2 Air Liquide 6.0), the autoclave was pressurized with H_2 high purity (Air Liquide 6.0) to 8 MPa at ambient pressure and closed. The gas supply was then disconnected from the autoclave before the reaction. The magnetic gas injection stirrer (torque 80 Ncm, Premex AG) was adjusted to 1000 rpm in order to improve the hydrogen transfer to the reaction mixture (Figure 15), and possibly to improve the hydrogenation pathway [77], reducing polymerization [49]. The reactor was heated by cartridges in a brass mantle. The temperature difference between the heating cartridge and the temperature inside the reactor was 10 °C.

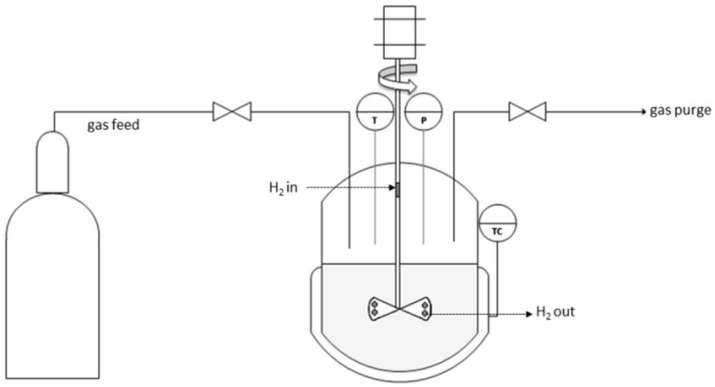

Figure 15. Schematic diagram of the experimental device used for the experiments. Autoclave picture is available in the Supplementary Material. Reproduced from reference [117] according to the terms of Creative Commons Attribution License.

The influence of the reaction time was investigated and the upgrading experiments were conducted for a total time of 2 hours and 4 hours (including the heating ramp). The reactions were mainly conducted at the temperatures of 175 °C and 225 °C; however, based on our investigation [96,116] presented in Chapter 4, a temperature of 325 °C was selected for the second upgrading of UBWBO, aiming a higher deoxygenation degree. The second upgrading step was conducted with Ni-Cr catalyst. The catalyst was selected for the 2-step upgrading based on the parameters as hydrogen consumption, degree of deoxygenation, pyrolysis oil yield and reaction pathways observed in the 1-step upgrading. For the conditions of temperature and reaction time, the set point was reached in a rate of 5 °C·min^{-1}. Once the reaction is completed, the reactor is rapidly cooled to approximately 40-30 °C by pressurized air flow and then further cooled to 20-23 °C with an ice bath. At this point the reactor is depressurized and the gas is collected for further composition analysis. The initial and final pressures were recorded for calculation of the hydrogen consumed (mol of H_2·Kg^{-1} of pyrolysis oil) during the reaction (equation S.1).

3.2.3.2 Liquid products and feedstock characterization

The liquid products and feedstock characterization were performed using a variety of analytical techniques. Carbon, hydrogen and nitrogen content were determined by elemental analysis using a CHN analyzer 628 Leco. When very low amount of sample was available, the elemental analysis was performed by a Vario El cube micro-elemental analyzer. In both cases the oxygen content was obtained by the difference and the concentration used for determination of the degree of deoxygenation (equation S. 6).

The pH value was determined using a pH-meter 691 and the water content by Karl Fischer Tritando 841. The calorific value was determined by calorimeter IKA C5000. Sulfur and metal content (leached after the reactions), were obtained by inductively coupled plasma optical emission spectrometer Agilent, 725. For this measurement the upgraded aqueous phase samples were filtrated using a 0.2 μm polytetrafluoroethylene filter.

The distribution of functional groups in the products as well as in the feedstock were obtained by proton NMR (^{1}H-NMR). The samples were prepared diluting 0.1 g of sample (after centrifugation for solids removal for 3 minutes, neoLab mini centrifuge D-6015) with 0.7 g of deuterated methanol (Sigma Aldrich, 99.8 at.% D) containing 2 g of sodium 3-trimethylsilyl-2-2',3,3'-tetradeuteropropionate in 1 L of solution, as internal standard. The spectrum treatment was performed using the software MestReNova by integration the spectra in pre-defined regions.

Further quantitative and qualitative investigation of the liquid fractions was performed by GC MS/FID at Thünen Institute in Hamburg, Germany. 1 μl of sample diluted in acetone with fluoranthene as internal standard was injected at 250 °C into a HP 6890 gas chromatograph. The instrument was equipped with a cyanopropyl-phenyl-methylpolysiloxane column (60 m x 0.25 mm x 0.25 μm) and the heating ramp was programmed as follow: the program started at 45 °C and was kept for 4 minutes; heated to 280 °C at 4 °C·min^{-1} and kept at this temperature for 20 minutes. Eluted compounds were analyzed by a mass spectrometry detector (HP 5972 ms) and a flame ionization detector (FID). The compounds were analyzed qualitatively comparing the spectra with a NIST and an in-house developed library.

3.2.3.3 Gas product characterization

The gaseous components after the upgrading reactions were analyzed by gas-chromatography. After collection, 100 μl of sample was injected at the gas chromatograph (Agilent 7890A), at the following conditions: injector temperature of 250 °C, oven set at initial temperature of 50 °C (10 min), heated at 3 °C·min^{-1} to 90 °C, then at 20 °C.min^{-1} until 150 °C (16 min) and finally heated at a rate of 50 °C.min^{-1} (10 min). Separation of the compounds was

performed by two columns: Molsieve 5A and Hayesep 57096, Restek and the compounds detected by a thermal conductivity (TCD) and flame ionization (FID) detectors.

3.2.3.4 Characterization of Ni-based catalysts

The catalysts structure was analyzed by complementary analytical techniques before (as received) and after the upgrading reactions. The Ni-based catalysts were analyzed in situ by X-ray absorption spectroscopy (XAS) at the CAT-ACT beamline at and the synchrotron radiation source at KIT (Karlsruhe, Germany). The samples were finely sieved in the range of 90-200 μm and diluted with SiO_2 sieved in the same range. Ni catalyst was diluted 1:2 whereas Ni-Cr catalyst was diluted 1:8. The XAS-TPR measurements were conducted with 50 ml·min^{-1} of 5% H_2 in Helium, heating rate of 5 °C·min^{-1} until 450 °C. The measurement of Ni (Ni K edge 8333 eV) was performed in transmission mode. The software Athena was used for analysis of the spectra. The linear combination fitting was performed using Ni, NiO standards.

Temperature programmed reduction with ammonia (NH_3-TPD) was used in order to evaluate the acidity of the nickel catalysts. The measurement was performed at Ruhr University Bochum in a BELCAT II (fully automated TPD set up, BEL Japan), coupled with online QMS detector (GAM 400 quadrupole mass spectrometer, Balzers Germany). An amount of 100 mg of sample was pretreated by flushing with Helium (Nml/min) for 30 min at 40 °C and 30 min with 3.5 % H_2/Ar (50 Nml/min) at 40 °C. The sample was then heated to 250 °C in a rate of 5 K·min^{-1} and reduced for 120 min at this temperature. In the sequence, the sample was flushed with He (50 Nml·min^{-1}) at 250 °C for 30 min and cooled down to 100 °C. The NH_3 adsorption was conducted at 100 °C using a mixture of 10 % NH_3/He for 60 min. The residual NH_3 adsorbed in internal piping was removed by flushing the system for 60 min with 50 Nml·min^{-1} of He. The measurement was then performed heating the sample from 100 °C to 600 °C at a rate of 5 K·min^{-1} in He (30 Nml·min^{-1}) and the desorbed compounds were detected by the online QMS detector.

X-ray diffraction (XRD) of the catalysts before and after reaction was measured in a diffractometer X'Pert PRO MPD PANalytical equipped with a copper anode (Cu Kα 1.54060 Å). The measurements were performed from 5° to 120° (step size of 0.017°) in a 2θ range. The total measurement time was 60 min. The Scherrer equation was used to calculate the average crystallite size (shape factor K=0.9) considering the reflection with highest intensity. The instrument line broadening was corrected before the calculation. The software X'PertHighscore Plus was used for data analysis.

The solid deposition on the spent Ni-based catalyst was determined by a Vario El cube micro-elemental analyzer, considering that the solid deposition was mainly composed by carbon,

with negligible concentration of oxygen [96]. The difference between the carbon concentration in the fresh and spent catalyst was used for the calculation. In the case of Ru/C, the solid was determined by the difference in weight of fresh catalyst loaded in the batch autoclave and the weight after the upgrading. The moisture content, determined by thermogravimetric analysis (TGA) was discounted for the calculation. This measurement was performed in a TGA analyzer Netzsch STA 409, heating the sample at 10 °C·min^{-1} from 20 °C to 105 °C at air flow of 70 ml·min^{1}. The sample remained at 105 °C for an hour and the moisture was obtained by the mass loss recorded.

Further characterization of the catalysts before and after reaction was performed by transmission electron microscopy (TEM). The measurements were performed at the Institute of Nanotechnology at KIT, with a Titan 80-300 (FEI, USA) transmission electron microscope with an acceleration voltage of 300 kV. Samples were prepared by depositing a small amount of powder on a carbon-coated copper grid. The software TIA was used for analysis to visualize the morphology and map the elemental distribution. Particle size distribution was derived with the support of FIJI software.

3.3 Results

In this section, the results of the upgrading of beech wood fast pyrolysis bio oil (BWBO) with Ru/C, Ni catalyst and Ni-Cr catalyst are presented. The performance of the catalysts in terms of upgraded oil yield, carbon, hydrogen and oxygen concentration, as well as reaction pathways and chemical composition of upgraded products is discussed. The influence of temperature (175 °C and 225 °C) and the reaction time of 2 and 4 h are evaluated. The attempt to reach deep levels of deoxygenation is presented by performing 2-step upgrading using a previously upgraded pyrolysis oil (UBWBO). This oil is the same BWBO which underwent a first hydrodeoxygenation step over Ni/SiO_2 with 7.9 wt.% Ni loading, 8 MPa of H_2 and 325 °C for 2 h, (details given in Chapter 5 and in the Supplementary Material Chapter 3 section S.1.1). In addition, the composition of gas and upgraded aqueous phase is discussed while Ni-based catalysts are characterized before and after upgrading reactions.

3.3.1 Hydrotreatment reactions: Catalytic performance

3.3.1.1 Products distribution, elemental analysis and physicochemical properties

The products distribution after the upgrading reactions is depicted in Figure 16. In all cases the main products are an upgraded oil phase (UOP) and upgraded aqueous phase (UAP) with minor formation of gaseous and solid products. At higher temperature the UOP yield is reduced with Ru/C catalyst (39.5 wt.% at 175 °C and 34.5 wt.% at 225 °C), whereas the opposite behavior is observed for both Ni based catalysts. Ni-Cr showed slightly higher UOP yields in comparison to Ni catalyst for both temperatures evaluated. At 175 °C the UOP fraction obtained with Ni was 44.3 wt.% whereas with Ni-Cr 50.2 wt.% of UOP was formed. At 225 °C 46.9 wt.% of UOP is obtained with Ni, while 51.5 wt.% of UOP is obtained with Ni-Cr, respectively. The highest UOP yield was observed for the 2-step upgrading conducted with Ni-Cr, with 69.5 wt.% of UOP formed. It can be explained by the lower water concentration of the UBWBO (5.1 wt.%), which resulted in low UAP (11.9 wt.%) after reaction, as observed. The amount of solid formed increased as the temperature increased, except for Ni catalyst. In this specific case, a reduction from 0.7 wt.% to 0.4 wt.% was observed. In general the solid yields were below 1 wt.%.

The influence of reaction time (2 h and 4 h) was also investigated and the results are presented in the Supplementary Material (Supplementary Material Chapter 3 S.1.3) using Ni catalyst. At longer reaction time slightly lower amounts of solid and higher UOP yields are found. The latter is in agreement with previous observations [77], although with a different catalyst. The 2-step upgrading conducted with Ni-Cr for two hours, resulted in a concentration of solid corresponding to 0.47 wt.% of the products. This concentration is 15 % lower compared to the

1-step reaction at 175 °C and 38 % lower at 225 °C, and comparable to the 1-step upgrading (0.44 wt.%) of BWBO at the same experimental conditions, as previously reported [116].

The gas product yield was lower for Ni-based catalysts in comparison to the Ru/C catalyst, with Ni-Cr showing the lowest gas production at 175 °C and 225 °C. At 325 °C the 2-step upgrading of UBWBO produced the highest yield of gaseous products; approximately 4 % of gas was produced, an indication of cracking reactions. Comparable gas yields were observed for both reactions times of 2 and 4 h. Further discussion regarding the composition of the gas fractions is available in section 3.3.1.3. Losses due to the viscosity of the upgraded oils and the difficulty to completely recover the products from the autoclave were in the range of 8-15 wt.%.

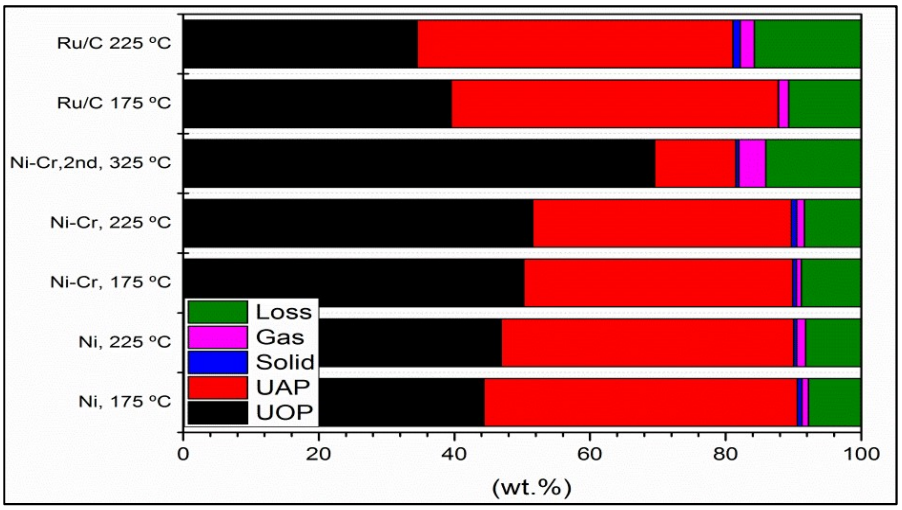

Figure 16. Products distribution after the first upgrading of beech wood fast pyrolysis bio-oil (BWBO) at 175 °C and 225 °C with Ni, Ni-Cr and Ru/C catalyst. The second upgrading of a previously upgraded beech wood fast pyrolysis bio-oil (UBWBO) is presented and referred as Ni-Cr, 2nd, 325 °C, considering the upgrading temperature of 325 °C with Ni-Cr catalyst. Upgraded aqueous phase is referred as UAP and upgraded oil phase as UOP. Reproduced from reference [117] according to the terms of Creative Commons Attribution License.

Analysis of the liquid fractions by elemental analysis (Table 3) showed a high carbon content (65.1-67.0 wt.% on dry basis), of upgraded oils from BWBO for all catalysts and temperatures tested. Slightly higher carbon content was observed at 225 °C for Ni-Cr (66.8 wt.%) and Ru/C (67.0 wt.%). In comparison to the feedstock (BWBO), the carbon content was increased by around 8-11.5 %. The 2-step upgrading reaction conducted with UBWBO increased the carbon content from 72.9 wt.% to 78.6 wt.%. When the initial carbon content is taken into account (from BWBO to $UOP^{2nd,Ni\text{-}Cr,325\ °C}$), an increase of 31.22% is observed. The hydrogen content also increased in the upgraded oils from BWBO. In this case, a positive effect of the temperature in the hydrogen concentration is observed for all catalysts tested. The highest hydrogen concentration was obtained Ni-Cr catalyst at 225 °C (7.9 wt.%), in contrast to 6.8 wt.% in the feed. The UBWBO, initially with 8.4 wt.% of hydrogen content, showed a value of 9.6 wt.% after upgrading. Carbon

and hydrogen were comparable at reactions conducted at 2 and 4 h. Nitrogen and sulfur concentrations were below the detection limit; for that reason no clear trends could be detected.

As expected, lower oxygen contents were observed in the upgraded oils. At 225 °C Ni-Cr and Ru/C reduced the oxygen content from 33 wt.% to 25.3 wt.% and 25.0 wt.%, respectively. UBWBO composed of 44.8 % less oxygen in comparison to BWBO, was further deoxygenated to 11.62 wt.%. Hence, the 2 step upgrading resulted in an $UOP^{2nd}{}_{,Ni\text{-}Cr,325\,°C}$ with 64.8% less oxygen in comparison to the initial BWBO. Similarly to carbon and hydrogen, the concentration of oxygen was comparable for reactions conducted for 2 and 4 h.

The water content in the upgraded oil was also significantly reduced. The BWBO contained 23 wt.% of H_2O, reduced to 10.1 wt.% with Ni-Cr at 225 °C (best performance observed for BWBO upgrading). A slightly higher concentration of H_2O was observed at reactions conducted for 2 h (11.6 wt.%) in comparison to 4 h. The UBWBO, initially with very low H_2O concentration (5.1 wt.%) showed a reduction of 54.9 %, resulting in a 2-step upgraded oil with 2.3 wt.% of H_2O. From the initial water concentration of BWBO, 90% could be removed by the 2-step upgrading. The high carbon and high hydrogen content as well as the lower water concentration and lower oxygen content resulted in higher heating values (HHV). That of the upgraded oils in comparison to BWBO was increased by 40.6 % with Ni-Cr at 225 °C and 37.5 % with Ru/C at the same temperature. The slightly lower HHV (26.12 MJ/Kg) obtained for the reaction conducted for 2 h is in agreement with the higher water (11.6 wt.%) concentration compared to 4 h reaction. The UBWBO already showed a HHV 59 % higher compared to the BWBO; after the second upgrading the HHV of $UOP^{2nd}{}_{,Ni\text{-}Cr,325\,°C}$ reached 36.93 MJ/Kg, 19.3 % higher compared to UBWBO and 90.1 % higher compared to BWBO.

The pH value increased in the upgraded oils in comparison to the feedstocks. The highest pH value of 4.9 was obtained after the 2-step upgrading. The correlation of the chemical composition with the pH value is later correlated with GC-MS/FID results.

A smaller content of carbon was observed in the upgraded aqueous phases (Supplemenraty Material Chapter 3 Table S.1.3). The higher the temperature the lower the carbon content in the UAP of BWBO, which is in this case desired. Ideally the highest recovery of carbon should be observed in the upgraded oil [49]. H_2O concentration in the upgraded aqueous phases was in the range of 42.6-52.0 wt.% for the upgrading reactions using BWBO (highest water concentration observed for Ru/C at 225 °C). The upgrading of UBWBO resulted in a colorless aqueous phase nearly free of carbon ([C]=1.6 wt.%) and with 97.0 wt.% of water (Figure S.4).

Table 3. Chemical composition of upgraded oils at different reaction conditions (8 MPa, 4h of reaction). Reproduced from ref [117] according to the terms of Creative Commons Attribution License.

	Ni, 175 °C 1-step UR		Ni, 225 °C 1-step UR		Ni-Cr, 175 °C 1-step UR		Ni-Cr, 225 °C 1-step UR		Ru/C, 175 °C 1-step UR		Ru/C, 225 °C 1-step UR		Ni-Cr, 325 °C 2-step UR[1]		BWBO[2]		UBWBO[3]	
	Upgraded oils and feedstocks - wet basis (wb) and dry basis (db)																	
	wb	*db*	*wb*	*db*	*wb*	*db*	*wb*	*db*	*wb*	*db*	*wb*	*db*	*wb*	*db*	*wb*	*db*	*wb*	*db*
C (wt.%)	57.9	65.9	58.3	65.1	58.5	65.5	60.1	66.8	57.6	65.2	59.9	67.0	76.8	78.6	46.1	59.9	69.1	72.9
H (wt.%)	8.0	7.6	8.0	7.6	8.0	7.6	8.2	7.9	7.9	7.5	8.1	7.7	9.6	9.6	7.8	6.8	8.5	8.4
O (wt.%)	34.1	26.5	33.7	27.2	33.5	26.8	31.7	25.3	34.4	27.2	31.8	25.0	13.4	11.6	46.0	33.0	21.8	18.2
N (wt.%)	<0.1	-	<1.0	-	<1.0	-	<1.0	-	<0.2	-	<0.2	-	<0.2	<0.2	<0.2	<0.2	0.3	0.3
S (wt.%)	<0.005		<0.005		<0.005		<0.005		<0.005		<0.005		<0.005		0.011	0.015	0.225	0.264
pH value	3.6	-	4.1	-	3.2	-	3.3	-	3.3	-	3.6	-	4.9	-	3^{LP};2.7^{HP}	-	3.0	-
H_2O (wt.%)	12.1	-	10.5	-	10.7	-	10.1	-	11.7	-	10.6	-	2.3	-	23.0	-	5.1	-
HHV (MJ/Kg)	26.3	-	26.3	-	26.2	-	27.3	-	25.5	-	26.7	-	36.9	-	19.41	-	30.93	-

[1] UR: Upgrading reaction; [2]Value calculated considering the mixture of 41 wt.% HP and 59 wt.% LP analyzed separately; [3]Value obtained as an average of four upgrading reactions. For more information see Supplementary Material.

A Van Krevelen diagram (Figure 17) was used in order to visualize the transformations occurring during the hydrotreatment reactions in terms of C, H and O content [37]. The reduction of the O/C ratio indicates hydrodeoxygenation, whereas an increase in the H/C ratio may indicate hydrogenation of the upgraded oils [52]. The upgrading reactions reduced the O/C ratio of BWBO from 0.47 to the range of 0.28-0.31. The lowest O/C ratios for these reactions were observed for Ni-Cr and Ru/C, both resulting in O/C of 0.28. The H/C ratios were reduced in comparison to BWBO, especially at low temperature (175 °C), while the higher temperature (225 °C) seems to promote the hydrogenation for both Ni-based catalysts [57].

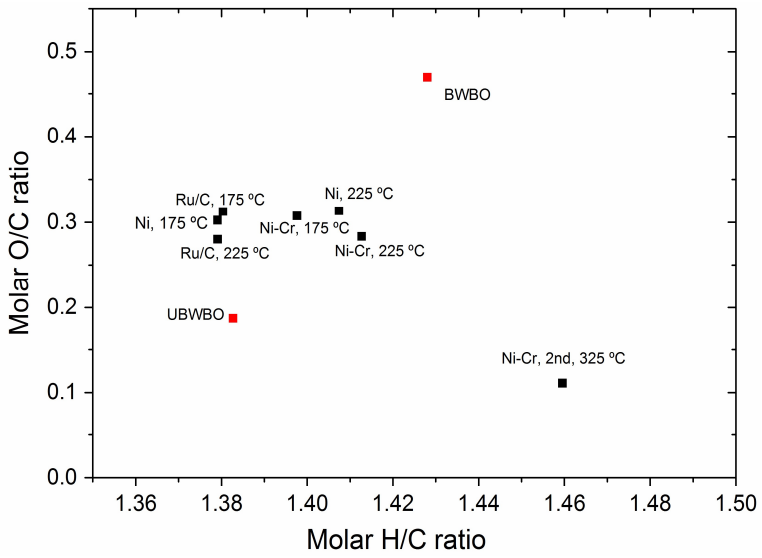

Figure 17. Van Krevelen diagram of the upgraded oils in comparison to the feed (dry basis). Reproduced from reference [117] according to the terms of Creative Commons Attribution License.

The UBWBO showed an O/C ratio of 0.19, much lower compared to the BWBO and to all the upgraded products obtained with all catalysts at 175 °C and 225 °C. The high hydrodeoxygenation activity of the Ni/SiO_2 catalyst used in the first upgrading reaction has been previously reported elsewhere [96]. After the reaction the O/C ratio was further reduced to 0.11 whereas the H/C ratio increased considerably from 1.38 to 1.46. This observation indicates that the catalyst was able to further hydrodeoxygenate and mainly hydrogenates the upgraded oil. A qualitative solubility test (1:100 in volume) with the 2-step upgraded oil showed slightly solubility in a nonpolar solvent (n-hexane), while easily solubilized in a polar solvent (tetrahydrofuran) in agreement with observations of Ardiyinati et al. [70]. Hence, if co-feeding with refinery streams is intended, H/C ratios should be at least in the crude-oil range of 1.5 to 2.0 while O/C ratio should be below 0.05 [37].

3.3.1.2 Detailed chemical composition of liquid products and feedstocks by ^{1}H-NMR and GC-MS/FID

- Characterization of upgraded liquid products and feedstocks by ^{1}H-NMR

An overview of the main functional groups in the upgraded liquid products (UOP and UAP) was obtained by ^{1}H-NMR (Table 4). Each integration range corresponds to a specific proton assignment. Considering that the BWBO was composed by two phases, the comparison among the upgraded oils and feedstock will be performed taking into account the HP_{BWBO}. In the case of the upgraded aqueous phase, the comparison will consider the LP_{BWBO}.

The mmol of protons in the alkanes region (0.5-1.5 ppm) increased in all upgraded oils. Initially the HP_{BWBO} showed 8.20 mmol·g^{-1} while the upgraded products of the 1-step upgrading reaction were in the range of 13.4-21.55 mmol·g^{-1}.The temperature increased the concentration of protons for all catalysts tested, especially for Ni-Cr, which produced the UOP with the highest concentration of protons in this region (21.55 mmol·g^{-1}) for 1-step reactions. The concentration of protons of the UBWBO (after the 2-step upgrading almost doubled, increasing from 22.0 mmol·g^{-1} to 41.80 mmol·g^{-1}). In the UAPs the integration values remained in the range of 4.90-7.47 mmol·g^{-1} for the upgrading conducted with BWBO, slightly higher compared to the initial LP_{BWBO} (3.0 mmol·g^{-1}). The lowest value (0.75 mmol·g^{-1}) was obtained in the aqueous phase obtained after the second upgrading of UBWBO. The protons in the integration region corresponding to α proton to carboxylic acid or keto-groups, α proton to unsaturated groups (1.5-3.0 ppm) also increased in the upgraded oils in comparison to HP_{BWBO}, especially at 225 °C. While HP_{BWBO} showed 17.8 mmol·g^{-1} the upgraded products were in the range of 20.3-25.94 mmol·g^{-1}. A slight decrease from 39.2 mmol·g-1 to 36.5 mmol·g^{-1} was observed after the second upgrading of UBWBO. These observations correlated to the GC-MS/FID results and are later discussed. UAP in general showed much lower concentration of protons in this range in comparison to UOPs; lowest concentrations were obtained with Ru/C at 225 °C (4.27 mmol·g^{1}) and with Ni-Cr at 325 °C (4.3 mmol·g^{-1}) using UBWBO.

Upgraded oils with Ni catalyst at 175 °C and 225 °C showed similar integration values to BWBO in the region of Ethers, dibenzenes, alcohols (3.0-4.3 ppm). The same was observed for Ru/C at 225 °C while slightly higher integration value obtained for this catalyst at 175 °C. Ni-Cr showed higher integration values, especially at 175 °C (16.45 mmol·g^{-1}). The UBWBO already showed lower integration values (11.5 mmol·g^{-1}) which was further reduced to 5.9 mmol·g^{-1} after the second upgrading. A correlation between GC-MS-FID and ^{1}H-NMR was observed for the upgrading reactions conducted with BWBO. However, in the case of the 2-step upgrading, the same tendency regarding the reduction in the alcohols concentration was not clear. Considering that only a small fraction of GC-detectable substances can be quantified [118], discrepancies between both techniques may occur. The UAPs showed higher values in

comparison to UOPs in this range correlating to the results of alcohols given by GC-MS/FID (Table 3). Especially with the second upgrading, very low concentration of protons is observed in the $UAP^{2nd}{}_{,Ni\text{-}Cr,325°C}$ (0.5 mmol·g^{-1}), which agrees with the very low amount of alcohols observed by gas chromatography.

In the range of carbohydrates, H_2O and OH exchange groups (4.3-6.0 ppm) the upgraded oils showed lower integration values in contrast to the UAP; due to the lower concentration of water in comparison to the feedstock, most of the water is concentrated in the UAP, reflecting in the high mmol of proton per g of sample, as observed. In agreement with the very low water content (2.3 wt.%) the product of the 2-step upgrading showed the lowest integration values for this range (6.3 mmol·g^{-1}); on the contrary, the UAP, mainly composed by water (97 wt.%) showed the highest integration range, approximately 8 times higher compared to UBWBO.

The range corresponding to (hetero-)aromatics compounds (6.0-8.5 ppm) slightly reduced after upgrading reactions, indicating low activity towards aromatic conversion, even in the case of UBWBO. UAPs were almost absent of protons belonging to this range (<0.1 mmol·g^{-1}).

Table 4. [1]H-NMR of upgraded oil and feedstock. Reproduced from ref [117] according to the terms of Creative Commons Attribution License (CC BY).

Integration Range (ppm)[1]	Ni, 1-step 175 °C mmol·g^{-1}		Ni, 1-step 225 °C mmol·g^{-1}		Ni-Cr 1-step 175 °C mmol·g^{-1}		Ni-Cr 1-step 225 °C mmol·g^{-1}		Ni-Cr 2-step 325 °C mmol·g^{-1}		Ru/C 1-step 175 °C mmol·g^{-1}		Ru/C 1-step 225 °C mmol·g^{-1}		UBWBO mmol·g^{-1}	BWBO mmol·g^{-1}	
	UOP	UAP	UOP	UAP	UOP	UAP	UOP	UAP	UOP	UAP	UOP	UAP	UOP	UAP	UOP	HP	LP
0.5-1.5	16.66	7.05	17.39	7.47	16.79	6.54	21.55	5.85	41.80	0.75	13.40	5.74	16.30	4.90	22.0	8.20	3.0
1.5-3.0	21.56	9.45	23.22	9.94	21.38	6.92	25.94	6.09	36.50	4.30	20.30	8.30	21.90	4.27	39.20	17.80	11.0
3.0-4.3	13.96	20.76	13.66	19.81	16.45	18.18	15.55	14.00	5.90	0.50	14.40	16.10	13.30	11.4	11.50	13.20	13.90
4.3-6.0	22.11	64.00	21.76	68.99	27.74	60.26	22.78	53.62	6.30	111.7	29.90	64.30	24.80	77.5	13.50	28.50	50.20
6.0-8.5	6.07	0.67	6.04	0.79	5.21	0.82	6.01	0.50	5.80	0.10	5.90	0.55	4.80	0.40	7.50	8.14	3.20
9.5-10.1	0.00	0.00	0.00	0.00	0.04	0.00	0.00	0.00	0.0	0.0	0.0	0.0	0.0	0.0	0.0	0.01	0.06

[1]Integration range of 0.5-1.5 ppm corresponds to alkanes; 1.5-3.0 ppm corresponds to α proton to carboxylic acid or keto-groups, α proton to unsaturated groups; 3.0-4.3 ppm to ethers, dibenzenes and alcohols; 4.3-6.0 ppm to water, O-H exchanging groups and carbohydrates; 6.0-8.5 ppm to (hetero-)aromatics; 9.5-10.1 ppm to aldehydes.

- Characterization of upgraded liquid products and feedstocks by GC-MS/FID

The samples upgraded with Ni-based catalysts at 225 °C and after the 2-step upgrading, as well as BWBO and UBWBO were further analyzed by GC-MS/FID (Table 5). A detailed list with the quantification of GC-detectable compounds is available in the Supplementary Material (Table S.4).

Eight different organic acids were identified in the BWBO. Acetic acid was in the highest concentration (7.2 wt.% dry basis). After upgrading of BWBO, only acetic acid, propionic acid and butyric acid were observed in the products with both catalysts. Slightly higher amount of total organic acids was observed in $UOP_{Ni,225\ °C}$ in contrast to $UOP_{Ni\text{-}Cr,225\ °C,}$ while more than double of acids was observed in the $UAP_{Ni,225\ °C}$ in comparison to $UAP_{Ni\text{-}Cr,225\ °C}$.

Considering the amount of acetic acid initially loaded into the autoclave (considering the amount of BWBO used in each reaction), and the amount of acetic acid after upgrading (considering the weight of UAP and UOP and theirs respective concentrations), nearly the same concentration of acetic acid was observed in the products obtained with Ni catalyst (sum of $UAP_{Ni,225\ °C}$ and $UOP_{Ni,225\ °C}$). On the other hand around 12.92 % of acetic acid was converted with Ni-Cr at 225 °C. In the case of Ni catalyst, it may indicate that even with some possible conversion of acetic acid to products such as methane [90], as a result of dehydrogenation to acetate followed by decarboxylation [66], or even esterification to products such as 2-hydroxyethyl acetate (higher concentration in the upgraded products in comparison to BWBO), some acetic acid is also formed, resulting in nearly the same amount before and after upgrading. It is known that the conversion of compounds such as levoglucosan results in formation of acetic acid [119]. As most of this compound was converted, it can be assumed that some acetic acid could be formed from this route. The higher methane formation observed for Ni-Cr (section 3.3.1.3), on the other hand, is in agreement with the higher acetic acid conversion [90] and may indicate higher activity of Ni-Cr for this reaction pathway.

In the case of consecutive reaction, a conversion of 97 % of acetic acid was obtained in the second upgrading reaction, only detected in the $UAP^{2nd}{}_{,Ni\text{-}Cr,325\ °C}$. Due to the high volume of methane produced, possibly this route was also favored as previously observed in the 1-step upgrading with Ni-Cr catalyst. Hence, the Cr_2O_3 in the catalyst formulation might play a role in this case, considering its reported activity to aliphatic acids conversion [120].

The concentration of propionic acid, the second most abundant acid in the BWBO (0.55 g), increased in the upgraded products especially with Ni (2.19 g) in comparison to Ni-Cr

(0.88 g) at 225 °C. The opposite behavior was obtained with UBWBO: Approximately 96.7 % of the initial propionic acid in the UBWBO was converted after the second upgrading and detected only in the $UAP^{2nd,Ni\text{-}Cr,325°C}$. We assume that while propionic acid is formed from the conversion of hemicellulose derivatives [121] under the upgrading conditions, it is further converted to compounds such as 1 propanol and propane [33,65], especially with Ni-Cr. This assumption explains the lowest concentration of propionic acid in the 1-step upgrading with Ni-Cr catalyst, as well as agrees with the high conversion observed in the second upgrading. In this case, possibly propionic acid is not formed, as most of the hemicellulose derivatives were converted in the first upgrading, resulting only in propionic acid conversion.

Esters observed in the BWBO were completely converted after upgrading, while new compounds were formed. The concentration of acetic acid 2-hydroxyethyl ester increased in the upgrading products with both catalysts (concentration 3.6 times higher with Ni and 2.1 times higher with Ni-Cr, 225 °C). This indicates that conversion of acetic acid is taking place with Ni catalyst, although nearly equal concentration of acetic acid before and after upgrading as discussed previously. Hence, Ni catalyst seems to be more selective towards esterification in comparison to Ni-Cr. The only ester observed in UBWBO (methyl ester propionic acid), was completely converted after the second upgrading.

The number and concentration of alcohols in the upgraded fraction increased significantly after the upgrading of BWBO. Initially only four alcohols were identified in the BWBO, with ethylene glycol in highest concentration (2.81 wt.% dry basis). After upgrading, 24 different alcohols were formed with Ni catalyst and 29 alcohols were formed with Ni-Cr at 225 °C. The most abundant alcohols were ethylene and propylene glycol in both cases. The ethylene glycol concentration increased from 0.97 g in the feed to 3.77 g with Ni and 3.25 g with Ni-Cr. Propylene glycol was formed with both Ni and Ni-Cr, resulting in 0.72 g and 0.64 g, mostly concentrated in the upgraded aqueous phases. In agreement with our previous finding and other investigations, the formation of propylene glycol is attributed to the hydrogenation of acetol [96,122]. Moreover, its hydrodeoxygenation may lead to formation of 1-propanol, compound only identified in the upgraded fractions. Further hydrodeoxygenation of 1-propanol could result in formation of propane, observed in upgrading reactions conduct with Ni-Cr. Ethylene glycol formation, on the other hand, has been reportedly attributed to hydrogenation of hydroxyacetaldehyde [85,95]. UBWBO was almost free of alcohol, with minor concentration of 2,4-dimethylcyclopentanol, product of hydrogenation of 2,4-dimethyl cyclopentanone.

Aldehydes are very reactive at very mild conditions and can be easily converted [61,93]; Consequently they were completely converted after upgrading. The concentration of ketones was reduced from 3.04 g in the BWBO to 0.43 g and 0.12 g with Ni and Ni-Cr, respectively. Hydroxypropanone or acetol (5.8 wt.% dry basis) and 1-hydroxy-2-butanone (0.52 wt.% dry basis) were the compounds in the highest concentration in the BWBO and possibly converted to propylene glycol and 1,2-butanediol, both identified in the products.

The UBWBO showed initially 22 non-aromatic ketones with 2-methylcyclopentanone in the highest concentration (1.22 wt.% dry basis). The highest conversion of ketones with Ni-Cr catalyst during the 1-step upgrading was one of the motivating criteria adopted for selection of this catalyst for the 2-step upgrading reaction. After the second upgrading reaction only 8 ketone compounds were observed in the upgraded products, most of them initially observed in the UBWBO, indicating only partial conversion. From the initial 1.16 g in the UBWBO, the 2-step upgraded oil was composed by 0.65 g of ketones, respectively.

Non-aromatic hydrocarbons were absent in the feedstocks as well as in the upgraded products using BWBO. However, cyclic hydrocarbons, such as methylcyclohexane (0.62 wt.% dry basis), cyclohexane (0.54 wt.% dry basis), and ethylcyclohexane (0.36 wt.% dry basis) were the hydrocarbons in highest concentration identified in the $UOP^{2nd}{}_{,Ni\text{-}Cr,325\ °C}$. Long chain aliphatic compounds such as n-pentadecane (0.03 wt.% dry basis) and n-heptadecane (0.11 wt.% dry basis) were also formed after upgrading.

Analogous to the observation for ketones, most of the furans in the BWBO (around 1.0 g) were converted with upgrading, while new furans were formed after 1-step upgrading. The final concentration in the $UOP_{Ni,225\ °C}$ (0.91 g) and $UOP_{Ni\text{-}Cr,225\ °C}$ (0.87 g) was in the similar range of BWBO, despite the conversions observed. The second upgrading of UBWBO reduced nearly by half the concentration of furans in the $UOP^{2nd}{}_{,Ni\text{-}Cr,\ 325\ °C}$.

The BWBO was composed by 5.81 wt.% dry basis aromatic compounds, meaning 2.23 g of aromatics in total. The conversion with Ni catalyst resulted to 1.97 g of aromatics in the upgraded products whereas the upgrading with Ni-Cr resulted in 1.43 g of aromatics. In respect to the 2-step upgrading, 1.39 g of GC-detectable aromatics initially in the UBWBO were reduced to 0.42 g in the $UOP^{2nd}{}_{,Ni\text{-}Cr,325\ °C}$. These findings contradict the ^{1}H-NMR observation, in which the concentration of aromatics remained nearly in the same range for all the reactions. Hence, as just a small fraction of the sample is quantified by GC-MS/FID, in the range of 23 % for 1-step and only 7.6 % for $UOP^{2nd}{}_{,Ni\text{-}Cr,325\ °C}$, it may indicate that the aromatics underwent polymerization during the upgrading treatment, as the ^{1}H-NMR analyzes the complete liquid sample. Further

characterization to support this hypothesis was not performed due to the limited amount of samples available and the priority given to other analytical techniques. However, it was visually possible to observe higher viscosity of 2-step upgraded oil in comparison to the feedstock.

The total amount of compounds belonging to the benzene group, remained nearly in the same range after 1-step upgrading with Ni-Cr (around 0.02 g in the feed and products), whereas nearly 40 % less was observed in the products obtained with Ni catalyst (0.013 g). The products obtained after the second upgrading, on the other hand, showed a total amount of benzene around 5.6 times higher compared to UBWBO.

Although very low, the concentration of toluene increased after the 1-step upgrading (feed: 0.003 g, Ni-Cr: 0.006 g; Ni: 0.005 g). Initially absent of toluene, the 2-step upgraded oil was composed by 0.017 g of toluene. It was previously reported that toluene is among the plausible products of guaiacol conversion [123,124], in agreement with the lower guaiacol concentration in the upgraded products in comparison to the feed. The concentration of benzene also increased in the $UOP^{2nd}{}_{,Ni\text{-}Cr,325\ °C}$ from 0.006 g to 0.0181g. Other six compounds belonging to the benzene group were observed in the 2 step upgraded oil with 1-methyl-naphtalene, the heterocyclic aromatic compound in the highest concentration (0.038 g), a evidence of aromatics condensation taking place.

Most of the lignin derived phenols were converted, with nearly the same compounds observed mostly in the UOPs for both Ni-based catalysts. Among the products, phenol was observed in higher concentration in the $UOP_{Ni,225\ °C}$ (0.114 wt.% dry basis), in comparison to the $UOP^{2nd}{}_{,Ni\text{-}Cr,325\ °C}$ (0.022 wt.% dry basis). The highest concentration of cyclohexanol in the products obtained with Ni-Cr may be an indication of the aromatic ring hydrogenation of phenol as a possible reaction pathway [99]. This assumption can be extrapolated to $UOP^{2nd}{}_{,Ni\text{-}Cr,325\ °C}$, considering the absence of phenol and high concentration of cyclohexanol (0.469 wt.% dry basis). Furthermore, o-cresol was not observed in the upgraded products with Ni, whereas it was among the most abundant lignin derived phenols in the $UOP^{2nd}{}_{,Ni\text{-}Cr,325\ °C}$ (0.11 wt.% dry basis). Most of the studies have reported toluene and methylcyclohexane as the main product obtained from o-cresol [125].

A number of 24 compounds belonging to the guaiacol group were identified in the BWBO, with guaiacol (0.621 wt.% dry basis), 4-methyl-guaiacol (0.683 wt.% dry basis), eugenol (0.22 wt.% dry basis), cis-isoeugenol (0.32 wt.% dry basis), vanillin (0.47 wt.% dry basis) and acetoguaiacone (0.34 wt.% dry basis) among the main compounds. Eugenol and isoeugenol were hydrogenated to 4-propylguaiacol, as previously reported [85,96]. The concentration of

guaiacol reduced slightly to 0.18 g with Ni and 0.17 g with Ni-Cr. The concentration of acetoguaiacone in the products obtained with Ni catalyst increased to 0.20 g, while completely converted with Ni-Cr. It can be an evidence of lignin depolymerization [76] with Ni catalyst, whereas further conversion probably took place with Ni-Cr. Only three compounds belonging to the guaiacol group were identified in the UOP^{2nd}, $_{Ni\text{-}Cr,325\,°C}$ resulting in 0.68 wt.% on dry basis.

The number of syringol belonging compounds was reduced from 8 in the BWBO to 5 and 3 compounds with Ni and Ni-Cr catalyst. The initial concentration of 0.10 g increased to 0.22 g with Ni, mainly due to the formation of dihydrosinapyl alcohol (0.18 g), in this case attributed to further depolymerization of lignin oligomers [125,126], whereas the concentration of syringols was reduced to 0.03 g with Ni-Cr. Compounds belonging to syringol group were absent in the UBWBO as well as in the 2 step upgraded products.

The carbohydrate fraction of BWBO was mainly composed by sugars (9.96 wt.% dry basis, 3.4 g). Levoglucosan was the main sugar compound and completely converted with both catalysts. A complex reaction pathway is attributed to levoglucosan conversion, leading to CO_2, alcohols such as ethyleneglycol, propyleneglycol, 1,2-butanediol, acetic acid as well as polymerization products [8,95,109]. After the upgrading, 0.313 g still remained in the $UAP_{Ni,225\,°C}$ whereas 0.049 g remained unconverted with Ni-Cr in both cases mostly unknown sugars. Hence, Ni-Cr is more active for sugars conversion in comparison to Ni. By analogy to glucose conversion previous observed [127], the higher conversion of sugars with Ni-Cr catalyst may be attributed to Cr_2O_3 in the catalyst formulation In this case, the adsorption of molecules is preferentially done through oxygen adsorption to Cr^{3+} by the oxygen lone pairs of electrons [8,128–130]. Further discussion is given is section 3.3.3.

Table 5. Quantification of GC-MS/FID detectable compounds in the feedstock and upgraded liquid products. Reproduced from ref [117] according to the terms of Creative Commons Attribution License (CC BY).

Compounds	BWBO[1]		UBWBO		Ni, 225 °C, 1-step UR				Ni-Cr, 225 °C, 1-step UR				Ni-Cr, 325 °C, 2-step UR			
	wb[2] *(wt.%)*	*db*[3] *(wt.%)*	*wb*[2] *(wt.%)*	*db*[3] *(wt.%)*	*UOP wb*[2] *(wt.%)*	*UOP db*[3] *(wt.%)*	*UAP wb*[2] *(wt.%)*	*UAP db*[3] *(wt.%)*	*UOP wb*[2] *(wt.%)*	*UOP db*[3] *(wt.%)*	*UAP wb*[2] *(wt.%)*	*UAP db*[3] *(wt.%)*	*UOP wb*[2] *(wt.%)*	*UOP db*[3] *(wt.%)*	*UAP wb*[2] *(wt.%)*	*UAP db*[3] *(wt.%)*
Nonaromatic compounds	**17.41**	**24.74**	**13.69**	**14.61**	**15.00**	**16.91**	**28.70**	**55.68**	**13.15**	**14.64**	**20.72**	**41.57**	**5.13**	**5.28**	**2.96**	**80.99**
Acids	5.56	7.87	9.71	10.37	8.64	9.73	10.02	19.45	7.96	8.86	4.55	9.14	-	-	2.73	74.72
Nonaromatic Esters	0.33	0.47	0.08	0.08	0.59	0.66	0.79	1.53	0.27	0.31	0.58	1.16	-	-	-	-
Nonaromatic Alcohols	1.96	2.89	0.18	0.19	4.16	4.69	17.51	33.97	4.34	4.83	15.54	31.17	0.46	0.47	0.11	3.12
Nonaromatic Aldehydes	3.49	4.99	-	-	-	-	-	-	-	-	-	-	-	-	-	-
Nonaromatic Ketones	6.05	8.51	3.72	3.98	1.57	1.77	0.38	0.73	0.58	0.65	0.05	0.10	1.84	1.89	0.12	3.15
Hydrocarbons	-	-	-	-	0.04	0.05	-	-	-	-	-	-	2.84	2.92	-	-
Heterocyclic compounds	**2.39**	**3.30**	**0.70**	**0.75**	**2.41**	**2.72**	**1.88**	**3.66**	**2.52**	**2.80**	**1.85**	**3.71**	**0.34**	**0.35**	**0.16**	**4.44**
Furans	2.19	3.04	0.70	0.75	2.23	2.51	1.76	3.42	2.27	2.53	1.70	3.41	0.34	0.35	0.16	4.44
Pyrans	0.19	0.27	-	-	0.18	0.20	0.12	0.24	0.25	0.27	0.15	0.29	-	-	-	-
Aromatic Compounds	**4.46**	**5.81**	**4.47**	**4.77**	**7.27**	**8.2**	**1.54**	**2.98**	**6.25**	**6.95**	**0.93**	**1.87**	**1.94**	**1.99**	**-**	**0.09**
Benzenes	0.05	0.05	0.07	0.08	0.06	0.06	-	-	0.10	0.11	-	-	0.60	0.62	-	-
Aromatic Alcohols	-	-	-	-	-	-	0.05	0.11	-	-	-	-	-	-	-	-
Aromatic Aldehydes	0.03	0.04	-	-	-	-	-		-	-	-	-	-	-	-	-
Aromatic Ketones	0.01	0.01	-	-	-	-	-		-	-	-	-	-	-	-	-
Aromatic Esters	-	-	-	-	-	-	0.05	0.10	0.08	0.09	-	-	-	-	-	-
Lignin Derived Phenols	0.5	0.64	0.86	0.91	0.70	0.79	0.06	0.11	0.71	0.79	0.03	0.07	0.68	0.70	-	-
Guaiacols	3.68	4.81	3.54	3.78	5.53	6.23	1.37	2.67	5.21	5.80	0.90	1.80	0.66	0.68	-	-
Syringols	0.19	0.25	-	-	0.23	0.26	-	-	0.15	0.17	-	-	-	-	-	-
Carbohydrate	**6.79**	**9.96**	**-**	**-**	**-**	**-**	**1.31**	**2.54**	**-**	**-**	**0.19**	**0.39**	**-**	**-**	**-**	**-**
Sugars	6.79	9.96	-	-	-	-	1.31	2.54	-	-	0.19	0.39	-	-		
Other organic compounds[4]	**0.68**	**0.03**	**0.07**	**0.07**	**0.45**	**0.51**	**0.65**	**1.26**	**0.20**	**0.22**	**0.56**	**1.11**	**0.20**	**0.21**	**0.01**	**0.16**
Total (wt.%)[5]	**34.61[LP] 28.14[HP]**	**53.66[LP] 32.83[HP]**	**18.93**	**20.21**	**34.08**	**66.12**	**25.14**	**28.33**	**24.25**	**48.66**	**22.12**	**24.62**	**3.14**	**85.68**	**7.61**	**7.84**

[1]Value obtained from the mixture of LP and HP as described in section 3.1; [2]wb: wet basis; [3]db: dry basis; [4]Unknown compounds, N-compounds, acetates and terpenes. [5]Total of the sample quantified by GC-MS/FID. The total quantified of HP and LP from BWBO are presented separately.

3.3.1.3 Degree of deoxygenation (DOD), H_2 consumption and gaseous products of upgrading reactions

The hydrogen consumption and the degree of deoxygenation (DOD) were correlated in Fig. 3. The DOD ranged from 24 % with Ni at 225 °C to 30.2 % with Ru/C at 225 °C. The experimental deviation was considered of ±1.2 estimated from four measurements (Supplementary Material Chapter 3 Table S.1). The two highest DOD were obtained with Ni-Cr and Ru/C at 225 °C. In the case of Ru/C, it can be partly attributed to the highest amount of CO_2 production among all the reactions, combined to the highest yield of gas for the 1-step reaction (2.1 %). The amount of gas formed in this case was circa 60 % higher in comparison to Ni catalyst and 85 % higher in relation to Ni-Cr, whereas the amount of CO_2 produced was 55.6 % higher compared to Ni and 126 % higher compared to Ni-Cr catalyst at 225 °C. The influence of temperature over the DOD can be noticed for 1-step reaction with both Ni-Cr and Ru/C catalyst whereas not clear tendency was observed with Ni catalyst. In this case, the DOD and hydrogen consumption (considering the experimental deviation of ±0.35) are considered the same in both temperatures. Similar observation of higher oxygen concentration obtained at higher temperature was reported elsewhere, although over different hydrotreatment conditions [127]. Overall, the highest DOD for 1-step reactions and Ni-based catalysts was obtained with Ni-Cr at 225 °C, reaching 29.5 % of oxygen removed.

Ni-based catalysts showed higher hydrogen uptake in comparison to Ru/C, especially the Ni catalyst, attributed to the higher metal loading [102] (see section 3.2.2 Catalysts), as well as the highest amount of NiO. The comparable H_2 at 175 °C and 225 °C agrees with the DOD observed. In the 1-step reactions with Ni-Cr and Ru/C, the highest consumption was observed at 225 °C, as usually higher consumption of hydrogen are observed at higher temperatures [77,88,104].

The consumption of hydrogen in the 2-step reaction was significantly higher compared to 1-step reactions. The highest hydrogen uptake correlated to the H/C ratio given in the Van Krevelen plot (Figure 17). However, the higher hydrogen consumption not necessarily influenced the DOD (26.4 %). In this case, the catalytic reaction seems to prefer other reaction pathways, considering the significant amount of CH_4 formed (Figure 18 b). Ethane, propane, n-butane and i-butane were also produced in higher concentration in comparison to 1-step reactions, whereas CO_2 was minimized in comparison to 1-step reactions, in agreement with previous studies [127]. The highest cracking activity observed for Ni-Cr catalyst may be attributed to strong acid sites, reported to be very active for cracking reactions [107].

Some assumptions arise in regard to the high amount of gaseous hydrocarbon formed; the high temperature is reportedly attributed to increase the yields of gaseous products [104] which is in agreement to the highest gas yield (3.9 %) at 325 °C among all reactions; However, not just the temperature but the bio-oil composition plays a role in the gas formation, considering that reactive species were stabilized in the UBWBO [8] and competitive reactions might be minimized. As example, the high conversion of acetic acid in the 2-step upgrading (97 % converted, see section 3.3.1.2) can be one of the reaction pathways leading to CH_4 formation [90]. High reaction temperature, and lower concentration of water in the UBWBO compared to BWBO may act synergistically, contributing to the decarboxylation of acetic acid, leading to CH_4 and CO_2 formation, as reported elsewhere [59]. Cracking reactions most probably also contributed to the high concentration of CH_4 and C2-C4 gaseous compounds. The lowest concentration of CO_2 in the gas phase in contrast to the highest consumption of hydrogen may be correlated to methanation reaction [69,131]. Furthermore, CO may also contribute to methane formation, as CO undergoes methanation easily compared to CO_2 [132].

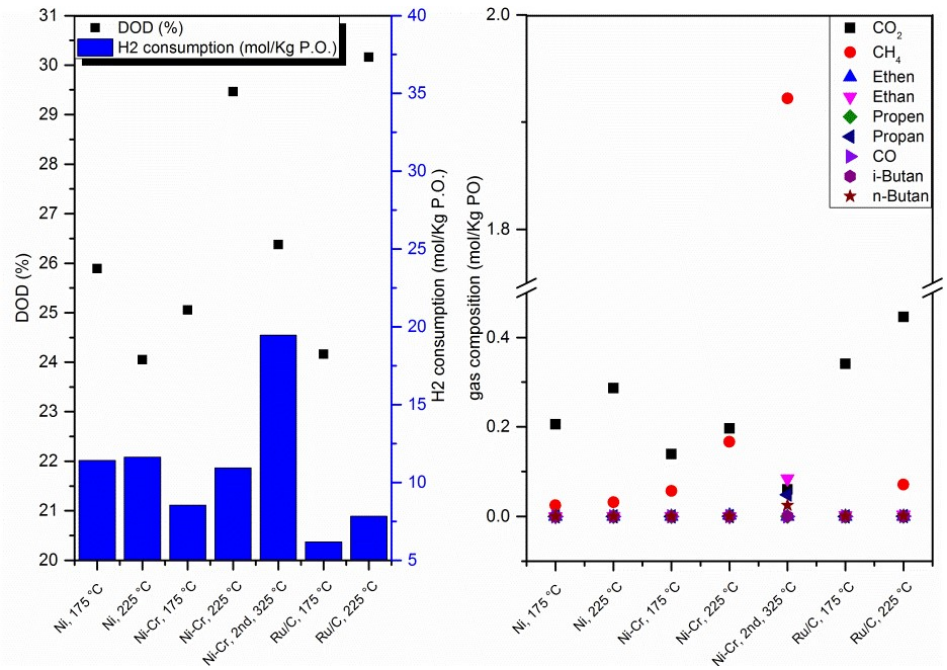

Figure 18. Degree of deoxygenation vs. hydrogen consumption and gas composition for the upgrading reactions conducted with BWBO and UBWBO. Reproduced from reference [117] according to the terms of Creative Commons Attribution License.

3.3.2 Catalysts characterization

The Ni-based catalysts were characterized in detail by a variety of analytical techniques in order to correlate the catalytic activity and their characteristics. Considering that both Ni-based catalysts consisted of metallic nickel and nickel oxide, the oxidation state transformation over reductive atmosphere was followed by in situ X-ray absorption

spectroscopy, depicted in Figure 19. Ni catalyst was initially composed by 55 at.% of NiO and 44 at.% of Ni, whereas Ni-Cr catalyst was initially composed by 23 at.% of NiO and 77 at.% of Ni, respectively. Under the reductive atmosphere the reduction of NiO in the Ni catalyst started close to 250 °C, close to bulk NiO [69], whereas the reduction of the NiO present in the Ni-Cr catalyst was observed already at around 100 °C. The complete reduction of NiO in both Ni and Ni-Cr catalyst was reached at 450 °C and 275 °C, respectively. This observation may only partially explain the highest consumption of H_2 observed to Ni catalyst during the hydrotreatment reactions, as a small amount of H_2 was possibly consumed for reduction of NiO to Ni. Moreover, the lowest temperature required for complete reduction of NiO in the Ni-Cr catalyst may be attributed to the higher metallic nickel loading, lowering the reduction temperature [102,133] whereas the small amount of Al_2O_3 in the catalyst formulation may interact with nickel, retarding the reduction in the Ni catalyst [68] in addition to the highest NiO concentration. Surface properties possibly also play a role in this case.

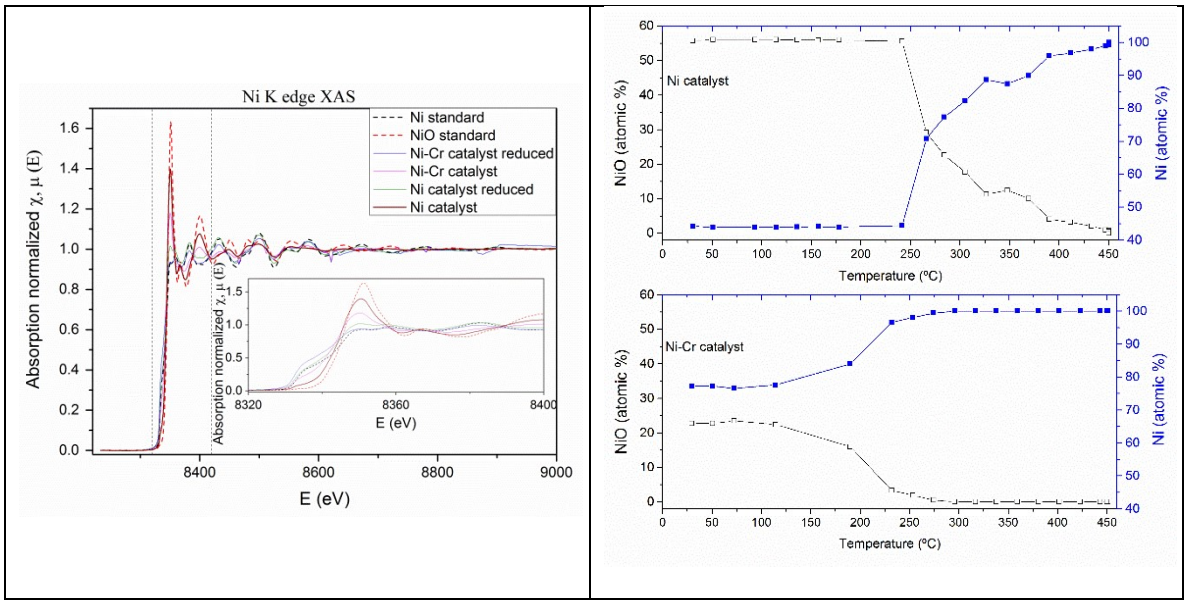

Figure 19. X-ray absorption spectroscopy of both Ni-based catalysts before and after in situ reduction. Ni and NiO standards also included. Reproduced from reference [117] according to the terms of Creative Commons Attribution License.

The strength and density of acid sites were obtained by NH_3-TPD (Figure 20). For both fresh catalysts two desorption peaks were observed. For Ni catalyst the first desorption peak was around 150 °C and the second desorption peak around 300 °C. In the case of Ni-Cr the low temperature desorption peak was observed at around 180 °C whereas the high temperature desorption peak was observed around 355 °C. The amount of NH_3 desorbed in both low and high temperature peak are given in Table 6. The peaks at lower temperatures (up to 205 °C) are attributed to weak acid sites while the peaks at higher temperature are attributed to moderate (250-350 °C) to strong acid sites (higher than 350 °C) [134,135].

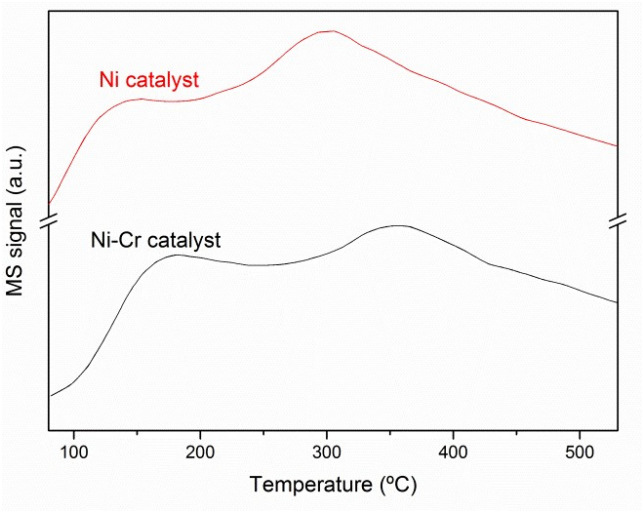

Figure 20. NH_3-TPD of Ni and Ni-Cr catalysts. m/e=17. Reproduced from reference [117] according to the terms of Creative Commons Attribution License.

Although higher amount of NH_3 desorbed at low and high temperatures observed for Ni catalyst, the broader peak observed for Ni-Cr at higher temperature is an indication of sites with stronger acidity, similar to observations of Yang et al. [83] for Ni/γ-Al_2O_3 and Ni/CeO_2 catalysts. Hence, it may indicate the presence of stronger acid sites in this catalyst, in comparison to Ni catalyst. The presence of chromium is reported to increase the acidity of Ni-based [107], due to strong acid sites of Cr_2O_3 [136] which are essential for HDO reactions [52], although also related to coke formation and deactivation mechanisms. Although different BET surface area, the density of acid sites is nearly the same for both catalysts.

Table 6. NH_3 desorption at low and high temperature. Reproduced from ref [117] according to the terms of Creative Commons Attribution License (CC BY).

Sample	Low Temperature NH_3 desorption ($mol.g^{-1}$)	High temperature NH_3 desorption ($mol.g^{-1}$)	Density of acid site ($\mu mol/m^2$)[1]
Ni	3.32×10^{-4}	1.00×10^{-3}	7.01
Ni-Cr	1.92×10^{-4}	4.65×10^{-4}	6.99

[1] Sum of mols of NH_3 desorbed at low and high temperature/BET surface area

The particle size distribution of Ni-based catalysts (Figure 21) was obtained by scanning electron transmission (STEM), with at least 377 particles measured for the particle size distribution determination. The fresh Ni catalyst showed an average particles size of 7.9±4.9 nm, reaching 10.9±7.2 nm after upgrading; on the other hand, the average particle size of Ni-Cr increased from 8.7±4.2 nm to 16.9±11.6 nm after the reaction at 225 °C and reached 18.2±12.6 nm after the 2-step upgrading at 325 °C. Both catalysts showed high heterogeneity of particles sizes after upgrading reactions, revealing that sintering and agglomeration took place.

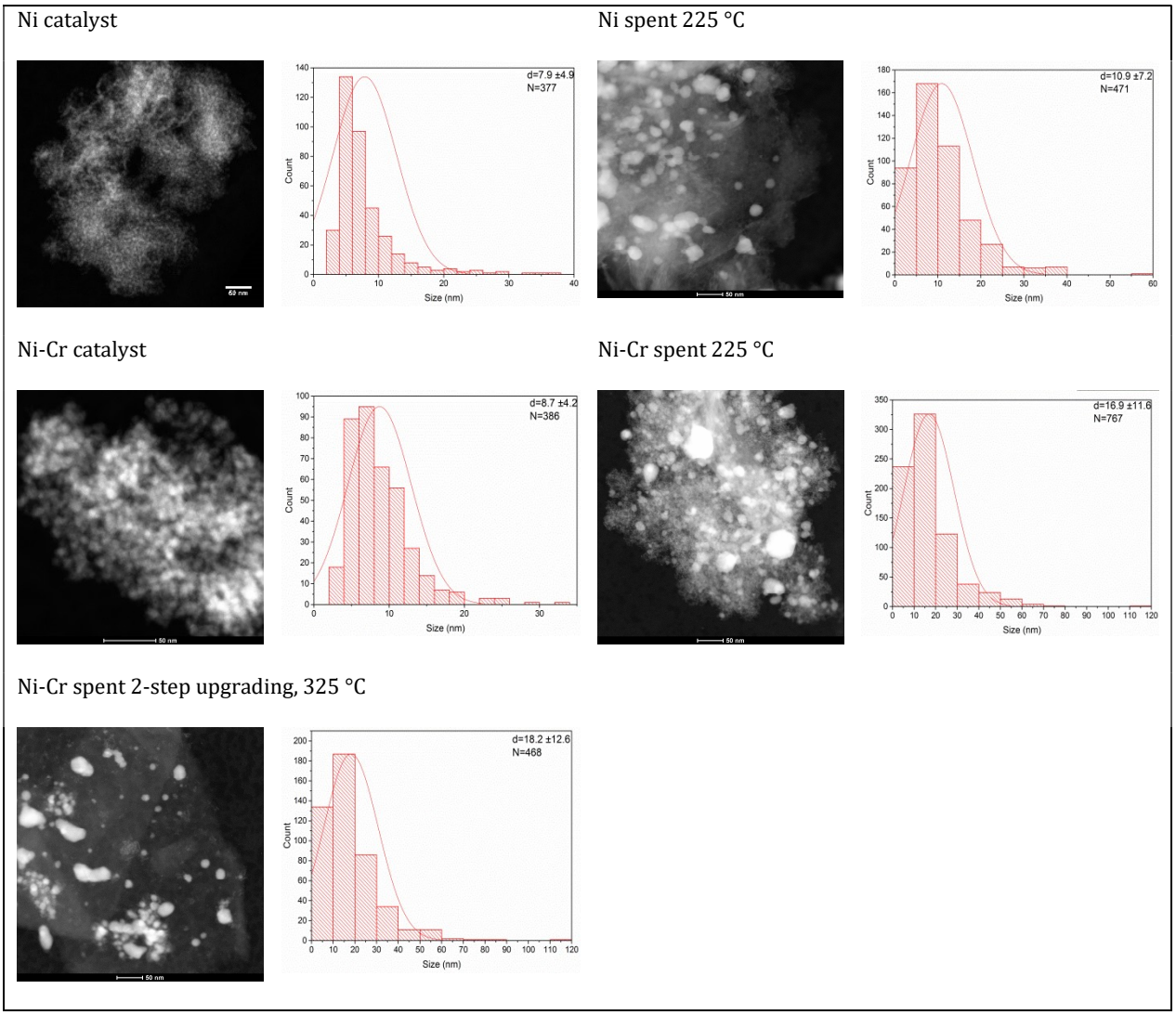

Figure 21. STEM image and particle size distribution of the catalysts before and after reaction. d= average diameter; N= number of particles. Reproduced from reference [117] according to the terms of Creative Commons Attribution License.

Similar concentration of carbon determined by elemental analysis was deposited over the spent Ni-Cr catalyst, in the range of 11 wt.%, whereas around 7.4 wt% of carbon was deposited over spent Ni catalyst. The concentration of sulfur, on the other hand, was below the quantification limit (<0.5 wt.%) in all catalysts used in the first step upgrading, except the Ni-Cr after the second upgrading, with a sulfur concentration of 0.2 wt.%. This observation agrees with the higher concentration of sulfur in the UBWBO (0.225 wt.% wet basis) in comparison to BWBO (0.011 wt.% wet basis). As previously stated that Cr_2O_3 may act as a trap for sulfur molecules [107], a STEM-EDX of spent Ni-Cr catalyst at 325 °C was performed (Figure 22 and Table 7). Considering that chromium is homogenously distributed over the particle analyzed and surroundings, no clear preference for sulfur adsorption is observed. Additionally, carbon deposition is also homogeneously distributed over the spent catalyst particle.

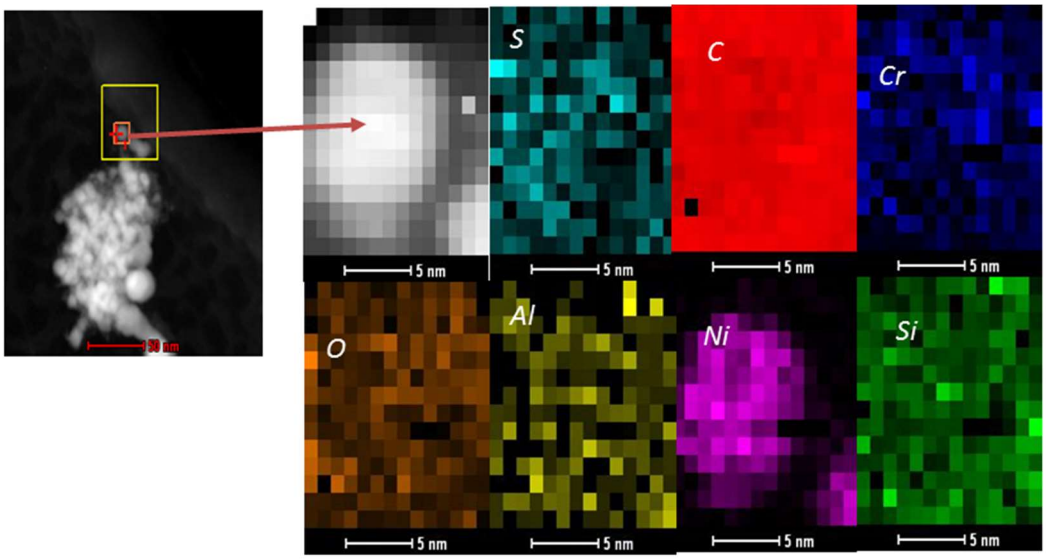

Figure 22. STEM image of spent Ni-Cr catalyst after the second upgrading at 325 °C. Reproduced from reference [117] according to the terms of Creative Commons Attribution License.

Table 7. STEM-EDX spent Ni-Cr after the second upgrading at 325 °C. Reproduced from ref [117] according to the terms of Creative Commons Attribution License (CC BY).

Element	**C**	**O**	**Al**	**Si**	**Ni**	**Cr**	**S**
at.%	88.46	5.49	0.37	1.10	2.63	0.60	0.50

The X-ray powder diffraction for fresh and spent catalysts is depicted in Figure 23. The broad reflections attributed to highly dispersed NiO disappeared after the upgrading reaction for both catalysts at 225 °C, indicating reduction to metallic nickel under H_2 atmosphere. The sharper diffractions observed after the 1-step upgrading reaction indicate bigger crystallite sizes of metallic nickel in the catalysts [133]. Reflections attributed to crystalline chromium oxide were absent in the fresh and spent catalysts, due to the high dispersion as well as indicating an amorphous phase. Broader peaks are observed in the spent catalyst after the 2-step upgrading; it may indicate high dispersion of metallic nickel, whereas the very low diffraction peaks of NiO may indicate oxidation of metallic nickel. The crystallite size of Ni catalyst increased from 3.5 nm to 29.2 nm whereas Ni-Cr increased from 4.4 nm to 61.3 nm after the 1-step reaction and to 7.6 nm after the 2-step upgrading.

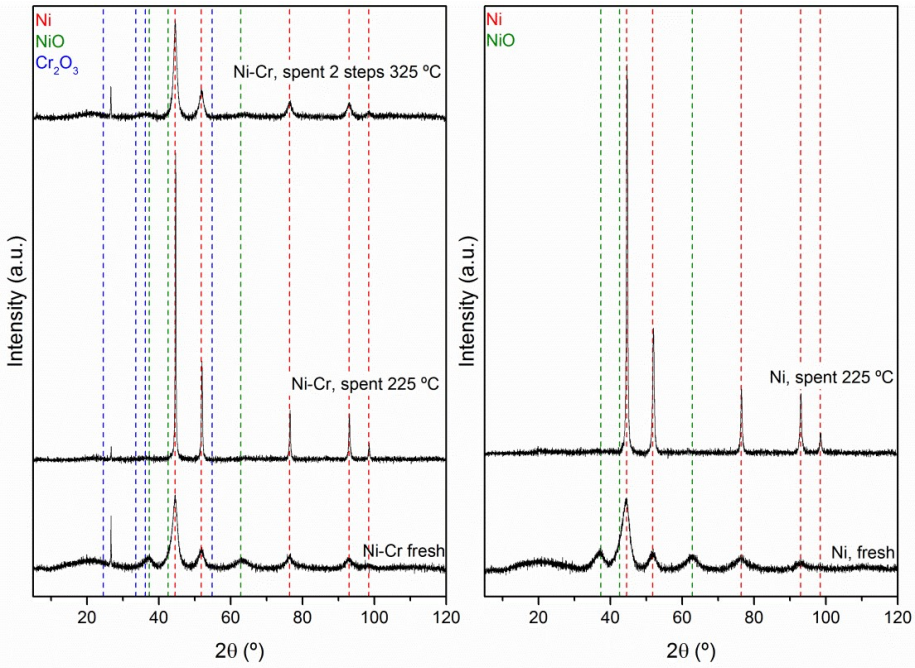

Figure 23. XRD powder diffraction of fresh and spent Ni-based catalysts. Reproduced from reference [117] according to the terms of Creative Commons Attribution License.

In terms of leaching, less than 0.7 wt.% of Ni was leached from both catalysts to the upgraded aqueous phase at 175 °C and 225 °C. The lowest concentration of nickel leached was observed at the second step upgrading, with 0.1 wt.% of Ni leached at 325 °C. It can be attributed to the low concentration of water of UBWBO, and the highest pH in comparison to BWBO. For all reactions, chromium was below the quantification limit of 0.011 wt.% in the upgraded aqueous phase, meaning that the amount of chromium leached was below 0.2 wt.% of the total chromium added to the autoclave.

3.3.3 Correlation of catalytic performance vs. properties of Ni-based catalysts

The highest catalytic activity of Ni-Cr catalyst, especially at 225 °C, may be explained not just by the strongest acid sites observed by NH_3-TPD (considering that the density of acid sites was nearly the same for both catalysts (Table 6), but also in terms of metal oxygen bonding, as suggested by Mortensen et al. [68]. According to the authors, the lower the oxygen-metal bond strength, the higher the hydrogenation activity of oxides due to the facility to generate oxygen vacancy in the support and/or in the promoters. In the current study, the oxygen metal bond strength of the oxides in both Ni-based catalysts formulation decreases in the following order [137]: SiO_2>Al_2O_3>Cr_2O_3. Hence, the lower the oxygen-metal bond strength, the higher the propensity to form strong acid sites and more oxygen vacancies are available therewith increasing not just the hydrogenation activity as reported by the previous authors, but in our case also increasing the hydrodeoxygenation activity. This assumption agrees to the observations for Ni-Cr catalyst, due to the promoter effect of Cr_2O_3.

Additionally the presence of NiO in both Ni-based catalysts also plays a role in the catalytic activity. NiO acts synergistically with Ni catalyst and the support, contributing in higher extent to hydrogenation as well as to hydrodeoxygenation pathways due to oxygen vacancies [138]. However, due to the reductive atmosphere, NiO is reduced to metallic along the hydrotreatment reaction, confirmed by XRD results, and its contribution is reduced as the reaction time increases. The metallic Ni originally in the catalyst composition, as well as formed after NiO reduction, promotes the dissociation of H_2 which will further hydrogenate the molecules adsorbed over the catalyst surface [139]. The highest atomic percentage of metallic nickel available at Ni-Cr catalyst in contrast to Ni catalyst at the reaction conditions may result in higher availability of dissociated H_2, also contributing to the highest hydrogenation activity observed for this catalyst.

Hence, the reaction pathways including hydrogenation and hydrodeoxygenation in both Ni based catalyst involves a complex system, in which support and promoters acid sites and metallic centers act synergistically. The hydrodeoxygenation simplified in Figure 24 is reported to initiate by the adsorption of oxygen containing compounds over the catalyst support surface, while the hydrogen is adsorbed and dissociated over the reduced metal. The adsorption of oxy compounds is facilitated by the oxygen vacancy in the oxide surface and the new oxygen vacancies generated after the elimination of water formed due to the H_2 atmosphere [8,68]. The cleavage of the C-O bond occurs then due to electron donation. The hydrodeoxygenated molecule is desorbed and the active acid site is restored. The differences in selectivity observed are then correlated to the composition of both Ni-based catalysts [8].

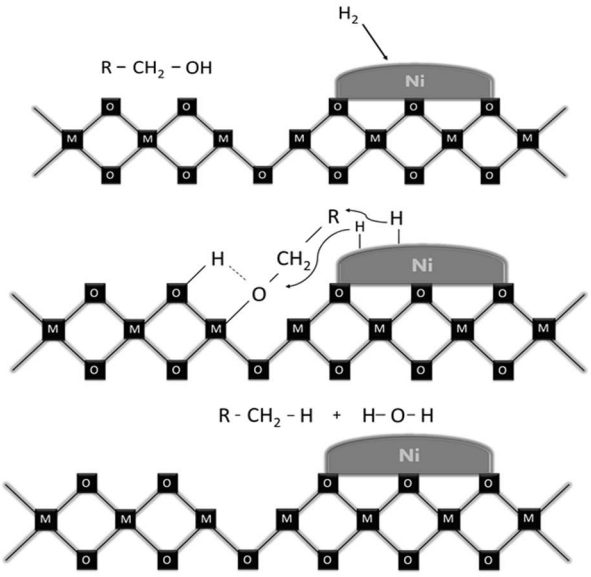

Figure 24. Simplified representation of hydrodeoxygenation over Ni-based catalysts. R-CH_2-OH represents the molecules to be hydrodeoxygenated and M-O represents the support material (SiO_2 and SiO_2-ZrO_2-Al_2O_3), NiO and Cr_2O_3. NiO is completely reduced during the hydrotreatment reaction. The particles size of Cr_2O_3 are smaller compared to metallic nickel (not represented in the Figure) but the mechanism of hydrodeoxygenation is assumed the same as the support material. Reproduced from reference [117] according to the terms of Creative Commons Attribution License.

Other characteristics of the catalysts are also correlated to the catalytic activity. The metallic particle size is considered to play a role during the hydrotreatment, by the cleavage of C-O bonds in the step and corner sites [73] as well as by promoting the hydrogenation pathway [140]. However, the similar particle size for both Ni-based catalysts, leads to the assumption that other parameters such as chemical composition and strength of acid sites contributed to the differences observed in terms of selectivity, H_2 consumption, and other parameters discussed previously.

3.4 Conclusion

The hydrotreatment of a beech wood fast pyrolysis bio-oil applying two Ni-based catalysts with high loading of Ni was evaluated in comparison to Ru/C catalyst. The influence of promoters, temperature and reaction time was correlated with the composition and yields of upgraded products. The evaluation of 2-step upgrading for deep deoxygenation level was also investigated.

The upgraded oil yields achieved at 1-step upgrading were higher with Ni-based catalysts in comparison to Ru/C. The highest upgraded oil yield of 51.5 wt.% with Ni-Cr catalysts contrasted to 34.5 wt.% with Ru/C at 225 °C. The lowest yield in this case correlates to the highest gas production with the noble metal catalyst. Comparable deoxygenation values, carbon and hydrogen content were observed in the upgraded oils with Ni-Cr and Ru/C. However, highest H/C ratios for the oils upgraded with Ni-based catalysts agrees to the highest hydrogenation activity in comparison to Ru/C, especially Ni-Cr at 225 °C. Hence, the increase in the temperature showed a positive effect over 1-step upgraded oil.

Both Ni-based catalysts reduced significantly the concentration of ketones and showed activity towards alcohols formation. The highest conversion of ketones, organic acids and sugars and the highest amount of alcohols in the upgraded liquid products with Ni-Cr in contrast to Ni catalyst is attributed to the difference in formulation as well as to the strength of acid sites promoted by Cr_2O_3.

The influence of reaction time showed that the longer the reaction time is, the higher were the oil yield, solid yield and the hydrogen consumption while the water content is reduced. The chemical composition of upgraded oils in terms of elemental analysis, gas production and gas composition are comparable at 2 and 4 h of reaction.

Particularly interesting is a 2-step upgrading. The upgraded oil after 2-step upgrading showed 90 % less water, 64.8 % less oxygen and a higher heating value 90.1 % higher compared to the original beech wood fast pyrolysis oil. The increase in methane formation in comparison to 1-step reaction may correlate to nearly total conversion of acetic acid, considering that only 3 % remained in the 2-steps

upgraded liquids. On the other hand, the discrepancy of aromatics compounds quantified by ^{1}H-NMR and GC-MS/FID may indicate that polymerization of aromatics took place during the second upgrading step.

The solids formation for 1-step and 2-step reactions was below 1 % and evenly distributed over the catalysts used for 1-step reactions. Carbon and sulfur were observed to be homogeneously distributed over the 2-step spent Ni-Cr catalyst surface.

Thus both high loading Ni-based catalysts produce high yields of upgraded oils with properties comparable to oil upgraded with Ru/C. However, further investigation should address the optimization of 2-step upgrading to reach deeper levels of hydrodeoxygenation while the resistance of both Ni-based catalysts to sulfur poisoning should be investigated, considering especially the influence of Cr_2O_3. For this investigation a continuously operated experimental-setup is proposed.

Chapter 4. Hydrotreatment of Fast Pyrolysis Bio-oil Fractions over Nickel-Based Catalyst

Chapter redrafted after:

Schmitt, C. C., Raffelt, K., Zimina, A., Krause, B., Otto, T., Rapp, M., Grunwaldt, J.D., Dahmen, N. (2018). Hydrotreatment of Fast Pyrolysis Bio-oil Fractions over Nickel-based Catalyst. *Topics in Catalysis*, 61, 1769-1782.

Declaration of contributions:

Caroline Carriel Schmitt performed the experimental design, conducted the hydrotreatment reactions, evaluated the data, discussed the results and wrote the manuscript.

Anna Zimina and Bärbel Krause supported with the X-ray photoelectron spectroscopy measurements and discussion of the results.

Thomas Otto performed the BET surface area measurements.

Michael Rapp supported with the discussion of the results.

Klaus Raffel, Jan-Dierk Grunwaldt and Nicolaus Dahmen supervised the work, contributed to the discussion and corrected the manuscript.

List of abbreviation Chapter 4

BWBO: Beech wood fast pyrolysis bio-oil

DOD: degree of deoxygenation

FPBO: Fast pyrolysis bio-oil

HDO: Hydrodeoxygenation

HP: Heavy Phase

LP: Light Phase

ULP: Upgraded light phase

UO: Upgraded oil

$UO_{FBBO,\ 325\ °C,\ 80\ bar}$: Upgraded complete BWBO at 325°C and 80 bar

$UO_{HP,\ 325\ °C,\ 80\ bar}$: Upgraded isolated HP at 325°C and 80 bar

Abstract Chapter 4

Residual biomass shows potential to be used as a feedstock for fast pyrolysis bio-oil production for energetic and chemical use. Although environmentally advantageous, further catalytic upgrading is required in order to increase the bio-oil stability, by reducing reactive compounds, functional oxygen-containg groups and water content. However, bio-oils may separate in fractions either spontaneously after ageing or by fractionated condensation. Therefore the effects of upgrading on different fast pyrolysis bio-oil (FPBO) fractions obtained from a commercially available FPBO were studied by elemental analysis, GC-MS and ^{1}H-NMR. Not only the FPBO was upgraded by catalytic hydrotreatment as received, but also the heavy phase fraction formed after intentional aging and phase separation. The reactions were conducted between 175 °C - 325 °C and 80 - 100 bar by using a nickel-chromium catalyst in batch experiments. The influence of the hydrotreatment conditions correlated with the composition of the upgraded products. Higher oxygen removal was obtained at higher temperatures, whereas higher pressures resulted in higher hydrogen consumption with no significant influence on deoxygenation. At 325 °C and 80 bar 42 % of the oxygen content was removed from the FPBO. Compounds attributed to pyrolysis oil instability, such as ketones and furfural were completely converted while the number of alcohols detected in the upgraded products increased. Coke formation was observed after all reactions, especially for the reaction with the fraction rich in lignin derivatives, likely formed by polymerization of phenolic compounds mainly concentrated in this phase. Independently of the feedstock used, the upgraded bio-oils were very similar in composition, with reduced oxygen and water content, higher energy density and higher carbon content.

4.1 Introduction

Accordingly to the introduction given in Chapter 1 FPBO is a complex mixture of more than 300 mostly oxygenated compounds with different functional groups, such as carboxylic acids, aldehydes, furfurals, alcohols, carbohydrates, and ketones including high amounts of water. In addition, various lignin derivative compounds i.e. phenol and guaiacol are present, limiting its direct application as fossil fuel replacement [65,93,141]. The amount of these compounds is dependent on various parameters, in particular, the selected biomass as well as its moisture content. Reactor design, residence time, mixing behavior and heat transfer rates as well as condensation temperature also play a significant role in the product yield and composition, which can result in single-phase or multiphase pyrolysis condensates [11].

If separation in two phases occurs, a water rich phase consisting mostly of polar compounds such as organic acids, alcohols, aldehydes, ketones and sugar derivatives and a more dense organic phase with mostly high molecular compounds, such as phenolic, lignin-derived compounds are formed [11]. Also inorganic, hetero-atom containing compounds may be present in the pyrolysis condensates.

The present work investigates the catalytic hydrotreatment of a FPBO and its fractions obtained by separation in two phases (light and heavy phase) after storage at elevated temperatures, considering that the long term storage or aging of bio-oils can result in natural separation in two phases. Therefore, the upgrading of the heavier fraction, rich in lignin derivative compounds was particularly investigated. Using nickel-chromium based catalyst we report on the influence of temperature and pressure on the HDO activity.

4.2 Materials and methods

4.2.1 Feedstock: Fast pyrolysis bio-oil and phase rich in lignin derivatives

The same intentionally aged (24 h, 80 °C) BWBO used in Chapter 3 was used in this study. The BWBO is spontaneously separated in two phases after storage. The oil was composed by 59 wt.% of light phase (LP) and 41 wt.% of heavy phase (HP). Table 8 shows an overview of the main compounds in both fractions, obtained by solvent extraction [115]. While the LP concentrates most of the organic compounds rich in oxygen and water, the HP contains most of the lignin depolymerization products with lower oxygen content.

Table 8. Distribution of the main compounds in the pyrolysis-oil fractions by solvent extraction [115]. Reproduced from ref [116] according to the terms of Creative Commons Attribution License (CC BY).

Compounds	LP (wt.%)	HP (wt.%)
Water	35.30	14.50
Solid	n.d.	0.79
Extractives	0.10	9.99
Aldehydes, ketones, furan, lignin monomers and volatile acids	30.71	1.72
Sugars, hydroxyacids	24.94	26.09
Aging products, low molecular weight lignin	4.24	35.30
Aging Products, high molecular weight lignin	3.15	11.05
Ethylenglycol	1.67	0.76

4.2.2 Catalyst

Based on the previous results observed in Chapter 3, the Ni-Cr catalyst was selected for this study. The catalyst is composed of Ni (30 wt.%), NiO (26 wt.%) and Cr_2O_3 (15 wt.%), graphite (1.5 wt.%) in diatomaceous earth support (27 wt.%).

4.2.3 Hydrotreatment Setup

The reactions were performed in the same 200 ml autoclave described in Chapter 3. The autoclave was in-house designed and built for temperatures of up to 400 °C and pressure up to 360 bar. In order to promote a better transfer of hydrogen into the bio-oil, avoiding mass transfer limitation, the autoclave was equipped with a gas injection stirrer.

The experiments were performed at two different pressures (80 and 100 bar, set at room temperature), four different temperatures (175 °C, 225 °C, 275 °C and 325 °C) and two feedstocks: the original FPBO as well was as the heavy phase (HP). All the experiments were performed twice. Approximately 2.5 g of catalyst and 50 g of feedstock were added into the autoclave. For the

experiments using FPBO, 20.5 g of HP and 29.5 g of LP were weighted (after phase separation, the phases were stored separately), according to the composition given in section 4.2.1. The autoclave was closed, purged with nitrogen for five minutes for air removal and then pressurized with hydrogen. The autoclave was heated to the reaction temperature with a heating ramp of 5 °C/min. The reaction duration was 2 h. After the reaction, the autoclave was cooled down to approximately 40 °C using a pressurized air flow and then cooled down to approximately 20 °C using an ice bath. The gas sample was collected for further chemical analysis. The remaining mixture of upgraded liquid products, composed of upgraded light phase (ULP), upgraded oil phase (UO), solids and spent catalysts was collected, centrifuged (7000 rpm, 40 min, Thermo Scientific Heraeus Biofuge Stratos), separated and weighted . The spent catalyst was vacuum filtrated and washed with acetone several times, in order to remove any bio-oil residue.

The pressure was recorded before and after the reaction. The hydrogen consumed during the hydrotreatment was determined by using the ideal gas law, considering the amount of hydrogen before and after the reaction (determined by gas chromatography, section 4.2.4) at room temperature [70,142].

4.2.4 Characterization techniques: feedstock, upgraded products and catalyst.

The FPBO fractions (LP and HP) and upgraded products, upgraded light phase (ULP) and upgraded oil (UO) were characterized using the same analytical techniques. The elemental composition, hydrogen, carbon and nitrogen, was obtained by CHN 628 Leco. The oxygen was obtained by the difference. The high heating value (HHV) was obtained by Channiwala's equation [143]:

$$HHV\ (MJ/Kg) = 0.3491C + 1.1783H - 0.1034O - 0.0151N + 0.1005S - 0.0211\ ash \quad (1)$$

Titration using the Karl Fischer Tritando 841, Metrohm was employed for water content determination; pH and density were obtained using a pH-meter 691, Metrohm and densimeter Anton Paar DMA4500M, respectively. Sulfur content and leached metals (upgraded products) were measured with an Inductively Coupled Plasma Optical Emission Spectrometer (ICP-OES, Agilent, 725).

Selected samples were analyzed using a gas chromatography–mass spectrometer (GC-MS HP G1800A) aiming a qualitative investigation of the main compounds in pre-selected samples. The GC-MS was equipped with a Restek stabilwax column (30 m x 0.25 mm x 0.25 μm) and the identification of the compounds was obtained matching the mass spectra with the NIST 2005 library. The sample was diluted 1:20 in methanol, filtrated (0.25 μm filter), injected (1 μl, split 1:20) at 250 °C (injector temperature) and measured using the temperature program starting at 40 °C (kept for 5 minutes), heated to 250 °C at 8 °C/min, (kept 10 minutes at this temperature).

The distribution of functional groups was measured by proton nuclear magnetic resonance (^{1}H-NMR). The samples were measured in a Bruker Biospin spectrometer composed by a 5.45 T magnet, 250 MHz frequency, pulse of 90°, 10.0633 s of acquisition time: 1.0 s of relaxation delay, 24 scans and 3255.2 Hz of spectral width and time domain of 32 k. The solutions were prepared diluting approximately 0.1 g of sample in deuterated methanol (about 800 µl) containing 2 g/l of internal standard (sodium 3-trimethylsilyl-2-2',3,3'-tetradeuteropropionate). The spectra were integrated in pre-defined regions in order to calculate the millimoles of protons with respect to the internal standard. The software MestReNova was used for spectrum processing.

The gaseous products were quantified using a gas chromatograph Agilent 7890A equipped with two detectors – flame ionization detector (FID) and thermal conductivity detector (TCD) – and two columns – Restek Molsieve 5A and Restek 57096 Hayesep Q. The sample (100 µl, split 28:1) was injected at 250 °C (injector temperature) and measured using the temperature program starting at 50 °C kept for 10 min, heated to 90 °C at 3 °C/min, 20 °C/min to 150 °C, kept for 16 mins, heated to 230 °C/min at 50 °C/min and kept at this temperature for 10 min.

The catalyst used in this study was characterized before and after the hydrotreatment reactions. Metals and sulfur content were obtained by inductively coupled plasma optical emission spectrometry (ICP-OES). The catalyst was digested in a microwave oven for 45 minutes in a mixture of 0.5 ml of hydrogen peroxide (H_2O_2), 2 ml of hydrochloric acid (HCl) and 6 ml of nitric acid (HNO_3) prior the measurement. The X-ray diffraction spectra and the average crystallite size were obtained by the XRD (X'Pert PRO MPD PANalytical diffractometer, copper anode Cu Kα 1.54060 Å). The sample was measured in a 2θ range between 5° and 120° for 60 min and 0.017° step size. The crystalline size was obtained using the Scherrer equation (k factor=0.9). The data were analyzed using the software X'PertHighscore Plus.

The specific surface area was determined by BET method (Belsorp Mini II), recording the nitrogen isotherm at 77 K. Fresh and spent catalysts were analyzed.

The carbon deposition over the spent catalysts was obtained by thermogravimetric analysis (Netzsch STA 409). The catalyst samples were heated in air (70 mL/min) from 20 °C to 105 °C at 10 °C/min and kept for an hour (moisture determination); heated then to 1100 °C at 10 °C/min and finally kept at this temperature for 30 minutes [144]. The results of mass loss (discounting the mass loss attributed to moisture), were used to determine the amount of solids produced during the reactions.

The surface analysis of the fresh and spent catalysts was performed using a Scanning electron microscopy (SEM) (GeminiSEM 500, Zeiss; software: SmartSEM Version 6.01) with a thermal Schottky

field emitter cathode. For the quantitative analysis of micro areas and the distribution of the elements, an energy dispersive X-ray spectrometer X-MaxN from Oxford with a silicon drift detector (80 mm^2 and resolution of 127 eV) was employed (software: Aztec 3.3).

Furthermore the surfaces of the catalysts were analyzed by x-ray photoelectron spectroscopy (XPS). A layer of catalyst powder was uniformly distributed in a carbon tape and fixed in a molybdenum sample holder. The measurements were performed in an ultra-high vacuum chamber (base pressure 10^{-8} Pa) equipped with an unmonochromated XR-50 Mg K alpha X-ray source and a Phoibos 150 analyzer (manufacturer SPECS). The angle between the analyzer and the X-ray source was 45°. The electrons originating from a samples were detected along the surface normal of the sample (sample area: 2 mm diameter); the energy scale was calibrated using the Ag 3d peak of a silver reference sample. Peak shifts due to charging effects were compensated using the flood gun FG 15/40 (SPECS). The chemical composition was quantified with the software CasaXPS [145], using the integrated database for sensitivity factors. For the quantification, a Shirley background was subtracted from the peaks Ni 2p 3/2, Cr 2p, and C1s. For O 1s, Si 2s, and Al 2s a linear background was assumed.

4.3 Results

4.3.1 Hydrotreated products distribution

The products distribution for each condition tested is summarized in Table 9. Mainly two product phases are obtained, i.e. the upgraded light phase (ULP) and the upgraded oil phase (UO). Gas and solid phase were present in lower concentrations. Comparing firstly the reaction performed at 175 °C, 225 °C and 275 °C with FPBO, the oil yield slightly increased with the increase of temperature for reactions performed at 80 bars whereas a small reduction in the oil yield was observed at 100 bars. In general, for these conditions the oil yield amounted to 39.3-43.7 wt.% with higher UO yields at 275 °C and 80 bar (43.7 wt.%) and lower water concentration (Table 10).

The products obtained using the isolated heavy phase (HP) showed the opposite behavior: the higher the temperature, the lower the UO yield. Among the reactions performed at 175 °C, 225 °C and 275 °C, the lower yields of UO were observed for the reactions performed at 275 °C and 80 bar (65.5 wt.%) resulting also in an UO with the lower water concentration (7.2 wt.%) compared to the reactions performed at 275 °C, 100 bar (7.5 wt.%).

The following reaction performed at 325 °C, 80 bar for FPBO feedstocks showed UO yields (43.6 wt.%) comparable to the results with 275 °C, 80 bar (43.7 wt.%). At the same time, the upgrading at this condition resulted in an UO with the lowest water content observed for this feedstock (6.5 wt.%). The upgrading of the HP at this conditions also resulted in an UO with the lowest water

concentration for this feedstock and the lowest UO yield (63.10 wt.%), which can also be attributed to the lowest water content.

Regarding the gas production, an increase in the gas yield was observed with the temperature. For reactions performed at 325 °C and 80 bar, the gas production was approximately ten times higher than the gas yield at 175 °C, for both feedstocks. The gas composition is further discussed in the section 4.3.2.

For all of the reactions performed, the solid concentration ranged between 0.44 wt.% and 1.28 wt.%. Although a small amount of solid products was observed, the higher yields were obtained for the reactions using the isolated HP. This can be related to the fact that higher concentration of oligomeric phenolic compounds in the HP might lead to a higher amount of polymerization products, resulting in higher amount of coke formation [60,88,91]. In general the losses obtained during the reaction were below 12 wt.% and are mainly due to upgraded products which could not be completely recovered from the reactor walls.

Table 9. Hydrotreated products distribution for both feedstocks (FPBO and HP) and different reaction conditions. Reproduced from ref [116] according to the terms of Creative Commons Attribution License (CC BY).

Reaction conditions	**Feed: FPBO**					**Feed: HP**				
	ULP* (wt.%)	UO** (wt.%)	Gas (wt.%)	Solid (wt.%)	Loss (wt.%)	ULP* (wt.%)	UO** (wt.%)	Gas (wt.%)	Solid (wt.%)	Loss (wt.%)
175 °C, 80 bar	50.33 ±1.83	40.60 ±0.42	0.72 ±0.014	0.51 ±0.02	7.84 ±2.29	14.93 ±0.19	74.89 ±1.25	0.63 ±0.03	1.18 ±0.02	8.35 ±1.31
225 °C, 80 bar	50.75 ±0.35	40.77 ±0.18	1.14 ±0.13	0.48 ±0.03	6.86 ±0.69	18.84 ±0.08	70.52 ±0.74	0.99 ±0.13	1.19 ±0.01	8.36 ±0.52
275 °C, 80 bar	48.63 ±0.38	43.74 ±0.36	2.44 ±0.15	0.57 ±0.10	4.63 ±0.99	20.44 ±0.65	65.49 ±0.44	1.16 ±0.19	1.05 ±0.07	11.86 ±1.35
325 °C, 80 bar	43.19 ±1.27	43.61 ±0.53	7.10 ±0.01	0.44 ±0.01	5.65 ±0.71	20.45 ±1.78	63.10 ±1.27	6.93 ±0.23	1.28 ±0.12	8.25 ±3.40
175 °C, 100 bar	48.10 ±0.42	42.42 ±0.81	0.65 ±0.08	0.97 ±0.17	7.85 ±1.32	15.50 ±2.12	72.33 ±3.16	0.50 ±0.11	1.27 ±0.18	10.40 ±5.56
225 °C, 100 bar	52.54 ±0.33	40.12 ±0.88	0.78 ±0.03	0.56 ±0.09	6.0 ±1.29	21.26 ±0.37	72.23 ±3.15	0.64 ±0.08	0.66 ±0.04	5.21 ±2.74
275 °C, 100 bar	47.61 ±0.29	39.30 ±1.12	2.86 ±0.05	0.65 ±0.07	9.58 ±0.95	21.92 ±2.71	68.13 ±0.18	2.90 ±0.27	0.79 ±0.13	6.27 2.76

*ULP: Upgraded light phase

**UO: Upgraded oil

4.3.2 Upgraded products

The upgraded liquid products were analyzed in detail. The elemental composition of the products (dry basis) obtained for both feedstocks are summarized in Table 10 and Table 11. The concentration of carbon in the UOs increased according to the upgrading temperature whereas the oxygen content decreased.

Firstly, the hydrotreatment reactions of both feedstocks were evaluated at 175 °C, 225 °C and 275 °C at 80 and 100 bar. At these conditions the carbon was mainly concentrated in the UO for both feedstocks (63.13-68.69 wt.%), resulting in an increase in the energy density in the upgraded products (28.06-32.37 MJ/Kg) in comparison to the feedstocks (FPBO=24.33 MJ/Kg and HP=27.23 MJ/Kg). The hydrogen consumption varied from 205 NL/Kg of feed at 175 °C at 80 bar to 365 NL/Kg of feed at 275 °C, 100 bar.

Although higher hydrogen consumption was observed for the reactions performed at 100 bars in comparison to the reactions performed at 80 bars for the same temperature, no significant effect of pressure on the hydrodeoxygenation was observed for both feedstocks. For example, the degree of deoxygenation (DOD) obtained at 275 °C, 80 bars for the upgrading of FPBO was 40.7 % while at 100 bar the DOD obtained was 38.0 %. Consequently, we consider that the temperature exhibits a higher influence on the hydrodeoxygenation degree.

Table 10. Characterization of the elemental composition of the products after hydrotreatment over different conditions upon applying the fast pyrolysis bio-oil (FPBO). Reproduced from ref [116] according to the terms of Creative Commons Attribution License (CC BY).

Reaction conditions		**C (wt.%)**	**H (wt.%)**	**O (wt.%)**	**N*** **(wt.%)**	**HHV (MJ/Kg)**	**H_2O (wt.%)**	**H_2 consumption (NL/kg of feed)**	**DOD** (%)**
Feed	LP	53.25 ±0.11	6.77 ±0.01	39.96 ±0.11	<0.2	22.44 ±0.05	35.30 ±0.28	-	-
	HP	63.68 ±0.41	6.89 ±0.17	29.24 ±0.58	<0.2	27.31 ±0.40	14.55 ±0.07	-	-
175 °C, 80 bar	ULP	49.55 ±0.25	8.17 ±0.14	42.27 ±0.11	<1.0	22.55 ±0.06	43.5 ±0.28	205.51 ±4.05	25.36 ±0.43
	UO	65.43 ±0.11	7.67 ±0.06	26.75 ±0.16	<0.3	29.13 ±0.08	10.9 ±0.28		
225 °C, 80 bar	ULP	49.56 ±0.40	8.47 ±0.50	41.94 ±0.37	<1.0	22.94 ±0.84	48.45 ±0.18	261.97 ±1.35	27.20 ±3.25
	UO	65.97 ±0.62	7.80 ±0.05	26.09 ±0.58	<1.0	29.54 ±0.33	10.50 ±0.28		
275 °C, 80 bar	ULP	50.83 ±0.08	9.19 ±0.01	39.24 ±0.10	<0.3	24.51 ±0.04	57.7 ±0.07	288.41 ±2.97	40.74 ±0.23
	UO	69.76 ±0.10	8.67 ±0.04	21.24 ±0.05	<0.3	32.37 ±0.10	9.4 ±0.01		
325 °C, 80 bar	ULP	50.58 ±0.58	8.09 ±0.82	40.2 ±0.97	<0.3	23.01 ±0.85	72.8 ±2.69	286.48 ±10.75	42.05 ±0.99

	UO	70.43 ±0.42	8.48 ±0.07	20.77 0.35	<0.3	32.42 ±0.10	6.5 ±0.14		
175 °C, 100 bar	ULP	49.80 ±0.16	7.90 ±0.25	42.28 ±0.07	<0.3	22.32 ±0.25	43.5 ±0.28	210.76 ±10.73	19.95 ±7.44
	UO	63.13 ±3.13	7.58 ±0.37	28.69 ±2.67	<0.3	28.06 ±1.72	13.2 ±2.97		
225 °C, 100 bar	ULP	49.82 ±0.05	8.70 ±0.18	41.37 ±0.31	<0.3	23.37 ±0.27	48.1 ±0.14	286.6 ±10.12	32.39 ±1.0
	UO	66.76 ±0.01	8.45 ±0.13	24.23 ±0.18	<0.3	30.79 ±0.17	11.25 ±0.25		
275 °C, 100 bar	ULP	51.15 ±0.55	9.55 ±0.20	38.50 ±0.37	<0.3	25.15 ±0.01	60.9 ±0.28	365.51 ±4.72	38.06 ±0.60
	UO	68.69 ±0.21	8.78 ±0.01	22.20 ±0.21	<0.3	32.03 ±0.10	9.3 ±0.07		

*Variation in the limit of detection due to the calibration of the equipment

**Calculated on dry basis as follow: DOD (%) = (1- $O_{upgraded\ oil}/O_{feed}$).100

Hence, additional reactions were performed at 325 °C and 80 bars. At this condition the carbon content in the UOs increased ($UO_{FPBO,\ 325\ °C\ ,\ 80\ bar}$=70.4 wt.%; $UO_{HP,\ 325\ °C,\ 80\ bar}$ =71.6 wt.%) in comparison to the other conditions tested. Furthermore the DOD was also higher compared to the reactions performed previously. For the FPBO a reduction of 42.05 % in the oxygen content was observed while for the HP the DOD achieved was 32.0 % (Table 11).

Comparing the results of the experiments at 325 °C, 80 bar and 275 °C, 100 bars confirms that a temperature increase of 50 °C has more beneficial effects than a pressure increase of 20 bars: At 325 °C, 80 bar DOD, the H content of UO and the H/C ratio of UO is higher, whereas 22 – 28 % less H_2 is consumed compared to the reaction at 275 °C, 100 bar.

The pH of the upgraded products remains very similar in the feeds while the density decreased in comparison to the feedstocks (pH_{HP}= 3.1 ρ_{HP}=1.19 g/cm^3; pH_{LP}= 2.8 ρ_{LP}=1.18 g/cm^3). For the upgrading at 325 °C, 80 bar FPBO the upgraded oil showed a pH_{UO}=3.2 and ρ_{UO}=1.08 g/cm^3 and the ULP showed pH_{ULP}= 3.2 ρ_{ULP}=1.02 g/cm^3. The upgraded products of the reaction with HP showed pH_{UO}=3.7 ρ_{UO}=1.09 g/cm^3 and pH_{ULP}= 3.4 ρ_{ULP}=1.02 g/cm^3 respectively.

For all evaluated conditions, the water content in the UOs dropped with higher temperature, while it increased in the light phases considerably (41.5-80.1 wt.%). Furthermore, for all the upgraded products, including ULP and UO, the nitrogen content was below 1 wt.% and therefore no significant changes could be detected.

Table 11. Characterization of the elemental composition of the products after hydrotreatment over different conditions upon applying the phase rich in lignin derivatives (HP). Reproduced from ref [116] according to the terms of Creative Commons Attribution License (CC BY).

		C (wt.%)	H (wt.%)	O (wt.%)	N* (wt.%)	HHV (MJ/Kg)	H_2O (wt.%)	H_2 consumption (NL/kg of feed)	DOD** (%)
Feed:	HP	63.51	6.89	29.59	<0.2	27.23	14.5	-	-
175 °C, 80 bar	ULP	49.31 ±0.10	8.15 ±0.01	42.54 ±0.08	<1.0	22.42 ±0.04	42.20 ±0.11	196.65 ±2.20	11.76 ±0.10
	UO	66.33 ±0.05	7.56 ±0.10	26.11 ±0.03	<1.0	29.36 ±0.08	9.70 ±0.07		
225 °C, 80 bar	ULP	49.41 ±0.10	7.96 ±0.07	42.62 ±0.01	<0.3	22.23 ±0.06	65.20 ±0.11	247.01 ±2.3	16.80 ±0.16
	UO	67.25 ±0.16	8.13 ±0.01	24.62 ±0.20	<0.3	30.51 ±0.10	9.0 ±0.01		
275 °C, 80 bar	ULP	49.54 ±0.62	7.73 ±0.89	42.72 ±0.26	<0.3	22.00 ±0.86	67.1 ±0.42	295.55 ±5.86	23.89 ±0.10
	UO	69.40 ±0.10	8.08 ±0.04	22.52 0.05	<0.3	31.42 ±0.01	7.20 ±0.04		
325 °C, 80 bar	ULP	48.37 ±0.90	7.30 ±1.80	44.32 ±2.70	<0.3	22.84 ±2.72	80.1 ±0.21	282.06 ±19.69	32.00 ±0.52
	UO	71.64 ±0.60	8.24 ±0.01	20.12 ±0.16	<0.3	32.64 ±0.06	5.50 ±0.21		
175 °C, 100 bar	ULP	49.06 ±0.24	8.02 ±0.11	42.92 ±0.12	<0.3	22.13 ±0.06	41.50 ±0.14	203.81 ±2.21	10.44 ±0.24
	UO	65.54 ±0.03	7.96 ±0.04	26.50 ±0.10	<0.3	29.52 ±0.10	10.90 ±0.05		
225 °C, 100 bar	ULP	49.7 ±0.23	8.90 ±0.04	41.4 ±0.19	<0.3	23.56 ±0.05	49.7 ±0.95	277.98 ±35.82	19.26 ±2.29
	UO	67.88 ±0.31	8.23 ±0.04	23.89 ±0.34	<0.3	30.92 ±0.08	9.40 ±0.11		
275 °C, 100 bar	ULP	50.79 ±0.30	8.54 ±0.13	40.67 ±0.16	<0.3	23.58 ±0.04	68.5 ±0.18	344.87 ±10.63	26.09 ±0.33
	UO	69.73 ±0.10	8.40 ±0.04	21.87 ±0.05	<0.3	31.97 ±0.30	7.50 ±0.10		

*Variation in the limit of detection due to the calibration of the equipment.
**Calculated on dry basis as presented in Table 10.

The changes in the distribution of functional groups as a function of the upgrading reaction conditions were determined by ^{1}H-NMR. For comparison purposes, the ULP will be related to the initial LP whereas the UO will be compared to the initial HP. The same tendencies were observed for the reactions performed at 80 and 100 bar; hence, the results obtained at 100 bar are only reported in the supplementary material (Figure S.10).

The integration regions for the upgraded oils (Figure 25 a and b) show that the concentration of protons belonging to the alkane region (0.5-1.5 ppm) increased significantly in the UOs (16.78-22.68 mmol/g sample) compared to the initial concentration of the HP (8.25 mmol/g sample), as well as the proton concentration in the region of α proton to carboxylic acid or keto-group, α proton to unsaturated group ($feed_{HP}$= 17.81 mmol/g sample; products= 18.23 to 32.54 mmol/g sample).

The concentration of protons in the alcohols, ethers and dibenzenes (3.0-4.3 ppm) regions increase with the temperature up to 225 °C. For the reactions performed at higher temperatures (275 °C and 325 °C) the concentration of protons then decreased (11.76-8.63 mmol/g sample) for values below the feed (HP= 13.17 mmol/g sample). The decrease in the concentration of protons at higher temperatures can be attributed to the fact that compounds such as alcohols, ethers and dibenzenes tend to react at approximately 250-300 °C, as also reviewed by Elliot [61].

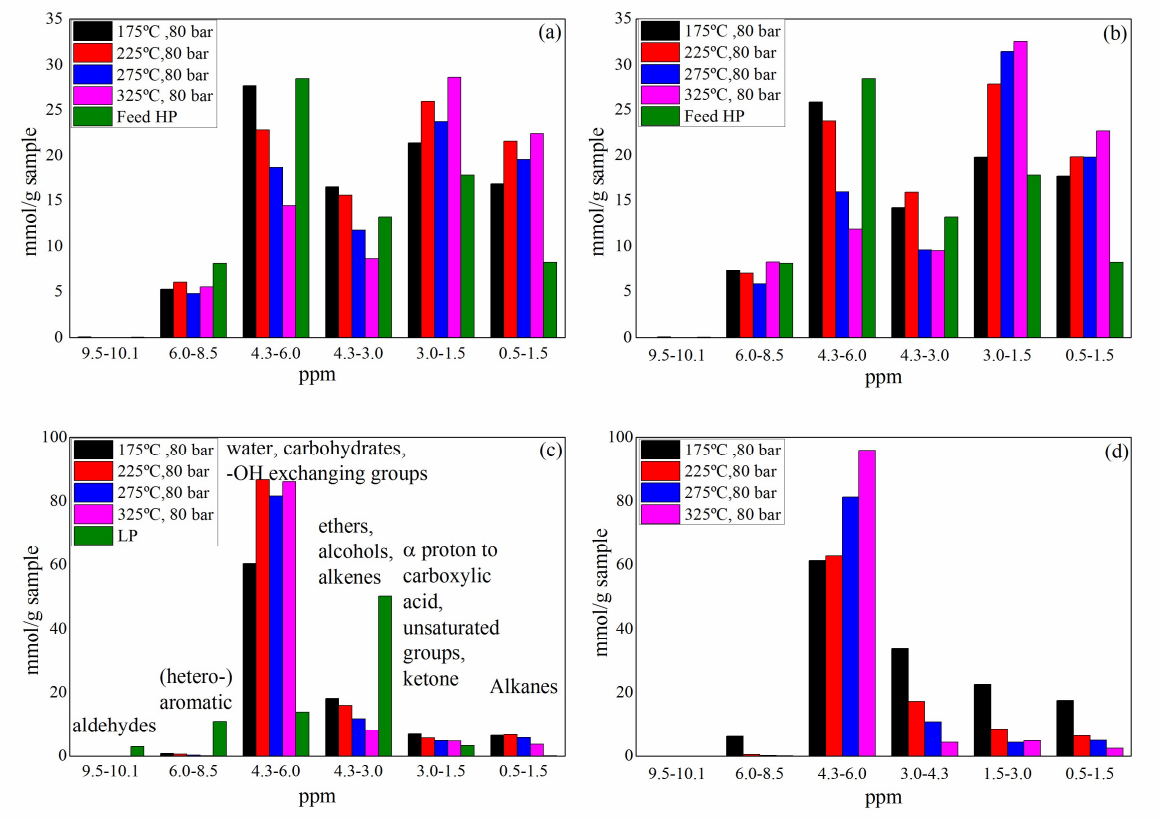

Figure 25. ^{1}H-NMR spectra integration of the upgraded products at different temperatures and 80 bar. a) UO, Feed: FPBO; b) UO, Feed: HP; c) ULP, Feed: FPBO; d) ULP, Feed: HP. Reproduced from reference [116] according to the terms of Creative Commons Attribution License.

The concentration of protons belonging to the carbohydrates, water and O-H exchanging groups (4.3-6.0 ppm) showed a considerable reduction compared to the feed (HP). A clear tendency is observed with the increase of the temperature: the higher the temperature, the lower the concentration of protons in this region. Such a tendency can be explained considering that at higher temperatures the water content in the upgraded oil is reduced; in addition, conversion of sugars molecules during the hydrotreatment could also contribute to the reduction of protons in this region [99,146]. A reduction of protons in the region of (hetero)-aromatics was observed for all upgraded oils in comparison to the feed, although the concentration in the UO was similar for all the conditions tested. The only exception was observed to the oil upgraded at 325 °C, 80 bar, feed: HP, which showed the higher concentration of protons in this region (8.29 mmol/g sample), with a slightly higher concentration. Protons attributed to aldehydes (9.5-10.1 ppm) were present in very small amount in

the feed and were not observed in the products; These reactive compounds usually react at mild temperatures and can be reduced completely by hydrogen [61,147].

The integration regions for the upgraded light phases (Figure 25 c and d) show that the concentration of protons belonging to the alkane region (0.5-1.5 ppm) increased in the ULPs in comparison to the LP (0.056 mmol/g sample), especially in reactions performed at lower temperatures. At 325 °C, the concentration of protons is the lowest compared to all the conditions evaluated, which could indicate migration of these compounds to the upgraded oil. The protons concentration in the region between 1.5-3.0 ppm has also increased in comparison to the original LP (3.26 mmol/g sample).

The concentration of protons in the range of 3.0-4.3 (alcohols, ethers and dibenzenes) reduced significantly in comparison to the feed (LP=50.25 mmol/g sample), especially for the reactions performed at 325 °C, 80 bar (FPBO= 8.26 mmol/g ULP). It can be assumed that there is a tendency of alcohols, ether and dibenzenes of being converted at higher temperatures.

The protons in the range of 4.3-6.0 ppm increased considerably in the ULPs in comparison to the LP of the feed (13.88 mmol/ g sample). Furthermore the highest concentrations were observed for the reactions performed at more severe conditions (325 °C, 80 bars). This could be explained considering that the water removed from the upgraded product is concentrated in the ULPs; the higher the temperature the lower the water concentration in the upgraded oil and consequently the higher the water concentration in the upgraded light phase. For example, this assumption is in agreement with the results observed to the reactions applying the heavy phase at 325 °C and 80 bar: the highest water concentration was observed in the ULPs at this condition (80.1 wt.%), in agreement with the highest concentration of protons (95.91 mmol/g ULP) among all the ULPs evaluated.

The protons in the (hetero)-aromatic range also decreased considerably in the upgraded products while aldehydes, initially present in the LP, were not observed in the ULPs.

In order to identify the main compounds obtained at different reaction conditions, as well as to compare the feedstock and upgraded products, a qualitative investigation by GC-MS was performed. The main compounds in selected samples are depicted in Figure 26 and correlated with the retention time given in the Table 12. More detailed information, including the chromatograms for all the conditions tested is available in the supplementary material (Figure S.6, S.7, S.8 and S.9).

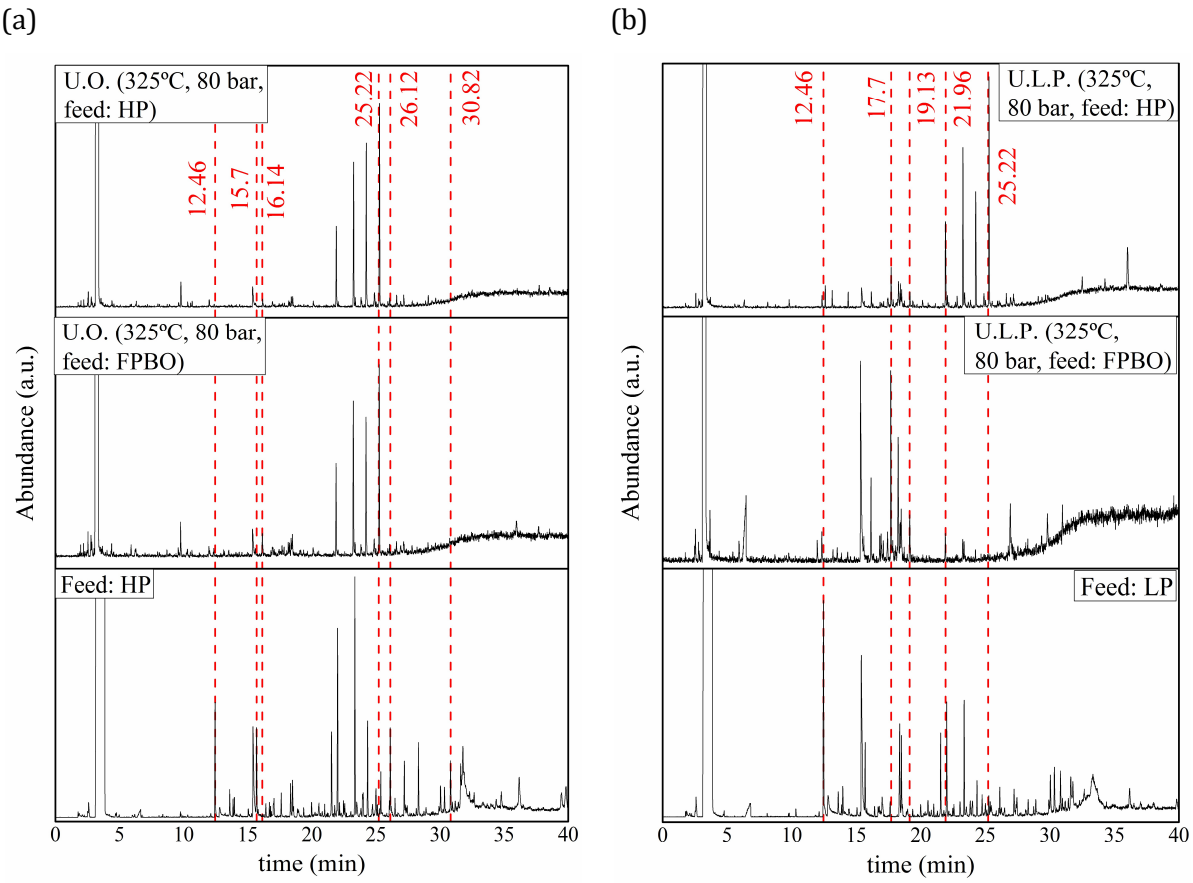

Figure 26. Chromatograms obtained for upgraded oils (a) and upgraded light phases (b) in comparison to the feeds (LP and HP). Reproduced from reference [116] according to the terms of Creative Commons Attribution License.

Some relevant peaks were identified and correlated with the data given in Table 12. Furthermore the main reaction pathways identified are available in the Figure S.13. The appearance of alcohols in cyclic structure in the UOs as well as in the ULPs, such as cyclopentanol, 2-methyl-cyclopentanol, and cyclohexanol is observed in the upgraded product while ketones (1-hydroxy-2-propanone; 2-cyclopenten-1-one; 2-methyl-2-cyclopenten-1-one), initially present in the feeds, are not observed in any of the upgraded products. This indicates that keto groups reacted mainly by hydrogenation of the carbonyl groups producing alcohols [65]. Furfural was converted for all of the reaction conditions tested. The presence of tetrahydrofurfuryl alcohol (RT:16.14 min) in the UOs and ULPs, observed for the reactions performed at T> 175 °C, indicates that furfural was hydrogenated to tetrahydrofurfuryl alcohol [65,148]. This selectivity was previously observed by Boscagli et al. [99] for a Ru/C catalyst while for a bimetallic nickel catalyst ($NiCu/Al_2O_3$) the ring opening seems to be more favorable. Further investigations are presently undertaken to investigate whether this significant difference in selectivity may be the results of chromium in the catalyst.

Table 12. Retention time of the main compounds identified by GC-MS. Reproduced from ref [116] according to the terms of Creative Commons Attribution License (CC BY).

Retention time (min)	Compound	Retention time (min)	Compound
6.61	water	**21.54**	2-hydroxy-3-methyl-2-cyclopenten-1-one
9.8	2-methyl-cyclopentanone	**21.96**	2-methoxy-phenol
12.36	cyclopentanol	**22.68**	1,4-butanediol
12.46	1-hydroxy-2-propanone	**23.20**	2-methoxy-5-methylphenol
12.6	2-methyl-cyclopentanol	**23.24**	1,4-dimethoxy-benzene
13.6	2-cyclopenten-1-one	**23.36**	2-methoxy-4-methyl-phenol
13.85	2-methyl-2-cyclopenten-1-one	**24.01**	phenol
13.96	3-butene-1,2-diol	**24.32**	4-ethyl-2-methoxy-phenol
14.38	cyclohexanol	**25.0**	4-methyl-phenol
15.36	acetic acid	**25.22**	2-methoxy-4-propyl-phenol
15.7	furfural	**26.12**	eugenol
16.14	tetrahydro-2-furanmethanol	**27.23**	2-methoxy-4-(1-propenyl)-phenol
16.82	2,3-butanediol	**28.32**	2-methoxy-4-(1-propenyl)-phenol
17.7	propylene glycol	**30.04**	5-(hydroxymethyl)-2-furancarboxaldehyde
18.30	1,2-ethanediol	**30.82**	vanillin
18.46	1,2-ethanediol, monoacetate	**31.62**	1-(3-hydroxy-4-methoxyphenyl)-ethanone
19.13	1,2-butanediol		

Propylene glycol was present in the upgraded products, especially in the ULPs. Most likely hydroxypropanone (RT: 12.46 min), detected in the feeds but not in the upgraded products, was hydrogenated to propylene glycol. Furthermore, the increase in the propylene glycol, and other diols such as 1,2-butanediol (Figure S.6 and S.7) can be associated to the sugar molecules of the feedstock; the hydrogenation of xylose and glucose leads to the formation of xylitol and sorbitol which can undergo further hydrogenolysis resulting in the alcohols such as propylene glycol, 1,2-ethanediol and 1,2-butanediol [146], present in the ULPs.

Aromatic compounds such as 2-methoxyphenol (guaiacol) and 2-methoxy-4-ethylphenol (4 ethylguaiacol) were identified in the products as well as in the feed. Molecules with higher retention time, such as eugenol, vanillin and isoeugenol were not identified in the products. Vanillin, derived of the guayacyl units in the polymeric lignin structure [76] and observed in the feed, was completely converted after the reactions. It can be converted to vanyllil alcohol by hydrogenation and then to guaiacol by demethoxylation [149,150]. Guaiacol can further undergo demethoxylation and hydrogenation resulting in cyclic alcohols [147,151]. For the whole temperature range, eugenol was completely converted: the hydrogenation of the double bonds leads to the conversion to propylguaiacol, identified in the upgraded products (RT: 25.22 min) [147]. A small peak related to phenol was observed in the chromatogram of the HP. After the reaction the peak disappeared, suggesting that phenol was completely converted: the hydrogenation of the aromatic ring of phenol leads to the conversion to cyclohexanol (compound detected in the upgraded products) [61,99].

Moreover the peak at 25.22 min in the upgraded products can also suggest the hydrogenation of the double bond in the isoeugenol molecule.

For the conditions tested, the hydrogenation of the molecules was more likely to occur compared to hydrodeoxygenation. Furthermore, the compounds identified in the upgraded light and heavy phases were for all the reaction conditions very similar. Keto groups, furfural and compounds such as vanillin and eugenol were completely converted.

Table 13. Distribution of the main compounds in the gas phase. Reproduced from ref [116] according to the terms of Creative Commons Attribution License (CC BY).

	CO_2 (mol/Kg feed)		**CO (mol/Kg feed)**		**CH_4 (mol/Kg feed)**		**C_2H_6 (mol/Kg feed)**		**C_3H_8 (mol/Kg feed)**	
	Feed: FPBO	Feed: HP	Feed: FPBO	Feed: HP	Feed: FPBO	Feed: HP	Feed: FPBO	Feed: HP	Feed: FPBO	Feed: HP
175 °C, 80 bar	0.14 ±0.01	0.13 ±0.01	n.d.	n.d.	0.06 ±0.01	0.05 ±0.01	n.d.	n.d.	n.d.	n.d.
225 °C, 80 bar	0.20 ±0.01	0.18 ±0.02	n.d.	n.d.	0.15 ±0.01	0.11 ±0.04	n.d.	n.d.	n.d.	n.d.
275 °C, 80 bar	0.40 ±0.01	0.46 ±0.04	0.04 ±0.01	n.d.	0.39 ±0.04	0.45 ±0.01	0.010 ±0.002	0.013 ±0.002	n.d.	n.d.
325 °C, 80 bar	1.30 ±0.09	1.16 ±0.17	0.05 ±0.03	0.02 ±0.01	0.69 ±0.09	0.64 ±0.04	0.046 ±0.03	0.046 ±0.01	0.013 ±0.001	0.015 ±0.002
175 °C, 100 bar	0.12 ±0.01	0.97 ±0.06	n.d.	n.d.	0.06 ±0.01	0.05 ±0.01	n.d.	n.d.	n.d.	n.d.
225 °C, 100 bar	0.11 ±0.01	0.11 ±0.04	n.d.	n.d.	0.18 ±0.01	0.11 ±0.04	n.d.	n.d.	n.d.	n.d.
275 °C, 100 bar	0.38 ±0.01	0.38 ±0.07	n.d.	n.d.	0.68 ±0.01	0.70 ±0.04	0.015 ±0.01	0.017 ±0.01	n.d.	n.d.

n.d: not detected.

The main compounds in the gas phase (excluding hydrogen, which was the main compound detected), are presented in Table 13. CO_2 was the main compound, followed by methane, and in smaller amounts ethane, propane and CO.

The concentration of CO_2 increased with the temperature for both feedstocks, with a slightly higher concentration for the reactions with (FPBO). The reactions performed at higher pressures lead to lower amounts of CO_2, when comparing reactions performed at the same temperature. CO_2 is mainly

obtained by decarboxylation, whereas CO forms by decarbonylation [52]. CH_4 can be produced as a result of carbohydrates conversion, C-C bonds cleavage as well as methanation of CO_2 [65,99].

4.3.3 Catalyst Characterization

Based on the results above, the spent catalyst of reactions conducted with FPBO and HP at 325 °C and 80 bar was selected for further characterization, considering the higher degree of deoxygenation, chemical composition and hydrogen consumption (reducing excess of hydrogen consumption), respectively. The characterization of fresh catalyst is presented for comparison.

The metal leaching was obtained by ICP-OES measuring the content of Ni and Cr in the ULPs. 0.73 wt.% of Ni (in relation to the initial concentration of metal in the catalyst) was leached after the reaction with FPBO whereas 0.43 wt.% was leached for the reaction with HP. The high amount leached for the FPBO can be related to the higher water concentration in this feedstock [53,105]. The amount of chromium leached was lower compared to Ni; 0.010 wt.% of Cr was leached for FPBO feed and 0.014 wt.% for reaction with HP.

Table 14. Solid residue, BET surface area and approximate elemental distribution over the Ni-Cr catalyst surface by SEM-EDX. Reproduced from ref [116] according to the terms of Creative Commons Attribution License (CC BY).

		Ni-Cr Fresh	Spent (FPBO)	Spent (HP)
Solid residue (wt.%) TGA		-	7.6	15.5
BET area (m^2/g)		94	92	75
SEM-EDX approximate surface composition	Ni (wt.%)	40.8	51.4	32.8
	Cr (wt.%)	4.3	5.4	3.6
	C (wt.%)	12.9	19.3	34.8
	S* (wt.%)	n.d.	0.2	0.2
	Mg** (wt.%)	n.d.	0.2	0.2
	Ca*** (wt.%)	n.d.	0.2	0.3
	Cr/Ni	0.1	0.1	0.1

*$[S]_{FPBO}$=0.012 wt.%; $[S]_{HP}$=0.009 wt.%
**$[Mg]_{FPBO}$= 0.003 wt.%; $[Mg]_{HP}$=0.003 wt.%
***$[Ca]_{FPBO}$= 0.005 wt.%; $[Ca]_{HP}$= 0.008 wt.%;
n.d.: not detected.

The amount of solid deposition over the catalyst was measured by thermogravimetric analysis (TGA) and the results were presented in section 4.3.1, as the percentage of solid formed. The TGA measurements are available in the supplementary material (Figure S.19). The catalyst used for HP upgrading showed after the reaction approximately the double of the solid deposition compared to the catalyst used for the FPBO upgrading and also smaller specific surface area (Table 14) although

approximately 80 % of the original specific surface area was preserved. Furthermore, in order to investigate the surface of the catalysts after the reaction, the approximate composition of the fresh and spent catalysts was analyzed by SEM-EDX.

The elemental distribution of the catalyst is shown in Table 14. The carbon content in the spent catalyst increased in relation to the fresh catalyst, due to coke deposition, especially for the catalyst used in the HP upgrading, in agreement with the solid residue results (Table 9). Condensation of phenolic compounds (present in higher concentration in the heavy phase), can lead to ring condensation, being responsible for the coke formation [67,152]. The higher concentration of these compounds in the heavy phase (Table 7) could result in higher amounts of coke, as observed. Furfural, present is both feedstocks, tends to polymerize under high temperatures, which could also contribute to formation of the solid deposition observed [144,153].

Furthermore, catalyst poisons were detected in the spent catalysts. Sulfur was present in the catalysts tested in both conditions, in very similar concentration, despite of their different concentration in the feedstocks (0.012 wt.% FPBO; 0.009 wt.% HP). Due to the poisoning effect over Ni catalysts the presence of sulfur should be taken into account especially if long term applications are intended [53]. This topic is object of investigation in Chapter 7.

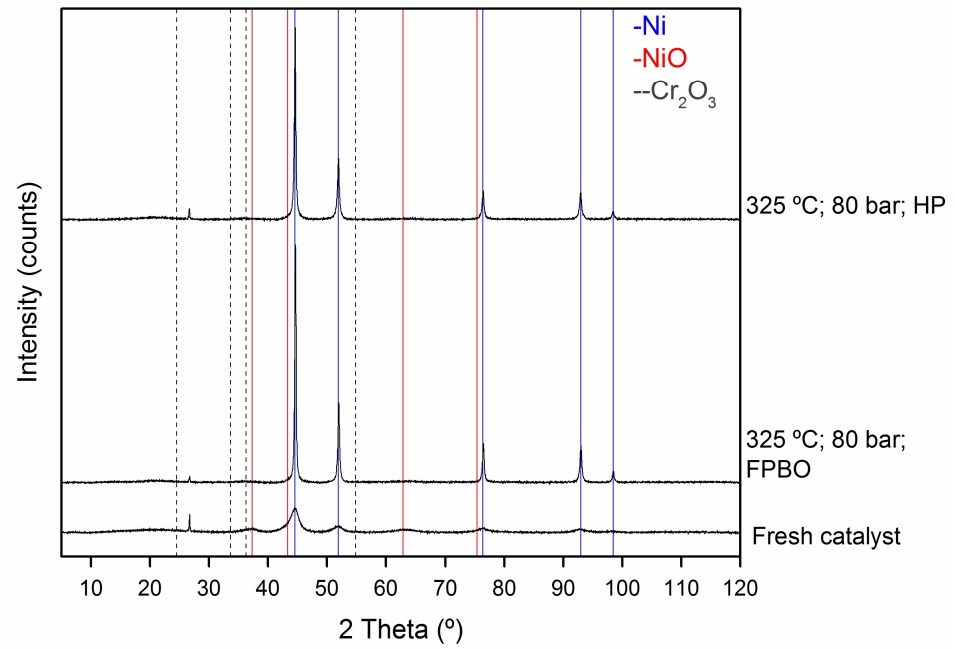

Figure 27. X-ray powder diffraction patterns of fresh and spent catalysts. Reproduced from reference [116] according to the terms of Creative Commons Attribution License.

Compounds such as Mg and Ca were also observed in the spent catalyst. Magnesium was present in higher concentration for the reaction with FPBO whereas higher concentration of calcium was observed for the spent catalyst applying HP. Usually compounds such as magnesium and calcium

are present in small concentrations in pyrolysis-oils and are attributed to catalyst poisoning, reducing its activity in the same way that sulfur and nitrogen compounds [53].

The X-ray powder diffraction patterns are depicted in Figure 27. The passivated/fresh catalyst shows broad reflections which could indicate a highly dispersed metal distribution [107]. Reflections attributed to metallic nickel could be observed in the passivated/fresh catalyst (2θ = 44.5°, 51.8°, 76.4°, 92.95° and 98.45°) as well as small broad reflections attributed to nickel oxide (2θ = 37.2°, 42.6° and 62.8°). Although present in high concentration, reflections attributed to Cr_2O_3 (JCPDS 381479) could not be observed, indicating a high dispersion of chromium oxide or an amorphous chromium phase [99,107,154]. After the reaction, the catalysts show sharper reflections attributed to metallic nickel for both conditions tested, indicating the reduction of the nickel oxide under the reductive conditions of the upgrading reactions.

The average crystallite size estimated by Scherrer equation increased after the reaction. While the average crystallite size for the fresh catalyst was about 4.4 nm, the spent catalysts used for HP and FPBO upgrading increased to 18 and 16 nm, respectively. This indicates some sintering of the Ni particles [53], as previously observed for nickel catalyst at high temperature [155].

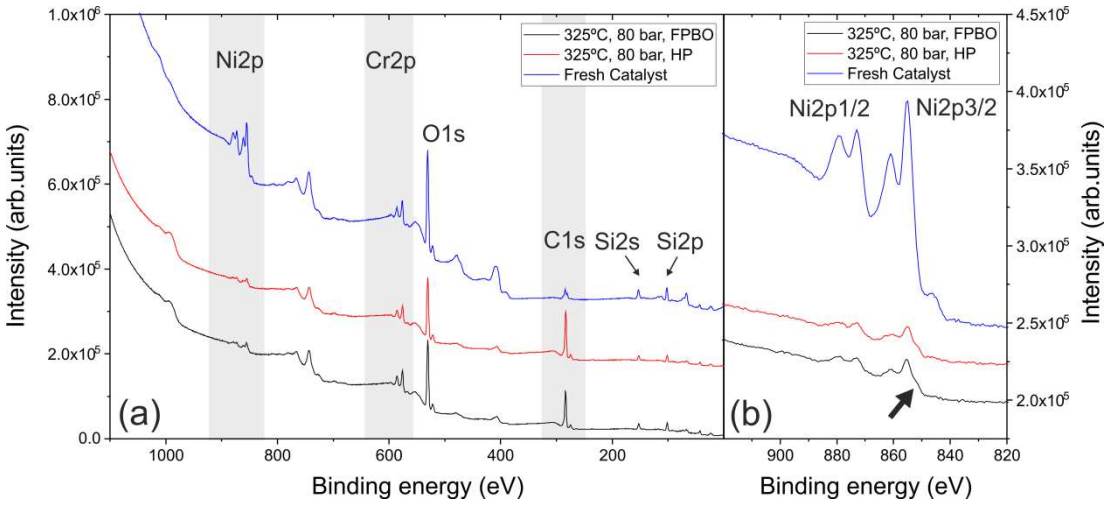

Figure 28. a) XPS spectra for the fresh and the spent catalysts. b) Zoom into the Ni2p region (offset adapted for better comparison). Reproduced from reference [116] according to the terms of Creative Commons Attribution License.

Further surface characterization of the catalyst was performed by XPS. Figure 28 a shows the survey spectra of the fresh and the spent catalysts. The characteristic XPS peaks for Ni, Cr, O, Cr, and Si are indicated. For all samples, the Cr $2p_{3/2}$ peak was observed at 276 eV, as expected for Cr_2O_3 [107,156,157]. Figure 28 b shows a zoom into the Ni 2p region. The Ni $2p_{3/2}$ peak was observed at 855 eV, with a pronounced satellite peak at 861 eV. [158], reported similar peak positions for $Ni(OH)_2$ and NiO. The small peak around 846 eV, visible only for the intense peak of the fresh catalyst, originates

from the Mg $K\alpha_3$ line of the non-monochromatized x-ray beam. For the spent catalyst, an additional shoulder was observed at 851.5 eV (indicated by an arrow), which is close expected peak position of metallic nickel at 852.6 eV [158,159]. This is consistent with XRD observations suggesting a reduction of NiO to Ni for the spent catalysts.

The O 1s peak at 530.5 eV results from a superposition of NiO, Cr_2O_3, silica (used as support material for the catalyst), and adventitious oxygen due to the sample exposure to air [158,160]. The C 1s peak at 284 eV is also a superposition of carbonaceous deposition due to the catalytic process, adventitious carbon. However, in agreement with the EDX measurements the carbon content determined by XPS is significantly increased for the spent catalysts, indicating that for the spent catalysts the C 1s peak is dominated by the carbonaceous deposition. Due to the lower concentration of species previously observed by SEM-EDX and the limitation of the XPS to concentrations below 0.1 atomic percentage (at. %), S, Ca and Mg were not identified in the XPS of spent catalyst samples.

The chemical composition within the top most few nm of the catalyst samples was determined assuming a homogeneous material distribution within this layer. The relative atomic concentration is summarized in Table 15. In agreement with the EDX results, the carbon content increased for the spent catalysts. The reduction of the oxygen content is consistent with the reduction of nickel oxide species to metallic nickel, as observed by XRD. However, in contrast to the EDX results and the low degree of metal leaching, the Cr/Ni ratio increased significantly for the spent catalyst. This can be explained with the larger Ni grain size observed for the spent catalyst or encapsulation of Ni by carbonaceous compounds. With increasing grain size, the surface/volume ratio decreases. XPS is only sensitive to the surface region, underestimating thus the Ni content of the spent catalyst. In addition to the main components of the catalyst, small amounts of silicon and aluminum where detected. They can be are attributed to the support material.

Table 15. Atomic percentages obtained by XPS. Reproduced from ref [116] according to the terms of Creative Commons Attribution License (CC BY).

	Fresh Catalyst	**325 °C, 80 bar feed: FPBO**	**325 °C, 80 bar feed: HP**
Cr (2p) (at.%)	4.58	4.21	2.79
O (1s) (at.%)	51.44	34.58	28.44
C (1s) (at.%)	18.97	49.87	59.90
Si (2s) (at.%)	14.40	9.39	7.25
Al (2s) (at.%)	1.10	0.64	0.56
Ni ($2p_{3/2}$) (at.%)	9.51	1.32	1.05
Cr/Ni	0.48	3.18	2.65
Ni/Si	0.66	0.14	0.14

4.4 Conclusion

The complete beech wood pyrolysis-oil and the isolated heavy phase were upgraded at different conditions of temperature and pressure applying a nickel-chromium catalyst. The hydrotreatment of both feedstocks resulted in upgraded oils with higher carbon content and lower oxygen content, mainly at higher temperatures (275 – 325 °C). At higher pressure (100 bar compared to 80 bar), higher consumption of hydrogen was observed with no significant reduction in the oxygen content, indicating mainly hydrogenation reactions are favored thereby not hydrodeoxygenation. Higher gas production was observed for the reactions at higher temperatures, resulting in a gas product composed by carbon dioxide (decarboxylation product) and methane (C-C bond cleavage) for both feedstocks. The ^{1}H-NMR showed an increase in the aliphatic region by hydrogen treatment whereas the aromatics remained in the upgraded oil. Furthermore, gas chromatography showed that compounds such as ketones, furfural and aldehydes were completely converted while aromatics were stable, which is in agreement with the ^{1}H-NMR results. The increase in the number of alcohols detected can indicate hydrogenation of the carbonyl groups.

The higher solid deposition over the spent catalyst was observed for the catalyst used for HP upgrading although no significant reduction in the specific surface area was observed. It is assumed that the higher concentration of phenolic compounds in the HP leads to condensation reactions of the aromatic rings resulting in coke formation. In addition to carbon, small amounts of poisoning substances such as sulphur, calcium and magnesium were also detected in the spent catalysts. Furthermore, small amounts of leached metal were observed in the upgraded light phase.

In summary, the results demonstrate that the upgrading of complete pyrolysis oil or isolated heavy phase leads to upgraded oils with very similar properties, with lower oxygen and water content and higher energy density. The nickel-chromium catalyst was active for the conditions tested and further investigations will elucidate the influence of poisoning substances, such as sulfur, carbon and magnesium over the long term stability of the catalyst.

Chapter 5. Synthesis and Regeneration of Nickel-Based Catalysts for Hydrodeoxygenation of Beech Wood Fast Pyrolysis Bio-Oil

Chapter redrafted after:

Schmitt, C. C., Reolon, M.B.G., Zimmermann, M., Raffelt, Grunwaldt, J.D., Dahmen, N. (2018) Synthesis and Regeneration of Nickel-based Catalysts for Hydrodeoxygenation of Beech Wood Fast Pyrolysis Bio-oil. *Catalysts*, 8 (10), 449-477.

Declaration of contributions:

Caroline Carriel Schmitt performed the experimental design, conducted part of the experiments, analyzed the data, discussed the results and wrote the manuscript.

María Belén Gagliardi Reolon performed most of the experiments, analyzed the data and discussed the results.

Michael Zimmermann contributed with the scanning electron microscopy measurements.

Klaus Raffel, Jan-Dierk Grunwaldt and Nicolaus Dahmen supervised the work, contributed to the discussion and corrected the manuscript.

List of abbreviation – Chapter 5

CD_3OD: Deuterated methanol

GC-MS: Gas chromatography–mass spectrometry

HDO: Hydrodeoxygenation

^{1}H-NMR: proton NMR

HP: Heavy phase beech wood fast pyrolysis bio-oil

H_2-TPR: Temperature programmed reduction

ICP-OES: Inductively coupled plasma atomic emission spectroscopy

SEM-EDX: Scanning Electron Microscopy/Energy Dispersive X-ray spectroscopy

XRD: X-ray diffraction

Abstract Chapter 5

In this chapter four nickel-based catalysts were synthesized by wet impregnation and evaluated for the hydrotreatment/hydrodeoxygenation of beech wood fast pyrolysis bio-oil. Parameters such as elemental analysis, pH value, water content, as well as heating value of the upgraded bio-oils were taken into account for the evaluation of the catalysts activity and catalyst reuse in cycles of hydrodeoxygenation after regeneration. The reduction temperature, selectivity and hydrogen consumption were distinct among them, although all catalysts tested produced upgraded bio-oils with reduced oxygen concentration, lower water content and higher energy density. Especially Ni/SiO_2 was able to remove more than 50 % of the oxygen content and reduced the water content by more than 80 %, with low coke and gas formation. The evaluation over four consecutive hydrotreatment reactions and catalyst regeneration showed a slightly reduced hydrodeoxygenation activity of Ni/SiO_2, mainly attributed to deactivation caused by sintering and adsorption of poisoning substances, such as sulfur. After the fourth catalyst reuse, the upgraded bio-oil showed 43 % less oxygen in comparison to the feedstock and properties comparable to the upgraded bio-oil obtained with the fresh catalyst. Hence, nickel-based catalysts are promising for improving the hard wood fast pyrolysis bio-oil properties, especially monometallic nickel catalysts supported on silica.

5.1 Introduction

The fast pyrolysis bio-oil obtained after fast pyrolysis has poorer physical and chemical characteristics if compared to liquid fossil fuels. The heating value is usually lower, only 40–50 % compared to conventional fossil fuels (42–45 MJ/Kg), mainly due to the high oxygen and water content. Additionally, it shows high viscosity, low chemical stability and solid particles [34,161,162] due to incomplete solid separation or polymerization reactions during storage, for example. Carboxylic acids present in the bio-oil composition lead to high acidity (pH value around 2–3.7), resulting in a bio-oil with potentially corrosive properties. Furthermore, it is highly unstable during storage due to ongoing chemical reactions, resulting in larger molecules by polymerization, etherification and esterification [161], for example. Additionally, it is immiscible with fossil fuels and tends to undergo phase separation when stored for a long time.

Considering these poor fuel properties, the direct application of bio-oil is limited to furnaces and boilers, being unsuitable for application in gas turbines, diesel engines and other applications without further treatment [91]. Concerning bio-oil production today, wood with low ash content is used, leading to relatively "well-natured" bio-oils. Through the use of ash-rich feedstocks, bio-oil yield and quality is decreased, while the tendency for phase separation increases.

To improve these properties and obtain a product resembling diesel fuel, bio-oil requires an additional upgrading treatment. Upgraded bio-oil can then be used as feedstock for producing chemicals, such as phenols for resin production, additives for fertilizers and pharmaceutical industries, as well as flavoring agents in the food industry [163]. Regarding terms of energetic use, upgraded bio-oil might be used as feedstock in oil refineries and fuels in engines [23].

A variety of upgrading techniques already have been proposed, such as catalytic cracking, hydrodeoxygenation (HDO) and esterification in supercritical fluids [18]. Among them, HDO appears to be a propitious route, due to its flexibility with respect to the biomass feed, the good economy of the input materials, and its compatibility with refinery infrastructures [52]. HDO is a high-pressure catalytic treatment in which oxygen is removed by hydrogen resulting in water, which is environmentally benign [164]. Usually, sulfides, noble metals and transition metal catalysts are used [165]. Noble metals such as Pt, Pd and Ru have been evaluated widely for HDO and are often the first choice in hydrogenation reactions. Additionally, they have a low tendency to be poisoned by the sulfur present in the bio-oil [166]. Their relatively high costs, however, prevent them from being widely used. Recently, nickel-based catalysts have become more attractive, considering their lower price, availability, activity and reduced hydrogen consumption [162,167]. Jin et al. [82] evaluated a series of nickel-based catalysts on different supports (SiO_2, Al_2O_3, AC and SBA–15 mesoporous silica) for the HDO of anisole, used as a model compound. Boscagli et al. [99] investigated the HDO of the bio-oil light

phase over a variety of nickel-based catalysts ($NiCu/Al_2O_3$, Ni/SiO_2, Ni/ZrO_2, Ni/TiO_2 and NiW/AC). Dongil et al. [101] studied the HDO of guaiacol over nickel-based catalysts, using different carbon-based supports.

The combination of nickel in bimetallic catalysts has also attracted attention for HDO, especially in combination with copper. Ardiyanti et al. [71] evaluated the application of NiCu at different loadings supported in δ–Al_2O_3 for upgrading of model compounds and fast pyrolysis bio-oil. Dongil et al. [123] investigated the effect of Cu loading on nickel catalysts supported in carbon nanotubes over the HDO of guaiacol. Mortensen et al. [68] screened different catalysts, including $NiCu/SiO_2$ for phenol HDO and, more recently, Boscagli et al. [53] tested $NiCu/Al_2O_3$ for the HDO of phenol and bio-oils reusing the catalyst after a regeneration step.

The investigation of nickel and nickel–copper catalysts on SiO_2 and ZrO_2 supports with real feedstock (fast pyrolysis bio-oil) is of interest, especially with respect to the lower acidity in comparison to Al_2O_3, a commonly studied support for HDO catalysts [39]. Many studies are focused on alumina-supported catalysts (Al_2O_3) [53,71] and upgrading applying model compounds [82,101] but supports with higher stability are required. The alumina-support is well known for its acidity, tendency for increased coke formation, low water tolerance, and conversion to boehmite, resulting in the oxidation and deactivation of the active metal [52,61,65]. He et al. noted [65] the selection of the support for HDO of bio-oils, consequently, must consider the resistance to the water content, the supports to acidity to reduce coke formation, the porosity of the support and its ability to keep the active metal dispersed for the activation of hydrogen. Hence, the investigation of different supports, such as SiO_2 and ZrO_2, appears interesting, especially when including catalyst regeneration in consecutive cycles of HDO-regeneration, evaluating the thermal stability of the catalyst [168]. Presently, only a few works have investigated the regeneration and evaluation of the reuse of the catalyst [53]. Most works, in fact, only consider one regeneration step and do not contemplate Ni catalysts [53,169,170]. It is an essential step to reduce costs, minimizing the waste generation at the same time helping to increase the reusability and recyclability of the catalysts, extending its lifetime [171]. Additionally, previous studies considered the HDO of model compounds whereas others considered the application of pyrolysis oil. Usually, different temperature, pressure and reactor designs are used, which makes the comparison of the performance of different nickel-based catalysts difficult.

The current work synthesizes four nickel-based catalysts, characterizes them and uses them for a multi-phase fast pyrolysis bio-oil upgrading. Supports with higher stability (SiO_2 and ZrO_2) are selected. The catalyst with the best performance is then selected and reused in subsequent

HDO-regeneration steps, resulting in four consecutive reactions. Finally, the performance and the catalytic activity along the HDO-regeneration steps are assessed and discussed.

5.2 Materials and methods

5.2.1 Catalyst syntheses

The four nickel-based catalysts, Ni/SiO_2, Ni/ZrO_2, $NiCu/SiO_2$ and $NiCu/ZrO_2$, were synthesized by wet impregnation as follows. Both supports (silica and zirconia from Alfa Aesar) were milled to 0.125–0.250 mm and added to the metal solution in a ratio of 1:10. The metal precursors were $Ni(NO_3)_2.6H_2O$ (Sigma–Aldrich) and $Cu(NO_3)_2.2H_2O$ (Alfa Aesar). The water was evaporated at 35 °C, 45 mbar, 100 rpm in a rotary evaporator (Hei-VAP Advantage ML/G3) and the formed catalyst was dried for 12 h at 105 °C. The catalysts were then calcined at 450 °C for 4 hours after reaching the set point, with a heating ramp of 10 °C/min (Thermolyne F6010) and later reduced in a 25% H_2/N_2 flow of 3L/min, heating ramp of 5K/min, during 4 h. The reduction temperatures were defined by temperature programmed reduction (H_2-TPR) experiments (see Sections 5.2.5 and 5.3.1). Regarding the monometallic Ni catalyst, the metal concentration in the catalyst was defined in 8.6 wt.% [172] while, for the bimetallic catalysts, the metal concentration was defined in 28 wt.% of Ni and 3.5 wt.% Cu [71].

5.2.2 Beech wood fast pyrolysis bio-oil

The experiments were carried out with a beech wood fast pyrolysis bio-oil, previously used in Chapter 3 and Chapter 4. Following intentional aging (24 h, 80 °C) two phases were observed (41 wt.% of heavy phase and 59 wt.% of light phase), respectively. Both phases were separated, and previously characterized separately, as presented elsewhere [115]. The main physicochemical properties and elemental analyses are presented (Table 16).

Table 16. Physicochemical properties and elemental analysis of the HP and LP of aged beechwood bio-oil [115]. Reproduced from ref [96] according to the terms of Creative Commons Attribution License (CC BY).

	Beechwood fast pyrolysis bio-oil	
	HP	**LP**
Carbon (wt.%) (wet basis; dry basis)	54.3; 63.7	34.3; 52.4
Hydrogen (wt.%) (wet basis; dry basis)	7.5; 6.9	8.3; 6.8
Nitrogen (wt.%) (wet basis; dry basis)	<0.2	<0.2
Oxygen (wt.%) (wet basis; dry basis)	38.2; 29.2	57.3; 39.9
H_2O (wt.%)	14.5	35.3
HHV (MJ/kg) (wet basis; dry basis)	23.1; 27.3	14.1; 22.4
pH value	3	2.7
Density (g/cm^3)	1.19	1.17

5.2.3 Hydrodeoxygenation Reactions

The HDO experiments were conducted in a 200 ml volume batch reactor. More details about the reactor are given in Chapter 3 and Chapter 4. The conditions selected for this study were fixed to 325 °C and 80 bar of H_2 based on the current authors' previous investigation [116], presented in Chapter 4. Fifty grams of bio-oil (composed of the mixture of the LP and HP, in the proportion advised in Section 5.2.2) and 5 wt.% of catalyst in relation to the amount of the bio-oil were added to the autoclave. The reactor was closed and purged with N_2 for 5 min and pressurized with H_2 (Air liquid Alphagaz 2, purity 6.0) at ambient temperature. The stirrer was switched to 1000 rpm and the heating program was started at a rate of 5 °C/min. The global reaction time, including the heating ramp, was 120 minutes. When this time was reached, the reaction was quenched first using a flow of compressed air and, later, in a cold water bath with ice, until reaching ambient temperature. Two experiments were performed for each set of conditions and are presented as an average.

Following the reaction, the final pressure was recorded for hydrogen consumption determination and the gas phase was collected for gas-chromatography analysis. The mixture of spent catalyst, carbon rich solid, upgraded bio-oil and aqueous phase was collected, centrifuged for 40 min at 7000 rpm (Thermo Scientific Heraeus Biofuge Stratos) and then separated for further characterization. The H_2 consumption was calculated using the ideal gas law, as the difference of the moles of hydrogen loaded to the reactor and the remaining moles after the hydrotreatment, from the pressure before and after the reaction and the gas composition determined by gas chromatography [70].

5.2.4 Products characterization

The gas composition was determined by collecting and analyzing the gaseous fraction by gas chromatography. A 100 µl sample was injected at 250 °C (split 28:1) in an Agilent 7890A (two detectors: thermal conductivity and flame ionization detector, TCD and FID respectively) equipped with two columns: Restek 79,096 Hayesep Q and Restek Molsieve 5A. The oven temperature was programmed as follows: the initial temperature was set to 50 °C maintained for 10 minutes; increased to 90 °C at a heating rate of 3 °C per minute and then increased to 150 °C at a heating rate of 20 °C per minute, maintained at this temperature for 16 minutes and finally heated to 230 °C at 50 °C per minute and kept for 10 minutes.

The liquid products (aqueous phase and upgraded bio-oil) were characterized using the same methodology, except the higher heating value (HHV), which was not determined for the aqueous phases. The pH values were measured with a pH-meter from Metrohm. The HHV was determined using a calorimeter IKA C5000 control and the water content using a volumetric Karl–Fischer titrator from

Metrohm (Titrando 841, titration reagents Composite 5 and dry Methanol). Carbon, hydrogen and nitrogen content were measured using a micro-elemental analyzer Elementar Vario el Cube. The content of oxygen was estimated by the difference.

Quantitative ^{1}H-NMR was employed to characterize the functional groups in the product molecules, based on the number of protons in the corresponding ^{1}H-shift range [173]. ^{1}H-NMR spectra were recorded at 25 °C on a Bruker Biospin spectrometer, equipped with a 5.47 T magnet (^{1}H frequency 250 Hz). Sample preparation consisted of 0.1 g of either upgraded bio-oil or aqueous phase and their dilution in 0.7 g of deuterated methanol (CD_3OD) containing TMSP-d4 [3-(trimethylsilyl)-2,2,3,3-tetradeuteropropionic acid sodium salt] as an internal standard (0.1 g TMSP in 50 ml CD_3OD). Subsequently, the samples were centrifuged (removal of particles not solubilized) and placed in NMR tubes.

The liquid samples also were analyzed qualitatively using a gas chromatography mass spectrometer (GC-MS) HPG1800A, with a Restek stabilwax column. Prior to measurement, the samples were diluted in methanol and filtrated using a 0.25 µm filter. A 1 µl sample was injected at 250 °C, with a split of 1:20. The oven temperature was programmed as follows: the initial temperature was set to 40 °C, maintained for 5 minutes; increased to 300 °C with a heating rate of 20 °C per minute and maintained for 20 minutes at this condition.

5.2.5 Catalysts characterization

The concentration of metal in the catalysts was analyzed by ICP-OES (Agilent 725 ICP-OES Spectrometer). The sample was dissolved using a mixture of HNO_3 (2 ml), HCl (6 ml) and H_2O_2 (0.5 ml) and digested in a microwave oven for 45 minutes at 240 °C.

To determine the reduction temperature profile of the active metal, an Autochem HP 2950 (Micrometrics) was used for the temperature programmed reduction by hydrogen (H_2-TPR). The measurements were performed at a heating rate of 1 K/min until 500 °C and 5% H_2 in Ar at 30 ml/min. The samples were dried in a 30 ml/min flow of Ar at 300 °C for 3 hours before the measurement.

The total specific surface area of the catalyst was determined by nitrogen physisorption with a Belsorp Mini II at 77K and calculated by applying the BET theory in the fitting rate between 0.05-0.30 p/p0 (12 points). Powder X-ray diffraction (XRD) was measured using an X'Pert PRO MPD instrument (PANalytical GmbH) equipped with a Cu anode (Cu Kα 1.54060 Å). The XRD patterns were recorded in a 2θ range between 5–120° (1 hour, step size 0.017°). The average crystallite size was estimated using the Scherrer equation (shape factor K = 0.9) after correcting the instrumental line broadening.

Leaching of the catalyst was monitored by analyzing the aqueous phase by ICP-OES. Sample preparation involved the filtration with a 0.2 μm PTFE membrane of the produced aqueous phase after each reaction.

To identify the elements present on the particles of fresh and spent catalysts, SEM/EDX (Scanning Electron Microscopy/Energy Dispersive X-ray spectroscopy) was applied. The equipment for this technique was a GeminiSEM 500, Zeiss, software SmartSEM Version 6.01, with a thermal Schottky field-emitter cathode. An energy dispersive X-ray spectrometer X-Max^N from Oxford with a silicon drift detector (80 mm^2 and resolution of 127 eV) was employed for the quantitative analysis of micro areas and the distribution of the elements, in addition to the software Aztec 3.3. The C, H, N and S of the spent catalysts were measured by a micro-elemental analyzer Elementar Vario el Cube. The solid over the spent catalysts (coke) was calculated by the carbon concentration over the spent catalyst (determined by elemental analysis), considering oxygen concentration negligible [88]. More detail is given in the supplementary material (Equation S7).

5.2.6. Catalysts regeneration

Based on the experimental results, such as oxygen content, water concentration, solid and gas production as well as upgraded bio-oil yield, one of the catalysts was selected for further application in cycles of HDO and regeneration. The cycles each consisted of an HDO reaction, calcination of the spent catalyst (as described in Section 5.2.1), followed by a reduction and a subsequent HDO reaction. Altogether, the catalyst was used four times. To evaluate the behavior of the catalyst over the consecutive uses, the spent catalyst was analyzed through SEM-EDX and XRD between the regenerations: EDX was performed for the spent and reduced catalysts, whereas XRD was performed for the spent, calcined and reduced catalysts. Furthermore, the upgraded products also were characterized along the cycles, as described in Section 5.2.4.

5.3 Results

5.3.1 Characterization of the synthesized catalysts

The results obtained from the temperature programmed reduction (H_2–TPR), in Figure 29, were useful to identify the catalysts' reduction temperatures before the hydrodeoxygenation (HDO) reactions. The H_2–TPR profile for Ni/SiO_2 showed a clear peak at 350 °C, while the peak for Ni/ZrO_2 is found between 350–400 °C, in agreement with literature [99,174,175]. Since the reduction of bulk Ni-oxide occurs around 400–450 °C [176,177], the reduction temperature of Ni/SiO_2 and Ni/ZrO_2 was set to 500 °C to ensure a full reduction before hydrodeoxygenation (HDO) reactions. The addition of Cu to Ni [176,177], as well as the higher loading of Ni [102,133] seems to promote the reduction of Ni

oxide, as for both bimetallic NiCu catalysts the temperature of reduction is lower compared to monometallic Ni catalysts. Concerning $NiCu/SiO_2$, it occurs at 300 °C, while for $NiCu/ZrO_2$ it was closer to 200 °C. Different peaks are present in the H_2–TPR profiles, attributed to bulk nickel oxide reduction, reduction of Cu(II) to Cu(0) (below 250 °C), as well as reduction of bimetallic NiCu species which, according to Ardiyanti et al. [70], should occur approximately in the range of 290–390 °C. Regarding the current catalysts, most of the reduction was observed at lower temperatures. Consequently, the reduction of NiCu catalyst was set at 350 °C.

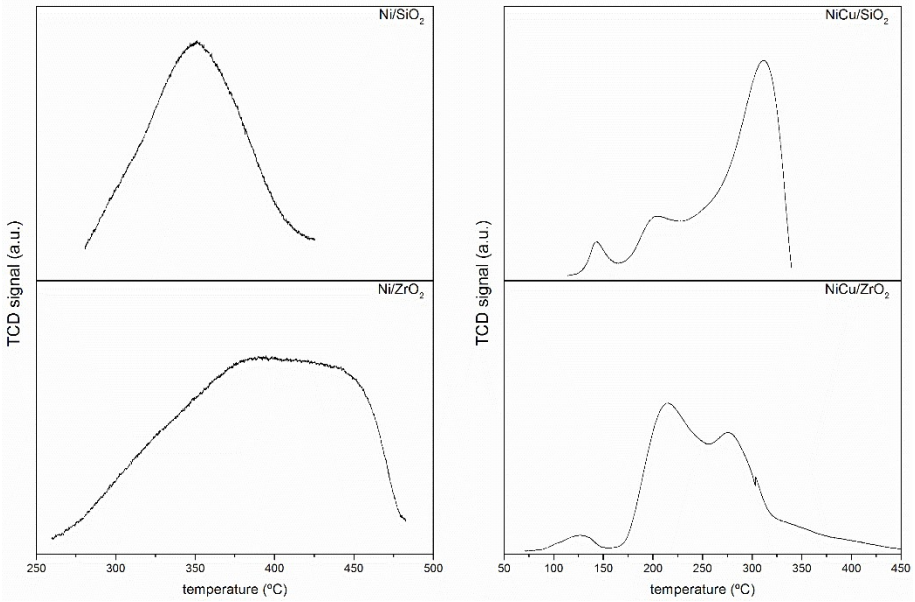

Figure 29. Temperature programmed reduction profile for the nickel-based catalysts. (TCD: Thermal conductivity detector; a.u.: arbitrary units). Reproduced from reference [96] according to the terms of Creative Commons Attribution License.

Powder X-ray diffraction (XRD), provided information about the crystalline structure of the catalyst (Figure 30). Both SiO_2-supported catalysts show similar XRD patterns. The reflections located at 37.25° and 43.29° indicate the presence of Ni oxide (NiO) in the calcined catalysts. Additionally, metallic Ni was identified due to the reflections at 44.49°, 51.85°, 76.38°, 92.93° and 98.44°. Following the reduction, reflections attributed to NiO disappeared, remaining just metallic Ni reflections. A similar behavior can be seen for Ni/ZrO_2 and $NiCu/ZrO_2$ (Figure 30). Both NiO and metallic Ni are present in the calcined catalyst. Subsequently, the reduction reflections of NiO are no longer observed for Ni/ZrO_2 and showed a reduced intensity for $NiCu/ZrO_2$. Reflections attributed to copper were not observed in the bimetallic catalysts, which can be a result of high dispersion of the metal, as well as low concentration [71,99].

The crystallite sizes were estimated using the Scherrer equation. The crystallite size was 17.7 nm for Ni/SiO_2, whereas for $NiCu/SiO_2$, the value was estimated to be 21.4 nm. $NiCu/ZrO_2$ showed a crystallite size of 43.3 nm and the crystallite size of Ni/ZrO_2 was estimated at 9.7 nm.

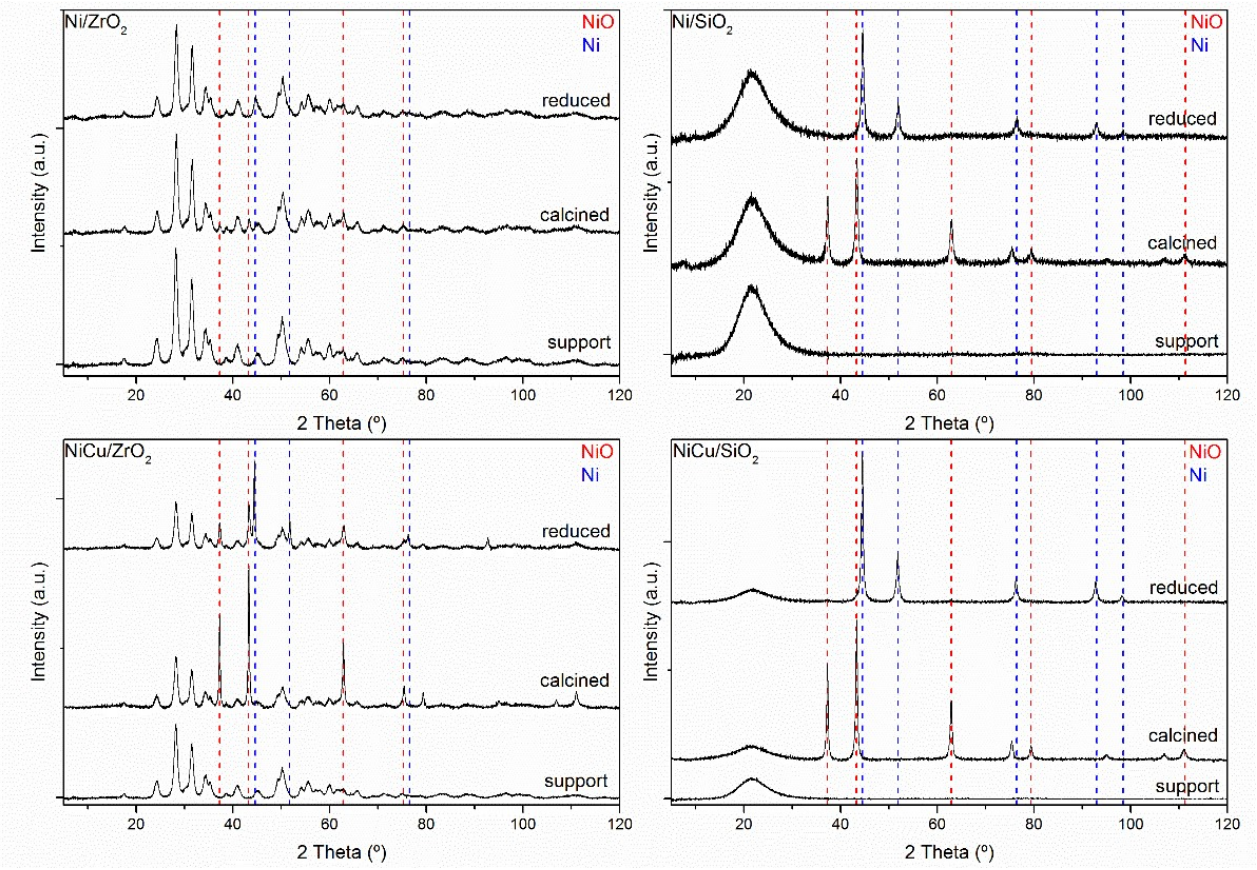

Figure 30. X-ray powder diffraction of the freshly synthesized catalysts. Ni/ZrO_2, Ni/SiO_2, $NiCu/ZrO_2$ and $NiCu/SiO_2$. a.u.: arbitrary units. Reproduced from reference [96] according to the terms of Creative Commons Attribution License.

The metal concentration, as well as the specific surface area, is compiled in Table 17. The Ni/SiO_2 catalyst displays the highest specific surface area (215 m^2/g), while $NiCu/ZrO_2$ shows the lowest (50 m^2/g). Usually, SiO_2-supported catalysts show higher surface areas in comparison to ZrO_2-supported catalysts [178]. The BET surface area of the catalysts, as well as the micropore area and volume, is reduced with the addition of Cu and higher nickel loading. This behavior was also observed by Dongil et al. [123] and Zhang et al. [179]. Furthermore, no micropores were observed in the zirconia supported catalysts.

Table 17. BET surface area, pore area, volume, diameter and metal content in the freshly synthesized catalysts. Reproduced from ref [96] according to the terms of Creative Commons Attribution License (CC BY).

	Ni/SiO_2	**Ni/ZrO_2**	**$NiCu/SiO_2$**	**$NiCu/ZrO_2$**
BET surface area (m^2/g)	215	65	156	50
Micropore area (m^2/g)	24	0	12	0
Micropore volume (cm^3/g)	0.009	0	0.004	0
Pore diameter (nm)	17.1	12.7	17.1	10.2
Ni (wt.%)	7.9	8.0	27.9	27.3
Cu (wt.%)	-	-	3.2	3.1

5.3.2 Hydrotreatment reactions

5.3.2.1 Upgraded bio-oil yields and properties

The HDO reactions with Ni/SiO_2 showed the highest yield of upgraded bio-oil (49.36 wt.%), and the lowest yields of the aqueous phase (35.57 wt.%) and solids (Table 18). These tendencies were not clear for the remaining catalysts. The lowest yield of upgraded bio-oil (45.32 wt.%) was obtained with Ni/ZrO_2, while $NiCu/ZrO_2$ showed the highest production of solids (0.32 wt.%) and aqueous phase (43.52 wt.%). The highest production of gas was obtained with Ni/ZrO_2 (4.54 wt.%) whereas the lowest was obtained with $NiCu/SiO_2$ (3.56 wt.%).

Table 18. Mass balance, elemental analysis and physicochemical properties of the upgraded bio-oils obtained with fresh Ni-based catalysts. Reproduced from ref [96] according to the terms of Creative Commons Attribution License (CC BY).

	Ni/SiO_2	**Ni/ZrO_2**	**$NiCu/SiO_2$**	**$NiCu/ZrO_2$**
Mass balance				
Upgraded bio-oil (wt.%)	49.36 ±0.07	45.32 ±0.03	49.03 ±0.03	46.39 ±0.04
Aqueous phase (wt.%)	35.57 ±0.07	42.72 ±0.01	41.45 ±0.01	43.52 ±0.03
Gas (wt.%)	4.29 ±0.06	4.54 ±0.05	3.56 ±0.07	3.87 ±0.03
Solids (wt.%)	0.23 ±0.11	0.31 ±0.06	0.31 ±0.22	0.32 ±0.29
Losses (wt.%)	10.54 ±0.17	7.10 ±0.05	5.65 ±0.47	5.90 ±0.49
Upgraded bio-oil (dry basis; wet basis)				
Carbon (wt.%)	73.15 ± 0.06; 69.75 ± 0.21	72.22± 0.01; 68.10 ± 0.21	72.37 ± 0.58; 66.80 ± 0.85	72.15 ±1.01; 67.25 ± 0.21
Hydrogen (wt.%)	8.42 ± 0.07; 8.55 ± 0.07	8.25± 0.01; 8.40± 0.01	8.51 ± 0.31; 8.70 ± 0.28	8.55 ± 0.31; 8.70 ± 0.28
Oxygen (wt.%)	17.86 ± 0.05; 21.30 ± 0.01	19.46 ± 0.15; 23.00 ± 0.14	19.00 ± 0.91; 24.10 ± 1.13	20.35± 0.01; 23.60 ± 1.41
Nitrogen (wt.%)	0.32 ± 0.01; 0.30 ± 0.01	0.32 ± 0.01; 0.30 ± 0.01	0.32 ± 0.01; 0.30 ± 0.01	0.32 ± 0.01; 0.30 ± 0.01
Physicochemical properties				
H_2O (wt.%)	4.85 ± 0.07	5.10± 0.01	7.30 ± 0.42	5.95 ± 0.35
HHV (MJ/kg)	31.18 ± 0.08	30.85 ± 0.02	29.86 ± 0.26	30.27 ± 0.31
pH value	3.55 ± 0.35	3.05 ± 0.35	3.35 ± 0.07	3.20 ± 0.14
Density (g/cm^3)	1.11 ± 0.01	1.12 ± 0.01	1.09 ± 0.01	1.11 ± 0.01

The elemental composition of the upgraded bio-oils by the different nickel-based catalysts is presented in Table 18. The concentration of carbon increases in all upgraded bio-oil in comparison to the concentration in the feed (57.31 wt.% dry basis) [115]. The highest carbon content (73.15 wt.% dry basis) was obtained applying Ni/SiO_2. The remaining oils upgraded with the other catalysts displaying a concentration of around 72.25 wt.% in dry and 67.38 wt.% in wet basis, respectively. The hydrogen concentration was slightly higher in the upgraded bio-oils in comparison to the initial feed,

while the oxygen content was reduced in comparison to the original beech wood bio-oil (35.84 wt.% in dry basis). The upgraded bio-oil over Ni/SiO_2 shows the lowest oxygen concentration (17.86 wt.% dry basis), followed by $NiCu/SiO_2$ (19.00 wt.% dry basis), Ni/ZrO_2 (19.46 wt.% dry basis) and $NiCu/ZrO_2$ (20.35 wt.% dry basis).

The water content in the upgraded bio-oils was reduced significantly from 26.77 wt.% in the original feed to values between 4.85 and 7.30 wt.% in the upgraded bio-oils. More than 70 % of the water content in the original oil was removed by the hydrotreatment, in fact. The upgraded bio-oil over Ni/SiO_2 showed the lowest water content (4.85 wt.%), while $NiCu/SiO_2$ had the highest value (7.30 wt.%). The opposite was observed for the upgraded aqueous phase. While the upgraded aqueous phase obtained with Ni/SiO_2 showed 74.35 wt.% of water, the aqueous phase obtained with $NiCu/SiO_2$ showed 67.15 wt.% of H_2O (Table S8). This is due to the fact that the water removed from the upgraded bio-oils mainly was concentrated in the aqueous phase.

The higher heating value (HHV) also changed by the reactions. Seen in the feedstock, this value was 24.33 MJ/kg, whereas, for the upgraded bio-oils, the HHV increased to values ranging from 29.86 MJ/kg to 31.18 MJ/kg in the case of SiO_2 supported catalysts. A slight increase in the pH value was observed, except for the upgraded bio-oil with Ni/ZrO_2. The density of the upgraded bio-oils decreased after the hydrotreatment. Comparing the density of the upgraded bio-oils with the density of the heavy phase, for example, the value was reduced from 1.19 g/cm^3 to values between 1.09 and 1.12 g/cm^3. The upgraded bio-oil over $NiCu/SiO_2$ displayed the lowest density (1.09 g/cm^3), while the highest corresponded to Ni/ZrO_2 (1.12 g/cm^3).

Further information regarding the upgraded bio-oils composition was obtained by proton nuclear magnetic resonance (^{1}H-NMR), depicted in Figure 31. Table 19 shows the assignment of chemical groups to the integration range of the spectra [173]. , The aqueous phases are compared to the light phase (LP) of the feedstock, whereas the upgraded bio-oil is compared to the heavy phase (HP) of the feedstock.

Table 19. Integration ranges of ^{1}H-NMR spectra and their corresponding proton assignment [173]. Reproduced from ref [96] according to the terms of Creative Commons Attribution License (CC BY).

Integration range of ^{1}H–NMR spectra	**Proton assignment**
10.1–9.5	Aldehydes
8.5–6.0	(Hetero-)aromatics
6.0–4.3	Carbohydrates, water, O-H exchanging groups
4.3–3.0	Alcohols, ethers, dibenzenes
3.0–1.5	α proton to carboxylic acid or keto-groups, α proton to unsaturated groups
1.5–0.5	Alkanes

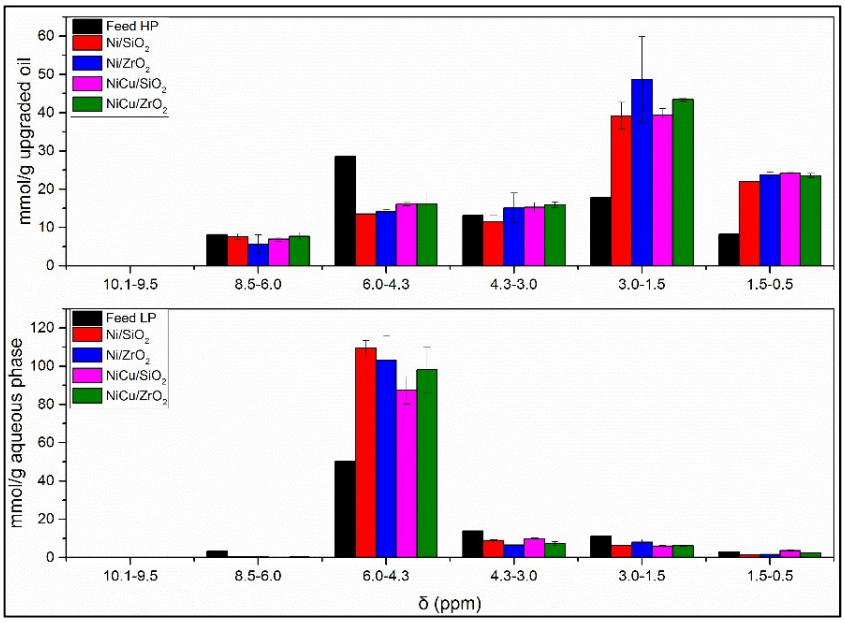

Figure 31. ^{1}H–NMR integrals of the bio-oil components, HP (top) and LP (bottom), in contrast to the products (upgraded bio-oil and aqueous phase) obtained by different catalysts. Reproduced from reference [96] according to the terms of Creative Commons Attribution License.

The signals for aldehydes (10.1–9.5 ppm) are very small in the feed, especially in the LP. They were not observed in the upgraded products as they are very reactive even at mild conditions and, therefore, are hydrogenated quickly to alcohols [180]. The main signals for the upgraded bio-oil were found in the region of α-protons to carboxylic acid or keto-groups and α-protons to unsaturated groups (3.0–1.5 ppm) with a concentration of 37.7 mmol/g sample.

The aromatic (8.5–6.0 ppm) were concentrated mostly in the upgraded bio-oil and almost absent in the aqueous phase (7.2 versus 0.8 mmol/g sample). No significant differences among catalysts were observed. A slight increasing tendency could be observed for the concentration of alcohols, ethers and dibenzenes (4.3–3.0 ppm), although it was not significantly different among all tested catalysts. The concentration of protons in this region was more abundant in the upgraded bio-oil (14.2 mmol/g sample) in comparison to the aqueous phase (9.3 mmol/g sample). The abundance of alkanes (1.5–0.5 ppm) almost triples in comparison to the feed (heavy phase) and was significantly higher in the upgraded bio-oil than in the aqueous phase (20.3 versus 2.4 mmol/g sample).

The accumulation of water in the aqueous phase is also confirmed by the ^{1}H-NMR measurements, considering that the main signal obtained for the aqueous phase was found in the carbohydrates, water and O-H exchanging groups (6.0–4.3 ppm). The high concentration of protons in this region (89.7 mmol/g sample) is attributed to the removal of water from the bio-oil [88,116], in agreement with Karl–Fisher results. To contrast, the proton in this region decreases in all upgraded bio-oils, especially for Ni/SiO_2, which produced the upgraded bio-oil with the lowest water concentration (Table 18).

To identify the main compounds in the upgraded bio-oils, as well as to investigate differences in selectivity among the catalysts tested, the upgraded bio-oils were analyzed qualitatively by gas chromatography-mass spectrometer (GC-MS), depicted in Figure 32 and Table 20. To compare, the chromatograms of the upgraded bio-oils are discussed in comparison to the chromatograms of the heavy phase (feedstock), available in the supplementary material (Figure S.22).The chromatograms of the upgraded aqueous phases, as well as the light phase of the feedstock, are also available as supplementary material (Figure S.22 and Figure S.23).

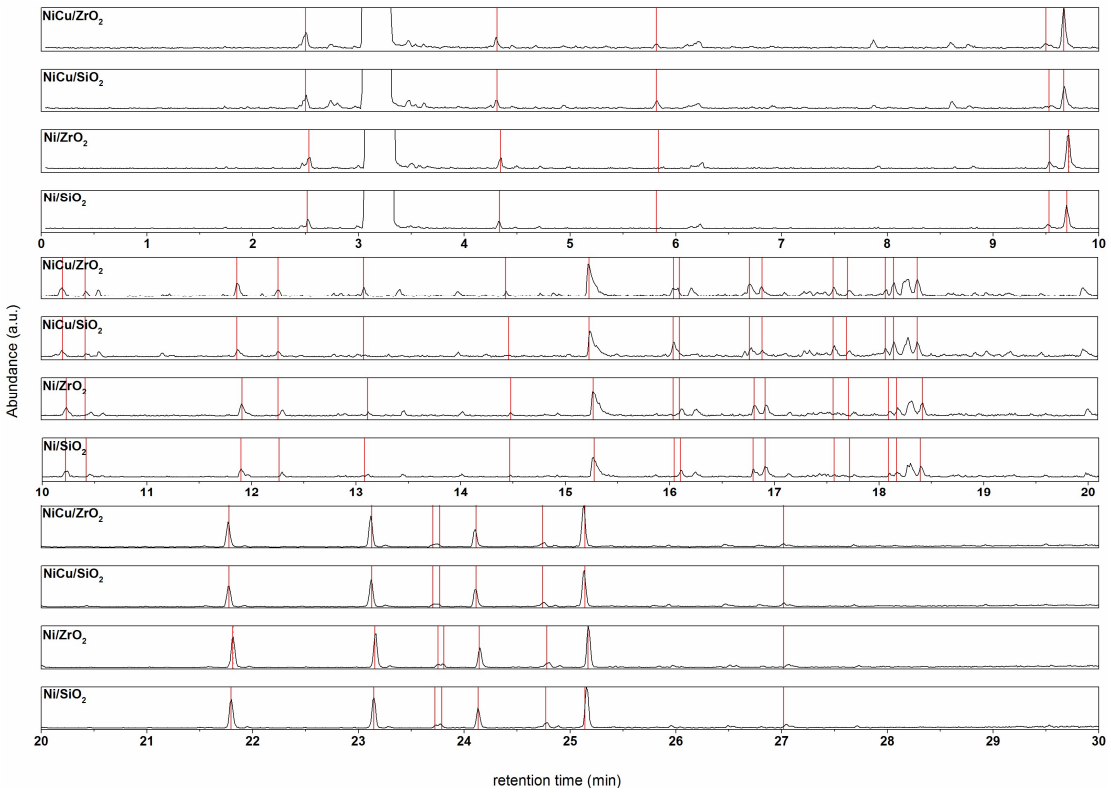

Figure 32. Chromatograms of the upgraded bio-oils over different nickel-based catalysts. Reproduced from ref [96] according to the terms of Creative Commons Attribution License (CC BY).

Typical compounds were observed in the upgraded bio-oils, such as carboxylic acids, ketones, phenolic compounds and others [98]. The main reaction pathways identified and later discussed are available in Figure S.18.

A variety of ketones, especially but not limited to cyclic forms, were identified in all the upgraded bio-oils, such as 2-pentanone, cyclopentanone, 3-methyl-cyclopentanone, 2-ethyl-cyclohexanone, cycloheptanone and others, in agreement with Boscagli et al. [88] and Ardiyanti et al. [71]. They are attributed as products of sugar conversion and its derivatives.

Aromatic compounds initially present in the feedstock also were observed in the upgrade-oil, such as guaiacol (2-methoxy-phenol), phenol and 4-ethyl-2-methoxy-phenol. Acetic acid also was present in the feedstock as well as in the upgraded products.

Subsequent to the upgrading reaction, compounds initially present in the bio-oil mixtures, such as furfural, were completely converted for all the catalysts tested. The same was observed for eugenol and compounds with GC retention times higher than 30 min, such as vanillin. Although very similar to compositions of all upgraded bio-oils, some differences in selectivity were observed for the catalysts. Observed in the oils upgraded with bimetallic catalysts was 1-propanol (5.82 min), similar to the peak at 16.04 min, attributed to tetrahydro-2-furanmethanol (tetrahydrofurfuryl alcohol), was observed in the oils upgraded with NiCu catalysts. It shows that furfural is completely hydrogenated to tetrahydrofurfuryl alcohol over these catalysts [153]. Earlier studies observed the selectivity of copper-containing catalysts for furfural hydrogenation, particularly at high temperatures [148]. Furfural also can be converted to cyclopentanone [98,153] and 2-pentanone [34,181], both identified in the products, as well as other cyclopentanones [182]. Compounds such as methane, identified in the gas phase and later discussed, also can be derived from furfural conversion; the conversion of furfural to furfuryl alcohol and later to furan leads to methane formation [183]. Furthermore, the peak at 17.57 min, attributed to propylene glycol, was observed only in the upgraded bio-oils as well as in the aqueous phases (Figure S.23) upgraded with NiCu catalysts. Propylene glycol can be obtained from hydrogenation of hydroxy acetone [184], which was converted completely after the HDO reactions (see peak at 12.46 min Figure S.9). While copper-containing catalysts seem to favor the production of propylene glycol in comparison to other catalysts [157], nickel catalysts seems to follow a different pathway. Resulting from the C-O bond cleavage of propylene glycol was 1-propanol [184] which also was observed in the oils upgraded with bimetallic catalysts. Furthermore, compounds initially absent in the feedstock, such as 2-methoxy-4-propyl-phenol, resulting from the hydrogenation of the double bond of eugenol, were identified in the upgraded bio-oil [116]. A peak at a retention time of 26.9 min was observed in the upgraded aqueous phases obtained with bimetallic catalysts, although the identification of the compound was not possible.

Differences among the feed (LP) and upgraded products (aqueous phases), as well as among the products obtained with different catalysts, were observed. Observed in all upgraded aqueous phases, except for $NiCu/SiO_2$ was 2-methyl-propanol (13.08 min). The peak attributed to tetrahydro-2-furanmethanol increased significantly, mainly in the aqueous phases obtained by bimetallic catalysts, in the same way as observed in the upgraded bio-oils. Propanoic acid (16.77 min) was observed for all aqueous phases.

Table 20. Retention time of the main compounds in the upgraded bio-oil identified by GC-MS. Reproduced from ref [96] according to the terms of Creative Commons Attribution License (CC BY).

Retention time (min)	Compound
2.51	Acetic acid, methyl ester
4.32	2-pentanone
5.82	1-propanol
9.46	Cyclopentanone
9.64	2-methyl-cyclopentanone
10.20	3-methyl-cyclopentanone
10.42	(R)-3-methyl-cyclohexanone
11.84	2-ethyl-cyclopentanone
12.23	Cycloheptanone
13.08	2-methyl-2-propanol
14.47	6-hepten-1-ol
15.23	Acetic acid
16.04	Tetrahydro-2-furanmethanol
16.10	2,3,4-trimethyl-cyclopent-2-ene-1-one
16.77	Propanoic acid
16.87	2,3-dimethyl-2-cyclopenten-1-one
17.57	Propylene glycol
18.07	Dihydro-5-methyl-2(3H)-furanone
18.13	1,2-ethanediol
18.40	γ-butyrolactone
19.05	3-pentanol
21.74	2-methoxy-phenol
23.09	2-methoxy-4-methyl-phenol
23.67	4-methyl-phenol
23.70	Phenol
24.07	4-ethyl-2-methoxy-phenol
24.72	2-ethyl-phenol
25.1	2-methoxy-4-propyl-phenol
27.02	2-propyl-phenol

5.3.2.2 Hydrogen consumption and gaseous products

The hydrogen consumption was considered for the evaluation of the different catalysts. $NiCu/SiO_2$ presented the highest consumption (239.3 NL/kg bio-oil), followed by $NiCu/ZrO_2$ (201.6 NL/kg bio-oil), Ni/SiO_2 (186.2 NL/kg bio-oil) and Ni/ZrO_2 (181.9 NL/kg bio-oil). Yin et al. [175] reported, higher hydrogenation activity can be seen when adding copper to Ni catalysts, due to changes in the catalytic activity and selectivity, favoring some hydrogenation reactions [185]. The hydrogen consumption can be correlated to the H/C molar ratio. A higher H/C molar ratio and lower O/C molar ratio indicates an upgraded bio-oil with improved properties [52]. The catalysts evaluated resulted in H/C ratios between 1.37 (Ni/ZrO_2) to 1.53 ($NiCu/SiO_2$), showing a tendency between the hydrogen uptake and the H/C molar ratio. The same tendency was not observed for the O/C ratio. The lowest ratio was observed using Ni/SiO_2 (0.18) whereas the highest was for $NiCu/ZrO_2$ (0.28). This indicates that a higher consumption of H_2 does not reflect in the HDO of the feedstock.

Although a very similar total gas production (Figure 33) was obtained for all tested catalysts, Ni/ZrO_2 showed the highest total gas production (1.06 mol/kg bio-oil), followed by Ni/SiO_2

(0.99 mol/kg bio-oil), $NiCu/ZrO_2$ (0.90 mol/kg bio-oil) and $NiCu/SiO_2$ (0.86 mol/kg bio-oil). The total gas production was determined mainly by the production of CO_2, the most abundant gas product for all four catalysts, in agreement with other studies [70,88,109,178]. Decarboxylation of carboxylic acids can result in CO_2 formation [88]. Carbon monoxide, methane and other gases such as propane, propene, ethane and ethene were formed in smaller amounts.

Monometallic Ni catalysts produced the highest amount of CO_2, followed by $NiCu/ZrO_2$ and, later, by $NiCu/SiO_2$. According to Gallakota et al. [18], in an ideal scenario all C atoms should be converted to hydrocarbons without CO_2 formation. Nevertheless, since the total gas production of the four catalysts represented around 4 wt.% (see mass balance Table 18), the produced amounts of CO_2 are, in general, quite reduced in these four cases. The formation of CO_2 might indicate lower hydrogen consumption [59]. This effect was observed when the CO_2 production was compared to the hydrogen consumption—both variables were inversely proportional (Figure S.21), as reported by Boscagli et al.[88]. This tendency only was noticed in the CO_2 production, but not for the remaining produced gases.

The formation of methane was observed mainly for $NiCu/SiO_2$. The smallest concentration of methane was obtained for Ni/SiO_2. Methane resulted from the hydrogenation of carbohydrates, acetic acid decomposition, cleavage of C-C bonds of alcohols or even from methoxy groups demethylation [59]. It is important to highlight that the higher methane production was observed with $NiCu/SiO_2$, the catalyst that showed the highest H_2 consumption. This is an indication of hydrocracking of the molecules and excessive hydrogen consumption [109,186].

CO formation was more abundant in the SiO_2-supported catalysts. $NiCu/SiO_2$ displayed the highest amount, followed by Ni/SiO_2, Ni/ZrO_2 and $NiCu/ZrO_2$. The formation of CO can be a result of the C-O cleavage of different groups, such as carboxylic acids, aldehydes and alcohols. The loss of C via CO (de-carbonylation), is less advantageous than the loss of CO_2 (decarboxylation), considering more O is removed per mole of lost carbon [59].

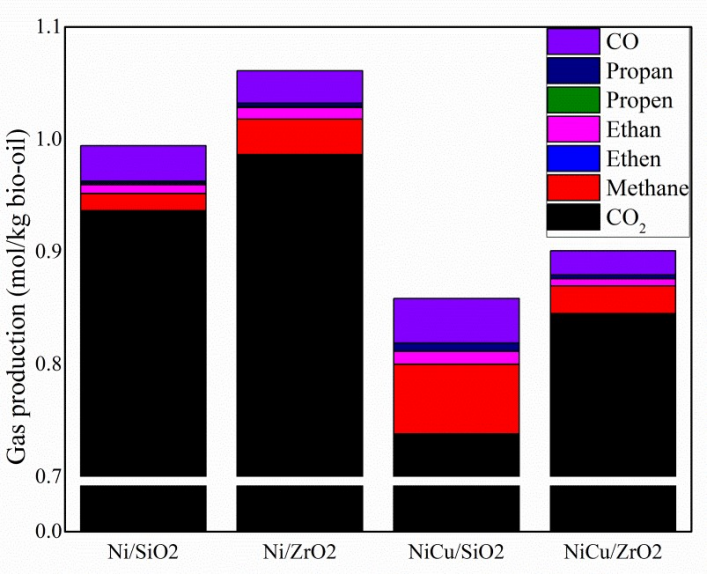

Figure 33. Gas fraction composition obtained for the nickel-based catalysts tested. Reproduced from reference [96] according to the terms of Creative Commons Attribution License.

5.3.3 Catalysts characterization

The spent catalysts were evaluated mainly in terms of metal leaching, XRD, sintering, carbon deposition as well as surface area and composition. Inductively Coupled Plasma Emission Spectroscopy (ICP-OES) was further used to evaluate the metal content present in the upgraded aqueous phases and determine the metal leaching. Ni/SiO_2 presented 0.8% of Ni leached while using Ni/ZrO_2 0.43% of Ni was washed into the aqueous phase. Both NiCu catalysts showed 0.16% of Ni leached while $NiCu/SiO_2$ and $NiCu/ZrO_2$ displayed 0.08% and 0.04% of Cu leached, respectively. Similar leaching levels also were found by Boscagli et al.[53] in a reaction at 240 °C compared to a $NiCu/Al_2O_3$ catalyst. The extent of leaching seems to correlate to the support. The lowest proportions of metals leached were observed in ZrO_2-supported catalysts. Reported previously, ZrO_2 seems to be stable in the harsh reaction conditions [65,70,179,187]. Due to the severity of the HDO reactions, the structure, morphology and texture of the catalysts might be affected [70], therefore, the spent catalysts were analyzed by XRD after the reactions. No significant differences were observed between the X-ray diffraction patterns of the fresh and spent catalysts, except for $NiCu/ZrO_2$. The small diffractions attributed to NiO disappeared in the spent catalysts, indicating further nickel reduction. The XRD patterns are available in Figure S.20 (supplementary material). The crystallite sizes were calculated for the spent catalysts. The crystallite size of $NiCu/SiO_2$ increased from 21.4 nm to 43.0 nm after the reaction. Such an increase in the crystallite size was previously observed [188] and is an indication of sintering, which might result in loss of the catalyst activity [75]. Conversely, the crystallite size of Ni/ZrO_2, Ni/SiO_2 and $NiCu/ZrO_2$ remained in the same range observed for the fresh catalysts. The composition of selected particles was analyzed by EDX (Energy Dispersive X-ray spectroscopy) and the results obtained for the fresh and spent catalysts are presented in Table 21.

Table 21. Composition of selected particles of different Ni-based catalysts (fresh and spent) obtained by EDX. Reproduced from ref [96] according to the terms of Creative Commons Attribution License (CC BY).

Catalyst		Ni (wt.%)	Cu (wt.%)	Si (wt.%)	Zr (wt.%)	C (wt.%)	S (wt.%)	Ca (wt.%)	Fe (wt.%)
Ni/SiO_2	Fresh	11.2	-	38.6	-	3.6	-	-	-
	Spent	7.3	-	44.9	-	12.1	0.2	-	-
Ni/ZrO_2	Fresh	8.6	-	-	60.9	6.4	-	-	-
	Spent	6.3	0.7	-	45.5	26.3	0.1	0.1	1.3
$NiCu/SiO_2$	Fresh	30.0	2.9	29.2	-	3.2	-	-	-
	Spent	26.9	2.4	18.2	-	26.7	0.2	-	-
$NiCu/ZrO_2$	Fresh	55.8	6.3	-	20.0	4.0	-	-	-
	Spent	44.0	4.5	-	16.4	24.3	0.1	0.1	0.7

Carbon deposition was observed for all catalysts after HDO, with lower concentration observed in Ni/SiO_2. Poisoning substances, such as sulfur and calcium, were observed near the detection limit in the spent forms. Sulfur appeared in all spent catalysts, whereas calcium and iron were observed only in zirconia-supported catalysts. The Ni proportion over the catalysts' surfaces decreased, attributed mainly to the carbon deposits of higher molecular weight polymerization products [175]. The specific surface areas of the spent catalysts were reduced in comparison to the fresh ones, especially for the silica-supported catalysts. The specific surface area of Ni/SiO_2 was reduced to 46 m^2/g, a sharp reduction in comparison to the original surface area (215 m^2/g). $NiCu/SiO_2$ showed a reduction from 156 m^2/g to 36 m^2/g. It can be attributed to the fact that the pores probably were blocked by carbonaceous deposition. The micropore area of Ni/SiO_2 was reduced to 8 m^2/g, whereas the micropore area of $NiCu/SiO_2$ was reduced to 3 m^2/g. The reduction in the surface area of the zirconia-supported catalyst was less significant. Ni/ZrO_2 showed a reduction to 57 m^2/g (original: 65 m^2/g), whereas $NiCu/ZrO_2$ was reduced from 50 to 36 m^2/g. The reduction of the surface area is attributed to deposition of carbon in all cases, as already documented by many authors [178,189–191].

Considering that SEM-EDX (Scanning Electron Microscopy/Energy Dispersive X-ray spectroscopy) provides the elemental mapping of only selected regions [192], further composition analysis was performed measuring the active metals and poisoning substances in the bulk catalyst (Table 22).

Table 22. Metal content and poisoning substances on the catalyst before and after the reaction. Reproduced from ref [96] according to the terms of Creative Commons Attribution License (CC BY).

Catalyst		Ca* (wt.%)	S* (wt.%)	Mg* (wt.%)	Ni* (wt.%)	Cu* (wt.%)	C** (wt.%)
Ni/SiO_2	Fresh	0.03	0.01	0.01	7.94	-	-
	Spent	0.03	0.12	0.01	7.05	0.01	4.2
Ni/ZrO_2	Fresh	0.01	0.01	-	8.02	-	-
	Spent	0.06	0.13	0.01	6.94	0.07	5.6
$NiCu/SiO_2$	Fresh	0.02	0.01	0.01	27.90	3.25	-
	Spent	0.02	0.13	0.01	25.90	2.76	8.6
$NiCu/ZrO_2$	Fresh	0.01	0.01	-	27.30	3.10	-
	Spent	0.05	0.14	0.01	25.25	2.72	7.1

* Results obtained by ICP-OES.

** Results obtained by elemental analysis.

Agreeing with EDX results, an increase in the calcium concentration over both zirconia-supported catalysts was observed. Sulfur, considered a very persistent poisoning substance of nickel [53,72], increased in all catalysts tested after the reaction, with slightly lower concentrations at Ni/SiO_2. Interestingly, no differences were observed in the XRD spectra, such as nickel sulfide formation [72]. The concentration of active metals (Ni and Cu) was reduced in the spent forms in comparison to the fresh catalyst. This behavior correlates to the carbon deposition. Accompanying a higher concentration of carbon, which initially is absent in the fresh catalysts, the average concentration of nickel and copper in the spent catalyst decreases. Furthermore, leaching also can play a role in the reduction of active metal in the catalyst, as discussed previously. The carbon concentration obtained by elemental analysis shows the same tendencies as observed with the EDX measurements.

5.3.4 Cycles of HDO and regeneration: Catalyst and product behavior

Ni/SiO_2 was selected for further consecutive HDO reactions as soon as the original reactions with the fresh catalyst were carried out. Key parameters were considered for selection of this catalyst for consecutive HDO-regeneration cycles: HDO activity, water and carbon concentration in the upgraded bio-oil, hydrogen consumption as well as solid formation. The upgraded bio-oil obtained with Ni/SiO_2 showed the highest carbon content and the lowest oxygen content in comparison to other catalysts, an indication of the improvement of the oil quality (higher energy density and better chemical stability). Additionally, upgrading with Ni/SiO_2 resulted in an upgraded bio-oil with the lowest water concentration, low hydrogen consumption, lowest amount of solids formed, highest HHV and pH (Table 18). Finally, the smallest production of methane also was obtained for this catalyst (Figure 33). Therefore, Ni/SiO_2 was selected to carry out the following regeneration steps.

Along the cycles of HDO-regeneration, the catalyst was characterized in the intermediate steps of the process: spent, calcined and reduced form. Only a small amount of sample was available for characterization, considering that the catalyst needed to be reused in the following experiments. Due

to that reason, two techniques which require low sample amounts showing meaningful results were selected to monitor the catalyst along the cycles— SEM-EDX and XRD. The upgraded products were characterized using the same techniques as described previously.

Looking at the SEM-EDX results, it was possible to follow the main changes occurring on the catalyst surface (Figure 34). The fresh catalyst showed a good dispersion of nickel particles over the support surface (Figure S.26 fresh a). Along the cycles, sintering of the nickel particles was observed. Specific regions were analyzed by EDX to estimate the composition. While the fresh catalyst mainly was composed of nickel, silica and a low concentration of carbon, the spent catalysts clearly showed a small concentration of sulfur (near the detection limit) located in the area of the nickel particles. Interestingly, in the regions with very low nickel concentration or even absent of nickel, no sulfur was identified. Al and Fe were also observed in the EDX spectrum, although in very small concentrations (below 0.1 wt.%). Aluminum was observed in small concentrations (support composition) but the authors cannot discard the possibility of contamination during the removal of the catalyst from the autoclave (aluminum paste is used to seal the reactor).

Considering that EDX measurements can be made either as element mapping or point analysis, both methods were used. Further compilation of images, as well as the mapping of the catalyst surface along the cycles, is available in the supplementary material (Figure S.26, Figure S.27 and Table S.10).

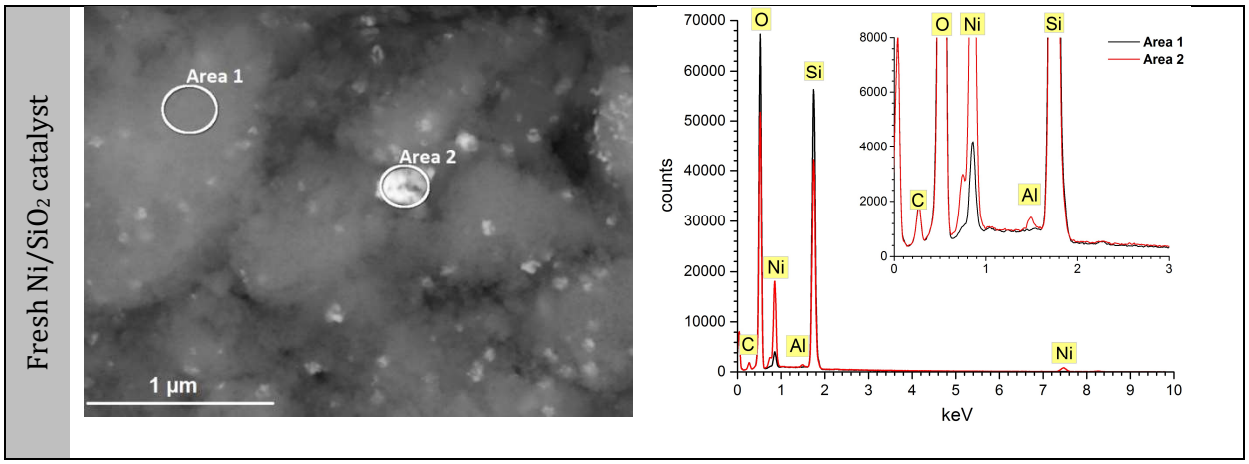

1st reaction-spent

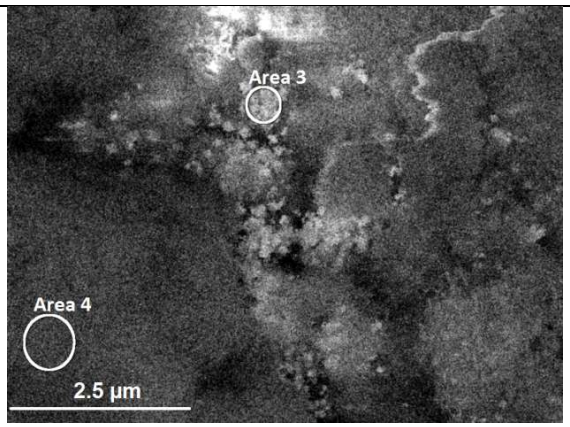

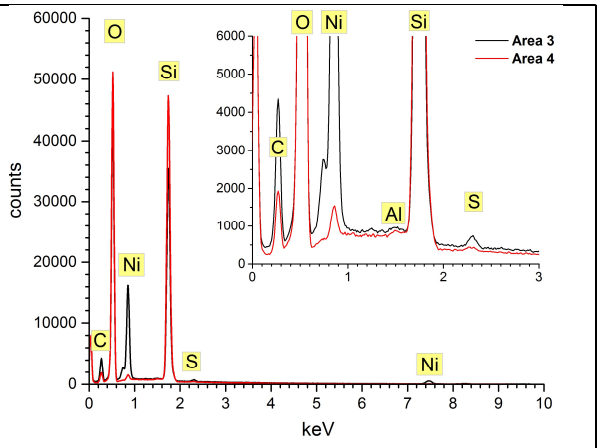

2nd reaction-spent

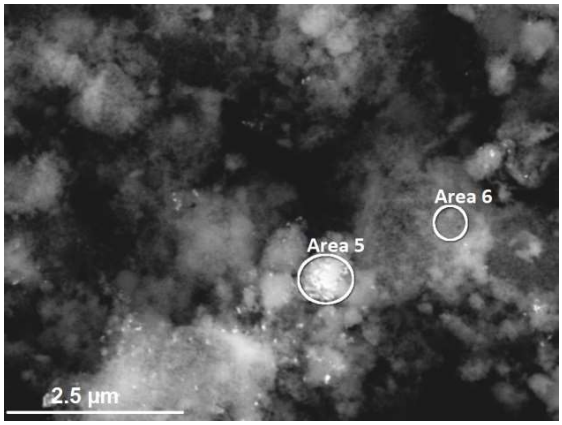

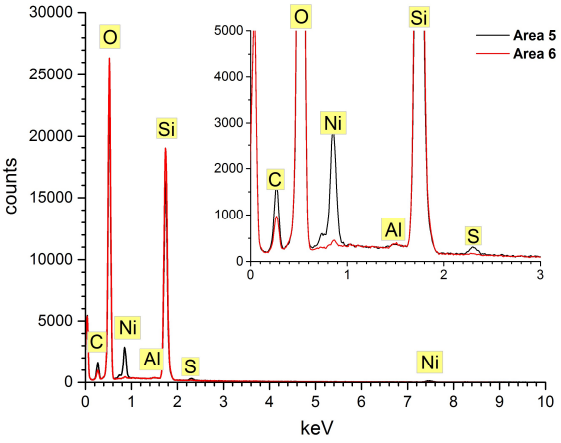

3rd reaction-spent

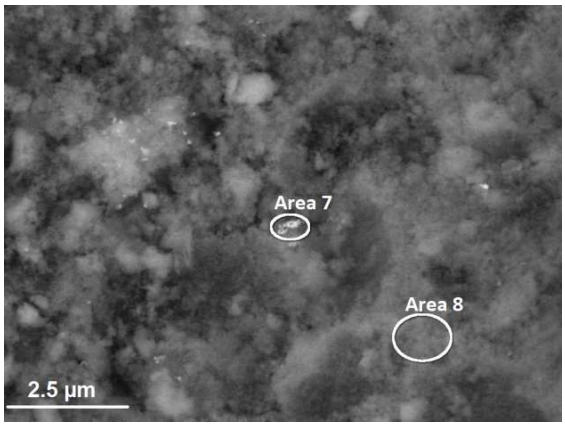

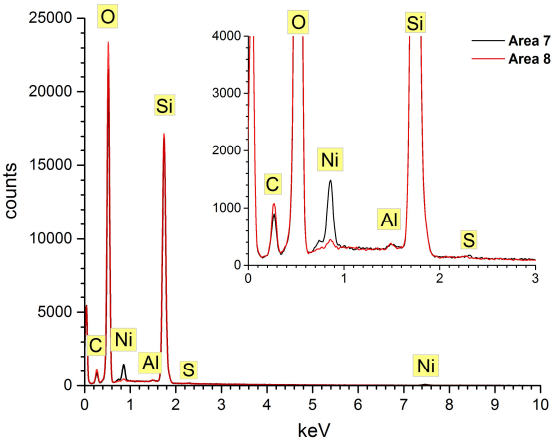

4th reaction-spent

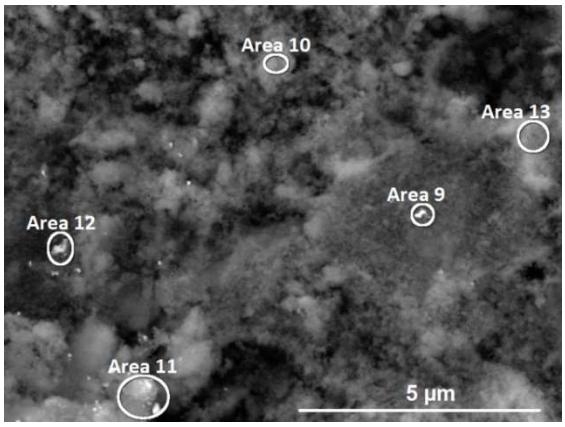

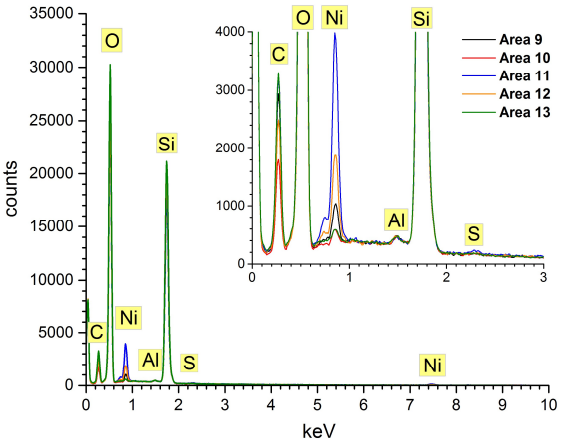

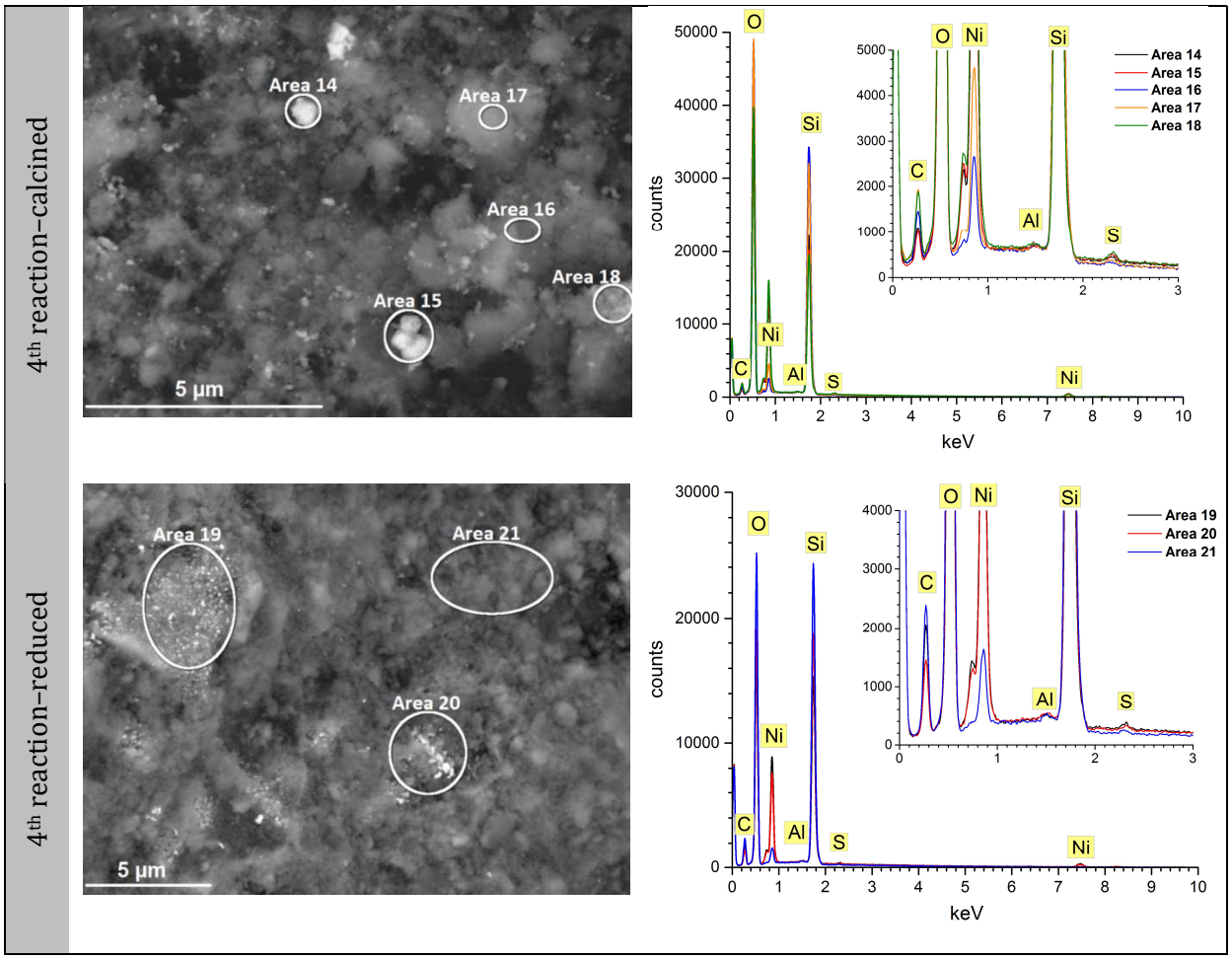

Figure 34. SEM-EDX images and spectra of Ni/SiO_2 along the consecutive cycles. Reproduced from reference [96] according to the terms of Creative Commons Attribution License.

Table 23. SEM-EDX scan composition of selected regions of Ni/SiO_2 over consecutive cycles. Reproduced from ref [96] according to the terms of Creative Commons Attribution License (CC BY).

Spectrum	C (wt.%)	Si (wt.%)	S (wt.%)	Ni (wt.%)
1 – Fresh Ni/SiO_2	4.1	41.5	-	3.1
2 – Fresh Ni/SiO_2	2.6	24.9	-	44.9
3 – 1st reaction (spent)	8.4	24.5	0.3	37.1
4 – 1st reaction (spent)	6.0	42.8	-	1.2
5 – 2nd reaction (spent)	8.2	29.3	0.4	19.8
6 – 2nd reaction (spent)	5.8	38.6	<0.1	0.6
7 – 3rd reaction (spent)	5.5	35.4	0.1	13.6
8 – 3rd reaction (spent)	7.61	38.1	-	-
9 – 4th reaction (spent)	14.1	32.5	-	4.2
10 – 4th reaction (spent)	10.1	37.0	-	1.0
11 – 4th reaction (spent)	14.2	27.5	0.1	17.4
12 – 4th reaction (spent)	12.3	32.8	-	7.7
13 – 4th reaction (spent)	14.7	32.8	-	0.7
14 – 4th reaction (calcined)	2.4	22.3	0.1	41.6
15 – 4th reaction (calcined)	2.3	21.0	0.2	45.2
16 – 4th reaction (calcined)	4.6	38.7	<0.1	1.4
17 – 4th reaction (calcined)	5.7	34.7	0.1	7.1
18 – 4th reaction (calcined)	4.5	20.6	0.3	37.5
19 – 4th reaction (reduced)	9.1	23.6	0.2	40.4
20 – 4th reaction (reduced)	6.8	28.9	0.2	33.8
21 – 4th reaction (reduced)	12.6	37.7	0.1	5.0

Following the fourth reaction, the catalyst was analyzed by SEM-EDX in three different situations— spent, after the calcination and, finally, after the reduction step. Although punctual analyses were performed (Table 23), some trends could be observed. Regarding carbon, an expected lower concentration was observed after the calcination step (spectrum 14–16), in comparison to the spent catalyst (spectrum 9–13). Furthermore, the sulfur remained over the reduced catalyst, mainly in the regions with higher nickel concentration, indicating a persistent adsorption. Further structural investigation along the cycles was obtained by XRD and, in this case, the catalyst was analyzed along each new regeneration cycle, in the spent, calcined and reduced forms (Figure 35). Metallic Ni reflection was observed in the fresh, spent and reduced catalysts along the consecutive reactions. Due to the calcination step, reflections attributed to NiO were observed which disappeared after the reduction. Considering the low concentration of sulfur over the spent catalyst surface, reflections attributed to Ni_3S_2 as found by other authors [53,193,194] were not observed, even after the fourth reaction.

An increase in the crystallite sizes could be observed, as also identified by other authors [53]. Ni/SiO_2 showed initially a crystallite size of 17.7 nm and increased to 21.0 nm after the reaction. Following subsequent regenerations, the crystallite size reached 37.3 nm (fourth reaction), due to particle sintering occurring after each reaction [180], in agreement with the SEM-EDX observations.

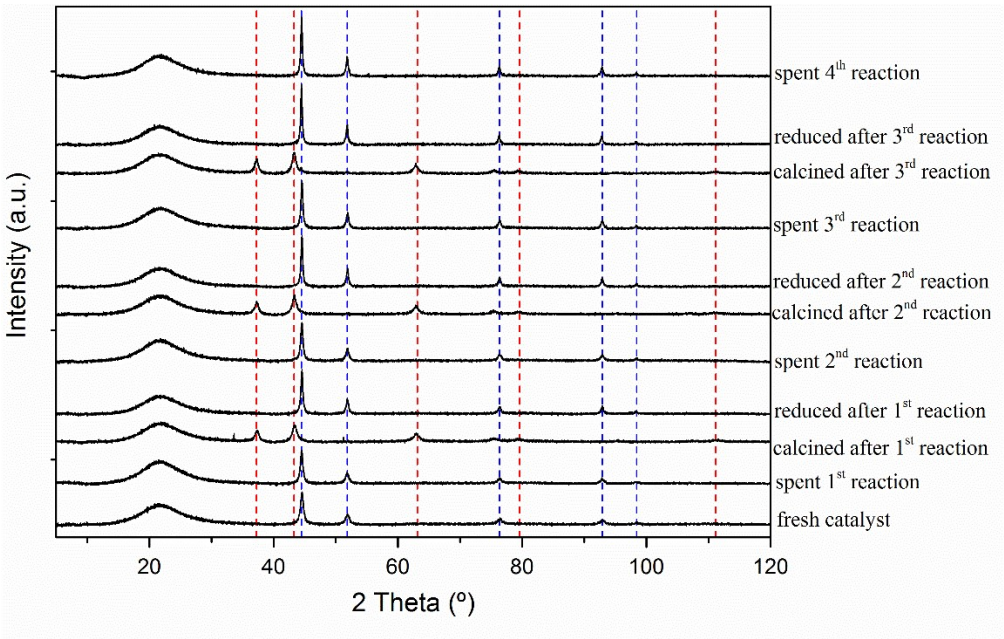

Figure 35. XRD pattern diffraction of Ni/SiO_2 catalyst along consecutive reactions and regeneration steps. Dashed blue lines refer to Ni and dashed red lines refer to NiO. Reproduced from reference [96] according to the terms of Creative Commons Attribution License.

Due to the small amount of sample available, the BET surface area was measured only after the fourth reaction (spent catalyst). The original catalyst had a surface area of 215 m^2/g of catalyst, reduced to 46 m^2/g after the first reaction and later to 39 m^2/g after the fourth reaction (spent catalyst), slightly lower compared to the first use. Furthermore, the amount of nickel leached to the light phase was calculated also. It could be noticed that along the cycles the amount of nickel leached was being reduced as follows: during the 1st reaction 0.8% of nickel was leached, followed by 0.6% in the 2nd, 0.12% in the 3rd reaction and, finally, in the 4th only 0.10% of nickel was leached.

The physicochemical properties of the upgraded bio-oils over consecutive reactions also were determined (Table 24). The carbon content remained above 72 wt.%, although a slight decrease was observed. The water concentration slightly increased after the second reaction, remaining in the same range over the following reactions (around 5.4 wt.%). The HHV and pH remained in the same range as observed in the reaction performed with the original catalyst. The oxygen concentration increased after the third reaction, reaching 20.35 wt.% after the fourth reuse of the catalyst. Similar tendencies were found by Boscagli et al. [53] evaluating the performance of regenerated catalysts, although, in their study, only one regeneration was considered and a different catalyst ($NiCu/Al_2O_3$) was used. As the number of consecutive reactions increased, the hydrogen consumption decreased, mainly between the first and second reuse. A reduction of 17.18% in the consumption of hydrogen between the original reaction and the first regeneration, 6.28% between the first and the second, and just 0.66% between the second and third regenerations was observed. The lower consumption of hydrogen indicates a decline in the hydrotreatment activity, which can be a result of the sintering, leaching and due to the poisoning substances [75] observed by XRD, ICP-OES and EDX measurements.

Table 24. Physicochemical properties, elemental analysis (in dry basis) of the upgraded bio-oil, hydrogen consumption and total gas production over consecutive HDO reactions and catalyst regeneration. Reproduced from ref [96] according to the terms of Creative Commons Attribution License (CC BY).

Property	1st reaction	2nd reaction	3rd reaction	4th reaction
Carbon (wt.%)	73.15	73.54	72.37	72.15
Hydrogen (wt.%)	8.42	8.25	8.51	8.55
Oxygen (wt.%)	17.86	17.74	19.00	20.35
Nitrogen (wt.%)	0.32	0.32	0.32	0.32
H_2O (wt.%)	4.85	5.4	5.5	5.3
HHV (MJ/kg)	31.18	30.92	31.11	31.26
pH value	3.6	2.8	3.5	3.4
H_2 consumption(NL/kg)	186.21	154.22	144.53	143.58
Gas production (mol/kg)	0.99	1.23	1.31	1.35

Furthermore, as the number of consecutive reactions increased, higher amounts of CO_2 were produced (Figure 36). Discussed previously, the consumption of hydrogen seems to be inversely proportional to the amount of CO_2 produced; Additionally, as the number of consecutive reactions

increased, the higher the amounts of CO, propene, ethane and ethene were produced, although less significant in comparison to CO_2. Methane remained constant along the cycles.

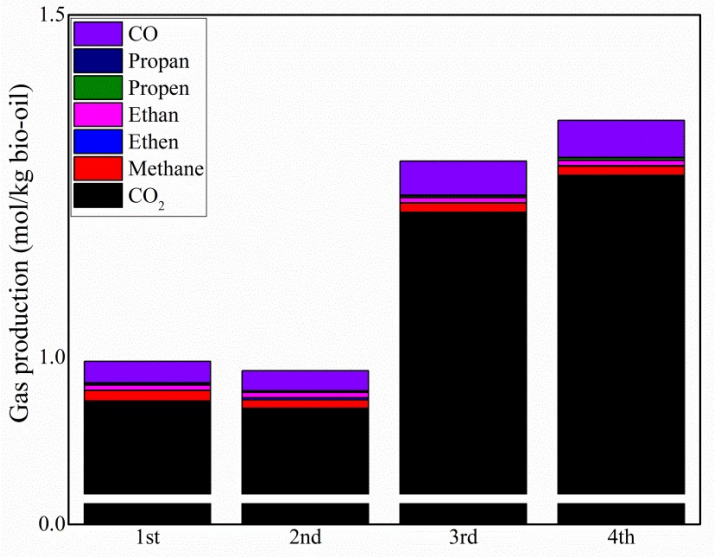

Figure 36. Gas composition obtained for the cycles of hydrotreatment-regeneration. Reproduced from reference [96] according to the terms of Creative Commons Attribution License.

The changes over consecutive reactions also were monitored by ^{1}H-NMR (Figure 37). Some trends observed for the original reaction also were observed along the cycles. The signal for aldehydes (10.1–9.5 ppm), already absent in the first reaction due to its high reactivity at low temperatures [180], was not observed in any of the phases for all regeneration stages. The highest signal for the upgraded bio-oil was found in the α protons to unsaturated, carboxylic acids and keto-groups (3.0–1.5 ppm) while, for the aqueous phase, it was located in the water, O-H exchanging and carbohydrate groups (6.0–4.3 ppm). Aromatics (8.5–6.0 ppm) mostly were concentrated in the upgraded bio-oil and almost absent in the aqueous phase (8.9 mmol/g sample versus 0.2 mmol/g sample on average). Dibenzenes, alcohols and ethers (4.3-3.0 ppm) were concentrated in the upgraded bio-oil (10.6 mmol/g sample versus 6.3 mmol/g in the aqueous phase on average). The same was observed for alkanes (1.5-0.5 ppm), 23.0 mmol/g bio-oil versus 1.1 mmol/g aqueous phase on average. Found in the upgraded bio-oil, it could be seen that the concentration of aromatics remained similar along the reactions. The values also were similar as observed for the feedstock (HP). A similar trend was observed for the carbohydrates, water and O-H exchanging groups. The increase in this region can be attributed to the higher water concentration in the upgraded products, as well as a lower conversion of compounds belonging to this region. As the number of reactions increased, the concentration of alcohols, ether and dibenzenes decreased. The α proton to unsaturated groups in the products was much higher in comparison to the feedstock. An increase of protons was observed until the second reaction, dropping in the following third and fourth reaction. Alkanes were also in higher concentration compared to the feedstock and the values were quite similar among all the reactions. Conversely, within the aqueous phase, the opposite tendency was observed for the carbohydrates,

water and O-H exchanging groups A decline along the regenerations was seen, probably due to the increase of the water content in the upgraded bio-oil. The signal for alcohols, ethers and dibenzenes also dropped, from 8.66 mmol/g after the first reaction to 5.19 mmol/g after the fourth regeneration. The signals for α proton to carboxylic acid or keto-groups, α proton to unsaturated groups, and for alkanes displayed a very small reduction after each reutilization of the catalyst.

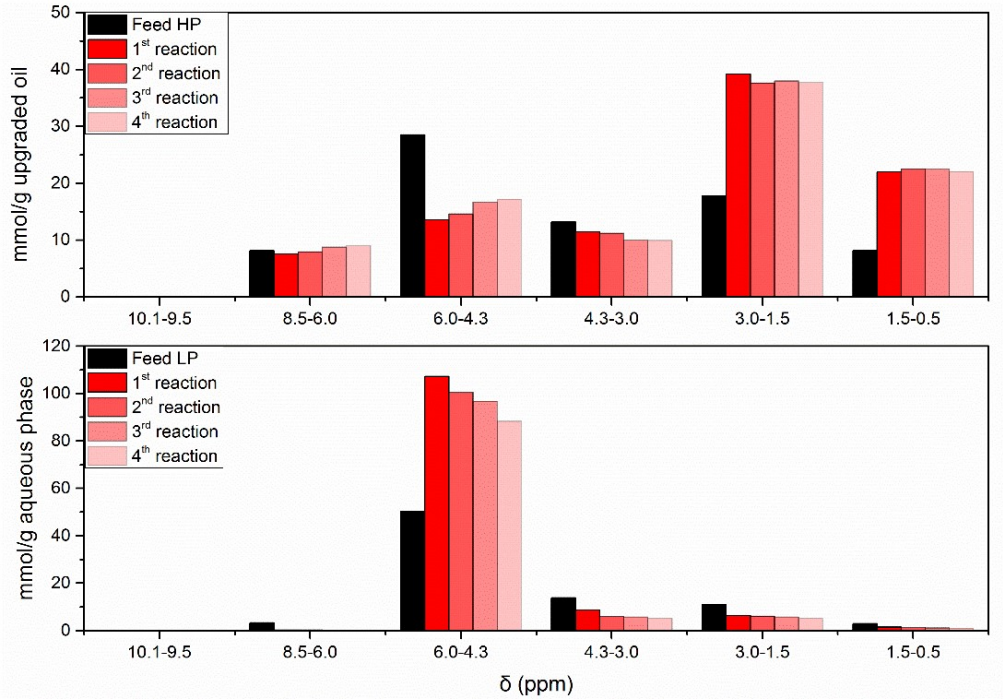

Figure 37. ^{1}H-NMR of upgraded bio-oil and HP (top) and aqueous phase and LP (bottom) along the HDO-regeneration cycles. Reproduced from reference [96] according to the terms of Creative Commons Attribution License.

Further qualitative investigation was performed with GC-MS. The composition of the upgraded bio-oils along the cycles was very similar, although some changes could be observed. The intensity of the peaks attributed to cycloheptanone (12.23 min) and 2-methyl-2-propanol (13.08 min) was reduced along the cycles. The same was observed for two more substances: dihydro-5-methyl-2-(3H)-furanone was being reduced until disappeared in the fourth reaction while a visible reduction in the γ-butyrolactone peak (18.4 min) was visible.

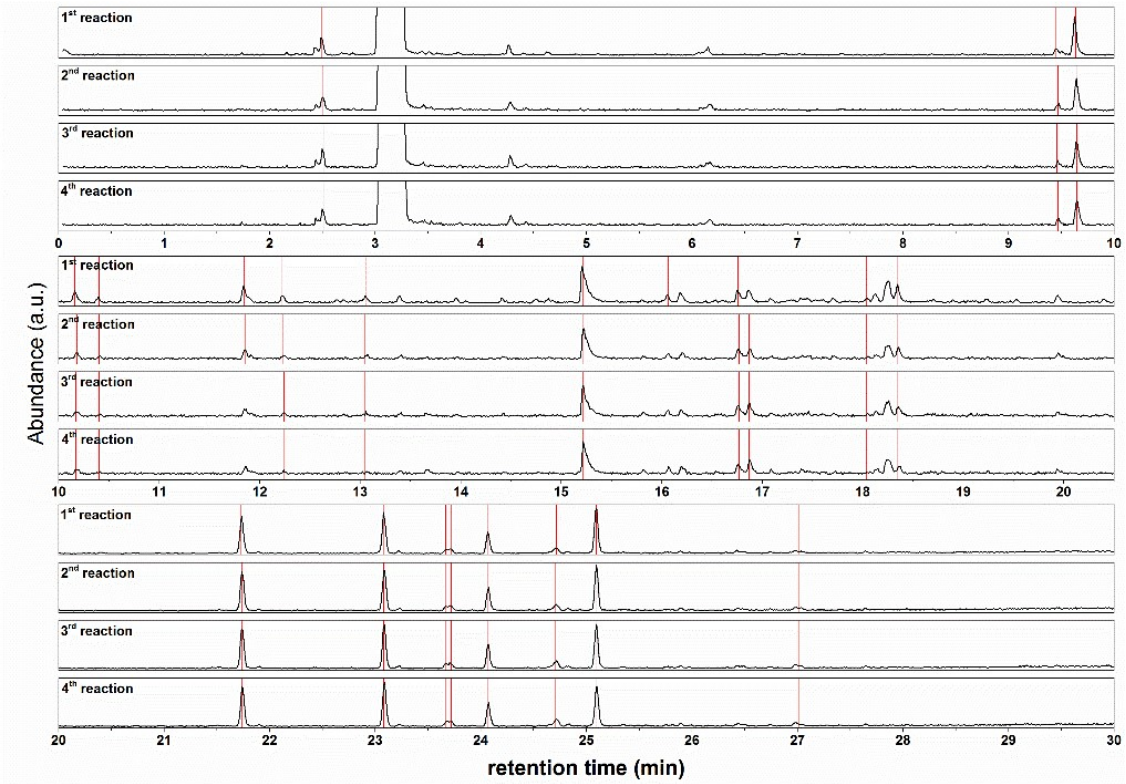

Figure 38. GC-MS upgraded bio-oil along the regeneration cycles. Reproduced from reference [96] according to the terms of Creative Commons Attribution License.

The dehydration of C6 sugars, such as glucose, results in compounds such as hydroxymethylfurfural [122]. The following conversion of hydroxymethylfurfural resulted in 5-(Hydroxymethyl)dihydro-2(3H)-furanone which was further converted to γ-valerolactone (Dihydro-5-methyl-2(3H)-furanone) through hydrogenation and direct deoxygenation [95]. Conversely, γ-butyrolactone is obtained through hydrogenation of 2(5H)-furanone [95]. These sugar derivative compounds then can be further converted to ketones and alcohols [65,122]. Based on these results, a correlation between ^{1}H-NMR and GC-MS could be proposed to explain these findings: Considering the higher signal obtained for the protons belonging to the carbohydrates, water and O-H exchanging groups, the current authors can assume that the upgraded bio-oils along the cycles showed higher concentration of not just of water, but also sugars, in comparison to the first reaction. Furthermore, based on the lower intensity of the GC-MS peaks of sugar derivative compounds, such as γ-valerolactone, γ-butyrolactone as well as 2-methyl-2-propanol, the current authors can assume that the conversion of sugars along the upgrading cycles is reduced. The peak intensity of 2-ethyl-cyclopentanone in the light phases (Figure S.24) is also reduced along the cycles. It also is evidence of lower conversion of sugars along the cycles, considering that this compound can be obtained from a compound with similar structure to furfural [93].

5.3.5 Discussion

The synthesis and evaluation of nickel-based catalysts showed differences among the catalysts evaluated. The temperature programmed reduction (H_2-TPR) showed that the catalysts, with the addition of copper as a promoter and higher loading of nickel, had a lower reduction temperature than the nickel oxides, which is in agreement with previous studies [133,168].

The evaluation of the catalysts for hydrodeoxygenation (HDO) reactions showed that upgraded bio-oil obtained with Ni/SiO_2 showed the best properties in terms of low oxygen concentration, low water concentration and high HHV (higher heating value). The higher HDO activity for this catalyst can be correlated to its higher surface area in comparison to the other catalysts tested in this study, which could be beneficial to increase the dispersion of the active components, resulting in a more active catalyst [82,191]. Coincidently, the ZrO_2-supported catalysts showed a lower HDO activity, which might be attributed to the lower surface area of this support [179]. Similar to the current study's findings, Dongil et al. [123] observed lower HDO activity for NiCu catalysts in comparison to monometallic Ni catalysts. The authors attributed the lower guaiacol HDO to the larger particle size, the presence of NiO particles as well as to copper particles located at the nickel active sites. Furthermore, a higher crystallite size of bimetallic catalysts, as observed for both NiCu catalysts, also might play a role in the lower HDO activity; the higher crystallite size decreases the number of step/corner sites, which, according to Mortensen et al. [52], are more active for breaking C-O bonds.

Coke formation is another important parameter for the selection of the catalyst. Observed for both Ni/SiO_2 and $NiCu/SiO_2$, the volume of the micropores was reduced significantly after the reactions. Coke is known for blocking the pores, covering the catalyst active sites, resulting in partial or even complete loss of activity [75], therefore, it is considered one of the main causes of deactivation in HDO reactions [34,52,65]. Considering that the catalyst acidity is connected directly to coke formation [34], the lower coke formation observed with Ni/SiO_2 could be related to the low acidity of silica [65]. Due to the amphoteric nature of ZrO_2, reduced coke formation would be expected [65]; However, SiO_2 was more resistant to coke formation. The addition of Cu also seems to contribute to the slightly higher amount of coke deposited on the bimetallic catalysts. Stated by Zhang et al. [179], the addition of copper increases the acidity of the catalyst, which can result in higher coke deposition [39], as observed. Hence, the lowest coke deposition observed for Ni/SiO_2 can be related to the lower acidity compared to $NiCu/SiO_2$ and higher resistance of SiO_2 in comparison to ZrO_2.

Reactive compounds, such as aldehydes, were converted completely after the upgrading. The reduction of these very reactive compounds results in a more stable oil [52,61]. The lower conversion of aromatic compounds over all the catalysts evaluated also is interesting; if further upgrading is

intended, aiming at fuel production, the presence of aromatic compounds could result in a high octane number gasoline [61].

Different selectivity among mono and bimetallic catalysts was attributed mostly to the addition of copper [122], with a minor contribution of nickel loading [101]. Furfural, also a very reactive compound [195], mainly seemed to be hydrogenated to tetrahydrofurfuryl alcohol over NiCu catalysts. Additionally, the presence of propylene glycol leads to the conclusion that hydroxy-acetone mainly was hydrogenated to this compound over bimetallic catalysts. Concurring with other authors, the addition of copper seems to increase the hydrogenation [123], increasing the hydrogen consumption. Furthermore, the higher hydrogen consumption observed for NiCu catalysts is in agreement with literature [71,99] giving evidence that the addition of a second metal can increase the hydrogenation activity of the catalyst [122]. Stated by Mortensen et al. [52], the H/C and O/C is used to evaluate the quality of the upgraded product. A higher H/C ratio is intended, whereas a lower O/C ratio is desired. During this case, it was observed that the higher H/C ratio for $NiCu/SiO_2$ agrees with the higher consumption of H_2 observed for this catalyst, but it was not reflected in the O/C ratio. The lowest O/C was obtained for Ni/SiO_2 (0.18) in fact, being much lower in comparison to the O/C ratio of the feed (0.47). It is important to note higher hydrogenation results in higher consumption of hydrogen [59,196], but it is not necessarily reflected in the reduction of the oxygen content. Moreover, the higher consumption of hydrogen also can result in higher methane formation [109], considering that during the hydrocracking the consumption of hydrogen is higher compared to hydrotreating [197]. This behavior was observed for $NiCu/SiO_2$. The catalyst showed not just the higher hydrogen consumption, but also a higher methane formation. The desired catalyst should be able to remove the larger amount of oxygen with minimal hydrogen consumption [123] as hydrogen consumption, bio-oil yield and catalyst deactivation are among the most important parameters to be considered in the HDO process [198]. Ni/SiO_2, therefore, was considered the more appropriate catalyst in terms of H_2 consumption and HDO activity.

Subsequent to the reaction, compounds such as calcium (only over ZrO_2) and sulfur were observed on the spent catalysts by two different analytical techniques, Inductively Coupled Plasma Emission Spectroscopy (ICP-OES) and Scanning Electron Microscopy/Energy Dispersive X-ray spectroscopy (SEM-EDX). Calcium, observed in higher concentrations in comparison to sulfur over the zirconia-supported catalysts, on the one hand acts as a poisoning agent, reducing the mobility and redispersion of the active metal centers over the support and, on the other hand, can reduce sintering, due to the reduction in the atom mobility, resistance to dissociation and migration [75].

Despite the detection of sulfur on the catalyst's surface, structural changes were not observed after the reactions by Powder X-ray diffraction (XRD), as observed in previous investigations.

Mortensen et al. [72] observed a reflection at approximately 2θ= 45.2°, attributed to NiS during the evaluation of the influence of sulfur over the conversion of guaiacol with Ni/ZrO_2. Boscagli et al. [53] observed the formation of Ni_3S_2, which was persistent to regeneration and changed the catalyst structure. The concentration of sulfur in the feed, in this case, varies significantly in both works. While Mortensen et al. used a model mixture containing 0.05 wt.% of sulfur, Boscagli et al. used feedstocks with a higher concentration of sulfur (light bio-oil phase with 0.05 wt.% of sulfur and straw bio-oil obtained at 450 °C with 0.3 wt.% of sulfur). The high concentration of sulfur resulted in a spent catalyst with a much higher concentration of sulfur on the catalyst (0.6–2.0 wt.%, SEM-EDX), in comparison to the current study's findings (feed sulfur concentration = 0.012 wt.% and spent catalysts = <0.1-0.4 wt.%, SEM-EDX). Even without structural changes, sulfur is one of the most persistent poisons for nickel catalysts. It is irreversibly chemisorbed and responsible for blocking the reaction-adsorption active site, modifying electronically the neighbor atom of metals and, thereby, reducing the ability to adsorb and dissociate H_2, at the same time influencing the diffusion or reactants, blocking their contact with the active site [75].

Along with the consecutive reactions with catalyst recycling, comparable carbon and hydrogen concentrations in the upgraded bio-oils and a slightly higher oxygen concentration was observed (20.34 wt.%) after the fourth reaction. It was higher compared to the first reaction (17.86 wt.%) but still much lower compared to the feed (35.84 wt.%, dry basis). It gives evidence of a low rate of deactivation and the reuse of the catalyst is possible. The increase in the oxygen concentration can be correlated with the reduction in the H_2 uptake, in agreement with lower HDO activity of Ni/SiO_2 in comparison to the fresh catalyst [54]. The current authors assumed that the reduced activity can be correlated mainly to sintering, poisoning and coke deposition (although easily removed during the calcination step), as the leaching was negligible. The crystallite size increased over the cycles in the same proportion that the HDO activity was reduced along the consecutive reactions. The fresh catalyst showed a crystallite size of 17.7 nm, reaching 37.3 nm after the fourth reuse. Thus, the number of active surfaces available were reduced with the increase of the crystallite size [75]. Furthermore, the lower H_2 uptake also can result in a higher amount of CO_2 formation, as observed along the cycles, considering the higher the hydrogen uptake, the lower the CO_2 production [88]. Curiously, the sulfur concentration remained approximately constant along the cycles. Furthermore, no differences were observed in the XRD diffractions. The current authors concluded that sulfur was strongly adsorbed on the catalyst, affecting surface-sensitive reactions, resulting only in partial loss of activity of the catalytic surface [75].

The results obtained by ^{1}H-NMR showed that the concentration of protons in the region related to water and carbohydrates increased along the cycles. Moreover, the gas chromatography-mass spectrometer (GC-MS), showed that the peak of some sugar derivatives became smaller over the

consecutive cycles. It was assumed that the catalytic conversion of sugars was affected by the lower activity of Ni/SiO_2 along the cycles. This assumption corroborates the results of GC-MS, from which the intensity of sugar derivative compounds (γ-valerolactone γ-butyrolactone 2-ethyl-cyclopentanone 2-methyl-2-propanol) have been reduced as the number of cycles increased. Considering the assumption that the conversion of sugars through hydrogenation is reduced with the increase in the number of consecutive reactions, higher amounts of coke formation could be expected, considering that the thermal polymerization of the sugar fraction can lead to increased char deposition [37,88,175] over the cycles. The results of SEM-EDX showed a slightly higher carbon deposition over the spent catalyst after the fourth reaction.

Since poisoning substances might affect some specific reactions [75], the investigation of model compound conversions as well as the effect of poisonings, over single compounds, could contribute to the understanding of the selectivity changes observed along the cycles. Considering the difficulty for regeneration of sulfur-poisoned catalysts, due to the harsh conditions required (700 °C in steam) [75], its influence over the conversion of model compounds should be investigated in detail. Since deactivation mechanisms are difficult to be monitored in batch experiments [72], continuously operated reactors are more appropriate for this investigation.

5.4 Conclusion

Four nickel-based catalysts on different supports were synthesized and evaluated for the HDO of a multi-phase beech wood fast pyrolysis bio-oil. The bimetallic catalysts showed lower reduction temperature, attributed to the addition of copper and higher metal loading. Furthermore, NiCu catalysts presented higher consumption of hydrogen and different selectivity toward the conversion of compounds such as furfural, compared to monometallic catalysts. Upgraded bio-oils with reduced concentration of oxygen, lower water concentration and higher carbon content were obtained after the HDO reactions. Ni/SiO_2, in particular, showed the highest HDO activity, reducing more than 50 % of the oxygen content and more than 80% of the water content, thus selected for application in cycles of regeneration-reaction. During the consecutive reactions, the activity of the catalyst decreased, attributed mainly to sintering and poisoning by sulfur, as coke was removed easily during the regeneration steps. Lower hydrogen consumption and higher carbon dioxide production were observed in comparison to the reactions when applying the fresh catalyst. Correlating the results obtained by ^{1}H-NMR and GC-MS, it was possible to observe that compounds known as sugar derivatives were being reduced along the consecutive reactions at the same time that the concentration of protons in the region attributed to water, carbohydrates and O-H exchange was increased. The partial loss of activity seemed to lower the conversion of sugars.

Accompanying that, the catalysts evaluated seemed to be suitable for HDO of hardwood fast pyrolysis bio-oil, especially Ni/SiO_2. Further investigation will be addressed, considering a detailed investigation of model compound conversions and the effect of sulfur and calcium over HDO of single compounds. The influence of sintering over the activity and selectivity will be investigated also. Due to the limitation of the batch reactor for deactivation mechanism studies, the application of a trickle bed reactor in future studies is intended.

Chapter 6. From agriculture residue to upgraded product: The thermochemical conversion of sugarcane bagasse for fuel and chemical products

Chapter redrafted after:

Schmitt, C. C., Moreira, R., Neves, R.C., Richter, D., Funke, A., Raffelt, K., Grunwaldt, J.D., Dahmen, N. (2020). From agriculture residue to upgraded product: The thermochemical conversion of sugarcane bagasse for fuel and chemical products. Fuel Processing Technology, 197, 106199.

Declaration of contributions:

Caroline Carriel Schmitt performed the experimental design, conducted part of the experiments, analyzed the data, discussed the results and wrote the manuscript.

Renata Moreira and Renato Cruz Neves selected, prepared and characterized the biomass.

Daniel Richter and Axel Funke performed the fast pyrolysis experiments

Klaus Raffelt, Jan-Dierk Grunwaldt and Nicolaus Dahmen supervised the work, contributed to the discussion and corrected the manuscript.

List of abbreviation – Chapter 6

DOD: degree of deoxygenation

E.P: Electrostatic precipitator

FPBO: Fast pyrolysis bio-oil

IUP: Intermediate upgraded phase

$IUP_{Ni\text{-}Cr/SiO2}$: upgraded intermediate phase using benchmark Ni-Cr/SiO_2 catalyst

SCB: sugarcane bagasse

SCBPO: sugarcane bagasse fast pyrolysis bio-oil

ULP: upgraded light phase

$ULP_{Ni/SiO2}$: upgraded light phase using Ni/SiO_2 catalyst (7.9 wt.% Ni, synthesis Chapter 5)

$ULP_{Ni\text{-}Cr/SiO2}$: upgraded light phase using benchmark Ni-Cr/SiO_2 catalyst

UOP: upgraded oil phase

$UOP_{Ni/SiO2}$: upgraded oil phase using Ni/SiO_2 catalyst (7.9 wt.% Ni, synthesis Chapter 5)

$UOP_{Ni\text{-}Cr/SiO2}$: upgraded oil phase using benchmark Ni-Cr/SiO_2 catalyst

Abstract Chapter 6

A holistic investigation considering the sugarcane bagasse characterization, fast pyrolysis and upgrading of bio-oil applying two nickel-based catalysts is presented. The bio-oil composition is correlated to the bagasse building blocks, and the hydrotreatment reaction pathways are identified. Despite the high ash content of 6.75 wt.%, 54.6 wt.% of bio-oil was obtained by fast pyrolysis, attributed to low concentration of potassium (0.08 wt.%) and low humidity (2.80 wt.%) observed in the bagasse. Upgraded bio-oil with 60.3 % less water and 43.3 % less oxygen was obtained with Ni/SiO_2, resulting in an HHV 63 % higher compared to bagasse. $Ni\text{-}Cr/SiO_2$ showed the highest hydrogenation activity and the highest conversion of acids, converting 25.7 % of acetic acid and 14.95 % of propionic acid while Ni/SiO_2 was more active for conversion of compounds containing aromatic groups. The higher viscosity of upgraded oils in comparison to the fast pyrolysis bio-oil indicates that the stabilization during the heating ramp can be improved to suppress polymerization. Hence, sugarcane bagasse is an attractive feedstock with an overall final yield of 30.5 wt.% of the upgraded product.

6.1 Introduction

Sugarcane crops play a significant role in sugar and ethanol production worldwide. The annual production around the globe was recently estimated in approximately 1.6 billion tons [199] tons, mainly used for sugar and ethanol production by fermentation (first generation ethanol, 1G). Brazil, considered the biggest sugarcane producer in the world, has an approximate production in 2018/2019 of 635.51 million tons of sugarcane with 30.41 billion of litre of ethanol produced [200]. Considering that for each ton of sugarcane produced, 0.28 tons of sugarcane bagasse (SCB) are generated as byproduct [201], 448 million tons of bagasse are generated annually worldwide. Approximately 178 million tons are generated in Brazil. Usually the bagasse is destined for bioelectricity generation, mostly used in the production unit, with the surplus transferred to the electric grid [202,203]. New alternatives have been studied in the last years, in order to use the sugarcane bagasse as a feedstock for ethanol production, so called second generation (2G) ethanol by making use of the feedstock´s polycarbohydrates. Conventional 1G ethanol production is relatively simple compared to the complex 2G ethanol production, which requires first separation from the lignin fraction, hydrolysis and then the fermentation of monomeric sugars to ethanol [204,205]. Many efforts are being dedicated in order to reduce the costs and increase the efficiency of the second generation ethanol [203,204].

An alternative for biochemical sugarcane bagasse conversion is the 2G thermochemical conversion, e.g. by fast-pyrolysis. To carry out fast pyrolysis, the dry biomass (moisture content below 10 wt. %) is ground to a particle size of <3 mm, thermally decomposed at approximately 500 °C in inert atmosphere with a hot gas residence time of a few seconds, resulting in a fast pyrolysis bio-oil (FPBO) as the main product [23,206]. FPBO is a brown liquid with high water content and high viscosity [1]. In contrast to fermentation products, the pyrolysis oil is composed of hundreds of oxygenated compounds such as carboxylic acids, ketones, aldehydes, alcohols, phenols, sugars, ethers, and esters already identified [1,8,33,52]. FPBO can be used to supply power and heat or it can be further processed towards fuel and chemical products [23,52].

Relatively clean (i.e. ash-free) wood is the state-of-the-art feedstock for industrial applications of fast pyrolysis. A variety of other types of biomass have been applied as feedstocks for FPBO production, such as wheat straw [16], corn stover [207], palm empty fruit bunches [208] and many other biomasses such as pine wood or switchgrass and rice straw [9]. Some studies performed with sugarcane bagasse do exist for the case of slow pyrolysis [208–210], but there is little information on fast pyrolysis of SCB [206].

Although the use of different types of biomass results in FPBOs with different composition [23,37,208], in general, the FPBO show similarities. FPBO has approximately half of the heating value of crude oil, shows high acidity (pH value below 3), high water concentration (15-35 wt.%),

polymerization due to secondary reactions which results in aging phenomena, and high oxygen content (35-50 wt.%), which limits its direct application as boiler fuel [1,8,23]. Consequently, if application as a transportation fuel or even some chemicals in the context of a bio-based refinery is targeted, upgrading is required.

Different strategies are used for FPBO upgrading and conditioning: solvent addition for viscosity reduction, emulsification or extraction with diesel fuel, esterification, hydrotreatment and others [23]. The hydrotreatment is performed at high pressures of hydrogen, and applying catalysts aiming at stabilization and hydrodeoxygenation of the FPBO [8,39]. In this way, the FPBO can be practically completely deoxygenated to hydrocarbons and/or partially deoxygenated to a range of fuel intermediates or profitable chemicals [8,33,81]. Hence, the catalyt plays an important role in the hydrotreatment reactions. For that reason, the choice and development of catalyst for FPBO hydrotreatment has been a subject of many investigations. Particularly nickel-based catalysts showed to be active for conversion of model compounds [82,103,196,211] and fast pyrolysis bio-oil of different feedstocks [96,102]. Additionally to the low cost, high degree of deoxygenation, possibility of inclusion of promoters in the catalyt formulation whether for different selectivity [131] or higher resistance to poisoning substances and deactivation [212] have been previously reported as advantages of nickel-based catalysts.

Although some groups have already considered the pyrolysis of sugarcane bagasse, only very few have worked on the hydrotreatment of the liquid product fraction [213] and up to now not considered the whole process chain from SCB. However, this represents an essential step in order to evaluate the viability of the 2G thermochemical conversion integration to the 1G ethanol unit depicted in Figure 39. The use of SCB is especially advantageous in comparison to other biomasses or sugarcane leaves, as it is already centrally collected in the sugar mill. Sugarcane leaves are usually left in the field, which would require an efficient and cheap collection system [204,214]. Hence, the centralized sugarcane conversion unit would be beneficial from an economic point of view, allowing bigger scale units, without the need to transport the feedstock or an intermediate product, as usually suggested for biomass derived bio-oils production [37]. Additionally, the high concentration of lignin (17-32 wt.%) [214,215], considered a limitation for carbohydrate hydrolysis [214] makes the sugarcane bagasse especially interesting for thermochemical valorisation [2], as not just hydrocarbons but also funcionalized aromatics monomers are interesting target products [81]. This approach is especially relevant for countries such as Brazil, with record production of sugarcane ethanol in 2019 and perspective of increased production until 2030 [216]. The high volumes of agriculture residues generated, can undergo thermochemical conversion followed by hydrotreatment, resulting in products with potential to be blended to aviation kerosene, in the concentration of 10 %, as defined by the Brazilian national biofuel policy (RenovaBio) for 2030 [217]. Furthermore a new range of

functionalized chemicals, i.e. functionalized aromatic compounds can be produced, expanding the range of chemicals obtained in the sugarcane refinery.

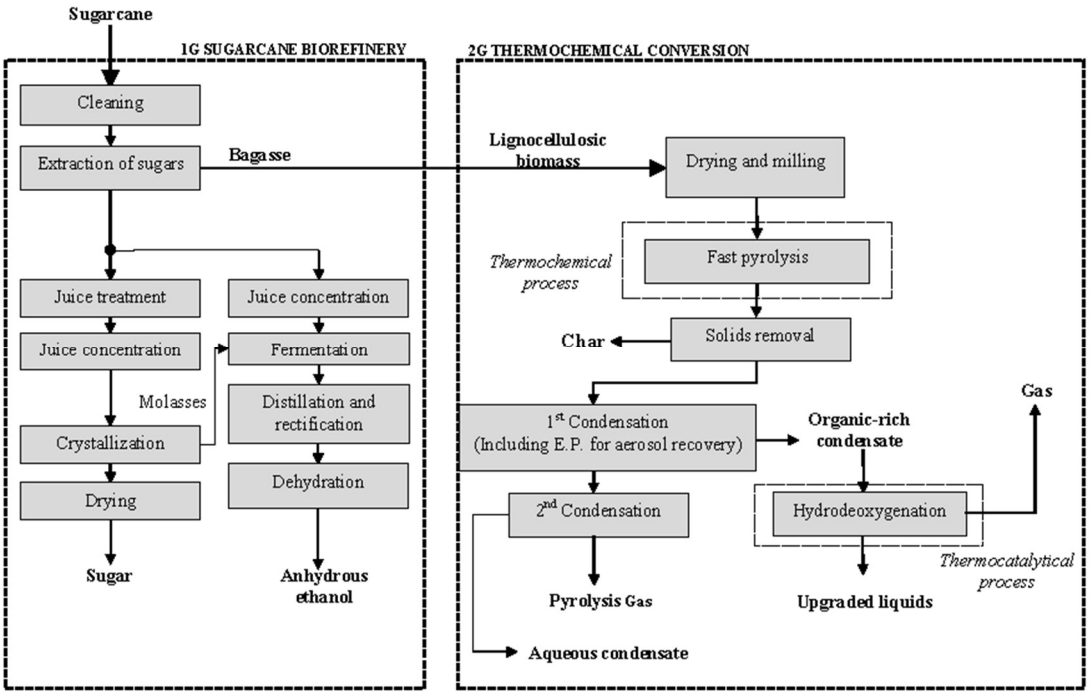

Figure 39. Integration of 1G and 2G thermochemical conversion route for sugarcane biorefinery. E.P: Electrostatic precipitator. Reproduced from reference [85] according to the terms of Creative Commons Attribution License.

The aim of this study is to present for the first time a comprehensive investigation, from the bagasse characterization, followed by fast pyrolysis and hydrotreatment to the final upgraded products. The experimental work is conducted in the same laboratory and analytical methods are aligned so that maximum consistency is achieved. Specific focus is set on conversion of SCB by fast pyrolysis to maximize organic liquid yield, subsequent hydrotreatment of the produced FPBO, correlation between the sugarcane bagasse building blocks and the main compounds observed in the bio-oil. Additionally, the main chemical reactions taking place during the hydrotreatment are identified and discussed. This approach allows identification of feedstock specific characteristics, advantages, and disadvantages of the whole process chain.

6.2 Materials and methods

6.2.1 Sugarcane bagasse collection, preparation and characterization

The sugarcane bagasse was collected at Iracema biorefinery, located in Iracemápolis, São Paulo, Brazil, in June, 2016. The SCB was pre-dried at 105 °C overnight (FABBE oven) to a moisture content of 46.2 %. This procedure was performed at IUT (Institute for Technological Research, São Paulo, Brazil). In the sequence, the samples were shipped to Germany in plastic bags.

The SCB was further dried in Germany for 3 days at room temperature (moisture content below 10 wt.%), chopped (Viking GE260) and milled to ≤ 2mm with a cross-beater mill SK100. Approximately one third of the sample was further milled to fine powder using a cryogenic mill (Freezer/Mill® Cryogenic grinder 6875), in order to be characterized in terms of moisture and ash content, elemental analysis, volatile matter, higher heating value and major elements. Pictures of dry and milled SCB are depicted in the Supplementary Material (Figure S.28 a and S.28 b).

The moisture and ash content were determined using a thermogravimetric analyzer (TGA 701, LECO). For moisture determination, the sample was maintained at constant temperature of 105 °C in air until constant weight (mass loss is then attributed to the sample's moisture content). The ash content was obtained under the following conditions: the sample was heated from ambient to 250 °C at a heating rate of 4.5 °C/min and maintained at this temperature for 30 min. In the sequence, the SCB was heated to 550 ºC ± 10 °C at a heating rate of 10 °C/min and maintained at this temperature for 120 min. The residue is then considered as the ash content.

The volatile matter content was obtained placing 1 g of sample for seven min in a furnace (Nabertherm model LV9/11) at 900 °C ± 10 °C in inert atmosphere. The volatile matter is the difference between the sample's weight before and after the thermo treatment.

The higher heating value (HHV) was determined using the calorimeter IKA C 5000 at 25 °C and at constant volume. Carbon, hydrogen and nitrogen content were determined using a CHN 628 Leco. Sulfur content was obtained by Eltra CS-2000 elemental analyzer. The concentration of oxygen was calculated by difference, as follow:

$$[O]_{wt.\%}=100 - ([C]_{wt.\%}+ [H]_{wt.\%}+ [N]_{wt.\%}+ [S]_{wt.\%} + [ash]_{wt.\%}) \quad \text{Equation (1)}$$

The fixed carbon content (FC) was obtained by the difference considering the moisture, ash and volatile matter content.

$$FC_{wt.\%}= 100 – M_{wt.\%} - A_{wt.\%} - VM_{wt.\%} \quad \text{Equation (2)}$$

Where M is the moisture content, A is the ash content and VM is the volatile matter content in weight percent.

Major inorganic elements (Al, Ca, Fe, Mg, P, K, Si, Na and Ti) present in the SCB were quantified by ICP-OES (Agilent 725, Inductively Coupled Plasma Emission Spectrometer). The samples were prepared by microwave digestion (Anton Paar, Multiwave 3000) by mixing approximately 0.5 g of dry bagasse with 6 ml of HNO_3 (65 vol.%, Merck Millipore), 2 ml HCl (37 vol.%, Merck Millipore), 1 ml HF

(40 vol.%, Merck Millipore) and 0.5 ml of H_2O_2 (35 vol.%, Merck Millipore). The digestion is performed at 240 °C for 1 hour.

Additionally, the SCB was characterized by Py-GC/FID (pyrolysis gas chromatography/flame ionization detector) and by Py-GC-MS (pyrolysis gas chromatography/mass spectrometer) at Instituto Superior de Agronomia (ISA), University of Lisbon, Portugal. For the Py-GC/FID measurements, approximately 76 mg of sample was pyrolyzed by a CDS Pyroprobe 1000 (650 °C, 10 seconds), coupled to a gas chromatograph (Agilent 7820) by a heated interface at 270 °C. The compounds were injected at 270 °C (split 1:20), separated in a low/mid-polarity column (J&W Scientific DB-1701, 60 m x 0.25 mm x 0.25 μm), and detected by a FID detector at 270 °C. The oven was programmed starting at 45 °C for 4 min, heated to 270 °C at a heating rate of 4 °C/min and kept at this temperature for 6 min. The area of each peak was used for quantification of compounds [218]. The qualitative analysis of the pyrolysis products was performed by a HP 6890 connected to an Agilent 5973 MS detector (sample pyrolysed by a CDS Pyroprobe 100 as described previously). The compounds were identified by comparison with literature and the NIST library. More information regarding the methodology can be found elsewhere [219].

6.2.2 Fast pyrolysis

The SCB conversion was performed at the Python process development unit located at the Institute of Catalysis Research and Technology, Karlsruhe, Germany. More details regarding the fast pyrolysis unit (feedstock conversion capacity of 10 kg/h of biomass) as well as the method description can be found elsewhere [26]. The dry biomass was used as obtained from <2 mm screening after milling in a cross beater mill. In the pyrolysis unit, the feedstock was mixed with preheated heat carrier (1 mm steel beads) in a twin-screw mixer reactor. The mechanical mixing is designed to ensure the high heating rate required for fast pyrolysis at around 500 °C [13,220]. After pyrolysis, solids are recovered from gas cyclones at reactor temperature before the gas phase is recovered from two condensers. The first condenser is designed as a quench system to instantly cool down the gas phase from reactor temperature to around 90 °C. In this stage an organic-rich condensate is collected, further cooled down and recirculated to act as quenching medium for the incoming hot pyrolysis vapour. The second condenser is operated at ambient temperature at around 20 °C to obtain the water rich aqueous condensate. The condensate is also recirculated to the condenser after cooling to form a film inside its tube bundle, i.e. there is direct contact of incoming pyrolysis gas and recirculated condensate. The remaining non-condensable gas is vented after analysis by a GC/FID (Emerson, Daniel Modell 700).

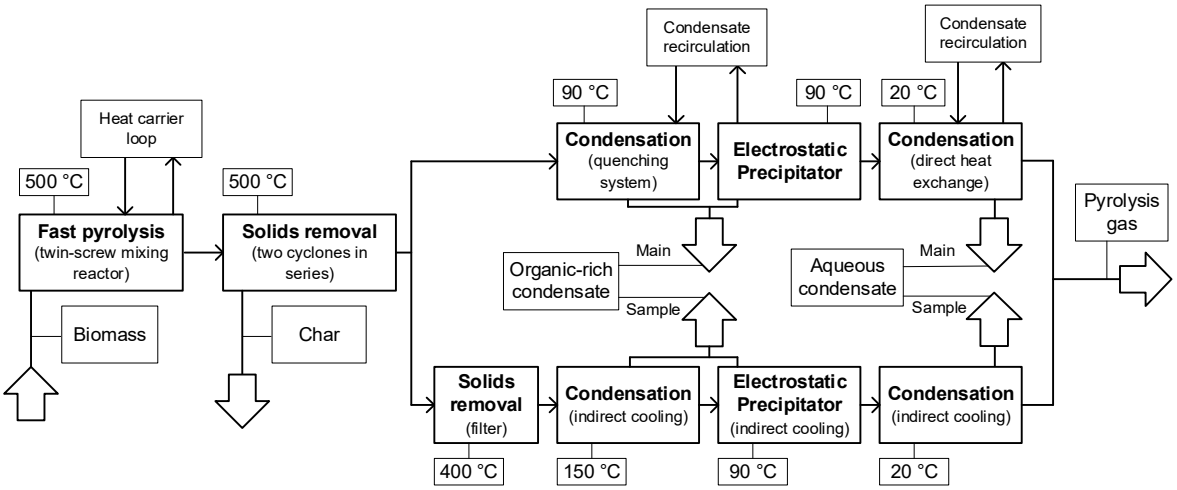

Figure 40. Block flow scheme of the pyrolysis and the product (upper line) and sample (lower line) recovery system. Reproduced from reference [85] according to the terms of Creative Commons Attribution License.

The FPBO samples collected for subsequent hydrotreatment have been obtained from a modified condensation system which was operated parallel to the main pyrolysis product flows (see Figure 40). The reason for this procedure is the fact that both condensation loops require a start-up material to initiate condensation (ethylene glycol and water for first and second condenser, respectively). This start-up material is not being displaced during one experimental day and thus represents a significant fraction of the obtained FPBO. The results of hydrotreatment would inevitably be obscured by the start-up material. Instead, hot pyrolysis gas is extracted between the cyclones and the first condensers at reactor temperature and condensed by indirect cooling. In this sampling train, hot gases initially pass a ceramic filter (operated at 400 °C) to remove remaining particles. Most of the sensible heat is removed in a jacketed tube operated with cooling water. The gases leave this condenser at around 100-150 °C despite the low cooling temperature. This first condensation step is followed by an electrostatic preciptator where aerosols are removed and the gas further cools down to the desired temperature (around 90 °C in analogy to the first condensation stage in the main system). Condensate of the first two condensation steps is merged in one collection vessel and represents the organic condensate. The aqueous condensate is obtained subsequently in a condenser with a cooling coil (operated at 4 °C) so that the outlet gas leaves slighly below 20 °C. Remaining gases are merged after the final condensation step and vented after analysis.

For subsequent hydrotreatment, only the organic condensate (Figure S.28 c), obtained at 90 °C from the sampling train is used and further denoted as sugarcane bagasse fast pyrolysis bio-oil (SCBPO).

6.2.3 Hydrotreatment Reactions conditions and analysis

In order to upgrade the SCBPO, batch reactor experimentss using different catalysts were performed. The hydrotreatment was performed using a self-designed and built 200 ml autoclave. The catalysts as well as the upgrading condition (325 °C and 90 bar of H_2) were selected as reference case used in our previous investigations [96,116]. Two Ni-based catalysts, one commercially available and the other prepared by wet impregnation technique at IKFT, were used for the upgrading reactions. The commercially available catalyst is composed of 30 wt.% of Ni, 26 wt.% of NiO, 1.5 wt.% graphite and 15 wt.% of Cr_2O_3, supported on diatomaceous earth (mainly composed by SiO_2) with a specific surface area of 94 m^2/g. The commercially available catalyst is denoted as Ni-Cr/SiO_2 in the following. The second catalyst, denoted Ni/SiO_2 (7.9 wt.% Ni, specific surface area of 215 m^2/g), was prepared by wet impregnation in a rotary evaporator (Hei-VAP Advantage ML/G3). More details are given in Chapter 5.

Approximately 50 g of SCBPO was mixed with 2.5 g of catalyst in the autoclave. The mixture was purged with nitrogen for 5 min and then pressurized with H_2 (Air Liquide ALPHAGAZ 2, 6.0) at ambient temperature to 90 bar. The reactor was heated at 5 °C/min until 325 °C and constantly mixed along the reaction (gas injector stirrer at 1000 rpm). The overall reaction time was around 120 min, including the heating ramp. Due to the limited amount of SCBPO, a single hydrotreatment reaction was performed for each condition tested. Once the reaction was finished, the reactor was cooled down with a flow of compressed air to approximately 50 °C and further cooled down to ambient temperature (approximately 25 °C) using an ice/water bath. A gas sample was collected for quantification of the main gaseous products and hydrogen by gas chromatography (GC-TCD/FID Agilent 789A, columns Restek 57096 and Resteck Molsieve 5A). More information is given in the Chapter 4. In addition, the H_2 consumption was calculated using the ideal gas equation, the hydrogen concentration given by GC-TCD/FID as well as the reactor's pressure registered before and after reaction [180]. The remaining liquid and solid fractions were collected, centrifuged (7000 rpm, 40 min, Thermo Fisher Heraeus Biofuge Stratos) and separated. The reactions conducted with Ni/SiO_2 resulted in two upgraded liquid phases, a light phase (ULP) and heavier oil, denominated upgraded oil phase (UOP). The reactions conducted with Ni-Cr/SiO_2 resulted in three liquid phases: ULP, an intermediate phase (IUP), and UOP. The liquid samples (ULP, IUP, UOP as well as SCBPO) were characterized in terms of elemental analysis (CHN 628 Leco), pH (Metrohm pH-meter 691), water content (Metrohm, Karl Fischer Tritando 841), higher heating value (IKA C 5000 1/10 Control Calorimeter) and sulfur (Agilent Inductively Coupled Plasma Emission Spectrometer 725). The higher heating values presented in dry basis were calculated based on Channiwala's equation [143]:

$$HHV(MJ/kg) = 0.3491\times C + 1.1783\times H - 0.1034\times O - 0.0151\times N + 0.1005\times S - 0.0211\times ash \quad \text{Equation (3)}$$

In order to further understand the chemical composition of the upgraded liquids in comparison to the SCBPO, a qualitative investigation was performed by GC-MS HP G1800A. The samples were prepared by dilution in methanol (1:20 or 1:10), filtrated (0.25 μm polytetrafluoroetylene filter) and 1 μl was injected at 250 °C (injector temperature) with split of 1:20. The oven was programmed to start at 40 °C maintained for 5 min, heated at a rate of 8 °C/min to 250 °C and maintained at this temperature for 10 min. The separation of the compounds was performed by a Restek stabilwax column (30 m x 0.25 mm x 0.25 μm).

A quantitative analysis of the main compounds in the SCBPO as well as in the upgraded products was performed by GC-MS/FID. The measurement was conducted at Thünen Institute in Hamburg, Germany. A volume of 1 μl of sample containing fluoranthene as internal standard was measured in a HP 6890. The sample is injected splitless at 250 °C (injector temperature), in a 14% cyanopropyl-phenyl-methylpolysiloxane column (60 m x 0.25 mm x 0.25 μm). The oven temperature started at 45 °C maintained for 4 min, heated to 280 °C at 4 °C/min and maintained at this temperature for 20 min. The GC was equiped with two parallel detectors: a FID and a MS detector (HP 5972). The qualitative analysis was performed comparing the compounds spectra with a NIST and a home-made library. Further information about the methodology can be found elsewhere [221].

Additionally measurements of viscosity, molecular weights, number average (Mn) and weight average (Mw) and polydispersity (Mw/Mn), obtained by Size Exclusion Chromatography (SEC) were performed. The dynamic viscosity measurements were conducted at Institute for Mechanical Process Engineering and Mechanics at KIT, using an Anton Paar rheometer at 40 °C. The SEC was performed at DWI Leibniz Institute for Interactive Materials in Aachen, Germany. The measurement was conducted using an HPLC pump (1260 Infinity II, Agilent), an UV-detector (UV-2075plus, Jasco), a refractive index detector (1290 Infinity II, Agilent) and a multi angle light scattering (MALS) (SLD 7100, Polymer Standards Service). Further information is available in the Supplementary Material (S.6.9).

The solid samples (composed by spent catalyst and solid residue), were separated from the liquid fractions by centrifugation. The residual solid in the autoclave was washed with acetone, collected and mixed with the solid from centrifugation. The samples (solid from autoclave + centrifugation), were then vacuum filtrated and washed several times with acetone, until all remaining UOP was completely removed. The spent catalyst was analyzed in terms of elemental composition, using the same methodology described for the liquid samples. Sulfur, nickel and chromium concentration were determined by ICP-OES sample preparation using a mixture of 2 ml of HNO_3 (37 %, Merck Millipore), 6 ml of HCl (37 %, Merck Millipore) and 0.5 ml of H_2O_2 (35 %, Merck Millipore), followed by digestion in a Anton Paar, Multiwave 3000 microwave oven for 45 min at 240 °C) and crystalline structure analysis by powder X-ray diffraction (spectrometer X'Pert PRO MPD PANalytical

instrument, cooper anode Cu Kα 1.54060 Å). The measurements were recorded in a 2 theta range of 5° to 120° for 1h (step size 0.017°). The Scherrer equation was used for determination of the crystallite size (shape factor K= 0.9) after line broadening. Additonally, the fresh Ni-Cr/SiO_2 catalyst was analyzed by temperature programmed reduction using an Autochem HP 2950 (Micrometrics). The sample was previously dried in-situ in Ar flow of 30 mL/min for 3 hours at a constant temperature between 200 °C. For the measurements a flow of 30 ml/min of 5% H_2 in Ar was applied and a heating rate of 1 K/min until 400 °C. A mass spectrometer (MKS Cirrus 2) was used for recording TPR profiles. The H_2-TPR of Ni/SiO_2 can be found elsewhere [96]. The solid deposition over the catalyst was determined considering that it is mainly composed by carbon, as other compounds are considered negligible [88,96]. The carbon content in the spent catalyst, determined by elemental analysis (micro-elemental analyzer Elementar Vario el Cube) was used for the calculation as follow:

$$m_{solid} = ([C_{spcat}]_{wt.\%} \times m_{cat})/(100-[C_{spcat}]_{wt.\%}) \quad \text{Equation (4)}$$

Where the m_{solid} is the mass of coke (g) in the spent catalyst; $[C_{spcat}]$ is the carbon deposited on the spent catalyst (wt.%) obtained by elemental analysis and m_{cat} is the amount of catalyst (g) loaded to the reactor.

6.3 Results

6.3.1 Sugarcane bagasse characterization

The analytical results including the proximate and elemental analysis, inorganic compounds and other physicochemical properties are presented in Table 25.

Table 25. Characterization results for the sugarcane bagasse. Reproduced from ref [85] according to the terms of Creative Commons Attribution License (CC BY).

	SCB*
Residual moisture (wt. %)	2.80
HHV (MJ/kg)	18.51
Proximate analysis	
Ash (wt.%)	6.75
Volatile matter (wt.%)	80.32
Fixed carbon (wt.%)	10.14
Elemental analysis	
Carbon (wt.%)	47.40
Hydrogen (wt.%)	6.14
Nitrogen (wt.%)	0.28
Sulfur (wt.%)	< 0.1
Oxygen (wt.%)	46.18
Inorganic Compounds	
Al (wt.%)	0.11
Ca (wt.%)	0.05
Fe (wt.%)	0.19
K (wt.%)	0.08
Mg (wt.%)	0.04
Mn (wt.%)	<0.01
Si (wt.%)	1.79
Ti (wt.%)	0.04
Zn (wt.%)	<0.01

*Values are the average of two measurements. Methodologies performed accordingl to the standards described in Supplementary Material (Table S.11).

The sugarcane bagasse showed low moisture content (2.80 wt.%) when received for the analytics, after the drying process. The water content is one of the main parameters for biomass characterization, considering that the pyrolysis process can be affected and the efficiency reduced if the moisture content is >10 wt.% [210]. Hence, in this case the drying process was very successful. The high volatile matter observed (80.32 wt.%) is an indication of the ability of the biomass to be devolatilized [222]. The SCB shows an ash content of 6.75 wt.%. Compared to woody biomass, grassy biomass generally shows higher ash content, being responsible for lower liquid yields, high water and gas formation in the pyrolysis process [25,223,224]. Furthermore, high ash content and high fixed carbon results in high solid formation [209]. The elemental analysis (Table 25) uncovers carbon, hydrogen and oxygen as main constituents, whereas sulfur and nitrogen are found to be lower in comparison to other studies. For example, Rabiu et al. [225] found sulfur and nitrogen concentrations of 0.80 wt.% and 1.60 wt.%, while Sukumar et al. [226] observed sulfur and nitrogen concentrations of 0.19 wt.% and 0.69 wt.%, respectively. As presented by Islam et al. [209] the concentration of these

compounds can differ significantly among sugarcane samples. Sulfur is well known as a poisoning agent for catalysts [108] during the upgrading treatment step [53,96]. Hence, the lower concentration observed in this case can be considered an advantage, as the pyrolysis oil is expected to have lower sulfur in comparison to other residual biomasses, i.e. wheat straw [53,104]. Regarding the inorganic compounds identified, Si is present in highest amount, followed by iron and aluminum. Potassium is observed in smaller concentration (0.08 wt.%), but still requires attention due to its catalytic activity during the pyrolysis process, reducing the liquid yield [23] and increasing solids formation [2].

The characterization of SCB by Py-GC-MS and Py-GC/FID provides information about the main building blocks contributing to the lignocellulosic biomass composition [227]. A total of 71 compounds was detected (Table 26). Among them, 19 compounds were linked to polysaccharides (c), 7 compounds linked to hexoses (ch), 4 compounds to pentose (cp), 3 compounds to hydroxyphenyl (h), 22 compounds to guaiacyl (g), 9 compounds linked to syringyl (s) units while 7 peaks could not be precisely assigned. The pyrogram is available in the Supplementary Material (Figure S.29 and Table S.12). Compounds derived from hexoses and polysaccharides were obtained with the highest relative abundance (Table S.12). Hydroxyacetaldehyde, the major compound identified (12.52 %), is derived from cellulose depolymerization (ring fragmentation), in the same way as levoglucosan, obtained by transglycosylation of cellulose and one of the compounds with the highest relative abundance (6.12 %) [228,229]. Compounds such as propanal-2-one (8.93 %), acetic acid (8.19 %) and 2-hydroxy-3-oxobutanal (4.46 %) and hydroxypropanone (2.23 %) derived from polysaccharides units [230], also showed high relative abundance.

The ring scission of holocellulose (cellulose and hemicellulose) results in ketones and aldehydes, such as propanal and 2-hydroxy-3-oxobutanal [121,231], observed in significant quantities. Acetic acid is mainly derived from hemicellulose (elimination of acetyl group linked to xylose) [229,232], but can be also formed by the cracking of lignin side chains as well as be formed as a by-product of levoglucosan scission [229,230]. Other compounds obtained from cellulose decomposition, as furans [231] were also observed among the products.

The high number of small volatile compounds observed is a result of the pyrolysis temperature, leading to fragmentation to volatile products, mainly ketones and aldehydes [231], as observed (Table 26).

In addition, typical lignin derived compounds were identified [214,219,227,231,233,234] (Table 26 and Figure 43). Guaiacyl derived compounds, such as guaiacol, 3-methylguaiacol, 4-methylguaiacol, eugenol and 4-vinylguaiacol corresponded to the majority of all lignin derived compounds, with major contribution of 4-vinylguaiacol (3.92%). Usually softwood lignin is rich is guayacyl units, as reported elsewhere [235]. The main syringyl derived compounds identified were

syringol, 4-methylsyringol and 4-vinylsyringol while the hydroxyphenyl derived compounds were phenol, p-cresol and m-cresol.

The lignin content was calculated as the sum of the hydroxyphenyl+guaiacyl+syringyl areas divided by the sum of all peaks area. This method has been previously described elsewhere [219] and validated for woody biomass. Due to the differences in the feedstocks, the amount of lignin in the SCB sample was roughly estimated as 18 wt.%, within the expected range [215] for this type of biomass. The syringyl/guaiacyl ratio of 0.49 is well in agreement with previous studies [236].

Table 26. Compounds obtained by Py-GC of the SCB. Reproduced from ref [85] according to the terms of Creative Commons Attribution License (CC BY).

Compound	%*	Compound	%*
Acetaldehyde[c]	1.86	Eugenol[g]	0.26
2-Propenal (acrolein) [c]	1.95	4-Propylguaiacol[g]	0.07
Propanal[c]	8.93	5-Hydroxymethyl-2-furaldehyde[ch]	0.98
2,3-Butandione[c]	2.26	gamma-Lactone derivative[c]	0.53
Butanone-(2) or unknown[c]	1.37	Syringol[s]	1.21
Hydroxyacetaldehyde[ch]	12.52	Isoeugenol (cis)[g]	0.14
Acetic acid[c]	8.19	Pyran-(4H)-4-one, 2-hydroxymethyl-5-hydroxy-2,3-dihydro[ch]	1.35
Hydroxypropanone[ch]	2.23	1,5-Anhydro-b-D-xylofuranose[cp]	0.10
Unknown[u,c]	0.27	Isoeugenol (trans)[g]	0.54
3-Hydroxypropanal[c]	3.15	Syringol, 4-methyl-[s]	0.69
3-Butenal-2-one[c]	1.03	Vanillin[g]	0.75
(3H)-Furan-2-one[c]	0.98	Indene, 6-hydroxy-7-methoxy-, 1H-[g]	1.19
2-Hydroxy-3-oxobutanal[c]	4.46	Indene, 6-hydroxy-7-methoxy-, 2H-[g]	0.58
Furfural[c]	2.86	Homovanillin[g]	0.31
Dihydro-methyl-furanone[c]	3.95	Acetoguaiacone[g]	0.25
Isomer of 4-Hydroxy-5,6-dihydropyran-(2H)-one[cp]	1.43	Syringol, 4-vinyl-[s]	0.89
2(5H)-Furanone[c]	1.52	Guaiacyl acetone[g]	0.16
Gamma-Lactone and unknown [c]	0.24	Unknown [g/s]	0.25
4-Hydroxy-5,6-dihydropyran-(2H)-2-one[cp]	5.18	Propioguaiacone[g]	0.07
2-Hydroxy-1-methyl-cyclopenten-(1)-3-one [ch]	1.23	Isomer of coniferyl alcohol[g]	0.19
Phenol[h]	0.57	G-CO-CH=CH_2[g]	0.20
Guaiacol[g]	0.95	G-CO-CO-CH_3[g]	0.05
Methyl-butyraldehyde derivative[c]	0.61	1,6-Anydro-b-D-glucopyranose (levoglucosan) [ch]	6.12
p-Cresol[h] /	0.32	Syringol, 4-propenyl- (trans)[s]	1.37
m-Cresol[h]	0.07	Dihydroconiferyl alcohol[g]	0.11
3-Methylguaiacol[g]	0.24	Syringaaldehyde[s]	0.57
Gamma-lactone derivative [c]	1.49	Coniferyl alcohol (cis)[g]	0.16
4-Methyl guaiacol[g]	0.73	Homosyringaaldehyde[s]	0.17
Anhydrosugar[c]	1.44	Anhydrosugar: unknown[c]	0.42
Overlapping spectra; 4-ethyl-guaiacol[gc]	1.25	Acetosyringone[s]	0.32
Unknown[u,c]	0.45	Coniferyl alcohol (trans)[g]	0.07
Unknown[u,c]	0.31	Coniferylaldehyde[g]	0.76
1,4:3,6-Dianhydro-glucopyranose[ch]	0.28	Isomer of sinapyl alcohol	0.12
1,5-Anhydro-arabinofuranose[cp]	0.41	Sinapyl alcohol (trans)[s]	0.01
4-Vinylguaiacol[g]	3.92	Sinapinaldehyde[s]	0.40

*Calculated as follow: $[A_i/A_t]\cdot 100$ where A_i is the area of the peak of the compound i and A_t is the sum of the areas of all the compounds. The superscripts ^{c}, ^{ch}, ^{cp}, ^{h}, ^{g}, ^{s} and ^{u} correspond to compounds derived from polysaccharides, hexoses, pentose, hydroxyphenyl, guaiacyl, syringyl and unknown, respectively.

6.3.2 Fast-pyrolysis

The fast pyrolysis reactions resulted mainly in liquid products (60.1 wt.%), followed by non-condensable gas (19 wt.%) and solids (13.5 wt.%) (Table 27). The organic liquid yield, i.e. the liquid yield excluding water, was 48.7 wt.% on a dry feedstock basis. The results indicate that SCB is a very good feedstock for FPBO production – it yields almost as much organic liquids as poplar wood in the same experimental setup [13]. This high yield is observed despite the higher ash content of SCB as compared to the previously used poplar wood. Consequently, the results from SCB fast pyroylsis are outside the typically observed tendency that higher ash content in the feedstock lowers organic liquid yield [25,224]. This observation can be explained with the low potassium content in the feedstock. Most inorganics are due to silicium which can be regarded inert for pyrolysis. Sulfur was below de detection limit, which is in accordance with the low concentration in the SCB previously presented in section 6.3.1.

Table 27. Fast-pyrolysis product yields and SCBPO physicochemical properties. Reproduced from ref [85] according to the terms of Creative Commons Attribution License (CC BY).

	Sugarcane bagasse fast-pyrolysis products
Mass Balance (as received basis)	
Solids (wt.%)	13.5
Organic condensate (SCBPO) (wt.%)	54.6
Aqueous condensate (wt.%)	5.5
Gas (wt.%)	19.0
Loss (wt.%)	7.4
Physicochemical properties and elemental analysis - SCBPO (wet basis; dry basis) *	
Solid (wt.%)	0.8
pH value	2.9
H_2O (wt.%)	20.9
Density (g/cm^3)	1.18
HHV (MJ/kg)	18.73; 23.79
Carbon (wt.%)	45.0; 56.89
Hydrogen (wt.%)	7.50; 6.55
Oxygen (wt.%)**	47.50; 36.56
Nitrogen (wt.%)	<0.2; <0.2

Sulfur below de detection limit.
* Values are the average of two measurements.
** Determined according to Equation (1).

The SCBPO exhibits comparably high water content given the gas temperature of around 90 °C after the first condensation step. This observation is attributed to the cooling water temperature of 30 °C in the first condenser of the SCBPO sampling train which potentially leads to condensate

temperatures <90 °C at the tube's wall and thus increased condensation of water vapor. However, this fact has limited effects on subsequent hydrotreatment.

The SCBPO was deeply characterized in terms of chemical composition by GC-MS/FID as well as by GC-MS and later discussed (see Figure 43 and 44 section 6.3.3.3). Its composition is in line with the low amount of lignin in the feedstock as indicated by the results from the Py-GC-MS (see Table 26), i.e. there is a slightly higher amount of sugar derivatives and lower amount of lignin derived dimethoxyphenols as typically observed for woody feedstocks.

6.3.3 Hydrotreatment reactions and product characterization

6.3.3.1 Physicochemical properties and mass balance

The upgrading reactions with the Ni/SiO_2 catalyst for the SCBPO resulted in four main phases: gas phase, solid phase, upgraded light phase (ULP) and upgraded oil phase (UOP) as the main product (55.79 wt.%). A photograph of both liquid upgraded fractions is available (Figure S.28 c and d). A different product composition was observed after hydrotreatment with $Ni\text{-}Cr/SiO_2$. The upgrading step also resulted in gas, solid, ULP and UOP but an additional intermediate upgraded phase was observed (Table 28). This extra phase is denoted IUP, considering that after centrifugation (see section 2.3) this additional phase was concentrated between the heavy (UOP) and the light phase (ULP). The IUP was visibly less viscous compared to the UOP (paste-like upgraded product). The main product obtained with $Ni\text{-}Cr/SiO_2$ was the ULP, corresponding to 35.56 wt.%. Higher amounts of solid were also obtained with $Ni\text{-}Cr/SiO_2$, almost 5 times higher compared to the amount generated with Ni/SiO_2. The losses for both catalysts were around 9.5 wt.%, possibly due to the difficulty to completely recover the upgraded products from the autoclave, as previously reported [116].

For the viscosity measurements, the SCBPO, $UOP_{Ni/SiO2}$ and $IUP_{Ni\text{-}Cr/SiO2}$ were analyzed (Figure S.31). Due to the low sample amount and the priority for the mass related analytical techniques, it was not possible to measure the viscosity of $UOP_{Ni\text{-}Cr/SiO2}$. The SCBPO and the upgraded products showed a non-newtonian behavior (shear thinning) as previously observed in other studies [237]. Additionaly, an increase of viscosity after hydrotreatment was observed for both upgraded products analyzed in comparison to SCBPO, with highest viscosity observed in this case of $UOP_{Ni/SiO2}$. Although not analized, the $UOP_{Ni\text{-}Cr/SiO2}$ had a paste-like consistency, which most probably indicates a higher viscosity when compared to the SCBPO and the highest viscosity among the upgraded products presented here. Hydrotreatment has been usually suggested as a step for polymerization elimination [238], reducing the pyrolysis oil viscosity, as previously reported elsewhere [98]. Jahromi et al. [102] observed that the lower viscosity values were obtained with nickel-based catalysts with higher nickel loading. These finds are the opposite of our observations for SCBPO, even with the high loaded nickel catalyst

($Ni\text{-}Cr/SiO_2$). In our specific case, the behavior of SCBPO under hydrotreatment condition was different from previous observations for beech wood FPBO, which visually showed lower viscosity after upgrading [96,116]. In the previous study, we assumed that the stabilization step of FPBO took place during the heating ramp [99,104]. The stabilization is usually suggested in order to reduce reactivity and to avoid excessive char production and polymerization and is performed at mild temperature conditions [48,90]. However, in the present study on SCBPO it seems that the stabilization during the heating ramp is not enough to avoid polymerization which competed with hydrotreating reactions. Differences in composition among the beech wood and SCB bio-oil may explain the difference in the products obtained from upgrading. In order to unravel whether in fact polymerization reactions occur during the upgrading, the molecular weight distribution was measured by size exclusion chromatography (Table 28). The measurements were conducted with SCBPO, $UOP_{Ni/SiO2}$, $IUP_{Ni\text{-}Cr/SiO2}$ and $UOP_{Ni\text{-}Cr/SiO2}$. SEC plots are available in the Supplementary Material (Figure S.34).

Table 28. Product yields and physicochemical properties of upgraded liquid products. Reproduced from ref [85] according to the terms of Creative Commons Attribution License (CC BY).

	Ni/SiO_2	**$Ni\text{-}Cr/SiO_2$**
Mass Balance		
Upgraded oil phase UOP (wt.%)	55.79	24.71
Intermediate upgraded phase IUP (wt.%)	-	21.12
Upgraded light phase ULP (wt.%)	29.99	35.56
Solid (wt.%)	0.24	1.14
Gas (wt.%)	5.24	7.12
Loss (wt.%)	8.73	10.36
DOD (%)*	$43.3^{(UOP)}$	$38.0^{(IUP)}$;$32.2^{(UOP)}$

Size Exclusion Chromatography	**SCBPO**	**$UOP_{Ni/SiO2}$**	**$IUP_{Ni\text{-}Cr/SiO2}$**	**$UOP_{Ni\text{-}Cr/SiO2}$**
Mn (g/mol)	177.9	248.8	226.6	235.21
Mw (g/mol)	257.9	419.2	381.9	431.76
Polydispersity (Mw/Mn)	1.4	1.7	1.7	1.8

Physicochemical properties and elemental analysis (wet basis; dry basis) ***	**$ULP_{Ni/SiO2}$**	**$UOP_{Ni/SiO2}$**	**$ULP_{Ni\text{-}Cr/SiO2}$**	**$IUP_{Ni\text{-}Cr/SiO2}$**	**$UOP_{Ni\text{-}Cr/SiO2}$**
H_2O (wt.%)	71.2	8.3	68.4	8.8	8.6
pH value	2.6	-	3.0	3.8	-
HHV (MJ/kg)	-	30.17; 31.89	-	29.04; 31.73	26.32; 30.42
Carbon (wt.%)	13.1; 45.48	65.2; 71.1	15.2; 48.1	62.3; 68.31	60.9; 66.63
Hydrogen (wt.%)	10.2; 7.94	8.1; 7.83	10.2; 8.23	8.9; 8.69	8.5; 8.25
Oxygen (wt.%)**	76.5; 45.87	26.4; 20.74	74.4; 43.0	28.5; 22.67	30.30; 24.79
Nitrogen (wt.%)	<0.2; <0.2	0.3; 0.33	0.2; 0.63	0.3;0.33	0.3; 0.33

* DOD (degree of deoxygenation) determined in dry basis as follow: $DOD\ (\%) = (1 - O_{UOP}/O_{SCBO}) \cdot 100$

** Determined according to Equation (1)

***values are the average of two measurements

A closer look was given to the molecular weight tail, which provides information regarding polymerization [239,240]. The upgraded products caused higher intensity in higher molecular weight ranges when compared to the un-treated SCBPO. These observations are in agreement with the Mn and Mw from SEC given in Table 28. Although interaction of different chemical groups present in the sample may also influence the retention times during the SEC measurement [241], the Mn and Mw

number were used as a rough indication of polymerization reactions taking place during the hydrotreatment, especially in the case of the $UOP_{Ni\text{-}Cr/SiO2}$. The SEC results are in agreement with the viscosity. Therefore, the upgraded products with higher viscosity show the higher molecular weight.

A reduction of around 60.3 % of the water content was observed in the UOP applying the Ni/SiO_2 catalyst in comparison to SCBPO. In the case of $Ni\text{-}Cr/SiO_2$, an IUP with 57.9 % less water in comparison to the feed was obtained, whereas the UOP showed 58.8 % less water compared to the feed. The highest degree of deoxygenation (DOD) was obtained with Ni/SiO_2, resulting in a reduction of the oxygen content of around 43.3 %. In the case of the products obtained with $Ni\text{-}Cr/SiO_2$, a higher DOD was observed for the IUP (38.0 %), compared to the UOP (32.2 %). In total, 2.52 g of H_2O were formed with Ni/SiO_2, whereas 3.66 g of H_2O were formed with $Ni\text{-}Cr/SiO_2$. Although higher water formation with $Ni\text{-}Cr/SiO_2$ (35.5 % extra H_2O formed in total) in comparison to Ni/SiO_2 (24.4 % extra H_2O formed in total), the lowest O/C ratios in the Van Krevelen plot (Figure 41) as well as the highest DOD were observed for the second catalyst. Two hypotheses can be raised regarding the high water formation: usually char formation due to polymerization leads to water production [37]. Hence, as the highest solid formation was observed for $Ni\text{-}Cr/SiO_2$ (later discussed in section 6.3.3.4), it can be expected that also the highest water formation occurs. Secondly, the presence of oxides (NiO and Cr_2O_3) in the catalyst composition can lead to water formation due to the reduction of the oxide over H_2 atmosphere. In this case a maximum of approximately 0.26 g of water would be obtained, if the reduction of both NiO and Cr_2O_3, would take place. Consequently, this pathway of water formation does not reflect the water formation during UOP's deoxygenation.

Most of the carbon was recovered in the UOP obtained with both catalysts and in the $IUP_{Ni\text{-}Cr/SiO2}$. Considering the carbon initially present in the FBPO, 80.8 % was recovered in the UOP with Ni/SiO_2, whereas 62.7 % was recovered with $Ni\text{-}Cr/SiO_2$ in the organic rich fractions (sum of 33.45 % of carbon recovered in the $UO_{Ni\text{-}Cr/SiO2}$ and 29.3 % in the $IUP_{Ni\text{-}Cr/SiO2}$) after the upgrading. An overall carbon recovery from SCB to upgraded oil phase of 41.9 % was obtained with Ni/SiO_2 and 32.5 % with $Ni\text{-}Cr/SiO_2$ (sum of 17.3 % recovered in the UOP and 15.2 % recovered in the IUP).

Nitrogen was observed in low concentration in all upgraded liquid product phases, whereas sulfur was not observed in the upgraded products, which is in agreement with the low sulfur content in SCB as well as the absence of sulfur in the SCBPO, as reported in section 6.3.1 and section 6.3.2. In addition to the lowest water and oxygen content of the UOP obtained with Ni/SiO_2, the reaction also resulted in the upgraded product with the highest carbon content (71.1 wt.%). As a consequence, the HHV for this fraction was slightly higher (31.89 MJ/kg) compared to the value obtained to the IUP (31.73 MJ/kg) and the UOP (30.42 MJ/kg), both obtained with $Ni\text{-}Cr/SiO_2$ catalyst. In all cases, the HHV increased significantly in comparison to the feed (23.79 MJ/kg_{SCBPO}, dry basis).

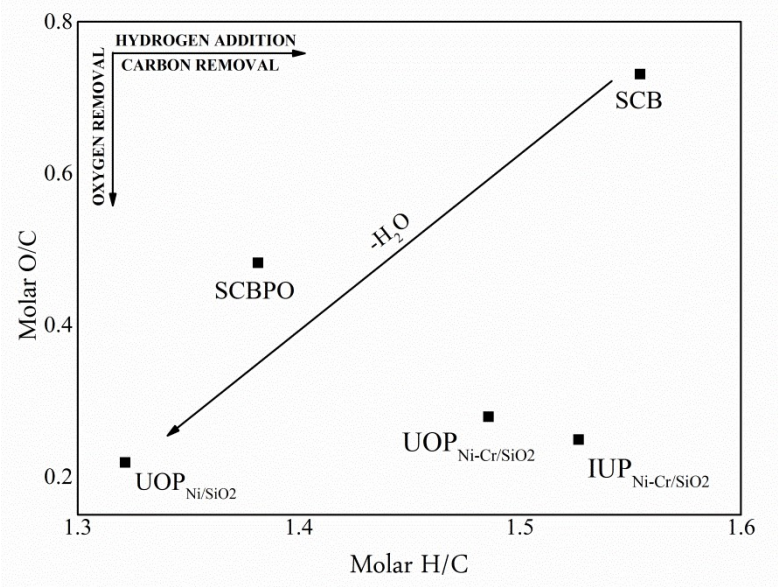

Figure 41. Van Krevelen diagram of sugarcane bagasse, fast pyrolysis bio-oil (dry basis) and upgraded products (dry basis). Reproduced from reference [85] according to the terms of Creative Commons Attribution License.

The Van Krevelen diagram considering the upgraded fractions (light phases are not included), as well as SCB and SCBPO is shown in Figure 41. The O/C ratio is significantly reduced in the SCBPO in comparison to SCB. A clear reduction of O/C ratio after hydrotreatment reactions is observed with both catalysts, especially with Ni/SiO_2 (0.22). The H/C ratio is reduced after the fast-pyrolysis step (1.55 to SCB and 1.38 to SCBPO), as well as in the UOP obtained with Ni/SiO_2, indicating hydrodeoxygenation [37] and dehydration due to polymerization [18]. It is in agreement with the DOD results previously discussed. Upgraded products obtained with $Ni\text{-}Cr/SiO_2$ showed higher values of H/C ratios. It indicates high hydrogenation activity [175] and agrees with the highest hydrogen consumption (Table 29) observed for reactions conducted with this catalyst.

6.3.3.2 Gas fraction characterization: consumption of hydrogen and chemical composition

The gas composition was taken into account in order to investigate the main products as well as the H_2 consumption. Experiments with $Ni\text{-}Cr/SiO_2$ showed the highest consumption of hydrogen (Table 29) and also the highest gas production (7.12 wt.%) compared to Ni/SiO_2 (5.24 wt.%). For both catalysts, carbon dioxide was the main product, followed by carbon monoxide and methane. Smallamounts of C2-C4 compounds were also detected. Similar to our previous findings with $NiCu/SiO_2$ catalysts [96], high hydrocracking activity was observed for the catalyst which consumed the highest amount of hydrogen, leading higher methane formation [59,102], possibly resulting in excessive consumption of hydrogen during this step [49].

Table 29. Hydrogen consumption and chemical composition of the gas fraction. Reproduced from ref [85] according to the terms of Creative Commons Attribution License (CC BY).

	Ni/SiO_2	**$Ni\text{-}Cr/SiO_2$**
Hydrogen consumption (NL/Kg feed)	199.43	326.2
Gas composition		
Carbon dioxide (mol/kg feed)	1.146	1.263
Carbon monoxide (mol/kg feed)	0.041	0.058
Methane (mol/kg feed)	0.016	0.718
Propane (mol/kg feed)	*	0.015
Ethane (mol/kg feed)	0.007	0.045
n-butane (mol/kg feed)	*	0.007

*Values below the limit of quantification.

The internal pressure and temperature of the autoclave were recorded along the reaction (Figure 42). The catalysts showed different pressure profiles. While the pressure profile for Ni/SiO_2 increased close to linearity during the heating ramp (even with consumption of hydrogen taking place), more pronounced hydrogen consumption was observed for $Ni\text{-}Cr/SiO_2$. A rough trend was plotted using the ideal gas and Soave Redlich Kwong equations to estimate the theoretical H_2 pressure in the autoclave without gas consumption. After 20 min of reaction at 97.7 °C with Ni/SiO_2, the recorded autoclave pressure is lower compared to the theoretical values, which gives an indication of H_2 consumption started already at lower temperatures [48,99]. Even if gaseous compounds are formed during this step (neglected in this approach), the H_2 consumption is still visible, considering the distance from the theoretical plots. At 50 min of reaction (159 bar and 257.5 °C) the pressure recorded is higher compared to the theoretical plots. It can be attributed to cracking reactions, mostly occuring at higher HDO temperatures [116,242], resulting mainly in decarboxylation [90], considering that CO_2 is the main gaseous product (Table 29). At 324.3 °C (approximately 77 min of reaction) the reaction with Ni/SiO_2 reached the highest pressure recorded for this catalyst (202.6 bar). A slightly decreased was observed after this point, reaching 194.4 bar (measured at 324.9 °C) at the end of the reaction (indication of H_2 consumption).

The hydrogen consumption profile with $Ni\text{-}Cr/SiO_2$ was more pronounced compared to Ni/SiO_2, in agreement with Table 29. After 22 min of reaction time, the reactor reached 88.8 °C and 104.3 bar. The pressure then decreased to approximately 95.6 bar, remaining at this range for about 9 min (temperature from 143.5 °C to 189 °C). A second pronounced pressure decrease is observed as the temperature continues to rise; a new plateau was observed at approximately 85.7 bar from 219.2 °C to 270.5 °C. After 57.4 min of reaction a sharp pressure increase could be noticed, reaching 140.1 bar (324.2 °C) in approximately 26 min (rate of 1 bar/°C), similar to the behaviour observed to Ni/SiO_2. After reaching the set point (325 °C), the pressure remained in the range of 146 bar. The highest pressure of 147.8 bar was recorded at the end of the reaction with $Ni\text{-}Cr/SiO_2$ (46.6 bar below Ni/SiO_2). It is an indication of higher catalytic activity and higher hydrogen consumption [99].

Based on the pressure profiles obtained for both catalysts, H_2-TPR result (Figure S.33) and our previous investigation of the influence of temperature (175 °C, 225 °C, 275 °C and 325 °C) on the conversion of a beech wood FPBO [116], some conclusions can be derived (further discussed in section 6.3.3.3). The H_2-TPR of Ni-Cr/SiO_2 (Supplementary material Figure S.33), showed very little H_2 consumption and H_2O production, starting mostly at around 83 °C and reaching the maximum H_2 consumption at 210 °C. This observation could partly explain the H_2 consumption behavior during the upgrading reaction (reduction of oxides). In the sequence, the H_2 consumption and water production are reduced during the TPR measurement, althought some H_2 is still being consumed in even lower amounts. In the case of the upgrading reactions, the hydrogen consumption takes already place at low temperatures, around 88.8 °C with Ni-Cr/SiO_2 and around 97.7 °C with Ni/SiO_2, might be an indication of hydrogenation of reactive compounds such as olefins, aldehydes and ketones, as these compounds are usually the first to be hydrogenated [8,61,104]. Furthermore, the low hydrogen uptake temperatures observed in both cases, but especially for Ni-Cr/SiO_2, are in agreement with the observations of Yin et al. [180]; the authors observed an H_2 uptake at around 80 °C, also using a high loaded Ni-based catalyst (NiCu/SiO_2). Mercader et al. 2011 [48] also reported hydrogen consumption taking place at this temperature. The plateaus observed at different temperature ranges for Ni-Cr/SiO_2 could be correlated to the reactivity range of some bio-oil components [61]. While very reactive compounds react at lower temperature, compounds with intermediate reactivitiy react mainly in the second plateau (219.2 °C to 270.5 °C). For example, Boscagli [104] observed that some ketones can be formed at slightly higher temperature ranges, whereas according to Elliott [61] some aliphatic alcohols can undergo thermal dehydration at moderate temperatures forming olefins (in our case olefins were only observed in the UOP with Ni-Cr/SiO_2 and later discussed at section 6.3.3.3). Hydrocracking and decarboxylation can be a plausible explanation for the sharp pressure increase with both catalysts at very similar temperatures (257.5 °C and 270.5 °C), as C2-C3 gaseous compounds, methane and carbon dioxide concentration are directly related to the increase of the reaction temperature [104,116].

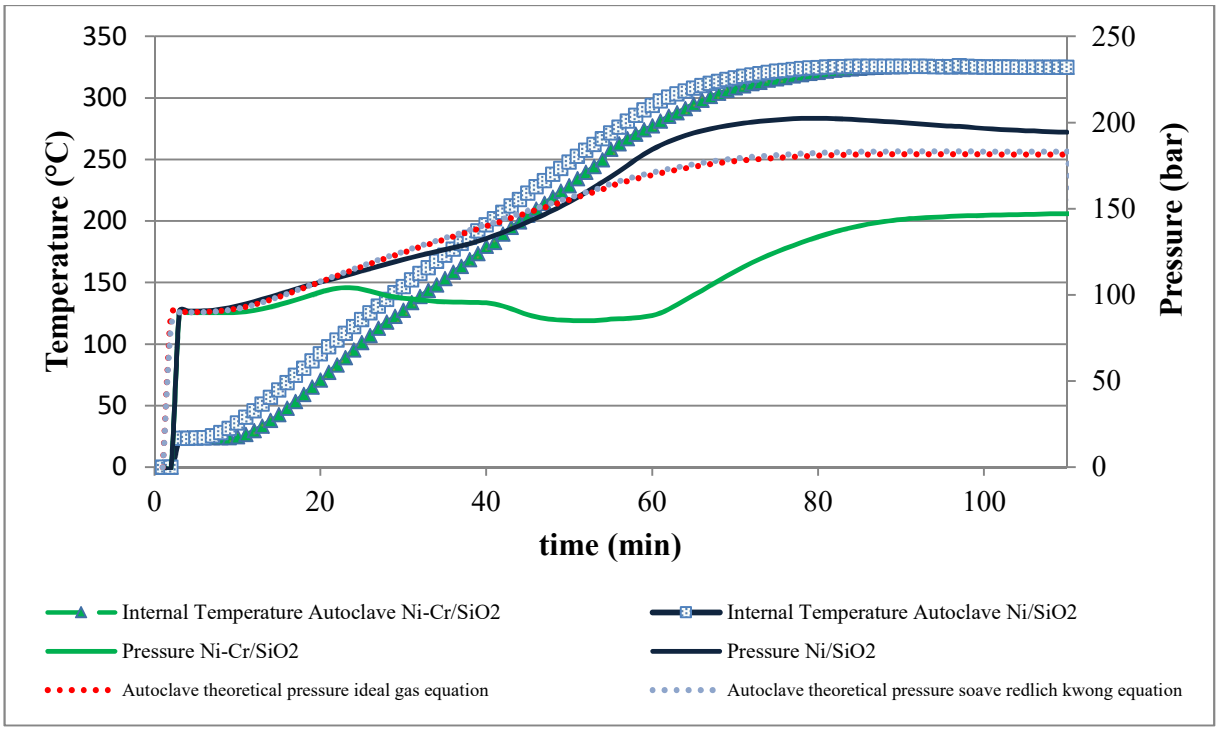

Figure 42. Pressure and temperature registered during the upgrading reactions as well as the theoretical hydrogen pressure expected if no consumption of H_2 would occur. Ideal gas equation and Soave Redlich Kwong equation were used for the theoretical calculation. Reproduced from reference [85] according to the terms of Creative Commons Attribution License.

6.3.3.3 Chemical composition of sugarcane bagasse fast pyrolysis bio-oil and upgraded liquid fractions

In the following the main chemical transformations which took place during the upgrading reactions of SCBPO in terms of GC detectable fraction are described. Usually around 20-40 % of all the compounds can be identified by gas chromatography [118,173]. Additionally, the Py-GC results of SCB and the main constituents of the SCBPO are correlated and discussed in comparison to the upgraded products. The compounds identified by GC-MS/FID are grouped and presented in Figure 44, whereas the detailed quantification of single compounds is given in Table S.14 together with the GC-MS measurements (Figure S.30 and Table S.13).

The main chemical compounds observed in the SCBPO (Table S.14) are in agreement with the Py-GC measurements with SCB (Table 26). In total, 28 compounds obtained by this analytical technique (from a total of 71) are observed in the SCBPO. In both cases, acetic acid, hydroxyacetaldehyde, hydroxypropanone and levoglucosan are observed as the main pyrolysis products, as well as furfural, 2(5H)furanone, 3-hydroxypropanal. In minor concentration, 9 of the 10 compounds belonging to the guaiacol group were observed in both cases. Some lignin derived phenols (phenol, p-cresol and m-cresol) and some of syringol's group belonging compounds (syringol, 4-methylsyringol, 4-vinylsyringol and syringaldehyde) were also obtained as products from the analytical and technical scale pyrolysis. All the sugars identified in the SCBPO pyrolysis experiment

were in agreement with this analytical technique. Due to the operational differences between both methods, as residence time and temperature, different fragmentation products are expected [231] and in fact observed. The main pyrolysis products and the precursor building blocks are highlighted in Figure 43, in brown and black color, respectively.

In terms of the upgraded products, the ULPs concentrated most of the water and most of the nonaromatic compounds (Figure 44). Considering the concentration on dry basis, the $ULP_{Ni/SiO2}$ was composed by 63.88 wt.% of nonaromatic compounds (sum of acids, non-aromatic alcohols, non-aromatic aldehydes, non-aromatic ketones, and hydrocarbons), whereas the $ULP_{Ni-Cr/SiO2}$ was composed by 48.85 wt.% of nonaromatic compounds. Among the nonaromatics in the ULPs, organic acids contributed to 49.24 wt.% of $ULP_{Ni/SiO2}$ and 34.11 wt.% of $ULP_{Ni-Cr/SiO2,}$ reflecting the lower pH value [243] observed (Table 28). The lowest pH was observed for the reaction with Ni/SO_2 (pH value 2.6), the fraction with highest concentrations of acetic acid. On the other hand, UOPs with both catalysts as well as the $IUP_{Ni-Cr/SiO2}$ showed similar concentration of organic acids (around 12.30 wt.%), mainly acetic and propionic acid. Initially, the feed contained 3.35 g of acetic acid while the liquid products showed lower amounts (calculated as the sum of acetic acid in the liquid upgraded fractions). The conversion with Ni/SiO_2 resulted in 3.10 g of acetic acid in the products while reactions performed with $Ni-Cr/SiO_2$ resulted in 2.49 g of acetic acid in the upgraded products. Considering the initial concentration, 7.5 % of the acetic acid was converted with Ni/SiO_2, while 25.7 % was converted by $Ni-Cr/SiO_2$. The conversion was calculated considering the initial moles of acetic acid in the SCBPO and the sum of moles of acetic acid in the upgraded liquid products. The possibility of acetic acid formation, for example, as a byproduct from levoglucosan scission [229,230] was not considered in this case. Acetic acid, mainly formed from depolymerization of hemicellulose [2,148], and as just previously mentioned from levoglucosan, can follow different reaction pathways during the bio-oil upgrading (Fig. 43 H, R_1). It can be converted to CH_4 and CO_2 by deprotonation to acetate followed by decarboxylation to methane [34]. After dehydroxylating to acetyl species followed by C-C bond cleavage results in CO and CH_4 [66]. The lower concentration of acetic acid and higher production of CH_4 observed with $Ni-Cr/SiO_2$ could be correlated to the methane formation pathway (higher methane concentration observed with this catalyst). Additionaly, the acetyl species can undergo hydrogenation to ethanol (not detected), which can be further hydrodeoxygenated to ethane or follow esterification to ethylacetate [66,90], both identified in the products.

Propionic acid, derived from hemicellulose pyrolysis [34,121], was observed in the SCPBO, as well as in the upgraded products. Considering the initial loading of SCBPO (around 50 g) and the concentration of propionic acid (3.73 wt.%), 1.84 g of propionic acid was loaded in the batch reactor. After the upgrading reaction a total of 1.81 g and 1.56 g of propionic acid were observed in the upgraded products with Ni/SiO_2 and $Ni-Cr/SiO_2$, respectively. Lower conversion (1.56 %) was

observed with Ni/SiO_2 in comparison to $Ni\text{-}Cr/SiO_2$ (14.95 % of conversion). Propionic acid can be converted (i) to ethane through dehydrogenation followed by decarboxylation [244], can (ii) undergo dehydroxylation and hydrogenation resulting in 1-propanol [65], identified mainly in the products with $Ni\text{-}Cr/SiO_2$, and can (iii) also undergo esterification, resulting in products such as propanoic acid, methyl ester, observed in the products [18] and shown in Figure 43 H, R_2. Similarly to acetic acid, propionic acid can also be decomposed to CH_4 [65], which could be another explanation for the higher concentration of methane (Table 29) observed with $Ni\text{-}Cr/SiO_2$.

Butyric acid and pentanoic acid, initially absent in the SCPBO, were observed in the products, mainly in the ULP obtained with Ni/SiO_2 and in all the products obtained with $Ni\text{-}Cr/SiO_2$ (pentanoic acid is not observed in the UOP with $Ni\text{-}Cr/SiO_2$). Although observed in lower concentration compared to acetic and propionic acids, the high concentration of these acids in the upgraded oils are in agreement with other studies [70,93] and can be considered a limitation for further applications, due to UOP's corrosiveness attributed by the high composition of organic acids [245].

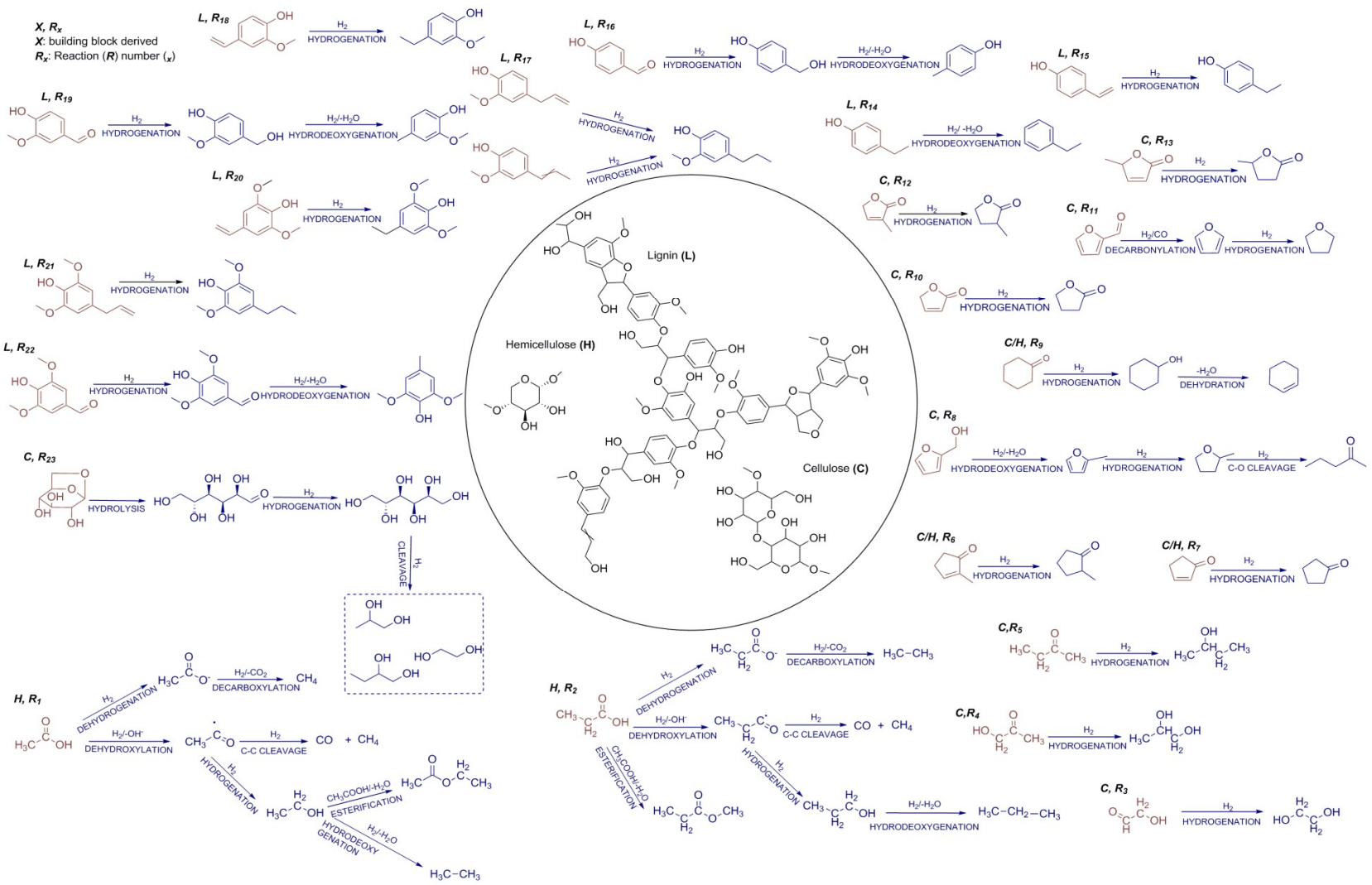

Figure 43. Some of the main SCB pyrolysis products are depicted (brown color) and some of the reaction pathways observed during the upgrading treatment (blue color).The building blocks of SCB are represented in black color (hemicellulose represented by α-D-Xylopyranose). Esterification reactions in H, R_1 and H, R_2, and the pathways from cyclohexanol to cyclohexene in C/H R_9 are mostly observed for Ni-Cr/SiO_2 catalyst. The molecules are identified in regard to the main source from which are derived (H: hemicellulose; C: celullose and L: lignin) as well as by the reaction (R) number. Reproduced from reference [85] according to the terms of Creative Commons Attribution License.

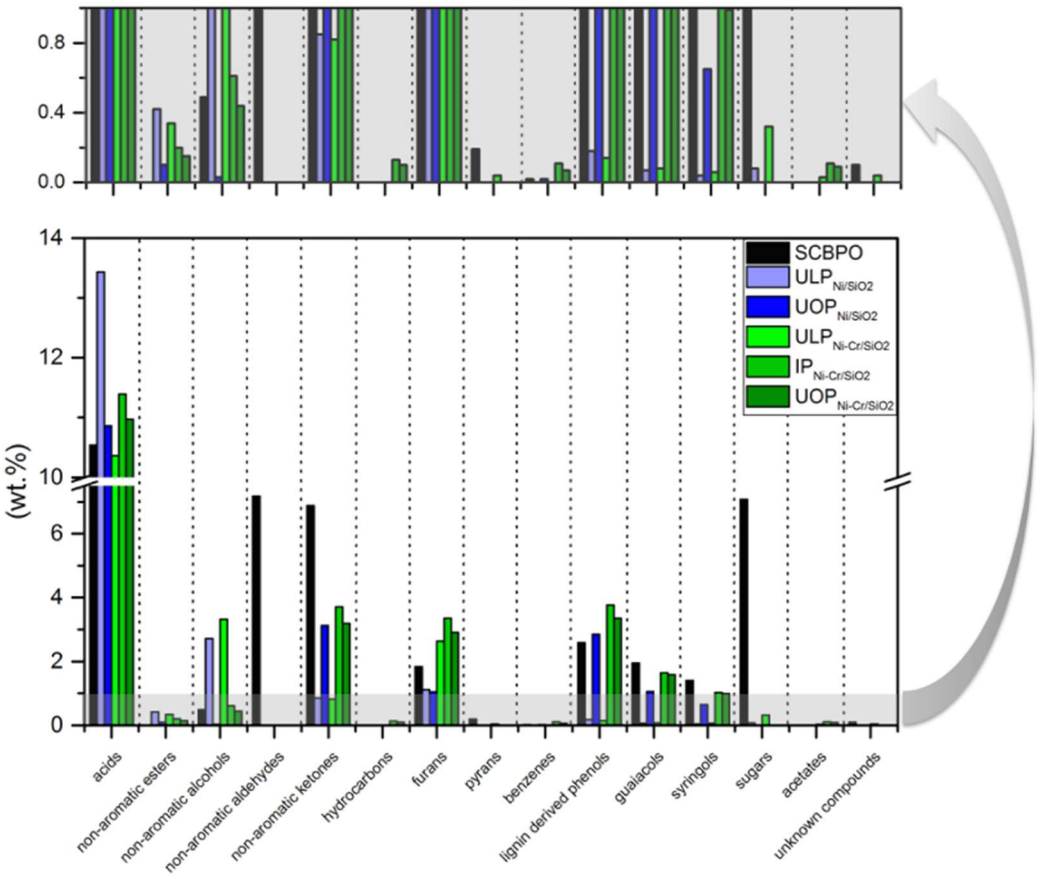

Figure 44. Distribution of the main chemical compounds in the SCBPO and upgraded products. Reproduced from reference [85] according to the terms of Creative Commons Attribution License.

Nonaromatic esters were observed in both phases obtained with Ni/SiO_2 (Figure 44), but with higher concentration found in the $ULP_{Ni/SiO2}$ (1.55 wt.% dry basis), followed by $UOP_{Ni/SiO2}$ (0.11 wt.% dry basis). The upgraded products with $Ni\text{-}Cr/SiO_2$ also showed nonaromatic esters in all three phases. The highest concentration was observed in the $ULP_{Ni\text{-}Cr/SiO2}$ (1.12 wt.% dry basis), followed by $IUP_{Ni\text{-}Cr/SiO2}$ (0.22 wt.% dry basis) and lower concentrations in the $UOP_{Ni\text{-}Cr/SiO2}$ (0.17 wt.% dry basis), although higher compared to $UOP_{Ni/SiO2}$ (0.11 wt.% dry basis). The esterification has been proposed to reduce the acidity of the pyrolysis oils [246]. Propanoic methyl ester was observed in the upgraded products with both catalysts, whereas acetic acid butyl ester was just detected in the products obtained with $Ni\text{-}Cr/SiO_2$. Acetic acid 2-hydroxyethyl ester was only observed in both $ULP_{Ni\text{-}Cr/SiO2}$ and $ULP_{Ni/SiO2}$, while propanoic acid, 2-hydroxyethyl was exclusively observed in the $ULP_{Ni/SiO2}$.

In terms of non-aromatic alcohols, higher concentrations were observed in the ULP with both catalysts in comparison to the feedstock (Figure 44). Ethylenglycol was the only compound initially found in the SCBPO (0.49 wt.% dry basis), considering its application as start-up material mentioned in section 2.2. The reaction with Ni/SiO_2 resulted in an increased absolute

ethylenglycol content (0.24 g in the feed versus 0.41 g after reaction as sum of LP+HP), mainly concentrated in the ULP. A small concentration of 1-propanol was also observed in the ULP, as already discussed, whereas an unknown aliphatic alcohol was observed in the UOP. The reaction performed with Ni-Cr/SiO_2 followed a different pathway: 9 non-aromatic alcohols were identified in the ULP (Table S.14). Ethyleneglycol was the main alcohol (6.42 wt.% dry basis, 0.34 g), followed by propylenglycol (2.48 wt.% dry basis) and 1-propanol (1.06 wt.% dry basis). Other compounds were present in the ULP in smaller concentrations. 1-propanol and 2-methyl-1-propanol were observed in the IUP, whereas 1-propanol was only identified in the UOP. The high concentration of ethylenglycol in the products in comparison to the feed can be related to the complete hydrogenation of hydroxyacethaldehyde (Figure 43 C, R_3), the non-aromatic aldehyde initially present in the SCBPO in higher concentration (6.03 wt.% wet basis) [247]. Following the same pathway, propylene glycol most probably was formed by the hydrogenation of acetol (Figure 43 C, R_4) [96,157,247]. Initially present in high concentration in the SCBPO (6.20 wt.% dry basis, 2.44 g in total), it was mostly converted after the upgrading reactions, remaining only 0.04 g in the ULP. Ni-Cr/SiO_2 seems to favor the hydrogenation, considering that propylene glycol was the second most abundant alcohol in the ULP with this catalyst, whereas the upgrading with Ni/SiO_2 followed a different pathway, as no propylene glycol was observed in none of the fractions obtained with this catalyst. Aditionally, alcohols such as 2-butanol observed in the $ULP_{Ni\text{-}Cr/SiO2}$ can be a product of 2-butanone hydrogenation (Figure 43 C, R_5) [8]. In the same way, alcohols in smaller concentration, such as cyclohexanol, is a product of cyclohexanone hydrogenation.

Initially 12 ketones were identified in the SCBPO, with acetol as the main compound. In total, the SCBPO was composed by 8.65 wt.% (3.40 g) of ketones (Figure 44). Other compounds belonging to the ketone group, mostly unsaturated cyclic compounds, were in much lower concentration. In the same way as observed for acetol, which was most hydrogenated to propylenglycol [248], most of the compounds initially present were hydrogenated. For example, 2-methyl-2-cyclopenten-1-one was possibly hydrogenated to 2-methyl-cyclopentanone (Figure 43 C/H, R_6) , and 2-cyclopenten-1-one possibly hydrogenated to cyclopentanone (Figure 43 C-H, R_7) [93]. On the other hand, ketones such as 2-pentanone, initially absent in the SCBPO were identified in the products. It can be explained by the hydrodeoxygenation of 2-furfurylalcohol to 2-methylfuran, followed by hydrogenation/C-O bond cleavage, resulting in 2-pentanone (Figure 43 C, R_8) [34]. Additionaly, ketones can undergo hydrogenation to alcohols and dehydration to olefins [249], as exemplified in Figure 43 (C/H, R_9). In summary, the upgrading with Ni/SiO_2 reduced the initial total amount of ketones (3.40 g) to 0.99 g and to 0.92 g of ketones with Ni-Cr/SiO_2.

Hydrocarbons, initially absent in the SCBPO were observed only in the $IUP_{Ni\text{-}Cr/SiO2}$ (0.15 wt.% dry basis) and $UOP_{Ni\text{-}Cr/SiO2}$ (0.01 wt.% dry basis). The hydrocarbons identified in the IUP were cyclohexene and ethylcyclopentane in smaller concentration. Cyclohexene could be formed from the hydrogenation of cyclohexanone to cyclohexanol, followed by dehydration to cyclohexene (Fig. 5 C/H, R_9) [65]; both precursors, cyclohexanone and cyclohexanol, only observed in the upgraded products with Ni-Cr/SiO_2.

The number of molecules belonging to group of furans, products of carbohydrate depolymerization [8,121], increased after upgrading reactions (Figure 44). Initially, 8 molecules attributed to a furan group were identified in the SCBPO (2.31 wt.% dry basis, correponding to 0.91 g of furans), mainly composed by 2(5H)-furanone, 2-furaldehyde and γ-butyrolactone (Table S.14). After the upgrading reaction, a total of 10 compounds were identified in the upgraded phases with Ni/SiO_2 (resulting in 0.46 g of furans, sum of all fractions), as well as 17 compounds were identified in the products obtained with Ni-Cr/SiO_2 (1.17 g, sum of all fractions), mostly concentrated in the ULP (8.68 wt.% dry basis, 0.46 g).

Compounds initially present in the feedstock, such as 2-furfuryl alcohol, 2(5H)-furanone, 3-methyl-2(5H)-furanone, 2-furaldehyde, 4-methyl-(5H)-furan-2-one and 5-methyl-2(5H)-furanone were completely converted with both catalysts. On the other hand, compounds such as γ-butyrolactone were observed in higher concentration in the products, (0.27 g in the products with Ni/SiO_2 and 0.30 g in the products with Ni-Cr/SiO_2) in comparison to the feed (0.10 g). This may be attributed to the hydrogenation of 2(5H)-furanone, initially observed in the SCBPO and completely converted, resulting in γ-butyrolactone (Figure 43 C, R_{10}) [95,96].

Tetrahydrofuran, a molecule absent in the SCBPO, was observed in the upgraded products. The decarbonylation of furfural leads to the formation of furan which is further hydrogenated to tetrahydrofuran (Figure 43 C, R_{11}) [181]. α-methyl-γ-butyrolactone, observed only in the upgraded products, is a product of hydrogenation of 3-methyl-2(5H)-furanone (Figure 43 C, R_{12}). The hydrogenation of 5-methyl-2-furanone results in γ-valerolactone (Figure 43 C, R_{13}). Tetrahydro-2-methyl-furan was observed only in the upgraded products with Ni-Cr/SiO_2. The hydrodeoxygenation of furfuryl alcohol results in 2-methylfuran which is then further hydrogenated to tetrahydro-2-methyl-furan (Figure 43 C, R_8). A further pathway can be followed by which 2-methylfuran can be converted to 2 pentanone [181], which was identified in all upgraded liquids with both catalysts.

The GC-detectable aromatic compounds in the SCBPO as well as in the upgraded products were classified in four main groups: benzenes, lignin derived phenols, guaiacols and syringols (Figure 44 and Table S.14). Initially, the SCBPO was composed by 7.50 wt.% (dry basis) of GC

detectable aromatic compounds, considering the 30 compounds identified and quantified. The upgrading reactions with Ni/SiO_2 resulted in low concentration of aromatics (1.05 wt.% dry basis) in the ULP and UOP with 5.16 wt.% (dry basis), respectively. Considering the initial amount of SCBPO loaded to the autoclave, 2.95 g of aromatics were reduced to 1.30 g of aromatics (1.26 g in the UOP) with Ni/SiO_2. The reactions conducted with $Ni\text{-}Cr/SiO_2$ resulted in 1.46 g of aromatics, mostly concentrated in the IUP (7.16 wt.% dry basis, 0.68 g) and UOP (6.71 wt.% dry basis, 0.73 g) with minor concentration in the ULP (0.28 wt.% dry basis, 0.05 g).

Benzene was present in the SCBPO, as well as in the upgrading products. Small concentration of toluene and ethyl-benzene were obtained with $Ni\text{-}Cr/SiO_2$. Ethyl-benzene could be formed from hydrodeoxygenation of 4-ethylphenol molecule (Figure 43 L, R_{14}), analogous to the reaction pathway reported by Gandarias et al., [146] to 2-ethylphenol.

Lignin derived compounds were observed in the feedstock as well as in the products (Figure 44 and Table S.14). Molecules such as phenol, cresols and 4-ethyl-phenol, were mainly concentrated in the UOP (3.21 wt.% dry basis, 0.786 g and 3.75 wt.% dry basis, 0.41 g for Ni/SiO_2 and $Ni\text{-}Cr/SiO_2$,respectively) and in the $IUP_{Ni\text{-}Cr/SiO2}$ (4.12 wt.% dry basis, 0.392 g). 4-ethyl-phenol was the main lignin derived compound observed in the UOP with Ni/SiO_2 (1.83 wt.% dry basis, 0.50 g) and in the IUP (2.43 wt.% dry basis, 0.52 g) and UOP (2.39 wt.% dry basis, 0.29 g) with $Ni\text{-}Cr/SiO_2$. It seems that the molecules already present in the feed (0.55 wt.%, 0.27 g) were not further converted, whereas the complete hydrogenation of 4-vinyl-phenol contributed to the increased concentration of this compound in the products (Figure 43 L, R_{15}). 4-hydroxy-benzaldehyde was also completely converted with both catalysts. A possible pathway for its conversion could be the hydrogenation followed by hydrodeoxygenation, resulting in 4-methylphenol (p-cresol) (Figure 43 L, R_{16}).

Most of the guaiacols initially present were converted with both catalysts. Ni/SiO_2 was able to convert the highest amount of guaiacols (feed: 0.96 g; sum of products: 0.30 g) in comparison to $Ni\text{-}Cr/SiO_2$ (feed: 0.96 g; sum of products: 0.38 g). In this case, possible products formed from depolymerization of GC non-detectable fraction are not considered. Compounds such as eugenol, isoeugenol, 4-vinylguaiacol and vanillin were completely converted with both catalysts, whereas compounds such as guaiacol, 4-methylguaiacol and 4-ethylguaiacol were in the feed and in the product, mostly concentrated in the UOPs as well as in the $IUP_{Ni\text{-}Cr/SiO2}$. In agreement with our previous findings [96,116], eugenol, cis and trans isoeugenol were completely hydrogenated most probably to 4-propylguaiacol, identified only in the products (Figure 43 L, R_{17}). In the same way 4-vinylguaiacol was possibly completely hydrogenated to 4-ethylguaiacol (Figure 43 L, R_{18}). The complete conversion of vanillin after the upgrading and

higher concentration of 4-methylguaiacol found in the products suggests that hydrogenation followed by hydrodeoxygenation was a possible reaction pathway for the vanillin (Figure 43 L, R_{19}) [150].

Initially 11 compounds belonging to the syringol group are present in the SCBPO. After the upgrading reactions, 8 substances were completely converted with both catalysts and mostly concentrated in the UOPs and $IUP_{Ni\text{-}Cr/SiO2.}$ Both 4-vinyl-syringol and 4-allyl-syringol were completely hydrogenated to 4-ethyl-syringol and 4-propyl-syringol, respectively (Figure 43 L, R_{20} and L R_{21}); Syringaldehyde on the other hand, possibly underwent hydrogenation, followed by hydrodeoxygenation, resulting in 4-methyl-syringol (Figure 43 L R_{22}).

Sugars contained in SCBPO such as levoglucosan, 1,5-anhydro-ß-D-xylofuranose, and 1,5-anhydro-ß-D-arabinofuranose, were completely converted. Levoglucosan, derived from the thermal degradation of celullose [2] is considered to be converted to compounds such as ethyleneglycol, propyleneglycol and 1,2-butanediol [95,247], identified mainly in the products with Ni-Cr/SiO_2. Firstly levoglucosan is converted by hydrolysis to glucose [95,175], which is hydrogenated to sorbitol [49,146], and later undergoes hydrogenolysis to diols as observed in the products (Figure 43 L, R_{20} and C R_{23}) [77,146]. As previously stated, acetic acid is also one possible product from levoglucosan scission [229,230]. Sugars are also known for polymerization during the hydrotreatment reactions, leading the the formation of char and carbon dioxide [77]. This pathway cannot be discarded, considering the char deposition observed over the spent catalysts (later discussed in Section 6.3.3.4). Furthermore, gaseous products such as ethane and methane might be also generated from sugar conversion [99]. A small amount of unknown sugars were observed in the ULPs, as well as a small concentration of isosorbide in the $ULP_{Ni\text{-}Cr/SiO2}$.

Acetates were mostly observed in the upgraded liquid products obtained with Ni-Cr/SiO_2, mainly composed by tetrahydro-2-furanmethanol acetate and ethylacetate, respectively. Tetrahydro-2-furanmethanol acetate is formed from the esterification reaction of acetic acid and a furfural intermediate [248,250]. The reaction of carboxylic acids and 2-furanmethanol and derivatives, can result in a less corrosive and more stable pyrolysis oil [181]. Minor unknown compounds were observed in the samples as well.

6.3.4 Catalysts characterization

The catalysts were characterized before and after the upgrading reaction. Additionally, the ULP was analyzed for the amount of leached metal ions. The $ULP_{Ni\text{-}Cr/SiO2}$ showed 0.0047 wt.% of Ni and concentration of Cr below the detection limit (<0.0016 wt.%). In terms of the amount of catalyst loaded to the autoclave, 0.054 wt.% of the initial concentration of Ni and less than

0.09 wt.% of Cr were leached into the ULP, respectively. Ni (0.032 wt.%) and Cr (<0.0016 wt.%) were also identified in the $IUP_{Ni\text{-}Cr/SiO2}$, which accounts 0.22 wt.% of Ni and less than 0.09 wt.% of Cr in the $IUP_{Ni\text{-}Cr/SiO2}$. The concentration of Ni (1.05 wt.%) and Cr (0.34 wt.%) in the $UOP_{Ni\text{-}Cr/SiO2}$ were also analyzed, but these results cannot be considered leaching; due to the high viscosity of the $UOP_{Ni\text{-}Cr/SiO2}$, a complete separation of catalyst even after centrifugation was not possible. Similar difficulties were previously reported elsewhere [99]. So, the results presented here are most propably attributed to the catalyst particles dispersed in the $UOP_{Ni\text{-}Cr/SiO2}$. Hence, 10 % of catalyst initially loaded to the autoclave (initial load of 2.49 g) remained in the $UOP_{Ni\text{-}Cr/SiO2}$, which implies that the separation of catalyst from the reaction products has to be improved in future work. The upgraded fractions obtained with Ni/SiO_2 showed 0.01 wt.% and 0.014 wt.% of Ni in the $ULP_{Ni/SiO2}$ and $UOP_{Ni/SiO2}$, respectively. In this case, 0.73 wt.% of Ni was leached to the $ULP_{Ni/SiO2}$ (considering the 2.56 g Ni/SiO_2 with [Ni]=7.9 wt.% loaded to the autoclave). In the same way as discussed above, the complete separation of upgraded oil and the catalyst was difficult due to the high viscosity of $UOP_{Ni/SiO2}$.

In terms of carbon deposition, $Ni\text{-}Cr/SiO_2$ showed 18.5 wt.% of carbon whereas Ni/SiO_2 showed 0.36 wt.% of carbon after the upgrading reactions. Carbonaceous deposition can be formed due to a variety of polymerization reactions [180] caused but not limited to compounds such as sugars [77], furans and phenolic oligomers (pyrolytic lignin) [34,251]. Usually considered to be one of the main reasons for catalyst deactivation in hydrotreatment reactions [39,53], solids formation should be minimized. The higher carbon deposition observed to $Ni\text{-}Cr/SiO_2$ could be interlinked to the high metal loading, as previously reported [252], although some studies describe the opposite behavior [102].

The XRD of fresh and spent Ni/SiO_2 show similar patterns. The reflections of metallic Ni are observed in both cases, at 44.49°, 51.85°, 76.38°, 92.93° and 98.44° (Figure S.32, Supplementary Material) [96]. The $Ni\text{-}Cr/SiO_2$ show the same reflections attributed to metallic nickel and additionally reflections attributed to NiO (37.2°, 42.6° and 62.8°). After the reaction, the NiO reflections disappeared, due to the reduction into metallic nickel under H_2 atmosphere. No reflections for Cr_2O_3 were observed for this catalyst (amorphous or dispersed chromium phase).

No significant differences in the crystallite sizes of Ni/SiO_2 are observed between the fresh and spent catalyst (in both cases a value of 17.7 nm). On the other hand the crystallite size of $Ni\text{-}Cr/SiO_2$ increased from 4.4 nm to 38.2 nm after the reaction. In another investigation we observed an increase of the crystallite size to around 18 nm [116] with beech wood bio-oil. Furthermore, the $Ni\text{-}Cr/SiO_2$ high metal loading and medium surface area facilitates the migration

of the metal particles resulting in sintering. In future, the catalyst may be pre-conditioned to receive a medium Ni particle size.

6.4 Conclusion

A study from sugarcane bagasse characterization to upgraded products after hydrotreatment was presented. The low moisture content of 2.80 wt.% and low potassium content of 0.08 wt.% were reflected in the high yield of organic liquids (60.1 wt.%) obtained by fast-pyrolysis, outside the range expected for residual biomass. Hydrotreatment reactions resulted in upgraded oils with lower oxygen, lower water and higher carbon content in comparison to SCBPO. Nonetheless distinct selectivities among both catalysts were observed. Ni/SiO_2 showed the highest activity for deoxygenation, reaching 43.3 % of oxygen removed, as well as the highest activity for conversion of aromatics. $Ni\text{-}Cr/SiO_2$ on the other hand, revealed high hydrogenation activity and highest conversion of carboxylic acids, reaching conversions of 25.7 % of acetic acid and 14.95 % of propionic acid. Furthermore highest formation of alcohols and furans was observed with this catalyst. Around 41.9 % of the carbon content of sugarcane bagasse was recovered in the upgraded oil obtained with Ni/SiO_2 whereas 32.5 % was recovered $Ni\text{-}Cr/SiO_2$ (sum of upgraded oil and upgraded intermediate phase). Polymerization of upgraded fractions took place with both catalysts.

In general, sugarcane bagasse proved to be an attractive feedstock for 2G biorefineries, with an overall yield of 30.5 wt.% of upgraded oil. By the selection of the appropiate catalyst, the final composition of the upgraded oil can be adjusted. However, further studies should consider the minimazation of polymerization during hydrotreatment reactions and higher deoxygenation levels should be targeted.

Chapter 7. Evaluation of nickel-based catalysts for hydrotreatment of bio-oil model compound mixtures in a continuous flow reactor: selectivity and resistance to sulfur poisoning

List of abbreviation – Chapter 7

FPBO: Fast pyrolysis bio-oil

MM1: Model mixture 1 composed of 5 wt.% guaiacol in 1-octanol

MM2: Model mixture 2 composed of 0.05 wt.% of sulfur (as 1-octanethiol) and 5 wt.% guaiacol in 1-octanol

POC: Pyrolysis Oil Converter Unit

TOS: Time on stream

Abstract Chapter 7

The catalytic activity of two high loaded nickel-based catalysts was evaluated in a continuously operated trickle bed reactor. The conversion of model substances was evaluated with and without the presence of sulfur in the feedstock. Both catalysts were active for more than 48 h of time on stream without reduction of activity by the addition of sulfur to the feedstock, while the selectivity was affected. Formation of Ni_3S_2 was observed in both catalysts but the higher intensities of metallic nickel in the spent nickel-chromium catalyst might indicate higher resistance of this catalyst to sulfur poisoning. Overall both catalysts were active over the reaction time tested, although it was assumed that the hydrogenation capacity is reduced by sulfur poisoning.

7.1 Introduction

The development of catalysts for hydrotreatment of FPBO is currently a hot topic of research, as introduced in the previous chapters. This is mainly due to the search for highly active catalysts, which are stable and resistant to deactivation. In this case, deactivation promoted by sintering, poisoning, leaching and coke deposition [253] must be overcome.

Nickel-based catalysts are considered good candidates for FPBO hydrotreatment [72,96,99,102,116,117]. Referred as very active catalysts, the abundance and low cost also contributed to the interest to employ nickel for hydrotreatment reactions, whether used as single metal [101], or combined to others such as Cu [70], Mo [64], P [254] in the catalyst formulation.

However, deactivation of nickel catalyst by the influence of sulfur have been reported in many chemical processes, such as steam reforming and methanation [253] as well as in hydrotreatment of FBPO. Although present in concentration of usually below 0.05 wt.% [52], this is enough for catalyst deactivation. It should be taken into account that the concentration of sulfur in the FPBO may vary significantly, depending of the biomass pyrolyzed. Due to the irreversible adsorption and the practical difficulty of regeneration [255], the understanding of poisoning caused by sulfur and the development of sulfur-resistant catalysts is crucial for long-term operation of FBPO hydrotreatment units.

Usually the catalyst deactivation can be minimized by the addition of promoters and selection of specific supports [253,255]. Consequently, the design of stable, robust and resistant catalysts able to lower or prevent deactivation is necessary to allow the upscaling and industrial operation of upgrading units.

As previously mentioned in the introduction of Chapter 3, promoters of chromium, such as Cr_2O_3, may be an alternative to improve the resistance of nickel-based catalyst against sulfur poisoning, increasing the catalytic activity [42], preventing sintering [46,47] and hydrogenating carbonyl groups [48] related to FPBO instability phenomena [49].

Although the investigation with real FBPO is indispensable to upscaling of hydrotreatment units, the use of simplified systems using model compounds contributes to the understanding of important reaction pathways, potentially hidden by the complex composition of hundreds of substances present in the FBPO. Especially for deactivation studies, the use of model compounds facilitates the investigation [8,72,256,257].

While most of the basic investigation is performed in batch reactors, usually for catalysts screening, continuous operated units are required [33]. The investigation in continuous reactors,

such as trickle bed reactors, allows steady state reactions, better temperature control (usually limited in batch reactors, especially during heating and cooling steps). Furthermore, studies in continuously operated reactors give information required for further upscaling [50] and deactivation studies can be easily followed.

Thus, the present work investigates the activity and selectivity of two nickel-based catalyst. The influence of Cr_2O_3 in the Ni-based catalyst composition over the conversion of model compounds is compared to a monometallic Ni-based catalyst. Furthermore, the promoter effect of Cr_2O_3 towards sulfur poisoning resistance, previously reported elsewhere [107] is addressed. The influence of sulfur over the activity and selectivity is investigated and the resistance to poisoning of both catalysts is reported. By the investigation of model compounds conversion, the selectivity of different catalysts could be addressed while the behavior of some key molecules under different reaction conditions could be followed [65].

7.2 Materials and methods

7.2.1 Catalyts and model mixtures

The hydrotreatment reactions were conducted using benchmark Ni-based catalysts. The first one referred as Ni catalyst is composed of a high loading of Ni whereas the second catalyst contains 15 wt.% of Cr_2O_3. Detailed information is presented in Chapter 3.

The experiments in continuous flow were performed applying two distinct mixtures of model compounds. The first model mixture (MM1), was composed of 5 wt.% guaiacol (Sigma-Aldrich) in 1-octanol (Sigma-Aldrich). The influence of sulfur on the hydrotreatment and catalyst deactivation was evaluated by applying a second model mixture (MM2), composed of 5 wt.% guaiacol, 0.05 wt.% of sulfur (as 1-octanethiol) in 1-octanol.

7.2.2 Hydrotreatment Unit

The hydrotreatment reactions were conducted in continuous flow using a trickle bed reactor, a so-called Pyrolysis Oil Converter Unit(POC), located at the Technical University of Denmark [72]. The unit is divided in gas feed section, liquid feed section, reactor, gas and liquid treatment sections (Figure 45).

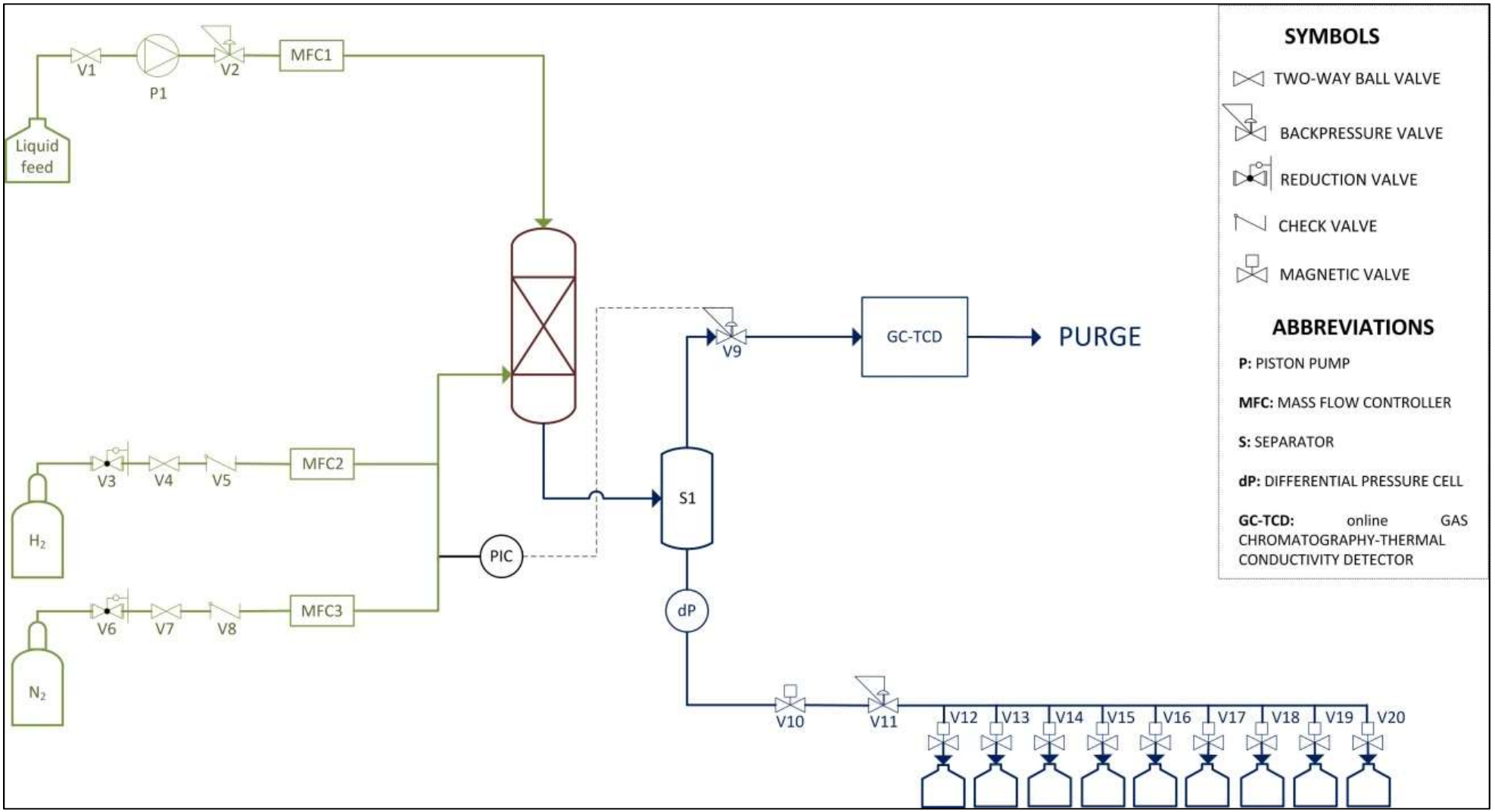

Figure 45. Simplified schematic diagram of the Pyrolysis Oil Converter unit. The gas and liquid feed sections are represented in green color, the reactor is represented in brown color and the liquid and gas treatment section is represented in blue color.

The POC unit operates at a maximum of 125 bar and 550 °C. The reactor is composed of an electrically heated oven, internal reactor tube (SS 316 stainless steel 91.5 cm length, outer diameter of 10 mm and inner diameter 8 mm, support pin for the catalytic bed at 42.5 cm from the bottom) and external pressure shell tube (SS 316 stainless steel 90.6 cm length including the flanges, inner diameter of 2 cm). The oven (Carbolite TVS12/600) has a heated zone of 60 cm.

The liquid was fed to the top of the inner reactor tube, while the gas was fed to the bottom of the pressure shell. The gas flowed to the top of the shell (flowing outside the internal reactor tube) to be pre-heated and entered the internal tube containing the catalytic bed (Figure S.35).

The liquid was fed to the setup using a piston pump (HPLC pump Knauer 100 A50102, 10 ml head) at a flow rate of 0.2 ml/min. The pump was calibrated prior the experiments (further information in the supplementary material, section b). A mass flow controller (Brooks Flomega 5882) was used to measure flow and as 'open and close' accessory, while the flow rate was controlled by the pump. The pressure was build up with a backpressure valve. The setup can be fed simultaneously with two gas lines of nitrogen and hydrogen, respectively, using mass flow controllers.

After the reaction part of the unit, the gas and liquid products were cooled before entering the separator tube S1. The line after the reactor was cooled by a WR recirculation chiller RC-10 basic, water cooling set at 7 °C. The separator tube was 49 cm long, and the gas/liquid products entered 27 cm from the bottom. The gas flowed to the top of the separator tube whereas the liquid was accumulated at the bottom of the separator tube. The height (h) of liquid was measured by the pressure difference (ΔP) between the top and bottom of the separator tube (differential pressure cell Honeywell STD924), liquid density (ρ) and gravitational acceleration (g) as follow:

$$h = \Delta P / \rho.g$$

A magnetic valve opened when a certain height of liquid was reached and a backpressure valve was manually set allowing a constant flow out of the POC unit to the vials. The samples were collected at approximately ambient pressure in pre-defined intervals. A valve manifold composed by eight magnetic two-way valves is programmed allowing unsupervised collection of liquid samples.

The gas flowed through a backpressure regulator (Baumann type 51000) responsible for controlling the pressure in the POC unit. The gas then flowed through a filter and was analyzed online every 22 minutes by a gas chromatograph with a thermal conductivity detector. Details are given in section 7.2.3.

7.2.3 Hydrotreatment reactions

An amount of 0.5 g of sieved catalyst (<125 μm) was mixed with 4 g of silicon carbide (150-250 μm) and transferred to the steel reactor. A layer of 1 cm of glass wool was placed in the bottom (support for the catalyst bed), followed by the mixture of catalyst + SiC (approximately 5 cm) and a final layer of glass wool (2 cm) was placed on top to achieve a homogeneous liquid distribution over the catalyst bed (Figure S.37).

Prior to the catalytic activity tests, the catalysts were reduced in-situ at 500 °C using a mixture of 10% H_2 in N_2 at ambient pressure. The total gas flow rate was kept at 500 Nml/min and the reduction took 90 minutes.

The hydrotreatment catalytic activity tests were conducted at 325 °C, 60 bar at a flow rate of 500 Nml/min of 90% H_2 and 10% N_2 with a liquid feed flow rate of 0.2 ml/min. All the tests were initiated applying the model mixture 1 (5 wt.% guaiacol in 1-octanol), called MM1. For runs where the evaluation of the influence of sulfur on the catalytic performance was evaluated, the model mixture (MM1) was switched after 5 h on stream (TOS) to a model mixture 2 (MM2), composed of 5 wt.% guaiacol, 0.05 wt.% 1-octanethiol in 1-octanol.

After the reaction was completed, the setup was fed with 100% N_2 (500 Nml/min) for 30 minutes at the reaction temperature and pressure. The pressure was reduced and any liquid remaining in the liquid treatment section was collected. The reactor was cooled to ambient temperature overnight. The spent catalyst was removed from the reactor tube and sieved in order to separate the catalyst from the glass wool and SiC for further characterization.

7.2.4 Liquid Products Characterization

The liquid products were analyzed using a GC-MS/FID (Shimadzu GC MS-GP 2010 Plus) after dilution with acetone (1:10). The GC was equipped with an Equity-5 column (Sigma Aldrich), 30 m x 0.32 mm x 0.5 μm. The program started at 40 °C kept for 8 minutes; the temperature was then increased at a rate of 10 °C/min to 250 °C and kept for 5 minutes. The injector and FID detector were maintained at 250 °C. A volume of 1 μl of sample was injected with a split of 1:80.

Qualitative data was obtained by comparing the MS spectra with the library (NIST 2008). The concentrations of compounds were obtained from the areas obtained with the FID detector. External calibration curves were used for quantification of guaiacol and 1-octanol, while the compositions of the liquid products were analyzed qualitatively.

7.2.5 Catalyst Characterization

The fresh and spent catalysts were analyzed by X-ray powder diffraction (XRD). The XRD patterns were recorded according to the methodology previously presented in Chapter 3. Further characterization was performed by Scanning Electron Microscopy/Energy Dispersive X-ray spectroscopy (SEM/EDX, GeminiSEM 500, equipped with a thermal Schottky field-emitter cathode, Zeiss, software SmartSEM 6.01). The catalysts were characterized before and after the reaction. Further details about the analytical techniques were already presented in Chapter 3.

7.3 Results

7.3.1 Conversion of guaiacol and 1-octanol

The conversion of guaiacol and 1-octanol as a function of time on stream (TOS) is depicted in Figure 46, considering a model mixture free of sulfur (MM1, see item 7.2.1) and a sulfur-containing mixture (MM2). While the conversion of guaiacol applying MM1 with Ni catalyst is higher than 80 %, the conversion with NiCr catalyst initially reaches 68.2 %, being reduced to around 41 % after 18 h of TOS, remaining in this range as the TOS increases. In terms of 1-octanol, the conversion remained above 70% along the reaction with Ni catalyst and MM1. NiCr catalyst, on the other hand, initially showed a conversion of around 60 %, being reduced to around 20 % after 28 h of TOS. The conversion stays in this range along all the reaction.

By the addition of sulfur to the model mixture, the conversion of guaiacol and 1-octanol with Ni catalyst is still higher compared to NiCr catalyst, while the conversion is slightly increased in comparison to MM1 for both catalysts. Hence, reduction of the catalytic activity was not inhibited by the addition of sulfur. Even with the formation of Ni_3S_2 (later discussed in section 7.3.3) and changes on the selectivity (discussed in section 7.3.2), both catalysts were active over the influence of sulfur along the TOS.

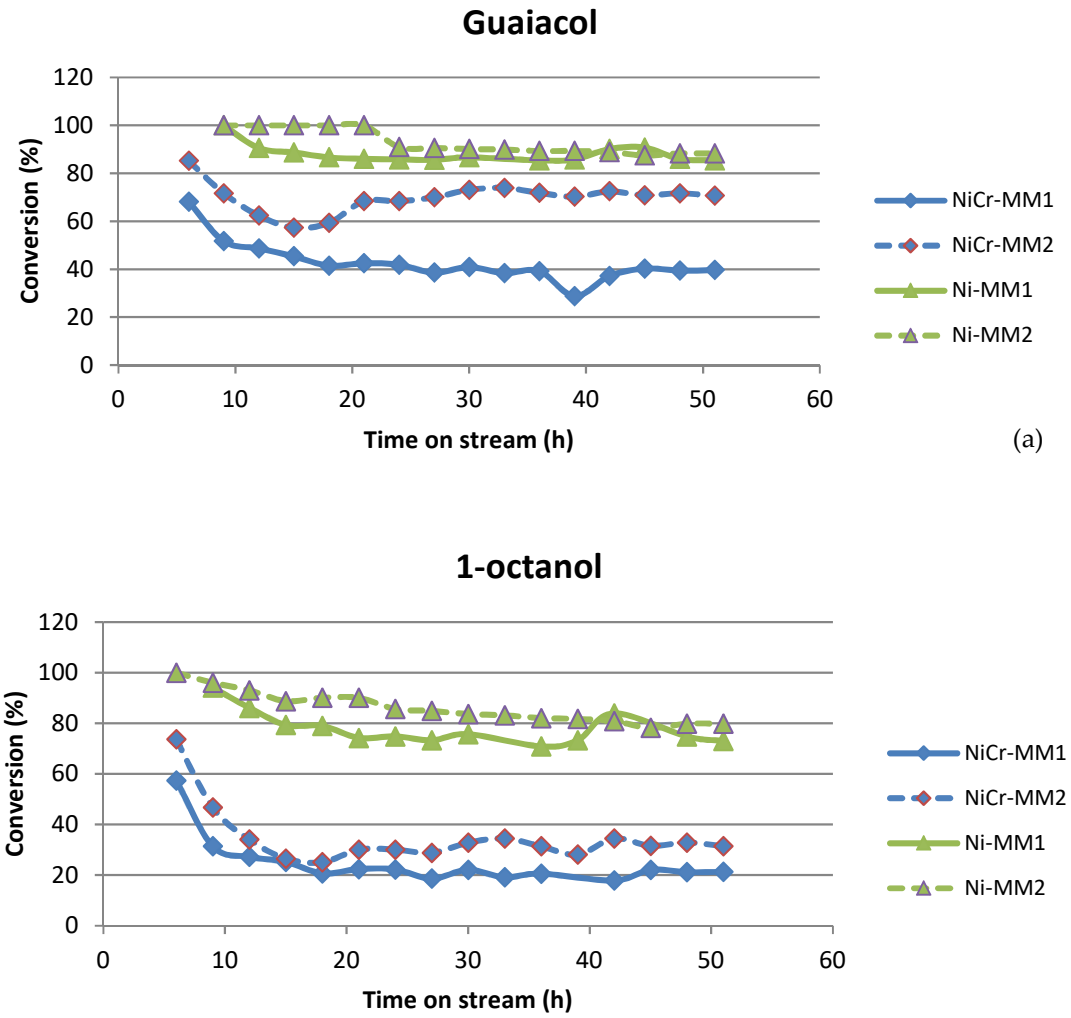

Figure 46. Conversion of (a) guaiacol and (b) 1-octanol with and without the addition of sulfur to the liquid feed as a function of time on stream. MM1: Model mixture without sulfur; MM2: Model mixture with sulfur.

7.3.2 Chemical composition of upgraded liquids: qualitative investigation of selectivity and reaction pathways

Differences in selectivity between both catalysts as well as by the addition of sulfur to the feed were observed in the liquid products. The main compounds observed in the liquid samples are shown in Figure 47 while minor compounds are available in the supplementary material (Figure S.38). To perform the evaluation, peaks of 15 compounds qualitatively identified by comparing the MS spectra to the NIST 2008 library were integrated based on the FID signal. N-octane was the main compound observed from 1-octanol conversion over Ni catalyst, as well as with NiCr catalyst, although the selectivity with monometallic nickel catalyst was much higher in comparison to NiCr. Compounds such as 3-methylheptane and 2-methylheptane were exclusively observed in the liquid products obtained with Ni catalyst, while n-hexane was mostly formed with

Ni catalyst. Branched hydrocarbons were most probably formed by hydrodeoxygenation of 1-octanol, followed by isomerization (Figure 48), while hydrocracking of 1-octanol resulted in n-hexane. The abundance of some of the main compounds observed in the liquid upgraded products with Ni catalyst and MM1 was significantly reduced by the addition of sulfur (MM2), although the conversion of guaiacol and 1-octanol was not reduced. As previously stated, changes in the selectivity are expected upon catalyst poisoning [255,258]. For example, 1-methoxyoctane formed by methylation of 1-octanol [259], was observed in the upgraded liquids with Ni catalyst and MM1; however, it was not observed in the upgraded liquids by the reactions conducted with Ni catalyst and MM2. In this case, the reaction follows another pathway.

The conversion route of 1-octanol to dioctylether, as a result of the dehydration of 1-octanol (Figure 48, reaction 5) [260] is suppressed by the addition of sulfur. The same is observed with the reaction route for octanal, octyl-cyclohexane and cyclohexane formation. Octanal was most probably formed by dehydrogenation of 1-octanol [261] while octyl-cyclohexane followed a more complex pathway. In this case, guaiacol undergoes demethoxylation to phenol, hydrogenation of the aromatic ring and dehydration. Hence the very reactive cycloalkene is reacted with 1-octene (formed by dehydrogenation of 1-octanol [257,261]) resulting in octyl-cyclohexane. Cyclohexane, on the other hand, was formed by the hydrogenation of guaiacol, followed by demethoxylation and hydrodeoxygenation, respectively [72]. The reaction pathways towards alkenes formation, such as cis-2-octene, 1-octene and trans-4-octene are preferred in the presence of sulfur. All alkene isomers are products of dehydration of 1-octanol [261], although higher abundance is observed for internal alkenes, such as cis-2-octene, as they are more stable than primary alkenes [262]. Formation of 2,3-dimethyl-1-hexene is only observed with MM2 as feedstock.

Differences in selectivity with the NiCr catalyst in contrast to Ni catalyst as well as selectivity change by the sulfur added to the feedstock were observed. N-octane was the main product observed, due to dehydration of 1-octanol followed by hydrogenation [256]. Dioctylether was the second most abundant compound. When sulfur was present in the feedstock, the selectivity to octanal (much higher with NiCr in contrast to Ni catalyst), 1-methoxyoctane, dioctylether and octyl-cyclohexane formation were significantly reduced, after 27 h, 12 h, 12 h and 27 h of TOS, respectively. The abundance of compounds such as cis-2-octene and trans-4-octene increased sharply, while 1-octene initially absent in the products with MM1 is formed with MM2. The highest formation of cis-2-octene, 1-octene, trans-4-octene for both catalysts and 1-octene for Ni catalyst observed with the sulfur-containing model mixture may be attributed to the formation of Ni_3S_2 in both catalysts, observed by XRD (Figure 49) and later discussed (section 7.3.3). As previously reported, the sulfur atom modifies the nearest Ni atoms electronically as well as blocks metallic sites, lowering the ability of dissociative adsorption of H_2 [108,255] and

reactant molecules [75]. Hence, it would explain the higher abundance of alkenes in the liquid products obtained with MM2; the ability to hydrogenate the alkenes and further isomerize the molecules for products such as 2,4-dimethylhexane (Ni catalyst) or formation of 1-1'oxobisoctane and 1-methoxyoctane with NiCr is reduced, resulting in the highest concentration of octenes, as observed. It should be taken into account, considering that alkenes are attributed to polymerization resulting in coke formation [65], responsible for further deactivate the catalyst by covering the active site [100,258] and reducing the upgraded liquid yields. Compounds such as phenol, para-tolyl octanoate, phenol and 1,2-benzenediol even in low abundances, were exclusively observed in the liquid products obtained with NiCr and MM2. As previously reported, the hydrogenation of aromatic rings can be also affected by the structural changes promoted by sulfur over nickel-based catalysts [53].

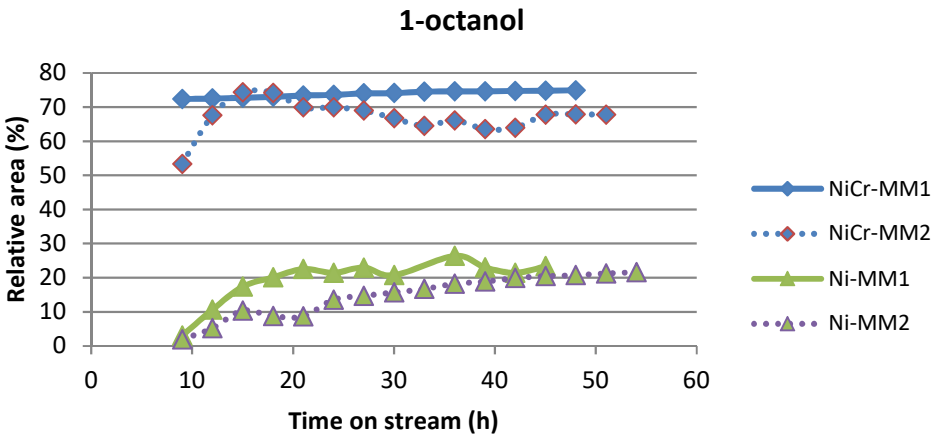
1-octanol
Relative area (%)
Time on stream (h)
NiCr-MM1
NiCr-MM2
Ni-MM1
Ni-MM2

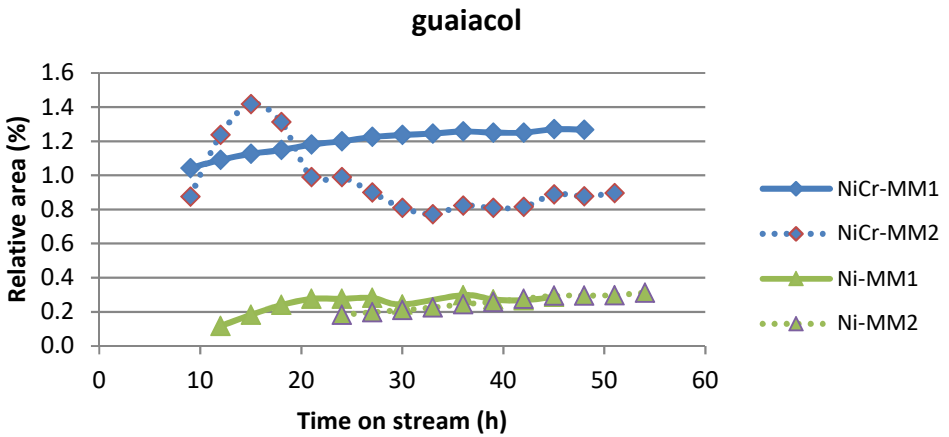
guaiacol
Relative area (%)
Time on stream (h)
NiCr-MM1
NiCr-MM2
Ni-MM1
Ni-MM2

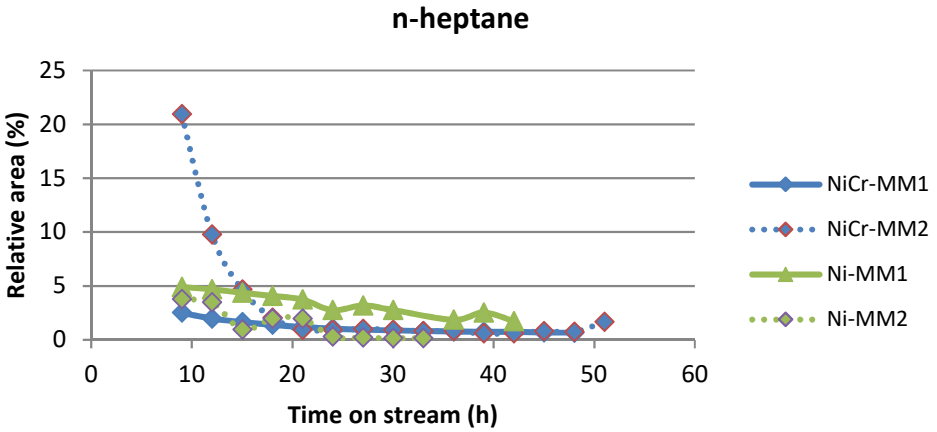
n-heptane
Relative area (%)
Time on stream (h)
NiCr-MM1
NiCr-MM2
Ni-MM1
Ni-MM2

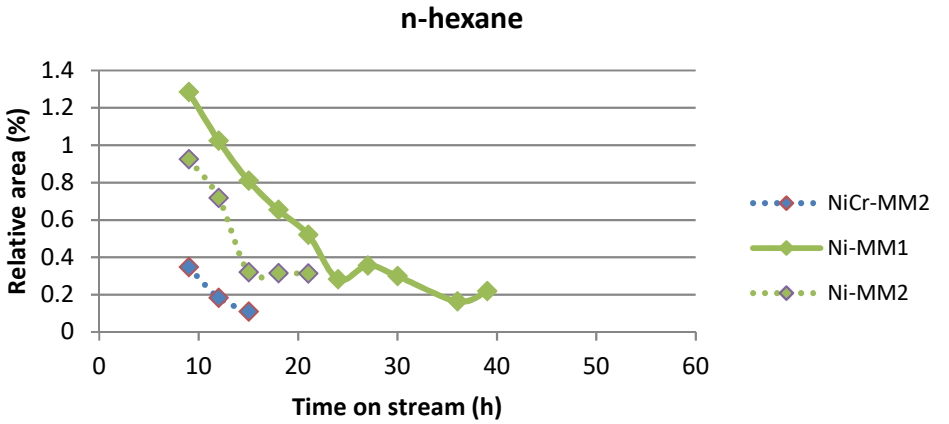
n-hexane
Relative area (%)
Time on stream (h)
NiCr-MM2
Ni-MM1
Ni-MM2

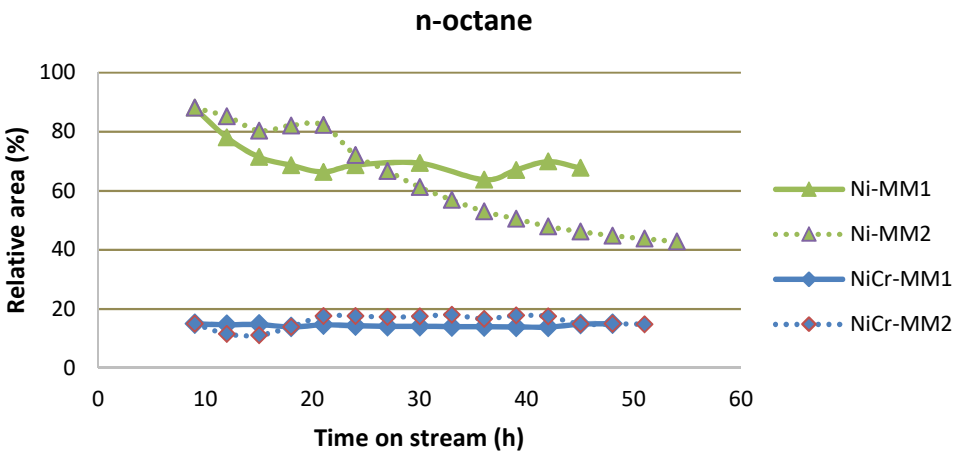
n-octane
Relative area (%)
100
80
60
40
20
0
0
10
20
30
40
50
60
Time on stream (h)
Ni-MM1
Ni-MM2
NiCr-MM1
NiCr-MM2

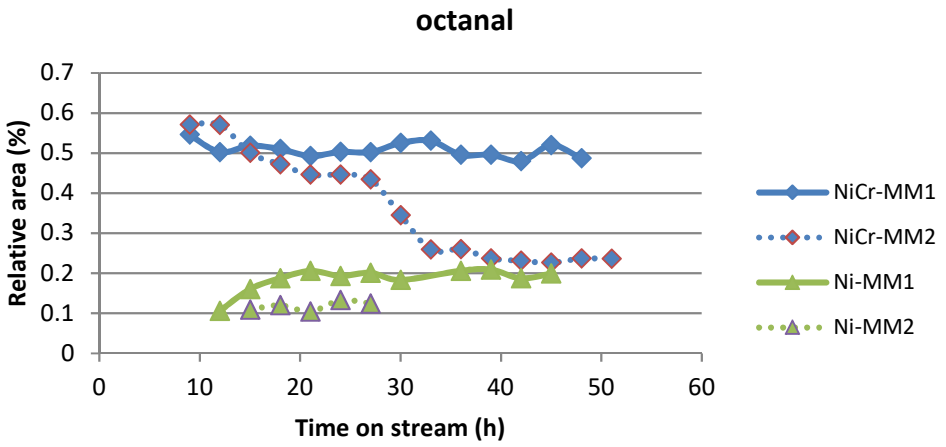
octanal
Relative area (%)
0.7
0.6
0.5
0.4
0.3
0.2
0.1
0
0
10
20
30
40
50
60
Time on stream (h)
NiCr-MM1
NiCr-MM2
Ni-MM1
Ni-MM2

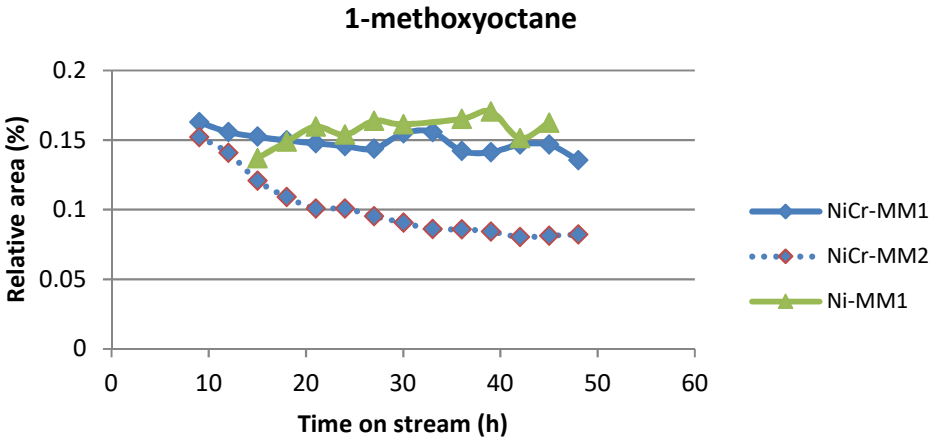
1-methoxyoctane
Relative area (%)
0.2
0.15
0.1
0.05
0
0
10
20
30
40
50
60
Time on stream (h)
NiCr-MM1
NiCr-MM2
Ni-MM1

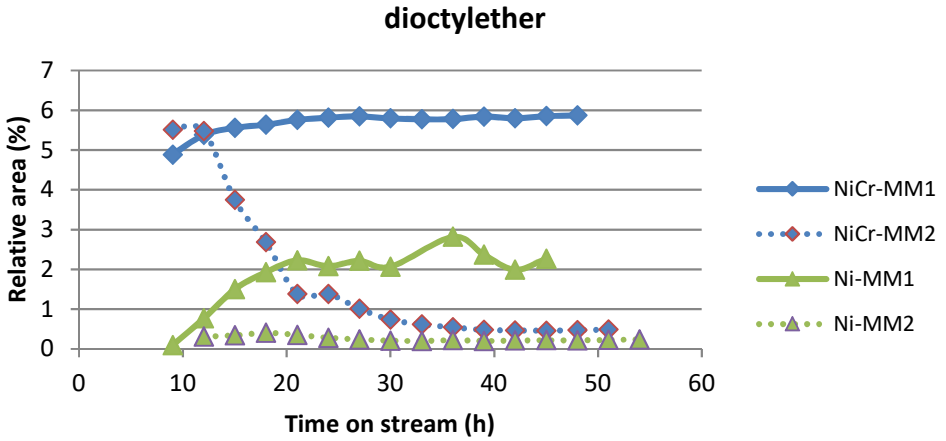
dioctylether
Relative area (%)
7
6
5
4
3
2
1
0
0
10
20
30
40
50
60
Time on stream (h)
NiCr-MM1
NiCr-MM2
Ni-MM1
Ni-MM2

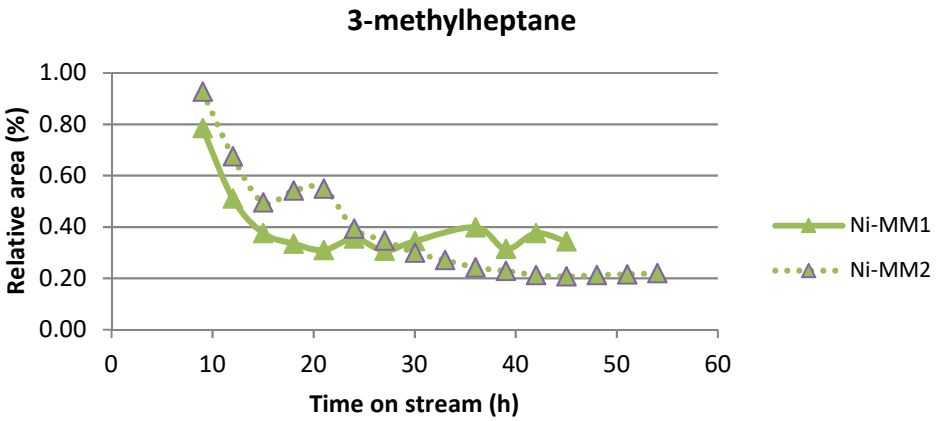
3-methylheptane
Relative area (%)
1.00
0.80
0.60
0.40
0.20
0.00
0
10
20
30
40
50
60
Time on stream (h)
Ni-MM1
Ni-MM2

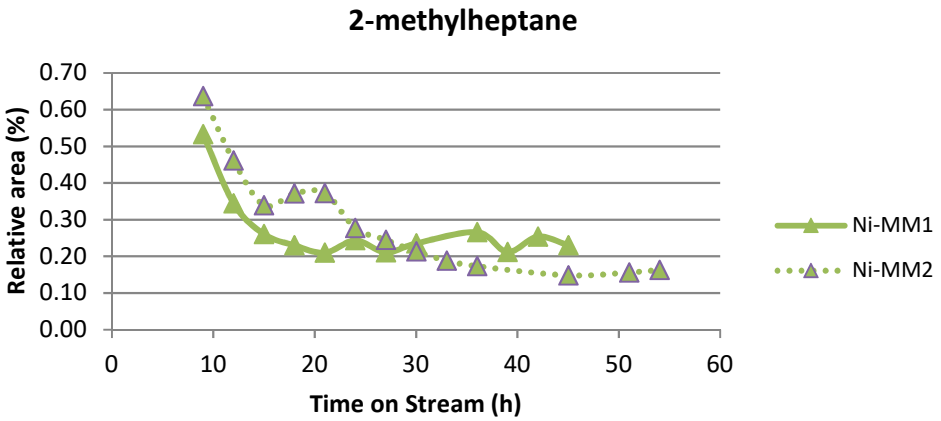
2-methylheptane
Relative area (%)
0.70
0.60
0.50
0.40
0.30
0.20
0.10
0.00
0
10
20
30
40
50
60
Time on Stream (h)
Ni-MM1
Ni-MM2

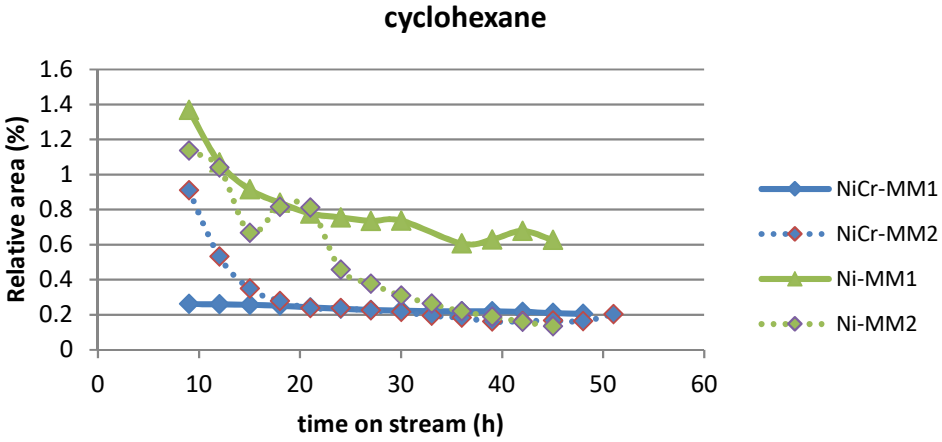
cyclohexane
Relative area (%)
1.6
1.4
1.2
1
0.8
0.6
0.4
0.2
0
0
10
20
30
40
50
60
time on stream (h)
NiCr-MM1
NiCr-MM2
Ni-MM1
Ni-MM2

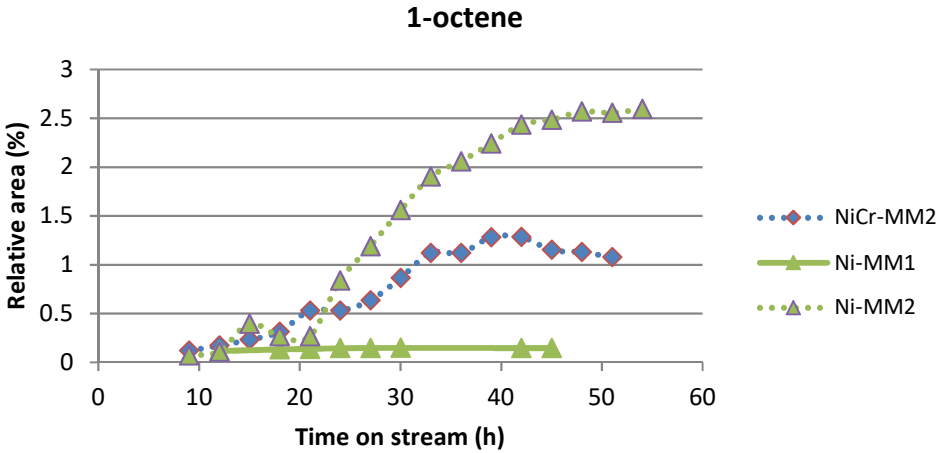
1-octene
Relative area (%)
3
2.5
2
1.5
1
0.5
0
0
10
20
30
40
50
60
Time on stream (h)
NiCr-MM2
Ni-MM1
Ni-MM2

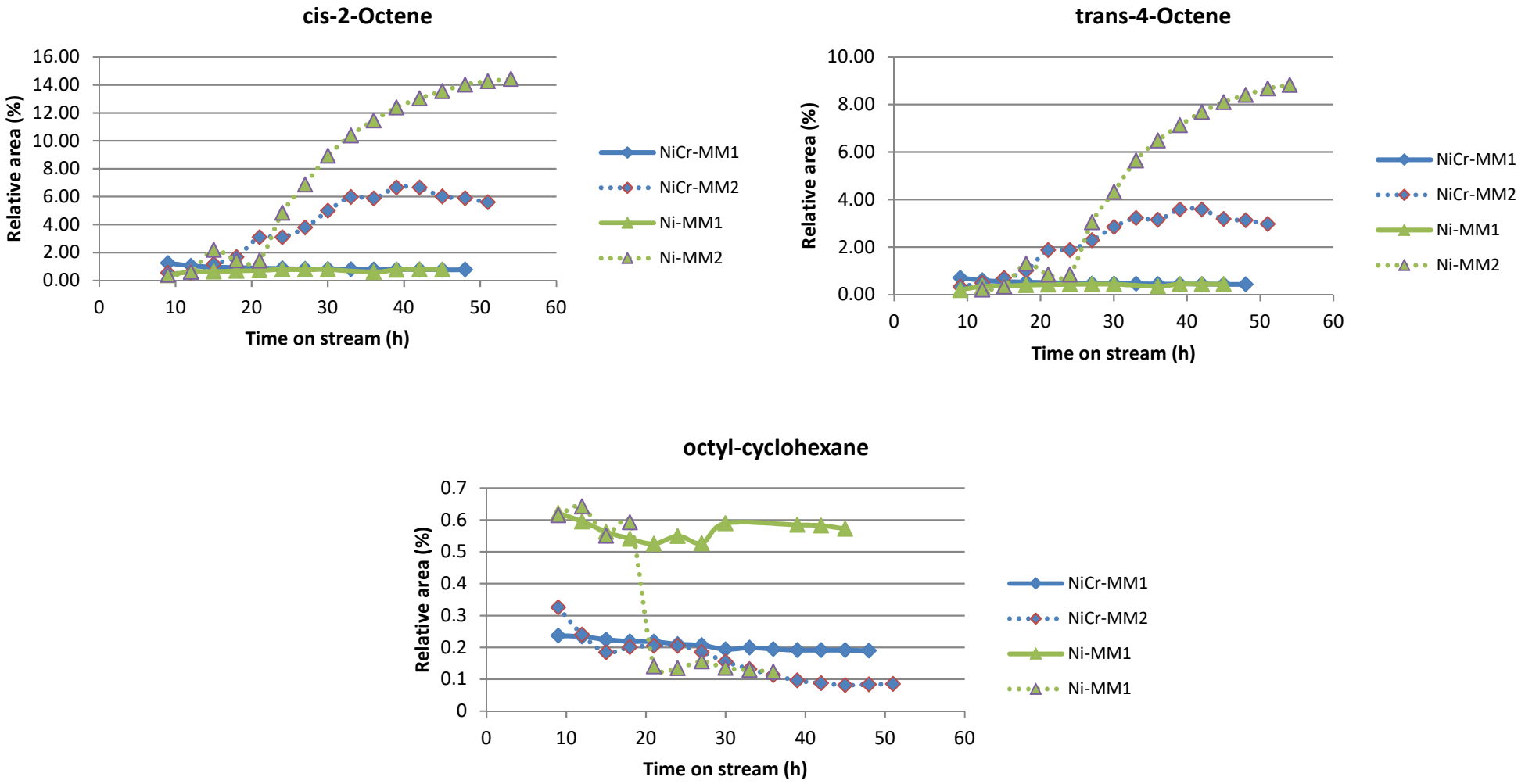

Figure 47. Main compounds identified in the upgraded liquids as function of time on stream. The samples collected at 3 h and 6 h are not depicted as residues remaining in the pipes could be present. The relative area was calculated by dividing the FID area of the compound A by the sum of the area of 15 main compounds (A_{15}) identified in the liquid products, as follow: $A/\Sigma A_{15}$. MM1: Model mixture without sulfur; MM2: Model mixture with sulfur.

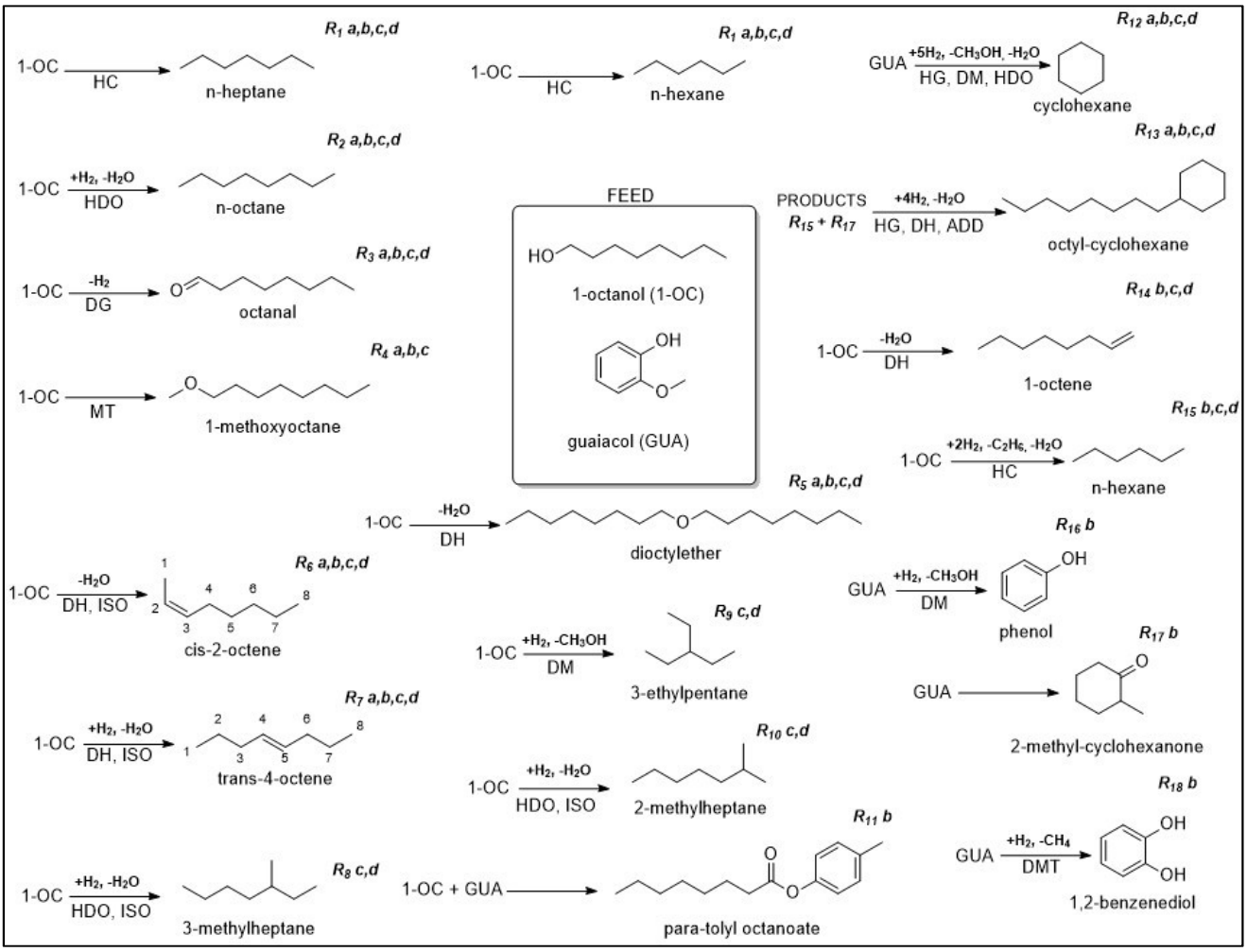

Figure 48. Reaction pathways observed during the reactions conducted with Ni and NiCr, MM1 and MM2. The reactions are identified by number (Rx: reaction number) and the conditions at which the reaction pathway was observed. a: NiCr, MM1; b: NiCr, MM2; c: Ni, MM1; d: Ni, MM2. HC: hydrocracking; HDO: hydrodeoxygenation; DH: Dehydration; DM: Demethoxylation; DMT: Demethylation; ISO: Isomerization; DG: Dehydrogenation; ADD: Addition; HG: Hydrogenation; MT: methylation.

7.3.3 Catalysts characterization

The X-ray powder diffraction of both Ni and NiCr catalysts (Figure 49) showed that the initial NiO present in both fresh catalysts is completely reduced after initial reduction treatment, in agreement with previous investigations [117]. Characteristic diffractions of NiO at 37.2°, 42.6° and 62.8° are no longer observed. The intensity of the diffractions attributed to metallic nickel (44.5°, 51.8°, 76.4°, 92.95° and 98.45°) is reduced in the spent catalysts, especially for Ni catalyst after hydrotreatment over the presence of sulfur (MM2). It shows that some metallic nickel active sites remained, not being completely modified, as described for poison substances [100]. On the other hand, the presence of bulk Ni_3S_2 shows that by the presence of sulfur the surface has been restructured causing changes in the catalytic properties [108]. Hence, the selectivity to some of the reaction pathways observed with MM1 is maintained, probably due to the remaining metallic nickel, whereas some changes in selectivity observed are probably related to Ni_3S_2. Diffractions

attributed to Ni_3S_2 are observed in both catalysts (21.756°, 31.102°, 37.496°, 49.726°, 50.114°, 55.157°).

The chromium containing catalyst showed highest diffraction intensity for metallic Ni, and lower diffraction intensity of Ni_3S_2. The presence of Cr_2O_3 in the catalyst composition may contribute to the sulfur poisoning resistance. As previously described, by combining Ni in the catalyst formulation with metals with higher free energy of sulfide formation, such as chromium, the resistance to sulfur poisoning may increase, although the stability of Cr_2O_3 ($\Delta G°$=-1046 kJ/mol) is higher than the chromium sulfide ($\Delta G°$=-109 kJ/mol) [255].

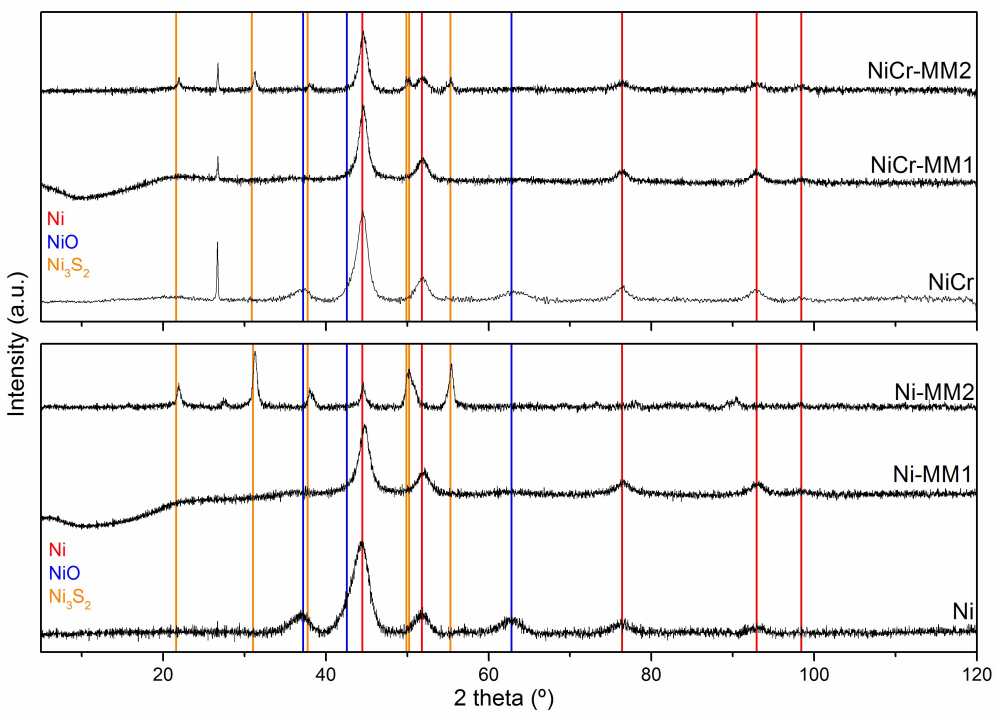

Figure 49. XRD powder diffraction of both catalysts before and after hydrotreatment reaction with MM1 (without sulfur) and MM2 (with sulfur).

The composition of the fresh and spent catalysts surfaces was determined by SEM-EDX. Carbon concentration remained near the same range for both catalysts. The significantly higher concentration of carbon observed for the NiCr-MM2 (27.9 wt.%) is probably due to SiC particles not completely separated from the catalyst after hydrotreatment, also confirmed by the high concentration of Si compared to other regions and samples analyzed. The difficulty in separate the catalyst and SiC was mainly due to the paste consistency of the catalyst after hydrotreatment reactions.

Table 30. SEM-EDX of selected areas of fresh and spent catalysts

Mixture		C (wt.%)	S (wt.%)	Ni (wt.%)	Si (wt.%)	Cr (wt.%)
NiCr	**Area 1**	10.4	-	25.5	10.8	4.7
	Area 2	7.7	-	28.6	9.6	5.4
NiCr-MM1	**Area 1**	10.8	1.6	45.4	11.3	7.5
	Area 2	11.5	1.6	52.3	6.8	9.2
NiCr-MM2	**Area 1**	27.9	3.8	9.8	46.8	1.4
	Area 2	12.9	15.3	32.9	14.1	3.1
Ni	**Area 1**	9.3	-	32.4	9.4	-
	Area 2	8.1	-	34.0	8.6	-
Ni-MM1	**Area 1**	8.9	2.4	57.0	8.5	-
	Area 2	8.7	2.0	60.5	7.2	-
Ni-MM2	**Area 1**	10.1	15.9	48.7	7.9	-
	Area 2	8.2	15.4	48.7	9.8	-

Both fresh catalysts were free of sulfur. After the reaction with MM1 a small amount of sulfur is detected in the catalyst surfaces. Considering that previously a catalyst which required sulfidation was tested in the POC setup, the residual sulfur present most probably resulted in a slight contamination of the samples. However, no changes were observed in the diffraction patterns, revealing that the low concentration of sulfur observed over the catalyst was not enough to result in structural changes. Hence, in this case we assumed that sulfur had no significant effect over the hydrotreatment reactions.

On the other hand, by the addition of sulfur into the feedstock a significant amount is observed over the catalyst surface, in agreement with the formation of Ni_3S_2 given by XRD results (Figure 49), with similar amounts observed in both catalysts.

7.4 Conclusion

The conversion of bio-oil model mixtures was evaluated in a continuous flow reactor. The differences in selectivity due to the catalysts composition and the addition of sulfur to the feedstock were evaluated. Both Ni and NiCr catalysts were active for conversion of 1-octanol and guaiacol for more than 48 h of time on stream. Higher conversions were obtained with the Ni catalyst. For both catalysts the conversion was not reduced by the addition of sulfur to the liquid feedstock, although the selectivity was affected. The Ni catalyst was mainly selective for n-octane, 3-methylheptane and 2-methylheptane, while NiCr produced n-octane and dioctylether as the main products. By the presence of sulfur to the feedstock, the selectivity towards alkenes significantly increased for both catalysts while the main pathways observed with Ni and NiCr were inhibited.

The formation of bulk Ni_3S_2 was observed in both spent catalysts after upgrading with sulfur-containing model mixtures. The highest metallic Ni diffraction intensity observed for the chromium-containing catalyst may reveal higher resistance to sulfur poisoning by this catalyst.

However, due to the higher abundance of alkenes in the liquid products with both catalysts, as well as the detection of aromatic compounds in the upgraded liquids with NiCr catalysts, it is assumed that the dissociation of H_2 molecules and further hydrogenation capacity of both catalysts was compromised.

Hence, both nickel-based catalysts proved to be active for hydrotreatment reactions. Considering that the conversion was not affected during the interval of time tested, the composition of the fast pyrolysis bio-oil may lead to a different range of products in the upgraded bio-oil by the presence of contaminants in the feed. Further studies should consider longer reaction periods and must investigate the influence of sulfur and other poisoning substances using fast pyrolysis bio-oil.

Chapter 8. Conclusions and Outlooks

Biomass shows a significant potential to be converted into fuels and chemicals through thermochemical conversion routes, especially by fast pyrolysis which already achieved commercial maturity. However, the application of fast pyrolysis bio-oil is still limited. This is mainly due to its high content of oxygen-containing organic compounds, high water content, low energy density, high acidity and its tendency towards ageing. All of these unfavourable properties must be overcome if replacement of crude oil based fuels is intended.

Hydrotreatment, considered a most promising technology to upgrade FPBO properties, still needs further investigation, as introduced in detail in Chapter 1. The research questions and issues raised in Chapter 2 must be answered, allowing the selection of the best catalyst for continuously operated hydrotreatment reactions, upscaling and stable operation of FPBO hydrotreatment units in biorefineries.

Thus, the present thesis studied the application of nickel-based catalysts for hydrotreatment of fast pyrolysis bio-oils. The influence of promoters, supports, feedstocks and poisoning substances was systematically investigated along the chapters.

In Chapter 3 the catalytic activity of both benchmark high loaded nickel-based catalysts was compared to Ru/C. The influence of promoters, temperature, reaction time and 2-step hydrotreatment was presented. In comparison to Ru/C, both nickel-based catalysts produced higher yields of upgraded oil. The oxygen removal was similar to Ru/C and nickel-chromium catalyst, as well as the concentration of carbon and hydrogen in the upgraded oils. However, highest hydrogenation activity was observed for both nickel-based catalysts. Consequently, nickel catalysts showed higher H/C ratio in comparison to Ru/C, especially at 225 °C, revealing the influence of temperature over the hydrogenation activity. In general, the concentration of ketones was significantly reduced with both nickel-based catalysts and both were selective towards formation of alcohols. Among them, nickel-chromium catalysts showed the highest conversion of organic acids, sugars and ketones, attributed to the presence of Cr_2O_3 in the catalyst formulation and the strength of the acid sites. Comparable composition of upgraded oils in terms of elemental analysis, as well as gas production and gas composition were obtained with 2 h and 4 h of reactions. The longer the reaction the higher the hydrogen consumption as well as the lower the water concentration in the upgraded oil. The 2-step upgrading resulted in an upgraded oil with 90 % less water, 64.8 % less oxygen and with 90 % higher HHV in comparison to the beech wood fast pyrolysis bio-oil. The solid formation for all the reactions was below 1 % and evenly distributed over the catalysts. In summary, both benchmark nickel-based catalysts proved to be active to hydrotreatment of beech wood fast pyrolysis bio-oil with activity comparable to Ru/C. Especially the nickel-chromium catalyst showed to be the most interesting option, due to the

highest degree of deoxygenation, highest H/C ratio at 225 °C and lower hydrogen consumption compared to monometallic nickel-based catalyst. Furthermore, the highest conversion of organic acids, ketones and sugars make nickel-chromium a good candidate for further investigation.

Due to the promissing results observed in Chapter 3, the upgrading reaction parameters in terms of reaction temperature, pressure and feedstock were optimized with nickel-chromium catalyst in Chapter 4, at a reaction time of 2 h. The multiphase beech wood FPBO was completely upgraded (mixture of light and heavy phase) was well as the isolated heavy phase. At higher temperatures (275 – 325 °C), lower oxygen content and higher concentration of carbon were obtained in the upgraded oils. The production of gas was also promoted by higher temperatures. The higher consumption of hydrogen observed at 100 bar had no influence over the degree of deoxygenation, although hydrogenation was favored. The upgraded oil characterization showed that reactive compounds were converted while aromatics remained in similar range in all conditions tested. Independent of the feedstock composition (light phase + heavy phase or isolated heavy phase) the upgraded oils showed similar composition in terms of elemental analysis as well as higher heating value and water content. The highest degree of deoxygenation of 42 % was obtained at 325 °C with the complete feedstock (light phase + heavy phase). The highest amount of solid over the spent nickel-chromium catalyst was obtained when the isolated heavy phase was employed as feedstock. It was assumed that its composition rich in lignin derivative compounds resulted in condensation of phenolic compounds leading to formation of coke. In general, the similarities of the upgraded oils in terms of chemical composition, independent of the feedstock, showed that the use of the complete beech wood FPBO is more favourable. The temperature of 325 °C proved to be the optimum temperature and pressure of 80 bars, due to the lower consumption of H_2, without influencing the deoxygenation rate obtained with nickel-chromium catalyst.

Due to the significant amount of oxygen still remaining in the upgraded oil, despite the high hydrogenation activity, even at optimized conditions in Chapter 4, the development of catalysts with higher deoxygenation activities was proposed in Chapter 5. Thus, in this chapter four nickel-based catalysts were synthesized and evaluated for hydrotreatment of beech wood fast pyrolysis bio-oil at 325 °C and 80 bar of H_2. Lower reduction temperatures were observed with the bimetallic catalysts $NiCu/SiO_2$ and $NiCu/ZrO_2$ in contrast to monometallic Ni/SiO_2 and Ni/ZrO_2, which correlates with the addition of copper and high concentration of metal. Overall, all the catalysts were active for hydrotreatment, resulting in upgraded oils with reduced oxygen and water content but both copper-containing catalysts showed higher consumption of H_2 and different selectivity compared to monometallic Ni catalysts. Especially the conversion of furfural was promoted when bimetallic catalysts were used for hydrotreatment. The highest

hydrodeoxygenation was obtained with Ni/SiO_2, with more than half of the original oxygen content of the feedstock removed. In this case the upgraded oil showed a reduction of 80 % in the water content. Due to the best hydrodeoxygenation activity, Ni/SiO_2 was selected for evaluation of consecutive cycles of hydrotreatment-regeneration. The catalytic activity slightly decreased over consecutive cycles, caused by sintering and poisoning. It was reflected in the consumption of hydrogen, which was reduced along the cycles. In addition, the partial loss of activity most probably reduced the conversion of sugars, as sugar derivative compounds were observed in the upgraded products in lower intensities. Thus, all catalysts synthesized by wet impregnation were active for hydrotreatment of beech wood fast FPBO. Especially Ni/SiO_2 showed the highest activity for hydrodeoxygenation and for other important properties, such as lowest water concentration in the upgraded oil and lowest yields of gas and solids.

Hence, based on the promising results with nickel-chromium catalyst in Chapter 3 and 4, as well as the results observed with Ni/SiO_2 in Chapter 5, the investigation of the catalytic activity using fast pyrolysis bio-oils from non-wood biomass was proposed in Chapter 6, aiming the evaluation of the catalytic behavior.

Thereby, in Chapter 6 an investigation of the complete value chain, from sugarcane bagasse characterization, fast pyrolysis and hydrotreatment applying both nickel-chromium and Ni/SiO_2 catalyst is performed. The work investigated not just the hydrotreatment pathway itself, but the integration of the thermochemical conversion route into the sugarcane biorefinery. A special focus was given to the evaluation of the catalytic activity of both catalysts during hydrotreatment of sugarcane bagasse fast pyrolysis bio-oil. The fast pyrolysis of sugarcane bagasse resulted in a high fast pyrolysis bio-oil yield of 60.1 wt.%, attributed to a low moisture content of 2.80 wt.% and low potassium concentration of 0.08 wt.% in the feedstock. Overall, the hydrotreatment of the sugarcane bagasse FPBO resulted in upgraded bio-oils with reduced oxygen and water content, while the carbon content was increased. However, different selectivities were observed with Ni/SiO_2 and nickel-chromium catalyst. In agreement to the hydrotreatment conducted with beech wood FPBO nickel-chromium showed the highest hydrogenation activity, largest conversion of organic acids, and highest formation of furans and alcohols, while Ni/SiO_2 showed largest deoxygenation activity, reaching 43.3 % of oxygen removal from the sugarcane bagasse FPBO. Furthermore, the highest conversion of aromatic compounds was obtained with Ni/SiO_2. Overall, 35.2 % of carbon originally in the sugarcane bagasse was recovered in the oil obtained with nickel-chromium (intermediate phase + heavy phase) whereas 41.9 % were recovered in the upgraded oil obtained with Ni/SiO_2. Polymerization took place during the hydrotreatment reaction with both catalysts, revealing to be more severe with sugarcane bagasse FPBO in comparison to polymerization observed with beech wood FPBO.

Overall, the integration of a thermochemical route for conversion of sugarcane bagasse in combination with catalytic upgrading proved to be a promising valorization route in the sugarcane biorefineries. However, the selection of the catalysts plays a role in terms of the upgraded product composition and strategies to minimize the competition between polymerization and hydrotreating reaction pathways must be considered.

Lastly, aiming at the evaluation of the catalytic performance in a continuously operated hydrotreatment unit, both high loaded benchmark nickel-based catalysts, nickel and nickel-chromium catalysts, were used for the conversion of model mixtures over the influence of sulfur in Chapter 7.

Both benchmark nickel-based catalysts were active along 48 h of time on stream for conversion of both guaiacol and 1-octanol, selected to compose the binary model mixture. The highest conversion was obtained with the benchmark nickel catalyst. By the addition of 1-octanethiol to the model mixture, the catalytic activity of both catalysts was not affected, while the selectivity was changed by the presence of sulfur. Initially nickel-chromium was more active towards n-octane and dioctylether formation, while nickel-based catalyst was mostly selective for n-octane and branched hydrocarbons, such as 3-methylheptane and 2,4-dimethylhexane. By the addition of sulfur to the feed mixtures, the selectivity towards alkenes formation increased significantly for both catalysts and the main reaction pathways were inhibited. The presence of sulfur in the feed leaded to the formation of bulk Ni_3S_2 in both spent catalysts. However, the highest diffraction intensity of metallic Ni observed in the spent nickel-chromium catalysts may indicate higher resistance to sulfur poisoning by this catalyst. Nevertheless, the higher abundance of alkenes in the upgraded products of both catalysts, in addition to the presence of aromatic compounds in the upgraded product obtained with nickel-chromium catalyst might indicate that the H_2 dissociation and the hydrogenation activity was compromised by the formation of Ni_3S_2.

Thus, both high loaded benchmark nickel-based catalysts proved to be active over 48 h of time on stream even with the presence of sulfur in the feedstock, although a different range of products was obtained by the presence sulfur-containing compound to the feed model mixture.

In summary all catalysts evaluated in this study were active for hydrotreatment of FPBO. Especially Ni/SiO_2 and nickel-chromium showed superior hydrodeoxygenation and hydrogenation activities, regardless of the feedstock. However, further studies in terms of catalyst formulation, long term stability and activity, allowing hydrotreatment in continuously operated reactors are required for future integration of a hydrotreatment unit in biorefineries

Further investigations should especially consider minimization of the polymerization occurring during hydrotreatment. The influence of sugars and lignin derivative compounds should be carefully studied aiming a better comprehension of the polymerization mechanism. The influence of organic acids over the conversion of sugars should be also consider in future investigations.

The addition of hydrogen donor solvents should also be an object of investigation in the future, in order to reduce the consumption of molecular H_2, as well as to explore milder hydrotreatment possibilities, in terms of H_2 pressure and temperature.

Continuously operating hydrotreatment facilities applying FPBO should be considered in further studies, in order to investigate the deactivation versus time on stream and in situ catalyst regeneration. Cycles of continuous hydrotreatment/regeneration should be performed for evaluation of long term stability of catalysts.

New catalysts formulations, based on nickel in combination to niobium could be considered in the future, due to the catalytic activity already demonstrated by this metal as well as the high availability of niobium in Brazil, one of the biggest producers of biomass worldwide.

Furthermore, 2-step hydrotreatment should be carefully considered in future studies, especially in continuous operating units, using two stages in upgrading. Combinations of catalysts for example Ni/SiO_2 and nickel-chromium used in the present work in sequential batch upgrading could be studied in detail in continuous reactors. Attention should be given to the final composition of the upgraded oil, selectivity of the catalysts and coke formation.

Overall efforts are still required in order to develop new catalysts formulations, promoters, supports and reactor designs in order to allow the development of new biorefineries, integration to biorefineries already stablished and co-processing in crude oil refineries worldwide.

References

1. Kan, T.; Strezov, V.; Evans, T. J. Lignocellulosic biomass pyrolysis: A review of product properties and effects of pyrolysis parameters. *Renew. Sustain. Energy Rev.* **2016**, *57*, 1126–1140, doi:10.1016/J.RSER.2015.12.185.

2. Mohan, D.; Pittman, C. U.; Steele, P. H. Pyrolysis of Wood / Biomass for Bio-oil : A Critical Review. *Energy & Fuels* **2006**, *20*, 848–889, doi:10.1021/ef0502397.

3. Demirbaş, A. Biomass resource facilities and biomass conversion processing for fuels and chemicals. *Energy Convers. Manag.* **2001**, *42*, 1357–1378, doi:10.1016/S0196-8904(00)00137-0.

4. Xiu, S.; Shahbazi, A. Bio-oil production and upgrading research: A review. *Renew. Sustain. Energy Rev.* **2012**, *16*, 4406–4414, doi:10.1016/j.rser.2012.04.028.

5. Goyal, H. B.; Seal, D.; Saxena, R. C. Bio-fuels from thermochemical conversion of renewable resources: A review. *Renew. Sustain. Energy Rev.* **2008**, *12*, 504–517, doi:10.1016/j.rser.2006.07.014.

6. Ching, D. Upgrading of biomass : alternative ways for biomass treatment, 2014.

7. Guedes, R. E.; Luna, A. S.; Torres, A. R. Operating parameters for bio-oil production in biomass pyrolysis: A review. *J. Anal. Appl. Pyrolysis* **2018**, *129*, 134–149, doi:10.1016/j.jaap.2017.11.019.

8. Dabros, T. M. H.; Stummann, M. Z.; Høj, M.; Jensen, P. A.; Grunwaldt, J.-D.; Gabrielsen, J.; Mortensen, P. M.; Jensen, A. D. Transportation fuels from biomass fast pyrolysis, catalytic hydrodeoxygenation, and catalytic fast hydropyrolysis. *Prog. Energy Combust. Sci.* **2018**, *68*, 268–309, doi:10.1016/j.pecs.2018.05.002.

9. Anwar, Z.; Gulfraz, M.; Irshad, M. Agro-industrial lignocellulosic biomass a key to unlock the future bio-energy: A brief review. *J. Radiat. Res. Appl. Sci.* **2014**, *7*, 163–173, doi:10.1016/j.jrras.2014.02.003.

10. Feng Xu, Jianming Yu, Tesfaye Tesso, Floyd Dowell, D. W. Qualitative and quantitative analysis of lignocellulosic biomass using infrared techniques : A mini-review. *Appl. Energy* **2013**, *104*, 801–809, doi:10.1016/j.apenergy.2012.12.019.

11. Oasmaa, A.; Fonts, I.; Pelaez-Samaniego, M. R.; Garcia-Perez, M. E.; Garcia-Perez, M. Pyrolysis Oil Multiphase Behavior and Phase Stability: A Review. *Energy & Fuels* **2016**, *30*, 6179–6200, doi:10.1021/acs.energyfuels.6b01287.

12. Collard, F. X.; Blin, J. A review on pyrolysis of biomass constituents: Mechanisms and composition of the products obtained from the conversion of cellulose, hemicelluloses and lignin. *Renew. Sustain. Energy Rev.* **2014**, *38*, 594–608, doi:10.1016/j.rser.2014.06.013.

13. Funke, A.; Tomasi, M.; Dahmen, N.; Leibold, H. Experimental comparison of two bench scale units for fast and intermediate pyrolysis. *J. Anal. Appl. Pyrolysis* **2017**, *124*, 504–514, doi:10.1016/j.jaap.2016.12.033.

14. James, A. K.; Thring, R. W.; Helle, S.; Ghuman, H. S. Ash management review-applications of biomass bottom ash. *Energies* **2012**, *5*, 3856–3873, doi:10.3390/en5103856.

15. Bridgwater, A. V. Renewable fuels and chemicals by thermal processing of biomass. *Chem. Eng. J.* **2003**, *91*, 87–102, doi:https://doi.org/10.1016/S1385-8947(02)00142-0.

16. Pfitzer, C.; Dahmen, N.; Tröger, N.; Weirich, F.; Sauer, J.; Günther, A.; Müller-Hagedorn, M. Fast Pyrolysis of Wheat Straw in the Bioliq Pilot Plant. *Energy and Fuels* **2016**, *30*, 8047–8054, doi:10.1021/acs.energyfuels.6b01412.

17. Polin, P. J. .; Carr, D. H. .; Whitmer, L. E. .; Smith, R. G. .; Brown, R. C. . Conventional and autothermal pyrolysis of corn stover: Overcoming the processing challenges of high-ash agricultural residues. *J. Anal. Appl. Pyrolysis* **2019**, *143*, 104679, doi:doi.org/10.1016/j.jaap.2019.104679.

18. Gollakota, A. R. K.; Reddy, M.; Subramanyam, M. D.; Kishore, N. A review on the upgradation techniques of pyrolysis oil. *Renew. Sustain. Energy Rev.* **2016**, *58*, 1543–1568, doi:10.1016/j.rser.2015.12.180.

19. Park, J.; Meng, J.; Lim, K. H.; Rojas, O. J.; Park, S. Transformation of lignocellulosic biomass during torrefaction. *J. Anal. Appl. Pyrolysis* **2013**, *100*, 199–206, doi:10.1016/j.jaap.2012.12.024.

20. Moreira, R.; Neves, R. C.; Schmitt, C. C.; Breunig, M.; Tambani, P. C.; Ushima, A. H.; Funke, A.; Rafelt, K. Characterization of Brazilian sugarcane bagasse and sugarcane straw based on European methodologies to evaluate the potential for energy conversion. In *European Biomass Conference and Exhibition Proceedings*; 2017; Vol. 2017.

21. Hornung, A. Intermediate pyrolysis of biomass. In *Biomass Combustion Science, Technology and Engineering*; Woodhead Publishing Limited, 2013; pp. 172–186 ISBN 9780857091314.

22. Shemfe, M. B.; Gu, S.; Ranganathan, P. Techno-economic performance analysis of biofuel production and miniature electric power generation from biomass fast pyrolysis and bio-oil upgrading. *Fuel* **2015**, *143*, 361–372, doi:10.1016/j.fuel.2014.11.078.

23. Bridgwater, A. V. Review of fast pyrolysis of biomass and product upgrading. *Biomass and Bioenergy* **2012**, *38*, 68–94, doi:10.1016/j.biombioe.2011.01.048.

24. Dahmen, N. Lecture: Energy from Biomass, Karlsruhe Institute of Technology: Karlsruhe, 2019.

25. Oasmaa, A.; Solantausta, Y.; Arpiainen, V.; Kuoppala, E.; Sipilä, K. Fast pyrolysis bio-oils from wood and agricultural residues. *Energy and Fuels* **2010**, *24*, 1380–1388, doi:10.1021/ef901107f.

26. Funke, A.; Richter, D.; Niebel, A.; Dahmen, N.; Sauer, J. Fast Pyrolysis of Biomass Residues in a Twin-screw Mixing Reactor. *J. Vis. Exp.* **2016**, doi:10.3791/54395.

27. Auersvald, M.; Shumeiko, B.; Vrtiška, D.; Straka, P.; Staš, M.; Šimáček, P.; Blažek, J.; Kubička, D. Hydrotreatment of straw bio-oil from ablative fast pyrolysis to produce suitable refinery intermediates. *Fuel* **2019**, *238*, 98–110, doi:10.1016/j.fuel.2018.10.090.

28. Funke, A.; Pfitzer, C. Fast Pyrolysis for the Thermochemical Conversion of Biomass Available online: https://www.ikft.kit.edu/english/255.php (accessed on Dec 4, 2019).

29. Fahmi, R.; Bridgwater, A. V.; Donnison, I.; Yates, N.; Jones, J. M. The effect of lignin and inorganic species in biomass on pyrolysis oil yields, quality and stability. *Fuel* **2008**, *87*, 1230–1240, doi:10.1016/j.fuel.2007.07.026.

30. Envergent Convert forest waste to renewable fuels Available online: https://www.envergenttech.com/technology/rtp/ (accessed on Jan 14, 2020).

31. Fortum Fortum Otso bio-oil Available online: https://www.fortum.com/products-and-

services/power-plant-services/fortum-otso-bio-oil (accessed on Jan 14, 2020).

32. BTG-BTL BTG-BTL pyrolysis process Available online: https://www.btg-btl.com/en/technology (accessed on Jan 14, 2020).

33. Elliott, D. C. Biofuel from fast pyrolysis and catalytic hydrodeoxygenation. *Curr. Opin. Chem. Eng.* **2015**, *9*, 59–65, doi:10.1016/j.coche.2015.08.008.

34. Si, Z.; Zhang, X.; Wang, C.; Ma, L.; Dong, R. An Overview on Catalytic Hydrodeoxygenation of Pyrolysis Oil and Its Model Compounds. *Catalysts* **2017**, *7*, 1–22, doi:10.3390/catal7060169.

35. Negahdar, L.; Gonzalez-Quiroga, A.; Otyuskaya, D.; Toraman, H. E.; Liu, L.; Jastrzebski, J. T. B. H.; Van Geem, K. M.; Marin, G. B.; Thybaut, J. W.; Weckhuysen, B. M. Characterization and Comparison of Fast Pyrolysis Bio-oils from Pinewood, Rapeseed Cake, and Wheat Straw Using 13C NMR and Comprehensive GC × GC. *ACS Sustain. Chem. Eng.* **2016**, *4*, 4974–4985, doi:10.1021/acssuschemeng.6b01329.

36. Wang, H.; Male, J.; Wang, Y. Recent advances in hydrotreating of pyrolysis bio-oil and its oxygen-containing model compounds. *ACS Catal.* **2013**, *3*, 1047–1070, doi:10.1021/cs400069z.

37. Venderbosch, R. H.; Ardiyanti, A. R.; Wildschut, J.; Oasmaa, A.; Heeres, H. J. Stabilization of biomass-derived pyrolysis oils. *J. Chem. Technol. Biotechnol.* **2010**, *85*, 674–686, doi:10.1002/jctb.2354.

38. Gollakota, A. R. K.; Reddy, M.; Subramanyam, M. D.; Kishore, N. A review on the upgradation techniques of pyrolysis oil. *Renew. Sustain. Energy Rev.* **2016**, *58*, 1543–1568, doi:10.1016/j.rser.2015.12.180.

39. Saidi, M.; Samimi, F.; Karimipourfard, D.; Nimmanwudipong, T.; Gates, B. C.; Rahimpour, M. R. Upgrading of lignin-derived bio-oils by catalytic hydrodeoxygenation. *Energy Environ. Sci.* **2014**, *7*, 103–129, doi:10.1039/C3EE43081B.

40. Elliott, D. C.; Wang, H.; French, R.; Deutch, S.; Iisa, K. Hydrocarbon liquid production from biomass via hot-vapor-filtered fast pyrolysis and catalytic hydroprocessing of the bio-oil. *Energy and Fuels* **2014**, *28*, 5909–5917, doi:10.1021/ef501536j.

41. Baldwin, R. M.; Feik, C. J. Bio-oil stabilization and upgrading by hot gas filtration. *Energy and Fuels* **2013**, *27*, 3224–3238, doi:10.1021/ef400177t.

42. Zhang, Q.; Xu, Y.; Li, Y.; Wang, T.; Zhang, Q.; Ma, L.; He, M.; Li, K. Investigation on the esterification by using supercritical ethanol for bio-oil upgrading. *Appl. Energy* **2015**, *160*, 633–640, doi:10.1016/j.apenergy.2014.12.063.

43. Xu, X.; Zhang, C.; Zhai, Y.; Liu, Y.; Zhang, R.; Tang, X. Upgrading of bio-oil using supercritical 1-butanol over a ru/c heterogeneous catalyst: Role of the solvent. *Energy and Fuels* **2014**, *28*, 4611–4621, doi:10.1021/ef500968a.

44. Tang, Z.; Lu, Q.; Zhang, Y.; Zhu, X.; Guo, Q. One step bio-oil upgrading through hydrotreatment, esterification, and cracking. *Ind. Eng. Chem. Res.* **2009**, *48*, 6923–6929, doi:10.1021/ie900108d.

45. Oasmaa, A.; Czernik, S. Fuel oil quality of biomass pyrolysis oils - state of the art for the end users. *Energy and Fuels* **1999**, *13*, 914–921, doi:10.1021/ef980272b.

46. Diebold, J. P. *A Review of the Chemical and Physical Mechanisms of the Storage Stability of Fast Pyrolysis Bio-Oils: Report NREL/SR-570-27613, Golden, CO*; 2000;

47. Oasmaa, A.; Kuoppala, E.; Selin, J. F.; Gust, S.; Solantausta, Y. Fast pyrolysis of forestry residue and pine. 4. Improvement of the product quality by solvent addition. *Energy and Fuels* **2004**, *18*, 1578–1583, doi:10.1021/ef040038n.

48. Mercader, F. D. M.; Koehorst, P. J. J.; Heeres, H.J.; Kersten, S. R. A.; Hogendoorn, J. A. Competition Between Hydrotreating and Polymerization Reactions During Pyrolysis Oil Hydrodeoxygenation. *AIChE J.* **2011**, *55*, 3160–3170, doi:10.1002/aic.12503.

49. Mercader, F. D. M. *Pyrolysis oil upgrading for co-processing in standard refinery units*; 2010; ISBN 9789036530859.

50. Yin, W.; Venderbosch, R. H.; Heeres, H. J. *Recent developments in the catalytic hydrotreatment of pyrolysis liquids*; Elsevier Ltd., 2018; ISBN 9780081010259.

51. Zacher, A. H.; Olarte, M. V.; Santosa, D. M.; Elliott, D. C.; Jones, S. B. A review and perspective of recent bio-oil hydrotreating research. *Green Chem.* **2014**, *16*, 491–515, doi:10.1039/c3gc41382a.

52. Mortensen, P. M.; Grunwaldt, J. D.; Jensen, P. A.; Knudsen, K. G.; Jensen, A. D. A review of catalytic upgrading of bio-oil to engine fuels. *Appl. Catal. A Gen.* **2011**, *407*, 1–19, doi:10.1016/j.apcata.2011.08.046.

53. Boscagli, C.; Yang, C.; Welle, A.; Wang, W.; Behrens, S.; Raffelt, K.; Grunwaldt, J. D. Effect of pyrolysis oil components on the activity and selectivity of nickel-based catalysts during hydrotreatment. *Appl. Catal. A Gen.* **2017**, *544*, 161–172, doi:10.1016/j.apcata.2017.07.025.

54. Elliott, D. C.; Hart, T. R.; Neuenschwander, G. G.; Rotness, L. J.; Olarte, M. V.; Zacher, A. H.; Solantausta, Y. Catalytic hydroprocessing of fast pyrolysis bio-oil from pine sawdust. *Energy and Fuels* **2012**, *26*, 3891–3896, doi:10.1021/ef3004587.

55. Wildschut, J.; Iqbal, M.; Mahfud, F. H.; Cabrera, I. M.; Venderbosch, R. H.; Heeres, H. J. Insights in the hydrotreatment of fast pyrolysis oil using a ruthenium on carbon catalyst. *Energy Environ. Sci.* **2010**, *3*, 962, doi:10.1039/b923170f.

56. Talmadge, M. S.; Baldwin, R. M.; Biddy, M. J.; McCormick, R. L.; Beckham, G. T.; Ferguson, G. A.; Czernik, S.; Magrini-Bair, K. A.; Foust, T. D.; Metelski, P. D.; Hetrick, C.; Nimlos, M. R. A perspective on oxygenated species in the refinery integration of pyrolysis oil. *Green Chem.* **2014**, *16*, 407–453, doi:10.1039/c3gc41951g.

57. Oasmaa, A.; Kuoppala, E.; Ardiyanti, A.; Venderbosch, R. H.; Heeres, H. J. Characterization of hydrotreated fast pyrolysis liquids. *Energy and Fuels* **2010**, *24*, 5264–5272, doi:10.1021/ef100573q.

58. Elliott, D. C.; Neuenschwander, G. G. Liquid fuels by low-severity hydrotreating of biocrude. *Dev. Thermochem. Biomass Convers.* **1996**, *1*, 611–621, doi:10.1016/S0140-6701(98)96316-0.

59. French, R. J.; Stunkel, J.; Black, S.; Myers, M.; Yung, M. M.; Iisa, K. Evaluate impact of catalyst type on oil yield and hydrogen consumption from mild hydrotreating. *Energy and Fuels* **2014**, *28*, 3086–3095, doi:10.1021/ef4019349.

60. Joshi, N.; Lawal, A. Hydrodeoxygenation of pyrolysis oil in a microreactor. *Chem. Eng. Sci.* **2012**, *74*, 1–8, doi:10.1016/j.ces.2012.01.052.

61. Elliott, D. C. Historical developments in hydroprocessing bio-oils. *Energy and Fuels* **2007**, *21*, 1792–1815, doi:10.1021/ef070044u.

62. Shafaghat, H.; Rezaei, P. S.; Ashri Wan Daud, W. M. Effective parameters on selective catalytic hydrodeoxygenation of phenolic compounds of pyrolysis bio-oil to high-value hydrocarbons. *RSC Adv.* **2015**, *5*, 103999–104042, doi:10.1039/c5ra22137d.

63. Şenol, O. I.; Viljava, T. R.; Krause, A. O. I. Hydrodeoxygenation of methyl esters on sulphided NiMo/γ-Al2O3 and CoMo/γ-Al2O3 catalysts. *Catal. Today* **2005**, *100*, 331–335, doi:10.1016/j.cattod.2004.10.021.

64. Gholizadeh, M.; Gunawan, R.; Hu, X.; Hasan, M. M.; Kersten, S.; Westerhof, R.; Chaitwat, W.; Li, C. Z. Different reaction behaviours of the light and heavy components of bio-oil during the hydrotreatment in a continuous pack-bed reactor. *Fuel Process. Technol.* **2016**, *146*, 76–84, doi:10.1016/j.fuproc.2016.01.026.

65. He, Z.; Wang, X. Hydrodeoxygenation of model compounds and catalytic systems for pyrolysis bio-oils upgrading. *Catal. Sustain. Energy* **2012**, *1*, 28–52, doi:10.2478/cse-2012-0004.

66. Wan, H.; Chaudhari, R. V.; Subramaniam, B. Aqueous phase hydrogenation of acetic acid and its promotional effect on p-cresol hydrodeoxygenation. *Energy and Fuels* **2013**, *27*, 487–493, doi:10.1021/ef301400c.

67. Gholizadeh, M.; Gunawan, R.; Hu, X.; De Miguel Mercader, F.; Westerhof, R.; Chaitwat, W.; Hasan, M. M.; Mourant, D.; Li, C. Z. Effects of temperature on the hydrotreatment behaviour of pyrolysis bio-oil and coke formation in a continuous hydrotreatment reactor. *Fuel Process. Technol.* **2016**, *148*, 175–183, doi:10.1016/j.fuproc.2016.03.002.

68. Mortensen, P. M.; Grunwaldt, J. D.; Jensen, P. A.; Jensen, A. D. Screening of catalysts for hydrodeoxygenation of phenol as a model compound for bio-oil. *ACS Catal.* **2013**, *3*, 1774–1785, doi:10.1021/cs400266e.

69. Ardiyanti, A. R.; Bykova, M. V.; Khromova, S. A.; Yin, W.; Venderbosch, R. H.; Yakovlev, V. A.; Heeres, H. J. Ni-Based Catalysts for the Hydrotreatment of Fast Pyrolysis Oil. *Energy and Fuels* **2016**, *30*, 1544–1554, doi:10.1021/acs.energyfuels.5b02223.

70. Ardiyanti, A. R.; Khromova, S. A.; Venderbosch, R. H.; Yakovlev, V. A.; Melián-Cabrera, I. V.; Heeres, H. J. Catalytic hydrotreatment of fast pyrolysis oil using bimetallic Ni-Cu catalysts on various supports. *Appl. Catal. A Gen.* **2012**, *449*, 121–130, doi:10.1016/j.apcata.2012.09.016.

71. Ardiyani, A. R.; Khromova, S. A.; Venderbosch, R. H.; Yakovlev, V. A.; Heeres, H. J. Catalytic hydrotreatment of fast-pyrolysis oil using non-sulfided bimetallic Ni-Cu catalysts on a δ-Al2O3 support. *Appl. Catal. B Environ.* **2012**, *117–118*, 105–117, doi:10.1016/j.apcatb.2011.12.032.

72. Mortensen, P. M.; Gardini, D.; Carvalho, H. W. P. de; Damsgaard, C. D.; Grunwaldt, J.; Jensen, P. A.; Wagner, J. B.; Jensen, A. D. Stability and resistance of nickel catalysts for hydrodeoxygenation: carbon deposition and effects of sulfur, potassium, and chlorine in the feed. *Catal. Sci. Technol.* **2014**, *4*, 3672–3686, doi:10.1039/c4cy00522h.

73. Mortensen, P. M.; Grunwaldt, J. D.; Jensen, P. A.; Jensen, A. D. Influence on nickel particle size on the hydrodeoxygenation of phenol over Ni/SiO2. *Catal. Today* **2016**, *259*, 277–284, doi:10.1016/j.cattod.2015.08.022.

74. Pinheiro Pires, A. P.; Arauzo, J.; Fonts, I.; Domine, M. E.; Fernández Arroyo, A.; Garcia-Perez, M. E.; Montoya, J.; Chejne, F.; Pfromm, P.; Garcia-Perez, M. Challenges and opportunities for bio-oil refining: A review. *Energy and Fuels* **2019**, *33*, 4683–4720, doi:10.1021/acs.energyfuels.9b00039.

75. Argyle, M. D.; Bartholomew, C. H. Heterogeneous Catalyst Deactivation and Regeneration: A Review. *Catalysts* **2015**, *5*, 145–269, doi:10.3390/catal5010145.

76. Bozell, J. J.; Holladay, J. E.; Johnson, D.; White, J. F. Top Value-Added Chemicals from Biomass Volume II - Results of Screening for Potential Candidates from Biorefinery Lignin PNNL-16983, Pacific Northwest National Laboratory, 2007, Vol. II.

77. Venderbosch, R.; Heeres, H. Stabilisation of Biomass derived Pyrolysis Oils by Catalytic Hydrotreatment. *Biocoup.Com* 1–28.

78. Valle, B.; Aramburu, B.; Santiviago, C.; Bilbao, J.; Gayubo, A. G. Upgrading of Bio-Oil in a Continuous Process with Dolomite Catalyst. *Energy & Fuels* **2014**, *28*, 6419–6428, doi:10.1021/ef501600f.

79. Graglia, M.; Kanna, N.; Esposito, D. Lignin Refinery: Towards the Preparation of Renewable Aromatic Building Blocks. *ChemBioEng Rev.* **2015**, n/a-n/a, doi:10.1002/cben.201500019.

80. Zakzeski, J.; Bruijnincx, P. C. A.; Jongerius, A. L.; Weckhuysen, B. M. The Catalytic Valorization of Ligning for the Production of Renewable Chemicals. *Chem. Rev.* **2010**, *110*, 3552–3599, doi:10.1021/cr900354u.

81. Sun, Z.; Fridrich, B.; De Santi, A.; Elangovan, S.; Barta, K. Bright Side of Lignin Depolymerization: Toward New Platform Chemicals. *Chem. Rev.* **2018**, *118*, 614–678, doi:10.1021/acs.chemrev.7b00588.

82. Jin, S.; Xiao, Z.; Li, C.; Chen, X.; Wang, L.; Xing, J.; Li, W.; Liang, C. Catalytic hydrodeoxygenation of anisole as lignin model compound over supported nickel catalysts. *Catal. Today* **2014**, *234*, 125–132, doi:10.1016/j.cattod.2014.02.014.

83. Yang, Y.; Ochoa-Hernández, C.; de la Peña O'Shea, V. A.; Pizarro, P.; Coronado, J. M.; Serrano, D. P. Effect of metal-support interaction on the selective hydrodeoxygenation of anisole to aromatics over Ni-based catalysts. *Appl. Catal. B Environ.* **2014**, *145*, 91–100, doi:10.1016/j.apcatb.2013.03.038.

84. Brown, R. C. PY REFINERY: THERMAL FRACTIONATION OF LIGNOCELLULOSIC BIOMASS INTO DIVERSE BIOBASED PRODUCTS Available online: http://www.frontiersinbiorefining.org/2014/Documents/Plenary/Py Refinery - RC Brown Iowa State Univ.pdf (accessed on Apr 11, 2020).

85. Carriel Schmitt, C.; Moreira, R.; Cruz, R.; Richter, D.; Funke, A.; Raffelt, K.; Grunwaldt, J.; Dahmen, N. From agriculture residue to upgraded product : The thermochemical conversion of sugarcane bagasse for fuel and chemical products. *Fuel Process. Technol.* **2020**, *197*, doi:10.1016/j.fuproc.2019.106199.

86. Izquierdo, U.; Barrio, V. L.; Cambra, J. F.; Requies, J.; Güemez, M. B.; Arias, P. L.; Kolb, G.; Zapf, R.; Gutiérrez, A. M.; Arraibi, J. R. Hydrogen production from methane and natural gas steam reforming in conventional and microreactor reaction systems. *Int. J. Hydrogen Energy* **2012**, *37*, 7026–7033, doi:10.1016/j.ijhydene.2011.11.048.

87. Dahmen, N.; Lewandowski, I.; Zibek, S.; Weidtmann, A. Integrated lignocellulosic value chains in a growing bioeconomy: Status quo and perspectives. *GCB Bioenergy* **2019**, *11*, 107–117, doi:10.1111/gcbb.12586.

88. Boscagli, C.; Raffelt, K.; Grunwaldt, J. D. Reactivity of platform molecules in pyrolysis oil and in water during hydrotreatment over nickel and ruthenium catalysts. *Biomass and Bioenergy* **2017**, *106*, 63–73, doi:10.1016/j.biombioe.2017.08.013.

89. Wild, P. J. De; Huijgen, W. J. J.; Kloekhorst, A.; Chowdari, R. K.; Heeres, H. J. Biobased alkylphenols from lignins via a two-step pyrolysis – Hydrodeoxygenation approach. *Bioresour. Technol.* **2017**, *229*, 160–168, doi:10.1016/j.biortech.2017.01.014.

90. Elliott, D. C.; Hart, T. R. Catalytic hydroprocessing of chemical models for bio-oil. *Energy and Fuels* **2009**, *23*, 631–637, doi:10.1021/ef8007773.

91. Li, X.; Gunawan, R.; Wang, Y.; Chaiwat, W.; Hu, X.; Gholizadeh, M.; Mourant, D.; Bromly, J.; Li, C. Z. Upgrading of bio-oil into advanced biofuels and chemicals. Part III. Changes in aromatic structure and coke forming propensity during the catalytic hydrotreatment of a fast pyrolysis bio-oil with Pd/C catalyst. *Fuel* **2014**, *116*, 642–649, doi:10.1016/j.fuel.2013.08.046.

92. Chaiwat, W.; Gunawan, R.; Gholizadeh, M.; Li, X.; Lievens, C.; Hu, X.; Wang, Y.; Mourant, D.; Rossiter, A.; Bromly, J.; Li, C. Z. Upgrading of bio-oil into advanced biofuels and chemicals. Part II. Importance of holdup of heavy species during the hydrotreatment of bio-oil in a continuous packed-bed catalytic reactor. *Fuel* **2013**, *112*, 302–310, doi:10.1016/j.fuel.2013.05.004.

93. Gunawan, R.; Li, X.; Lievens, C.; Gholizadeh, M.; Chaiwat, W.; Hu, X.; Mourant, D.; Bromly, J.; Li, C. Z. Upgrading of bio-oil into advanced biofuels and chemicals. Part I. Transformation of GC-detectable light species during the hydrotreatment of bio-oil using Pd/C catalyst. *Fuel* **2013**, *111*, 709–717, doi:10.1016/j.fuel.2013.04.002.

94. Lee, H.; Kim, H.; Yu, M. J.; Ko, C. H.; Jeon, J. K.; Jae, J.; Park, S. H.; Jung, S. C.; Park, Y. K. Catalytic Hydrodeoxygenation of Bio-oil Model Compounds over Pt/HY Catalyst. *Sci. Rep.* **2016**, *6*, 1–8, doi:10.1038/srep28765.

95. Sanna, A.; Vispute, T. P.; Huber, G. W. Hydrodeoxygenation of the aqueous fraction of bio-oil with Ru/C and Pt/C catalysts. *Appl. Catal. B Environ.* **2015**, *165*, 446–456, doi:10.1016/j.apcatb.2014.10.013.

96. Schmitt, C. C.; Reolon, M. G.; Zimmermann, M.; Raffelt, K.; Grunwaldt, J.-D.; Dahmen, N. Synthesis and Regeneration of Nickel-Based Catalysts for Hydrodeoxygenation of Beech Wood Fast Pyrolysis Bio-Oil. *Catalysts* **2018**, *8*, 449, doi:10.3390/catal8100449.

97. Jin, W.; Pastor- Pérez, L.; Shen, D.; Sepúlveda-Escribano, A.; Gu, S.; Ramirez Reina, T. Catalytic upgrading of biomass model compounds: Novel approaches and lessons learnt from traditional hydrodeoxygenation - a review. **2018**, doi:10.1002/cctc.201801722.

98. Oh, S.; Choi, H. S.; Choi, I.-G.; Choi, J. W. Evaluation of hydrodeoxygenation reactivity of pyrolysis bio-oil with various Ni-based catalysts for improvement of fuel properties. *RSC Adv.* **2017**, *7*, 15116–15126, doi:10.1039/C7RA01166K.

99. Boscagli, C.; Raffelt, K.; Zevaco, T. A.; Olbrich, W.; Otto, T. N.; Sauer, J.; Grunwaldt, J. D. Mild hydrotreatment of the light fraction of fast-pyrolysis oil produced from straw over nickel-based catalysts. *Biomass and Bioenergy* **2015**, *83*, 525–538, doi:10.1016/j.biombioe.2015.11.003.

100. Furimsky, E. Deactivation of hydroprocessing catalysts. *Catal. Today* **2002**, *52*, 381–495, doi:10.1016/s0920-5861(99)00096-6.

101. Dongil, A. B.; Ghampson, I. T.; García, R.; Fierro, J. L. G.; Escalona, N. Hydrodeoxygenation of guaiacol over Ni/carbon catalysts: effect of the support and Ni loading. *RSC Adv.* **2016**, *6*, 2611–2623, doi:10.1039/C5RA22540J.

102. Jahromi, H.; Agblevor, F. A. Hydrodeoxygenation of pinyon-juniper catalytic pyrolysis oil

using red mud-supported nickel catalysts. *Appl. Catal. B Environ.* **2018**, *236*, 1–12, doi:10.1016/j.apcatb.2018.05.008.

103. Sápi, A.; Rémiás, R.; Kónya, Z.; Kukovecz, Á.; Kordás, K.; Kiricsi, I. Synthesis and characterization of nickel catalysts supported on different carbon materials. *React. Kinet. Catal. Lett.* **2009**, *96*, 379–389, doi:10.1007/s11144-009-5527-3.

104. Boscagli, C.; Tomasi Morgano, M.; Raffelt, K.; Leibold, H.; Grunwaldt, J.-D. Influence of feedstock, catalyst, pyrolysis and hydrotreatment temperature on the composition of upgraded oils from intermediate pyrolysis. *Biomass and Bioenergy* **2018**, *116*, 236–248, doi:10.1016/j.biombioe.2018.06.022.

105. Huynh, T. M.; Armbruster, U.; Nguyen, L. H.; Nguyen, D. A. Hydrodeoxygenation of Bio-Oil on Bimetallic Catalysts : From Model Compound to Real Feed. *J. Sustain. Bioenergy Syst.* **2015**, *5*, 151–160, doi:http://dx.doi.org/10.4236/jsbs.2015.54014.

106. Olarte, M. V.; Zacher, A. H.; Padmaperuma, A. B.; Burton, S. D.; Job, H. M.; Lemmon, T. L.; Swita, M. S.; Rotness, L. J.; Neuenschwander, G. N.; Frye, J. G.; Elliott, D. C. Stabilization of Softwood-Derived Pyrolysis Oils for Continuous Bio-oil Hydroprocessing. *Top. Catal.* **2016**, *59*, 55–64, doi:10.1007/s11244-015-0505-7.

107. Gómez-Cazalilla, M.; Infantes-Molina, A.; Mérida-Robles, J.; Rodríguez-Castellón, E.; Jiménez-López, A. Chromium species as captors of sulfur molecules on nickel-based hydrotreating catalysts. *Energy and Fuels* **2009**, *23*, 101–110, doi:10.1021/ef800741n.

108. Bartholomew, C. H. Mechanisms of catalyst deactivation. *Appl. Catal. A Gen.* **2001**, *212*, 17–60, doi:10.1016/S0926-860X(00)00843-7.

109. Yin, W.; Venderbosch, R. H.; Alekseeva, M. V.; Figueirêdo, M. B.; Heeres, H.; Khromova, S. A.; Yakovlev, V. A.; Cannilla, C.; Bonura, G.; Frusteri, F.; Heeres, H. J. Hydrotreatment of the carbohydrate-rich fraction of pyrolysis liquids using bimetallic Ni based catalyst: Catalyst activity and product property relations. *Fuel Process. Technol.* **2018**, *169*, 258–268, doi:10.1016/j.fuproc.2017.10.006.

110. Huazhang, L. *Ammonia Synthesis Catalysts: Innovation and Practice*; World Scientific: Singapore, 2013; ISBN 978-981-4355-78-0.

111. Thi, Q.; Bui, P.; Kim, Y.; Pil, S.; Han, J.; Chul, H.; Woo, S.; Won, C. Applied Catalysis B : Environmental Steam reforming of simulated biogas over plate Ni Cr catalysts : Influence of pre-oxidation on catalytic activity. *"Applied Catal. B, Environ.* **2015**, *166–167*, 335–344, doi:10.1016/j.apcatb.2014.11.045.

112. Deutschmann, O.; Knözinger, H.; Kochloefl, K.; Turek, T. Heterogeneous Catalysis and Solid Catalysts, 3. Industrial Applications. *Ullmann's Encycl. Ind. Chem.* **2011**, doi:10.1002/14356007.o05_o03.

113. Rover, M. R.; Hall, P. H.; Johnston, P. A.; Smith, R. G.; Brown, R. C. Stabilization of bio-oils using low temperature, low pressure hydrogenation. *Fuel* **2015**, *153*, 224–230, doi:10.1016/j.fuel.2015.02.054.

114. Pucher, H.; Schwaiger, N.; Feiner, R.; Ellmaier, L.; Pucher, P.; Chernev, B. S.; Siebenhofer, M. Biofuels from liquid phase pyrolysis oil: A two-step hydrodeoxygenation (HDO) process. *Green Chem.* **2015**, *17*, 1291–1298, doi:10.1039/c4gc01741b.

115. Schmitt, C.C.; C. Boscagli; Rapp, M.; Raffelt, R.; Dahmen, N. Characterization of light and heavy phase of pyrolysis-oil from distinct biomass for further upgrading reactions. *Proc. Eur. Biomass Conf. Exhib.* **2017**, 12–15, doi:10.5071/25thEUBCE2017-3AV.3.15.

116. Schmitt, C. C.; Raffelt, K.; Zimina, A.; Krause, B.; Otto, T.; Rapp, M.; Grunwaldt, J. D.; Dahmen, N. Hydrotreatment of Fast Pyrolysis Bio-oil Fractions Over Nickel-Based Catalyst. *Top. Catal.* **2018**, *0*, 0, doi:10.1007/s11244-018-1009-z.

117. Carriel Schmitt, C.; Zimina, A.; Fam, Y.; Raffelt, K.; Grunwaldt, J.; Dahmen, N. Evaluation of High-Loaded Ni-Based Catalysts for Upgrading Fast Pyrolysis Bio-Oil. *Catalysts* **2019**, *9*, 784, doi:10.3390/catal9090784.

118. Stankovikj, F.; McDonald, A. G.; Helms, G. L.; Garcia-Perez, M. Quantification of Bio-Oil Functional Groups and Evidences of the Presence of Pyrolytic Humins. *Energy and Fuels* **2016**, *30*, 6505–6524, doi:10.1021/acs.energyfuels.6b01242.

119. Zhang, X.-S.; Yang, G.-X.; Jiang, H.; Liu, W.-J.; Ding, H.-S. Mass production of chemicals from biomass-derived oil by directly atmospheric distillation coupled with co-pyrolysis. *Sci. Rep.* **2013**, *3*, 1120, doi:10.1038/srep01120.

120. Yokoyama, T.; Fujita, N. Hydrogenation of aliphatic carboxylic acids to corresponding aldehydes over Cr2O3-based catalysts. *Appl. Catal. A Gen.* **2004**, *276*, 179–185, doi:10.1016/j.apcata.2004.08.004.

121. Martínez, J. D.; Veses, A.; Mastral, A. M.; Murillo, R.; Navarro, M. V.; Puy, N.; Artigues, A.; Bartrolí, J.; García, T. Co-pyrolysis of biomass with waste tyres: Upgrading of liquid bio-fuel. *Fuel Process. Technol.* **2014**, *119*, 263–271, doi:10.1016/j.fuproc.2013.11.015.

122. Alonso, D. M.; Wettstein, S. G.; Dumesic, J. A. Bimetallic catalysts for upgrading of biomass to fuels and chemicals. *Chem. Soc. Rev.* **2012**, *41*, 8075–8098, doi:10.1039/C2CS35188A.

123. Dongil, A. B.; Bachiller-Baeza, B.; Rodriguez-Ramos, I.; Fierro, J. L. G.; Escalona, N. Effect of Cu loading on Ni/carbon nanotubes catalyst for hydrodeoxygenation of guaiacol. *RSC Adv.* **2016**, *3*, 26658–26667, doi:10.1039/C6RA00041J.

124. Mäki-Arvela, P.; Murzin, D. Hydrodeoxygenation of Lignin-Derived Phenols: From Fundamental Studies towards Industrial Applications. *Catalysts* **2017**, *7*, 265, doi:10.3390/catal7090265.

125. Mu, W.; Ben, H.; Ragauskas, A.; Deng, Y. Lignin Pyrolysis Components and Upgrading-Technology Review. *Bioenergy Res.* **2013**, *6*, 1183–1204, doi:10.1007/s12155-013-9314-7.

126. Rencoret, J.; Del Río, J. C.; Nierop, K. G. J.; Gutiérrez, A.; Ralph, J. Rapid Py-GC/MS assessment of the structural alterations of lignins in genetically modified plants. *J. Anal. Appl. Pyrolysis* **2016**, *121*, 155–164, doi:10.1016/j.jaap.2016.07.016.

127. Elliott, D. C.; Hart, T. R.; Neuenschwander, G. G.; Rotness, L. J.; Zacker, A. H. Catalytic Hydroprocessing of Biomass Fast Pyrolysis Bio-oil to Produce Hydrocarbon Products. *Environ. Prog. Sustain. Energy* **2009**, *28*, 441–449, doi:10.1002/ep.10384.

128. Haibing, G.; Hexing, L.; Yeping, X.; Minghui, W. Liquid phase glucose hydrogenation over Cr-promoted Ru-B amorphous alloy catalysts. *Mater. Lett.* **2002**, *57*, 392–398.

129. Li, H.; Li, H.; Wang, M. Glucose hydrogenation over promoted Co-B amorphous alloy catalysts. *Appl. Catal. A Gen.* **2001**, *207*, 129–137, doi:10.1016/S0926-860X(00)00662-1.

130. Li, H.; Li, H.; Deng, J. F. Glucose hydrogenation over Ni-B/SiO2 amorphous alloy catalyst and the promoting effect of metal dopants. *Catal. Today* **2002**, *74*, 53–63, doi:10.1016/S0920-5861(01)00530-2.

131. Phimsen, S.; Kiatkittipong, W.; Yamada, H.; Tagawa, T.; Kiatkittipong, K.; Laosiripojana, N.;

Assabumrungrat, S. Nickel sulfide, nickel phosphide and nickel carbide catalysts for bio-hydrotreated fuel production. *Energy Convers. Manag.* **2017**, *151*, 324–333, doi:10.1016/j.enconman.2017.08.089.

132. Gao, J.; Wang, Y.; Ping, Y.; Hu, D.; Xu, G.; Gu, F.; Su, F. A thermodynamic analysis of methanation reactions of carbon oxides for the production of synthetic natural gas. *RSC Adv.* **2012**, *2*, 2358–2368, doi:10.1039/c2ra00632d.

133. Li, X.; Cheng, H.; Liang, G.; He, L.; Lin, W.; Yu, Y.; Zhao, F. Effect of Phosphine Doping and the Surface Metal State of Ni on the Catalytic Performance of Ni/Al2O3 Catalyst. *Catalysts* **2015**, *5*, 759–773, doi:10.3390/catal5020759.

134. Kathiraser, Y.; Wang, Z.; Ang, M. L.; Mo, L.; Li, Z.; Oemar, U.; Kawi, S. Highly active and coke resistant Ni/SiO2 catalysts for oxidative reforming of model biogas: Effect of low ceria loading. *J. CO2 Util.* **2017**, *19*, 284–295, doi:10.1016/j.jcou.2017.03.018.

135. Kirumakki, S. R.; Shpeizer, B. G.; Sagar, G. V.; Chary, K. V. R.; Clearfield, A. Hydrogenation of Naphthalene over NiO/SiO2-Al2O3 catalysts: Structure-activity correlation. *J. Catal.* **2006**, *242*, 319–331, doi:10.1016/j.jcat.2006.06.014.

136. Gervasini, A. Microcalorimetric Study of the Acidity and Basicity. *J. Phys. Chem.* **1990**, *94*, 6371–6379.

137. Aksel, S.; Eder, D. Catalytic effect of metal oxides on the oxidation resistance in carbon nanotube-inorganic hybrids. *J. Mater. Chem.* **2010**, *20*, 9149–9154, doi:10.1039/c0jm01129k.

138. Li, Y.; Zhao, Y.; Chen, B.; Wang, W. Synergetic Catalysis of Nickel Oxides with Oxygen Vacancies and Nickel Phosphide for the Highly Efficient Hydrodeoxygenation of Phenolic Compounds. *ChemCatChem* **2018**, *10*, 2612–2619, doi:10.1002/cctc.201800010.

139. Zhao, L.; Zhao, J.; Wu, T.; Zhao, M.; Yan, W.; Zhang, Y.; Li, H.; Wang, Y.; Xiao, T.; Zhao, Y. Synergistic Effect of Oxygen Vacancies and Ni Species on Tuning Selectivity of Ni/ZrO2 Catalyst for Hydrogenation of Maleic Anhydride into Succinic Anhydride and γ-Butyrolacetone. *Nanomaterials* **2019**, *9*, 406, doi:10.3390/nano9030406.

140. Ermakova, M. A.; Ermakov, D. Y. High-loaded nickel–silica catalysts for hydrogenation, prepared by sol–gel. *Appl. Catal. A Gen.* **2003**, *245*, 277–288, doi:10.1016/s0926-860x(02)00648-8.

141. Bridgwater, A. Report with a Process Scheme for Hydrotreating Catalytically Produced Bio-Oil and Esterifying Bio-Oil with Alcohols and Producing Fuel Gas for Power Production or Synfuels Production Contractual Deadline : M42 Date : 28 March 2013 Author : AV Bridgwater D. **2013**, 1–54.

142. Chen, W.; McClelland, D. J.; Azarpira, A.; Ralph, J.; Luo, Z.; Huber, G. W. Low Temperature Hydrogenation of Pyrolytic Lignin over Ru/TiO2 : 2D HSQC and 13 C NMR Study of Reactants and Products. *Green Chem.* **2016**, *18*, 271–281, doi:10.1039/C5GC02286J.

143. Channiwala, S. A.; Parikh, P. P. A unified correlation for estimating HHV of solid, liquid and gaseous fuels. *Fuel* **2002**, *81*, 1051–1063, doi:10.1016/S0016-2361(01)00131-4.

144. Reddy Kannapu, H. P.; Mullen, C. A.; Elkasabi, Y.; Boateng, A. A. Catalytic transfer hydrogenation for stabilization of bio-oil oxygenates: Reduction of p-cresol and furfural over bimetallic Ni-Cu catalysts using isopropanol. *Fuel Process. Technol.* **2015**, *137*, 220–228, doi:10.1016/j.fuproc.2015.04.023.

145. Fairley, N.; Carrick, A. *The Casa Cookbook: Recipes for XPS Data Processing*; 1st ed.; Acolyte

Science: Knutsford, 2005; ISBN 0954953304.

146. Gandarias, I.; Arias, P. L. Hydrotreating Catalytic Processes for Oxygen Removal in the Upgrading of Bio-Oils and Bio-Chemicals. *Liq. Gaseous, Solid Biofuels-Conversion Tech.* **2013**, 327–356, doi:10.5772/50479.

147. Jongerius, A. L. *Catalytic Conversion of Lignin for the Production of Aromatics*; 2013; ISBN 9789039360019.

148. Resasco, D. E.; Sitthisa, S.; Faria, J.; Prasomsri, T.; Ruiz, M. P. *Furfurals as chemical platform for biofuels production*; 2011; Vol. 661; ISBN 9788130804620.

149. Yang, X.; Liang, Y.; Cheng, Y.; Song, W.; Wang, X.; Wang, Z.; Qiu, J. Hydrodeoxygenation of vanillin over carbon nanotube-supported Ru catalysts assembled at the interfaces of emulsion droplets. *Catal. Commun.* **2014**, *47*, 28–31, doi:10.1016/j.catcom.2013.12.027.

150. Kayalvizhi, J.; Pandurangan, A. Hydrodeoxygenation of vanillin using palladium on mesoporous KIT-6 in vapour phase reactor. *Mol. Catal.* **2017**, *436*, 67–77, doi:10.1016/j.mcat.2017.04.002.

151. Wang, X. Valorization of lignin and bio-oil by catalytic hydrogenation with Ni catalyst. *Fak. für Chemie der Ruhr Univ. Bochum* **2013**, 221.

152. Valle, B.; Aramburu, B.; Santiviago, C.; Bilbao, J.; Gayubo, A. G. Upgrading of Bio - Oil in a Continuous Process with Dolomite Catalyst. *Energy & Fuels* **2015**, *28*, 2014–2015, doi:10.1021/ef501600f.

153. Nakagawa, Y.; Tamura, M.; Tomishige, K. Catalytic Conversions of Furfural to Pentanediols. *Catal. Surv. from Asia* **2015**, *19*, 249–256, doi:10.1007/s10563-015-9194-2.

154. Marchetti, L.; Miserque, F.; Perrin, S.; Pijolat, M. XPS study of Ni-base alloys oxide films formed in primary conditions of pressurized water reactor. *Surf. Interface Anal.* **2015**, *47*, 632–642, doi:10.1002/sia.5757.

155. Faculty, T. A.; Olarte, M. V.; Fulfillment, I. P. Base-catalyzed depolymerization of lignin and hydrodeoxygenation of lignin model compounds for alternative fuel production. **2011**, 233 pp.

156. Biesinger, M. C.; Brown, C.; Mycroft, J. R.; Davidson, R. D.; McIntyre, N. S. X-ray photoelectron spectroscopy studies of chromium compounds. *Surf. Interface Anal.* **2004**, *36*, 1550–1563, doi:10.1002/sia.1983.

157. Deutsch, K. L. Copper catalysts in the C-O hydrogenolysis of biorenewable compounds, Iowa State University, 2012.

158. Biesinger, M. C.; Payne, B. P.; Lau, L. W. M.; Gerson, A.; Smart, R. S. C. X-ray photoelectron spectroscopic chemical state Quantification of mixed nickel metal, oxide and hydroxide systems. *Surf. Interface Anal.* **2009**, *41*, 324–332, doi:10.1002/sia.3026.

159. Prieto, P.; Nistor, V.; Nouneh, K.; Oyama, M.; Abd-Lefdil, M.; Díaz, R. XPS study of silver, nickel and bimetallic silver-nickel nanoparticles prepared by seed-mediated growth. *Appl. Surf. Sci.* **2012**, *258*, 8807–8813, doi:10.1016/j.apsusc.2012.05.095.

160. Payne, B. P.; Biesinger, M. C.; McIntyre, N. S. Use of oxygen/nickel ratios in the XPS characterisation of oxide phases on nickel metal and nickel alloy surfaces. *J. Electron Spectros. Relat. Phenomena* **2012**, *185*, 159–166, doi:10.1016/j.elspec.2012.06.008.

161. Czernik, S.; Johnson, D. K.; Black, S. Stability of wood fast pyrolysis oil. *Biomass and*

Bioenergy **1994**, *7*, 187–192, doi:10.1016/0961-9534(94)00058-2.

162. Olbrich, W.; Boscagli, C.; Raffelt, K.; Zang, H.; Dahmen, N.; Sauer, J. Catalytic hydrodeoxygenation of pyrolysis oil over nickel - based catalysts under H2/CO2 atmosphere. *Sustain. Chem. Process.* **2016**, *4*, 1–8, doi:10.1186/s40508-016-0053-x.

163. Balat, M. An overview of the properties and applications of biomass pyrolysis oils. *Energy Sources, Part A Recover. Util. Environ. Eff.* **2011**, *33*, 674–689, doi:10.1080/15567030903228914.

164. Furimsky, E. Catalytic hydrodeoxygenation. *Appl. Catal. A Gen.* **2000**, *199*, 147–190, doi:10.1016/S0926-860X(99)00555-4.

165. Song, H.; Gong, J.; Song, H.; Li, F. A novel surface modification approach for synthesizing supported nickel phosphide catalysts with high activity for hydrodeoxygenation of benzofuran. *"Applied Catal. A, Gen.* **2015**, *505*, 267–275, doi:10.1016/j.apcata.2015.08.007.

166. Elliott, D. C. Biofuel from fast pyrolysis and catalytic hydrodeoxygenation. *Curr. Opin. Chem. Eng.* **2015**, *9*, 59–65, doi:10.1016/j.coche.2015.08.008.

167. Ewald, S.; Standl, S.; Hinrichsen, O. Characterization of nickel catalysts with transient methods. *Appl. Catal. A Gen.* **2018**, *549*, 93–101, doi:10.1016/j.apcata.2017.09.023.

168. Bykova, M. V; Ermakov, D. Y.; Kaichev, V. V; Bulavchenko, O. A.; Saraev, A. A.; Lebedev, M. Y.; Yakovlev, V. A. Applied Catalysis B : Environmental Ni-based sol – gel catalysts as promising systems for crude bio-oil upgrading : Guaiacol hydrodeoxygenation study. *"Applied Catal. B, Environ.* **2012**, *113–114*, 296–307, doi:10.1016/j.apcatb.2011.11.051.

169. Roldugina, E. A.; Naranov, E. R.; Maximov, A. L.; Karakhanov, E. A. Hydrodeoxygenation of guaiacol as a model compound of bio-oil in methanol over mesoporous noble metal catalysts. *"Applied Catal. A, Gen.* **2018**, doi:10.1016/j.apcata.2018.01.008.

170. Esmaeili, J.; Rahimpour, F. Regeneration of spent nickel catalyst from hydrogenation process of edible oils : Heat treatment with hydrogen injection. *Int. J. Hydrogen Energy* **2017**, *42*, 24197–24204, doi:10.1016/j.ijhydene.2017.07.171.

171. Ng, A.; Lup, K.; Abnisa, F.; Mohd, W.; Wan, A. A review on reactivity and stability of heterogeneous metal catalysts for deoxygenation of bio-oil model compounds. *J. Ind. Eng. Chem.* **2017**, *56*, 1–34, doi:10.1016/j.jiec.2017.06.049.

172. Zhao, H. Y.; Li, D.; Bui, P.; Oyama, S. T. Hydrodeoxygenation of guaiacol as model compound for pyrolysis oil on transition metal phosphide hydroprocessing catalysts. *Appl. Catal. A Gen.* **2011**, *391*, 305–310, doi:10.1016/j.apcata.2010.07.039.

173. Mullen, C. A.; Strahan, G. D.; Boateng, A. A. Characterization of various fast-pyrolysis bio-oils by NMR spectroscopy. *Energy and Fuels* **2009**, *23*, 2707–2718, doi:10.1021/ef801048b.

174. Koike, N.; Hosokai, S.; Takagaki, A.; Nishimura, S.; Kikuchi, R.; Ebitani, K.; Suzuki, Y.; Oyama, S. T. Upgrading of pyrolysis bio-oil using nickel phosphide catalysts. *J. Catal.* **2016**, *333*, 115–126, doi:10.1016/j.jcat.2015.10.022.

175. Yin, W.; Hendrikus, R.; Alekseeva, M. V; Bernardes, M.; Heeres, H.; Khromova, A.; Yakovlev, V. A.; Cannilla, C.; Bonura, G.; Frusteri, F.; Jan, H. Hydrotreatment of the carbohydrate-rich fraction of pyrolysis liquids using bimetallic Ni based catalyst : Catalyst activity and product property relations. *Fuel Process. Technol.* **2018**, *169*, 258–268, doi:10.1016/j.fuproc.2017.10.006.

176. Rodríguez, J. C.; Marchi, A. J.; Borgna, A.; Romeo, E.; Monzón, A. Gas Phase Selective Hydrogenation of Acetylene. Importance of the Formation of Ni-Co and Ni-Cu Bimetallic Clusters on the Selectivity and Coke Deposition. *Stud. Surf. Sci. Catal.* **2001**, *139*, 37–44, doi:https://doi.org/10.1016/S0167-2991(01)80178-6.

177. De Rogatis, L.; Montini, T.; Lorenzut, B.; Fornasiero, P. NixCuy/Al2O3 based catalysts for hydrogen production. *Energy Environ. Sci.* **2008**, *1*, 501–509.

178. Wang, Z.; Zeng, Y.; Lin, W.; Song, W. In-situ hydrodeoxygenation of phenol by supported Ni catalyst – explanation for catalyst performance. *Int. J. Hydrogen Energy* **2017**, *42*, 21040–21047, doi:10.1016/j.ijhydene.2017.07.053.

179. Zhang, X.; Wang, T.; Ma, L.; Zhang, Q.; Yu, Y.; Liu, Q. Characterization and catalytic properties of Ni and NiCu catalysts supported on ZrO2–SiO2 for guaiacol hydrodeoxygenation. **2013**, *33*, 15–19, doi:10.1016/j.catcom.2012.12.011.

180. Yin, W.; Kloekhorst, A.; Venderbosch, R. H.; Bykova, M. V.; Khromova, S. A.; Yakovlev, V. A.; Heeres, H. J. Catalytic hydrotreatment of fast pyrolysis liquids in batch and continuous set-ups using a bimetallic Ni–Cu catalyst with a high metal content. *Catal. Sci. Technol.* **2016**, *6*, 5899–5915, doi:10.1039/C6CY00503A.

181. Mariscal, R.; Maireles-Torres, P.; Ojeda, M.; Sádaba, I.; López Granados, M. Furfural: a renewable and versatile platform molecule for the synthesis of chemicals and fuels. *Energy Environ. Sci.* **2016**, *9*, 1144–1189, doi:10.1039/C5EE02666K.

182. Feng, J.; Yang, Z.; Hse, C. yun; Su, Q.; Wang, K.; Jiang, J.; Xu, J. In situ catalytic hydrogenation of model compounds and biomass-derived phenolic compounds for bio-oil upgrading. *Renew. Energy* **2017**, *105*, 140–148, doi:10.1016/j.renene.2016.12.054.

183. Agblevor, F. A.; Jahromi, H. Aqueous phase synthesis of hydrocarbons from furfural reactions with low molecular weight biomass oxygenates. *Energy and Fuels* **2018**, doi:10.1021/acs.energyfuels.8b02002.

184. Vispute, T. Pyrolysis Oils: Characterization, Stability Analysis, and Catalytic Upgrading to Fuels and Chemicals, University of Massachussets Amherst, 2011.

185. Khromova, S. A.; Smirnov, A. A.; Bulavchenko, O. A.; Saraev, A. A.; Kaichev, V. V.; Reshetnikov, S. I.; Yakovlev, V. A. Anisole hydrodeoxygenation over Ni-Cu bimetallic catalysts: The effect of Ni/Cu ratio on selectivity. *Appl. Catal. A Gen.* **2014**, *470*, 261–270, doi:10.1016/j.apcata.2013.10.046.

186. Huynh, T. M. Development of Novel Bimetallic Nickel-Cobalt Catalysts for Hydrodeoxygenation of Bio-oil producing a Co-feed for a Standard Refinery Unit, University of Rostock, 2015.

187. Ardiyanti, A. R.; Gutierrez, A.; Honkela, M. L.; Krause, A. O. I. I.; Heeres, H. J. Hydrotreatment of wood-based pyrolysis oil using zirconia-supported mono- and bimetallic (Pt , Pd , Rh) catalysts. *"Applied Catal. A, Gen.* **2011**, *407*, 56–66, doi:10.1016/j.apcata.2011.08.024.

188. Haasterecht, T. Van; Ludding, C. C. I.; Jong, K. P. De; Bitter, J. H. Toward stable nickel catalysts for aqueous phase reforming of biomass-derived feedstock under reducing and alkaline conditions. *J. Catal.* **2014**, *319*, 27–35, doi:10.1016/j.jcat.2014.07.014.

189. Oh, S.; Hwang, H.; Seok, H.; Weon, J. The effects of noble metal catalysts on the bio-oil quality during the hydrodeoxygenative upgrading process. *Fuel* **2015**, *153*, 535–543, doi:10.1016/j.fuel.2015.03.030.

190. Li, X.; Luo, X.; Jin, Y.; Li, J.; Zhang, H.; Zhang, A.; Xie, J. Heterogeneous sulfur-free hydrodeoxygenation catalysts for selectively upgrading the renewable bio-oils to second generation biofuels. *Renew. Sustain. Energy Rev.* **2018**, *82*, 3762–3797, doi:10.1016/j.rser.2017.10.091.

191. Chen, S.; Miao, C.; Luo, Y.; Zhou, G.; Xiong, K.; Jiao, Z. Study of catalytic hydrodeoxygenation performance of Ni catalysts: Effects of prepared method. *Renew. Energy* **2018**, *115*, 1109–1117, doi:10.1016/j.renene.2017.09.028.

192. González-Cobos, J.; de Lucas-Consuegra, A. A Review of Surface Analysis Techniques for the Investigation of the Phenomenon of Electrochemical Promotion of Catalysis with Alkaline Ionic Conductors. *Catalysts* **2016**, *6*, 15, doi:10.3390/catal6010015.

193. Hou, L.; Bu, Q.; Li, S.; Wang, D.; Xie, T. Ni3S2-Decorated TiO2 nanotube arrays as effective photoanodes for photoelectrochemical water splitting. *RSC Adv.* **2016**, *6*, 99081–99087, doi:10.1039/C6RA12598K.

194. Xiong, X.; Zhao, B.; Ding, D.; Chen, D.; Yang, C.; Lei, Y.; Liu, M. One-step synthesis of architectural Ni3S2 nanosheet-on-nanorods array for use as high-performance electrodes for supercapacitors. *NPG Asia Mater.* **2016**, *8*, e300, doi:10.1038/am.2016.126.

195. Sitthisa, S.; An, W.; Resasco, D. E. Selective conversion of furfural to methylfuran over silica-supported NiFe bimetallic catalysts. *J. Catal.* **2011**, *284*, 90–101, doi:10.1016/j.jcat.2011.09.005.

196. Jahromi, H.; Agblevor, F. A. Hydrotreating of guaiacol: A comparative study of Red mud-supported nickel and commercial Ni/SiO2-Al2O3 catalysts. *Appl. Catal. A Gen.* **2018**, *558*, 109–121, doi:10.1016/j.apcata.2018.03.016.

197. Miodrag Belosevic, M. G. E. D. Z. S. J. R. B. Degradation of Alizarin Yellow R using UV/H2O2 Advanced Oxidation Process. *Environ. Sci. Technol.* **2014**, *33*, 482–489, doi:10.1002/ep.

198. Srifa, A.; Faungnawakij, K.; Itthibenchapong, V.; Viriya-empikul, N.; Charinpanitkul, T.; Assabumrungrat, S. Production of bio-hydrogenated diesel by catalytic hydrotreating of palm oil over NiMoS2/γ-Al2O3 catalyst. *Bioresour. Technol.* **2014**, *158*, 81–90, doi:10.1016/j.biortech.2014.01.100.

199. Khattab, S. M. R.; Watanabe, T. Bioethanol From Sugarcane Bagasse: Status and Perspectives. In *Bioethanol Production from Food Crops*; Academic Press, 2019; pp. 187–212 ISBN 9780128137666.

200. Conab *Acompanhamento da safra brasileira Cana-de- açúcar Monitoramento agrícola - Cana-de- açúcar*; Brasília, 2018; ISBN 2318-7921.

201. Alcarde, A. R. Cana-de-Açúcar - Embrapa Available online: http://www.agencia.cnptia.embrapa.br/gestor/cana-de-acucar/arvore/CONTAG01_108_22122006154841.html (accessed on Nov 17, 2018).

202. Buckeridge, M. S.; de Souza, A. P.; Arundale, R. A.; Anderson-Teixeira, K. J.; Delucia, E. Ethanol from sugarcane in Brazil: A “midway” strategy for increasing ethanol production while maximizing environmental benefits. *GCB Bioenergy* **2012**, *4*, 119–126, doi:10.1111/j.1757-1707.2011.01122.x.

203. Dias, M. O. S.; Cunha, M. P.; Jesus, C. D. F.; Rocha, G. J. M.; Pradella, J. G. C.; Rossell, C. E. V.; Maciel Filho, R.; Bonomi, A. Second generation ethanol in Brazil: Can it compete with electricity production? *Bioresour. Technol.* **2011**, *102*, 8964–8971, doi:10.1016/j.biortech.2011.06.098.

204. Macrelli, S.; Galbe, M.; Wallberg, O. Effects of production and market factors on ethanol profitability for an integrated first and second generation ethanol plant using the whole sugarcane as feedstock. *Biotechnol. Biofuels* **2014**, *7*, 1–16, doi:10.1186/1754-6834-7-26.

205. Canilha, L.; Chandel, A. K.; Suzane Dos Santos Milessi, T.; Antunes, F. A. F.; Luiz Da Costa Freitas, W.; Das Graças Almeida Felipe, M.; Da Silva, S. S. Bioconversion of sugarcane biomass into ethanol: An overview about composition, pretreatment methods, detoxification of hydrolysates, enzymatic saccharification, and ethanol fermentation. *J. Biomed. Biotechnol.* **2012**, *2012*, doi:10.1155/2012/989572.

206. Al Arni, S. Comparison of slow and fast pyrolysis for converting biomass into fuel. *Renew. Energy* **2018**, *124*, 197–201, doi:10.1016/j.renene.2017.04.060.

207. Mullen C, Boateng A, Goldberg N, Lima I, Laird D, H. K. Bio-oil and bio-char production from corn cobs and stover by fast pyrolysis. *Biomass and Bioenergy* **2010**, *34*, 67–74, doi:https://doi.org/10.1016/j.biombioe.2009.09.012.

208. Vecino Mantilla, S.; Gauthier-Maradei, P.; Álvarez Gil, P.; Tarazona Cárdenas, S. Comparative study of bio-oil production from sugarcane bagasse and palm empty fruit bunch: Yield optimization and bio-oil characterization. *J. Anal. Appl. Pyrolysis* **2014**, *108*, 284–294, doi:10.1016/j.jaap.2014.04.003.

209. Islam, M. R.; Parveen, M.; Haniu, H. Properties of sugarcane waste-derived bio-oils obtained by fixed-bed fire-tube heating pyrolysis. *Bioresour. Technol.* **2010**, *101*, 4162–4168, doi:10.1016/j.biortech.2009.12.137.

210. Dewangan, A.; Pradhan, D.; Singh, R. K. Co-pyrolysis of sugarcane bagasse and low-density polyethylene: Influence of plastic on pyrolysis product yield. *Fuel* **2016**, *185*, 508–516, doi:10.1016/j.fuel.2016.08.011.

211. Shi, H.; Chen, J.; Yang, Y.; Tian, S. Catalytic deoxygenation of methyl laurate as a model compound to hydrocarbons on nickel phosphide catalysts: Remarkable support effect. *Fuel Process. Technol.* **2014**, *118*, 161–170, doi:10.1016/j.fuproc.2013.08.010.

212. Yakovlev, V. A.; Bykova, M. V.; Khromova, S. A. Stability of nickel-containing catalysts for hydrodeoxygenation of biomass pyrolysis products. *Catal. Ind.* **2012**, *4*, 324–339, doi:10.1134/S2070050412040204.

213. Charusiri, W.; Vitidsant, T. Upgrading bio-oil produced from the catalytic pyrolysis of sugarcane (Saccharum officinarum L) straw using calcined dolomite. *Sustain. Chem. Pharm.* **2017**, *6*, 114–123, doi:https://doi.org/10.1016/j.scp.2017.10.005.

214. del Río, J. C.; Lino, A. G.; Colodette, J. L.; Lima, C. F.; Gutiérrez, A.; Martínez, Á. T.; Lu, F.; Ralph, J.; Rencoret, J. Differences in the chemical structure of the lignins from sugarcane bagasse and straw. *Biomass and Bioenergy* **2015**, *81*, 322–338, doi:10.1016/j.biombioe.2015.07.006.

215. Arni, S. Al Extraction and isolation methods for lignin separation from sugarcane bagasse: A review. *Ind. Crops Prod.* **2018**, *115*, 330–339, doi:10.1016/j.indcrop.2018.02.012.

216. Agência Brasil Etanol deve alcançar recorde de produção com 33,14 bilhões de litros Available online: http://agenciabrasil.ebc.com.br/economia/noticia/2019-04/etanol-deve-alcancar-recorde-de-producao-com-3358-bilhoes-de-litros (accessed on May 22, 2019).

217. Moss, J. What to expect from Brazil's RenovaBio programme Available online: https://knect365.com/energy/article/e5560843-78a9-4034-81f7-25319afe103c/what-

to-expect-from-brazils-renovabio-programme (accessed on May 22, 2019).

218. Maria, A.; Alves, M. Mediante Pirólisis Analítica En Madera De Pinus Caribaea . Content and Quality Study of the Lignin By Analytical Pyrolysis in Pinus Caribaea. *Quality* **2007**, *9*, 179–188, doi:10.4067/S0718-221X2007000200008.

219. Alves, A.; Schwanninger, M.; Pereira, H.; Rodrigues, J. Analytical pyrolysis as a direct method to determine the lignin content in wood: Part 1: Comparison of pyrolysis lignin with Klason lignin. *J. Anal. Appl. Pyrolysis* **2006**, *76*, 209–213, doi:10.1016/j.jaap.2005.11.004.

220. Funke, A.; Grandl, R.; Ernst, M.; Dahmen, N. Modelling and improvement of heat transfer coefficient in auger type reactors for fast pyrolysis application. *Chem. Eng. Process. - Process Intensif.* **2018**, *130*, 67–75, doi:10.1016/j.cep.2018.05.023.

221. Windt, M.; Meier, D.; Marsman, J. H.; Heeres, H. J.; de Koning, S. Micro-pyrolysis of technical lignins in a new modular rig and product analysis by GC-MS/FID and GC × GC-TOFMS/FID. *J. Anal. Appl. Pyrolysis* **2009**, *85*, 38–46, doi:10.1016/j.jaap.2008.11.011.

222. Varma, A. K.; Mondal, P. Pyrolysis of sugarcane bagasse in semi batch reactor: Effects of process parameters on product yields and characterization of products. *Ind. Crops Prod.* **2017**, *95*, 704–717, doi:10.1016/j.indcrop.2016.11.039.

223. Augustínová, J.; Cvengrošová, Z.; Mikulec, J.; Vasilkovová, B.; Cvengroš, J.; Stu, F. Upgrading of biooil from fast pyrolysis. *46th Int. Conf. Pet. Process.* **2013**, *7*.

224. Nicole Tröger; Daniel Richter; Ralph Stahl Effect of feedstock composition on product yields and energy recovery rates of fast pyrolysis products from different straw types. *J. Anal. Appl. Pyrolysis* **2013**, *100*, 158–165, doi:https://doi.org/10.1016/j.jaap.2012.12.012.

225. Rabiu, S. D.; Auta, M.; Kovo, A. S. An upgraded bio-oil produced from sugarcane bagasse via the use of HZSM-5 zeolite catalyst. *Egypt. J. Pet.* **2018**, 1–6, doi:10.1016/j.ejpe.2017.09.001.

226. Sukumar, V.; Manieniyan, V.; Sivaprakasam, S. Bio oil production from biomass using pyrolysis and upgrading - A review. *Int. J. ChemTech Res.* **2015**, *8*, 196–206.

227. Lopes, F. J. F.; Silvério, F. O.; Baffa, D. C. F.; Loureiro, M. E.; Barbosa, M. H. P. Determination of Sugarcane Bagasse Lignin S/G/H Ratio by Pyrolysis GC/MS. *J. Wood Chem. Technol.* **2011**, *31*, 309–323, doi:10.1080/02773813.2010.550379.

228. Banyasz, J. L.; Li, S.; Lyons-Hart, J. L.; Shafer, K. H. Cellulose pyrolysis: The kinetics of hydroxyacetaldehyde evolution. *J. Anal. Appl. Pyrolysis* **2001**, *57*, 223–248, doi:10.1016/S0165-2370(00)00135-2.

229. Oh, S.; Choi, G.; Kim, J. Production of acetic acid-rich bio-oils from the fast pyrolysis of biomass and synthesis of calcium magnesium acetate deicer. *J. Anal. Appl. Pyrolysis* **2017**, *124*, 122–129, doi:10.1016/j.jaap.2017.01.032.

230. Shen, D.; Jin, W.; Hu, J.; Xiao, R.; Luo, K. An overview on fast pyrolysis of the main constituents in lignocellulosic biomass to valued-added chemicals: Structures, pathways and interactions. *Renew. Sustain. Energy Rev.* **2015**, *51*, 761–774, doi:10.1016/j.rser.2015.06.054.

231. Azeez, A. M.; Meier, D.; Odermatt, J. Temperature dependence of fast pyrolysis volatile products from European and African biomasses. *J. Anal. Appl. Pyrolysis* **2011**, *90*, 81–92, doi:10.1016/j.jaap.2010.11.005.

232. Patwardhan, P. R. Understanding the product distribution from biomass fast pyrolysis. *Chem. Eng.* **2010**, *Ph. D.*, 162, doi:Doctoral Thesis.

233. Lupoi, J. S.; Singh, S.; Parthasarathi, R.; Simmons, B. A.; Henry, R. J. Recent innovations in analytical methods for the qualitative and quantitative assessment of lignin. *Renew. Sustain. Energy Rev.* **2015**, *49*, 871–906, doi:10.1016/j.rser.2015.04.091.

234. Lin, X.; Sui, S.; Tan, S.; Pittman, C.; Sun, J.; Zhang, Z. Fast Pyrolysis of Four Lignins from Different Isolation Processes Using Py-GC/MS. *Energies* **2015**, *8*, 5107–5121, doi:10.3390/en8065107.

235. Wu, S. Estimation and comparison of bio-oil components from different pyrolysis conditions. **2015**, *3*, 1–11, doi:10.3389/fenrg.2015.00028.

236. Poelking, Viviane Guzzo De Carli; Giordano, A.; Ricci-Silva, M. E.; Williams, T. C. R.; Peçanha, D. A.; Ventrella, M. C.; Rencoret, J.; Ralph, J.; Barbosa, M. H. P.; Loureiro, M. Analysis of a modern hybrid and an ancient sugarcane implicates a complex interplay of factors in affecting recalcitrance to cellulosic ethanol production. *PLoS One* **2015**, *10*, doi:10.1371/journal.pone.0134964.

237. Oasmaa, A. .; Kuoppala, E. .; Gust, S. .; Solantausta, Y. Extractives on Phase Separation of Pyrolysis Liquids. *Energy & Fuels* **2003**, *17*.

238. George W. Huber David M. Ford, Surita R. Bhatia, Phillip C. Badger, A. A. U. Fast Pyrolysis Oil Stabilization: An Integrated Catalytic and Membrane Approach for Improved Bio-oils. **2011**, 72.

239. Yin, W.; Kloekhorst, A.; Venderbosch, R. H.; Bykova, M. V.; Khromova, S. A.; Yakovlev, V. A.; Heeres, H. J. Catalytic hydrotreatment of fast pyrolysis liquids in batch and continuous set-ups using a bimetallic Ni-Cu catalyst with a high metal content. *Catal. Sci. Technol.* **2016**, *6*, 5899–5915, doi:10.1039/c6cy00503a.

240. Kloekhorst, A.; Heeres, H. J. Catalytic Hydrotreatment of Alcell Lignin Using Supported Ru, Pd, and Cu Catalysts. *ACS Sustain. Chem. Eng.* **2015**, *3*, 1905–1914, doi:10.1021/acssuschemeng.5b00041.

241. Jiang, X. X.; Naoko, E.; Zhong, Z. P. Structure properties of pyrolytic lignin extracted from aged bio-oil. *Chinese Sci. Bull.* **2011**, *56*, 1417–1421, doi:10.1007/s11434-011-4465-4.

242. Payormhorm, J.; Kangvansaichol, K.; Reubroycharoen, P.; Kuchonthara, P.; Hinchiranan, N. Pt/Al2O3-catalytic deoxygenation for upgrading of Leucaena leucocephala-pyrolysis oil. *Bioresour. Technol.* **2013**, *139*, 128–135, doi:10.1016/j.biortech.2013.04.023.

243. Wang, J.; Chang, J.; Fan, J. Catalytic esterification of bio-oil by ion exchange resins. *J. Fuel Chem. Technol.* **2010**, *38*, 560–564, doi:10.1016/S1872-5813(10)60045-X.

244. Lugo-josé, Y. K.; Monnier, J. R.; Heyden, A.; Williams, C. T. Hydrodeoxygenation of propanoic acid over silica-supported palladium : effect of metal particle size. *Catal. Sci. Technol.* **2014**, *4*, 3909–3916, doi:10.1039/c4cy00605d.

245. Venderbosch, R.; Heeres, H. Pyrolysis Oil Stabilisation by Catalytic Hydrotreatment. In *Biofuel's Engineering Process Technology*; Bernardes, M. A. dos S., Ed.; InTech, 2011; pp. 385–410 ISBN 978-953-307-480-1.

246. Ardiyanti, A. *Hydrotreatment of fast pyrolysis oil: catalyst development and process-product relations*; 2013; ISBN 9789461822345.

247. Routray, K.; Barnett, K. J.; Huber, G. W. Hydrodeoxygenation of Pyrolysis Oils. *Energy*

Technol. **2016**, *5*, 80–93, doi:https://doi.org/10.1002/ente.201600084.

248. Xu, Y.; Zhang, L.; Chang, J.; Zhang, X.; Ma, L.; Wang, T.; Zhang, Q. One step hydrogenation-esterification of model compounds and bio-oil to alcohols and esters over Raney Ni catalysts. *Energy Convers. Manag.* **2016**, *108*, 78–84, doi:10.1016/j.enconman.2015.10.062.

249. Witsuthammakul, A.; Sooknoi, T. Selective hydrodeoxygenation of bio-oil derived products: ketones to olefins. *Catal. Sci. Technol.* **2015**, *5*, 3639–3648, doi:10.1039/C5CY00367A.

250. Chen, W.; Luo, Z.; Yang, Y.; Li, G.; Zhang, J.; Dang, Q. Upgrading of Bio-oil in Supercritical Ethanol: Using Furfural and Acetic Acid as Model Compounds. *BioResources* **2013**, *8*, 3934–3952.

251. Figueirêdo, M. B.; Jotic, Z.; Deuss, P. J.; Venderbosch, R. H.; Heeres, H. J. Hydrotreatment of pyrolytic lignins to aromatics and phenolics using heterogeneous catalysts. *Fuel Process. Technol.* **2019**, *189*, 28–38, doi:10.1016/J.FUPROC.2019.02.020.

252. Bykova, M. V.; Ermakov, D. Y.; Kaichev, V. V.; Bulavchenko, O. A.; Saraev, A. A.; Lebedev, M. Y.; Yakovlev, V. Ni-based sol-gel catalysts as promising systems for crude bio-oil upgrading: Guaiacol hydrodeoxygenation study. *Appl. Catal. B Environ.* **2012**, *113–114*, 296–307, doi:10.1016/j.apcatb.2011.11.051.

253. Moulijn, J. A.; Van Diepen, A. E.; Kapteijn, F. Catalyst deactivation: Is it predictable? What to do? *Appl. Catal. A Gen.* **2001**, *212*, 3–16, doi:10.1016/S0926-860X(00)00842-5.

254. Gonçalves, V. O. O.; de Souza, P. M.; Cabioc'h, T.; da Silva, V. T.; Noronha, F. B.; Richard, F. Hydrodeoxygenation of m-cresol over nickel and nickel phosphide based catalysts. Influence of the nature of the active phase and the support. *Appl. Catal. B Environ.* **2017**, *219*, 619–628, doi:10.1016/j.apcatb.2017.07.042.

255. Bartholomew, C. H.; Agrawal, P. K.; Katzer, J. R. Sulfur Poisoning of Metals. *Adv. Catal.* **1982**, *31*, 135–242, doi:10.1016/S0360-0564(08)60454-X.

256. Mortensen, P. M.; De Carvalho, H. W. P.; Grunwaldt, J. D.; Jensen, P. A.; Jensen, A. D. Activity and stability of Mo2C/ZrO2 as catalyst for hydrodeoxygenation of mixtures of phenol and 1-octanol. *J. Catal.* **2015**, *328*, 208–215, doi:10.1016/j.jcat.2015.02.002.

257. Hellinger, M.; Baier, S.; Mortensen, P.; Kleist, W.; Jensen, A.; Grunwaldt, J.-D. Continuous Catalytic Hydrodeoxygenation of Guaiacol over Pt/SiO2 and Pt/H-MFI-90. *Catalysts* **2015**, *5*, 1152–1166, doi:10.3390/catal5031152.

258. Forzatti, P. Catalyst deactivation. *Catal. Today* **2002**, *52*, 165–181, doi:10.1016/s0920-5861(99)00074-7.

259. Gooden, P. N.; Bourne, R. A.; Parrott, A. J.; Bevinakatti, H. S.; Irvine, D. J.; Poliakoff, M. Continuous acid-catalyzed methylations in supercritical carbon dioxide: Comparison of methanol dimethyl ether and dimethyl carbonate as methylating agents. *Org. Process Res. Dev.* **2010**, *14*, 411–416, doi:10.1021/op900307w.

260. Casas, C.; Bringué, R.; Ramírez, E.; Iborra, M.; Tejero, J. Liquid-phase dehydration of 1-octanol, 1-hexanol and 1-pentanol to linear symmetrical ethers over ion exchange resins. *Appl. Catal. A Gen.* **2011**, *396*, 129–139, doi:10.1016/j.apcata.2011.02.006.

261. Chandra Sekhar Palla, V.; Shee, D.; Maity, S. K. Kinetics of hydrodeoxygenation of octanol over supported nickel catalysts: A mechanistic study. *RSC Adv.* **2014**, *40*, 41612–41621, doi:10.1039/c4ra06826b.

262. Winterbottom, J. M. *Hydration and dehydration by heterogeneous catalysts*; 2007; Vol. 47; ISBN 9781847553164.

Supplementary Material

S.1 Supplementary Material – Chapter 3

S.1.1 Upgraded beech wood fast pyrolysis bio-oil with Ni/SiO_2 catalyst

The autoclave picture can be seen below (Fig. S.1).The upgrading was conducted at 325 °C and 80 bars for 120 minutes, including the heating ramp. Due to the low amount of upgraded oil produced in each experiment, it was necessary to repeat this procedure for at least four times. Hence, a significant amount of sample was produced, enough for characterization and further upgrading reactions. Some of the characterization results of upgraded light phases and upgraded oils are presented in Table S.1. The Ni/SiO_2 catalysts used for these reactions, synthesized by wet impregnation technique was composed by 7.9 wt.% of nickel. More information can be found in Chapter 5.

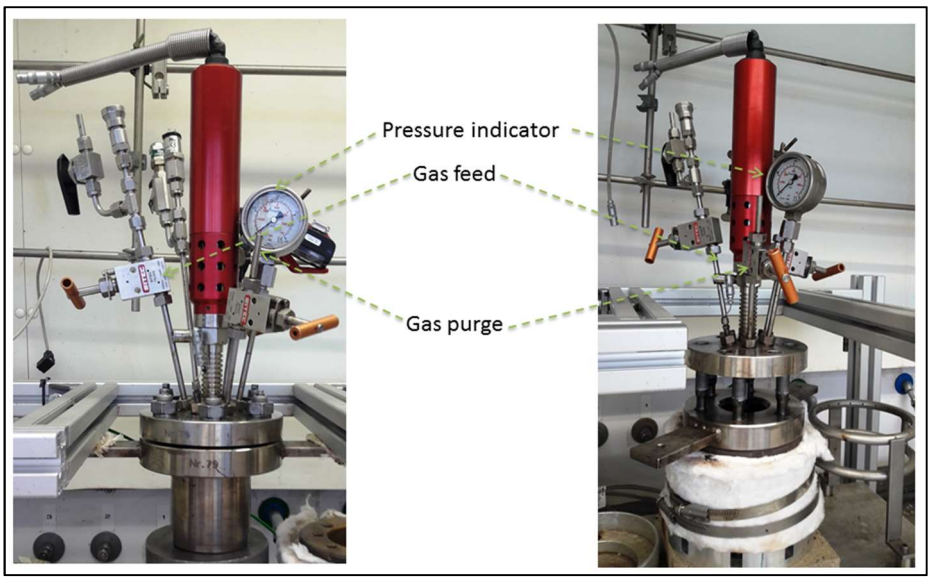

Figure S 1. Autoclave used during the experiments.

Table S 1. Characterization of upgraded beech wood fast pyrolysis bio-oils obtained with Ni/SiO_2.

Parameter	Reaction 1 (wet basis)	Reaction 2 (wet basis)	Reaction 3 (wet basis)	Reaction 4 (wet basis)	Average (wet basis)	Average (dry basis)	Standard Deviation (wet basis)
H_2 consumption (mol/Kg BWBO)	7.0	8.0	7.7	7.7	7.6	-	0.35
UPGRADED OIL							
Carbon (wt.%)	68.4	69.6	69.6	69.0	69.1	72.9	0.57
Hydrogen (wt.%)	8.2	8.6	8.5	8.7	8.5	8.4	0.21
Oxygen (wt.%)	22.8	21.3	21.4	21.8	21.82	18.18	0.68
Nitrogen (wt.%)	0.3	0.3	0.3	0.3	0.3	0.3	-
Sulfur (wt.%)	0.3	0.2	0.2	0.2	0.22	0.26	0.05
H_2O (wt.%)	5.6	4.9	4.8	5.2	5.1	-	0.36
HHV (MJ/Kg)	30.5	31.1	31.2	30.9	30.9	33.4	0.33
pH value	2.5	3.8	3.3	2.5	3.0	-	0.64
Density (g/cm^3)	1.12	-	1.11	-	1.11	-	0.005
Degree of deoxygenation (calculated in dry basis)	42.79	46.00	45.45	45.09	-	44.83	1.2
UPGRADED LIGHT PHASE							
Carbon (wt.%)	-	11.7	11.5	-	11.6	43.72	0.14
Hydrogen (wt.%)	-	11.5	11.4	-	11.45	12.39	0.071
Oxygen (wt.%)	-	73.8	74.0	-	73.9	42.19	0.141
Nitrogen (wt.%)	-	0.3	0.3	-	0.3	1.13	-
Sulfur (wt.%)	-	0.1	0.2	-	0.15	0.56	0.071
H_2O (wt.%)	-	74.5	74.2	71.7	73.47	-	1.537
pH value	-	3.1	3.1	2.9	3.03	-	0.115
Density (g/cm^3)	-	1.03	1.03	1.03	1.03	-	0.001

S.1.2 Upgraded products

The figure S.2 shows the detailed upgraded products after the centrifugation step. The UAP is concentrated on the top, upgraded oil in the bottom while the spent catalyst is concentrated in the tube's wall as well as in the bottom.

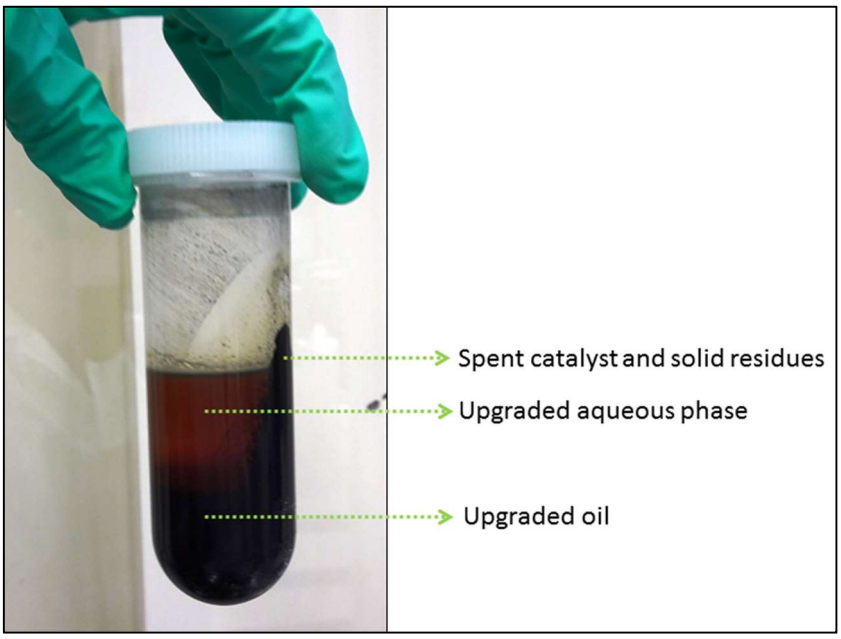

Figure S 2. Detailed of the upgraded products after the centrifugation step.

After the separation, the products are divided in tubes and later characterized. The Figure S.3 shows the typical upgraded products obtained after the upgrading of beech wood fast pyrolysis bio-oil with Ru/C, Ni catalyst and Ni-Cr catalyst.

Figure S 3. Upgraded products separated after centrifugation. From the left to the right: spent catalyst after filtration; upgraded aqueous phase and the two last samples in the right side are the upgraded oil.

The upgraded products obtained for the 2-step upgrading reaction are presented in Fig. S.4. A colorless upgraded aqueous phase was obtained in this case.

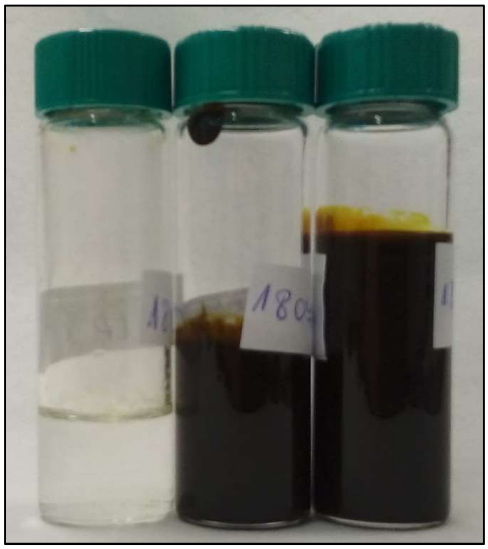

Figure S 4. Products obtained after the second upgrading performed with UBWBO. From the left: upgraded aqueous phase and two bottles containing the upgraded oil.

S.1.3 Evaluation of different reaction times

The comparison of different reaction times was conducted at 4 h and 2 h, respectively. The results obtained are demonstrated in Table S.2. Despite the higher H_2 consumption for the reaction conducted for 4 hours, the other parameters are comparable.

Table S 2. Comparison of reactions conducted with Ni catalyst at 225 °C for 2 h and 4 h, wet basis.

Upgraded oil composition	Ni, 225 °C, 4 hours of reaction[1]	Ni, 225 °C, 2 hours of reaction
C (wt.%)	58.3	58.2
H (wt.%)	8.0	8.5
O (wt.%)	33.1	33.0
pH value	4.1	3.9
H_2O (wt.%)	10.5	11.6
HHV (MJ/Kg)	26.3	26.1
Mass Balance		
Gas production (wt.%)	1.31	1.37
Upgraded aqueous phase (wt.%)	46.9	50.7
Upgraded oil (wt.%)	43.2	40.9
Solids (wt.%)	0.4	0.5
Loss (wt.%)	8.2	6.5
Gas composition		
CO_2 (mol/Kg PO)	0.29	0.30
CH_4 (mol/Kg PO)	0.03	0.03
H_2 consumption (mol/Kg PO)	11.62	9.48

[1]Already presented in the chapter, but in order to facilitate the comparison to the reader, the result is presented again in the Supplementary Material.

S.1.3 Elemental analysis and physicochemical characterization of the upgraded aqueous phases with Ni, Ni-Cr and Ru/C catalysts

Table S 3. Elemental analysis and physicochemical properties of upgraded aqueous phase upgraded with Ni, Ni-Cr and Ru/C catalysts.

	Ni, 175 °C 1-step UR	**Ni, 225 °C 1-step UR**	**Ni-Cr, 175 °C 1-step UR**	**Ni-Cr, 225 °C 1-step UR**	**Ru/C, 175 °C 1-step UR**	**Ru/C, 225 °C 1-step UR**	**Ni-Cr, 325 °C 2-step UR[1]**
C (wt.%)	28.5	26.5	28.0	25.5	27.8	23.8	1.6
H (wt.%)	9.7	9.9	9.5	9.4	9.2	9.7	14.5
O (wt.%)	61.7	63.5	62.3	64.9	62.9	66.3	82.1
N (wt.%)	<1.0	<1.0	<1.0	<1.0	<0.2	<0.2	<1.0
S (wt.%)	<0.5	<0.5	<0.5	<0.5	<0.5	<0.5	<0.5
pH value	3.5	3.5	3.5	3.6	3.0	3.1	3.7
H_2O (wt.%)	42.6	46.6	43.3	48.7	44.0	52.0	97.0
HHV (MJ/Kg)	12.8	12.2	12.6	11.8	12.4	[2]	[2]

[1]UR: upgrading reactions; [2]Not determined – high water concentration.

S.1.4 NH_3-TPD

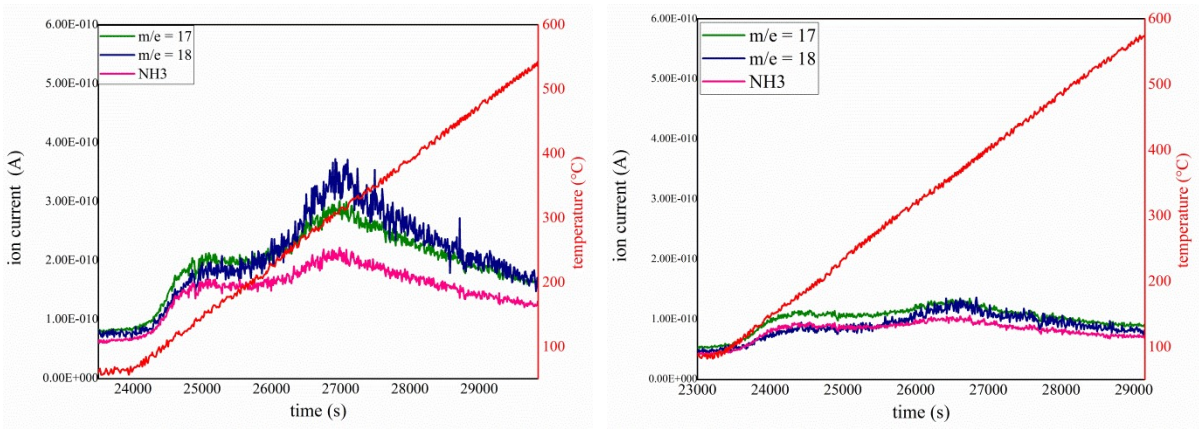

Figure S 5. NH_3-TPD of fresh nickel-based catalysts. Left: Ni catalyst; Right: Ni-Cr catalyst

For a quantitative analysis of the desorbed ammonia it is considered that the ammonia desorption is always accompanied by water desorption of in varying amounts. m/e = 17 is a trace of ammonia but inflected by the fragmentation of water in the ion source of the QMS detector. The general fragmentation pattern of water (library data) tells that the relative abundance of m/e =17 is 23% of the abundance of m/e = 18 for water.

Therefore a pure "NH_3" trace is created by assuming that (m/e = 17) – (0,23 * (m/e = 18)) is the ammonia amount of m/e =17 without the water inflection. This NH_3-trace is used for the quantitative calculations. The molar amount of desorbed ammonia is derived from a comparative

measurement with a substance with a known amount of NH_3 desorption. This is a H-ZSM5 sample (the high temperature peak is used).

S.1.5 Detailed chemical composition received from GC-MS/FID measurements

Table S 4. Single compounds identified by GC-MS/FID in the upgraded oils and feedstocks.

Compound *(wet basis; dry basis)*	**BWBO (wt.%)**		**UBWBO (wt.%)**	**Ni, 225 °C 1-step UR (wt.%)**		**Ni-Cr, 225 °C 1-step UR (wt.%)**		**Ni-Cr, 325 °C 2-step UR** (wt.%)**	
	LP	**HP**		**UAP**	**UO**	**UAP**	**UO**	**UAP**	**UO**
Nonaromatic Compounds	**19.81; 30.72**	**14.18; 16.54**	**13.69; 14.61**	**28.70; 55.68**	**15.0; 16.91**	**20.72; 41.57**	**13.15; 14.64**	**2.96; 80.99**	**5.13; 5.28**
Acids	**6.18; 9.59**	**4.643; 5.42**	**9.709; 10.37**	**10.025; 19.45**	**8.637; 9.73**	**4.554; 9.14**	**7.96; 8.86**	**2.735; 74.72**	**-**
Formic acid	n.q.	-	-	-	-	**-**	-	-	-
Acetic Acid[c]	4.732; 7.338	3.183; 3.714	4.388; 4.685	5.195; 10.08	3.693; 4.162	4.554; 9.138	3.232; 3.598	1.118; 30.53	-
Propionic Acid[c]	1.117; 1.732	1.062; 1.240	5.322; 5.682	4.776; 9.267	4.786; 5.395	-	4.625; 5.148	1.463; 39.96	-
Butyric Acid[c]	0.120; 0.187	0.151; 0.176	-	0.053; 0.103	0.158; 0.178	-	0.099; 0.111	0.125; 3.41	-
3-butenoic acid	0.025; 0.038			-		-		-	
(Z)-(cis)-2-butenoic Acid[#]	0.076; 0.117	0.093; 0.109	-	-	-	-	-	-	-
Pentanoic Acid[#]	0.021; 0.033	0.036; 0.042	-	-	-	-	-	-	-
4-pentenoic acid	0.038; 0.060			-		-		-	
Hexanoic Acid[#]	0.052; 0.081	0.118; 0.138	-	-	-	-	-	-	-
2-methyl-propanoic acid	-	-	-	-	-	-	-	0.030; 0.815	
Nonaromatic Esters	**0.388; 0.60**	**0.256; 0.30**	**0.079; 0.08**	**0.788; 1.53**	**0.589; 0.66**	**0.578; 1.16**	**0.275; 0.31**	**-**	**-**
Propanoic acid, methyl ester[#]	0.012; 0.019	0.021; 0.024	0.079; 0.084	-	-	-	-	-	-
Acetic acid 2-hydroxyethyl ester[c]	0.185; 0.287	0.103; 0.120	-	0.671; 1.303	0.517; 0.583	0.471; 0.944	0.209; 0.233	-	-
poss: Oxopropanoic acid methylester, 2-	0.091; 0.140			-	-	-		-	

Butenoic acid, dimethyl ester or isomer	0.014; 0.022			-	-	-		-	
Unknown aliphatic ester	0.059; 0.092			-	-	0.019; 0.037		-	
Poss: ethenyl ester propanoic acid#	0.021; 0.033	0.045; 0.053	-	-	-	-	-	-	-
Unknown aliphatic ester#	-	0.055; 0.064	-	-	-	-	-	-	-
7-oxodehydroabietic acid, methyl ester#	0.005; 0.008	0.032; 0.037	-	-	-	-	-	-	-
2-hydroxyethyl ester propanoic acid	-	-	-	0.030; 0.059	0.072; 0.081	0.017; 0.034	0.008; 0.008	-	-
Poss: butanoic acid, propyl ester	-	-	-	0.012; 0.023	-	-	0.025; 0.028	-	-
Similar to furancarboxylic acid, tetrahydro-3-methyl-5-oxo-,methyl ester	-	-	-	0.035; 0.068	-	0.071; 0.144	0.032; 0.036	-	-
Poss: furancarboxylic acid, tetrahydro-3-methyl-5-oxo-, methyl ester	-	-	-	0.039; 0.076	-	-	-	-	-
Nonaromatic Alcohols	**2.679; 4.15**	**0.926; 1.08**	**0.176; 0.19**	**17.507; 33.97**	**4.164; 4.69**	**15.537; 31.17**	**4.343; 4.83**	**0.114; 3.12**	**0.455; 0.47**
1-propanol	-	-	-	0.113; 0.220	0.134; 0.152	0.125; 0.251	0.132; 0.147	-	-
cyclohexanol#	-	-	-	0.011; 0.021	-	0.047; 0.093	0.215; 0.239	0.044; 1.190	0.455; 0.469
Ethylene glycol[c]	2.614; 4.053	0.88; 1.027	-	13.592; 26.371	2.382; 2.685	11.378; 22.829	1.729; 1.925	-	-
2-propen-1-ol#	0.021; 0.033	0.019; 0.022			-	-		-	-
Poss: 2-methyl-2-propanol#	0.013; 0.020				-	-		-	-
1,2-ethanediol, monoformate#	0.031; 0.048	0.027; 0.032			-	-		-	-
cyclopentanol[c]	-	-	-	0.048; 0.092	0.117; 0.132	0.060; 0.121	0.165; 0.184	0.011; 0.292	-
(n)-2-butanol#	-	-	-	0.008; 0.016	0.018; 0.020	0.031; 0.062	0.060; 0.067	0.060; 1.632	-
2-methyl-1-butanol#	-	-	-	0.010; 0.020	-	-	-	-	-
Poss: 2-methyl-1-butanol#	-	-	-	0.008; 0.016	0.031; 0.035	-	0.026; 0.029	-	-
Unknown aliphatic alcohol#	-	-	-	0.028; 0.054	0.028; 0.032	-	-	-	-

Propylene glycol#	-	-	-	2.326; 4.513	0.756; 0.852	2.034; 4.080	0.623; 0.694	-	-
2-methyl-cyclopentanol#	-	-	-	0.026; 0.051	0.105; 0.118	0.054; 0.108	0.217; 0.241	-	-
3-methyl-cyclopentanol#	-	-	-	0.011; 0.022	0.050; 0.056	0.014; 0.027	0.067; 0.074	-	-
2-methyl-trans-cyclopentanol#	-	-	-	0.012; 0.024	0.052; 0.058	0.042; 0.084	0.194; 0.216	-	-
Poss: 2,3-butanediol#	-	-	-	0.116; 0.224	0.053; 0.060	0.146; 0.292	0.051; 0.056	-	-
Poss: [R-(R*, R*)]-2,3-butanediol#	-	-	-	0.163; 0.317	0.069; 0.078	0.202; 0.405	0.095; 0.106	-	-
1,2-butanediol,(ñ) #	-	-	-	0.330; 0.641	0.165; 0.186	0.338; 0.677	0.143; 0.160	-	-
Poss: 1-methoxy-2-butanol#	-	-	-		0.056; 0.063	0.089; 0.179	0.101; 0.112	-	-
Isomer of 1-methoxy-2 butanol	-	-	-	-	-	0.166; 0.332	-	-	-
Unknown not identifiable aliphatic alcohol#	-	-	-	0.232; 0.456	0.107; 0.121	-	-	-	-
1,4-butanediol#	-	-	-	0.160; 0.311	0.042; 0.047	0.140; 0.282	0.025; 0.028	-	-
1,4-pentanediol#	-	-	-	0.020; 0.038	-	0.041; 0.083		-	-
Poss: Isomer of cyclopentane-1,2-diol	-	-	-	0.029; 0.057		0.047; 0.094		-	-
Unknown aliphatic alcohol#	-	-	0.078; 0.083	-	-	0.067; 0.134	-	-	-
2,4-dimethyl-cyclopentanol #	-	-	0.098; 0.105	-	-	-	-	-	-
(R)-(-)-2-pentanol	-	-	-	-	-	-	0.045; 0.050	-	-
Isomer of 1-methoxy-2-butanol	-	-	-	-	-	-	0.092; 0.102	-	-
Unknown aliphatic alcohol	-	-	-	-	-	0.040; 0.081	0.061; 0.067	-	-
Isomer of 3-methyl-1,2-cyclopentanediol	-	-	-	0.031; 0.059	-	0.024; 0.048	0.024; 0.027	-	-
glycerin	-	-	-	0.087; 0.168	-	0.063; 0.126	-	-	-
Isomer of 1,2,3-butanetriol	-	-	-	0.010; 0.019	-	-	-	-	-

Trans-1,2cyclohexanediol	-	-	-	-	-	0.227; 0.455	0.278; 0.309	-	-
1,2,4-butanetriol or Isomer	-	-	-	-	-	0.025; 0.050	-	-	-
Poss: trans-1,2-cyclohexanediol	-	-	-	-	-	0.074; 0.149	-	-	-
Unknown aliphatic alcohol#	-	-	-	0.133; 0.259		0.045; 0.091	-	-	-
Unknown not identiable aliphatic alcohol	-	-	-	-	-	0.020; 0.039	-	-	-
Nonaromatic Aldehydes	**4.133; 6.41**	**2.759; 3.22**	**-**	**-**	**-**	**-**	**-**	**-**	**-**
hydroxyacetaldehyde[c]	3.883; 6.021	2.428; 2.832	-	-	-	-	-	-	-
3-hydroxypropionaldehyde#	0.134; 0.207	0.115; 0.134	-	-	-	-	-	-	-
Butanal#	-	0.014; 0.016	-	-	-	-	-	-	-
2-butenal#	0.014; 0.022	0.024; 0.027	-	-	-	-	-	-	-
2-methyl-2-butenal#	-	0.029; 0.034	-	-	-	-	-	-	-
Poss: hexanal#	-	0.014; 0.016	-	-	-	-	-	-	-
Butanedial or propanal#	-	0.136; 0.158	-	-	-	-	-	-	-
Poss: 3-hydroxy-butanal	0.017; 0.027	-	-	-	-	-	-	-	-
Butanedial or Propanal	0.085; 0.132	-	-	-	-	-	-	-	-
Nonaromatic Ketones	**6.428; 9.97**	**5.594; 6.53**	**3.723; 3.98**	**0.378; 0.73**	**1.567; 1.77**	**0.051; 0.10**	**0.580; 0.65**	**0.115; 3.15**	**1.837; 1.89**
Acetol (hydroxypropanone)[c]	4.732; 7.338	3.171; 3.70	-	-	-	-	-	-	-
Acetonylacetone (2,5-hexandione) [c]	0.006; 0.009	0.035; 0.041	-	-	0.027; 0.031	-	-	-	-
2-butanone[c]	0.051; 0.079	0.082; 0.096	0.229; 0.245	0.022; 0.044	0.080; 0.090	-	-	-	0.387; 0.398
1-hydroxy-2-butanone[c]	0.412; 0.639	0.305; 0.356	-	-	-	-	-	-	-
2,3-butandione (diacetyl)[c]	0.127; 0.198	0.102; 0.119	-	-	-	-	-	-	-

3-hydroxy-2-butanone[c]	0.056; 0.086	0.053; 0.061	0,118; 0,126	0.101; 0.196	-	-	-	-	-
1-acetyloxy-propan-2-one[c]	0.071; 0.110	0.093; 0.109	-	-	-	-	-	-	-
cyclopentanone[c]	-	0.107; 0.125	0,283; 0,303	-	0.239; 0.269	-	0.183; 0.203	0.028; 0.766	-
2-cyclopenten-1-one[c]	0.132; 0.205	0.202; 0.236	-	-	-	-	-	-	-
2,3-dimethyl-2-cyclopenten-1-one[c]	0.062; 0.095	0.091; 0.106	0.149; 0.159	-	-	-	-	-	-
2-methyl-2-cyclopenten-1-one[c]	0.034; 0.053	0.09; 0.105	-	-	-	-	-	-	-
3-methyl-2-cyclopenten-1-one[c]	0.057; 0.089	0.097; 0.114	-	-	-	-	-	-	-
2-hydroxy-2-cyclopenten-1-one[#]	0.030; 0.046	0.023; 0.027	-	-	-	-	-	-	-
2-hydroxy-1-methyl-1-cyclopenten-3-one[c]	0.408; 0.632	0.578; 0.675	-	-	-	-	-	-	-
3-ethyl-2-hydroxy-2-cyclopenten-1-one[c]	0.054; 0.084	0.091; 0.106	-	-	-	-	-	-	-
2-cyclohexen-1-one[c]	0.004; 0.007	0.009; 0.011	-	-	-	-	-	-	-
Poss: 3-buten-2-one = 2-butenone[#]	0.008; 0.013	0.009; 0.011	-	-	-	-	-	-	-
Poss: 3-methyl-2-butanone[#]	-	0.020; 0.023	0.082; 0.088	0.008; 0.015	0.034; 0.038	-	-	-	-
3-methyl-3-buten-2-one[#]	0.016; 0.025	0.038; 0.044	-	-	-	-	-	-	-
2-pentanone[#]	-	0.024; 0.028	0.205; 0.219	-	0.119; 0.134	-	-	0.016; 0.447	0.152; 0.156
3-pentanone[#]	-	0.012; 0.014	0.160; 0.171	-	-	-	-	0.023; 0.620	0.131; 0.135
Poss: 2,3-pentanedione[#]	0.021; 0.033	0.027; 0.031	-	-	-	-	-	-	-
3-penten-2-one[#]	0.007; 0.011	0.011; 0.013	-	-	-	-	-	-	-
Poss: 4-hydroxy-2-pentanone	0.017; 0.026		-	0.036; 0.071	-	-		-	
2-methyl-cyclopentanone[#]	-	0.025; 0.029	-	-	-	-	0.223; 0.248	0.025; 0.695	-
Isomer of 3-methyl-2-cyclopenten-1-one[#]	0.006; 0.009	0.012; 0.015	-	-	-	-	-	-	-

1-hydroxy-3-methyl-2-butanone#	0.016;0.024	0.022; 0.026	-	-	-	-	-	-	-
Isomer of 3,4-dimethyl-cyclopentenone#	0.010; 0.015	0.026; 0.030	-	-	-	-	-	-	-
Poss: 1-(acetyloxy)-butan-2-one#	0.029; 0.044	0.067; 0.078	-	-	-	-	-	-	-
Ethyl-vinyl-cyclopentanone#	-	0.024; 0.028	-	-	-	-	-	-	-
Isomer of 3-ethyl-2-hydroxy-cyclopenten-1-one#	0.025; 0.038	0.042; 0.050	-	-	-	-	-	-	-
Poss: 2-cyclohexene-1,4-dione#	0.011; 0.017	0.021; 0.024	-	-	-	-	-	-	-
Poss: 2,4-dimethyl-1,3-cyclopentanedione#	0.015; 0.023	0.024; 0.028	-	-	-	-	-	-	-
3-ethyl-2-cyclopenten-1-one	-	0.036; 0.042	-	-	-	-	-		-
2-methyl-3-pentanone#	-	-	0.066; 0.070	-	-	-	-	-	-
3-hexanone#	-	-	0.018; 0.019	-	-	-	-	-	-
2-hexanone#	-	-	0.042; 0.045	-	-	-	-	-	-
4-methyl-3-hexanone#	-	-	0.026; 0.027	-	-	-	-	-	-
Dimethyl-cyclopentanone	-	-	-	0.008; 0.015	-	-	0.040; 0.045	-	-
2-hydroxy-3-pentanone#	-	-	0.069; 0.074	0.062; 0.121	-	-	-	-	-
2-methyl-cyclopentanone#	-	-	1.147; 1.225	0.140; 0.271	0.670; 0.755	0.051; 0.101	-	-	0.416; 0.429
3-methyl-cyclopentanone#	-	-	0.336; 0.359	-	-	-	-	-	0.158; 0.162
2,5-dimethyl-cyclopentanone#	-	-	0.043; 0.046	-	0.043; 0.049	-	0.013; 0.015	-	-
3,4-dimethyl-trans-cyclopentanone#	-	-	0.080; 0.085	-	-	-	-	-	-
Cyclohexanone#	-	-	0.075; 0.080	-	-	-	-	0.023; 0.624	0.243; 0.250
2-ethyl-cyclopentanone#	-	-	0.258; 0.276	-	0.106; 0.120	-	0.030; 0.033	-	-
2-methyl-cyclohexanone#	-	-	0.096; 0.103	-	-	-	-	-	-

Poss: 3-methyl-cyclohexanone	-	-	-	-	-	-	-	-	0.164; 0.169
2-ethyl-cyclohexanone#	-	-	0.032; 0.034	-	-	-	-	-	-
2,3,4-trimethyl-2-cyclopenten-1-one#	0.013; 0.020	0.022; 0.025	0.128; 0.137	-	-	-	-	-	-
Trimethyl-2-cyclopenten-1-one#	-	-	0.078; 0.083	-	-	-	-	-	-
Poss: dimethyl-cyclopentanone	-	-	-	-	0.124; 0.140	-	0.020; 0.022	-	-
Poss: trimethyl-cyclopentanone	-	-	-	-	0.037; 0.041	-	-	-	-
4-hydroxy-3-hexanone	-	-	-	-	0.088; 0.099	-	-	-	-
4-methyl-cyclohexanone	-	-	-	-	-	-	-	-	0.186; 0.192
Poss: 5-methyl-4-hexen-3-one	-	-	-	-	-	-	0.045; 0.050	-	-
Overlapping ethyl-cyclohexanone	-	-	-	-	-	-	0.027; 0.030	-	-
4-ethyl-cyclohexanone	-	-	-	-	-	-	-	-	0.079; 0.082
Hydrocarbons	-	**-**	**-**	**-**	**0.043; 0.05**	-	-	-	**2.836; 2.92**
n-pentadecane	-	-	-		-	-	-	-	0.031; 0.032
n-heptadecane	-	-	-	-	-	-	-	-	0.104; 0.108
cyclohexane	-	-	-	-	-	-	-	-	0.529; 0.544
Methyl-cyclohexane	-	-	-	-	-	-	-	-	0.608; 0.625
Poss: ethyl-cyclopentane	-	-	-	-	-	-	-	-	0.353; 0.363
1,3-dimethyl-cis-cyclohexane	-	-	-	-	-	-	-	-	0.096; 0.099
1-ethyl-3-methyl-trans-cyclopentane	-	-	-	-	-	-	-	-	0.088; 0.091
Poss: propyl-cyclopentane	-	-	-	-	-	-	-	-	0.270; 0.278
Ethyl-cyclohexane	-	-	-	-	-	-	-	-	0.355; 0.365

1-methyl-2-propyl-cyclopentane	-	-	-	-	-	-	-	-	0.063; 0.065
Propyl-cyclohexane	-	-	-	-	-	-	-	-	0.259; 0.267
Heterocyclic compounds	**2.33; 3.62**	**2.52; 2.94**	**0.70; 0.75**	**1.88; 3.66**	**2.41; 2.73**	**1.85; 3.71**	**2.52; 2.80**	**0.16; 4.44**	**0.34; 0.35**
Furans	**2.162; 3.35**	**2.29; 2.67**	**0.70; 0.75**	**1.761; 3.42**	**2.23; 2.51**	**1.702; 3.41**	**2.269; 2.53**	**0.163; 4.44**	**0.344; 0.35**
2(3H)-furanone#	0.083; 0.129	0.078; 0.091	-	-	-	-	-	-	-
2(5H)-furanone[c]	0.351; 0.545	0.406; 0.474	-	-	-	-	-	-	-
2-furaldehyde[c]	0.281; 0.436	0.491; 0.573	-	-	-	-	-	-	-
3-furaldehyde[c]	0.014; 0.022	0.021; 0.025	-	-	-	-	-	-	-
5-methyl-2-furaldehyde[c]	0.042; 0.065	0.081; 0.095	-	-	-	-	-	-	-
5-(hydroxymethyl)-2-furaldehyde[c]	0.441; 0.684	0.484; 0.565	-	-	-	-	-	-	-
1-(2-furanyl)-ethanone[c]	0.025; 0.039	0.041; 0.048	-	-	-	-	-	-	-
3-methyl-(5H)-furan-2-one[c]	0.088; 0.136	0.111; 0.129	-	-	-	-	-	-	-
x,x-dihydro-x-methyl-furan-x-on	0.075; 0.116	-	-	-	-	-	-	-	-
tetrahydro-2-methoxy-furan	0.004; 0.006	-	-	-	-	-	-	-	-
Poss: dihydro-4-hydroxy-2(3H)-furanone#	0.018; 0.029	0.013; 0.016	-	-	0.135; 0.152	-	-	-	-
Poss: 5-methyl-2(5H)-furanone#	0.043; 0.066	0.059; 0.069	-	-	-	-	-	-	-
3-methyl-furandione-2,5-#	0.034; 0.052	0.035; 0.041	-	-	-	-	-	-	-
4-methyl-(5H)-furan-2-one#	0.142; 0.219	0.138; 0.161	-	-	-	-	-	-	-
Lactone derivative poss: (S)-(+)-2',3'-dideoxyribonolactone#	0.076; 0.118	0.061; 0.071	-	-	-	-	-	-	-
Isomer of 2,5-dihydro-3,5-dimethyl-2-furanone#	0.037; 0.057	0.056; 0.065	-	-	-	-	-	-	-
Lactone derivative = furanone derivative#	0.022; 0.035	0.027; 0.032	-	0.30; 0.583	0.019; 0.021	-	0.129; 0.143	-	-

Lactone derivative[#]	0.072; 0.111	0.050; 0.058	-	-	0.150; 0.169	0.274; 0.549	-	-	-
γ-valerolactone	-	-	0.077; 0.083	-	-	-	-	0.022; 0.602	-
γ-butyrolactone[c]	0.135; 0.210	0.137; 0.160	0.475; 0.507	0.360; 0.699	0.450; 0.507	0.339; 0.680	0.416; 0.463	-	-
2-hydroxy- γ-butyrolactone[c]	0.178; 0.277	-	-	0.082; 0.158	-	0.049; 0.099	-	-	-
α-methyl-butyrolactone	-	-	0.036; 0.039	0.078; 0.151	0.129; 0.145	0.088; 0.176	0.142; 0.158	-	-
Tetrahydrofuran	-	-	0.038; 0.041	0.109; 0.211	0.313; 0.353	0.102; 0.205	0.308; 0.343	0.14; 3.838	0.133; 0.137
Tetrahydro-2-methyl-furan	-	-	-	-	-	0.064; 0.128	0.272; 0.303	-	0.088; 0.090
Tetrahydro-2,5-dimethyl-furan	-	-	-	-	-	-	0.071; 0.079	-	0.124; 0.127
Poss: tetrahydro-2-methyl-furan	-	-	-	0.031; 0.060	0.134; 0.151	0.322; 0.646	-	-	-
Tetrahydro-dimethyl-furan	-	-	-	-	0.026; 0.030	-	-	-	-
Unknown furan derivative	-	-	-	-	0.022; 0.025	-	0.050; 0.056	-	-
Poss: tetrahydro-2-methyl-2-furanol	-	-	-	0.391; 0.759	0.361; 0.407	-	0.320; 0.357	-	-
Poss: tetrahydro-2-furanmethanol	-	-	-	0.063; 0.122	0.085; 0.096	0.187; 0.376	0.221; 0.245	-	-
Poss: tetrahydro-derivative furan	-	-	-	-	0.027; 0.030	-	-	-	-
Unknown furanone derivative MW= 112	-	-	-	-	0.013; 0.015	-	-	-	-
Dihydro-5-methyl-2(3H)-furanone	-	-	-	0.053; 0.103	0.099; 0.111	0.079; 0.159	0.146; 0.163	-	-
Dihydro-3,5-dimethyl-2(3H)-furanone	-	-	-	0.021; 0.041	0.049; 0.056	-	0.035; 0.039	-	-
Poss: 5-ethyldihydro-2(3H)-furanone	-	-	-	-	0.218; 0.246	-	-	-	-
Dihydro-4-methyl-2(3H)-furanone	-	-	0.074; 0.079	0.103; 0.199	-	0.096; 0.192	0.141; 0.157	-	-
Tetrahydro-3-furanol	-	-	-	0.027; 0.053	0.018; 0.020	0.025; 0.050	-	-	-
Poss: Isomer of 3,4-furandiol, trans-	-	-	-	0.034; 0.066	-	-	-	-	-

Unknown furanol compound	-	-	-	0.109; 0.212	-	0.077; 0.154	-	-	-
Pyrans	**0.170; 0.26**	**0.230; 0.27**	**-**	**0.124; 0.24**	**-**	**0.147; 0.29**	**0.247; 0.27**	**-**	**-**
Poss: tetrahydro-2-[(tetrahydro-2-furanyl)methoxy]-2H-Pyran	-	-	-	0.089; 0.173	0.138; 0.156	0.147; 0.294	0.247; 0.27	-	-
Poss: tetrahydro-2H-pyran-2-methanol	-	-	-	0.035; 0.068	-	-	-	-	-
C5H8O2: poss. Tetrahydro-2H-pyran-2-one or dihydro-4-methyl-2(3H)-furanone	-	-	-	-	0.041; 0.046	-	-	-	-
2H-pyran-2-one#	-	0.023; 0.027	-	-	-	-	-	-	-
Maltol (3-hydroxy-2-methyl-4H-pyran-4-one)c	0.108; 0.168	0.146; 0.171	-	-	-	-	-	-	-
3-hydroxy-5,6-dihydro-(4H)-pyran-4-one#	0.062; 0.096	0.060; 0.070	-	-	-	-	-	-	-
Aromatic Compounds	**2.67; 4.14**	**7.07; 8.25**	**4.47; 4.77**	**1.54; 2.98**	**7.27; 8.2**	**0.93; 1.87**	**6.25; 6.95**	**0.00; 0.09**	**1.94; 1.99**
Benzenes	**0.006; 0.01**	**0.101; 0.12**	**0.075; 0.08**	**-**	**0.057; 0.06**	**-**	**0.099; 0.11**	**0.003; 0.09**	**0.599; 0.62**
toluenec	-	0.016; 0.019	-	-	0.024; 0.027	-	0.032; 0.036	-	0.077; 0.079
ethylbenzenec	-	-	-	-	-	-	0.022; 0.024	-	
Propyl-benzene	-	-	-	-	-	-	-	-	0.059; 0.060
1-methyl-naphtalene	-	-	-	-	-	-	-	-	0.177; 0.182
3,4-dimethoxy-toluenec	-	-	0.016; 0.017	-	-	-	-	-	-
2,3-dimethoxy-toluenec	-	0.018; 0.021	-	-	-	-	-	-	-
1-meythoxy-4-methyl-benzene#	-	0.023; 0.027	-	-	-	-	-	-	-
2,3-dihydro-1H-inden-1-onec	0.006; 0.009	0.014; 0.016	-	-	-	-	-	-	-
1-methoxy-2,3-dimethyl-benzene#	-	0.010; 0.012	-	-	-	-	-	-	-
Poss: dimethoxy-propyl-benzene	-	0.020; 0.023	-	-	-	-	0.027; 0.031	-	-
Benzene#	-	-	0.020; 0.021	-	-	-	-	0.003; 0.092	0.083; 0.085

1,2-dimethoxy-4-propyl-benzene#	-	-	0.015; 0.016	-	-	-	-	-	-
C18H22:Biphenyl, diisopropyl-#	-	-	0.023; 0.025	-	-	-	0.017; 0.019	-	-
C9H10: 2-propenyl-benzene or 2,3-dihydro-1H-indene#	-	-	-	-	0.033; 0.038	-	-	-	-
Octahydro-cis-1H-Indene	-	-	-	-	-	-	-	-	0.091; 0.094
1,2,3,4-tetrahydro-naphtalene	-	-	-	-	-	-	-	-	0.053; 0.054
1,2,3,4-tetrahydro-6-methyl-naphtalene	-	-	-	-	-	-	-	-	0.059; 0.061
Catechols	**n.q.**	**n.q.**	**-**	**n.q.**	**n.q.**	**n.q.**	**-**	**-**	**-**
catechol	Available n.q.	Available n.q.	-	-	-	-	-	-	-
3-methyl-catechol	-	Available n.q.	-	Available n.q.	-	-	-	-	-
hydroquinone	Available n.q.	Available n.q.	-	-	-	-	-	-	-
Methyl-benzenediol	Available n.q.	Available n.q.	-	-	n.q.	-	-	-	-
Aromatic Alcohols	-	-	-	**0.055; 0.11**	-	-	-	-	-
Poss: O-hexanoyl-1,2-benzendiol	-	-	-	0.055; 0.106	-	-	-	-	-
Aromatic Aldehydes	**0.022; 0.03**	**0.044; 0.05**	-	-	-	-	-	-	-
Benzaldehyde[c]	0.003; 0.005	0.013; 0.015	-	-	-	-	-	-	-
3-hydroxy-benzaldehyde#	0.019; 0.029	0.031; 0.036	-	-	-	-	-	-	-
Aromatic Ketones	**0.003; 0.005**	**0.008; 0.009**	**-**	-	-	-	-	-	-
acetophenone[c]	0.003; 0.005	0.008; 0.009	-	-	-	-	-	-	-
Aromatic Esters	-	**-**	**-**	0.050; 0.10	-	-	0.083; 0.09	-	-
Poss: homovanillic acid methyl ester	-	**-**	**-**	0.050; 0.096	-	-	0.083; 0.092	-	-
Lignin Derived Phenols	**0.269; 0.42**	**0.844; 0.98**	**0.856; 0.91**	**0.056; 0.11**	**0.70; 0.79**	**0.035; 0.07**	**0.707; 0.79**	**-**	**0.679; 0.70**

Phenol[c]	0.064; 0.099	0.114; 0.132	0.158; 0.168	0.025; 0.048	0.101; 0.114	-	0.020; 0.022	-	-
o-cresol[c]	0.040; 0.061	0.099; 0.115	0.076; 0.081	-	-	-	0.103; 0.114	-	-
p-cresol[c]	0.038; 0.059	0.097; 0.113	0.097; 0.104	0.017; 0.033	0.086; 0.097	0.017; 0.034	0.074; 0.083	-	0.077; 0.079
m-cresol[c]	0.026; 0.041	0.063; 0.073	0.076; 0.082	0.014; 0.026	0.060; 0.067	0.018; 0.036	0.070; 0.078	-	0.080; 0.083
2,5-dimethyl-phenol[c]	0.024; 0.038	0.040; 0.046	0.171; 0.182	-	-	-	-	-	0.141; 0.145
2,4-dimethyl-phenol[c]	0.016; 0.025	0.058; 0.068	-	-	0.089; 0.10	-	0.089; 0.099	-	-
2,6-dimethyl-phenol[c]	-	0.016; 0.019	-	-	-	-	-	-	-
2,3-dimethyl-phenol[c]	-	0.013; 0.015	-	-	-	-	-	-	-
3,5-dimethyl-phenol[c]	-	0.009; 0.010	-	-	-	-	-	-	-
3-ethyl-phenol[c]	-	0.033; 0.039	-	-	0.102; 0.115	-	0.109; 0.121	-	-
4-ethyl-phenol[c]	-	0.023; 0.027	0.031; 0.033	-	0.025; 0.029	-	0.026; 0.029	-	-
4-propyl-phenol[c]	-	0.041; 0.048	0.220; 0.235	-	0.181; 0.204	-	0.176; 0.196	-	0.317; 0.326
4-propenyl-trans-phenol[#]	-	0.023; 0.027	-	-	-	-	-	-	-
4-hydroxy-benzaldehyde[c]	0.009; 0.014	0.016; 0.019	-	-	-	-	-	-	-
Ethyl-methyl-phenol[#]	-	0.025; 0.030	-	-	0.031; 0.034	-	-	-	-
Poss: methoxy-trimethyl-phenol[#]	-	0.014; 0.017	-	-	-	-	-	-	-
Poss: allyl- or propenyl-phenol[#]	0.005; 0.007	0.022; 0.025	-	-	-	-	-	-	-
Phenolic dimere[#]	0.024; 0.037	0.041; 0.048	-	-	-	-	-	-	-
Unknown phenolic dimere compound[#]	0.023; 0.035	0.097; 0.113	-	-	-	-	-	-	-
Poss: x-methyl-x-propyl-phenol[#]	-	-	0.027; 0.029	-	0.026; 0.029	-	0.039; 0.044	-	-
C4-phenol	-	-	-	-	-	-	-	-	0.064; 0.066

Guaiacols (methoxy phenols)	**2.272; 3.52**	**5.788; 6.75**	**3.54; 3.78**	**1.375; 2.67**	**5.528; 6.23**	**0.898; 1.80**	**5.209; 5.80**	**-**	**0.660; 0.68**
Guaiacol[c]	0.330; 0.511	0.669; 0.780	0.797; 0.851	0.169; 0.328	0.648; 0.731	0.140; 0.282	0.704; 0.783	-	-
3-methyl-guaiacol[#]	0.014; 0.022	0.035; 0.040	-		0.049; 0.055	-	0.047; 0.052	-	-
4-methyl-guaiacol[c]	0.306; 0.475	0.842; 0.983	0.884; 0.944	0.169; 0.329	1.112; 1.253	0.137; 0.276	1.137; 1.266	-	0.178; 0.183
4-ethyl-guaiacol[c]	0.086; 0.134	0.299; 0.348	0.470; 0.502	0.052; 0.102	0.486; 0.548	0.065; 0.129	0.686; 0.764	-	0.174; 0.179
4-vinyl-guaiacol[#]	0.038; 0.059	0.107; 0.125	-	-	-	-	-	-	0.309; 0.318
4-propyl-guaiacol[c]	0.028; 0.044	0.140; 0.136	0.954; 1.019	0.071; 0.138	1.103; 1.243	0.069; 0.139	1.182; 1.316	-	-
eugenol[c]	0.080; 0.124	0.314; 0.366	-	-	-	-	-	-	-
Isoeugenol (4-propenyl-cis-guaiacol) [c]	0.110; 0.170	0.457; 0.533	-	-	-	-	-	-	-
Isoeugenol (4-propenyl-trans-guaiacol) [c]	-	0.594; 0.693	-	-	-	-	-	-	-
vanillin[c]	0.278; 0.431	0.461; 0.538	-	-	-	-	-	-	-
homovanillin[c]	0.049; 0.076	0.058; 0.068	-	-	-	-	-	-	-
Dihydroconiferyl alcohol[#]	0.187; 0.289	0.299; 0.349	-	0.492; 0.954	1.071; 1.207	0.413; 0.829	1.058; 1.178	-	-
Coniferyl alcohol (trans)[c]	0.116; 0.179	0.180; 0.210	-	-	-	-	-	-	-
Isomer of coniferyl alcohol[#]	0.130; 0.202	0.239; 0.279	-	-	-	0.038; 0.077	-	-	-
Acetoguajacone[#]	0.196; 0.304	0.344; 0.401	-	0.391; 0.758	0.485; 0.546	-	-	-	-
Propioguaiacone[#]	0.054; 0.084	0.068; 0.080	-	-	0.075; 0.085	-	-	-	-
coniferylaldehyde[c]	0.150; 0.233	0.353; 0.412	-	-	-	-	-	-	-
Guaiacol dimere[#]	0.004; 0.007	0.012; 0.014	-	-	-	-	-	-	-
Guaiacol dimere[#]	-	0.051; 0.059	-	-	-	-	-	-	-
Poss: Isomer of Propioguaiacone[#]	-	0.020; 0.023	-	-	-	-	-	-	-

Unknown guaiacol compound MW= 224#	0.013; 0.021	0.034; 0.040	-	-	0.088; 0.099	-	0.076; 0.085	-	-
Poss: dimere of guaiacyl compound MW= 274#	0.012; 0.018	0.036; 0.042	-	-	0.151; 0.170	-	0.156; 0.174	-	-
Guaiacyl acetone[c]	0.079; 0.122	0.131; 0.153	0.108; 0.116	-	0.070; 0.079	-	-	-	-
Poss:3-ethyl-guaiacol#	0.011; 0.018	0.046; 0.054	0.051; 0.055	-	0.043; 0.049	-	0.040; 0.045	-	-
Isomer of guaiacylacetone	-	-	-	-	0.046; 0.052	-	0.022; 0.024	-	-
Isomer of dihydroconiferyl alcohol	-	-	-	0.031; 0.059	0.063; 0.071	-	0.075; 0.083	-	-
Homovanillyl alcohol	-	-	-	-	0.038; 0.042	0.035; 0.071	0.025; 0.028	-	-
Syringols (dimethoxy phenols)	**0.099; 0.15**	**0.288; 0.34**	**-**	**-**	**0.988; 1.11**	**-**	**0.149; 0.17**	**-**	**-**
syringol	0.033; 0.052	0.066; 0.077	-	-	0.027; 0.030	-	-	-	-
4-methyl-syringol[c]	0.021; 0.033	0.043; 0.050	-	-	0.040; 0.045	-	0.049; 0.055	-	-
4-ethyl-syringol[c]	-	0.023; 0.027	-	-	0.020; 0.023	-	0.030; 0.034	-	-
4-allyl-syringol[c]	0.016; 0.025	0.032; 0.037	-	-	-	-	-	-	-
4-propyl-syringol[c]	-	0.016; 0.019	-	-	0.071; 0.080	-	0.069; 0.077	-	-
4-(1-propenyl)-cis-syringol#	-	0.023; 0.027	-	-	-	-	-	-	-
4-(1-propenyl)-trans-syringol#	-	0.040; 0.046	-	-	-	-	-	-	-
syringaldehyde[c]	0.028; 0.044	0.046; 0.054	-	-	-	-	-	-	-
Dihydrosinapyl alcohol	-	-	-	-	0.830; 0.936	-	-	-	-
Carbohydrates	**9.09; 14.09**	**3.72; 4.34**	**-**	**1.31; 2.54**	**-**	**0.19; 0.39**	**-**	**-**	**-**
Sugars	**9.088; 14.09**	**3.721; 4.34**	**-**	**1.311; 2.54**	**-**	**0.193; 0.39**	**-**	**-**	**-**
Levoglucosan[c]	5.591; 8.669	2.23; 2.60	-	-	-	-	-	-	-
1,6-anhydro-ß-D-glucofuranose,	0.064; 0.099	-		-	-	-		-	

1,6-anhydro-β-D-mannopyranose[c]	1.089; 1.689	0.311; 0.363	-	-	-	-	-	-	-
1,6-anhydro-ß-D-galactopyranose, (Levogalactosan)	0.173; 0.269	-		-	-	-	-	-	-
1,4:3,6-dianhydro-α-D-glucopyranose[#]	0.315; 0.488	0.160; 0.187	-	-	-	-	-	-	-
Anhydrosugar unknown[#]	0.614; 0.952	0.352; 0.410	-	0.236; 0.458	-	0.045; 0.089	-	-	-
Anhydrosugar unknown[#]	-	-		0.084; 0.162		0.092; 0.185	-	-	-
Poss; 1,4:3,6-dianhydro-D-glucitol	-	-	-	0.099; 0.193		0.057; 0.114	-	-	-
Poss: 2,3-anhydro-d-galactosan[#]	0.158; 0.245	0.093; 0.109	-	-	-	-	-	-	-
Poss: 2,3-anhydro-4-mannosan[#]	0.250; 0.388	0.162; 0.188	-	-	-	-	-	-	-
Unknown sugar derived compound[#]	0.046; 0.071	0.068; 0.079	-	0.101; 0.196	-	-	-	-	-
Unknown sugar derived compound[#]	0.049; 0.075	0.076; 0.089	-	0.132; 0.256	-	-	-	-	-
Anhydrosugar unknown[#]	0.469; 0.727	0.123; 0.143	-	0.659; 1.279	-	-	-	-	-
Anhydrosugar unknown[#]	0.073; 0.113	0.089; 0.104	-	-	-	-	-	-	-
Anhydrosugar unknown[#]	-	0.057; 0.067	-	-	-	-	-	-	-
Unknown sugar derived compound[#]	0.113; 0.176	-	-	-	-	-	-	-	-
-Other organic compounds	**0.71; 1.09**	**0.65; 0.76**	**0.07; 0.07**	**0.65; 1.26**	**0.45; 0.51**	**0.56; 1.11**	**0.20; 0.22**	**0.01; 0.16**	**0.20; 0.21**
N-compounds	**0.025; 0.04**	**0.016; 0.02**	-	**0.086; 0.17**	-	**0.115; 0.23**	-	-	-
Aliphatic Amide compound	-	-	-	0.086; 0.167	-	0.115; 0.23	-	-	-
Pyridine	0.025; 0.039	0.016; 0.019	-	-	-	-	-	-	-
Acetates	**0.041; 0.06**	**0.016; 0.016**	**-**	**0.006; 0.01**	**0.019; 0.02**	**-**	**0.030; 0.03**	**-**	**-**
Poss: 1,2,3-propanetriol, monoacetate	0.041; 0.064	0.016; 0.019	-	-	0.019; 0.021	-	-	-	-
Tetrahydro-2-furanmethanol-acetate	-	-	-	0.006; 0.012	-	-	0.021; 0.023	-	

Cyclopentanol acetate	-	-	-	-	-	-	0.009; 0.010	-	-
Terpenes	-	**0.014; 0.02**	**0.04; 0.04**	-	**0.054; 0.06**	-	-	-	-
Dehydroabietic acid methyl ester	-	-	-	-	0.018; 0.021	-	-	-	-
7-oxodehydroabietic acid, methyl ester	-	-	-	-	0.036; 0.040	-	-	-	-
Poss: diterpene	-	0.014; 0.017	-	-	-	-	-	-	-
Dehydroabietic acid methyl ester	-	-	0.040; 0.043	-	-	-	-	-	0.143; 0.148
18-norabieta-8,11,13-triene	-	-	-	-	-	-	-	-	0.033; 0.034
Unknown compounds	**0.527; 0.82**	**0.494; 0.58**	**-**	**0.247; 0.48**	**0.223; 0.25**	**0.247; 0.50**	**0.105; 0.12**	**-**	**-**
Miscellaneous	**0.112; 0.17**	**0.108; 0.13**	**0.026; 0.030**	**0.312; 0.61**	**0.158; 0.18**	**0.194; 0.39**	-	**0.006; 0.016**	**0.028; 0.03**
Poss: 1,2-epoxy-3-propoxy-propane	-	-	-	0.072; 0.139	0.046; 0.052	-	-	-	-
Poss: acetaldehyde, diisobutylacetal	-	-	-	0.098; 0.189	0.036; 0.040	0.168; 0.337	0.042; 0.047	-	-
Poss: Isomer of acetaldehyde, diisobutyl acetal	-	-	-	0.108; 0.209	0.050; 0.057	-	-	-	-
2,2'-Bi-1,3-dioxolane	0.078; 0.120	0.040; 0.047	-	-	-	-	-	-	-
Poss: 1,4-dioxin, 2,3-dihydro-	0.008; 0.012	0.011; 0.013	-	-	-	-	-	-	-
2-methyl-1,3-dioxolane	0.010; 0.015	0.021; 0.024	-	-	-	-	-	-	-
Silanol, trimethyl-, formate	0.008; 0.012	-	-	-	-	-	-	-	-
1-phenyl-naphtalene (impurity in IS= fluoranthene)	0.010; 0.016	0.036; 0.042	0.026; 0.028	0.025; 0.049	0.025; 0.029	0.026; 0.052	0.024; 0.027	0.006; 0.164	0.028; 0.029
Unknown acid anhydrife or furan acid ester	-	-	-	0.010; 0.019	-	-	-	-	-
Area of identified peaks (%)	**98.1**	**93.9**	**69.8**	**91.2**	**78.8**	**88.0**	**76.0**	**72.2**	**49.4**
Area of unknown peaks (%)	**1.9**	**6.1**	**30.2**	**8.8**	**21.2**	**12.0**	**24.0**	**27.8**	**50.6**
TOTAL (wt.%)	**34.61; 53.66**	**28.14; 32.83**	**18.93; 20.21**	**34.08; 66.12**	**25.14; 28.33**	**24.25; 48.66**	**22.12; 24.62**	**3.14; 85.68**	**7.61; 7.84**

Possi= possible compound; c= calibrated; n.q.= not quantified; #=estimated response factor; IS= internal standard; MW= molecular weight.

S.1.6 Hydrogen consumption determination, amount of gas generated, mass balance and degree of deoxygenation

The hydrogen consumption was approximated by the ideal gas equation, considering the volume of the gas constant and yielding moles of hydrogen before and after the reaction (equation S.2).

$H_{2\ consumed} = \frac{n_{H_2 i} - n_{H_2 f}}{m_{bio-oil}}$ (equation S.1)

$n_{H_{2i,f}} = \frac{y_{H_{2i,f}} \times p_{i,f} \times V_{cte}}{R \times T_{i,f}}$ (equation S.2)

n_{H2i} is the initial number of mols of H_2; n_{H2f} is the number of mols of H_2 after reaction; m is the amount of fast pyrolysis bio-oil transferred to the autoclave (kg). The number of mols of H_2 used in equation S.1 is obtained by the equation S.2, where $n_{H2i,f}$ is the initial or final number of H_2 mols before or after reaction; $y_{H2i,f}$ is the initial or final H_2 fraction in the gas composition; $p_{i,f}$ is the pressure recorded before and after the upgraded reaction (atm); V_{cte} is the gas volume in the autoclave in L (considered constant); R is the ideal gas constant (0.082 L.atm.K^{-1}.mol^{-1}) and $T_{i,f}$ are the temperatures in Kelvin at which the pressure was registered before and after the upgrading reactions. The amount of gas generated and later used for mass balance calculation was obtained by equation S.3, considering the gas composition obtained by gas-chromatography.

$gas\ (g) = \sum x_j \times MW_j \times n_{t,f}$ (equation S.3)

x_j is the mole fraction of gaseous compound j; MW_i is the molar mass of compound j (g.mol^{-1}) and $n_{t,f}$ is the total number of mols in the gas phase after the upgrading reaction. The remaining liquid mixture in the autoclave is composed by upgraded aqueous phase (UAP), upgraded oil (UOP), solid and spent catalyst. It was collected, weighted (in order to determine the recovery used in equation 4), and centrifuged (Thermo Fisher Heraeus Biofuge Stratos at 7000 rpm and 40 min). The liquid products obtained after centrifugation were separated and weighted for mass balance. The weight of UAP (g) was determined by weighting this phase, whereas the weight of UOP obtained was determined indirectly as follow:

$UO(g) = LR - (UAP + cat + solids)$ (equation S.4)

LR is the total liquid and solids mixture recovered (g) after the upgrading reaction, composed by UAP, UOP, solids and spent catalyst; UAP is the weight of upgraded light phase (g), obtained after centrifugation and separation; cat (g) is the amount of catalyst loaded to the reactor; and solids (g) is the amount of solids formed during the upgrading reaction (see equation

S.5). Additionally both liquid phases and spent catalyst were further characterized and more details are given in section 3.3.2.

The solid residue collected in the reactor (residual amount) and the solid sample obtained after centrifugation (containing residues of UOP) were mixed, washed with acetone and vacuum-filtrated (quantitative ashless filter paper Whatman, 589/3 blue ribbon). The amount of solid is given by equation S.5.

$$m_{solid}(g) = \frac{m_{cat} \times [C_{spcat}]}{100 - [C_{spcat}]} \text{ (equation S.5)}$$

Where the m_{solid} is the mass of solid (g) in the spent catalyst; m_{cat} is the amount of catalyst (g) loaded to the reactor; $[C_{\text{spcat}}]$ is the carbon concentration obtained by elemental analysis in the spent catalyst or by the difference in weight before and after reaction. The initial concentration of carbon in the fresh catalyst, if necessary, is discounted for solids calculation. The calculation for Ru/C considered the weight of catalyst added to the autoclave and the final weight recovered after the reaction. The difference is referred as the amount of solid deposited over the catalyst.

The degree of deoxygenation was obtained as follow:

$$DOD = \left(1 - \frac{[O_{UO}]}{[O_{feed}]}\right) \times 100 \text{ (equation S.6)}$$

DOD is the degree of deoxygenation (% g/g); $[O_{UOP}]$ is the concentration of oxygen in the upgraded oil (wt.%) and $[O_{feed}]$ is the concentration of oxygen in the feed (wt.%). The pH value was determined using a pH-meter 691 and the water content by Karl Fischer Tritando 841. The calorific value was determined by calorimeter IKA C5000. Sulfur and metal content (leached after the reactions), were obtained by inductively coupled plasma optical emission spectrometer Agilent, 725. For this measurement the upgraded aqueous phase samples were filtrated using a 0.2 μm polytetrafluoroethylene filter.

Supplementary Material – Chapter 4

S.4.1 Gas chromatography–mass spectrometry results

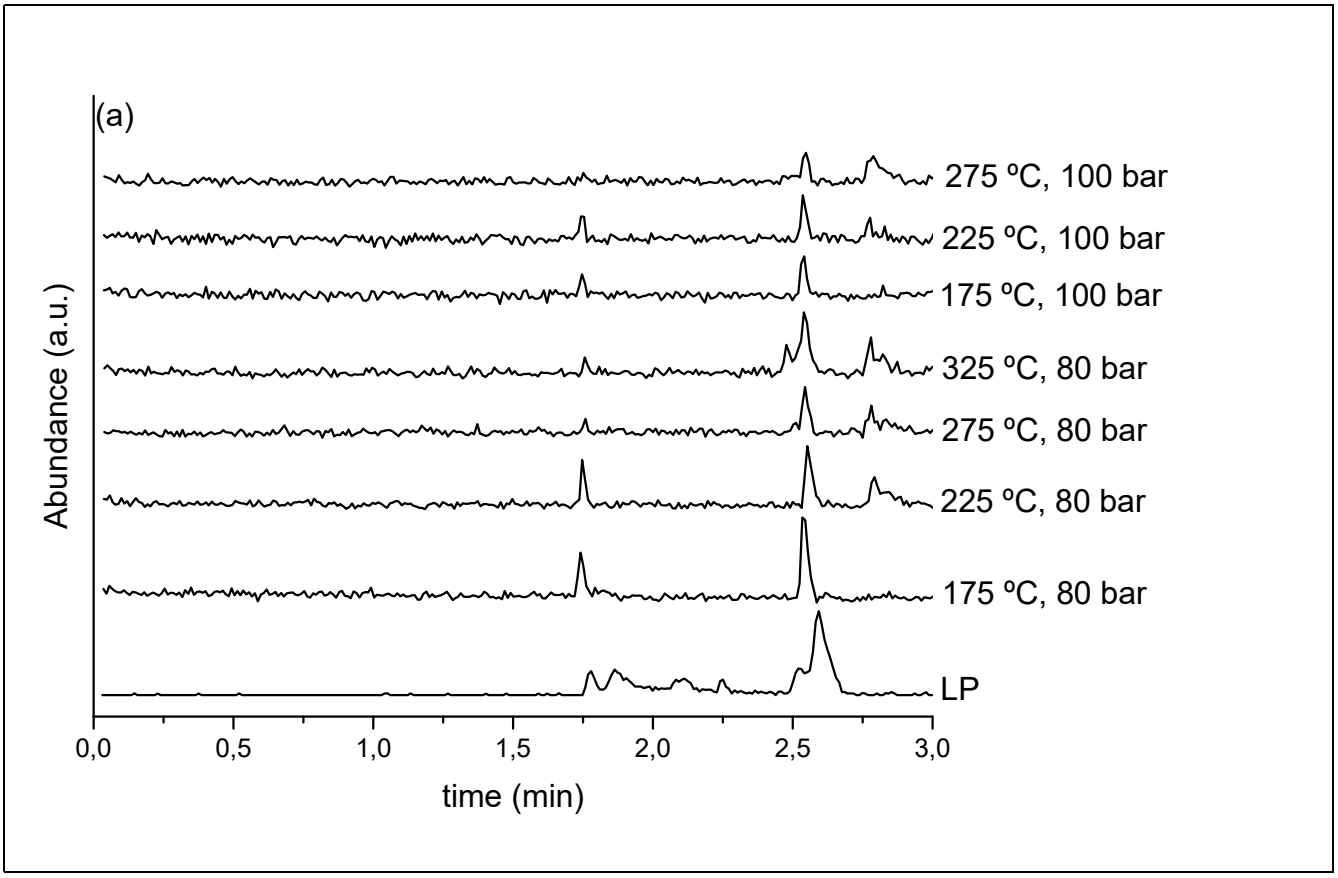

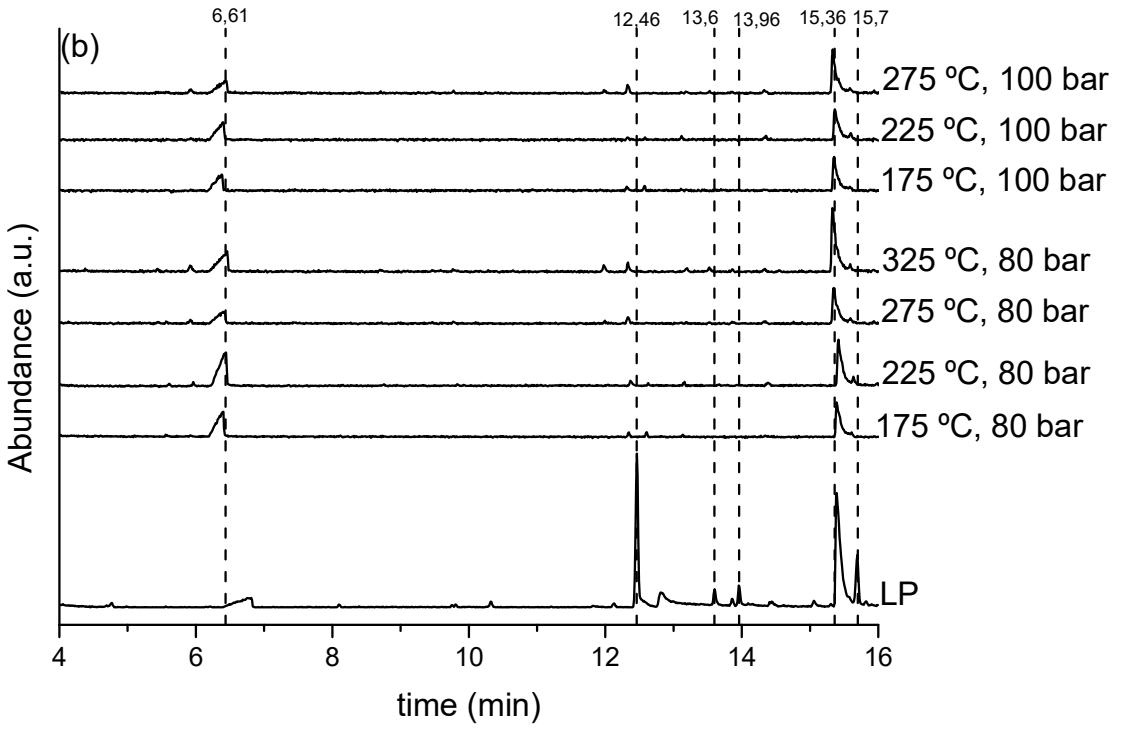
(b)
6,61
12,46
13,6
13,96
15,36
15,7
275 ºC, 100 bar
225 ºC, 100 bar
175 ºC, 100 bar
325 ºC, 80 bar
275 ºC, 80 bar
225 ºC, 80 bar
175 ºC, 80 bar
LP
Abundance (a.u.)
4
6
8
10
12
14
16
time (min)

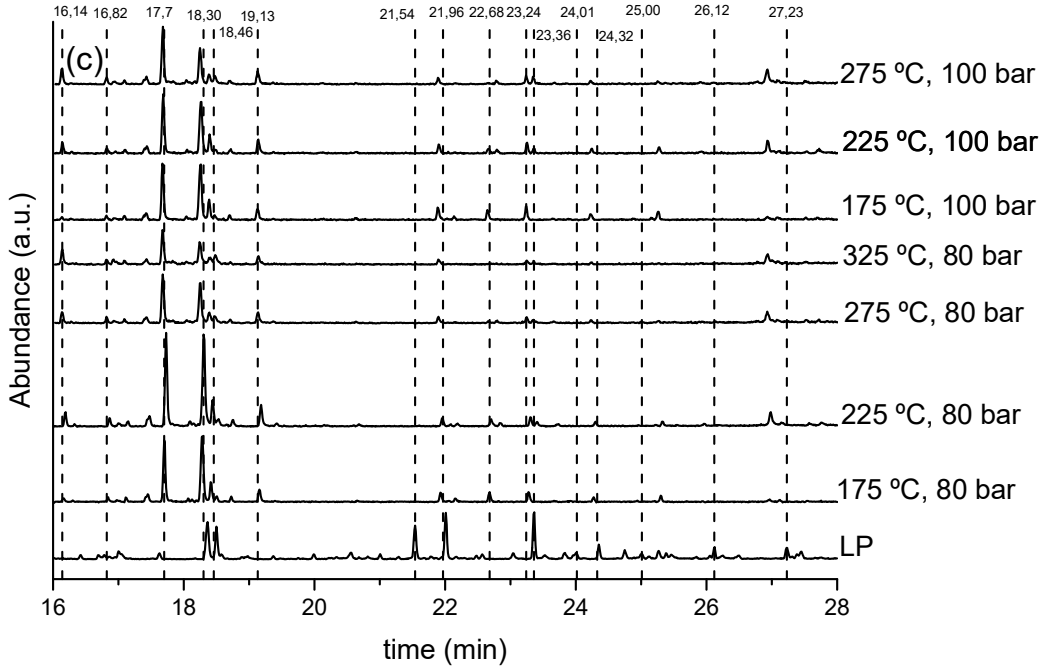
(c)
16,14
16,82
17,7
18,30
19,13
18,46
21,54
21,96
22,68
23,24
23,36
24,01
24,32
25,00
26,12
27,23
275 ºC, 100 bar
225 ºC, 100 bar
175 ºC, 100 bar
325 ºC, 80 bar
275 ºC, 80 bar
225 ºC, 80 bar
175 ºC, 80 bar
LP
Abundance (a.u.)
16
18
20
22
24
26
28
time (min)

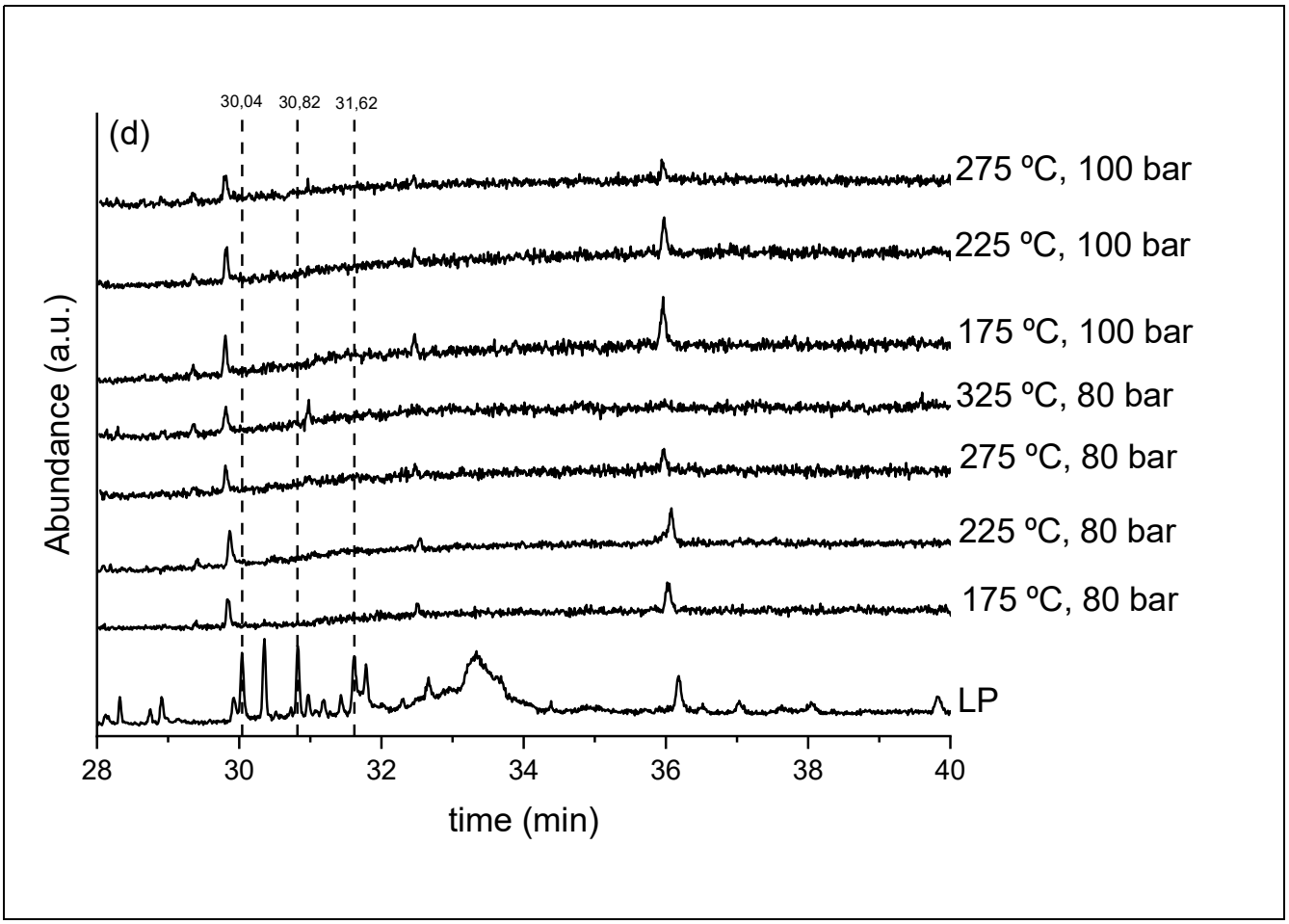

Figure S 6. Qualitative results obtained by GC-MS for the light phases products after upgrading at different conditions of pressure and temperature. Feed: FPBO, Product: ULP.

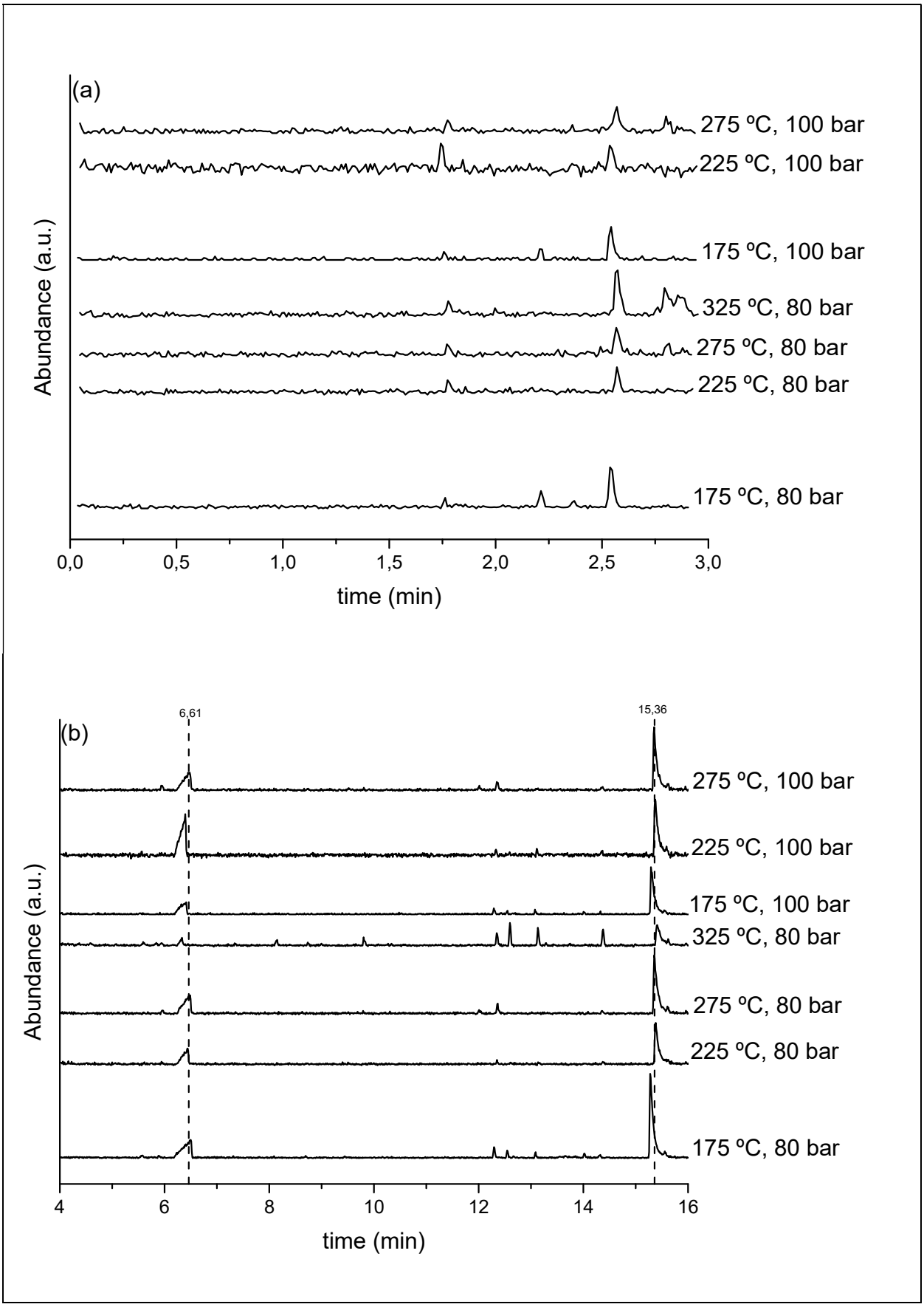
(a)
275 ºC, 100 bar
225 ºC, 100 bar
175 ºC, 100 bar
325 ºC, 80 bar
275 ºC, 80 bar
225 ºC, 80 bar
175 ºC, 80 bar
Abundance (a.u.)
0,0
0,5
1,0
1,5
2,0
2,5
3,0
time (min)
(b)
6,61
15,36
275 ºC, 100 bar
225 ºC, 100 bar
175 ºC, 100 bar
325 ºC, 80 bar
275 ºC, 80 bar
225 ºC, 80 bar
175 ºC, 80 bar
Abundance (a.u.)
4
6
8
10
12
14
16
time (min)

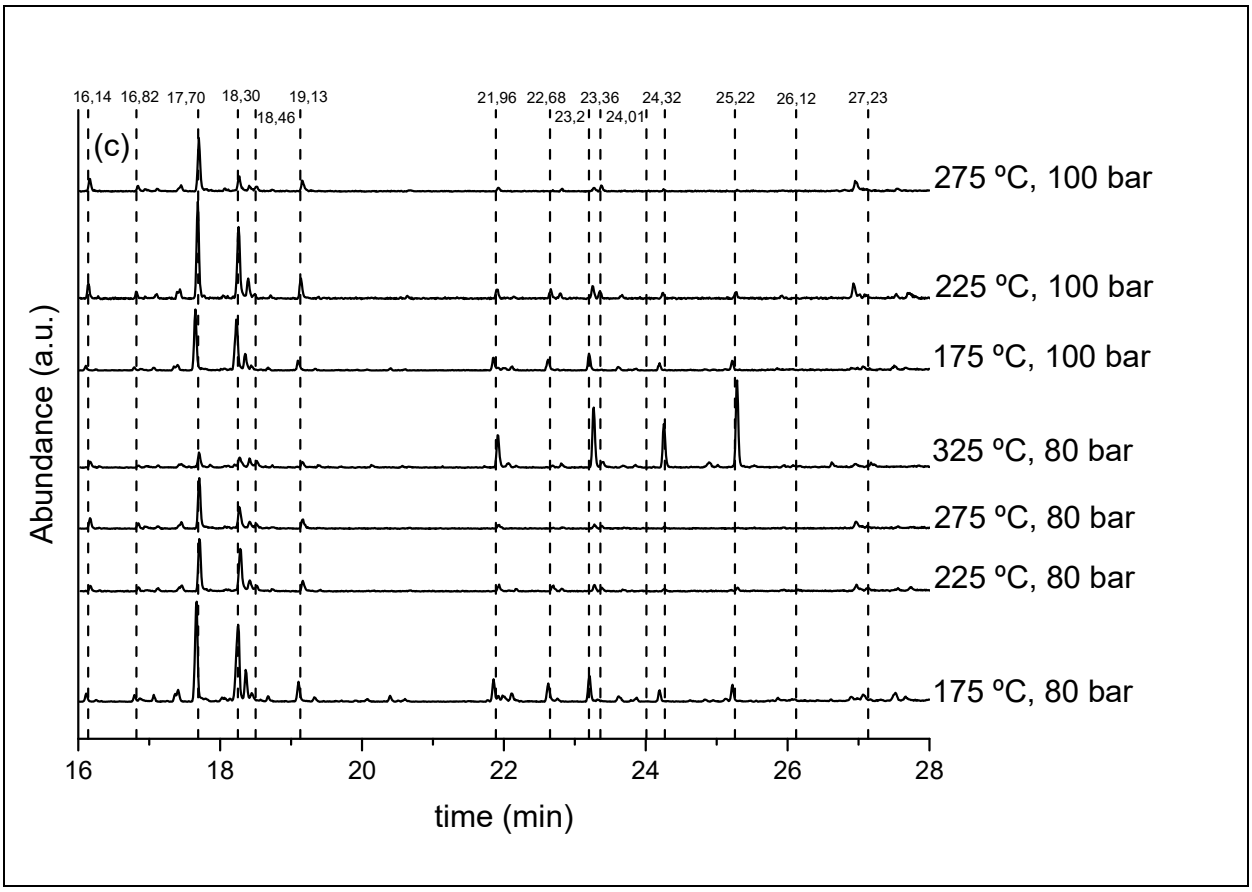
16,14
16,82
17,70
18,30
18,46
19,13
21,96
22,68
23,2
23,36
24,01
24,32
25,22
26,12
27,23
(c)
275 ºC, 100 bar
225 ºC, 100 bar
175 ºC, 100 bar
325 ºC, 80 bar
275 ºC, 80 bar
225 ºC, 80 bar
175 ºC, 80 bar
Abundance (a.u.)
16
18
20
22
24
26
28
time (min)

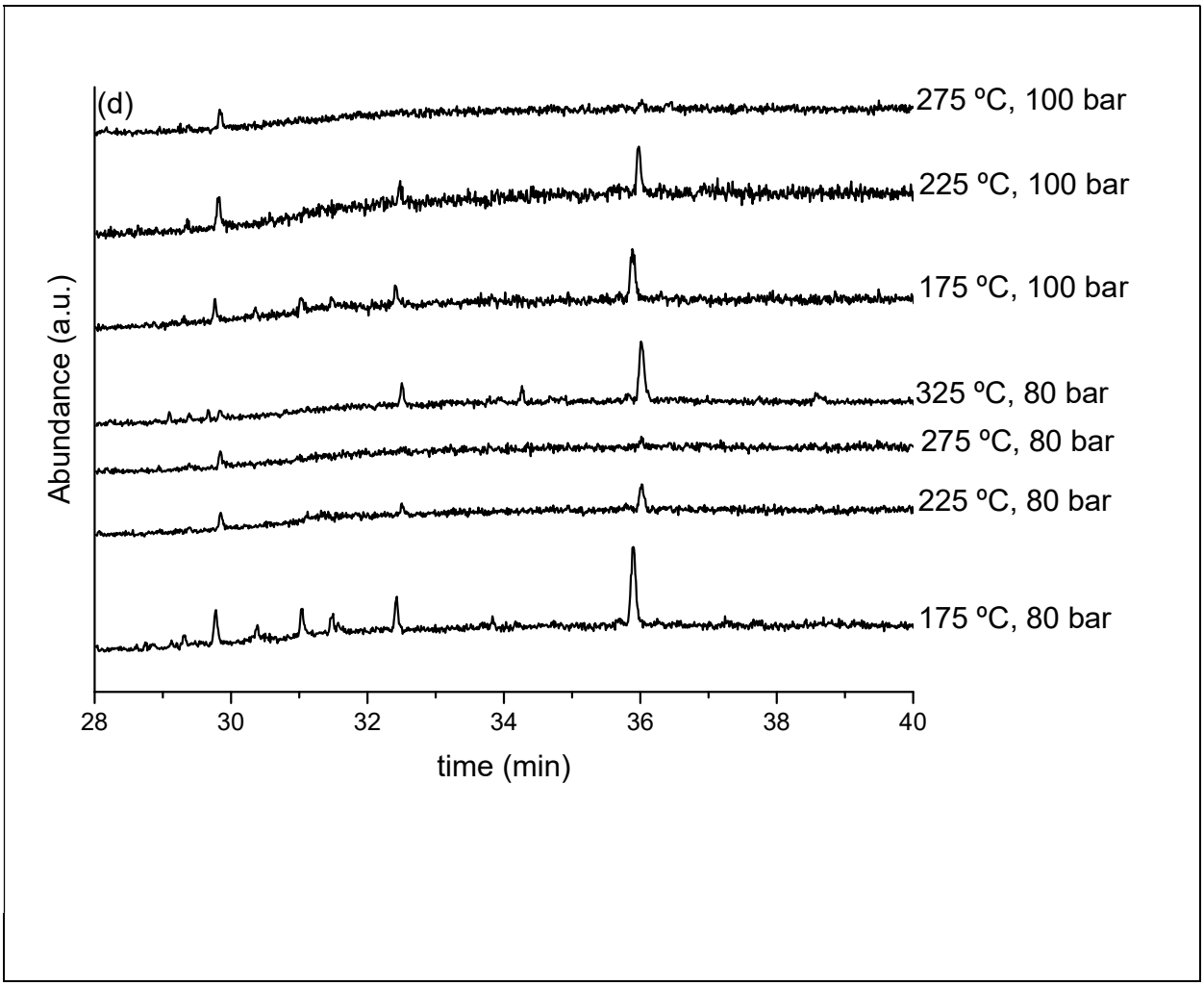

Figure S 7. Qualitative results obtained by GC-MS for the light phases products after upgrading at different conditions of pressure and temperature. Feed: HP, Product: ULP.

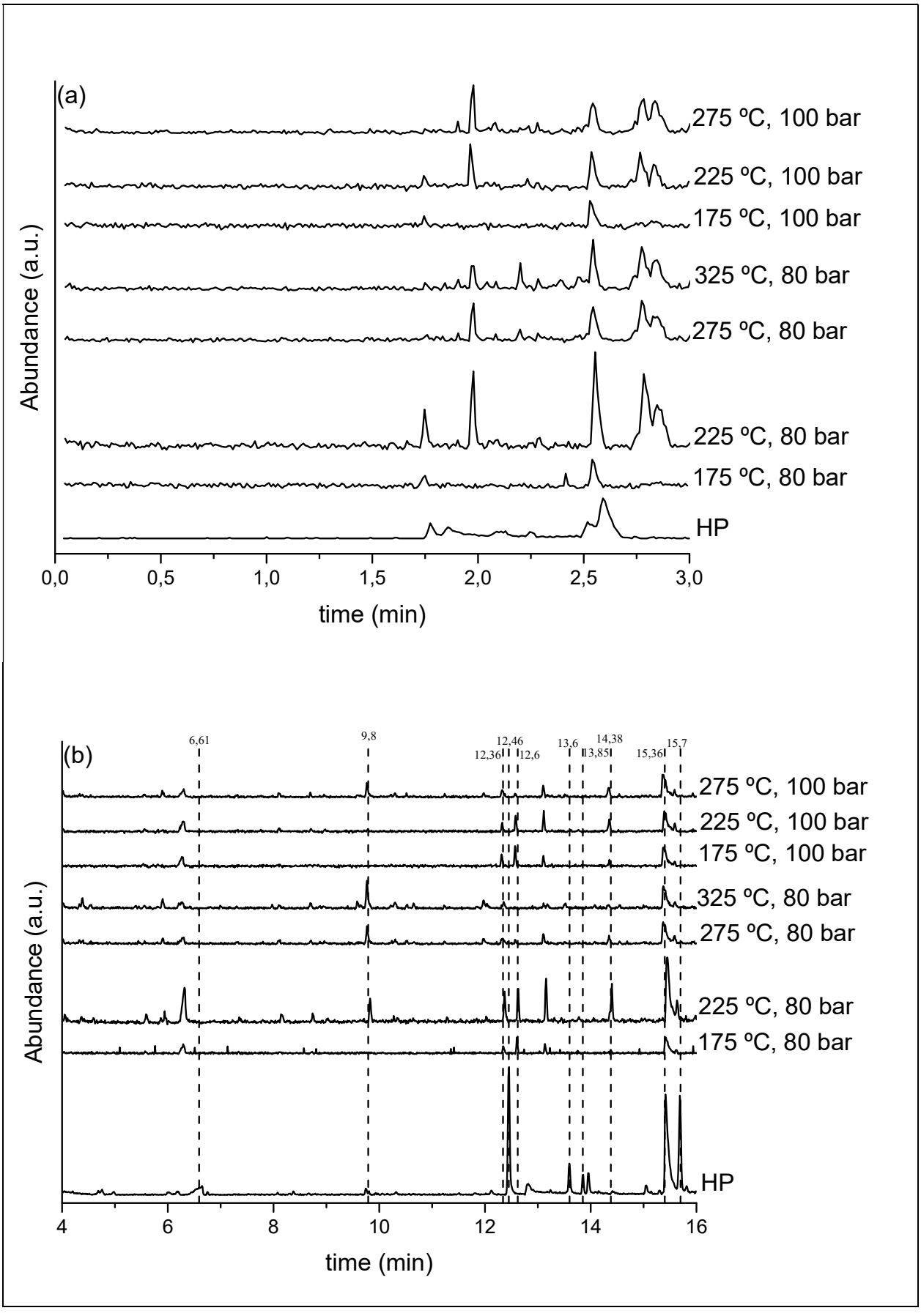
(a)
275 ºC, 100 bar
225 ºC, 100 bar
175 ºC, 100 bar
325 ºC, 80 bar
275 ºC, 80 bar
225 ºC, 80 bar
175 ºC, 80 bar
HP
Abundance (a.u.)
0,0
0,5
1,0
1,5
2,0
2,5
3,0
time (min)
(b)
6,61
9,8
12,36
12,46
12,6
13,6
13,85
14,38
15,36
15,7
275 ºC, 100 bar
225 ºC, 100 bar
175 ºC, 100 bar
325 ºC, 80 bar
275 ºC, 80 bar
225 ºC, 80 bar
175 ºC, 80 bar
HP
Abundance (a.u.)
4
6
8
10
12
14
16
time (min)

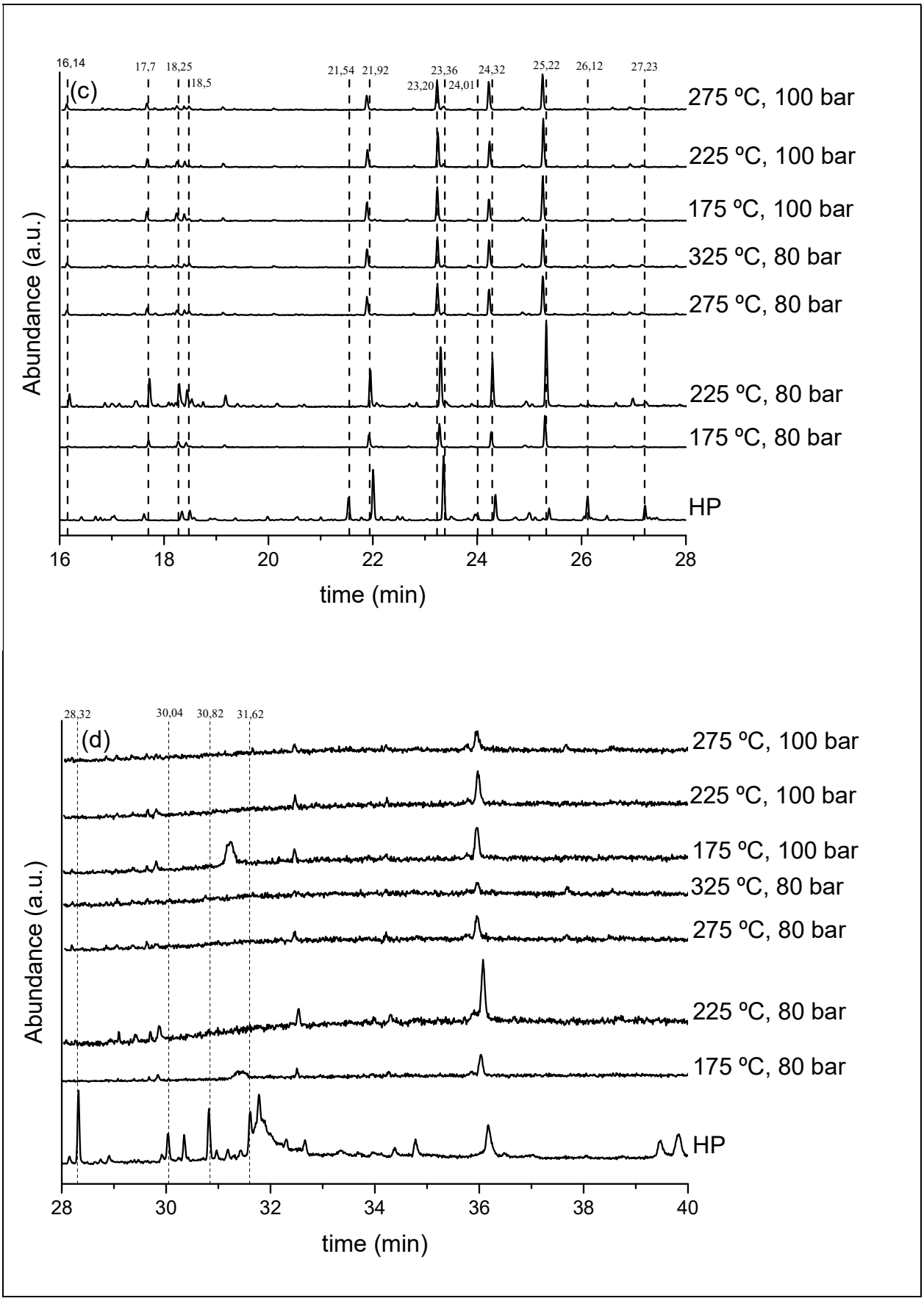

Figure S 8. Qualitative results obtained by GC-MS for the heavy phases products after upgrading at different conditions of pressure and temperature. Feed: FPBO, product: UO.

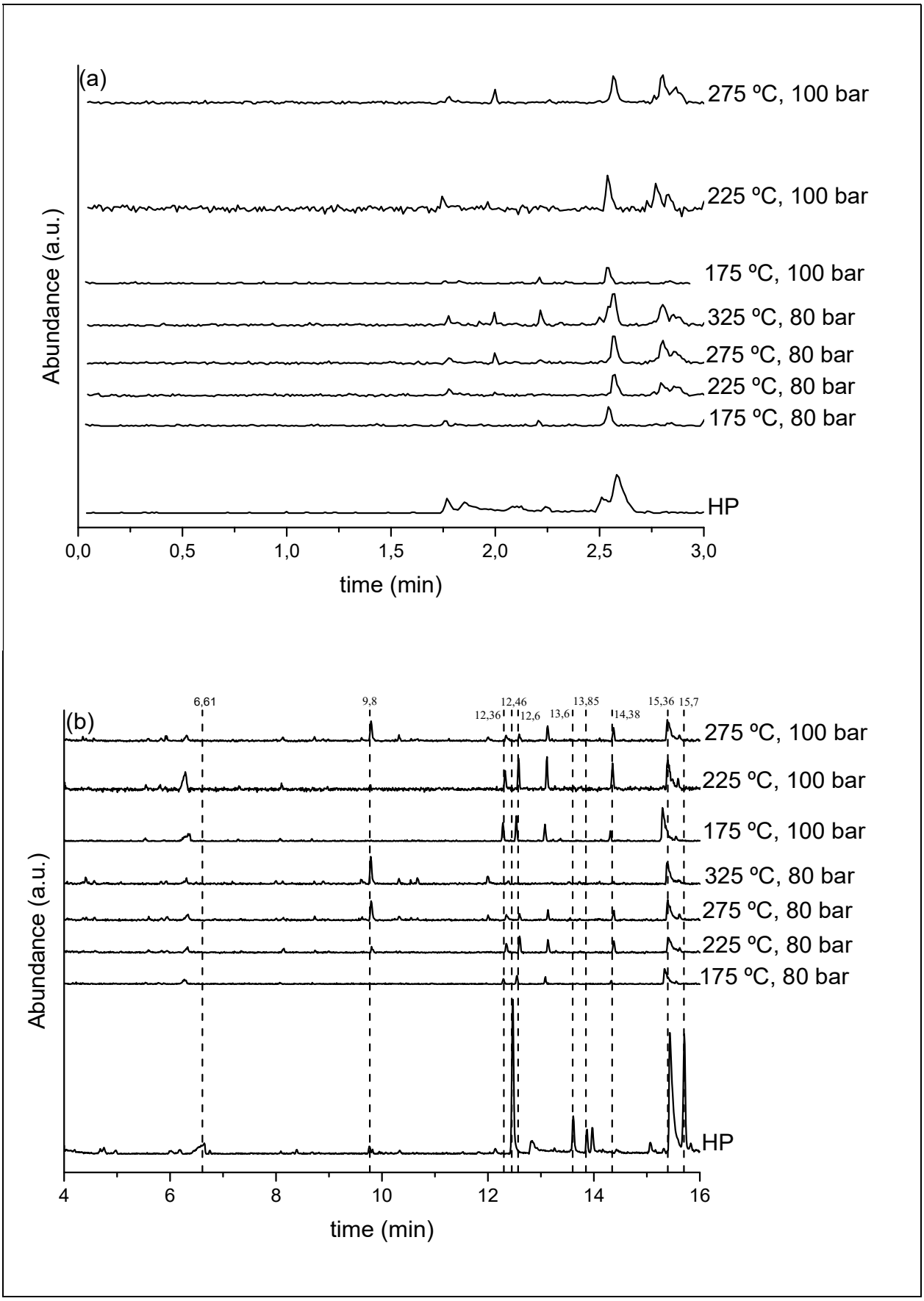
(a)
275 ºC, 100 bar
225 ºC, 100 bar
175 ºC, 100 bar
325 ºC, 80 bar
275 ºC, 80 bar
225 ºC, 80 bar
175 ºC, 80 bar
HP
Abundance (a.u.)
0,0
0,5
1,0
1,5
2,0
2,5
3,0
time (min)
(b)
6,61
9,8
12,36
12,46
12,6
13,6
13,85
14,38
15,36
15,7
275 ºC, 100 bar
225 ºC, 100 bar
175 ºC, 100 bar
325 ºC, 80 bar
275 ºC, 80 bar
225 ºC, 80 bar
175 ºC, 80 bar
HP
Abundance (a.u.)
4
6
8
10
12
14
16
time (min)

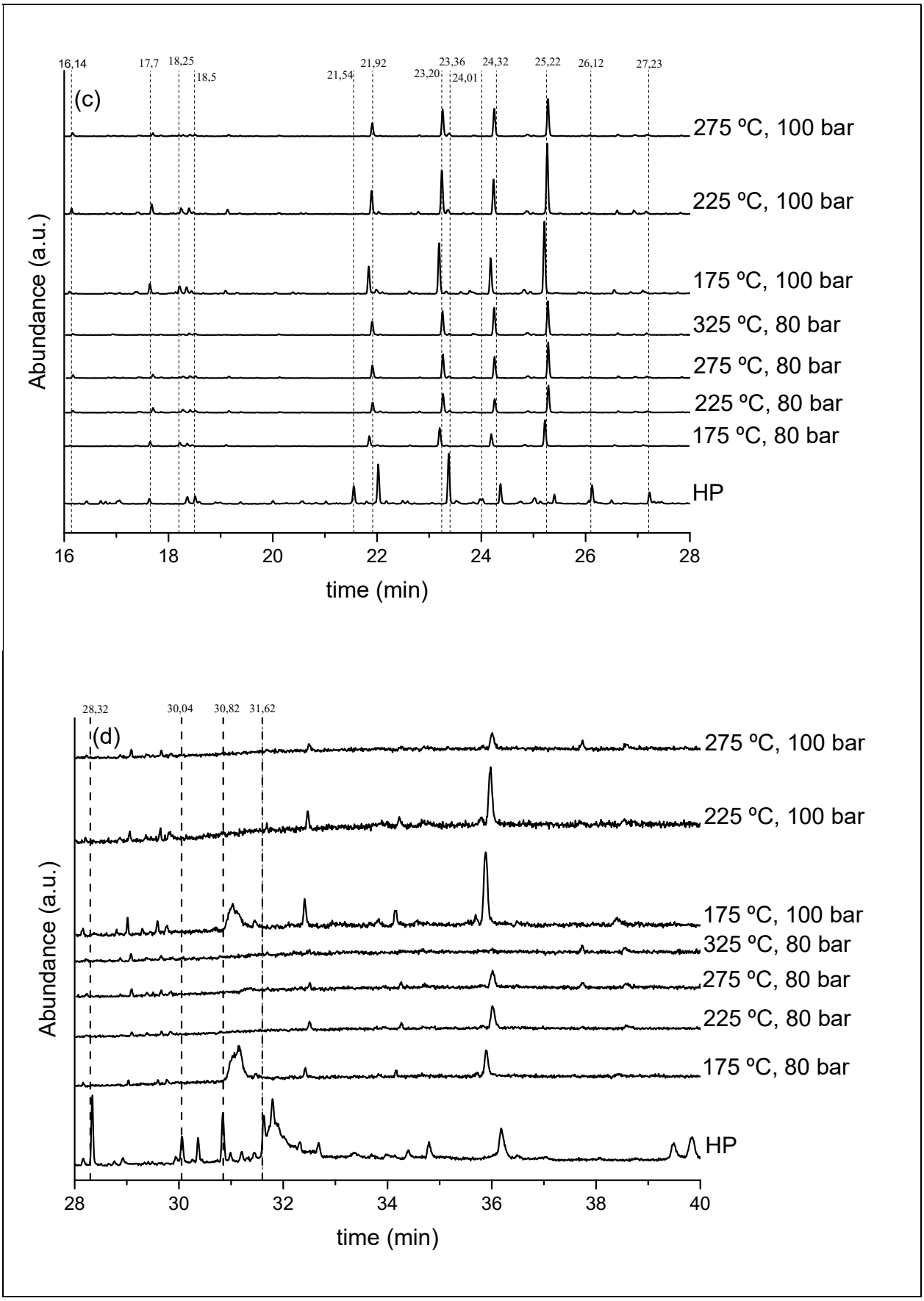

Figure S 9. Qualitative results obtained by GC-MS for the heavy phases products after upgrading at different conditions of pressure and temperature. Feed: HP, product: UO.

S.4.2 ^{1}H-NMR results

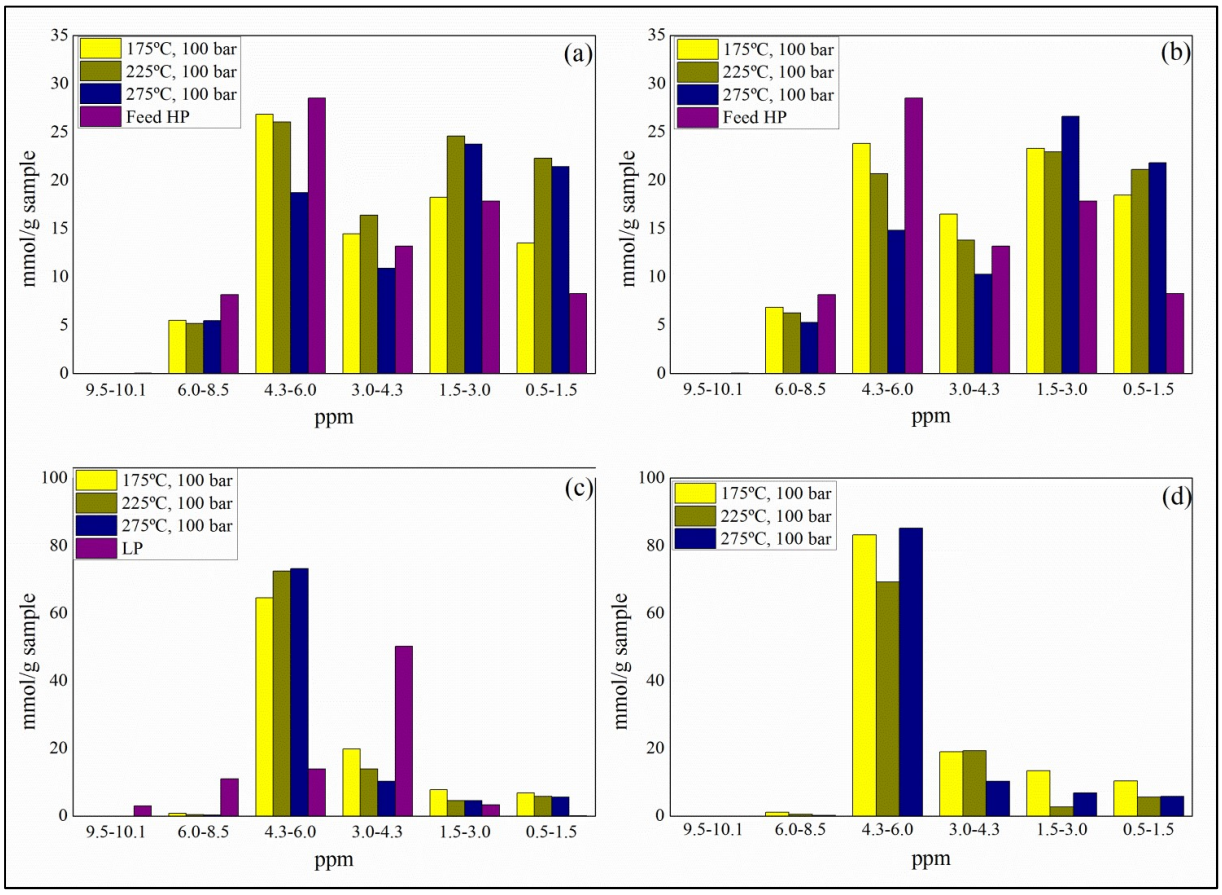

Figure S 10. ^{1}H-NMR spectra integration of the upgraded products at different temperatures and 100 bar. a) UO, Feed: FPBO; b) UO, Feed: HP; c) ULP, Feed: FPBO; d) ULP, Feed: HP; Integration regions: 0.5-1.5 ppm- alkanes; 1.5-3.0-α proton to carboxylic acid or keto-group, α proton to unsaturated group; 3.0-4.3-alcohols, ethers, dibenzenes; 4.3-6.0-carbohydrates, water, O-H exchanging group; 6.0-8.5-(hetero)-aromatic; 9.5-10.1-aldehydes.

S.4.3 SEM-EDX results

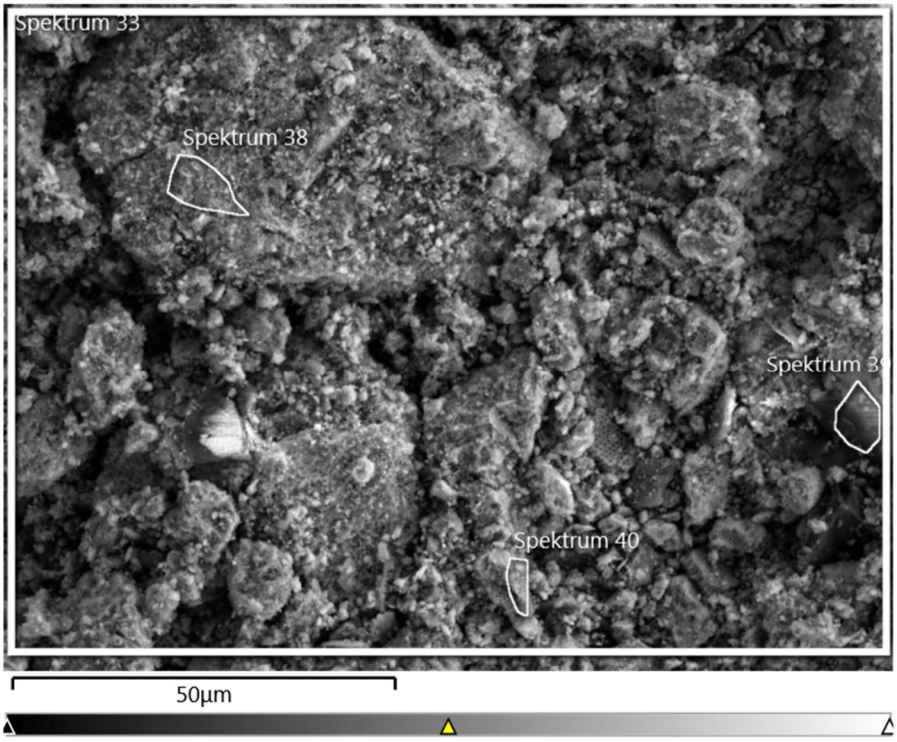

Figure S 11. SEM-EDX specific regions of the fresh Ni-Cr catalyst.

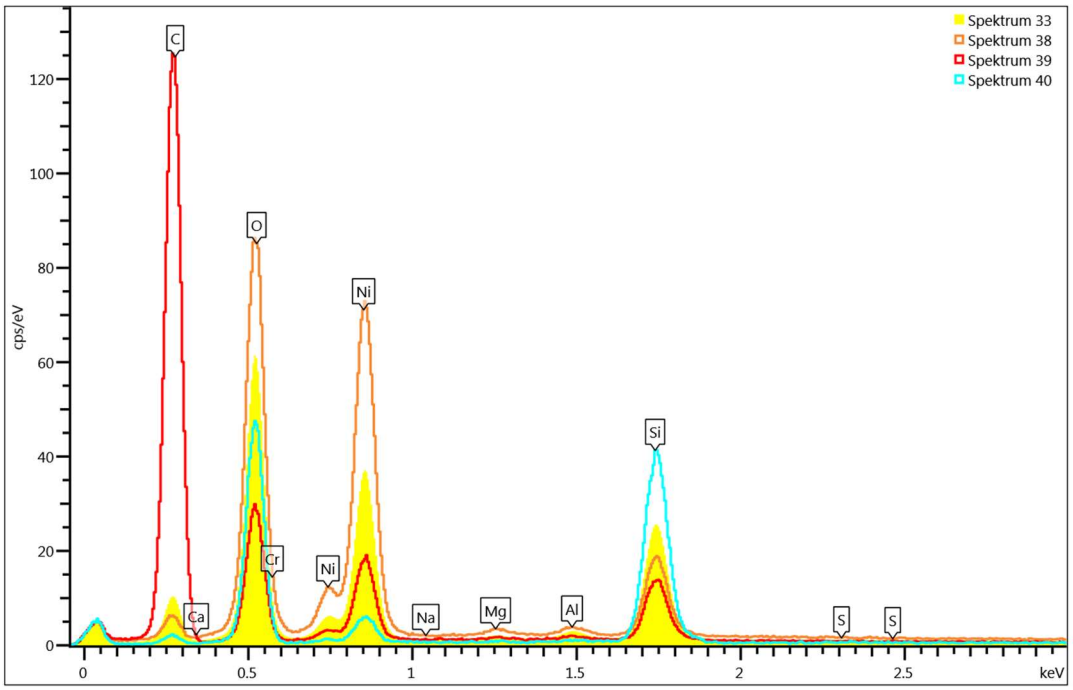

Figure S 12. EDX Spectra fresh Ni-Cr catalyst.

Table S 5. Elemental distribution over the catalyst surface by SEM-EDX. Fresh catalyst.

Compound	Spectra 38	Spectra 39	Spectra 40
C (wt.%)	4.3	63.8	5.7
O (wt.%)	24.6	15.9	44.4
Si (wt.%)	6.2	4.7	36.9
Cr (wt.%)	7.3	0.6	n.d.
Ni (wt.%)	56.4	14.6	12.4

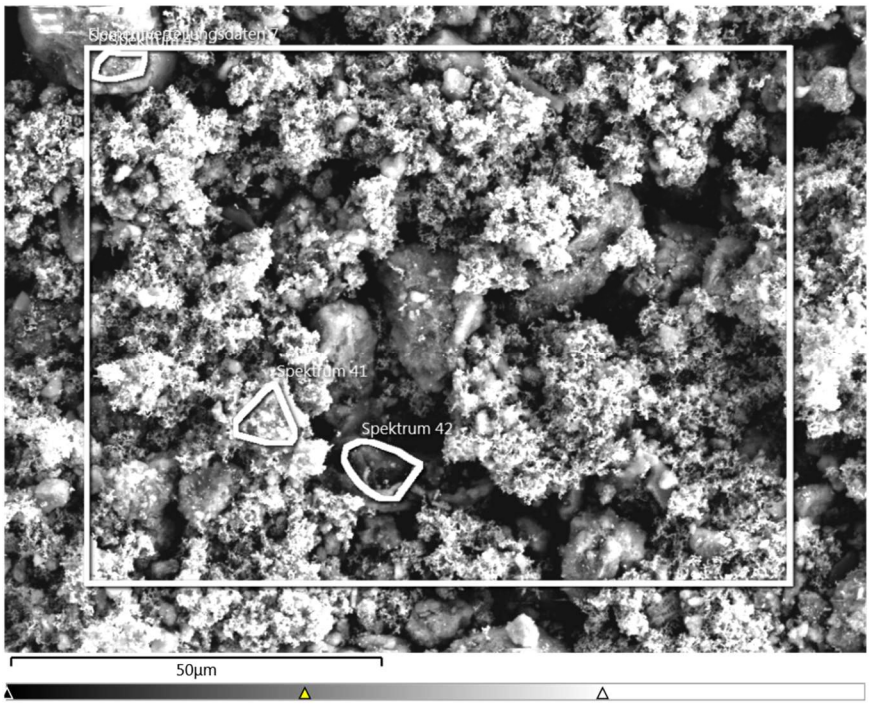

Figure S 13. SEM-EDX specific regions of the spent catalyst. Reaction conditions: 325ºC, 80 bar, Feed: FPBO.

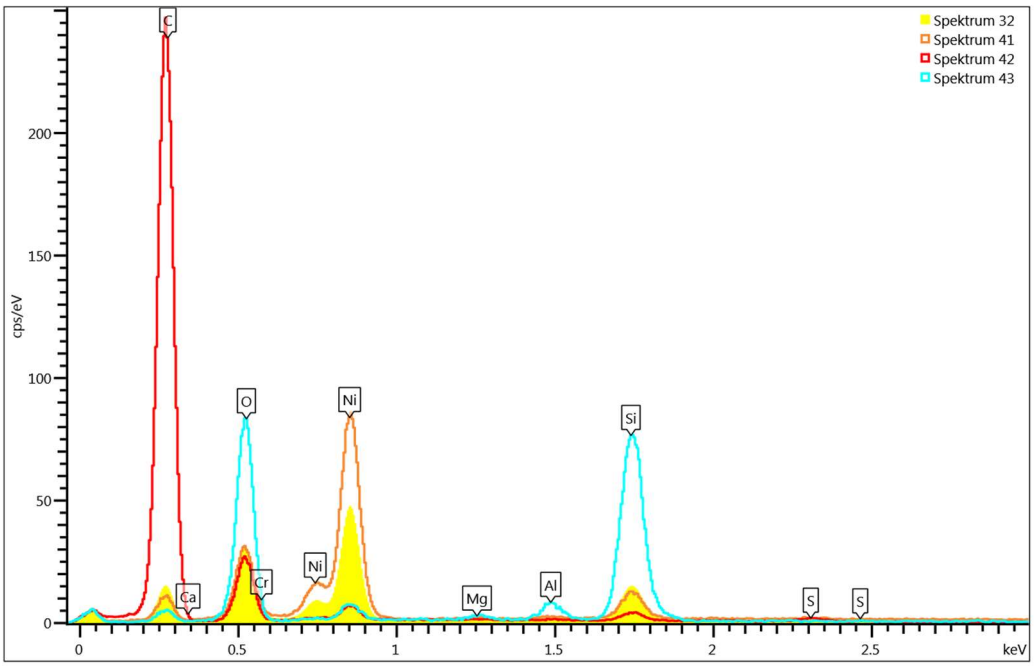

Figure S 14. EDX Spectra spent catalyst. Reaction conditions: 325ºC, 80 bar, Feed: HP+LP.

Table S 6. Elemental distribution over the catalyst surface by SEM-EDX. Spent catalyst. Reaction conditions: 325 °C, 80 bar, Feed: FPBO.

Compound	Spectra 41	Spectra 42	Spectra 43
C (wt.%)	10.1	76.8	8.3
O (wt.%)	10.1	13.9	42.8
Mg (wt.%)	0.2	0.1	0.7
Si (wt.%)	4.6	1.0	37.1
S (wt.%)	0.2	0.6	n.d.
Cr (wt.%)	6.1	2.2	n.d.
Ni (wt.%)	68.2	4.3	7.9
Ca (wt. %)	n.d.	0.9	0.3

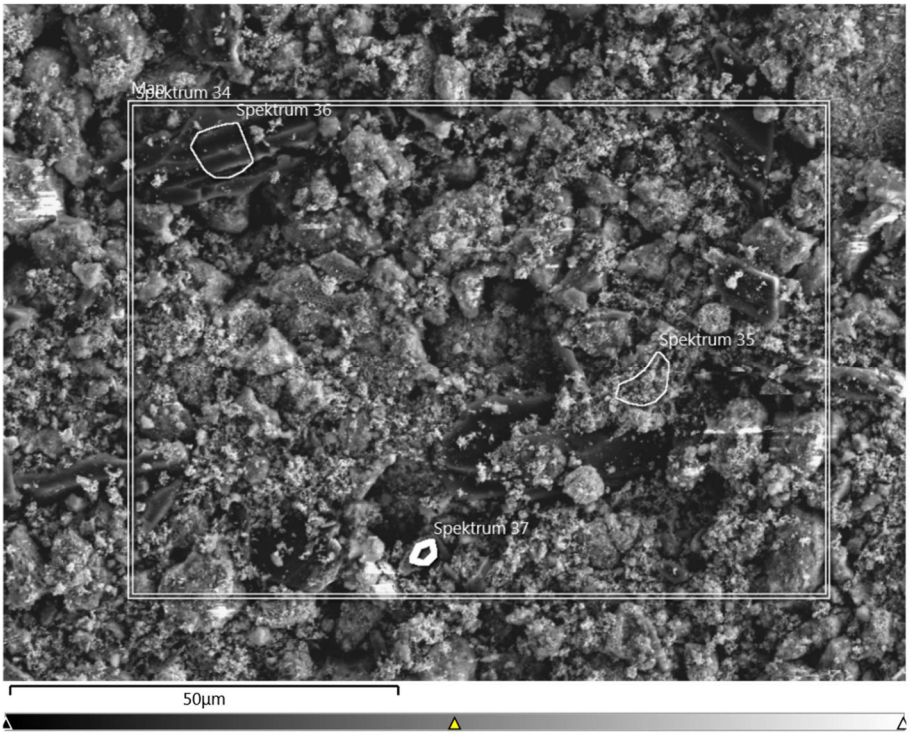

Figure S 15. SEM-EDX specific regions of the spent catalyst. Reaction conditions: 325 °C, 80 bar, Feed: HP.

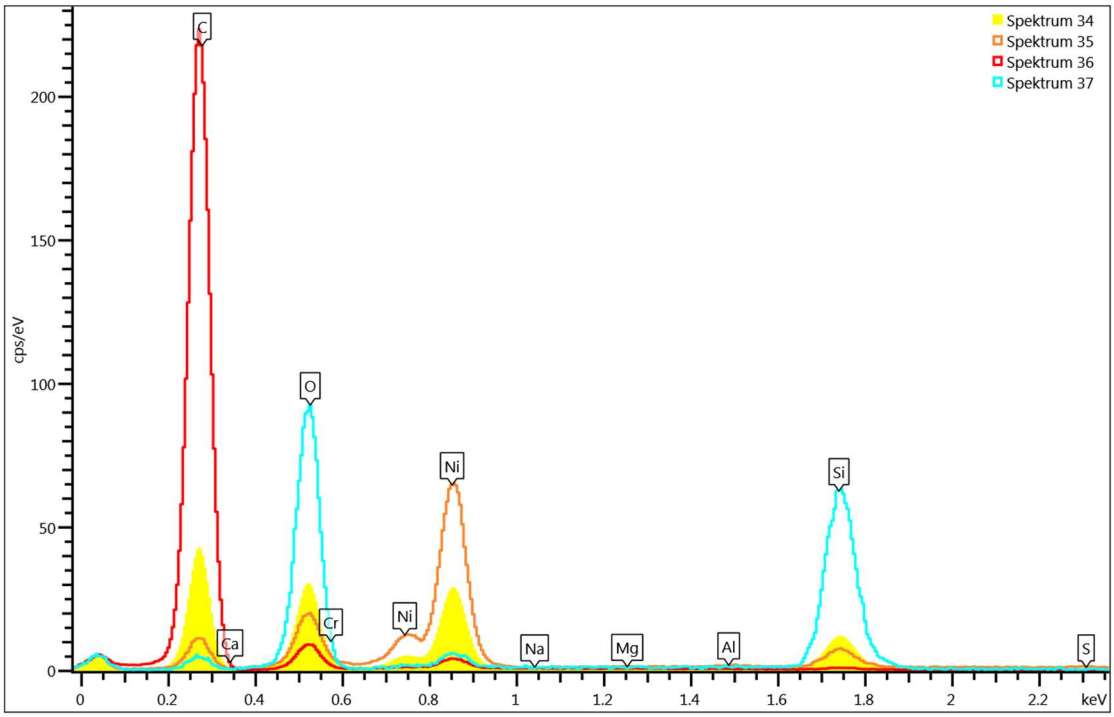

Figure S 16. EDX Spectra spent catalyst. Reaction conditions: 325 °C, 80 bar, Feed: HP.

Table S 7. Elemental distribution over the catalyst surface by SEM-EDX. Spent catalyst. Reaction conditions: 325 °C, 80 bar, Feed: HP.

	Spectra 34	**Spectra 35**	**Spectra 36**	**Spectra 37**
C (wt.%)	37.7	11.4	88.6	6.4
O (wt.%)	16.1	8.4	6.3	47.0
Mg (wt.%)	0.2	0.1	0.1	0.1
Si (wt.%)	7.3	4.2	0.3	40.0
Cr (wt.%)	5.5	4.9	1.1	n.d.
Ni (wt.%)	32.2	70.2	3.5	6.1
Ca (wt.%)	0.1	0.1	0.1	0.3
S (wt.%)	0.2	0.3	0.1	n.d.

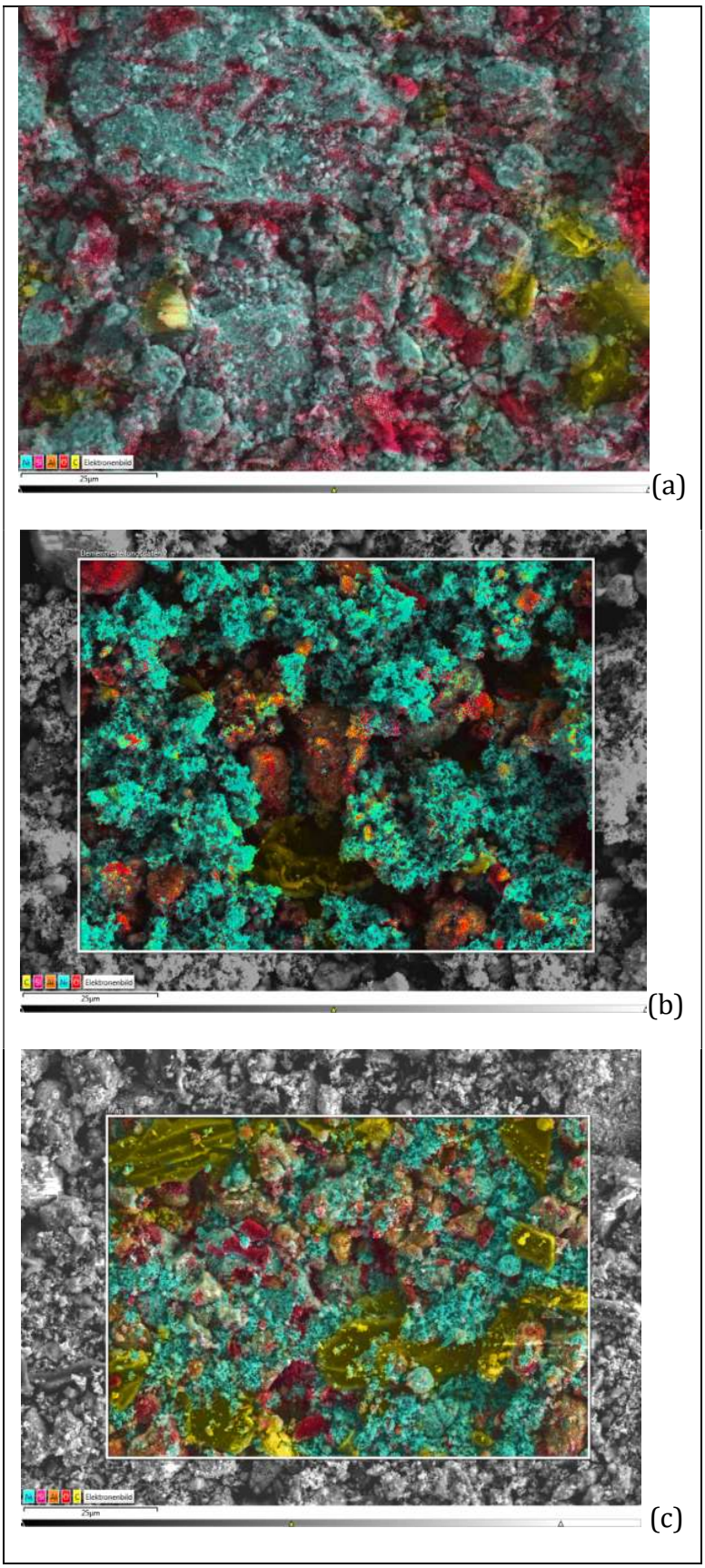

Figure S 17. Surface mapping of the main compounds in the catalysts surface. (a) Fresh catalyst; (b) Spent catalyst (325 °C, 80 bar, feed: FPBO); (c) Spent catalyst (325 °C, 80 bar, feed: HP).Yellow: carbon, green: nickel, pink: sulfur, red: oxygen.

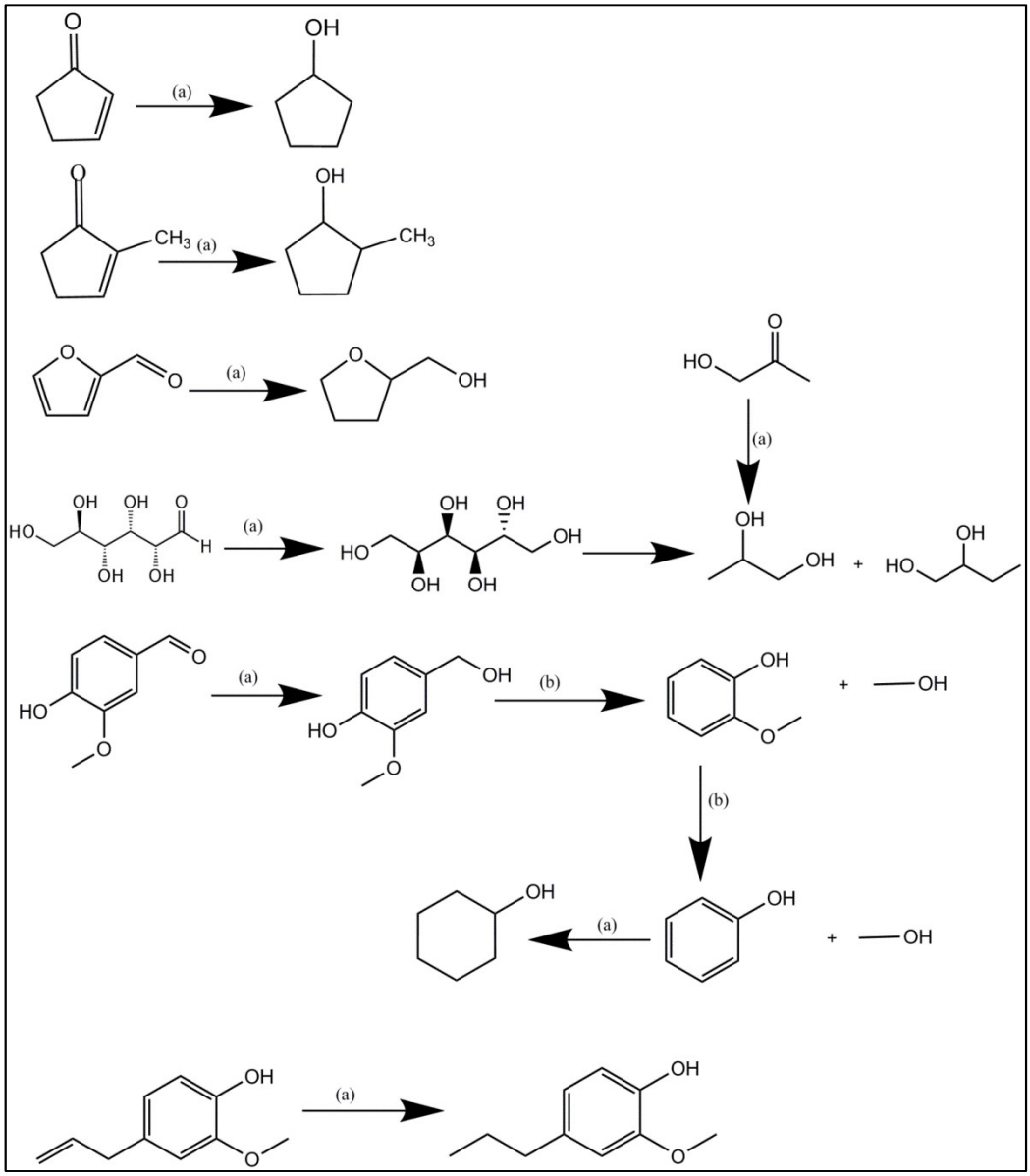

Figure S 18. Main reactions observed by GC-MS. (a) hydrogenation; (b) demethoxylation.

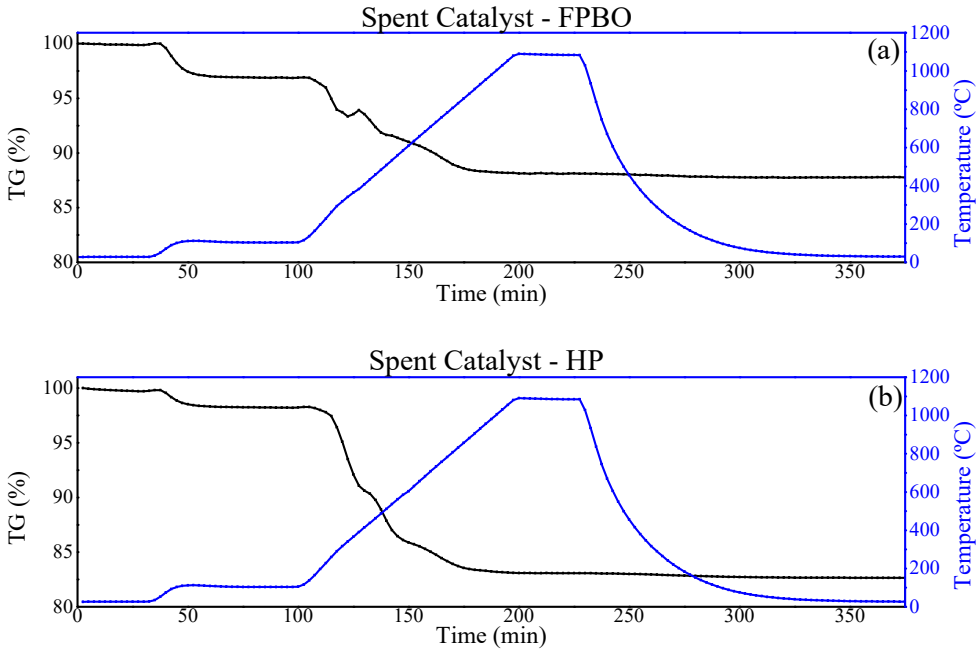

Figure S 19. Thermogravimetric analysis of spent catalysts. (a) Feed: FPBO; (b) Feed: HP.

Supplementary Material – Chapter 5

S.5.1 Coke calculation

The amount of solid (coke) over the spent catalyst was calculated following the equation below:

$$m_{solid} = \frac{\%C_{spentcat} \times m_{catalyst}}{100 - \%C_{spentcat}} \quad \text{Equation (S7)}$$

Where the m_{solid} is the mass of coke (g) in the spent catalyst; $\%C_{spentcat}$ is the concentration of carbon deposited over the spent catalyst obtained by elemental analysis and $m_{catalyst}$ is the amount of catalyst (g) loaded to the reactor.

S.5.2. Results

Table S 8. Elemental analysis and physicochemical properties of upgraded aqueous phases from different catalysts.

	Ni/SiO_2	**Ni/ZrO_2**	**$NiCu/SiO_2$**	**$NiCu/ZrO_2$**
Upgraded aqueous phase (wet basis)				
C (wt.%)	11.6 ±0.14	11.5±0.01	15.8 ±0.14	13.6±0.01
H (wt.%)	11.45 ±0.07	11.45 ±0.07	11.3±0.01	11.3±0.01
O (wt.%)	73.9 ±0.14	74.35 ±0.35	70.15 ±0.07	72.5±0.01
N (wt.%)	2.9±0.01	2.6 ±0.42	2.65 ±0.07	2.5±0.01
Physicochemical properties				
H_2O (wt.%)	74.35 ±0.21	74.5 ±0.028	67.15 ±0.21	72.35 ±1.20
pH	3.1±0.01	2.65 ±0.07	3.05 ±0.07	2.9±0.01
Density (g/cm^3)	1.028±0.07	1.026±0.01	1.034±0.01	1.031±0.01

S.5.3 XRD

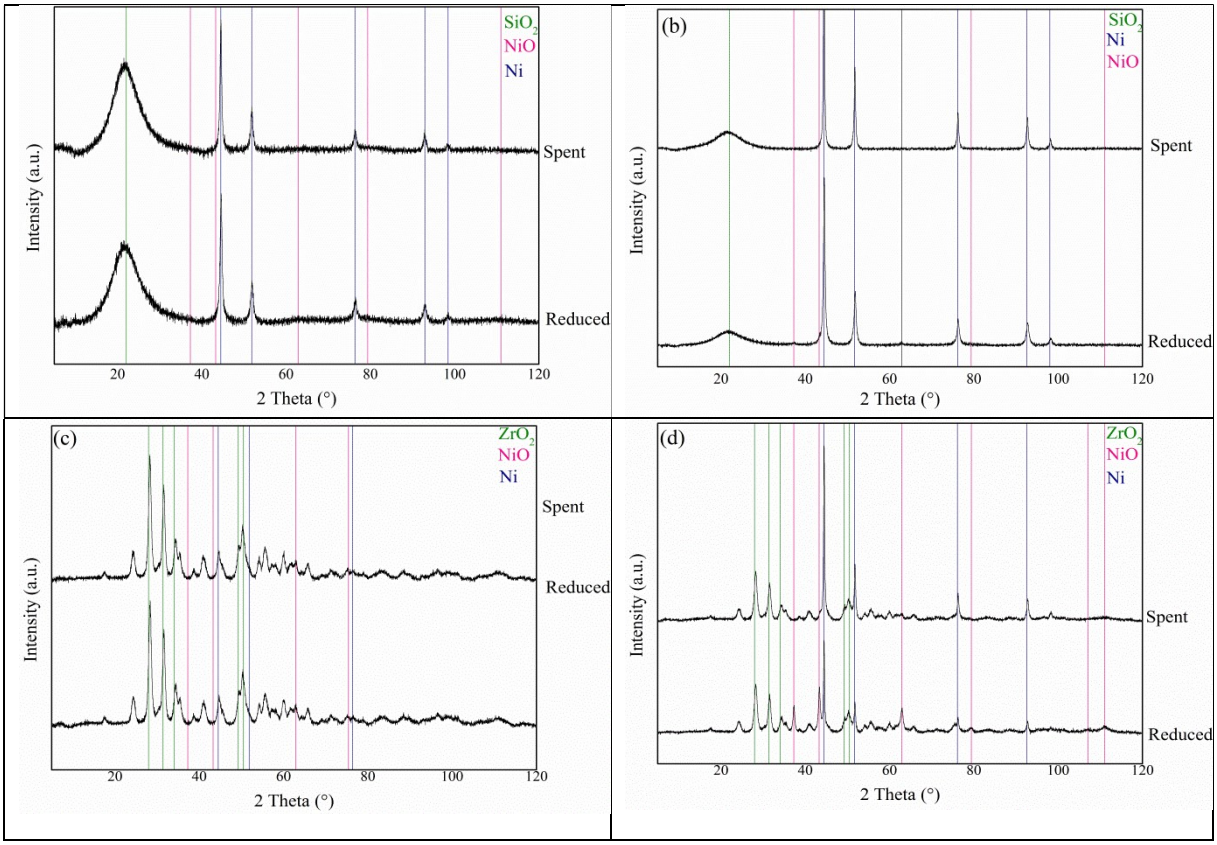

Figure S 20. Fresh and spent catalysts. a)Ni/SiO_2; b) NiCu/SiO_2; c)Ni/ZrO_2; d) NiCu/ZrO_2.

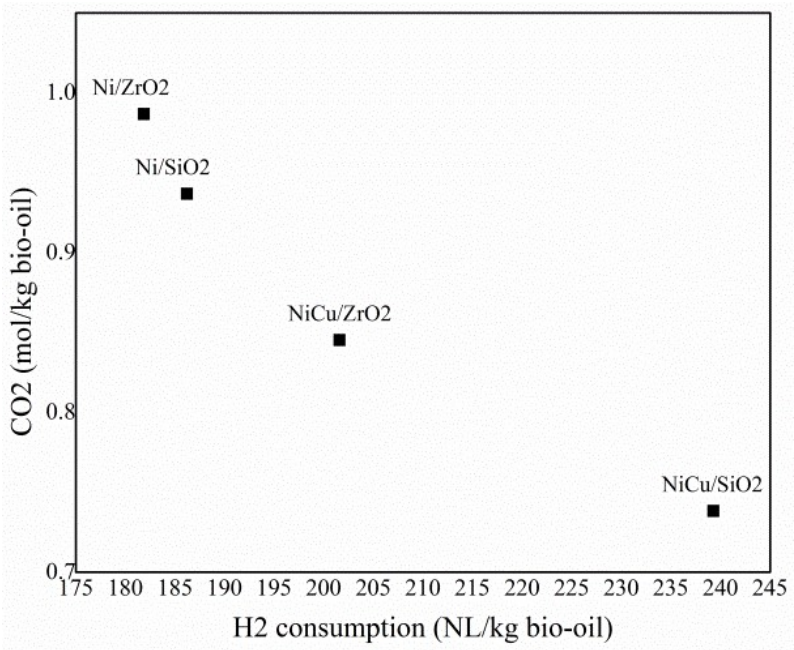

Figure S 21. Correlation between the H_2 consumption and CO_2 produced by different catalysts.

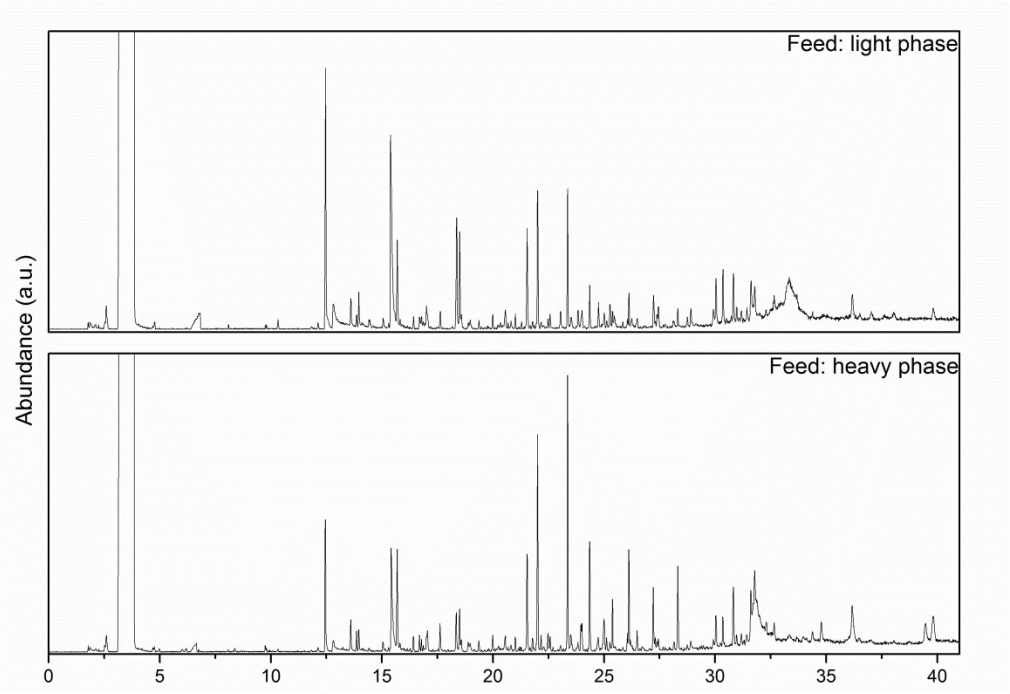

Figure S 22. GC-MS Feedstock (light phase and heavy phase).

Table S 9. Retention time of the main compounds identified in the feed (light and heavy phase).

Retention time (min)	Compound
12.46	1-hydroxy-2-propanone
13.6	2-cyclopenten-1-one
13.85	2-methyl-2-cyclopenten-1-one
15.36	Acetic acid
15.7	Furfural
16.42	1-(2-furanyl)-ethanone
16.7	3-methyl-2-cyclopenten-1-one
17.7	Propylene glycol
18.34	1,2-ethanediol
18.46	1,2-ethanediol, monoacetate
19.97	3-methyl-cyclopentanone
21.53	2-hydroxy-3-methyl-2-cyclopenten-1-one
22.0	2-methoxy-phenol
23.36	2-methoxy-4-methyl-phenol
23.954	2-methyl-phenol
24.0	Phenol
24.35	4-ethyl-2-methoxy-phenol
25.0	4-methyl-phenol
25.116	3-methyl-phenol
25.36	2-methoxy-4-propyl-phenol
26.114	Eugenol
27.23	2-methoxy-4-(1-propenyl)-phenol
28.314	2-methoxy-4-(1-propenyl)-phenol
30.04	5-(hydroxymethyl)-2-furancarboxaldehyde
30.82	Vanillin
31.62	1-(3-hydroxy-4-methoxyphenyl)-ethanone

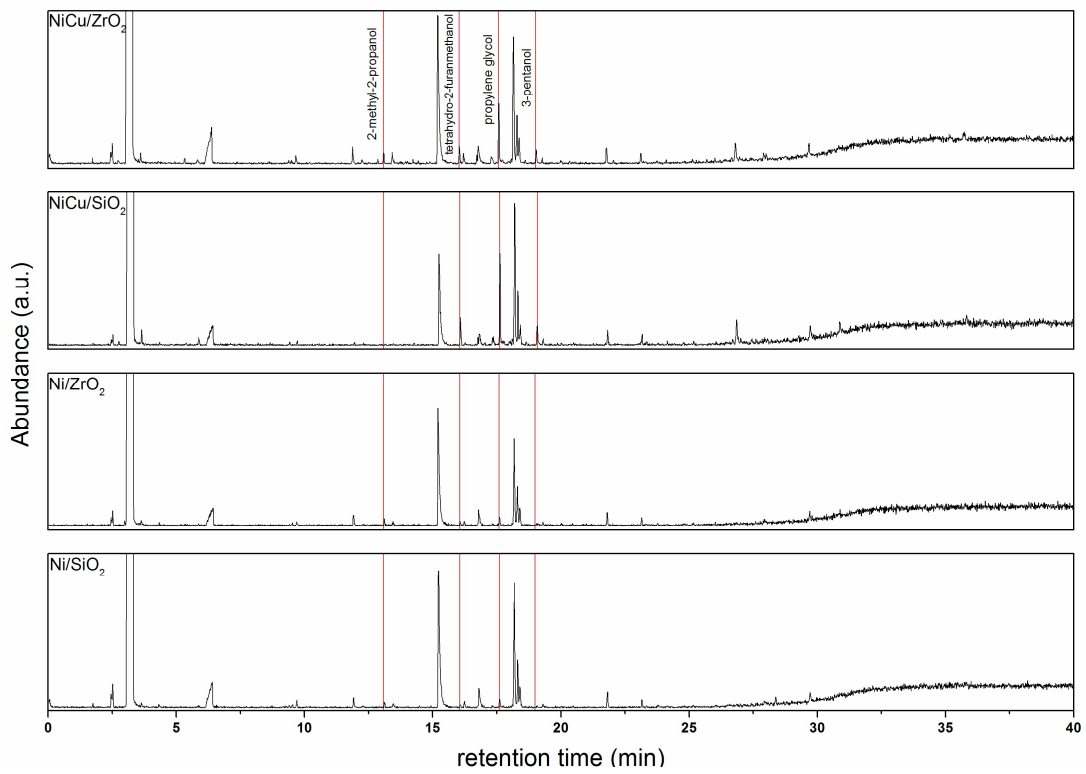

Figure S 23. GC-MS aqueous phase after hydrodeoxygenation with different catalysts.

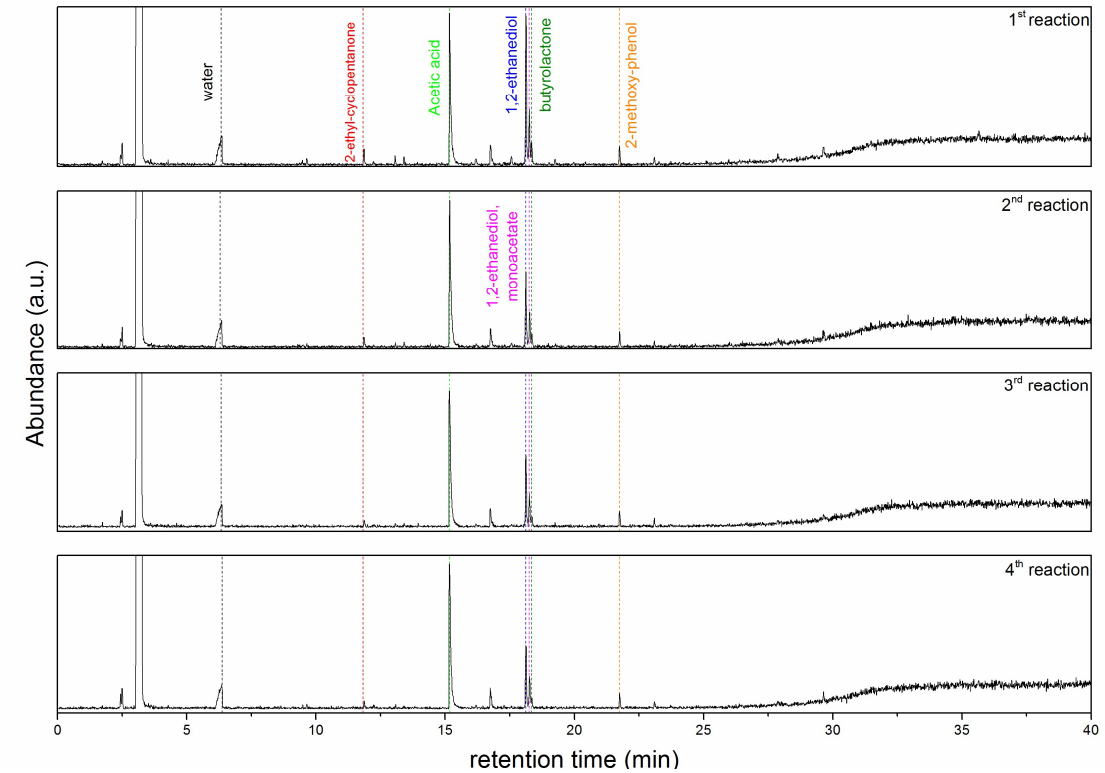

Figure S 24. GC-MS aqueous phase over the consecutive reactions.

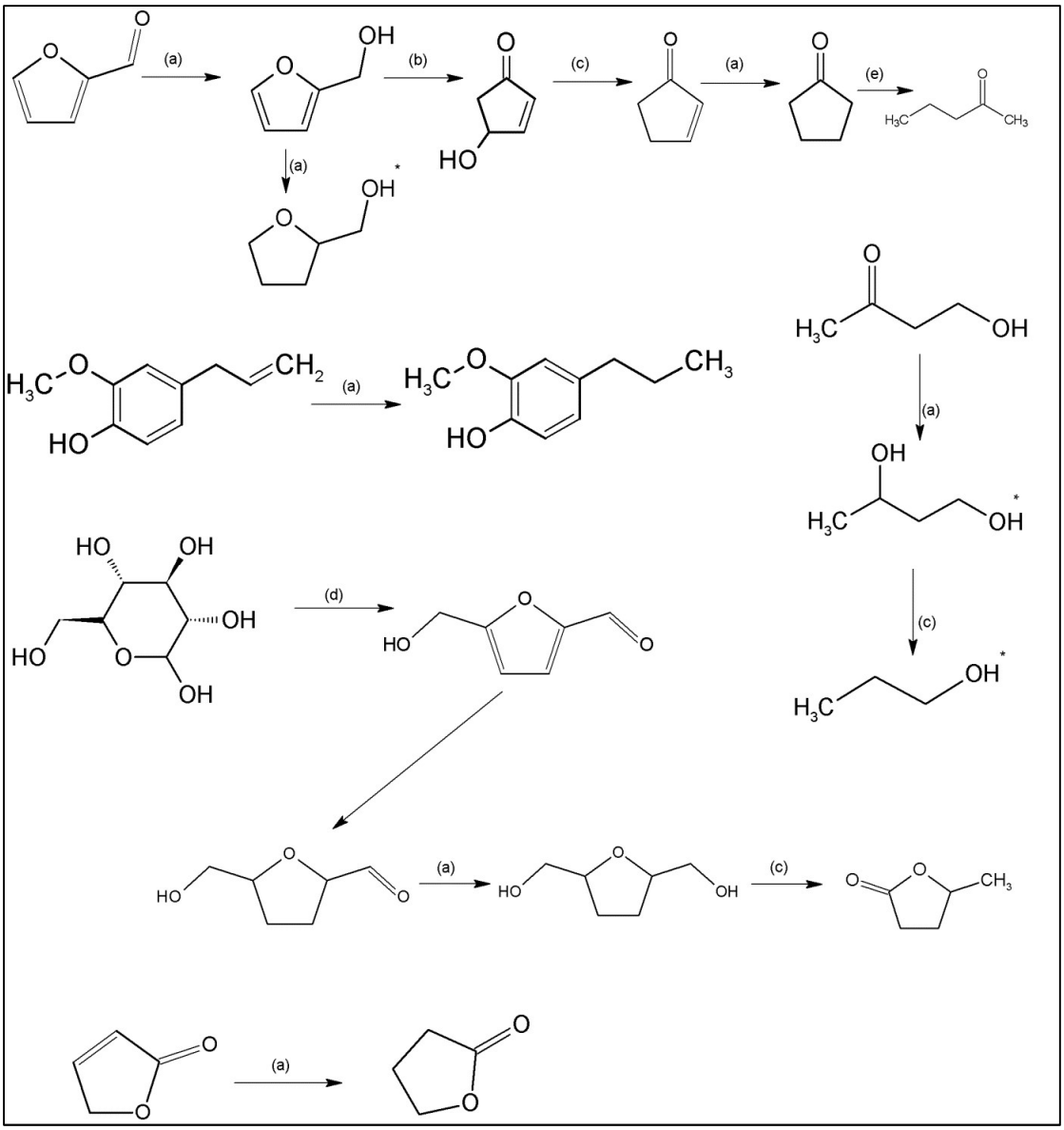

Figure S 25. Reaction pathways identified after HDO reactions.(a)-hydrogenation; (b)-rearrangement; (c)-direct deoxygenation; (d)-dehydration; (e)-ring opening; * Products obtained with $NiCu/SiO_2$ and $NiCu/ZrO_2$ catalysts.

Fresh Ni/SiO_2 catalyst

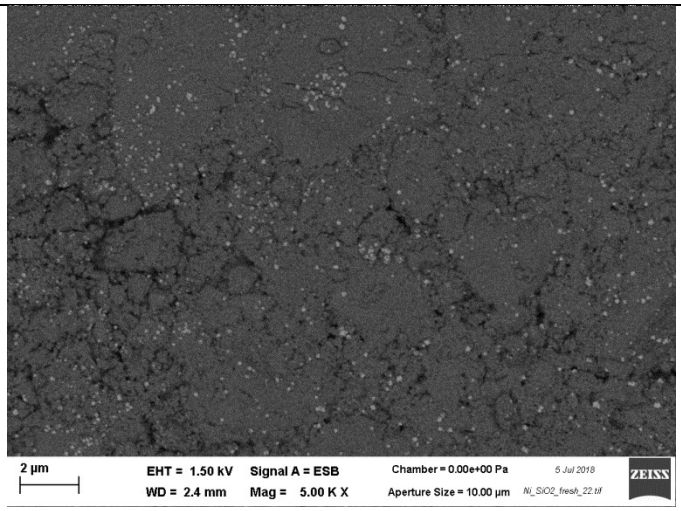

(fresh a)

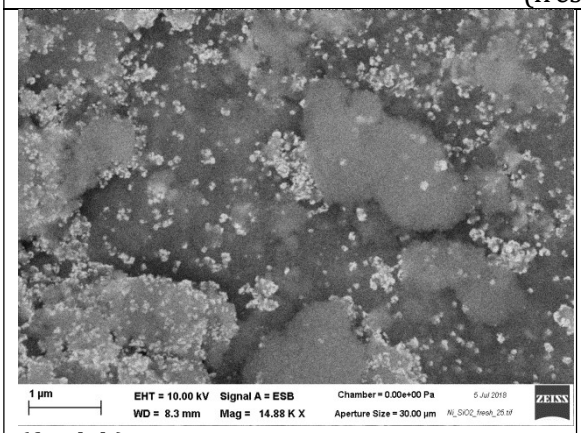

(fresh b)

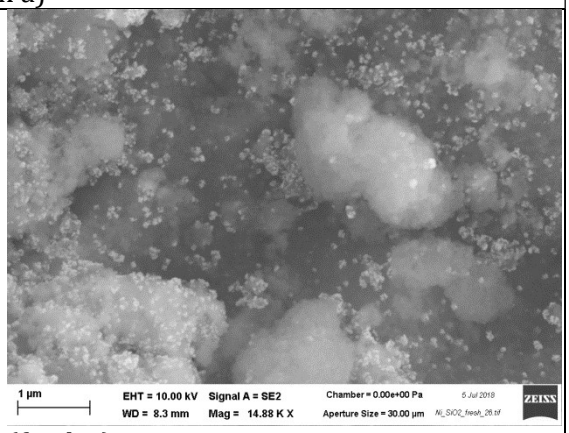

(fresh c)

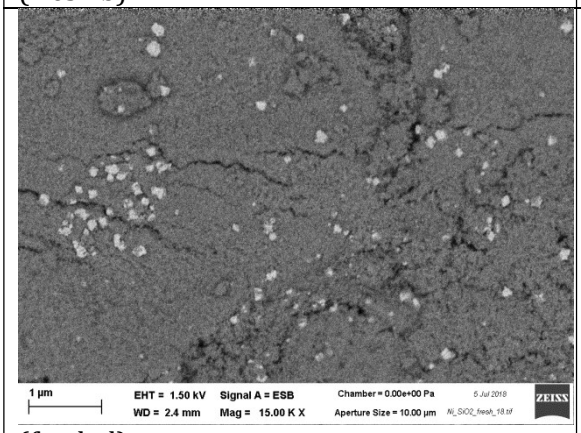

(fresh d)

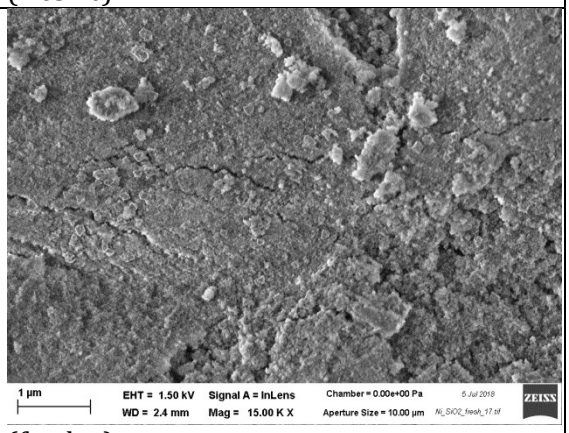

(fresh e)

1^{st} reaction

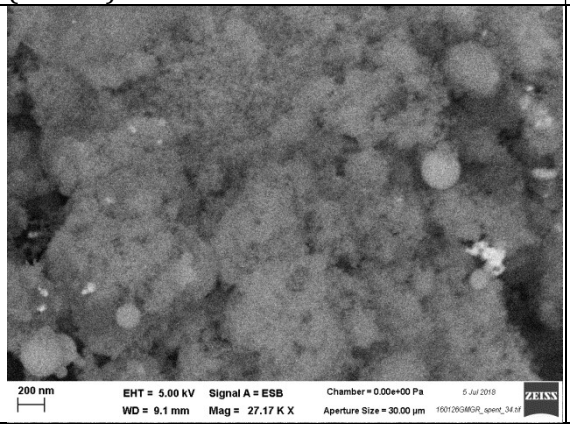

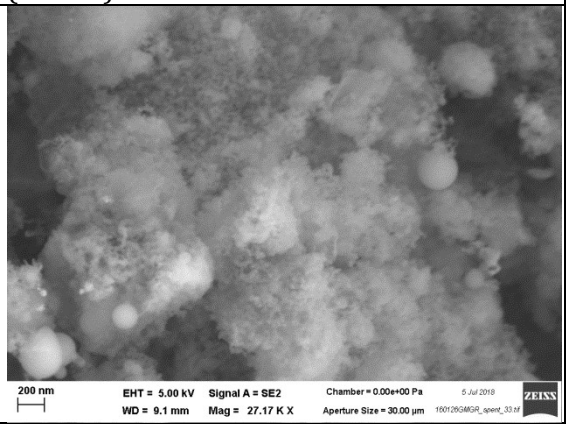

	(1st a)	(1st b)
	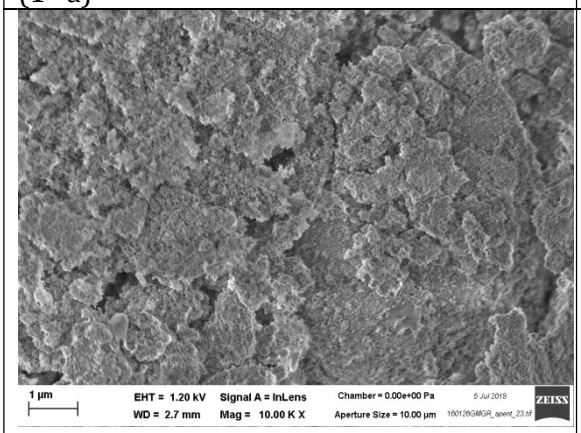	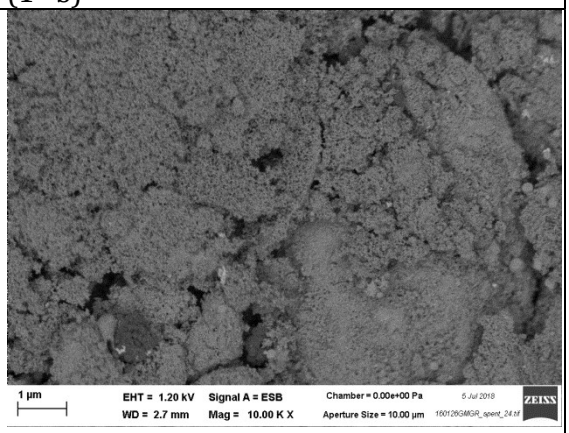
	(1st c)	(1st d)
2nd reaction - spent	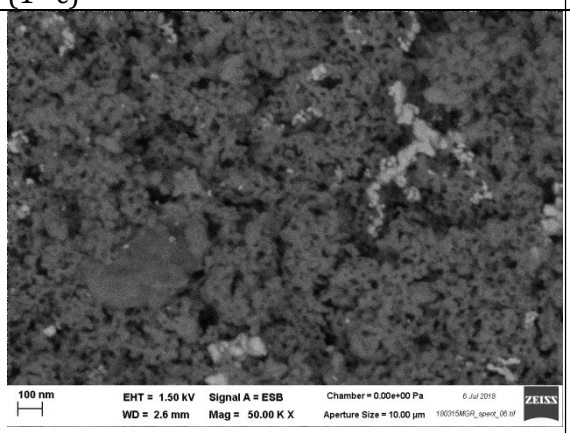	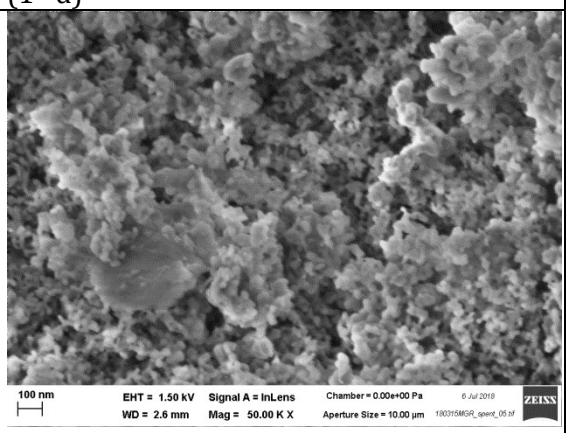
	(2nd a)	(2nd b)
	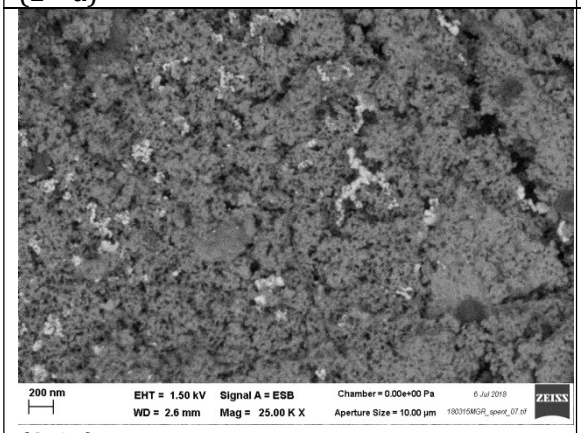	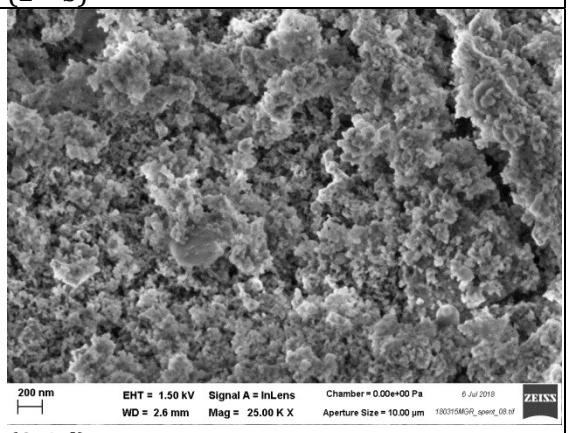
	(2nd c)	(2nd d)
	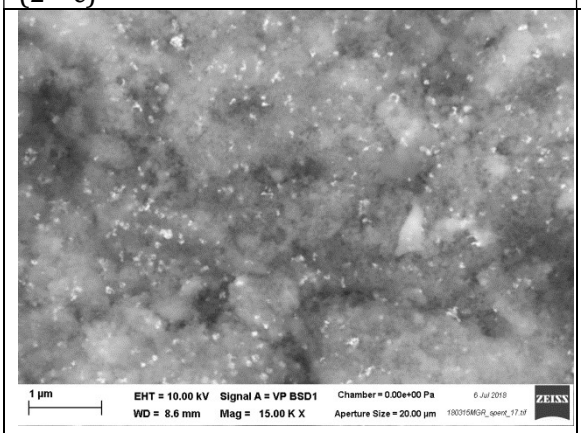	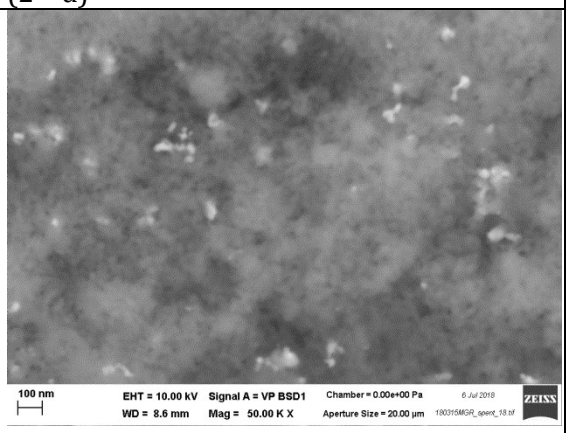
	(2nd e)	(2nd f)

3rd reaction - spent

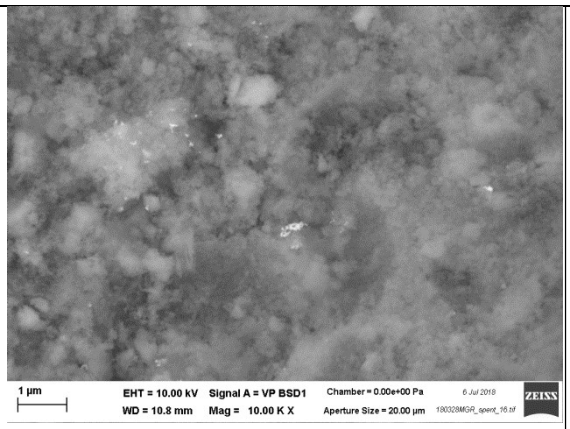

(3rd a)

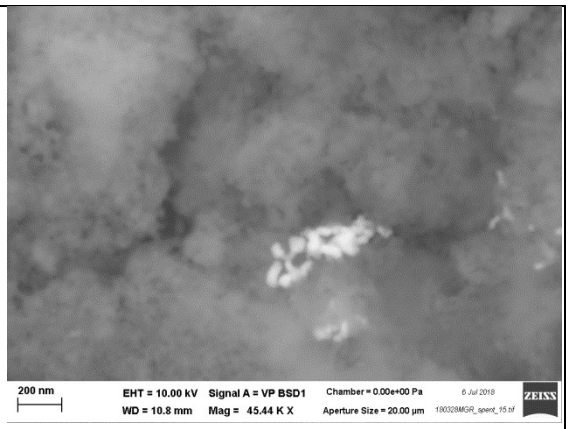

(3rd b)

4threaction - spent

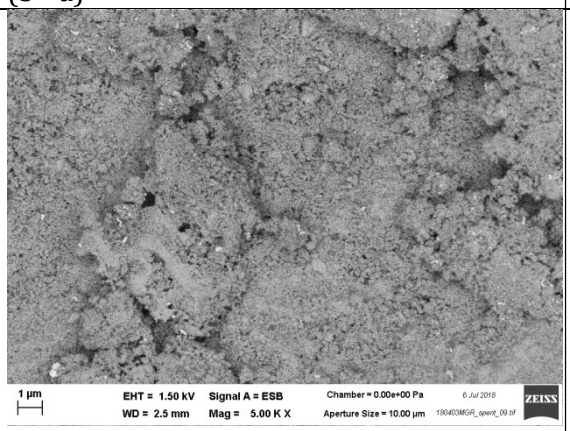

(4th spent a)

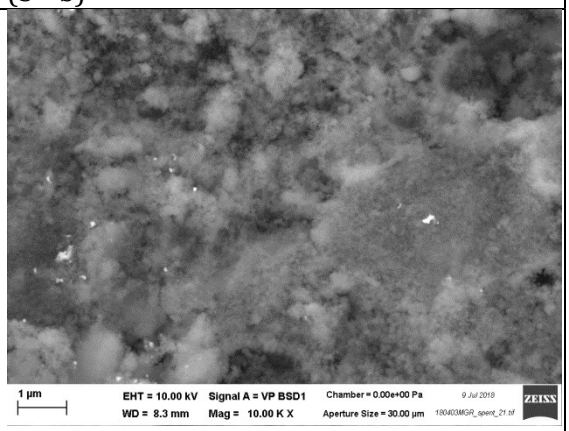

(4th spent b)

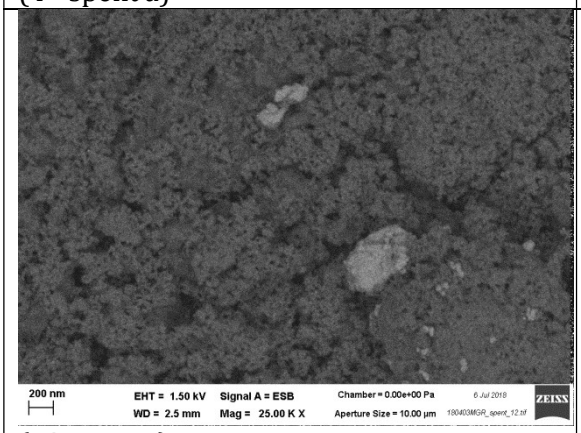

(4th spent c)

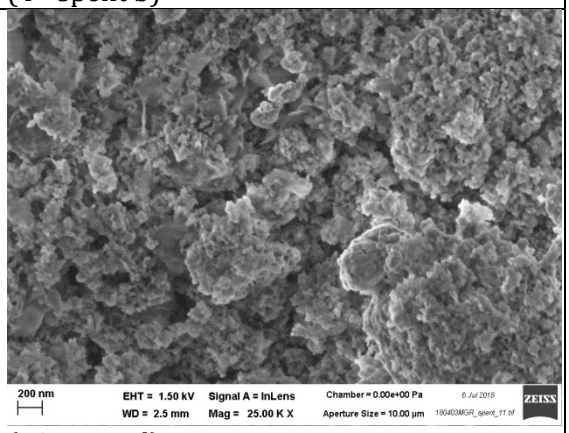

(4th spent d)

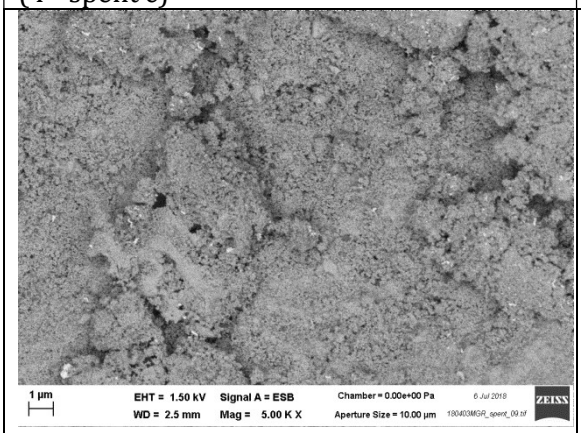

(4th spent e)

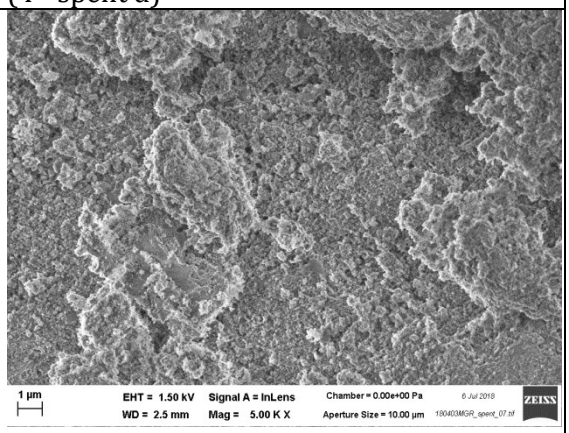

(4th spent f)

4th reaction – calcined

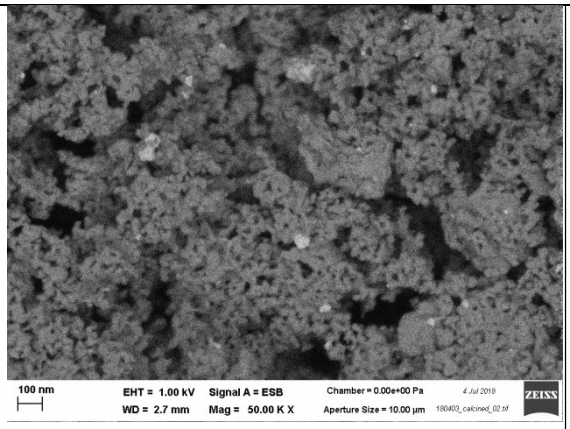

(4th calcined a)

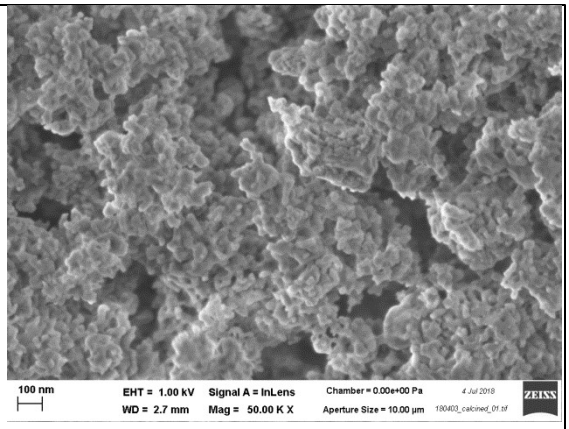

(4th calcined b)

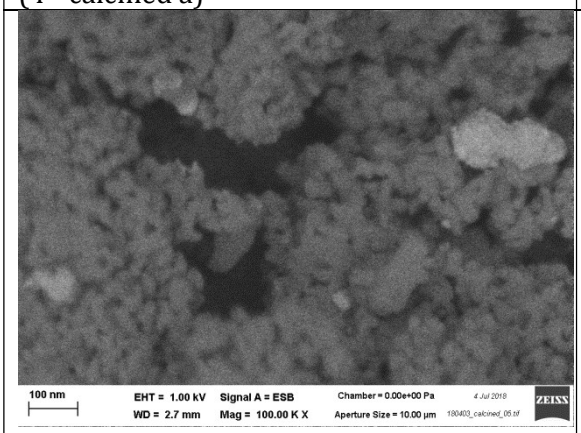

(4th calcined c)

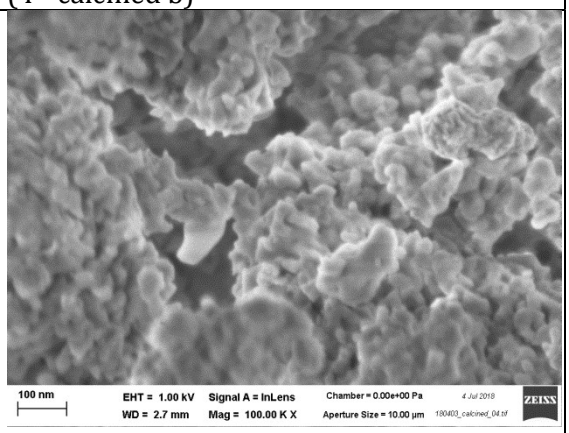

(4th calcined d)

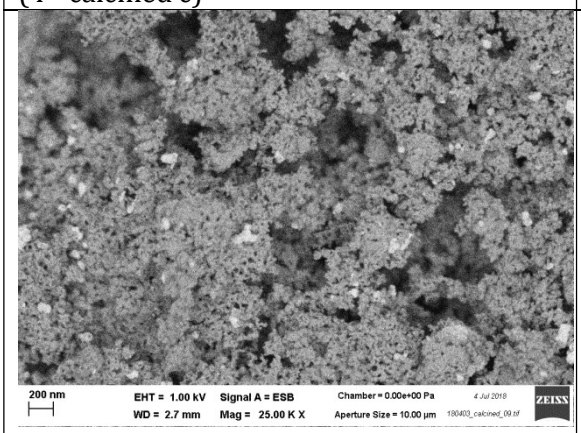

(4th calcined e)

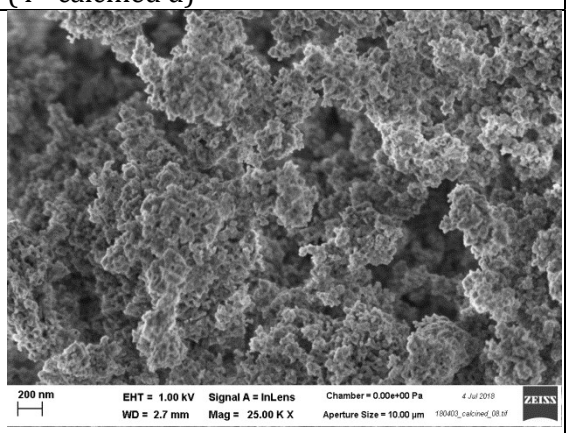

(4th calcined f)

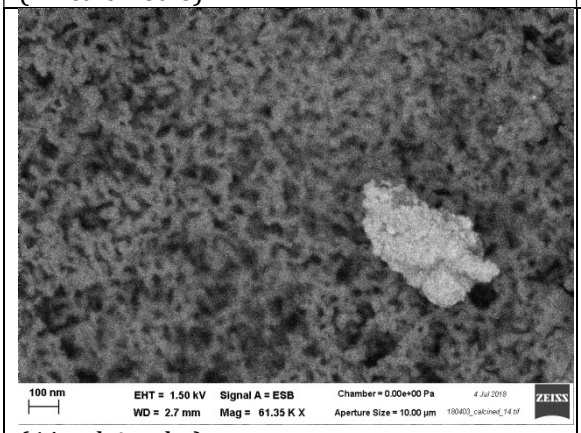

(4th calcined g)

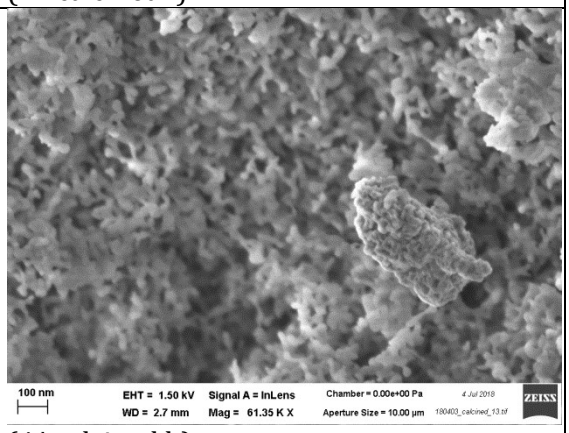

(4th calcined h)

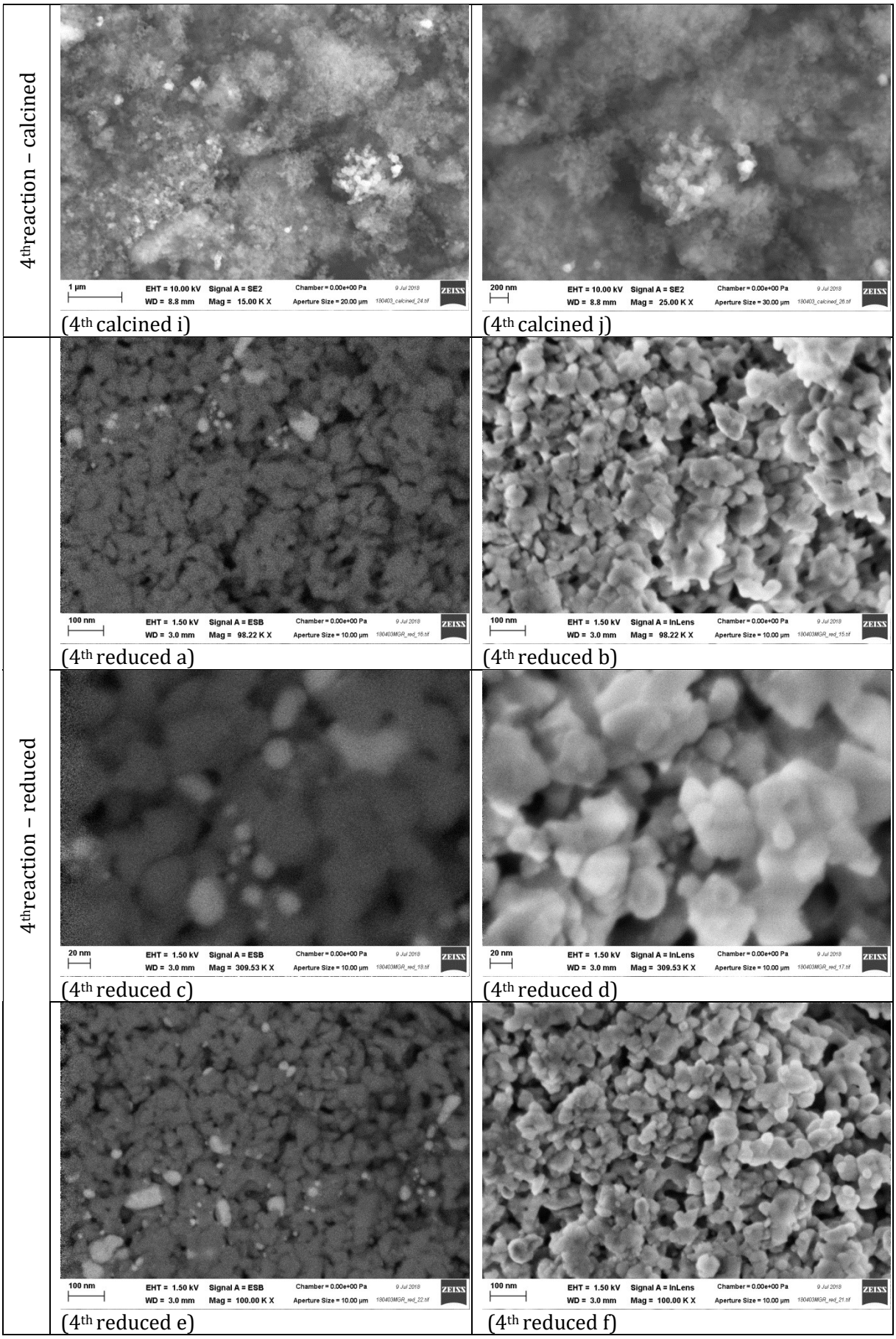

Figure S 26. Compilation of the main pictures obtained by SEM-EDX. Brighter parts are attributed to nickel particles.

Fresh Ni/SiO_2 catalyst

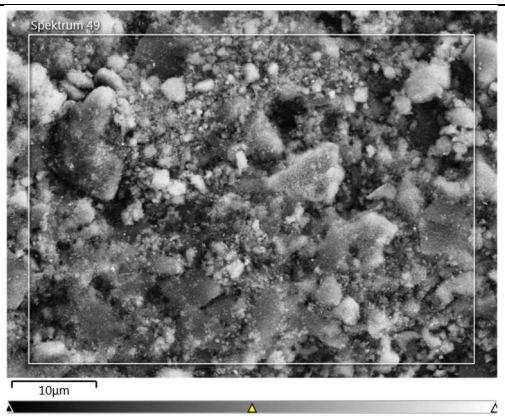

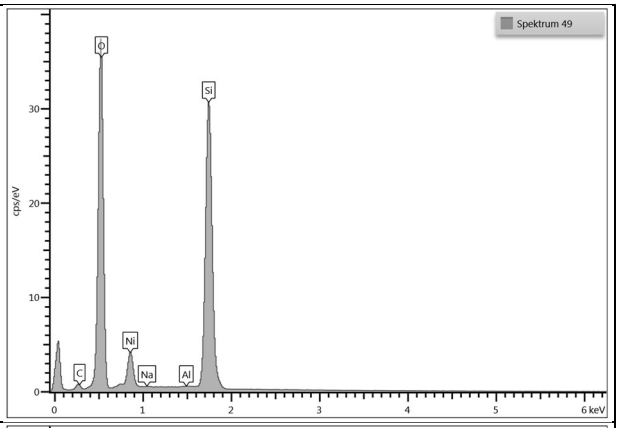

1st reaction - spent

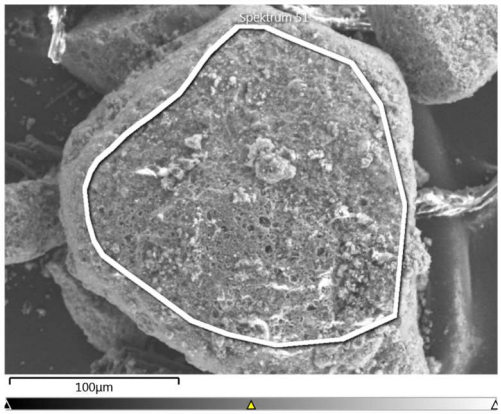

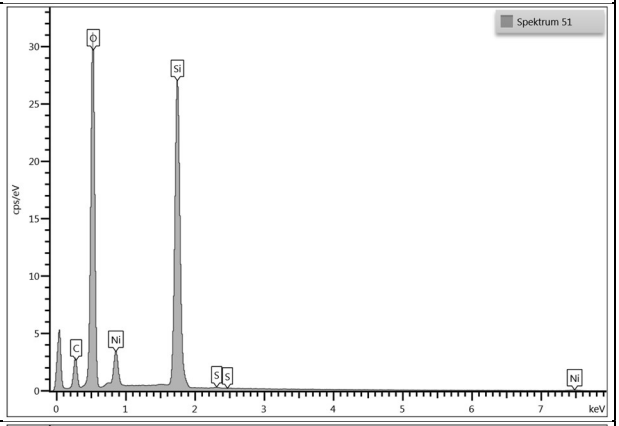

2nd reaction - spent

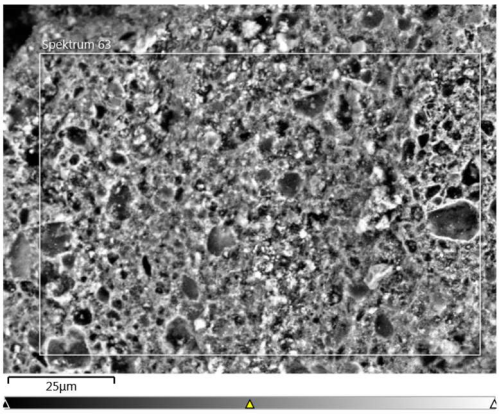

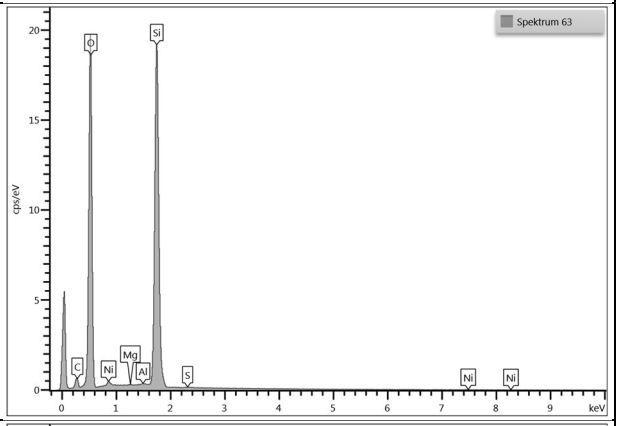

3rd reaction - spent

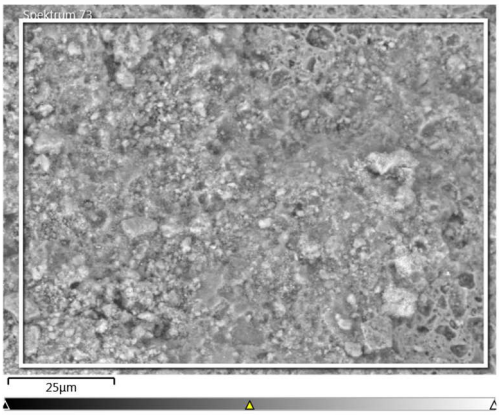

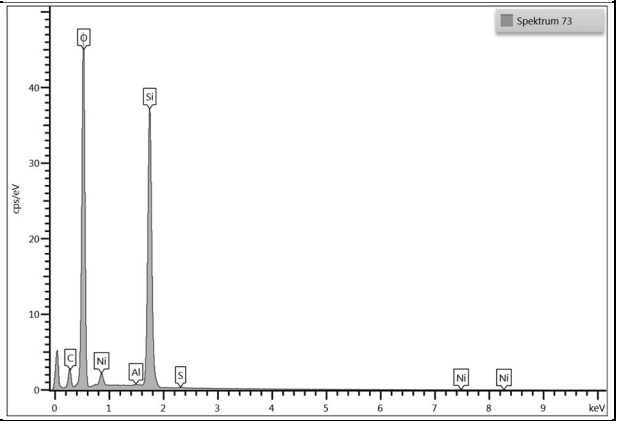

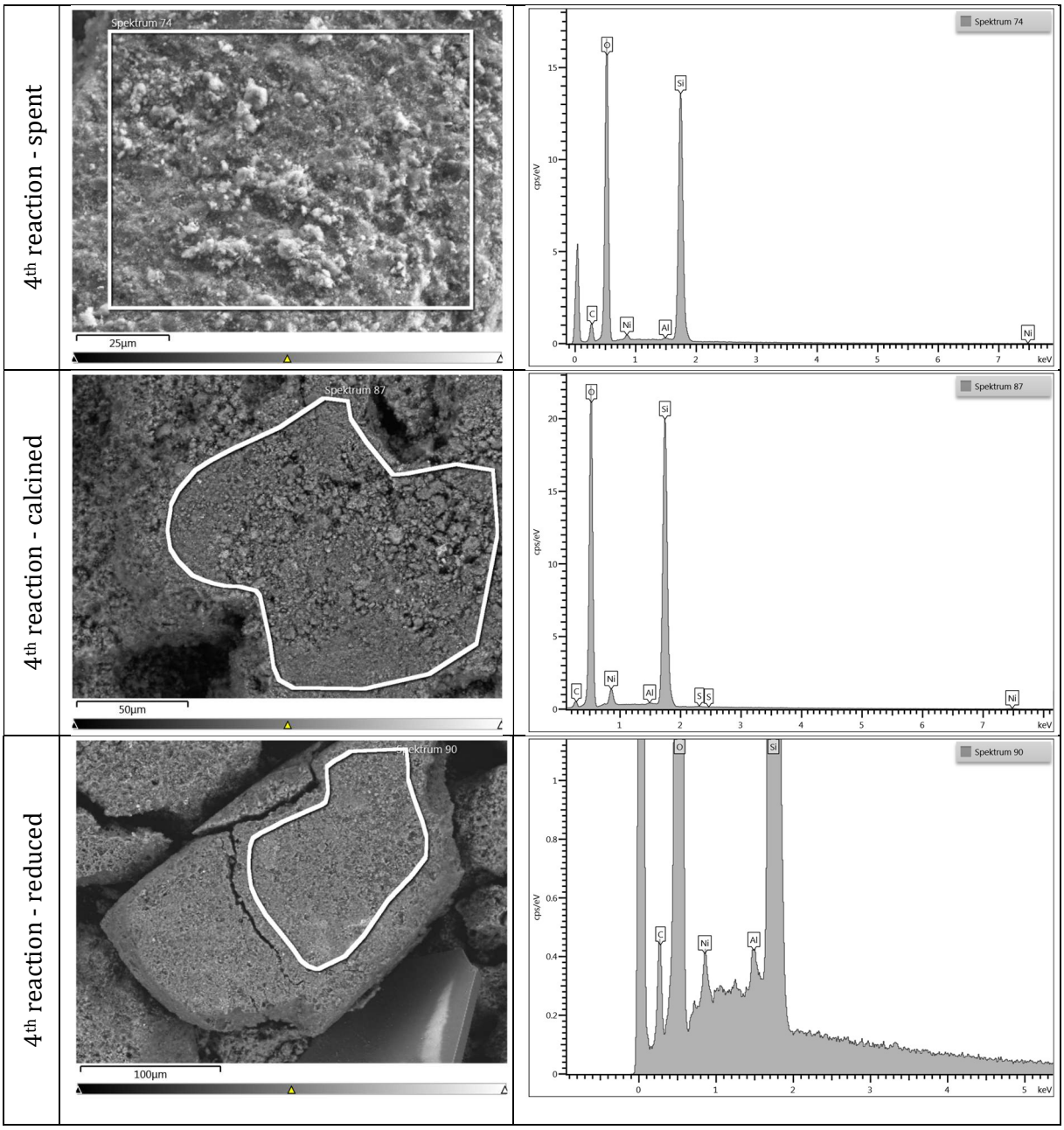

Figure S 27. EDX of selected regions

Table S 10. Elemental composition obtained by EDX of selected regions.

Spectrum	C (wt.%)	Si (wt.%)	S (wt.%)	Ni (wt.%)
Fresh Ni/SiO_2	2.9	39.5	-	9.6
1st reaction (spent)	12.1	44.9	0.2	7.3
2nd reaction (spent)	6.8	42.2	0.1	1.1
3rd reaction (spent)	9.1	37.4	0.1	2.4
4th reaction (spent)	10.1	37.9	-	1.8
4th reaction (calcined)	3.5	41.8	0.1	6.4
4th reaction (reduced)	3.6	44.5	-	1.2

Supplementary Material – Chapter 6

S.6.1 Sugarcane bagasse

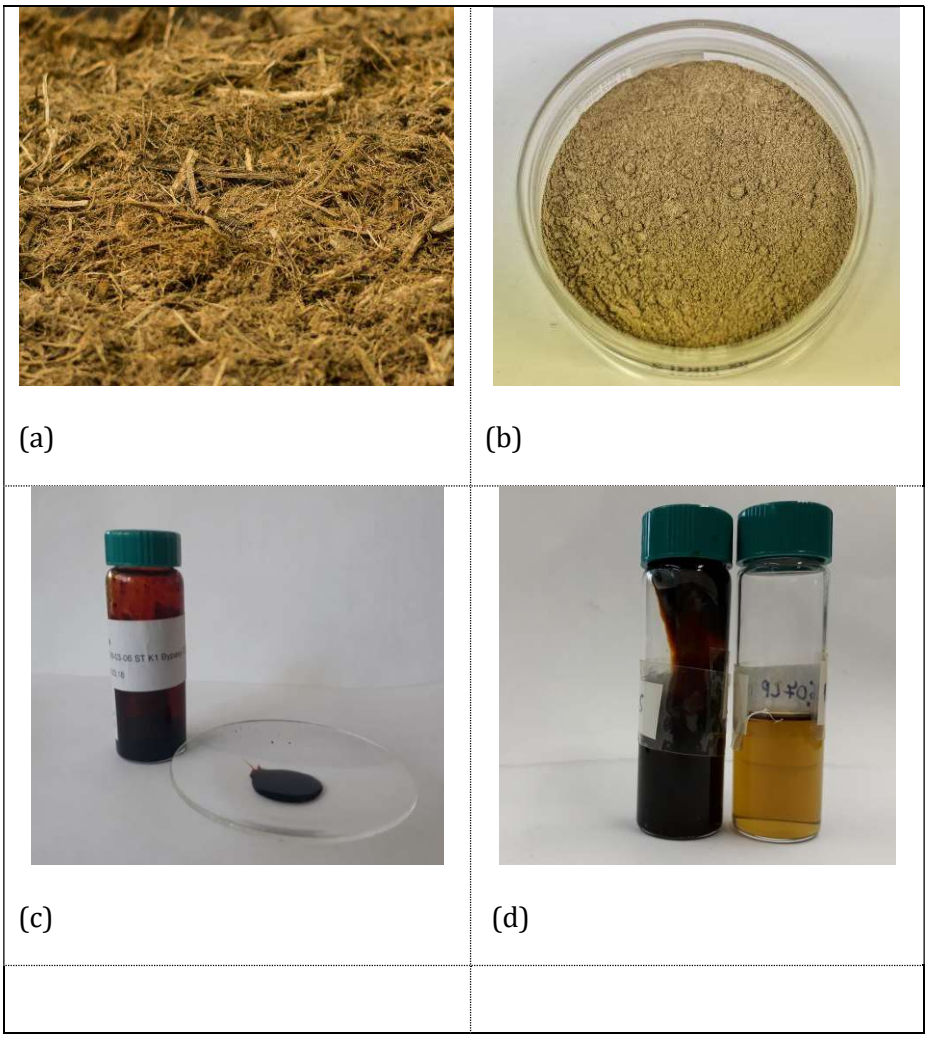

Figure S 28. Sugarcane bagasse dried (a) and milled (b), sugarcane bagasse pyrolysis-oil (c) and upgraded products (UOP and ULP) with Ni/SiO_2 (d).

S.6.2 The sugarcane bagasse (SCB) was characterized following the DIN norms listed below

Table S 11. Methodologies used for the sugarcane bagasse characterization and the respective norm.

Methodology	**Norm**
Moisture	DIN EN ISO 18134-3
Ash	DIN EN ISO 18122
Volatile Matter	DIN EN 18123
HHV	DIN EN ISO 18125 without acid-correction
CHN	DIN EN 16948
S	DIN EN 16994

S.6.3 Gas analysis methodology

The composition of the gas samples collected after the upgrading reactions was determined using a GC-TCD/FID (Gas Chromatography-Thermal conductivity detector/flame ionization detector). As soon as the reactor reached temperature below 25 °C, it was depressurized and a sample was collected. A volume of 100 µl was injected at 250 °C (injector temperature) and separated by two columns: Restek 57096 and Resteck Molsieve 5A. The oven was programmed at start temperature of 50 °C (10 minutes), increased to 90 °C at 3 °C/min, increased to 150 °C at 20 °C/min and maintained for 16 min and later increase to 230 °C/min at 50 °C/min and maintained for 10 minutes. The hydrogen consumption was calculated by the ideal gas law considering the moles of hydrogen before and after the reaction (based on the GC results) and the pressure before and after the reaction.

S.6.4 Sugarcane bagasse pyrogram

The pyrogram as well as the compounds identified are presented in Figure S.29 and Table S.12

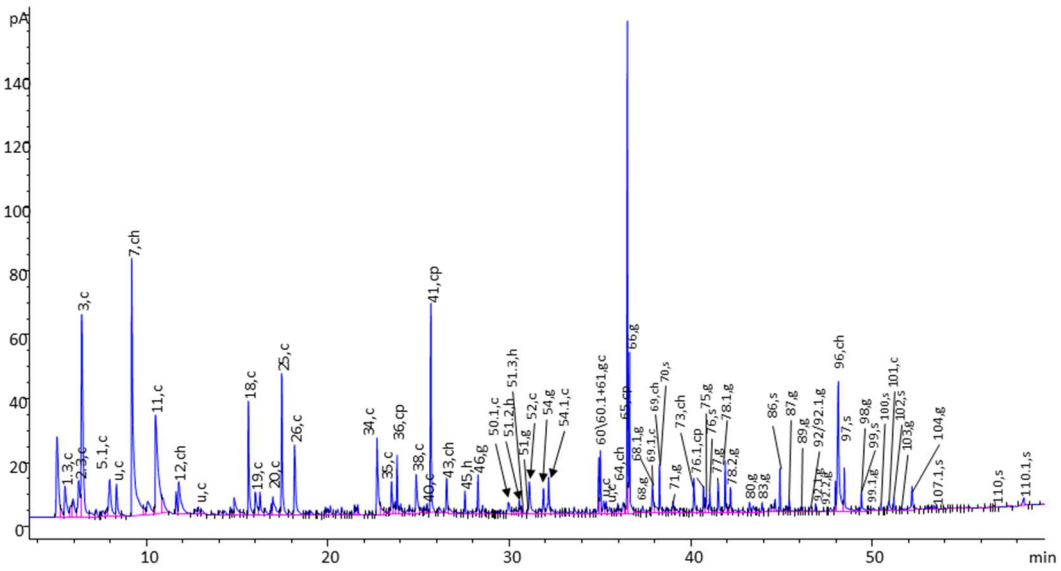

Figure S 29. Sugarcane bagasse pyrogram.

Table S 12. Compounds identified in the pyrogram.

Compound*	Compound
1.3,[c]	Acetaldehyde
2.3,[c]	2-Propenal (acrolein)
3,[c]	Propanal-2-one
5.1,[c]	2,3-Butandione
u,[c]	Butanone-(2) or unknown
7,[ch]	Hydroxyacetaldehyde
11,[c]	Acetic acid
12,[ch]	Hydroxypropanone
u,[c]	Unknown
18,[c]	3-Hydroxypropanal
19,[c]	3-Butenal-2-one
20,[c]	(3H)-Furan-2-one
25,[c]	2-Hydroxy-3-oxobutanal
26,[c]	2-Furaldehyde, 2-furfural
34,[c]	Dihydro-methyl-furanone
35,[c]	Dihydro-methyl-furanone
36,[cp]	Isomer of 4-Hydroxy-5,6-dihydropyran-(2H)-one
38,[c]	(5H)-Furan-2-one
40,[c]	Gamma-Lactone and unknown
41,[cp]	4-Hydroxy-5,6-dihydropyran-(2H)-2-one
43,[ch]	2-Hydroxy-1-methyl-cyclopenten-(1)-3-one
45,[h]	Phenol
46,[g]	Guaiacol
50.1,[c]	Methyl-butyraldehyde derivative
51.2,[h]/ 51.3,[h]	p-Cresol / m-Cresol
51,[g]	3-Methyl guaiacol
52,[c]	Gamma-lactone derivative
54,[g]	4-Methyl guaiacol
54.1,[c]	Anhydrosugar
60/60.1+61,[gc]	Overlapping spectra; 4-ethyl-guaiacol
u,[c]	Unknown
u,[c]	Unknown
64,[ch]	1,4:3,6-Dianhydro-glucopyranose
65,[cp]	1,5-Anhydro-arabinofuranose
66,[g]	4-Vinyl guaiacol
68,[g]	Eugenol
68.1,[g]	4-Propyl guaiacol
69,[ch]	5-Hydroxymethyl-2-furaldehyde
69.1,[c]	gamma-Lactone derivative
70,[s]	Syringol
71,[g]	Isoeugenol (cis)
73,[ch]	Pyran-(4H)-4-one, 2-hydroxymethyl-5-hydroxy-2,3-dihydro
76.1,[cp]	1,5-Anhydro-b-D-xylofuranose
75,g	Isoeugenol (trans)

76,s	Syringol, 4-methyl-
77,g	Vanillin
78.1,g	Indene, 6-hydroxy-7-methoxy-, 1H-
78.2,g	Indene, 6-hydroxy-7-methoxy-, 2H-
80,g	Homovanillin
83,g	Acetoguaiacone
86,s	Syringol, 4-vinyl-
87,g	Guaiacyl acetone
g/s	Unknown
89,g	Propioguaiacone
92.1,g	Isomer of coniferyl alcohol
92/92.1,g	G-CO-CH=CH_2
92.2,g	G-CO-CO-CH_3
96,ch	1,6-Anydro-b-D-glucopyranose (levoglucosan)
97,s	Syringol, 4-propenyl- (trans)
98,g	Dihydroconiferyl alcohol
99,s	Syringaaldehyde
99.1,g	Coniferyl alcohol (cis)
100,s	Homosyringaaldehyde
101,c	Anhydrosugar: unknown
102,s	Acetosyringone
103,g	Coniferyl alcohol (trans)
104,g	Coniferylaldehyde
107.1	Isomer of sinapyl alcohol
110,s	Sinapyl alcohol (trans)
110.1,s	Sinapinaldehyde

*The superscripts c, ch, cp, h, g, s and u correspond to compounds derived from polysaccharides, hexoses, pentose, hydroxyphenyl, guaiacyl, syringyl and unknown, respectively.

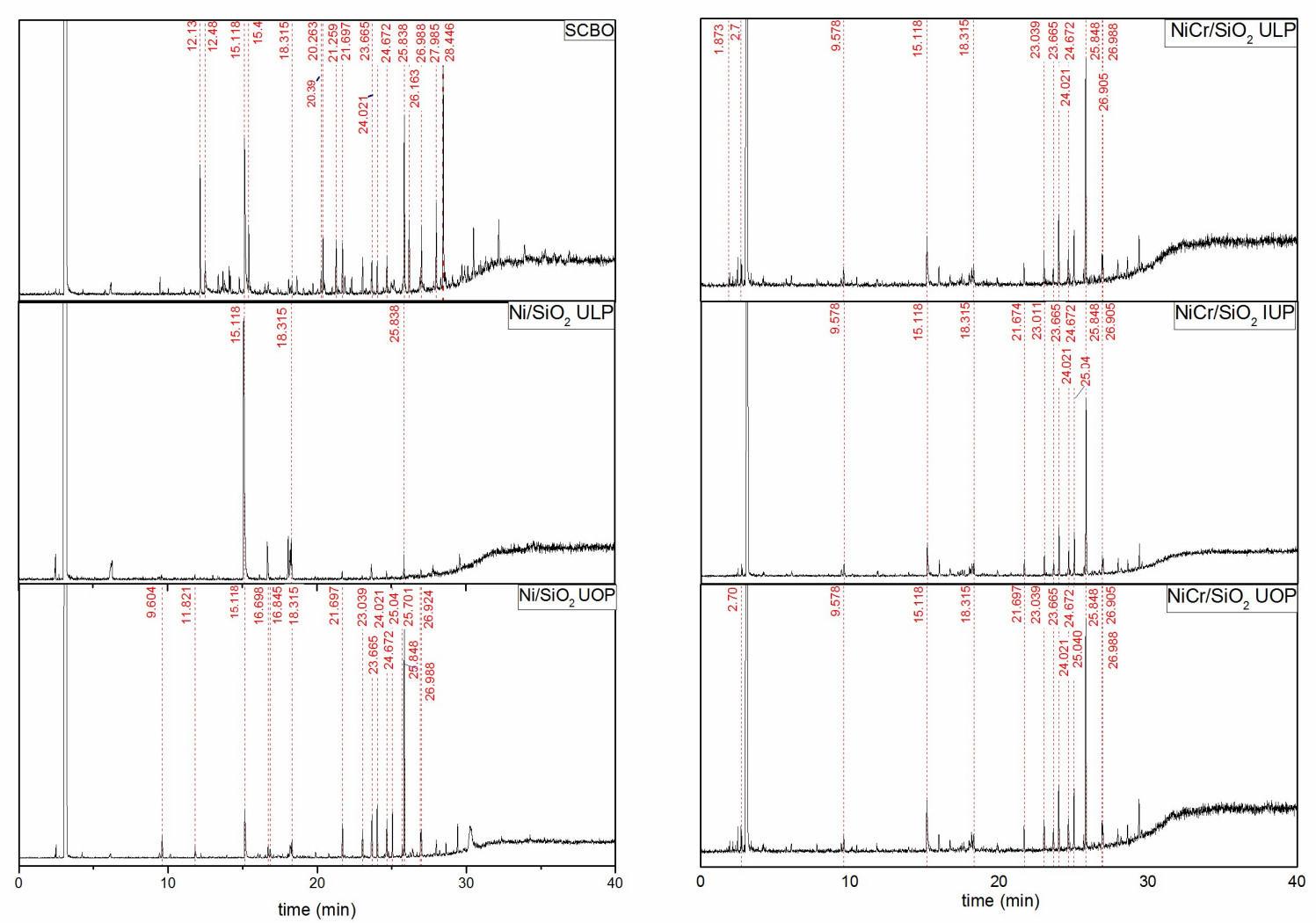

Figure S 30. Qualitative GC-MS chromatogram of SCBPO and upgraded fractions. Samples diluted 1:20 in methanol, except $IUP_{NiCr/SiO2}$, diluted 1:10 in methanol, respectively.

Table S 13. Qualitative evaluation of feedstock, and upgraded fractions with GC-MS.

Retention time (min)	Compound
1.873	Ethyl-cyclopropane
2.70	Tetrahydrofuran
9.578	Cyclohexanone
9.604	2-methyl-cyclopentanone
11.821	2-ethyl-cyclopentanone
12.134	1-hydroxy-2-propanone
12.480	1-propanol
15.118	Acetic acid
15.40	Furfural
16.698	Propanoic acid
16.845	2,3-dimethyl-2-cyclopenten-1-one
18.315	butyrolactone
20.263	2(5H)-Furanone
20.390	1,2-cyclopentanedione
21.259	3-methyl-1,2-cyclopentanedione
21.674	2,3,4-trimethyl-2-cyclopenten-1-one
21.697	2-methoxy-phenol
23.011	2-methoxy-5-methylphenol
23.039	2-methoxy-4-methylphenol
23.665	Phenol
24.021	4-ethyl-2-methoxy-phenol
24.672	4-methyl-phenol
25.040	2-methoxy-4-propyl-phenol
25.701	4-ethyl-2-methyl-phenol
25.838	2-ethyl-phenol
25.848	4-ethyl-phenol
26.163	1-(3-methoxyphenyl)-ethanone
26.905	2-propyl-phenol
26.924	4-propyl-phenol
26.988	2,6-dimethoxy-phenol
27.985	Eugenol
28.446	2,3-dihydro-benzofuran

S.6.5 GC-MS/FID

Table S 14. GC-MS/FID analysis of SCBPO and upgraded products.

Compound *(wet basis; dry basis)*	**SCBPO**	**Ni/SiO_2 ULP**	**Ni/SiO_2 UOP**	**Ni-Cr/SiO_2 ULP**	**Ni-Cr/SiO_2 IUP**	**Ni-Cr/SiO_2 UOP**
NONAROMATIC COMPOUNDS	**25.08;31.52**	**17.42; 63.88**	**14.11; 15.90**	**14.84; 48.85**	**16.04; 17.61**	**14.76;16.53**
Acids	**10.54;13.24**	**13.43; 49.24**	**10.86; 12.24**	**10.36; 34.11**	**11.39; 12.50**	**10.97;12.28**
Acetic acid[c]	6.80;8.55	10.67; 39.12	5.51; 6.21	8.10; 26.67	4.80; 5.27	4.69;5.25
Propionic acid[c]	3.73;4.70	2.29; 8.40	5.35; 6.03	1.89; 6.22	5.44; 5.97	5.45;6.1
Butyric Acid[c]		0.43; 1.57		0.32; 1.07	0.88; 0.96	0.84;0.94
Pentanoic Acid[#]	-	0.04; 0,15		0.05; 0.15	0.27; 0.30	-
Nonaromatic Esters	**-**	**0.42; 1.55**	**0.10; 0.11**	**0.34; 1.12**	**0.20; 0.22**	**0.15;0.17**
Propanoic acid, methyl ester[#] (NIST MQ 88)	-	0.04; 0.16	0.10; 0.11	0.16; 0.54	0.10; 0.11	0.08;0.08
Acetic acid, butyl ester[#]	-	-	-	-	0.10; 0.11	0.08;0.08

(NIST MQ 97)						
Acetic acid 2-hydroxyethyl ester[c]	-	0.37; 1.35	-	0.17; 0.58	-	-
Propanoic acid, 2-hydroxyethyl ester[#]	-	0.01; 0.05	-	-	-	-
Nonaromatic Alcohols	**0.49; 0.61**	**2.72; 9.98**	**0.03; 0.03**	**3.32; 10.91**	**0.61; 0.67**	**0.44;0.49**
Ethylene glycol[c]	0.49;0.61	2.68; 9.83	-	1.95; 6.42	-	-
1-propanol[#]	-	0.04; 0.15	-	0.32; 1.06	0.57; 0.63	0.44;0.49
2-butanol[#]	-	-	-	0.02; 0.06	-	-
Propylene Glycol[#]	-	-	-	0.75; 2.48	-	-
2,3-Butanediol[#]	-	-	-	0.03; 0.09	-	-
Cyclohexanol[#]	-	-	-	0.01; 0.03	-	-
1,2-Butanediol[#]	-	-	-	0.13; 0.44	-	-
Isomer of Cyclopentane-1,2-diol[#]	-	-	-	0.04; 0.14	-	-
1,2-Cyclohexanediol, cis-[#]	-	-	-	0.04; 0.14	-	-
1-Propanol, 2-methyl-[#]	-	-	-	-	0.04; 0.04	-
Unknown aliphatic alcohol[#]	-	-	0.03; 0.03	-	-	-
Nonaromatic Aldehydes	**7.18; 9.02**	-	-	-	-	-
Acetaldehyde, hydroxy-[c]	6.03;7.57	-	-	-	-	-
Propionaldehyde, 3-hydroxy[#]	0.59;0.75	-	-	-	-	-
Butanedial or Propanal [#]	0.56;0.70	-	-	-	-	-
Nonaromatic Ketones	**6.88;8.65**	**0.85; 3.11**	**3.12; 3.52**	**0.82; 2.71**	**3.71; 4.08**	**3.19;3.57**
Acetonylacetone (Hexadione, 2,5-)[c]	-	0.03; 0.13	-	0.01; 0.04	-	-
Acetoin (Hydroxy-2-butanone,3-)[c]	-	0.12; 0.45	-	0.16; 0.54	-	-
2-butanone[c]	-	-	-	-	0.40; 0.44	0,32; 0.36
Cyclopentanone[c]	-	-	0.35; 0.39	-	0.48; 0.53	0.44; 0.5
Cyclohexanone[#]	-	0.02; 0.07	-	0.04; 0.14	0.22; 0.24	-
Cyclohexanone, 2-hydroxy-[#]	-	-	-	0.02; 0.07	-	-
3-Hexanone, 4-hydroxy-[#]	-	-	-	0.03; 0.10	-	-
2-Pentanone[#]	-	0.10; 0.36	0.26; 0.30	0.15; 0.51	0.57; 0.63	0.45; 0.5
3-Pentanone, 2-hydroxy-[#]	-	0.03; 0.12	-	0.07; 0.22	-	-
2-methyl-3-pentanone[#]	-	-	0.04; 0.05	-	-	0.04; 0.04
3-hexanone[#]	-	-	0.02; 0.03	-	0.11; 0.12	0.07; 0.08
2-hexanone[#]	-	-	0.05; 0.05	-	0.12; 0.13	0.1; 0.12
2-methyl-cyclopentanone[#]	-	0.13; 0.47	0.89; 1.00	0.11; 0.37	0.86; 0.94	0.76; 0.85
Dimethylcyclopentanone[#]	-	-	0.05; 0.06	-	0.13; 0.14	0.07; 0.08
2,5-dimethyl-cyclopentanone[#]	-	-	-	-	0.04; 0.05	0.04; 0.04
Dimethyl-cyclopentanone[#]	-	-	-	-	-	0.05; 0.06
Methyl-cyclopentanone[#]	-	-	0.11; 0.12	-	-	0.2; 0.22
2-ethyl-cyclopentanone[#]	-	0.02; 0.06	0.28; 0.31	-	0.24; 0.27	0.22; 0.24
2-methyl-cyclohexanone[#]	-	0.01; 0.02	-	-	0.09; 0.10	0.08; 0.1
Acetol (Hydroxypropanone)[c]	4.94;6.20	0.26; 0.96	-	-	-	-
Butandione, 2,3- (Diacetyl) [c]	0.11;0.14	-	-	-	-	-
Propan-2-one, 1-acetyloxy- [c]	0.15;0.19	-	-	-	-	-
Cyclopenten-1-one, 2- [c]	0.20;0.25	-	-	-	-	-
Cyclopenten-1-one, 2-methyl-2- [c]	0.08;0.11	-	-	-	-	-
Cyclopenten-1-one, 3-methyl-2- [c]	0.08;0.11	0.02; 0.07	-	-	-	-
Cyclopenten-1-one, 2-hydroxy-2-[#]	0.39;0.49	-	-	-	-	-
Cyclopenten-3-one, 2-hydroxy-1-methyl-1-[c]	0.43;0.54	-	-	-	-	-
Cyclopenten-1-one, 2,3-dimethyl-2-[c]	-	0.02; 0.06	0.15; 0.17	-	-	-

3-Pentanone[#]	0.08;0.10	0.06; 0.23	0.25; 0.28	0.09; 0.30	0.30; 0.33	0.23; 0.26
2,3-Pentanedione[#]	0.05;0.06	-	-	-	-	-
1-Hydroxy-2-butanone[#]	0.26;0.32	-	-	0.13; 0.42	-	
poss: 2-Butanone, 3-methyl-	-	0.01; 0.05	0.06; 0.07	-		-
5,9-Dodecadien-2-one, 6,10-dimethyl-, (E,E))-[#]	0.11;0.14	-	-	-	-	-
1,4-Cyclohexanedione[#]	-	0.01; 0.02	-	-	-	-
Cyclopentanone, 2-acetonyl-[#]	-	0.01; 0.04	-	-	-	-
Unknown cyclic ketone compound[#]			-	-	0.15; 0.16	0.12; 0.13
3-methyl-cyclopentanone[#]	-		0.37; 0.41	-	-	-
Isomer of 2-methyl-cyclohexanone[#]	-	-	0.08; 0.10	-	-	-
2-cyclopenten-1-one, 2,3,4-trimethyl-[#]	-	-	0.07; 0.08	-	-	-
2-cyclopenten-1-one, trimethyl-[#]	-	-	0.09; 0.11	-	-	-
Hydrocarbons	**-**	**-**	**-**	**-**	**0.13; 0.15**	**0.01; 0.01**
Ethyl-cyclohexane[#]	**-**	**-**	-	-	-	0.01; 0.01
Cyclohexene[#]	**-**	**-**	-	-	0.13; 0.15	-
Cyclopentane, ethyl-[#]	**-**	**-**	-	-	0.03; 0.03	-
HETEROCYCLIC COMPOUNDS	**2.03; 2.55**	**1.12; 4.09**	**1.05; 1.18**	-	-	-
Furans	**1.84; 2.31**	**1.12; 4.09**	**1.05; 1.18**	**2.64; 8.68**	**3.35; 3.68**	**2.91; 3.26**
γ-valerolactone[#]	-	-	0.09; 0.10	0.18; 0.60	0.37; 0.40	-
α-methyl-γ-butyrolactone[c]	-	0.02; 0.07	-	0.09; 0.29	0.17; 0.19	0.16; 0.18
Tetrahydro-furan[#]	-	0.18; 0.66	0.31; 0.35	0.19; 0.64	0.70; 0.76	0.56; 0.62
Tetrahydro-2-methyl-furan[#]	-	-	-	0.07; 0.23	0.46; 0.50	0.37; 0.41
Tetrahydro-2,5-dimethyl-furan[#]	-	-	-	-	0.04; 0.05	-
Tetrahydro-2-methyl-2-furanol[#]	-	0.01; 0.04	-	0.54; 1.79	0.48;0.53	0.44; 0.5
Tetrahydro-3-methyl-furan[#]	-	-	-	-	0.08; 0.10	-
Tetrahydro-3-furanol[#]	-	-	-	0.06; 0.20	-	-
Tetrahydro-2-(methoxymethyl)-furan or isomere[#]	-	-	-	0.19; 0.62	-	-
Isomer of 2(3H)-furanone, dihydro-4-hydroxy-[#]	-	-	-	0.03; 0.10	-	-
2(3H)-furanone, dihydro-3,5-dimethyl-[#]	-	-	-	0.01; 0.04	-	-
Isomer of 2(3H)-furanone, dihydro-3,5-dimethyl-[#]	-		-	0.02; 0.05	-	-
3,4-furandiol, tetrahydro-,trans-[#]	-	0.01; 0.04	-	0.03; 0.08	-	-
Furfuryl alcohol, 2-[c]	0.10;0.12	-	-	-	-	-
Furanone, 2(5H)-[c]	0.63;0.79	-	-			
Furaldehyde, 2-[c]	0.56;0.71	-	-			
Furan-2-one, 3-methyl-, (5H)-[c]	0.04;0.05	-	-			
Furan-x-on, x,x-dihydro-x-methyl-[#]	0.10;0.13	-	-			
Butyrolactone, γ-[c]	0.21;0.26	0.68; 2.48	0.64; 0.72	0.68; 2.23	0.80; 0.87	0.79;0.88
2(5H)-Furanone, 5-methyl-(NIST MQ 84)[#]	0.07;0.09	-	-	-	-	-
Furan-2-one, 4-methyl-(5H)-(NIST MQ 88)[#]	0.13;0.16	-	-	-	-	-
2(3H)-furanone, dihydro-4-methyl-[#]	-	0.02; 0.07	-	0.10; 0.33	0.26; 0.28	0.24; 0.26

Lactone derivative = furanone[#]derivative (unspecific spectrum) [#]	-	-	-	0.42; 1.40	-	-
Lactone derivative (unspecific spectrum) [#]	-	0.13; 0.49	-	0.02; 0.08	-	-
Butyrolactone, 2-hydroxy-, γ-[c]	-	0.02; 0.07	-	-	-	-
2(3H)-furanone, dihydro-5-methyl-[#]	-	0.05; 0.17	-			
Pyrans	**0.19;0.24**	**-**	**-**	**0.04; 0.14**	**-**	**-**
Pyran-4-one, 3-hydroxy-5,6-dihydro-, (4H)- [#]	0.19;0.24	-	-	-	-	-
5-Valerolactone = 2H-pyran-2-one, tetrahydro[#]	-	-	-	0.04; 0.14	-	
AROMATIC COMPOUNDS	**5.97; 7.50**	**0.29; 1.05**	**4.57; 5.16**	**0.28; 0.93**	**6.52; 7.16**	**5.99; 6.71**
Benzenes	**0.02;0.03**	**0.0; 0.01**	**0.02; 0.02**	**-**	**0.11; 0.12**	**0.07; 0.08**
Benzene (NIST MQ 97) [#]	0.02;0.03	0.0; 0.01	0.02; 0.02	-	0.04; 0.05	0.03;0.04
Toluene[c]	-	-	-	-	0.05; 0.05	0.04; 0.05
Benzene, ethyl-[c]	-	-	-	-	0.02; 0.02	-
Lignin derived Phenols	**2.59; 3.26**	**0.18; 0.66**	**2.85; 3.21**	**0.14; 0.47**	**3.76; 4.12**	**3.35; 3.75**
Phenol[c]	0.16;0.20	0.08; 0.29	0.46; 0.52	0.03; 0.10	0.27; 0.29	0.25; 0.28
Cresol, o-[c]	0.06;0.07	0.01; 0.03	0.08; 0.08	0.01; 0.03	0.09; 0.10	0.08; 0.09
Cresol, p-[c]	0.11;0.13	0.02; 0.07	0.23; 0.26	0.02; 0.06	0.30; 0.33	0.3; 0.33
Cresol, m-[c]	0.04;0.05	0.01; 0.04	0.10; 0.11	0.01; 0.04	0.12; 0.14	0.12; 0.13
Phenol, 2,5-dimethyl-[c]	-	-	-	-	0.18; 0.20	-
Phenol, 2,4-dimethyl-[c]	-	-	-	-	-	0.11; 0.12
Phenol, 4-ethyl-[c]	0.55;0.69	0.06; 0.23	1.62; 1.83	0.07; 0.23	2.21; 2.43	2.14; 2.39
Phenol, 4-propyl-[c]	-	-	-	-	0.36; 0.39	-
Phenol, 4-vinyl-[#]	1.51;1.89	-	-	-	-	-
Phenol, 2-propyl-[c]	-	-	0.15; 0.17	-	-	0.17; 0.19
Benzaldehyde, 4-hydroxy-[c]	0.15;0.19	-	-	-	-	-
Phenol, ethyl-methyl-[#]	0.03;0.04	-	0.07; 0.08	-	0.12; 0.14	0.12; 0.13
Phenol, C4-[#]	-	-	0.06; 0.06	-	0.06; 0.06	0.06; 0.07
Poss: Phenol, x-methyl-x-propyl-[#]	-	-	-	-	0.04; 0.05	-
Phenol, 3,5-dimethyl-[c]	-	-	0.08; 0.09	-	-	-
Guaiacols (Methoxy phenols)	**1.95;2.45**	**0.07; 0.24**	**1.06; 1.20**	**0.08; 0.25**	**1.64; 1.80**	**1.58; 1.77**
Guaiacol[c]	0.14;0.18	0.03; 0.12	0.23; 0.26	0.03; 0.11	0.26; 0.29	0.25; 0.27
Guaiacol, 4-methyl-[c]	0.13;0.17	0.02; 0.06	0.20; 0.23	0.02; 0.06	0.32; 0.35	0.31; 0.35
Guaiacol, 4-ethyl-[c]	0.09;0.11	0.01; 0.05	0.34; 0.38	0.03; 0.08	0.58; 0.63	0.56; 0.62
Guaiacol, 4-propyl-[c]	-	0.0; 0.01	0.28; 0.32	-	0.48; 0.53	0.47; 0.52
Guaiacol, 4-vinyl-[#]	0.34;0.43	-	-	-	-	-
Guaiacol, 4-allyl- (Eugenol)[c]	0.06;0.07	-	-	-	-	-
Guaiacol, 4-propenyl- cis (Isoeugenol)[c]	0.16;0.20	-	-	-	-	-
Guaiacol, 4-propenyl-(trans) (Isoeugenol) [c]	0.30;0.38	-	-	-	-	-
Vanillin [c]	0.40;0.50	-	-	-	-	-
Phenylacetaldehyde, 4-hydroxy-3-methoxy- (Homovanillin) [c]	0.04;0.05	-	-	-	-	-
Phenylethanone, 4-hydroxy-3-methoxy- (Acetoguajacone) [#]	0.29;0.36	-	-	-	-	-
Syringols (Dimethoxy phenols)	**1.40;1.77**	**0.04; 0.14**	**0.65; 0.73**	**0.06; 0.21**	**1.02; 1.12**	**0.99; 1.1**
Syringol[c]	0.19;0.24	0.01; 0.04	0.21; 0.24		0.16; 0.17	0.15; 0.16

Syringol, 4-methyl-[c]	0.17;0.22	0.03; 0.10	0.14; 0.16	0.04; 0.13	0.24; 0.27	0.24; 0.27
Syringol, 4-ethyl-[c]	0.05;0.06	-	0.09; 0.10	0.01; 0.05	0.20; 0.22	0.2; 0.22
Syringol, 4-vinyl-[#]	0.15;0.19	-	-	-	-	-
Syringol, 4-propyl-[c]	-	-	0.21; 0.24	0.01; 0.04	0.42; 0.46	0.4; 0.45
Syringol, 4-allyl-[c]	0.13;0.16	-	-	-	-	-
Syringol, 4-(1-propenyl)-, cis[#]	0.09;0.11	-	-	-	-	-
Syringol, 4-(1-propenyl)-, trans[#]	0.28;0.35	-	-	-	-	-
Syringaldehyde[c]	0.15;0.19	-	-	-	-	-
Homosyringaldehyde[#]	0.02;0.03	-	-	-	-	-
Acetosyringone[c]	0.08;0.10	-	-	-	-	-
Syringyl acetone[#]	0.10;0.12	-	-	-	-	-
CARBOHYDRATES	**7.08;8.90**	**-**	-	-	-	-
Sugars	**7.08;8.90**	**0.08; 0.29**	**-**	**0.32; 1.06**	**-**	**-**
Anhydro-ß-D-arabinofuranose, 1,5-[#]	0.32;0.41	-	-	-	-	-
Anhydro-ß-D-xylofuranose, 1,5-[#]	0.73;0.92	-	-	-	-	-
Anhydro-ß-D-glucopyranose, 1,6-(Levoglucosan)[c]	5.40;6.79	-	-	-	-	-
Dianhydro-α-D-glucopyranose, 1,4:3,6-[#]	0.27;0.34	-	-	-	-	-
Anhydrosugar unknown[#](unspecific spectrum)[#]	0.35;0.44	-	-	-	-	-
Isosorbide[#]	-	-	-	0.25; 0.82	-	-
Unknown sugar[#]		0.08; 0.29	-	0.07; 0.24	-	
OTHER ORGANIC COMPOUNDS						
Acetates	**-**	**0.0; 0.01**	**-**	**0.03; 0.10**	**0.11; 0.12**	**0.09; 0.1**
Ethyl acetate[#]	**-**	0.0; 0.01	-	0.02; 0.05	0.06; 0.07	0.04; 0.04
2-Furanmethanol, tetrahydro-,acetate[#]	**-**	**-**	-	0.01; 0.04	0.05; 0.06	0.05; 0.05
unknown compounds	**0.10;0.13**	**-**	**-**	**0.04; 0.12**	**-**	**-**
Acetone derived compound = impurity in Acetone[#]	0.10;0.13	-	-	-	-	-
Unknown aliphatic alcohol[#]	-	-	-	0.03; 0.11	-	-
Isomer of 2(3H)-furanone, dihydro-dimethyl[#]	-	-	-	0.0; 0.02	-	-
Miscellaneous	**0.03;0.03**	**0.01; 0.02**	**0.03; 0.03**	**0.01; 0.02**	**0.03; 0.03**	**0.03; 0.03**
Naphthalene, 1-phenyl- (impurity in internal standarad= Fluoranthene) [#]	0.03;0.03	0.01; 0.02	0.03; 0.03	0.01; 0.02	0.03; 0.03	0.03; 0.03

c: calibrated compound; n.q.: not quantified; [#]: estimated response factor

S.6.6 Viscosity measurements

The dynamic viscosity results of SCBPO, $UOP_{Ni/SiO2}$ and $IUP_{Ni\text{-}Cr/SiO2}$ at 40 °C are depicted in the Figure S.31. Due to the low amount of sample available, the viscosity measurement of $UOP_{Ni\text{-}Cr/SiO2}$ was not performed.

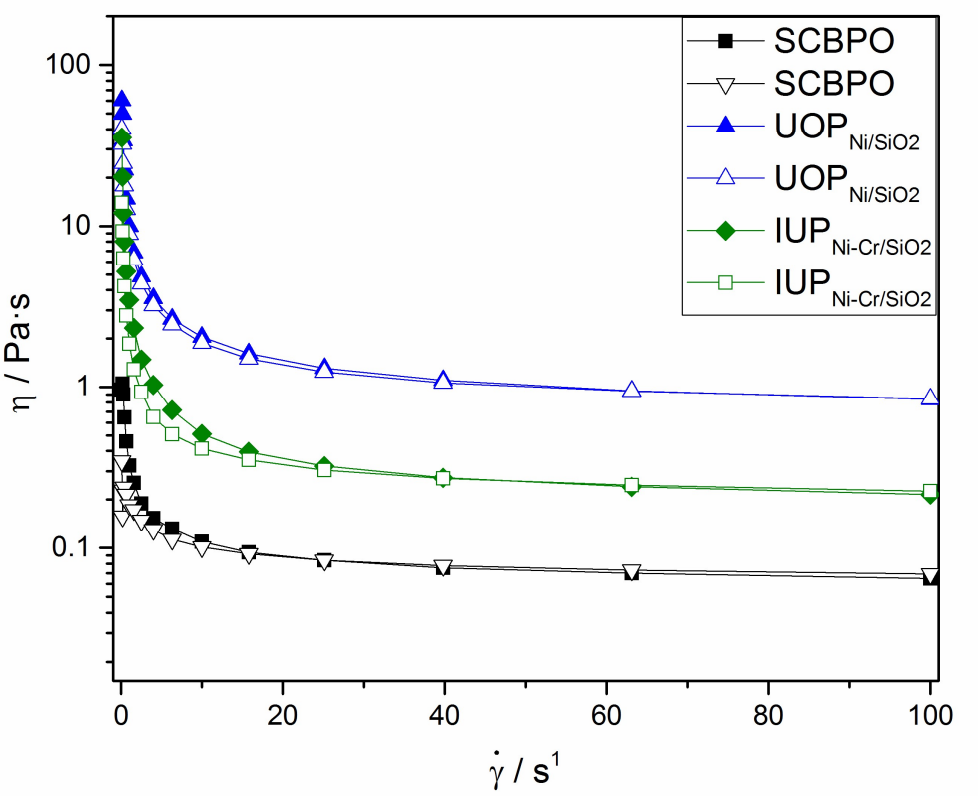

Figure S 31. Dynamic viscosity measured at 40 °C as a function of shear rate.

S.6.7 XRD fresh and spent catalysts

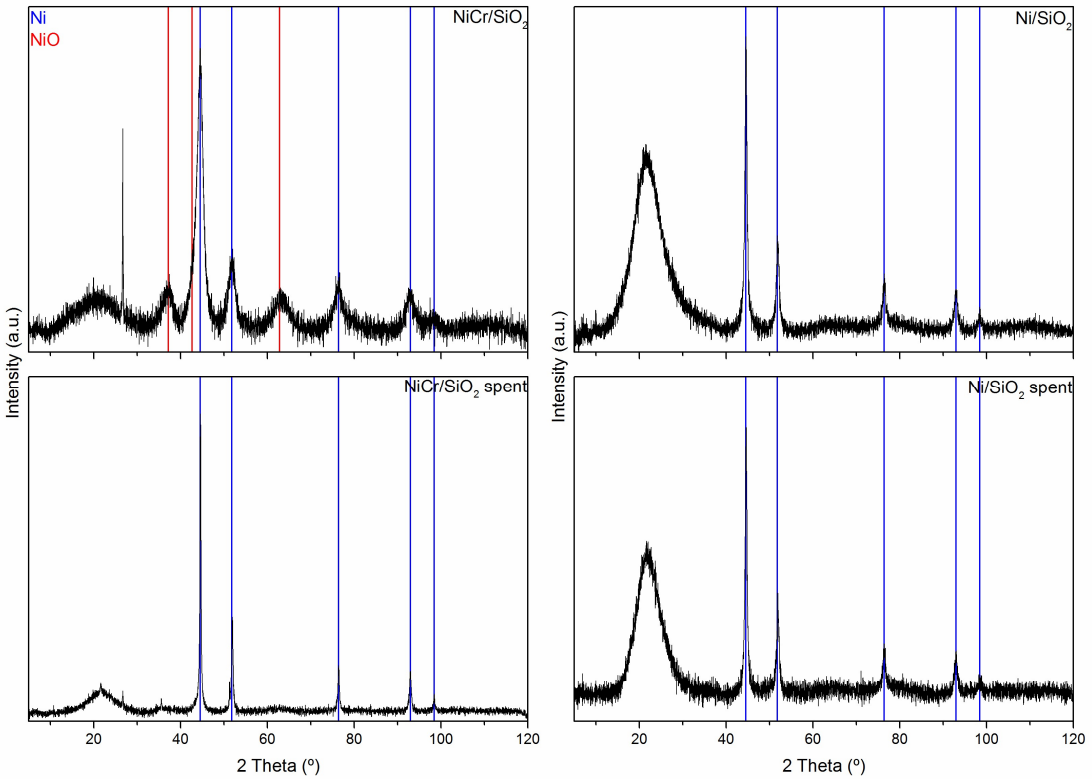

Figure S 32. XRD patterns before and after reactions. Ni diffractions are identified by blue lines and NiO by red lines.

S.6.8 Hydrogen temperature reduction (H_2-TPR) of Ni-Cr/SiO_2

The H_2-TPR measurement of Ni-Cr/SiO_2 is shown in Figure S.33.

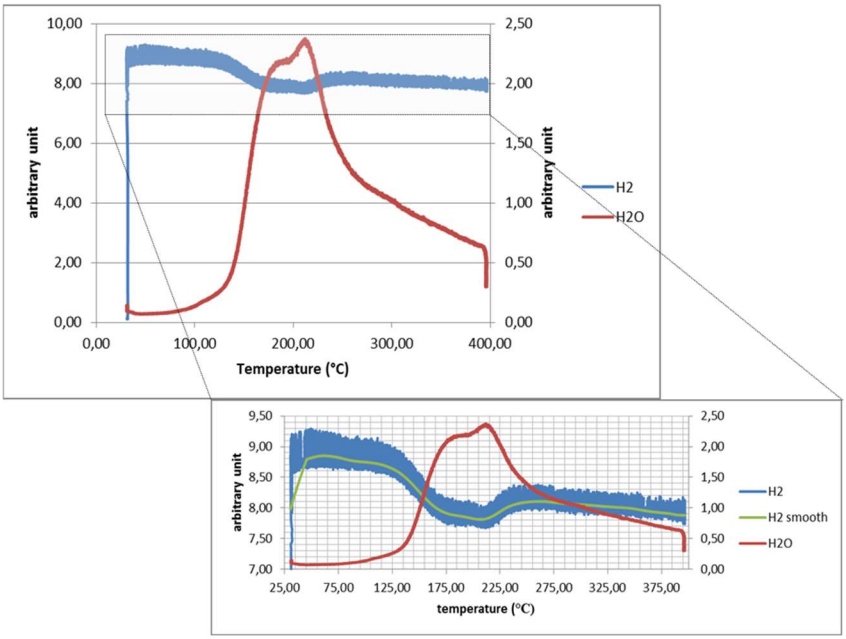

Figure S 33. H_2-TPR profile Ni-Cr/SiO_2 catalyst. H_2 consumption smoothed with Lowess method (zoomed area).

S.6.9 Size Exclusion Chromatgraphy

The SEC was performed at DWI Leibniz Institute for Interactive Materials in Aachen, Germany. The samples were prepare by dilution with tetrahydrofuran (≥99.7 %, unstabilized, HIUPerSolv CHROMANORM® HPLC grade, VWR), also used as eluent. The tetrahydrofuran used for sample preparation contained 250 mg/mL of 3,5-di-tert-4-butylhydroxytoluene (BHT, ≥99 %, Fluka) as internal standard. The measurement was conducted using an HPLC pump (1260 Infinity II, Agilent), an UV-detector (UV-2075plus, Jasco), a refractive index detector (1290 Infinity II, Agilent) and a multi angle light scattering (MALS) (SLD 7100, Polymer Standards Service). The device was composed by one pre-column (8x50 mm) and four SDplus gel columns (8x300 mm, SDplus, MZ Analysentechnik). Gel particles measured 5 µm with nominal pore widths of 50, 10^2, 10^3 and 10^4 Å. The flow rate was kept at 1.0 mL/min at 20 °C. Calibration was achieved using narrow distributed poly(methyl methacrylate) standards (Polymer Standards Service). The results were evaluated using the PSS WinGPC UniChrom software (Version 8.3.2).

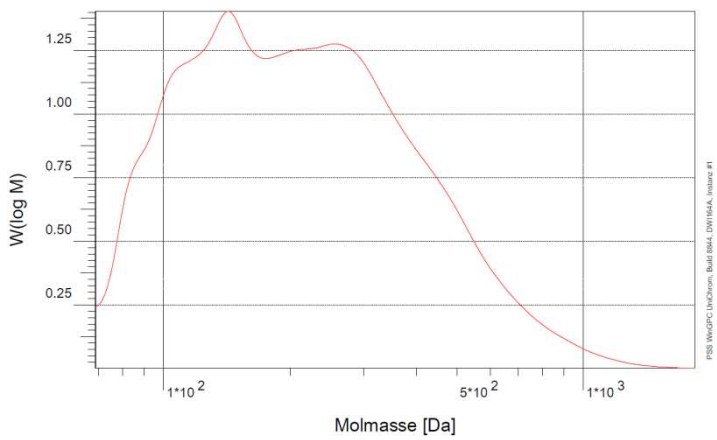

SCBPO

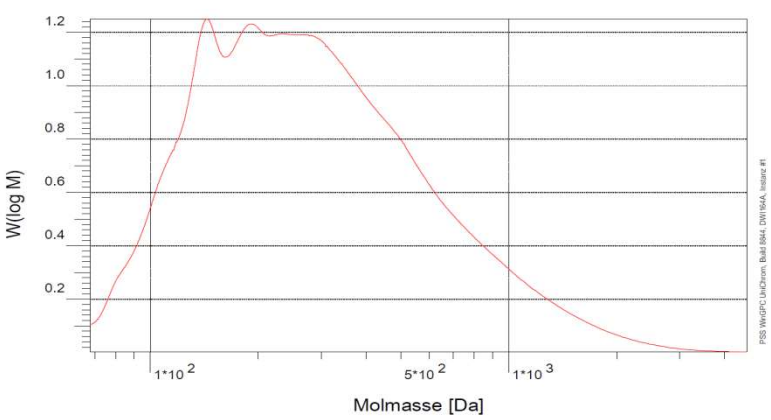

$IUP_{Ni\text{-}Cr/SiO2}$

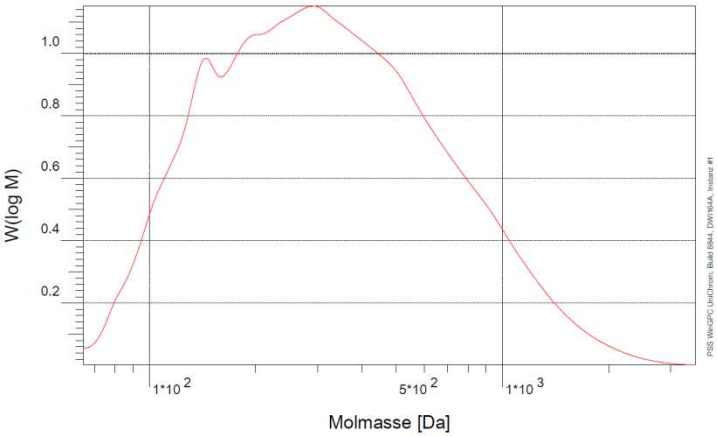

$UOP_{Ni/SiO2}$

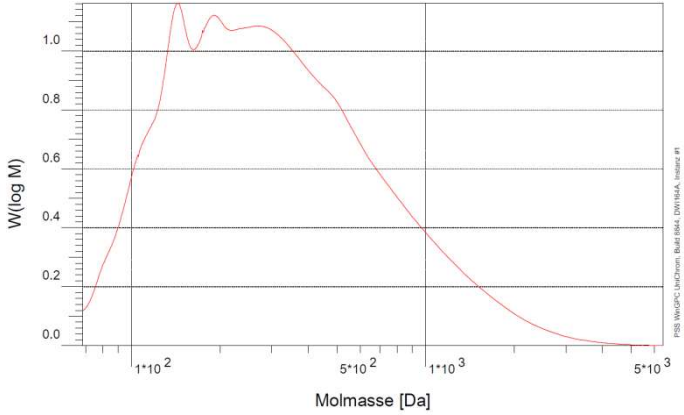

$UOP_{Ni\text{-}Cr/SiO2}$

Figure S 34. Size exclusion Chromatography of SCBPO and upgraded products

Supplementary Material – Chapter 7

S.7.1 Detail of the reactor used for the hydrotreatment/hydrodeoxygenation experiments.

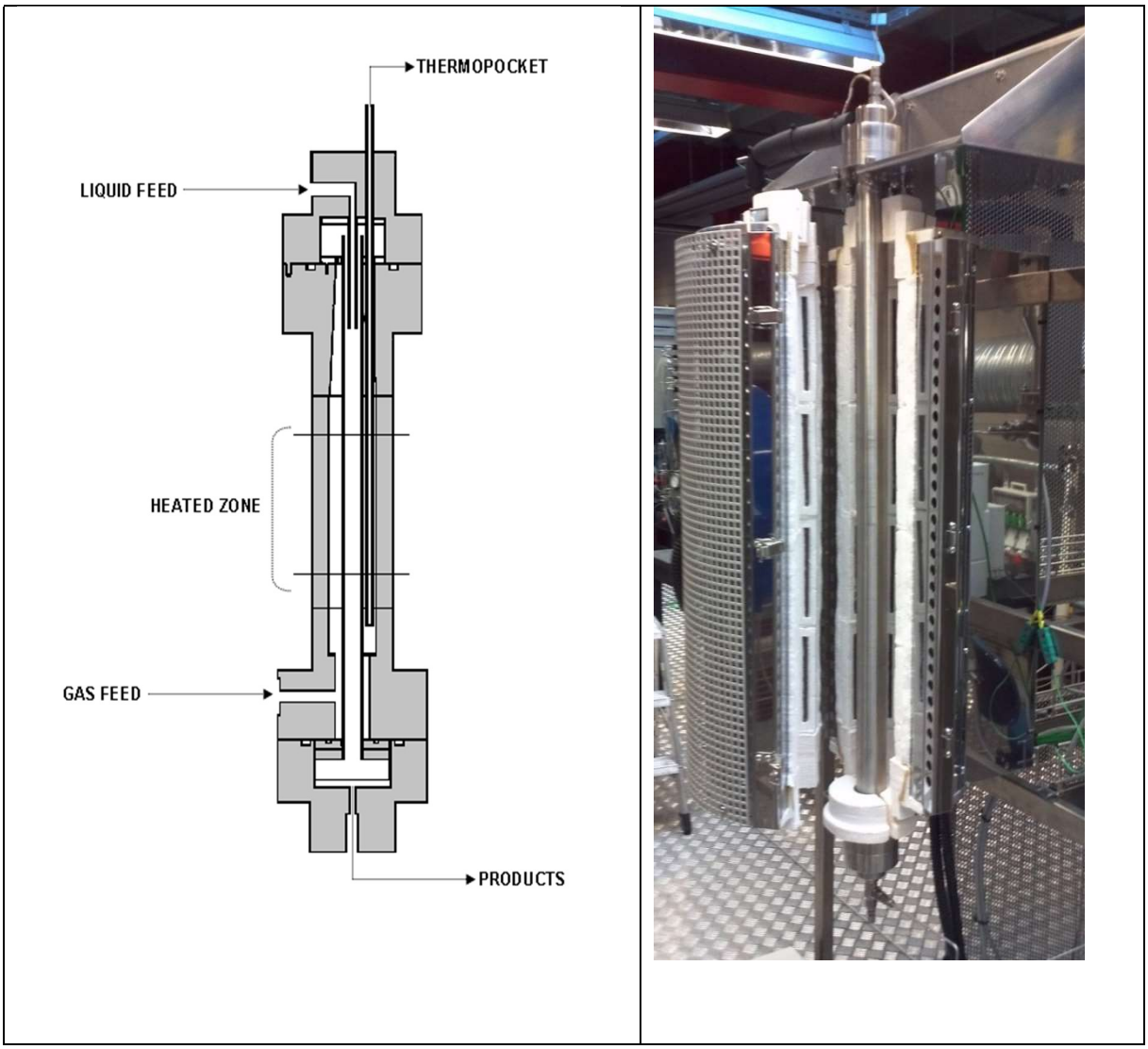

Figure S 35. Reactor details. (a) Reactor's schematic diagram (b) Oven and steel reactor.

S.7.2 Calibration piston pump

The piston pump was calibrated with the feed used for the experiments (5 wt.% guaiacol in 1-octanol). The flow was set at three different flow rate (0.1 ml/min, 0.2 ml/min and 0.3 ml/min) and the samples were collected in an interval of 5 minutes. For each flow rate evaluated, three samples were collected. The calibration curve was then plotted (Figure S.36).

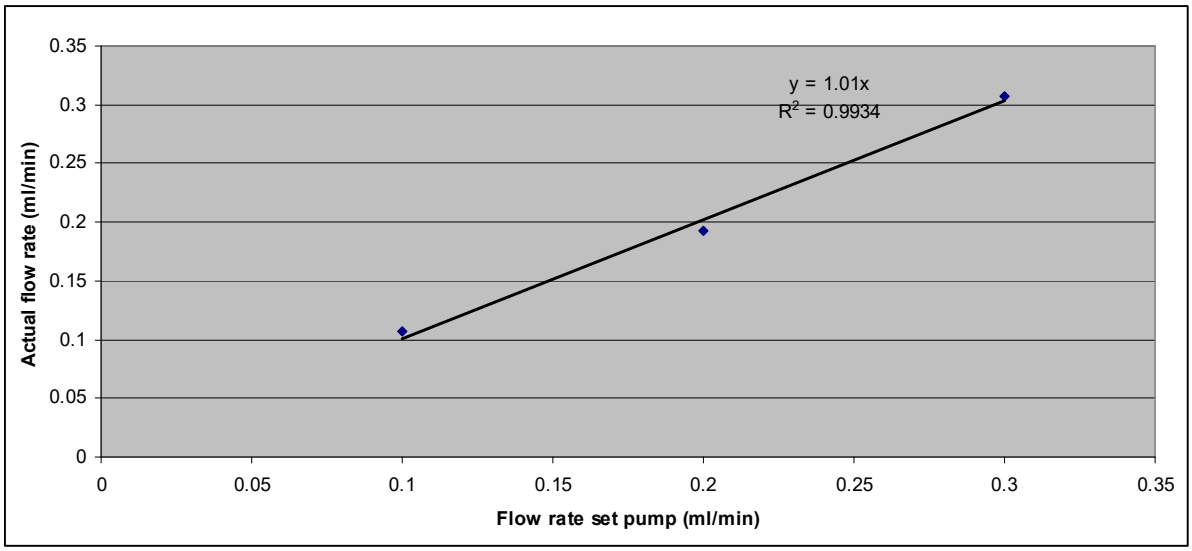

Figure S 36. Piston pump calibration.

S.7.3 Catalyst Bed

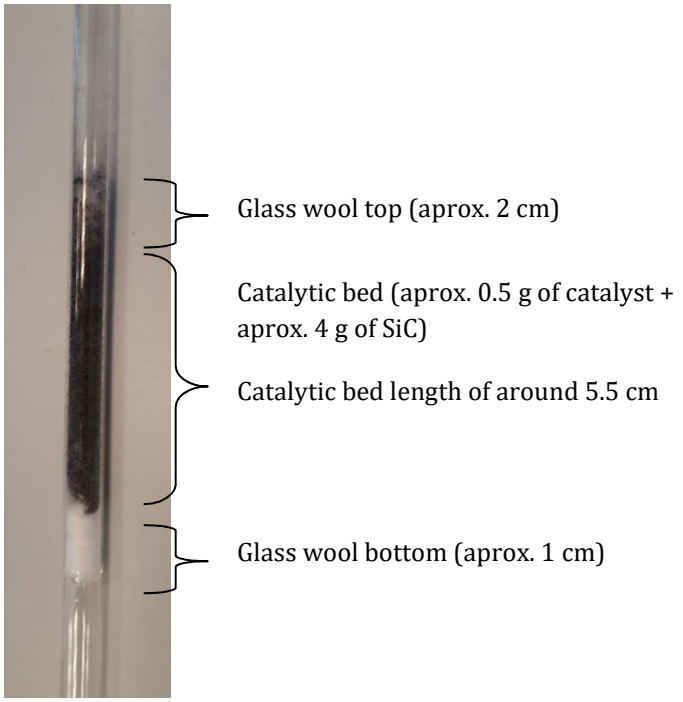

Figure S 37. Catalyst bed packed in a quartz tube for illustration of the packing procedure adopted for the hydrotreatment reactions.

S.7.4 Calibration curve for liquid products quantification

The external calibration of the compounds in the feedstock and in the upgraded liquids, described in Table S.15, as well as the R^2.

Table S 15. External calibration curve of guaiacol and 1-octanol.

Compound	Calibration curve	R^2
guaiacol	y=86871x-21975	0,9977
1-octanol	y=128166x-268504	0,9989

S.7.5 Chemical composition upgraded liquids

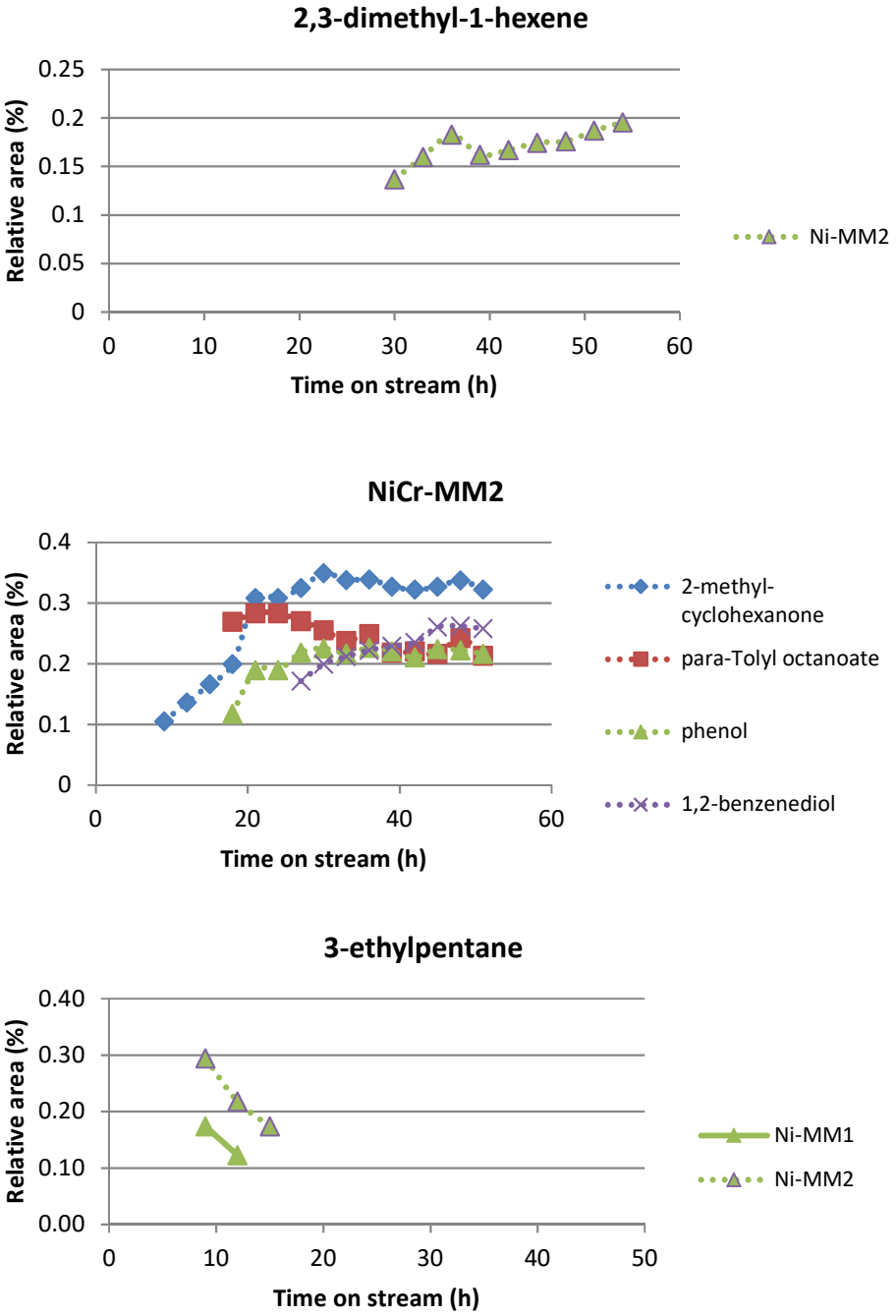

Figure S 38. Some of the minor compounds identified in the upgraded liquids as function of time on stream.

List of figures

List of Tables

Supplementary Material

List of supplementary Figures

List of Supplementary Tables